Classical and Quantum Dots Photoredox Catalyzed Synthetic Methods

Inaugural dissertation
of the Faculty of Science,
University of Bern

presented by

Eloïse Colson

from France

Supervisor of the doctoral thesis:
Prof. Dr. Philippe Renaud

Department of Chemistry, Biochemistry and Pharmaceutical Sciences
(University of Bern)

Classical and Quantum Dots Photoredox Catalyzed Synthetic Methods

Inaugural dissertation
of the Faculty of Science,
University of Bern

presented by

Eloïse Colson

from France

Supervisor of the doctoral thesis :
Prof. Dr. Philippe Renaud

Department of Chemistry, Biochemistry and Pharmaceutical Sciences
(University of Bern)

Accepted by the Faculty of Science.

Bern, 28.10.2022

The Dean
Prof. Dr. Marco Herwegh

«Le hasard ne favorise que les esprits préparés.»

Louis Pasteur

Abstract

Quantum dots are nanometer-sized semiconductors composed of an inorganic core and surrounded by an organic layer of ligands. Due to their nanometric size, quantum dots exhibit discrete atomic-like states and are able, upon light excitation, to engage in electron transfers with small organic molecules (Figure 1).
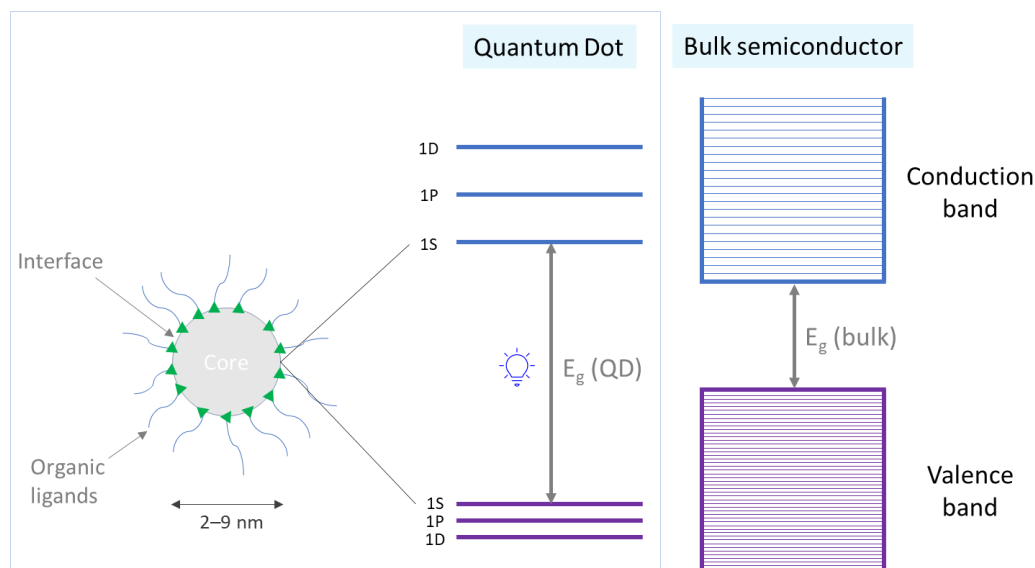

Figure 1. Quantum dot semiconductors – atomic-like states and general composition.

Their use as photocatalysts in preparative organic synthesis is developing rapidly but is largely limited to net reductive processes. In addition, quantum dots are still far from being adopted as common photocatalysts by organic chemists, despite the current craze for photoredox protocols. As part of a collaboration with a team of physical-chemists from the CEA in Grenoble (France), we had the objective to develop quantum dot photocatalysts (in Grenoble) and to use them for preparative organic chemistry (in Bern).

A first phase was devoted to the development of redox neutral photochemical methods using iridium photocatalysis. We investigated boronate complexes as radical precursors by one-electron oxidation and found that alcoholate-substituted boronate complexes where efficient at generating not the corresponding alkoxyl radical, but the phenyl radical (Figure 2). The alcohol substituent was important to reduce the formation of a biphenyl side-product. The utility of the generated phenyl radical was demonstrated by an allylation reaction as well as by its ability to engage in iodine abstraction. No substrate scope was investigated for these transformations and quantum dot photocatalysis was not applied in this case.
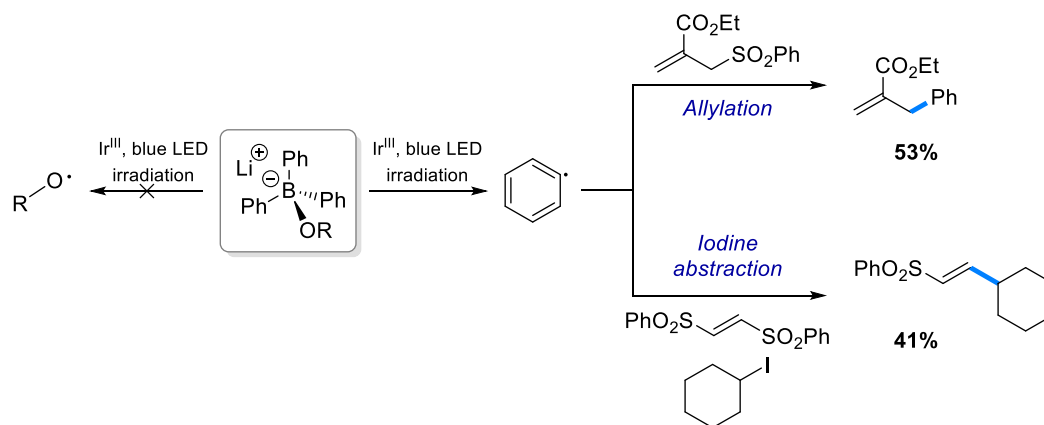
Figure 2. One-electron oxidation for alcoholate-substituted boronate complexes leading to the phenyl radical. Application for allylation and iodine abstraction reactions.

Next, we turned our intention to alpha-aminoalkyl radicals as key intermediates in a radical [3+3]-annulation reaction leading to biologically relevant tropane and related alkaloid skeletons (Figure 3). We demonstrated that a broad scope of aniline derivatives could be engaged in this transformation. The products are distinct from the Robinson annulated products and functional handles are available for further derivatization. In addition, important milestones towards the total synthesis of (+)-euphococcinine were achieved.
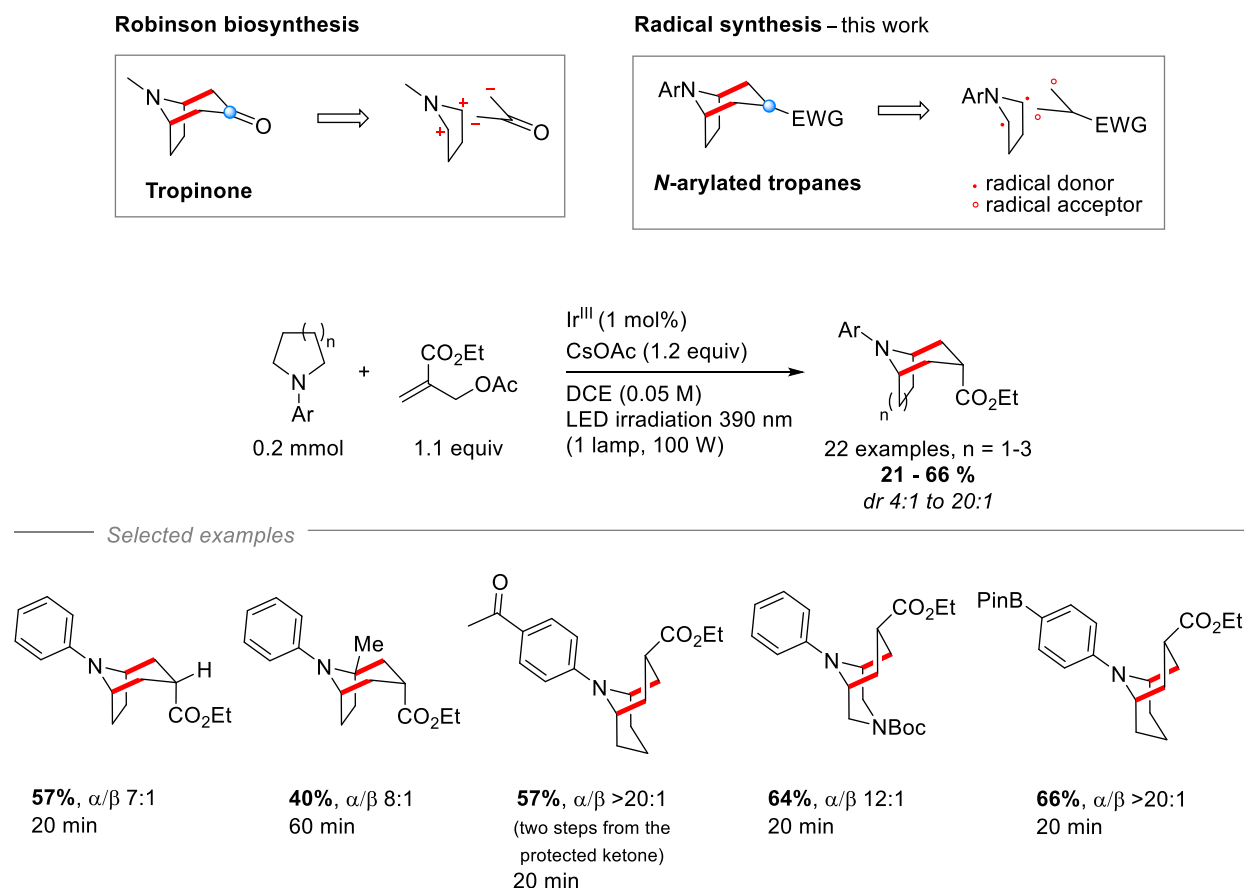
Figure 3. Selected scope of the radical [3+3]-annulation leading to tropane and homotropane derivatives.

After the development of suitable quantum dots in Grenoble, these photocatalysts were used for the radical annulation reaction. Despite limitations observed in the scope for reaction scale exceeding 0.05 mmol, promising results were obtained with *N*-phenylpyrrolidine on 0.2 mmol scale (Figure 4).

Photocatalyst
CsOAc (1.2 equiv)
⟶
LED irradiation 390 nm

0.2 mmol

With Ir^{III}: 1.1 equiv
With QDs: 1.3 quiv.

With Ir^{III}: **57%**, α/β 7:1, 20 min
With QDs: **46%**, α/β 6:1, 24 h
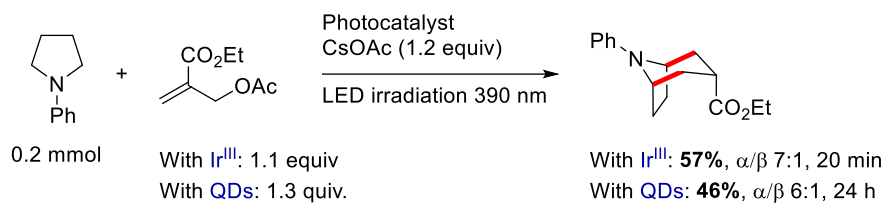
Figure 4. Radical [3+3]-annulation on *N*-phenylpyrrolidine. Comparison between the iridium-and the quantum dot-photocatalyzed reactions.

List of abbreviations and symbols

A or Abs	Absorbance
Ac	Acetyl
AIBN	Azobisisobutyronitrile
Alox	Aluminium oxide
aq.	aqueous
Ar	Aryl group
BDE	Bond Dissociation energy
Bn	Benzyl
brsm	Based on recovered starting material
C	Concentration
CB	Conduction Band
Cbz	Carboxybenzyl
Cy	Cyclohexyl
D	Diameter
DABCO	1,4-Diazabicyclo(2.2.2)octane
DCE	1,2-Dichloroethane
DCM	Dichloromethane
DIPEA	N,N-Diisopropylethylamine, or Hünig's base
DMAP	4-(Dimethylamino)pyridine
DME	Dimethoxyethane
DMF	N,N-dimethylformamide
DMPU	N,N'-Dimethylpropyleneurea
DMSO	Dimethylsulfoxide
dr	diastereomeric ratio
DTBHN	Di-tert-butyl hyponitrite
EDG	Electron Donating Group
ee	enantiomeric excess
Eg	Band gap

Eq.	Equation
equiv.	Equivalent
er	enantioemeric ratio
ESI	Electron Spray Ionization
EtOAc	Ethyl acetate
EWG	Electron Withdrawing Group
fcc	flash column chromatography
GC	Gas Chromatography
HAT	Hydrogen Atom Transfer
HOMO	Highest Occupied Molecular Orbital
HPLC	High Performance Liquid Chromatography
HRMS	High-Resolution Mass Spectrometry
hv	Irradiation
IR	Infrared spectroscopy
k	rate constant
LA	Lewis Acid
LB	Lewis Base
LED	Light Emitting Diode
LG	Leaving Group
LMCT	Ligand to Metal Charge Transfer
LUMO	Lowest Unoccupied Molecular Orbital
M	Molarity (mol/L)
m/z	mass-to-charge ratio
*m*CPBA	meta-chloroperbenzoic acid
MeCN	Acetonitrile
MLCT	Metal to Ligand Charge Transfer
mol%	0,01 equiv.
mp	melting point
MPA	3-mercaptopropionic acid
MVK	Methyl vinyl ketone

n.d.	not determined
NMP	N-Methyl-2-pyrrolidone
NMR	Nuclear Magnetic Resonance
Nu	Nucleophile
o.n.	Overnight
OlAc	Oleic acid
OlAm	Oleylamine
OMs	Mesylate
OPAc	Octylphosphonic acid
PCET	Proton Coupled Electron Transfer
Ph	Phenyl
Pin	Pinacol
PMP	Para-methoxyphenyl
PPAc	Phosphopropanoic acid
ppm	part per million
PPTS	Pyridinium para-toluenesulfonate
PT	Proton Transfer
pTsOH	para-toluenesulfonic acid
QD	Quantum Dot
R	Alkyl substituent
R_f	retention factor (TLC)
rt	room temperature
RT	Retention Time (GC)
SCE	Saturated Calomel Electrode
SET	Single Electron Transfer
SH	Homolytic substitution
S_H2	Homolytic substitution, 2nd order
S_N1	Nucleophilic Substitution, 1st order
S_N2	Nucleophilic Substitution, 2nd order
S_NAr	Nucleophilic Aromatic Substitution

SOMO	Singly Occupied Molecular Orbital
T	Temperature
TAEA	Tris(2-aminoethyl)amine
TEA	Triethylamine
TEM	Transmission Electron Microscopy
TFA	Trifluoroacetic acid
TFT	α,α,α-trifluorotoluene
THF	Tetrahydrofuran
THIQ	Tetrahydroisoquinoline
THP	Tetrahydropyran
TLC	Thin Layer Chromatography
TMS	Trimethylsilyl
UV	Ultraviolet
V	Volt
VB	Valence Band
vs	*versus*
Y	Functional group
ε	extinction coefficient

General table of contents

Chapter 1 – Quantum dots as photocatalysts in light-driven organic transformations

Chapter 2 – Photoredox mediated generation of radicals from boronate complexes

Chapter 3 – Tropane and related alkaloid skeletons *via* a radical [3+3]-annulation reaction

Chapter 4 – Quantum dots as photocatalysts in the radical [3+3]- annulation reaction

Chapter 1

Chapter 1 – Quantum dots as photocatalysts in light-driven organic transformations

This PhD thesis was initiated as part of a collaboration with Dr. Vincent Maurel, Dr. Jean-Marie Mouesca and Ali Dabbous from the CEA (Commissariat à l'énergie atomique et aux énergies alternatives) in Grenoble (France), with the objective to develop quantum dot photocatalysts and to use them for preparative organic chemistry. The responsibilities of each team in this project are multiple and well defined. In Bern, the first milestone is to develop innovative organic transformations using well known, classical photoredox catalysts such as organic dyes and/or metal polypyridyl complexes. In parallel, the task of the Grenoble team is to develop efficient quantum dots for C-C bond forming reactions, either using an already published model reaction or, if timely, using the reactions developed in Bern. The ultimate goal of the collaboration is to run the reaction developed in Bern with the quantum dots developed in Grenoble, and to do so on a meaningful scale in the organic chemistry lab. As part of this collaboration, the Bern lab should also provide the collaborators with the necessary starting materials as well as product and reaction intermediate references. The Grenoble lab is responsible for providing batch quantities of quantum dots as well as supporting the project with necessary calculations and analysis (fluorescence quenching experiments, electrochemical measurements, etc).

In the following chapter, general photoredox processes will be presented and the important characteristics of quantum dots will be summarized. Finally, the state-of-the-art in quantum dot photocatalyzed organic transformations will be surveyed.

1.1. General principles of photoredox chemistry

Since the first reports on the photoluminescence of ruthenium(II) complex Ru(bpy)$_3$ in the 1980s,[1] the literature on this topic has grown tremendously. In 1984, Deronzier and co-workers were the first to use Ru^{II}(bpy)$_3$ as photoredox catalyst in an organic transformation.[2] In the last decade photoredox chemistry has emerged has an essential tool in radical chemistry. It has rendered the generation of highly reactive radical species mild, safe and efficient – in a nutshell: accessible to all. The resurgence of this mode of reactivity has led to the development of numerous photocatalysts and a deeper understanding of physicochemical processes and mechanisms.

1.1.1. Reaching the photoexcited state in metal complexes

Photoredox chemistry is the process through which a photocatalyst can facilitate the conversion of visible light into chemical energy.[3,4] Many modern transition-metal catalysts (ruthenium- or iridium-based photocatalysts) operate in the blue light region. This absorption band in the visible region corresponds to a Metal-to-Ligand Charge Transfer (MLCT), meaning that an electron is transferred from a metal-based to a ligand-based orbital (see Figure 1 for a qualitative representation).[5] The resulting spatial separation of charges is crucial for the enhanced redox activity of the excited state compared to the ground state of the photocatalyst. Having promoted one electron to a higher lying orbital, the photocatalyst can now act as both an oxidant (Single Electron Transfer (SET) from the redox partner to the metal center) and as a reductant (SET from the ligand-based orbital to the redox partner), depending on the substrate.
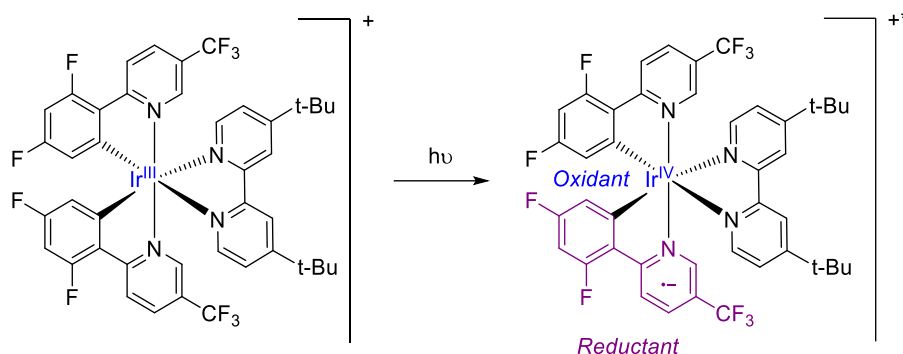
Figure 1. schematic representation of a MLCT in an iridium catalyst. The charge separation is critical for the redox activity of the photocatalyst.

From this reactivity it can easily be deduced that redox properties can be tuned through ligand design. Nowadays dozens of different iridium and ruthenium photocatalysts are commercially available and through them, a wide range of oxidation and reduction potentials can be accessed depending on the substrate to be activated.

1.1.2. Reactivity pathways for the photoexcited catalyst

In a reductive quenching cycle, the excited state of the photocatalyst acts as an oxidant by accepting an electron from the substrate (an electron donor (**D**)). This results in the reduction of the catalyst, which will need to give an electron back to an electron acceptor (**A**) in order to close the catalytic cycle (Figure 2a). In an oxidative quenching cycle, the photoexcited catalyst acts as a reductant which results in reduction of an electron acceptor and oxidation of the catalyst. A reduction event by an electron donor is necessary to close the catalytic cycle (Figure 2b). **A** and **D** can be, depending on the desired reaction, the substrate of interest, a reaction intermediate, or a sacrificial acceptor/donor. In some instances, it can also be a metal which has offered the possibility to develop dual-catalysis protocols.[6,7]
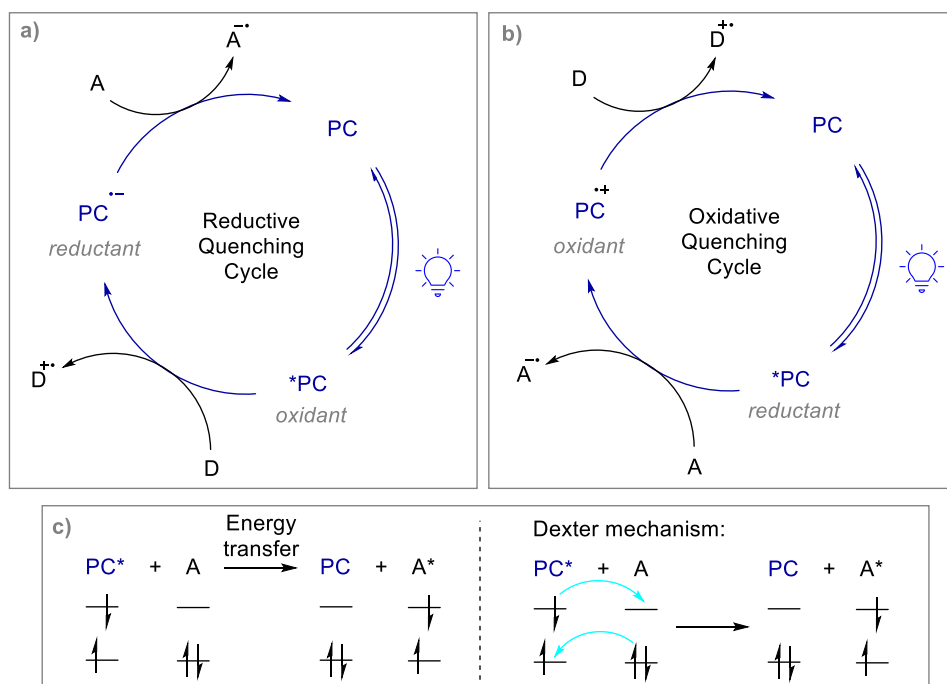
Figure 2. Three possible reaction pathways from a photocatalyst excited state. a) Reductive quenching by a reductant D. b) Oxidative quenching by an oxidant A. c) Energy transfer.

In its excited state, a photocatalyst can also act as an energy donor by donating its excess energy to another acceptor molecule (Figure 2c). This can occur through two nonradiative mechanisms known as the Förster and the Dexter energy transfer.[8] For the Förster energy transfer to occur, an overlap between the emission spectrum of the excited photocatalyst and the absorption spectrum of the acceptor is necessary. This is usually not the case between transition-metal photocatalysts and organic reactants so the Förster energy transfer is not a common pathway in photocatalyzed reactions. In the Dexter energy transfer mechanism, it is an orbital overlap that is necessary between the photoexcited catalyst and the acceptor. In other words, a bilateral exchange of electrons occurs between two molecules, and this requires a physical contact between the two entities. This is an important notion because molecular oxygen is a good quencher of the excited state of many transition-metal polypyridyl complexes following the Dexter mechanism.[9] As a result, photoredox reactions are oxygen sensitive and require to be carried out in strictly deoxygenated solutions.

1.1.3. Proton Coupled Electron Transfer – a specific mechanism for electron transfer

Proton Coupled Electron Transfer (PCET) is a redox mechanism in which an electron and a proton are exchanged within the same elementary step.[10] The important difference with a traditional hydrogen atom transfer (HAT) event is that in PCET, the electron and the proton travel to two different reagents: a proton transfer (PT) agent and an electron transfer (ET) agent. The scope of radical generation by HAT is thermodynamically limited by the difference in bond dissociation energy (BDE) between the two C-H bonds that are undergoing the hydrogen exchange.[11,12] To be favorable, the BDE of the bond being formed must be higher than the BDE of the bond being cleaved, and this is precisely the problem with the HAT from strong X-H bonds. This typically leads to the homolytic cleavage of the weakest or of the best polarity-matched bond in the substrate. Additionally, a HAT agent formally accepts both an electron and a proton. The acceptance of an electron will be favored by electron-withdrawing groups (higher oxidative power); but the acceptance of the proton will be disfavored by electron-withdrawing groups (lower Brønsted basicity). As a result of this inverse correlation, it is difficult to design potent HAT agents. By physically separating these two elemental steps, PCET allows for a much wider thermodynamical range. A number of redox values have been compiled by Knowles and co-workers in their recent review.[13]

Mechanistically, there are two possible pathways (Figure 3). Oxidative PCET involves the concerted transfer of an electron and a proton from the substrate to the PCET agents; this involves the hydrogen-bonding of the proton transfer reagent (base) with the substrate prior to electron transfer. This non-covalent pre-association allows for a selectivity towards strongly polarized heteroatom-hydrogen bonds over aliphatic C-H bonds. For example O-H bonds can be activated this way.[14,15] Reductive PCET involves the concerted transfer of an electron and a proton from the PCET agents to the substrate, usually a double bond. This involves the pre-association of the substrate with the acid (PT reagent) prior to electron transfer, thus achieving the selective reduction of ketones and imines over less polar olefines. Radicals alpha to secondary amines can be easily generated this way.[13,15]
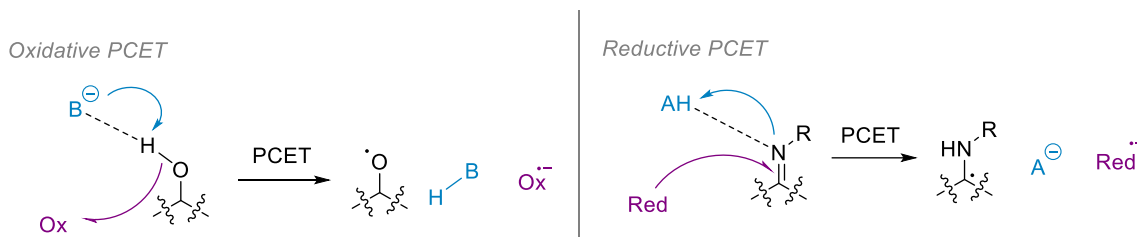
Figure 3. Mechanism of oxidative and reductive PCET.

1.1.4. Different types of photocatalysts

Photocatalysts can be of various nature but some common characteristics have emerged:

∴ Strong absorption of light in a specific region;
∴ Long-lived excited-state (typically longer than 10^{-9} s);
∴ Stability in solution;
∴ Reversible redox behavior with known or measurable redox potentials;
∴ Ease of synthesis and tunability of redox properties.

Transition-metal polypyridyl complexes such as presented in Figure 1 have been a convenient choice mostly because of the high tunability of their properties through ligand design. Although they have considerably contributed to the development of modern photoredox chemistry,[16–23] the sustainability of these rare-metal complexes, their price and lengthy synthesis have been more and more questioned. For these reasons the scientific community is heading back towards organic chromophores and more generally, metal-free photoredox catalysis.

Organic dyes have long been recognized for their ability to participate in photoinduced electron transfer (PET) because they can give rise to electronically excited molecules upon absorption of light. They can be used catalytically in organic synthesis and common organic photoredox catalysts include cyanoarenes, benzophenones, quinones, acridiniums (e.g. Fukuzumi's catalyst)[24,25] and xanthenes (with the famous fluorescein, eosin Y, Rose Bengal and Rhodamine),[26] to only name a few.[27–29] Significant advances in the field of organic photoredox catalysis have been made in the last 40 years, and this topic was extensively reviewed by Nicewicz and co-workers in 2016[30] and 2021 with a focus on C-H functionalization reactions.[31]

Electron Donor-Acceptor (EDA) complexes have been studied as early as 1952 by Mulliken who gave a precise nomenclature of electron donors and electron acceptors.[32] He defined donors D and acceptors A as entities whose interaction results in the transfer of a negative charge (an electron transfer) from D to A with the ultimate formation of an end-product, either as an additive combination of D and A, or of new entities (Figure 4). The interaction of D and A is typically described as a molecular aggregate in the ground-state. This EDA complex is able to absorb visible light even if the individual entities do not. This is due to the fact that new molecular orbitals are formed from the HOMO/LUMO coupling of the donor and the acceptor molecules, and this chemical entity is characterized by a new absorption band usually in the visible region.
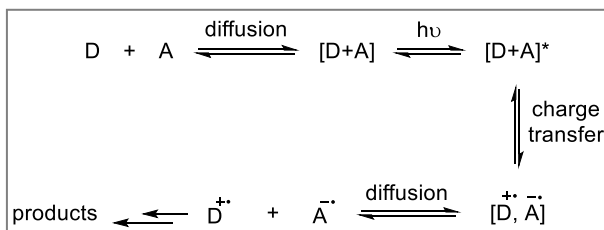
Figure 4. Electron transfer process in EDA complexes.

This reactivity has often been serendipitously identified through control experiments revealing that reaction could occur in the absence of photoredox catalyst. Nowadays this strategy has gained increased attention and is largely developed as part of a precise reaction design.[33,34] Melchiorre and co-workers are for example extensively developing this chemistry, but this strategy has been used by many others.[35–38]

In the last decade, **Quantum Dots (QD)** have also been recognized as sustainable photocatalysts and interesting alternatives to precious metal-based polypyridyl complexes. In this context, these entities have been for a long time in the hands of a physical-chemistry community using them mostly for CO_2 reduction and hydrogen generation.[39–43] More recently, quantum dots have proven to be able to replace metal polypyridyl complexes in key C-C bond formation reactions, and have gained increased attention from the organic chemistry community. The following sections aim at providing the reader with a general yet precise understanding of quantum dots from an organic chemistry point of view (section 1.2), and to display the range of organic transformations currently catalyzed by quantum dots (section 1.3).

1.2. Photophysics of quantum dots for the organic chemist

1.2.1. General description of quantum dots and underlying principles
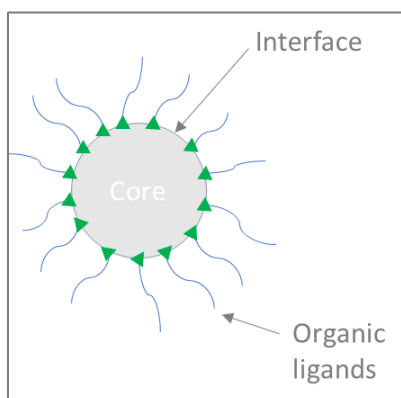
Figure 5: Schematic representation of a simple QD. Quantum dots are spherical nanoparticles surrounded by organic ligands.

A Quantum Dot (QD) is a nanometer-sized crystal of a semiconducting material with a defined composition, size and shape. A QD is composed of an inorganic core made up of a few hundred to a few thousand atoms, surrounded by an organic layer of ligands (Figure 5). The diameter of a quantum dot generally ranges from 2 to 10 nanometers. The core of common QDs is made of a non-rare metal cation such as cadmium (Cd^{2+}), indium (In^{3+}) or zinc (Zn^{2+}) with inclusions of elemental sulfur (S^{2-}), selenide (Se^{2-}), or tellurium (Te^{2-}) anions (CdS, CdSe, CdTe, etc). The structure and size of the core is defined by crystal growth during the synthesis. In solution, quantum dots have a colloidal nature and possess the advantages of a homogeneous catalyst (such as large extinction coefficients) while retaining the ability to be recovered by centrifugation.

These crystals of semiconductor are called quantum dots because their electronic wave function is under quantum confinement in all three dimensions. In a bulk semiconductor, the electron-hole pair (called an "exciton") has a characteristic length that is quantified through the "Bohr radius" parameter and that depends on the electronic structure of the material. This Bohr radius is defined as the most-probable distance between the electron and the hole within the exciton. When one or more spatial dimensions of the semiconductor are smaller than this distance, then the exciton becomes quantum-confined, and we talk about "quantum dots". This has several important consequences for QDs. While a bulk semiconductor has continuous conduction and valence energy bands and a fixed band gap, quantum dots have discrete atomic-like states and a size-dependent energy gap (Figure 6).[44]
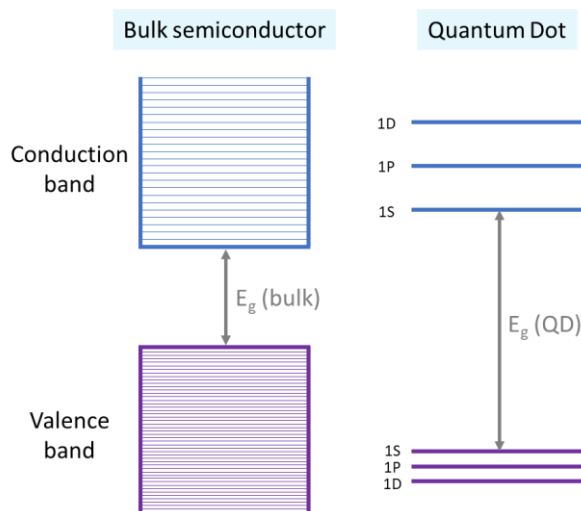
Figure 6. Discrete atomic-like energy state of a quantum dot compared to a bulk semiconductor. E_g = band gap.

Hence upon light excitation, an electron is promoted from the higher state of the valence band to the lower state of the conduction band, leaving a hole in the VB and bringing an electron into the CB (Figure 7). While for typical photocatalysts we refer to single electron transfers, for QDs we will call the charge carriers "holes" (h^+) and "electrons" (e^-). Similarly to common organic molecules, a high-lying CB will result in high reduction potential (easy transfer of an electron of the QD *to* the redox partner) while a low-lying VB will result in high oxidation potential (strong driving force and easy transfer of an electron *from* the redox partner).
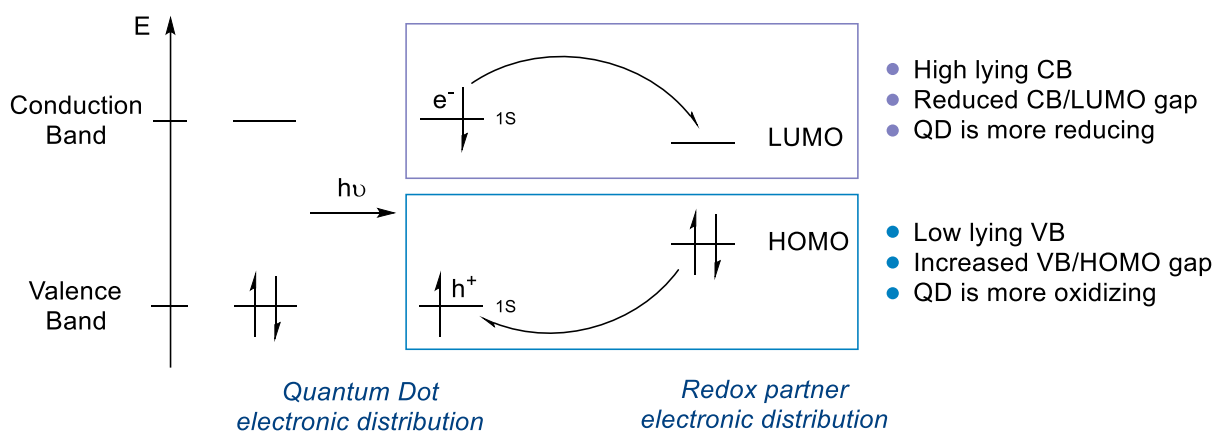
Figure 7. Simplified electronic structure of QDs and their interaction with organic redox partners. A hole transfer corresponds to an oxidation of the redox partner. An electron transfer corresponds to a reduction of the redox partner. We shall refer to the position of the VB as the oxidation potential of the QD (positive values); the position of the CB will correspond to the reduction potential (negative values).

1.2.2. Controlling the electronic properties of Quantum Dots

1.2.2.1. *Characterization of a quantum dot electronic properties*

The characterization of the electronic structure of quantum dots can be achieved through electrochemical measurements, optical absorbance, fluorescence, and electron microscopy measurements.[45] Cyclic voltammetry is a common experimental technique to determine the energies of conduction and valence band states of semi-conductors, but the interpretation of the cyclic voltammograms can be difficult. Because of their colloidal nature, QDs have low diffusion coefficients and therefore give rise to only small currents. Additionally, the measured potentials are dependent on

the surface functionalization due to the presence of potentially redox active ligands. It is possible to circumvent these problems, for example by using quantum-dot coated electrodes.[46] In numerous publications, the exact redox potentials is not calculated and/or measured. In some cases, it can be compared to literature known values; in many studies, the ability of specific quantum dots to exchange holes and electrons with a given substrate is apprehended through fluorescence quenching experiments.[47] Finally, the redox potentials of quantum dots can be estimated by reacting them with substrates of known and increasing oxidation potential (or reduction potential, depending on the reaction). The formation of product can be correlated to the redox potential of the substrate and therefore of the QDs, taking into account a small gap due to necessary driving force.[48]

The exact diameter of quantum dots as well as their extinction coefficient ε can be derived from the λ_{max} of absorption (easily determined by optical absorbance) through literature known formulas based on experimental polynomial fits,[49] or calculations.[50] This in turn allows the concentration of a QD sample to be determined by absorbance measurements using the Beer-Lambert law (equation 1).

$$A = \varepsilon l C \qquad \text{(Eq. 1)}$$

where   A is the absorbance;

ε is the extinction coefficient in $M^{-1}.cm^{-1}$;

l is the optical path length in cm;

C is the concentration of the absorbing species in $mol.L^{-1}$ (M).

Transmission Electron Microscopy (TEM) can also be used to determine the size of quantum dots as well as their size distribution. The size of the quantum dots is a critical parameter in their electronic properties, as will be demonstrated below.

1.2.2.2.   Size-dependent energy gap

The quantum-confinement of the exciton in the QDs results in high levels of energy for the holes and the electrons; hence the smaller the QD, the more oxidizing and reducing it becomes. In other words, the bigger the QD, the smaller the band gap (Eg) between conduction band and valence band (Figure 8). This band gap is an energy value and can thus be traced back to the wavelength of maximal absorption (through $E = hc/\lambda$). This can be used during the synthesis of the quantum dots to reach the desired size by simply measuring the position of the exciton by UV-Vis measurements.
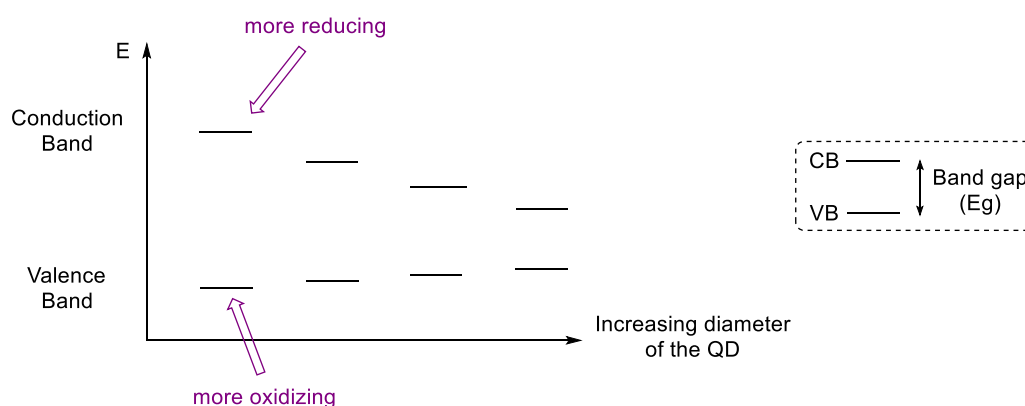
Figure 8. Shifting of conduction and valence bands with increasing diameter of the quantum dots. The shifting is stronger for the conduction band than for the valence band, meaning that the QDs become more reducing than they become oxidizing when their size is reduced (see also Table 1 below).

CdSe quantum dots belong to the most studied nanomaterials. Osterloh and co-workers have reported the energetic properties of CdSe QDs caped with 2-mercaptoethanol ligands as a function of their size.[46] Some indicative values are reported in Table 1 in V *vs* SCE to allow a facile comparison with values given for unimolecular photocatalysts. In addition, Weiss and co-workers have gathered an impressive number of values depending on QD composition, size, and capping ligands.[45]

diameter (nm)	E_{CB} (V *vs* SCE) – reduction potential of the QD	E_{VB} (V *vs* SCE) – oxidation potential of the QD
bulk, pH 9	-1.09	0.65
4.0	-1.29	0.76
3.0	-1.11	0.80
2.5	-1.61	0.97
2.0	-1.89	0.99

Table 1. Typical oxidation and reduction potentials of CdSe quantum dots depending on their size. With decreased diameter, the QD becomes more reducing (higher negative value) and more oxidizing (higher positive value). Values measured by Osterloh and co-workers.[46]

Although no systematic study has been conducted on CdS QDs, experimental estimations for the valence band energy of CdS QDs range from 1.24 to 1.9 V *vs* SCE,[51–53] significantly more oxidizing than for CdSe QDs. A conduction band edge energy was reported to be -1.19 V *vs* SCE, however the size of the QD was not specified.[53] Additionally, literature reports exist for quantum dots exhibiting highly reducing conduction band egde levels such as with ZnSe[54] and CuInS$_2$[48] based QDs.

The size of the quantum dot nanoparticle also has an influence on the extinction coefficient of this given nanocrystal. Peng and co-workers have shown a clear dependance in the case of CdTe, CdS and CdSe QDs where the bigger the nanoparticle, the higher the extinction coefficient.[49]

1.2.2.3. Interface engineering

A very important parameter in quantum dot photochemistry is the ability of holes and electrons to travel to the surface of the nanoparticle, to interact with a substrate, and to do so without first recombining. For a quantum dot, the source of the quantum confinement is the presence of a sharp dielectric interface between the crystalline core and the surrounding environment. In addition, the spherical structure of the nanoparticle has for consequent to increase its surface-to-volume area, which means that the majority of the atoms are at the interface with the surrounding environment. Therefore, modifications of the surface of the QD will have a strong and immediate influence on the overall electronic properties of the QD.[55]

Ligand tuning. Weiss and co-workers have compiled the valence band-edge energies of quantum dots of the same size and composition but being decorated with different surface ligands (typically oleate, oleylamine, alkyl amines, thiophenol, alkanethiols, trioctylphosphine oxide).[45] They have shown that energetic shifts ranging from 0.16 to 0.75 eV can be obtained depending on the electronic properties of the ligands. It was deduced that the greater the electron-donating character of the ligand's substituent attached to the surface, the more destabilized became both the valence and the conduction bands (shift to the higher E values). Therefore, electron transfer becomes more favorable. The reverse is true for electron-withdrawing groups.

But the ligands have far more importance than that with effects visible also on the stability of the quantum dots in solution, solubility, and more or less facile access of the substrate to the surface of the nanoparticle.[56,57] The ligands can be introduced on the nanoparticle during the synthesis but can also easily be exchanged post-synthesis due to the possibility to remove QDs from a solution through centrifugation or ultra-filtration. The ligands are an important parameter to study when developing quantum dots.

Core-shell QDs. Core-shell quantum dots are onion-like nanoparticles that contain two (or more) semiconductor materials with different band gaps (for example CdS/CdSe, CdSe/ZnS, etc) (Figure 9). These structures have been studied to facilitate spatial and wave function separation of electrons and holes.[58]

The band gap of the shell material compared to the core material can have important consequences. Although several possible combinations exist, we shall consider two main types of core-shell quantum dots (Figure 10).[59]
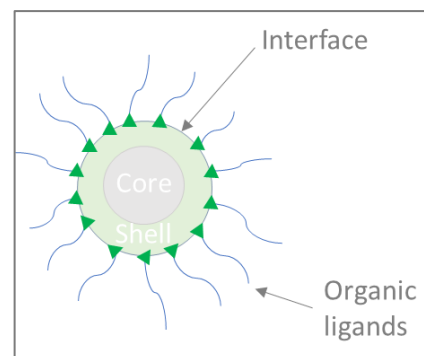
Figure 9: Schematic representation of a core-shell QD.

- In **type-I** QDs, the band gap of the shell is bigger than the band gap of the core. As a result, electrons in the valence band of the shell cannot populate the valence band of the core, and electrons in the conduction band of the core cannot populate the conduction band of the shell. Therefore, the charge carriers are both located in the core and will have difficulties to be transferred to the surrounding environment. This can be interesting when QDs are intended for photoluminescence. More interesting from an organic chemistry point of view are **inverted type-I** QDs. In this case, the band gap of the shell is smaller than the band gap of the core. Applying a similar reasoning as for the type-I QDs, we can deduce that holes and electrons will be located in the shell. Overall, this makes these types of QDs less oxidizing than their pure core counterparts, and more similar in properties to the shell material. At the same time, because holes are brought closer to the interface, this can be beneficial when the first step of the reaction is an oxidation (reductive quenching of the QD).

- In **type-II** QDs, both band gaps are similar in size, but the band gap of the shell is shifted down compared to the core. This means that the CB_{shell} and the VB_{shell} are lower than the CB_{core} and the VB_{core}. This results in electrons being located in the shell (as in inverted type-I QDs, they cannot transfer to the higher CB_{core}), and holes located in the core, which is ideal for charge separation and reduction as an initial step. **Quasi type-II** core-shell QDs are essentially type-II structures where the CB of the core and of the shell are very close, leading to the electrons being present not only in the shell but also in the core of the QD. In this type of QDs there is an enhanced charge separation. As a result, the hole can be relatively easily extracted as a first elemental step in the reaction, and subsequent electron transfer is easy due to the presence of electrons close to the interface

| Type-I | Inverted Type-I | Type-II | Quasi Type-II |
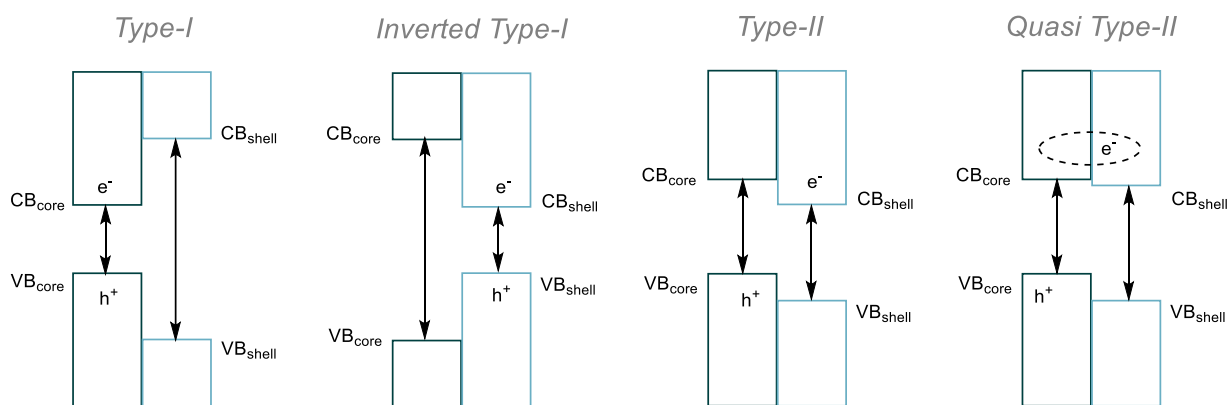
Figure 10. In inverted type-I core-shell QDs, the higher CB of the core forces the electrons to be located in the shell, while the lower VB of the core can be easily populated, leaving holes in the shell's VB. As a result, both charge carriers are located in the shell. In type II core-shell QDs, the lower CB of the shell is again populated by the electrons, but the holes are located in the higher VB of the core.

In addition to facilitate hole and electron transfer, the shell can provide a physical barrier between the optically activ core and the environment, making the colloid less sensitive to the environment (O_2, H_2O) and less prone to photo-oxidation.

Nanocomposites. Semiconductor-metal nanocomposites are core-shell structures where the shell is a noble metal such as Ag, Au, Pt. It has been shown that the metal in contact with the semiconductor enhances the photocatalytic efficiency of the composite by storing and shuttling photogenerated electrons from the semiconductor to an acceptor.[60–62] This has for consequence the decrease of charge recombination between the photogenerated holes and electrons. This can be done through coating of the QD with a metal layer; alternatively, the QD can be linked to a ligand-capped, metal nanoparticle *via* a molecular bridge (for example Metal-S-$(CH_2)_n$-S-QD).[63]

1.3. Quantum dots as photocatalysts for organic synthesis

The safe, scalable and efficient synthesis of colloidal solutions of quantum dots has been previously investigated.[64] A common method is the hot-injection approach where the injection of the semiconductor precursors is carried out at high temperatures (up to 320 °C) in a solution of a stabilizing ligand. The rate and order of addition as well as the temperature can be used to precisely control the size of the nanoparticles. The ligands can be exchanged after the synthesis and do not require lengthy synthesis. QDs have very high extinction coefficients (10^5–10^6 M^{-1} cm^{-1} versus 10^2 for typical iridium catalysts),[49] defined absorption and emission wavelengths, are photostable, and can easily be recovered from a reaction mixture.

For all these reasons, quantum dots have been investigated as suitable photocatalyst in place of transition metal polypyridyl complexes for organic synthesis. However so far, the use of quantum dots in organic synthesis has been largely limited to net oxidative or reductive reactions, with little applications in redox neutral C-C bond formations. Additionally, numerous methodologies still focus on the development of quantum dots using a model organic transformation without proposing a substrate scope or a scale-up protocol that would allow preparative chemistry to be carried-out. Although these studies are theoretically interesting and do give an insight into the capabilities of these photocatalysts, the following sections will solely focus on methodologies that do apply the use of quantum dots to preparative organic synthesis. Important parameters such as the reaction scale and the irradiation set-up are gathered and summarized in Table 2, when available. Studies focusing on the

development of organic transformations, including those without preparative synthesis, have been previously reviewed.[65–67]

1.3.1. Photooxidation and hydrogen evolution

This first section builds on the knowledge that was gained through the study of quantum dots as photocatalysts for the generation of hydrogen from water, and shows how this could be used to synthesize organic molecules.

The water splitting to H_2 and O_2 by single semiconducting material in solution is a known process that has been developed for the green generation of hydrogen.[68] The H_2-producing half-reaction is induced by the reduction of protons by photoexcited electrons at the surface of the semi-conductor (equation 2). The counterpart oxidative half-reaction involves the use of the photoexcited holes to generate O_2 and H^+ from H_2O (equation 3).

$$2H^+ + 2e^- \rightarrow H_2 \qquad \text{(Eq. 2)}$$

$$2H_2O \rightarrow O_2 + 4e^- + 4H^+ \qquad \text{(Eq. 3)}$$
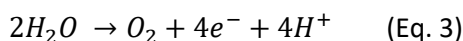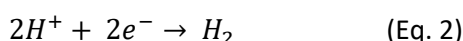
This later reaction involves a four-electron transferring process and as such, is often slow and significantly impairs the overall water splitting process. As a result, sacrificial reagents are often used to accelerate the rapid consumption of holes and electrons and through this, to accelerate the reduction/oxidation process. However, problems remain such as the production of useless by-products derived from these sacrificial reagents, the limited commercial value of O_2, and the necessary separation of explosive H_2-O_2 mixtures.[68]

The cooperative coupling of oxidative organic synthesis and hydrogen production has emerged as a powerful strategy to circumvent these issues.[69] From a hydrogen production perspective, the consumption of holes by organic reactants couples the hydrogen evolution with the production of value-added chemicals. From an organic synthesis point-of-view, the process can be used to synthesize these value-added compounds under mild conditions with hydrogen as the sole co-product of the reaction – a win-win situation. A semiconductor with a conduction band more negative than the reduction potential of H^+ (-0.41 V *vs* NHE) is necessary while the valence band has to be lower (more positive redox potential) than the oxidation potential of the organic substrate. In the very recent years, quantum dots have been recognized as possible photocatalysts for this transformation and have shown to allow the activation of X-H bonds (X = C, αN, S, αO) and the concomitant generation of hydrogen.[66,67,69] Very often (*vide infra*), it is proposed by the authors that two substrates are activated concurrently and are coupled *via* radical-radical coupling at the surface of the quantum dot (Figure 11).
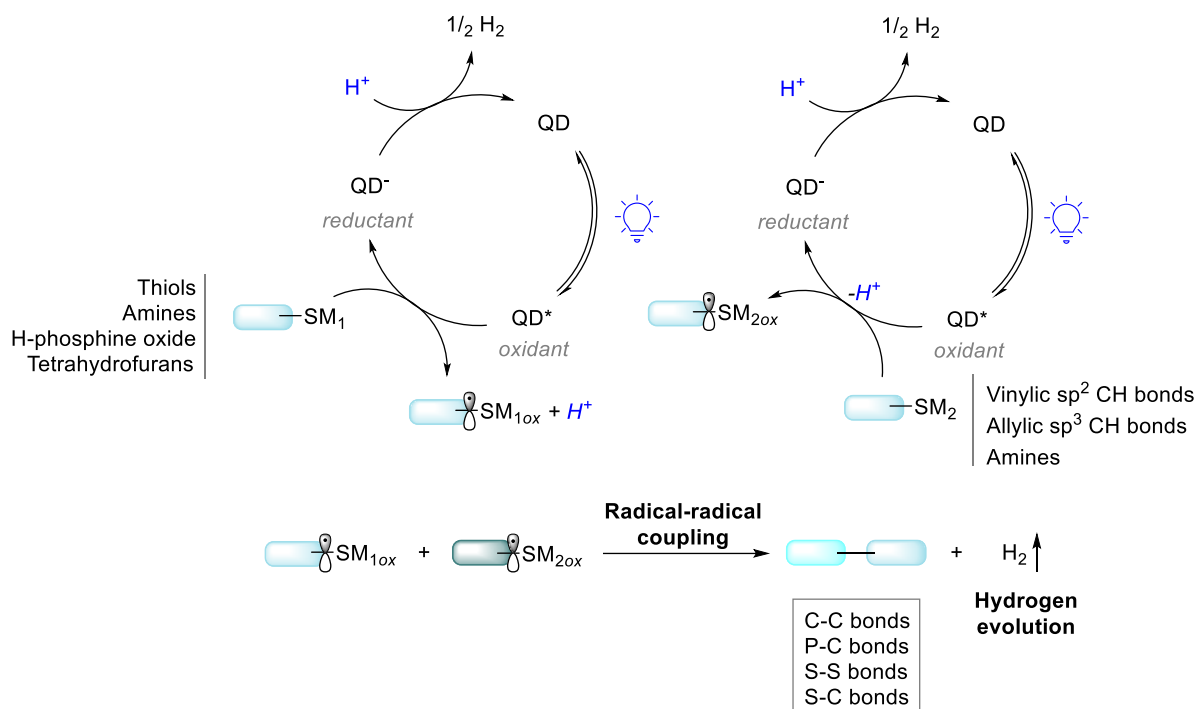
Figure 11. General mechanism for the cooperative oxidation of organic molecules and hydrogen evolution. For clarity purposes, two parallel catalytic cycles are drawn; because QDs can bind several substrates at once, it is possible that these two cycles take place on the same quantum dot.

In this type of reactivity, it has been observed that no reaction occurred with molecular catalysts such as iridium or ruthenium catalysts possessing suitable redox properties. It is postulated that the key parameter in quantum dot photocatalysis is the activation of several substrates at once, with immediate reduction of the proton at the surface of the QD. It is suggested that the protons do not diffuse in solution, allowing this reduction step that is otherwise considered not plausible using unimolecular catalysts. The absence of significant homo-coupling product formation could be explained by the fact that these radical species are generated simultaneously at equal rates; if they have different life-times, a persistent radical effect could explain why cross-couplings are observed in place of homo-coupling.[70] In some cases, alternative mechanism hypothesis not involving a radical-radical coupling step will be discussed.

This type of chemistry with quantum dots has been developed by Li-Zhu Wu and co-workers. In 2014, they reported the transformation of thiols into disulfides with concomitant hydrogen evolution using this method.[71] The authors suggested that the thiol substrates were bound to the quantum dots as thiolate anions (the reaction is run under basic conditions) so that the coupling reaction occurred on the QD's surface rather than in solution. The reaction was therefore more efficient when using naked quantum dots, i.e. whose ligands had been removed before reaction by an acidic treatment. Additionally, it was found that the coupling was facilitated by adding a nickel(II) cocatalyst for hydrogen evolution. It has been previously demonstrated that nickel(II) salts such as $NiCl_2$ or $Ni(OAc)_2$ are able to perform the reduction of H^+ into H_2.[72] It is thought that in this reaction, the excited states of the QDs are reductively quenched by the bound thiolates to give thiyl radicals, and that in the following reduction event electrons are first transferred to the nickel(II) ions. This cocatalyst in turn promotes a fast proton reduction. This strategy also helps to reduce recombination of holes and electrons by physically separating one charge carrier from the other.[61] Under these reaction conditions, the conversion of the thiol substrates and the rate of H_2 evolution were greatly improved and nearly quantitative yields were obtained within 4 hours. The authors also showed that when running the

reaction in D_2O instead of H_2O, D_2 was generated instead of H_2 with no loss of reaction efficiency. This indicated that the source of H atoms in the generation of H_2 was the aqueous solvent of the reaction. The reaction could be applied to thiophenols bearing electron-withdrawing and -donating groups but was very sensitive to steric hindrance (Figure 12). This is in accordance with the hypothesis of a QD/thiolate conjugate since steric hindrance would prevent attachment of the substrate on the surface of the QD. Aliphatic thiols having carboxyl, amino, methoxy and halide substituents were amenable to the reaction as well. Because the disulfide product is binding more weakly to the QD than the starting thiolate, the product detaches from the catalyst before further reaction occurs, avoiding overoxidation issues. Finally, the reaction was not impaired by the presence of oxygen and the quantum dots could be reused 4 times with minimal loss of yield. No scale-up was carried out above 0.25 mmol.
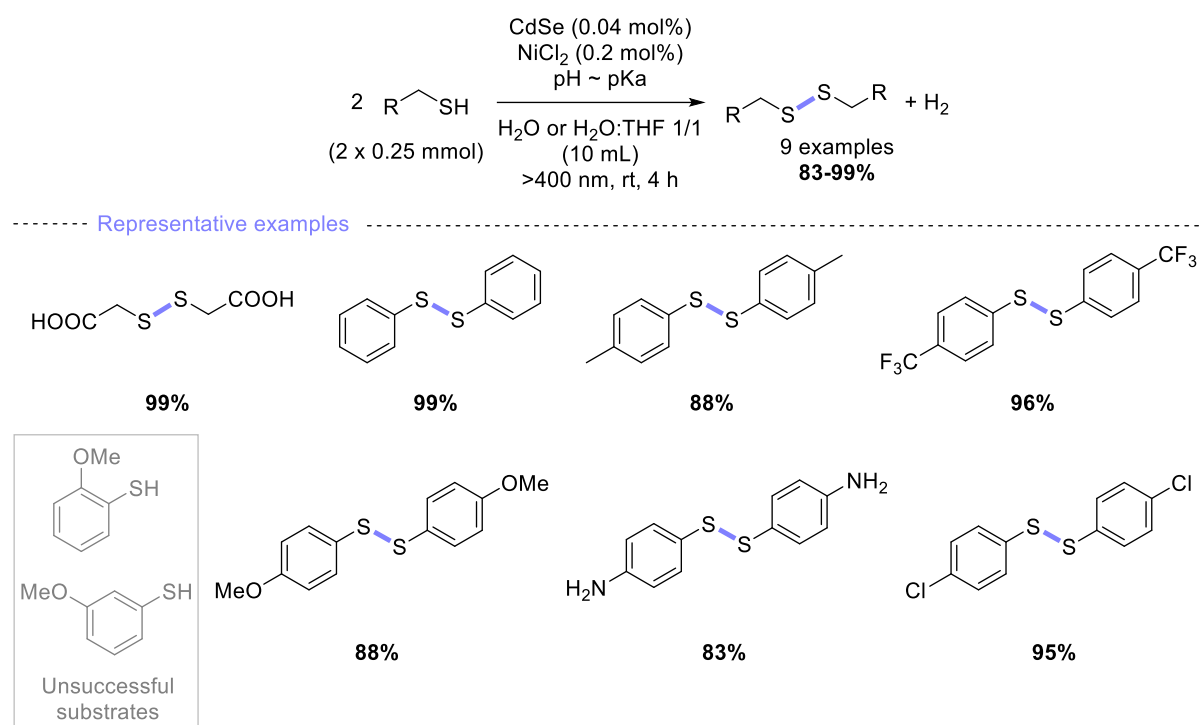
Figure 12. Transformation of thiols into disulfide and hydrogen by visible-light irradiation of quantum dots.

In 2017, the ability of thiolates to efficiently quench photoexcited holes and to generate thiyl radicals was used for the oxidation of primary and secondary benzylic alcohols to aldehydes and ketones.[73] The thiyl radicals were used as hydrogen atom abstraction agents to generate benzylic alpha-hydroxyl radicals (Figure 13A). Alternatively, the thiyl radicals could recombine to give the disulfide product, which was shown to be a suitable hole quencher able to generate a thiyl radical back. Disproportionation of two benzylic radicals was proposed for the formation of the desired oxidized product and benzyl alcohol, however this step seems less favorable than the possible competitive pinacol coupling. The possibility of a hole transfer to the α-hydroxybenzyl radical leading to the oxidized product was not discussed in this study but seems also more likely than the disproportionation step. This alternative mechanism was proposed by Weiss and co-workers who developed CdS QDs for the oxidation of benzylic alcohols to benzaldehyde.[74] Interestingly, the authors suggested that the first event in the mechanism was the electron transfer from the conduction band of the QD to the physically adsorbed Ni^{2+} ion, thus allowing the holes to be more long-lived. The quantum dots used in this study are directly caped with the 3-mercaptopropionic acid (MPA) ligands and $NiCl_2$ is used as nickel(II) cocatalyst.

13
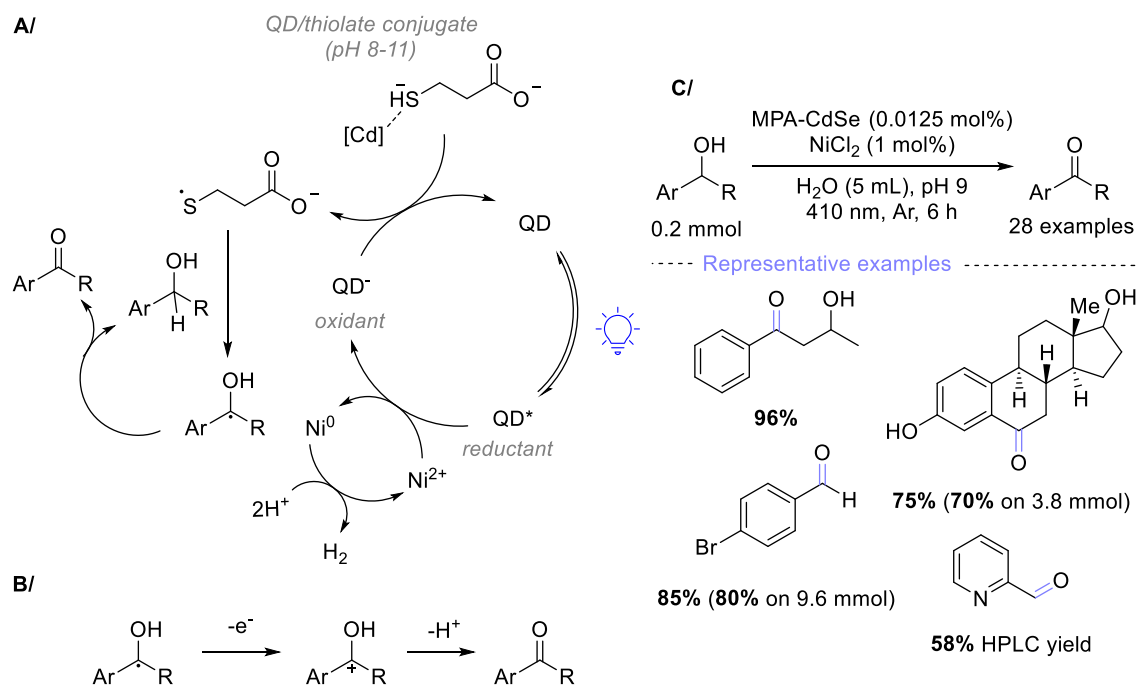
Figure 13. A/ Proposed mechanism for the thiyl radical mediated oxidation of benzylic alcohols under quantum dot photocatalysis. B/ Alternative mechanism leading to the product. C/ Scope of preparatively synthesized products.

The method could be successfully applied to polyhydroxylated compounds with a good selectivity for the benzylic position (Figure 13C). Not all products in the scope were isolated, however two gram-scale reactions were reported.

In 2021, the same group disclosed the direct alkylation and arylation of allylic bonds using quantum dots and visible light.[75] The scope was mostly limited to cyclic allylic systems of different sizes with the exception of one tetrasubstituted, linear alkene (Figure 14). Tetrahydroisoquinolines were found to be good partners for alpha-amino radical generation as well as alpha-amino esters. Notably a scale-up to 5 mmol could be carried out with minimal loss of yield (96% to 85% upon a 50-fold scale-up).

Figure 14. Representative conditions and substrate scope for the alkylation of allylic bonds.

It has been previously reported that a strong oxidant such as the photoexcited state of the 9-mesityl-10-methylacridinium ion ($E_{1/2}^*$ = + 2.06 V *vs* SCE in MeCN) was able to oxidize benzylic rings to the arene radical cation.[76,77] The acidity of π-C-H$^{•+}$ radical cation is inherently augmented compared to the starting material,[78] and deprotonation typically proceeds smoothly to give the desired benzylic radical. By choosing the right photocatalyst, overoxidation to the benzylic cation can be avoided. More recently, this chemistry was expanded to allylic sp³ C-H bonds by employing the same type of acridinium catalyst.[79] Li-Zhu Wu and co-workers found that holes generated from CdSe and CdSe/CdS quantum dots (1.9 nm diameter for the core) could drive the same type of transformation by generating allylic radicals. The proton liberated from the π-C-H$^{•+}$ radical cation can be efficiently reduced by a QD$^-$/Ni^{2+} system as previously described, leading to hydrogen evolution. The allylic radical is thought to be coupled *via* radical-radical coupling with alpha-amino radicals generated from alpha-amino C-H bonds. Alternatively, we could also propose that the alpha-amino radical is over-oxidized to the iminium ion, which would be a good radical trap for the allylic radical.[80] The resulting amine radical could be reduced to give the product and close the catalytic cycle.

Figure 15. Mechanistical hypothesis proposed by Wu and co-workers for the C-C bond formation between an allylic and a tertiary amine substrate under visible-light catalysis of quantum dots.

In this study, a Minisci reaction was developed as well. A wide range of isoquinoline substrates could be reacted with allylic bonds leaving functional groups such as alcohols, amides, esters and halogen untouched (Figure 16). Electron-poor pyridines were amenable to the reactions as well, but modest regioselectivity for the C2 over the C4 position was observed. Additionally, the high excess of allylic substrate necessary for the reaction let to bis-functionalization with some pyridine partners. The method could be used for the modification of natural products and drug molecules. The authors suggested that the high excess of the allylic substrate was necessary to favor the interaction of the substrates with the surface of the quantum dots and to enhance allylic radical formation. This is in accordance with the known difficulty to extract holes from quantum dots as the first step (reductive quenching). To facilitate interaction of the substrates with the surface, a pre-treatment of the quantum dots was used to remove all ligands.
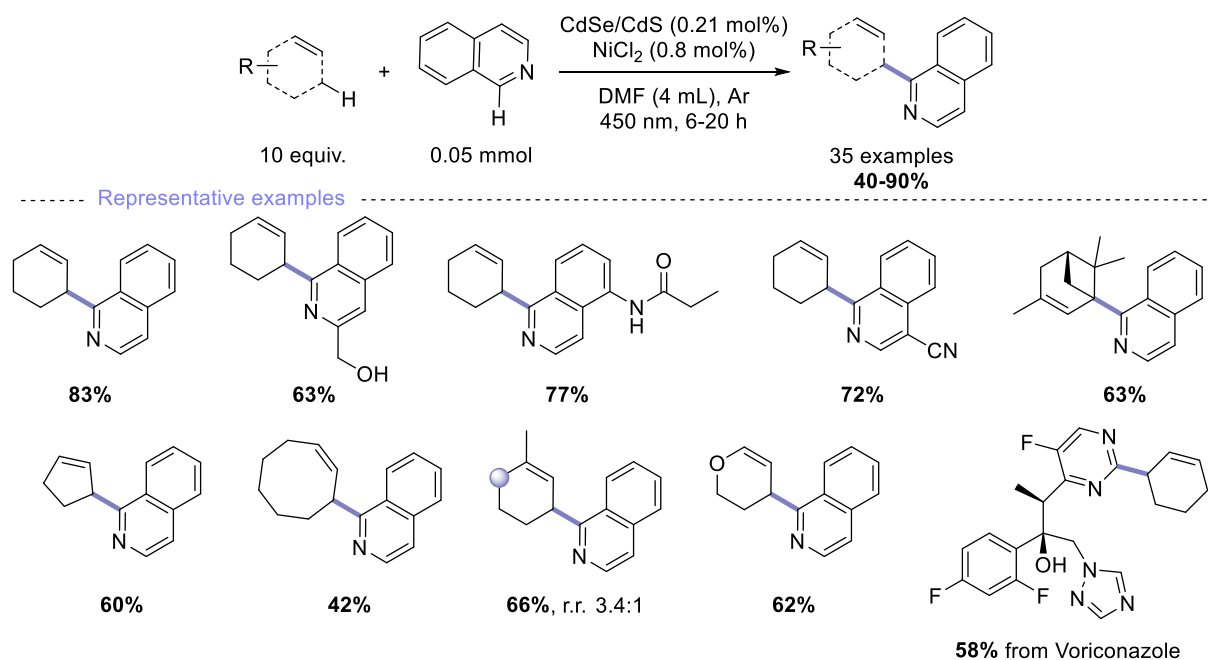
Figure 16. Representative conditions and substrate scope for the arylation of allylic bonds.

Mechanistically, it is probable that a first QD catalytic cycle generates the desired allylic radical, which can add to a variety of *N*-heteroarenes but in particular isoquinoline derivatives. For such a coupling to occur, the isoquinoline should be activated. It is not clear from the reaction conditions whether the pH would be acidic enough to protonate the nitrogen. Alternatively, $NiCl_2$ could play the role of a Lewis acid, or the QDs could be involved as well since the pretreatment with nitric acid creates cationic sites on the nanoparticle. A second oxidation event with loss of a proton yields the re-aromatized product.[81] Two reduction events from H^+ to H_2 regenerate the quantum dots (Figure 17).
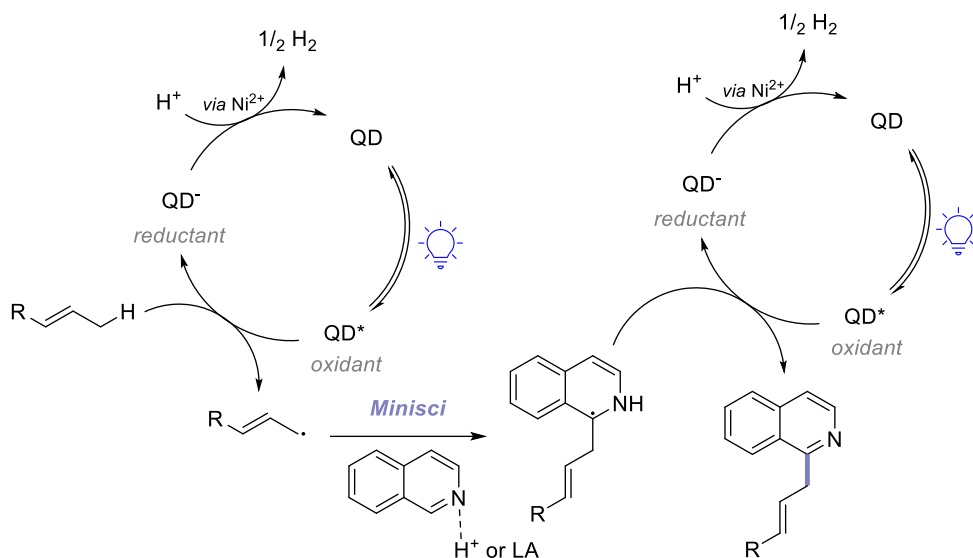
Figure 17. Mechanistical hypothesis for the Minisci reaction of allylic substrates under visible-light catalysis of quantum dots. For clarity purposes, two parallel catalytic cycles are drawn; because QDs can bind several substrates at once, it is possible that these two cycles take place on the same quantum dot.

The Wu group then reported a method devised from these two previous studies and proposed a direct allylic Csp^3-H and vinylic Csp^2-H thiolation under quantum dots photocatalysis.[82] The thiyl and allylic radicals are generated at the surface of the photocatalyst by quenching the holes of the excited state, while the released protons are reduced and account for the observed hydrogen evolution. No nickel(II) cocatalyst was required, and the authors suggest again a radical-radical coupling mechanism. However, thiyl radicals dimerization would give the disulfide, which is a good radical trap.[83] Hence it is also plausible that the desired product is obtained *via* radical addition of the allylic or vinylic radical to the accumulated disulfide compound.
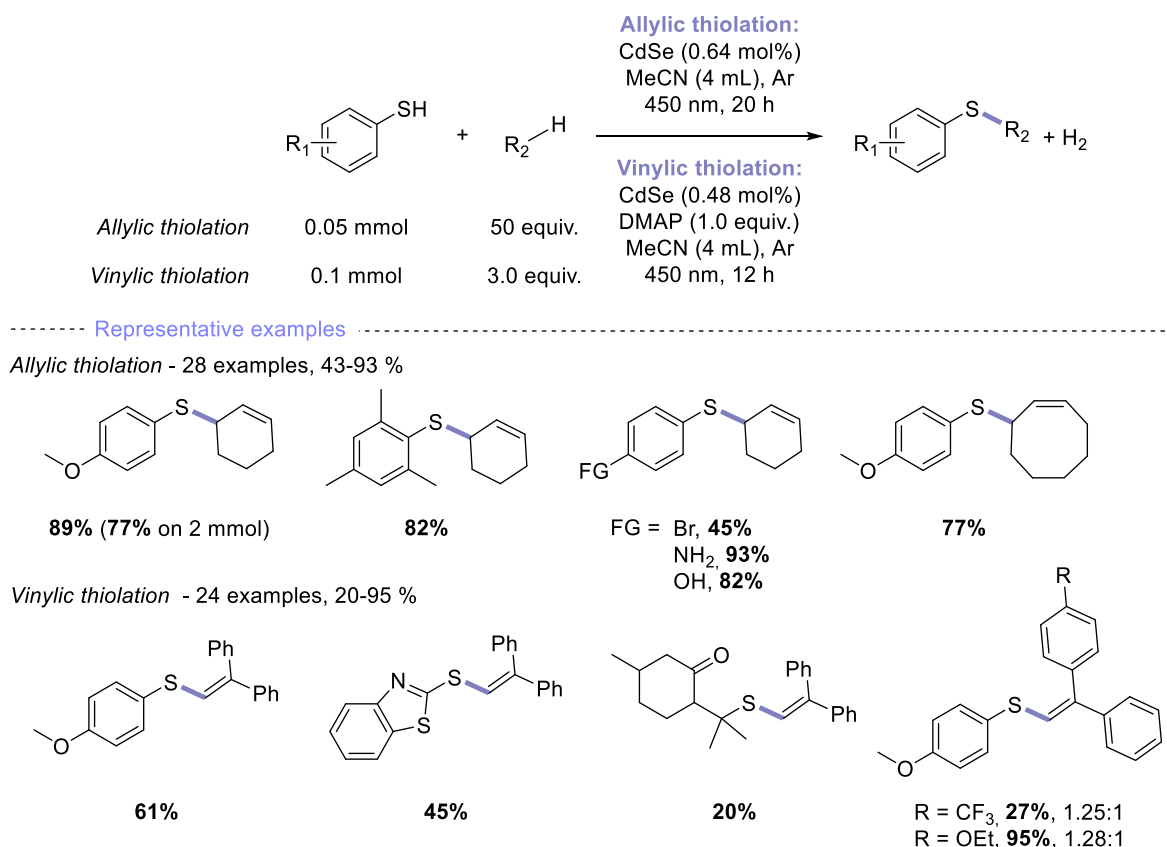
Figure 18. Allylic and vinylic thiolation under quantum dot photocatalysis.

Cyclic alkenes with an allylic C-H bond readily underwent allylic thiolation while electron-rich styrene derivatives without competing allylic positions underwent vinylic thiolation. As expected, electron-rich thiophenol derivatives were the best substrates for the transformation, and even *ortho* substituents were tolerated (Figure 18).

In a next publication, the Wu group reported that the conjugation of tetrahydrofuran (THF) at the surface of the quantum dots resulted in elongation of the α-C-H bond and reduction of the electron density, which allowed a so-called "proton coupled interfacial electron transfer".[84] While the authors suggest the transfer of both a proton and an electron from the α-C-H bond of THF/QD conjugates, it seems also probable that a radical cation is formed on the oxygen atom first, and that loss of the alpha proton occurs next. This could be facilitated by the coordination of THF on vacant sites of the QDs. These vacant sites have been shown be exposed by acidic treatment of the aqueous solution of quantum dots,[85] which could explain why the reaction efficiency was increased by employing two equivalents of benzoic acid. The alpha-oxy radical could be engaged in a radical-radical coupling reaction with alpha-amino radicals concurrently generated by the CdSe quantum dots (see Figure 15 for a similar example). Alternatively, the alpha-amino radical could be oxidized to the iminium ion and serve as radical trap for the alpha-oxy radical.[86] The scope for this transformation was large in number but limited to *N*-aryltetrahydroisoquinolines and alpha-ester secondary anilines; both electron-withdrawing and -donating groups were tolerated at all positions on the aromatic rings, except halogens and *ortho* substituents that proved problematic. No variation on the THF ring was reported (Figure 19).
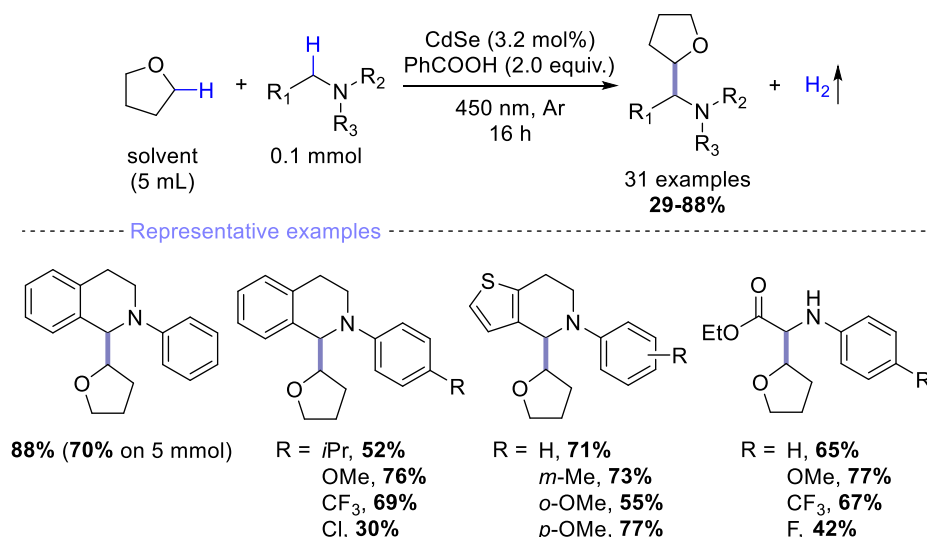
Figure 19. Radical-radical coupling of alpha-oxy and alpha-amino radicals from respectively THF and aniline derivatives.

Addition of the THF ring to chromone derivatives or terminal alkynes was demonstrated as well (Figure 20). In these two reactions, reduction of the intermediate radical by the QDs leads to the product without hydrogen evolution. The addition to alkenes seems limited to chromones and it is not discussed whether alternative electron-poor olefins could be used instead.[87,88] No details are given on the changes in the reaction conditions in these two protocols. The necessity to use core-shell quantum dots along with a base in the addition to alkynes is for example not rationalized. It could be related to the different reduction potentials required depending on the coupling partner – in the addition to chromones, an α-keto radical has to be reduced; in the addition to arylalkynes, a sp2-benzylic radical intermediate is involved. Alternatively, and considering the high excess of THF used in this reaction, it is possible that a radical chain mechanism is operative between the α-keto or benzylic radicals and the THF ring. The QDs would only be necessary to initiate the reaction.
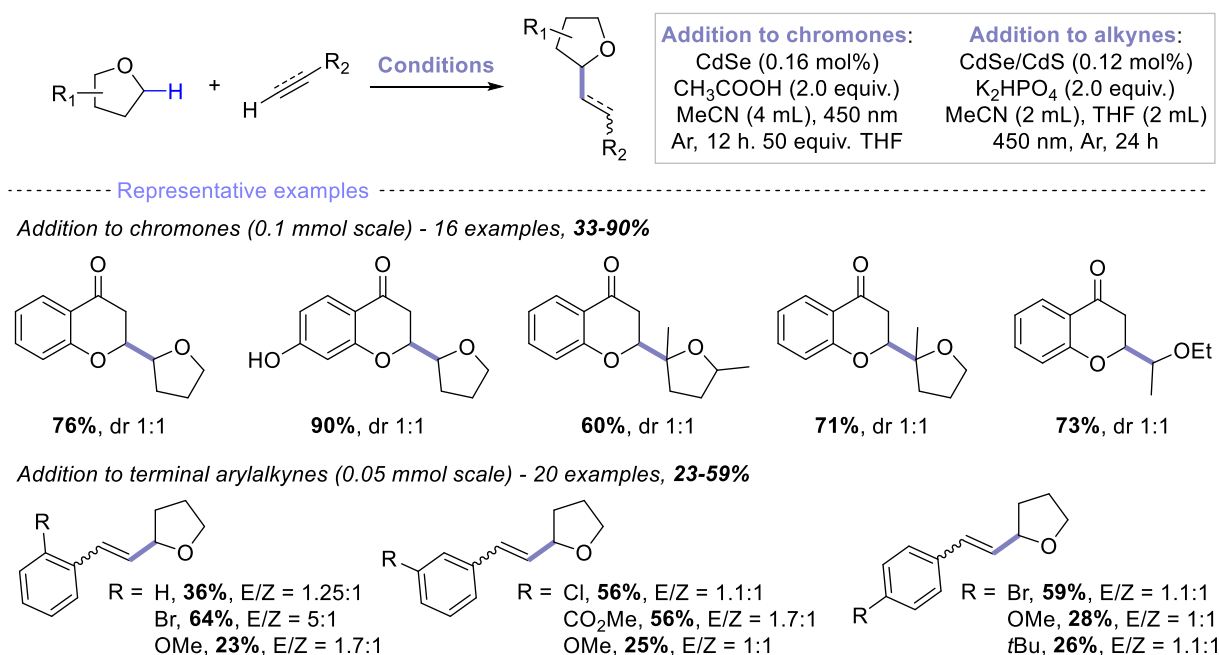
Figure 20. Addition of the alpha-oxy radical derived from THF on chromone derivatives and terminal arylalkynes.

Finally, a C-P bond formation driven by quantum dots was recently reported by the Zhu lab.[89] The authors showed that naked 1.9 nm CdSe quantum dots could oxidize H-phosphine oxides into phosphoryl radicals under visible-light photocatalysis. This radical species could undergo radical-radical coupling with alpha-amino radicals derived from *N*-aryltetrahydroisoquinolines with hydrogen evolution much like previously described (see Figure 15 and Figure 19). A different reactivity was observed when adding the phosphoryl radical to an unactivated alkene. This hydrophosphinylation reaction was demonstrated on 15 examples (0.1 mmol scale) with high yields of isolated products (Figure 21A). The authors proposed that the resulting C-centered radical could be trapped with the H• radical arising from reduction of a proton. The fact that no hydrogen evolution was observed in this reaction is probably rather to be attributed to a radical chain mechanism, a classical reactivity in radical phosphorylation reactions.[90] The resulting C-centered radical can abstract a hydrogen from the H-phosphine oxides to generate the phosphoryl radicals (Figure 21B). The QDs are necessary to initiate the chain.
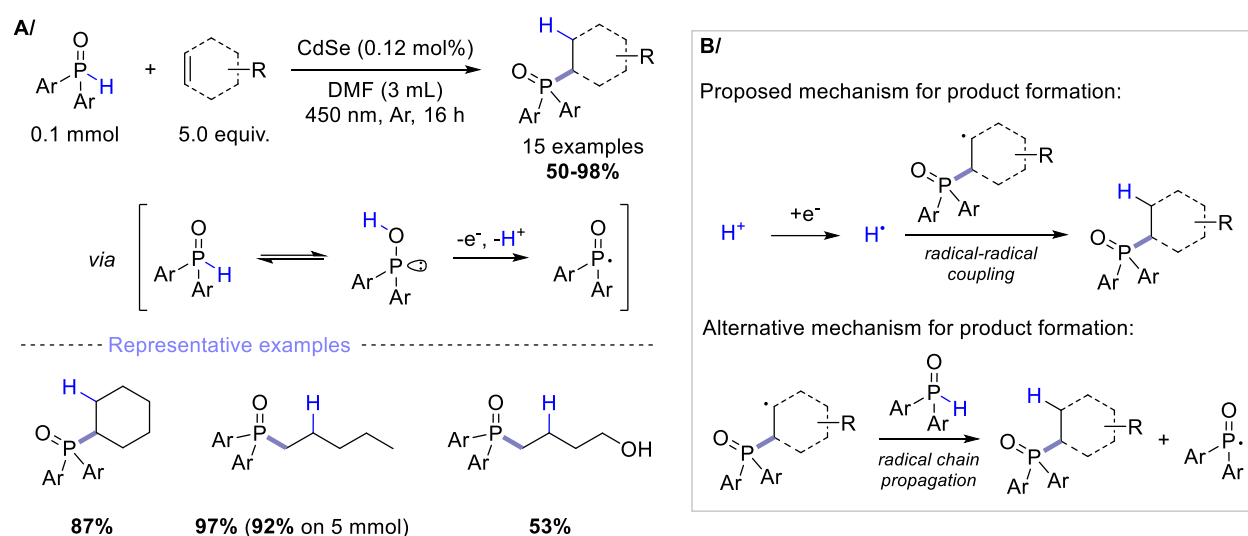
Figure 21. Hydrophosphinylation of unactivated alkenes. A/ Conditions and substrate scope. B/ Proposed versus alternative mechanism.

1.3.2. Redox neutral reactions

To demonstrate the ability of quantum dots to catalyze organic transformation, research groups have used them as photocatalysts in published transformations using iridium or ruthenium catalysts. This strategy allows the direct comparison of yield, catalyst loading and reaction time. In 2017, Krauss and Weix reported that oleate-capped, 3 nm CdSe QDs ($E_{1/2}^{red}$ = -1.52 V *vs* SCE) could be used for five different previously reported photoredox reactions, including C-C bond forming reactions, reactions with organic cocatalysts, and reactions with metal cocatalysts.[91] The authors showed that catalyst loadings as low as 0.0008 mol% could be used, a quantity significantly lower than for iridium and ruthenium catalysts (usually around 1 mol%). These low catalysts loadings required not only a robust and efficient catalyst, but also an optimal photochemical set-up that guaranties photon absorption. Notably, no changes in the reaction conditions were necessary at all, and the scale did not have to be reduced upon using the quantum dots. This should encourage the introduction of quantum dots as part of the catalyst screening in photoredox methodology developments. As a general conclusion for this study, it was found that most reactions following a reductive quenching pathway could be reproduced using oleate-capped 3 nm CdSe QDs. Although the isolated yields were often 10-20% lower with the QDs than with the compared photocatalysts, they should be evaluated in light of the catalyst loading. Considering the extremely low QD loading used in most reactions, the efficiency and turn-over

20

numbers were higher with the QDs than with the Ir or Ru photocatalysts. The limitations pointed out by Krauss and Weix concern the decomposition sometimes observed for the quantum dots, attributed to loss of ligands during the reaction. The authors suggest that using bi- or tri-dentate ligands could at least partially solve the problem. In the following section, three redox neutral reactions investigated in the study of Krauss and Weix will be presented.

1.3.2.1. Beta-functionalization of aldehydes and ketones via an enamine intermediate

The β-alkylation of aldehydes by combining photoredox and organocatalysis, initially proposed by MacMillan and co-workers with an iridium catalyst,[92] was successfully reproduced using quantum dots. Four examples are reported on preparative scale and the products were successfully isolated in 60-70% yields (Figure 22A). The elemental steps performed by the QD catalyst are a first oxidation step of the enamine intermediate, and a reduction step of a carbon radical intermediate after trapping with the activated olefin (Figure 22B). This is an elusive example of alpha-ester radical reduction by QDs.
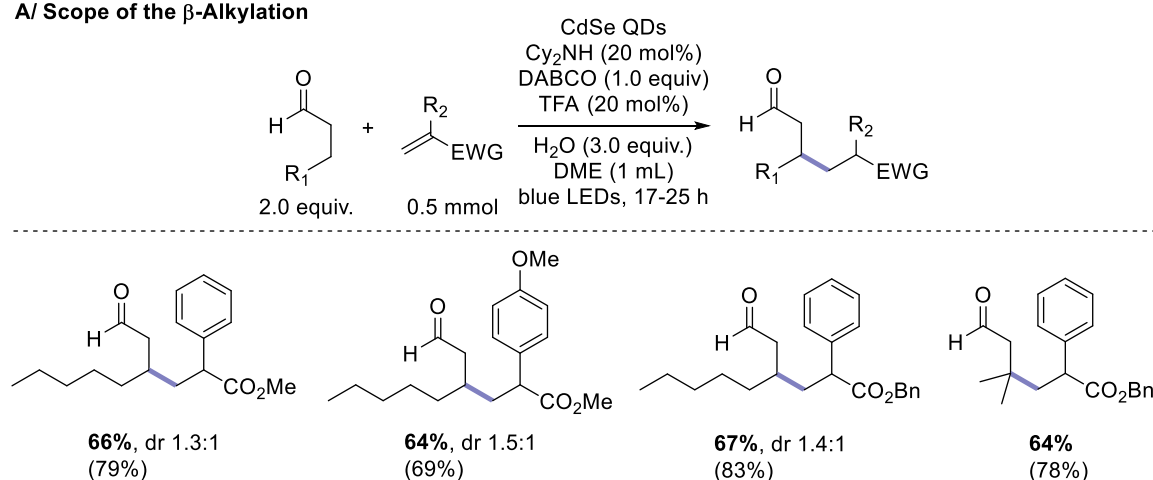
Figure 22. A/ Scope of the β-alkylation of aldehydes. Yields obtained with the CdSe QDs (yields with the Ir catalyst). B/ Elemental steps performed by the QD charge carriers.

A similar protocol was adapted from MacMillan and co-workers for the β-aminoalkylation of ketones.[93] The feasibility of the protocol using quantum dots was demonstrated on two examples (Figure 23A). Mechanistically it is proposed that DABCO is first oxidized by the quantum dots and serves as electron transfer agent to generate the enamine radical cation, and the vinylogous alpha-aminoalkyl radical by loss of a proton (Figure 23B). The imine is thought to be reduced by the QD electrons with concomitant proton transfer, although it is possible that the direct radical addition to the imine happens first and that the resulting intermediate is reduced by the quantum dots in a second step. Another possibility is that the vinylogous alpha-aminoalkyl radical is further oxidized and that the resulting cationic intermediate serves as radical trap. A final reduction event would deliver the product.

A/ Scope of the β-aminoalkylation
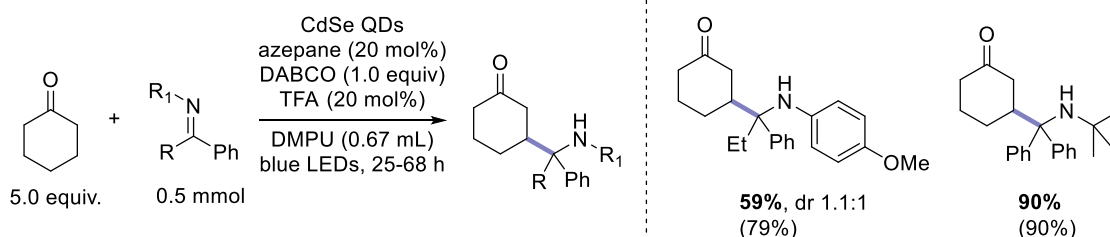
B/ Mechanism of the β-aminoalkylation
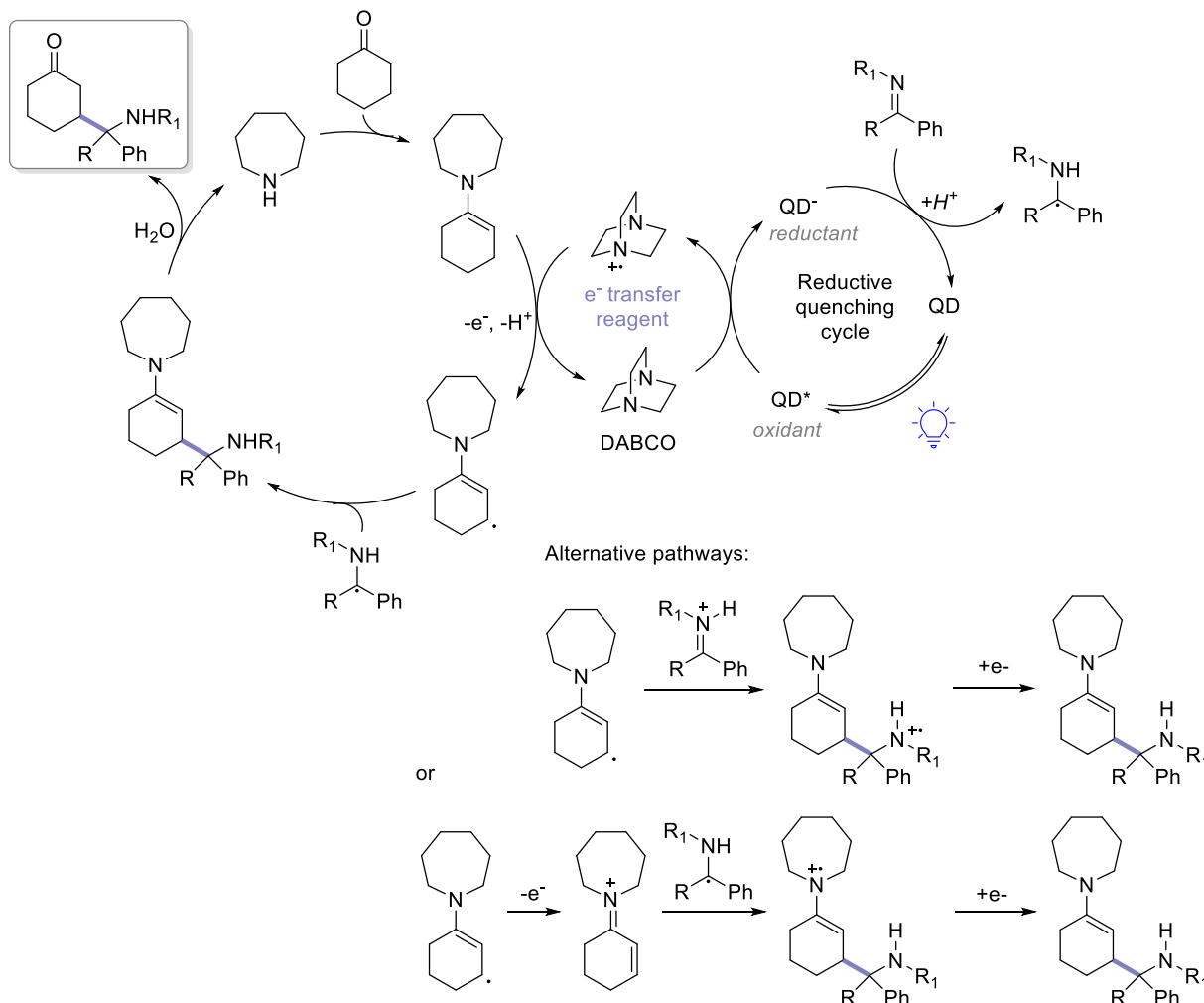
Figure 23. A/ Scope of the β-aminoalkylation of ketones. Yields obtained with the CdSe QDs (yields with the Ir catalyst). B/ Proposed mechanism and alternative radical addition pathways.

1.3.2.2.   Dual catalysis QD/Ni

Next, a metallaphotoredox amine arylation protocol was reproduced by Krauss and Weix, merging quantum dot and nickel catalysis.[94] It was proposed by the authors of the iridium-catalyzed protocol that the photoexcited catalyst was able to oxidize a nickel(II) complex into a nickel(III) complex, thus promoting a C-N reductive elimination without the need for additional ligands on the nickel metal center. The resulting nickel(I) species can be reduced back to the nickel(0) catalyst by the electrons of, in this case, CdSe (Figure 24). DABCO was present in this protocol as a base, not as an electron-transfer reagent. In their seminal publication on metallaphotoredox catalysis, MacMillan an co-workers proposed that the initial activation of the Ni^{II} into the Ni^0 species occurred via two discrete reduction events by the photocatalyst with the excess amine substrate playing the role of sacrificial oxidant.[95] The two electron reduction of Ni^{II} to Ni^0 was reported to be achieved at -1.1 V *vs* SCE in DMF.[96] Although the method using QDs was demonstrated on one example only, it shows the possibility to use quantum dots in metallaphotoredox protocols.
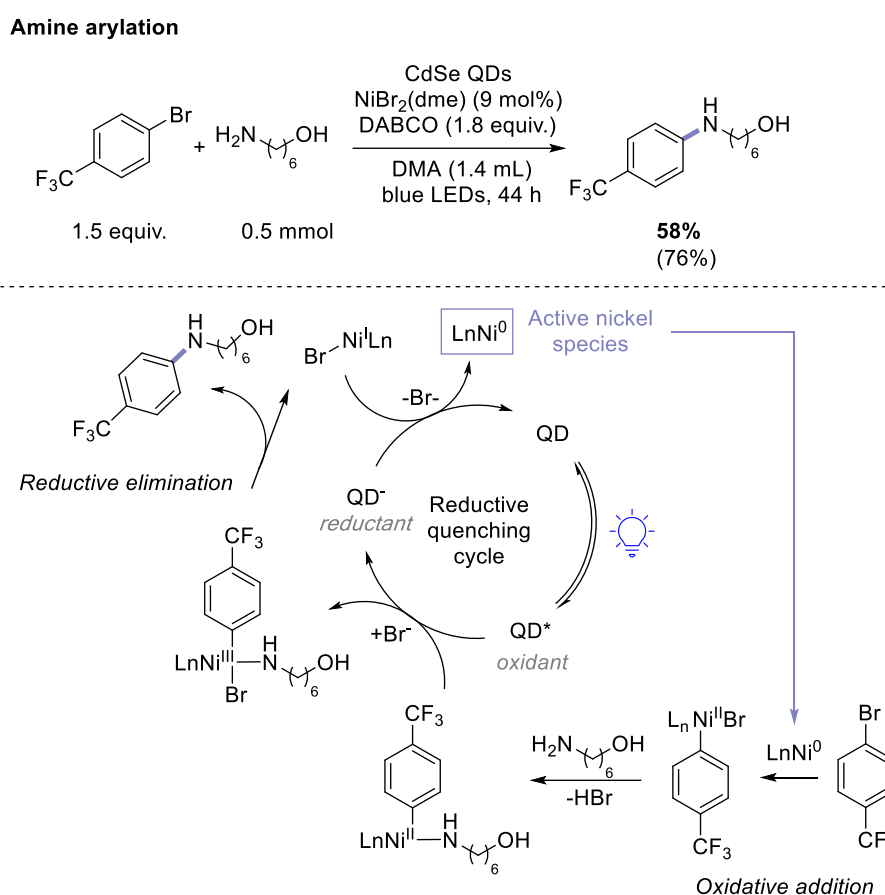
Figure 24. Amine arylation protocol using a dual QD/Ni catalytic system. Yield obtained with the CdSe QDs (yield with the Ir catalyst). The quantum dots are involved in the oxidation and reduction of the nickel complex intermediates.

1.3.2.3.   Alpha-functionalization of N-aryl pyrrolidine derivatives

The redox neutral alpha-functionalization of *N*-aryl tertiary amines has been extensively studied using iridium and ruthenium polypyridyl complexes (see Chapter 3). As a result, these studies have frequently been used as starting point and comparison for the development of quantum dots. For example, the α-vinylation of *N*-aryl pyrrolidine initially published by MacMillan and co-workers[97] was used as model reaction for the development of quantum dots by Weiss[52] and Pillai.[98] However, no

preparative synthesis for reported in these studies. Concomitantly to the preparation of this manuscript, Huang and Luo disclosed the potential of CdS quantum dot gels as photocatalysts for organic synthesis.[99] They based their study on the α-arylation of *N*-aryl pyrrolidine derivatives, a reaction initially developed by MacMillan and co-workers,[100] and demonstrated the synthetic utility of their photocatalytic system by a preparative protocol on 0.5 mmol scale. A quantum dot gel is a 3D nanoarchitecture of interconnected QDs, prepared by oxidation of thiolate-capped quantum dots. By doing so, the QD gel loses most of its surface ligands but retains the quantum confinement associated with QDs. Compared to the initial thiolate-capped quantum dots, the QDs in the gel retained their nanometric size (3.2 nm) and exciton peak (395 nm). Hence the band gap was unchanged, however the conduction and valence bands were shifted up by approximately 0.5 V due to the change in surface chemistry (see section 1.2.2). Importantly, the authors postulated that the gelation resulted in increased surface site exposition, which in turned resulted in increased adsorption of the reactants and easier charge transfer compared to the initial QDs. Indeed, the α-arylation of *para*-methoxyphenyl pyrrolidine proceeded with a 20% increase in NMR yield when using the gel rather than the thiolate-capped QDs (Figure 25). The protocol was used for the preparative synthesis of 8 α-arylated aniline derivatives in yields comparable to the iridium-catalyzed reaction. Interestingly, even electron-poor starting materials could be oxidized by the QD gel, and the quantum dot loading could be reduced to a very low 2 mmol%. In addition, the QD gel could be recovered from the reaction mixture by centrifugation and reused in another reaction with minimal loss of yield (10%).
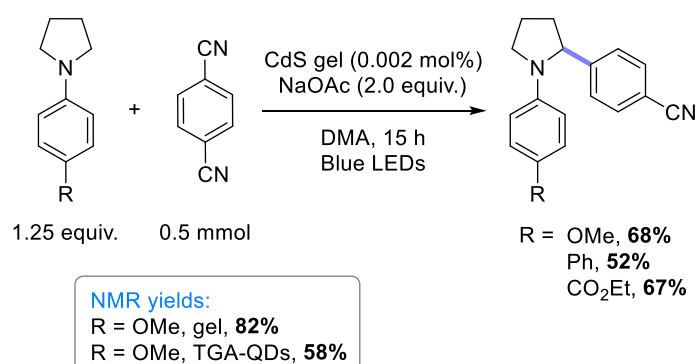
Figure 25. Alpha-arylation of aniline derivatives using a QD gel. TGA = thioglycolic acid.

When using *N*-arylated, tetrahydroisoquinoline (THIQ) derivatives as starting material, the authors observed that the QD gel gave rise to a ring-opened product. The authors postulated that the initial α-arylated product was able to bound to the surface of the gel, leading to a quaternary ammonium intermediate whose C–N bond was significantly weakened, allowing ring opening. This hypothesis was corroborated by the fact that this reaction was particularly efficient for electron-rich THIQ derivatives, who quaternary salt was stabilized (Figure 26). The exact mechanism of the ring opening is however still under investigation. This reactivity was not observed for non-gelated quantum dots.

Ring-opening arylation reaction (4 examples) via:

Ar =	product 1	product 2
OMe	n.d.	47%
(benzodioxane)	n.d.	14%
Ph	11%	21%
CF₃	40%	10%
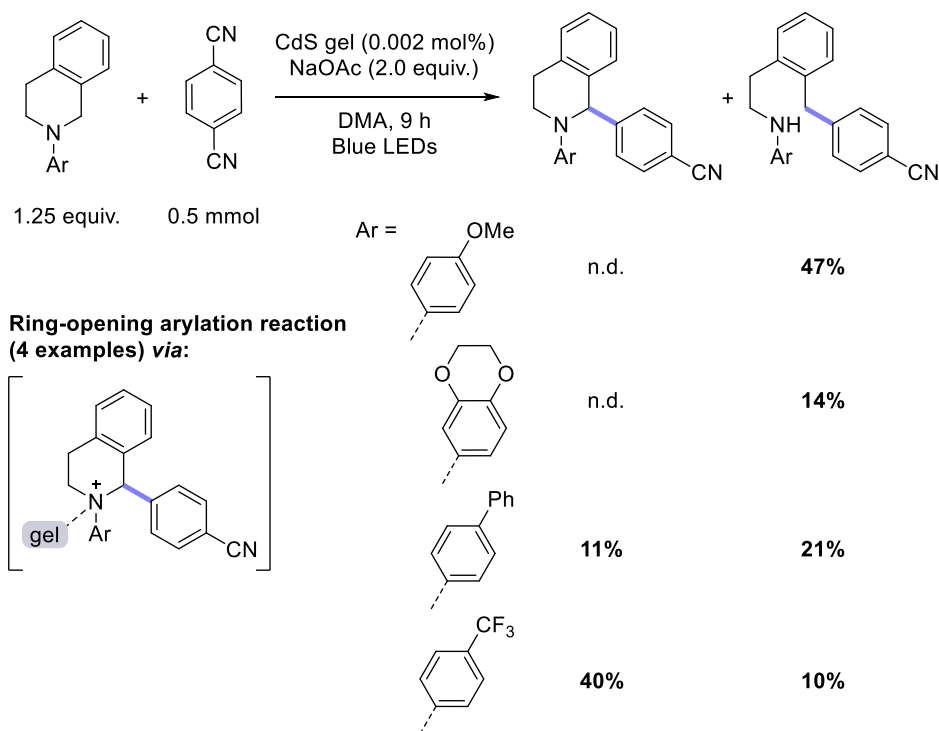
Figure 26. Ring opening of α-arylated N-aryl tetrahydroisoquinoline derivatives.

The mechanism of the α-arylation reaction was however based on the mechanism proposed by MacMillan and co-workers ().[100] Reductive quenching of the photoexcited QD gel leads to a radical cation, whose deprotonation gives the α-aminoalkyl radical. Reduction of the 1,4-dicyanobenzene coupling partner leads to the corresponding radical anion. Radical-radical coupling followed by loss of the cyano groups accounts for product formation.
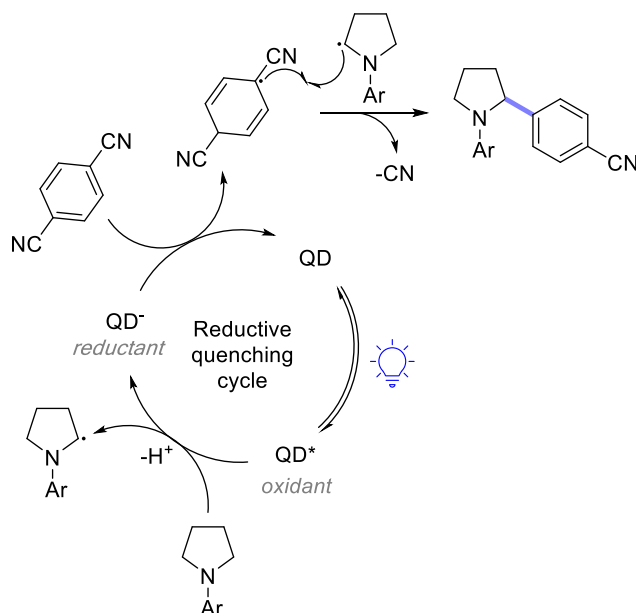
Figure 27. Mechanism of the α-arylation reaction based on MacMillan's hypothesis.

25

1.3.3. Net reductive reactions

The use of sacrificial reductants (usually trialkylamines or thiophenols) to quench the holes of the quantum dot can be a successful strategy to carry out a critical reduction step on the substrate of interest.

1.3.3.1.   Tertiary amines as sacrificial reductants

On their study on the broadness of organic transformations accessible by quantum dots, Krauss and Weix reported as well two net reductive reactions using tertiary amines as sacrificial reducants.[91] In a first protocol, the reduction event was used for the decarboxylative radical formation from N-acyloxyphthalimides and the following addition of this radical a on styrene derivative.[101] The recombination of benzylic radicals was observed as sole product (Figure 28). In the original publication using ruthenium catalysis, electron-poor olefins were used as well and resulted in alkylated products. However, these reactions were not reproduced with quantum dots (it is not specified in the paper of Krauss and Weix if they did not try, or if it did not work).

Figure 28. Decarboxylative radical addition to styrene from N-acyloxyphthalimide derivatives under CdSe photocatalysis. Yield obtained with the CdSe QDs (yield with the Ir catalyst). The quantum dots are involved in the reduction of the radical precursor. A sacrificial reductant quenches the holes of the QDs.

Then, a rather elusive oxidative quenching pathway was reproduced from Stephenson and co-workers[102] in the reductive dehalogenation of aryl halides. In this reaction, the photoexcited quantum dots are engaged in a reduction reaction with the aryl halide substrate, providing electrons as the first catalytical step. This required a high reduction potential for the photoexcited QDs, which was a limiting factor and restrained the scope to one electron-poor aryl iodide. The oxidized quantum dots were regenerated by a sacrificial amount of tributylamine, which was also involved in the hydrogen

abstraction step furnishing the product (Figure 29). Notably in this case, the scale was reduced from 0.6 to 0.25 mmol upon using quantum dots in place of the reported iridium catalyst.
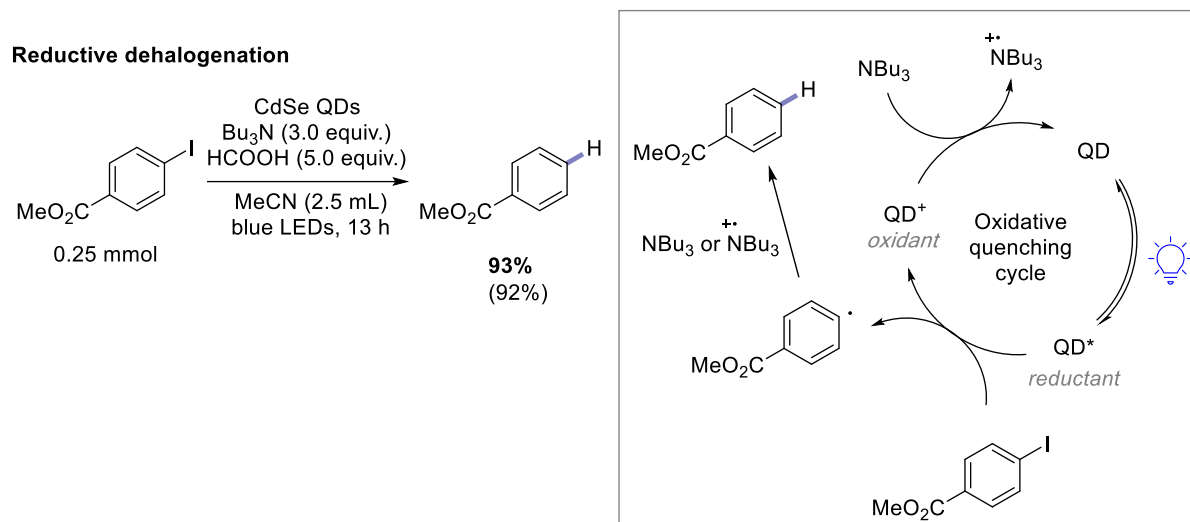
Figure 29. Reductive dehalogenation of aryl halides using an oxidative quenching pathway with CdSe quantum dots. Yield obtained with the CdSe QDs (yield with the Ir catalyst).

It is worthwhile noting here that König and co-workers developed significantly more reducing ZnSe/CdS quantum dots to achieve the same transformation.[54] They could enlarge the scope to a variety of electron-poor or neutral (hetero)aryl bromide derivatives. Four examples of coupling with pyrroles were reported as well, albeit in moderate yields of 40%. The protocol was not applied to preparative chemistry and the products were not isolated.

In close connection to these studies, Krauss and Weix explored the ability of CdS quantum dots to perform the reductive dehalogenation of electron-rich aryl chlorides with reduction potentials ranging from -2.5 to -3.5 V *vs* SCE.[103] The authors performed an extensive mechanism investigation and postulated that the catalytic cycle started by the reductive quenching of the photoexcited quantum dots by a tertiary amine (QD* to QD$^-$, Figure 30). The resulting anionic quantum dots were not reducing enough to directly transfer an electron to the aryl chloride derivatives. However, the possibility of exciting a second electron from the valence band to the conduction band in an anionic QD is retained (albeit with a much lowered absorbance compared to the excitation of the first electron).[44] This results in a "negative trion state"(QD^{-*}) consisting of two electrons in the conduction band and one hole in the valence band, and able to undergo a process known as the Auger recombination.[104] This is a nonradiative process in which the energy (E in Figure 30) liberated by the electron-hole recombination is transferred to the third charge carrier of the trion, exciting it to a higher-energy state. Depending on the band gap of the QD, and hence on the energy liberated by the electron-hole recombination, the excitation can promote the electron to a higher state (it is then called a "hot electron") or expel it completely from the QD into the solvent (ionization). Electron transfer of this highly reducing electron to the starting material brings the QD back to its initial state.
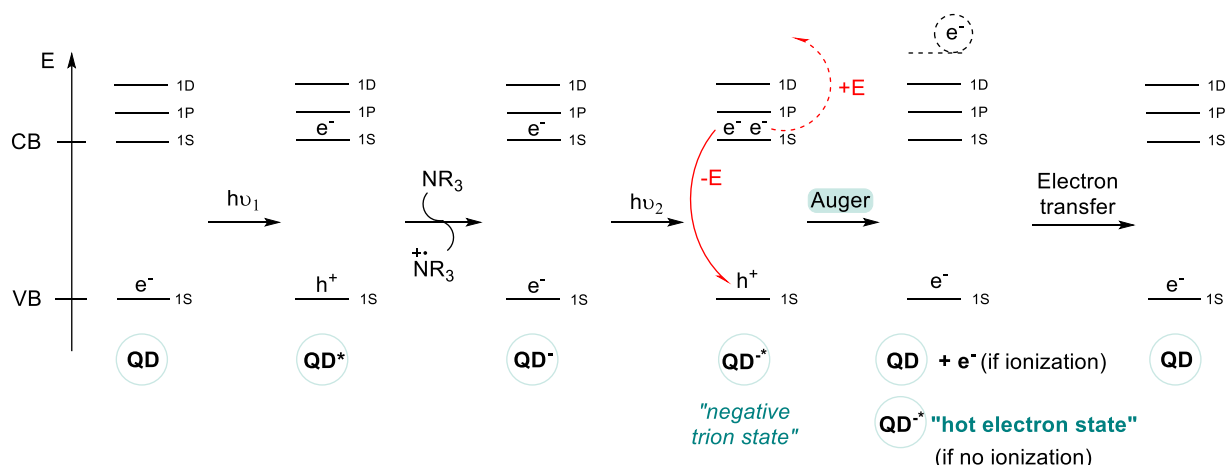
Figure 30. The Auger recombination mechanism conceptually explained using the simplified quantum dot electronic structure.

The quantum dots used in this study are relatively large, 5.6–5.8 nm CdS quantum dots capped with oleic acid ligands. The base tris(2-aminoethyl)amine (TAEA) proved to be a more efficient hole quencher than DIPEA due to its ability to anchor itself at the surface of the quantum dots. Ligand displacement experiments showed that TAEA was able to replace the native oleic acid ligands at the surface of the QDs upon reaction, and that this event was stabilizing for the nanoparticle. However, a large excess of TAEA was detrimental to the reaction outcome (>20% drop in yield compared to the optimized conditions), presumably due to an impaired access at the surface for the aryl chloride reactant. It is also interesting to note that the noncoordinating DIPEA resulted in less reproducible yields between different QD batches. The authors postulated that it was the exact surface chemistry which was likely responsible for the observed discrepancies between QD batches.

The aryl radicals obtained from this method were either trapped by a hydrogen atom donor (Figure 31A) or by aryl radical acceptors like B_2Pin_2 or *N*-methylpyrrole (Figure 31D). The strongly reducing conditions were used for challenging reductive deprotections of tosyl or benzyl groups and demonstrated good functional group tolerance (Figure 31B). In addition, the reductive ring opening of cyclopropyl carbonyl derivatives was performed (Figure 31C). The reactions were run on 0.25 to 0.5 mmol scale and a scale-up to 4 mmol was demonstrated. The quantum dots could be removed from the reaction media by precipitation and centrifugation to be used a second time without loss of yield.

Conditions A:
5.9 nm CdS (0.002 mol%)
TAEA (1.5 equiv.)
DMPU (0.25 M)
blue LEDs, rt
24 - 45 h

TAEA

A/ Hydrodechlorination

0.25 mmol

77%
(87% on 4 mmol)
E_{red} = -3.4 V *vs* SCE

80%
E_{red} = -2.9 V *vs* SCE

84%
E_{red} = -2.6 V *vs* SCE

B/ Reductive deprotection

R_2NTs → R_2NH
0.5 mmol

68%

68%
(89% NMR yield)

PMP→O→Bn → PMP→OH
0.25 mmol   79%

C/ Reductive ring opening (*Conditions A*)

71%

75% (NMR yield)

D/ Functionalization of aryl radicals

0.25 mmol

N-methylpyrrole
(50 equiv.)

42%

Figure 31. Scope and synthetic utility of the aryl radical generation using highly reducing QDs via the Auger process. PMP = para-methoxyphenyl.

In 2020, Weiss and co-workers had already reported a strategy for the reductive deprotection of aryl sulfonyl-protected phenols using $CuInS_2$/ZnS quantum dots exhibiting a high excited-state reduction potential (>-1.9 V *vs* SCE).[48] The two-photon, two-electron process required a high excess of triethylamine as a sacrificial terminal reductant (Figure 32). A series of electron-deficient aryl sulfonates with reduction potential below -1.8 V *vs* SCE could be deprotected as assessed by NMR on sub millimolar-scale reactions. Remarkably, the method supported the presence of NHBoc and toluenesulfonyl protecting groups, as well as proximate ketones. Only one isolated yield was reported on a low 0.022 mmol scale, making the method unpractical for preparative synthesis applications.

85% isolated yield of the deprotected product
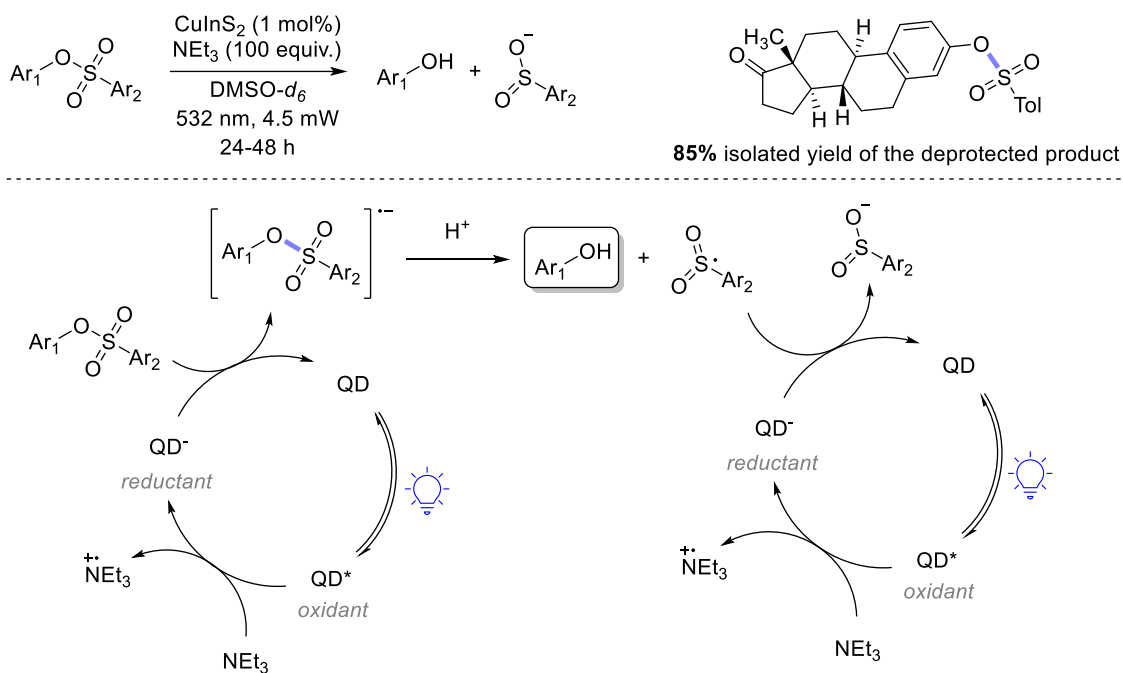
Figure 32. Reductive deprotection of aryl sulfonyl-protected phenols.

In 2019, Feng and co-workers reported a quantum dot photocatalyzed C(sp$_3$)-Cl bond cleavage of ClCF$_2$COOEt.[105] The resulting ethyl difluoroacetate radical was trapped by a variety of *N*-aryl allylamines, engaging in a cascade cyclization to provide medicinally relevant CF$_2$-containing azaheterocycles (Figure 33). The broadness of the reaction was demonstrated on a large substrate scope with good to excellent yields of fluorinated azaheterocycles. The reaction was not sensitive to the functional group electronic properties on the aromatic ring. The formation of 5, 6, and more challenging 7-membered rings was feasible. Diversely functionalized difluoromethyl chlorides were amenable to the reaction conditions including, additionally to ester groups, secondary and tertiary amides, benzoxazoles and oxadiazoles. A tricyclic product was obtained as well. The *in vitro* cytotoxicity of some of these medicinally relevant compounds was tested against two tumor cell lines and showed promising results, however the unusually high catalyst loading for this reaction (1 mol%) prevents its scalability.
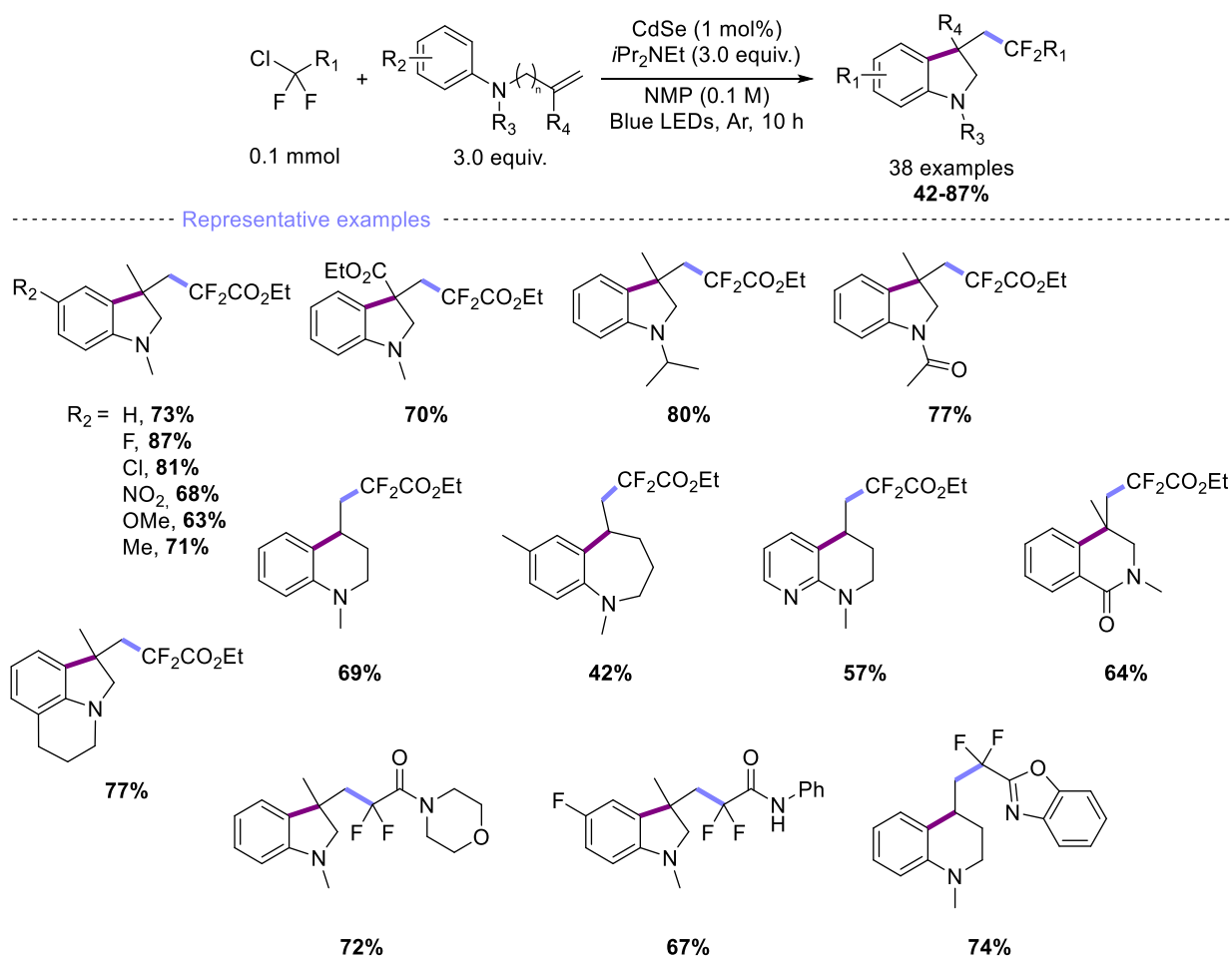
Figure 33. Examples of CF$_2$ containing azaheterocycles obtained through the quantum dot catalyzed method.

The employed 3.5 nm-CdS QDs were capped with octylphosphonic acid (OPA) ligands and are thought to enter in a rather classical catalytic cycle following a reductive quenching with iPr$_2$NEt. Subsequent electron transfer to ClCF$_2$COOEt afforded the desired radical that was electrophilic enough to add to the unactivated olefin of the N-arylamine substrate. Subsequent cyclization on the aromatic ring afforded an aryl radical that could be further oxidized either by the holes of the QD or by electron-transfer to the amminium radical cation of DIPEA. Loss of a proton afforded the rearomatized product. It is possible that the use of a simple N-aryl allylamine substrate required an excess of DIPEA as sacrificial reductant to avoid direct oxidation of the N-aryl moiety by the catalyst (see Chapter 3). A similar reaction was reported under iridium photocatalysis with a phosphonodifluoromethyl radical species [•CF$_2$PO(OEt)$_2$] reacting on N-arylacrylamides.[106] The mechanism followed in this latter case an oxidative quenching with final oxidation of the aryl radical by the iridium(IV) species, avoiding the use of a sacrificial reductant.
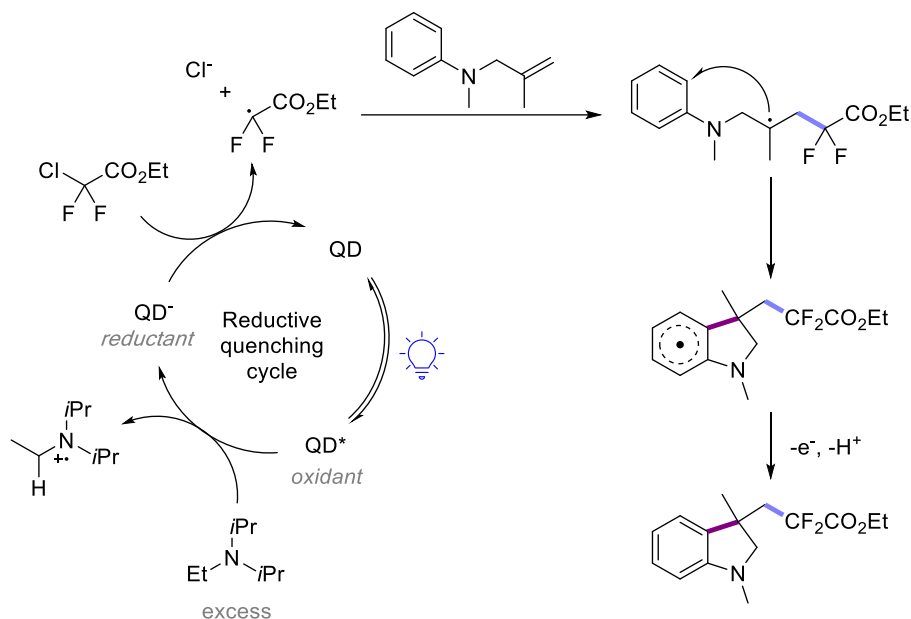
Figure 34. Mechanistic hypothesis for the quantum dot catalyzed C(sp$_3$)-Cl bond cleavage of ethyl chlorodifluoroacetate and following cascade cyclization with unactivated olefins.

1.3.3.2. Thiophenols as sacrificial reductants

Shen, Pu and Peng used thiophenols as sacrificial hole scavengers for the reduction of imines[107] and carbonyl compounds using quantum dots photocatalysts.[108] Additionally, thiophenols are very good hydrogen atom donors due to the stabilization of the aromatic thiyl radical by resonance.[83]

The reduction of aldimines to the corresponding secondary amines was developed in 2018 using oleylamine-capped, quasi type-II core-shell CdSe/CdS quantum dots as photocatalyst (refer Figure 10 for a definition) in presence of excess 4-fluorothiophenol in toluene. The reduction of a wide range of *N*-aryl benzaldimines was demonstrated, and it was found that *N*-alkyl benzaldimines were suitable substrates as well (Figure 35). In addition, the method was applied to the two-step synthesis of the antimycotic agent butenafine. Under optimal reaction conditions, the catalyst loading for this reaction could be lowered to 0.001 mol%, meaning that high TON numbers up to 10^5 could be obtained for the transformation. Additionally, QDs still had the ability to photocatalyze the reaction when more starting material was added to the reaction mixture after completion of the previous run. The reaction could be scaled-up from 0.4 to 6 mmol without loss of yield, and a one-pot reaction employing the appropriate benzaldehyde and aniline also afforded the desired product in retained high yield.
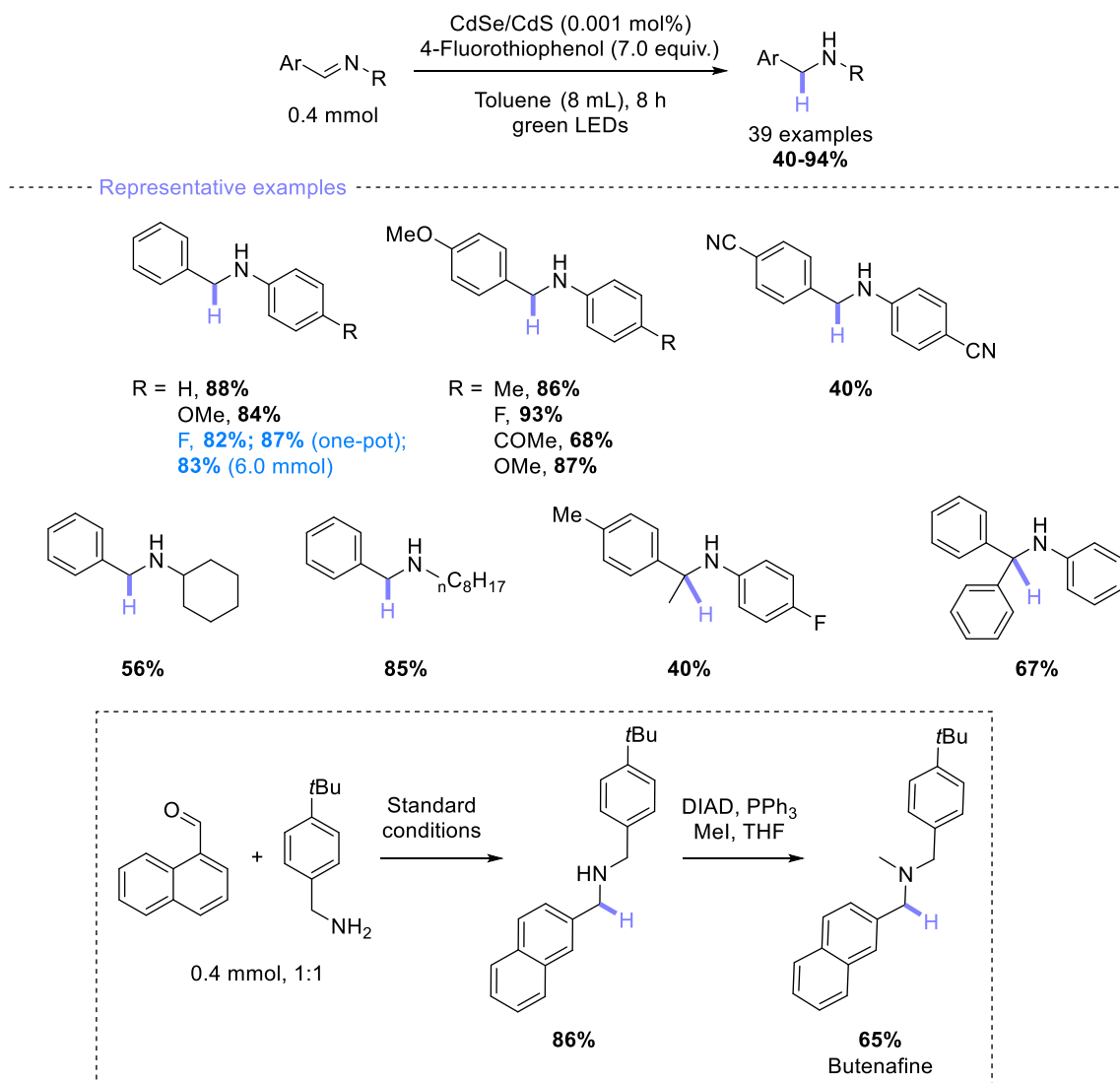
Figure 35. Substrate scope of the QD photocatalyzed reduction of imines.

The authors showed that in solution, proton transfer could take place between the acidic thiophenol and the native oleylamine ligands, leading to thiolate anions bound to the QDs. It is believed that these thiolates play a dominant role as hole trap, as exemplified by the good correlation between yields and acidity of the thiophenol employed as sacrificial reductant. Additionally, the oxidation potential of the thiolate anion (E_{ox} = + 0.85 V vs SCE) is lower than that of the neutral thiophenol (E_{ox} = + 0.95 V vs SCE)[109] and is in good correlation with the estimated oxidation potential of the valence band of the QDs (E_{ox} = + 0.9 V vs SCE). Hence a plausible mechanism for this reaction is the transfer of the holes from the valence band to the thiolate to generate a thiyl radical (Figure 36). Reduction of the neutral imine (E_{red} = − 2.0 V vs SCE)[110] by the electrons of the conduction band (E_{red} = − 1.2 V vs SCE) is thermodynamically unfavorable but is possible via a PCET pathway leading to the alpha-amino radical.[111] HAT from this nucleophilic radical to a second thiophenol molecule is a polarity-matched[112] process that affords the final product along with a another thiyl radical leading to a disulfide co-product.
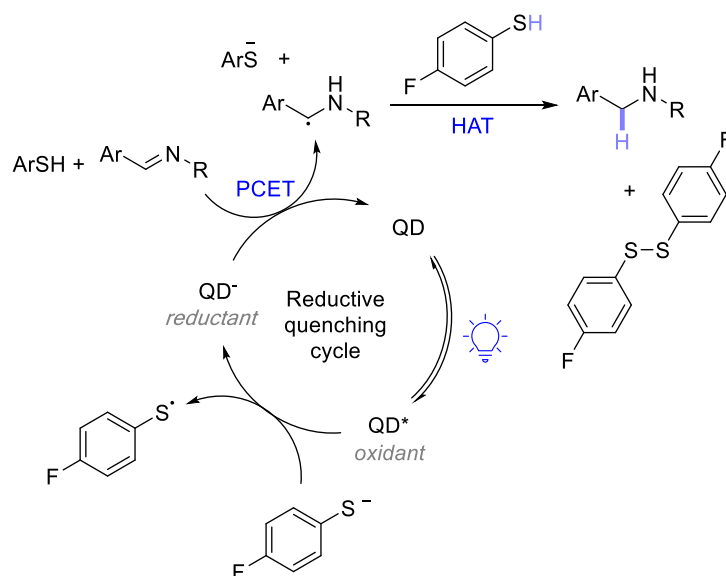
Figure 36. Proposed mechanism for the reduction of imines using core-shell QDs and a thiophenol derived sacrificial reductant.

The choice of catalyst and reagents is interesting to discuss. Running the reaction with plain-core CdS or CdSe QDs led to a decrease of yield compared to the core-shell CdSe/CdS (60% *vs* 87%). Importantly, plain CdSe precipitated during the reaction, indicating that the core-shell structure of the catalyst was not only important for the photocatalytic efficiency of the reaction but also for the stability of the QDs. The photocatalytic hydrogenation of diarylamines has been described using iridium catalysis with triethylamine as a sacrificial reductant.[113] It was found that under QD photocatalysis, triethylamine cannot be used as a hole scavenger, leading to no reaction at all. The authors suggested that triethylamine had a low ability to extract holes from quantum dots which seems to be in contradiction with previous studies, although DIPEA is indeed usually used instead of TEA (see Figure 28, Figure 41, Figure 34). It is possible that the high oxidation potential of the QD is not compatible with the easily oxidized TEA, leading to overoxidation and fast degradation of the QDs.

In 2021, the authors reported the same method expanded to the reduction of aryl aldehydes and ketones chemoselectively to either alcohols or pinacol products.[108] The scope of aromatic aldehydes was demonstrated on electron-rich and -poor substrates (Figure 37). Aromatic aldehydes substituted with a ketone or an ester substituent at the *para* position were well tolerated, albeit requiring a higher excess of *p*-toluenethiol. Heteroaromatic aldehydes could be reduced as well. The possibility of hydrogen abstraction of the aldehydic hydrogen by the thiyl radical, leading to the acyl radical, was not discussed by the authors but would be a non-productive, reversible process.[114] Aromatic ketones were suitable substrates providing that longer reaction times were applied, giving the desired mono-alcohols in high yields with electron-rich or -deficient substituents on the phenyl rings (Figure 37). Importantly, the formation of the pinacol product could not always be fully suppressed, especially for biarlyl ketones. As a matter of fact, the pinacol coupling reaction was mostly amenable to ketones, while aldehydes gave some amounts of mono-alcohol (Figure 38). This problem could be partially resolved by slowly injecting the thiophenol into the reaction mixture.

Ketones: 15 examples, **24-99%**
Aldehydes: 15 examples, **73-99%**
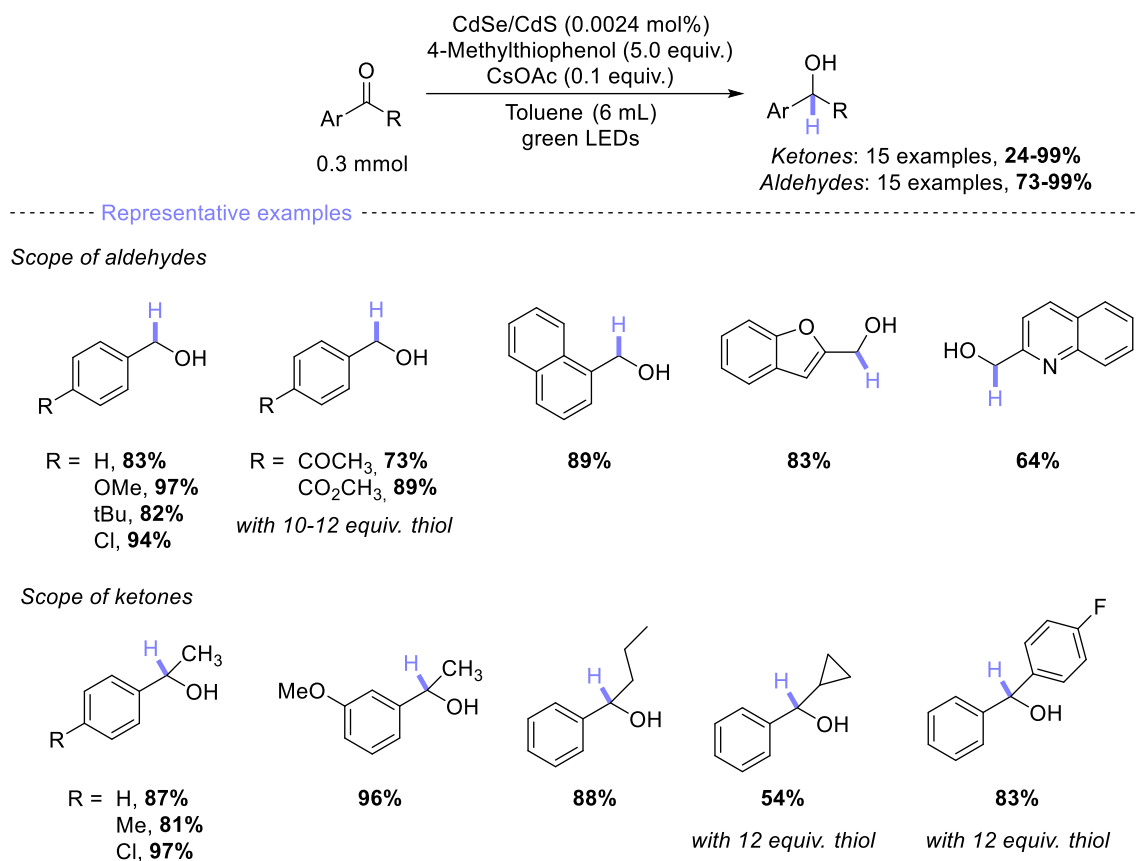
Figure 37. Scope of aromatic aldehydes and ketones in the reduction reaction mediated by QDs and 4-methylthiophenol.

Ketones: 6 examples, **84-99%**
Aldehydes: 5 examples, **44-83%**
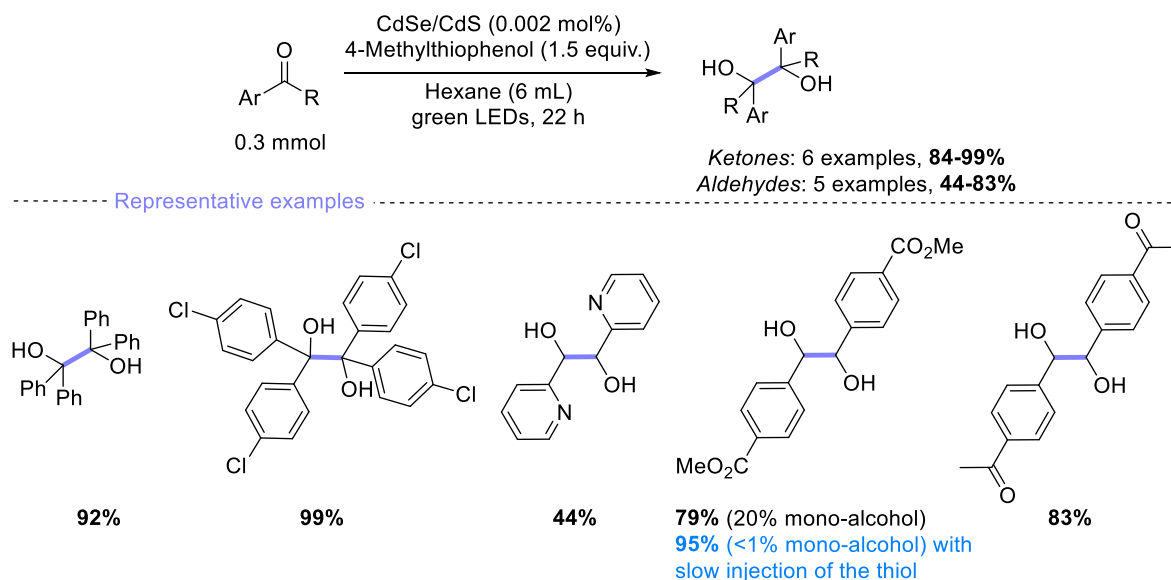
Figure 38. Scope of the pinacol coupling reaction.

Core-shell CdS/CdSe quantum dots were used in combination with *p*-toluenethiol as proton and hydrogen atom donor, as well as hole trap. The mechanism for the reduction of carbonyl compounds to the mono-alcohol is in all point similar to the one previously proposed for imines. Cesium acetate was used as a base to favor the formation of the thiophenolate anion, which is a good quencher of the photoexcited QDs compared to the neutral thiophenol derivative. Reduction of the neutral carbonyl

compound (-1.93 V *vs* SCE in MeCN for benzaldehyde and -2.11 V *vs* SCE in MeCN for acetophenone) by the electrons of the conduction band (~-1.2 V) is thermodynamically unfavorable but is possible *via* a PCET pathway leading to the ketyl radical.[115] HAT from excess thiophenol is a polarity-matched,[112] favored process that affords the mono-alcohol and suppresses completely the formation of the pinacol product. In presence of less thiophenol (1.5 instead of 5 equivalents), HAT to the ketyl radical is inefficient and dimerization becomes the main pathway for the ketyl radical intermediate, giving rise to the pinacol product (Figure 39). Alternatively, the same pinacol product could be obtained by addition of the ketyl radical to a second equivalent of the carbonyl compound,[116] leading to an alkoxyl radical that could abstract a hydrogen from thiophenol (at a rate of 10^9 M^{-1}s^{-1} at 298 K)[117] or that could be reduced to the oxyanion leading to the product. Probably because less thiol was used, no excess base was necessary in the pinacol coupling reaction. The basicity of the ligands is thought to be enough to generate the required thiolates.
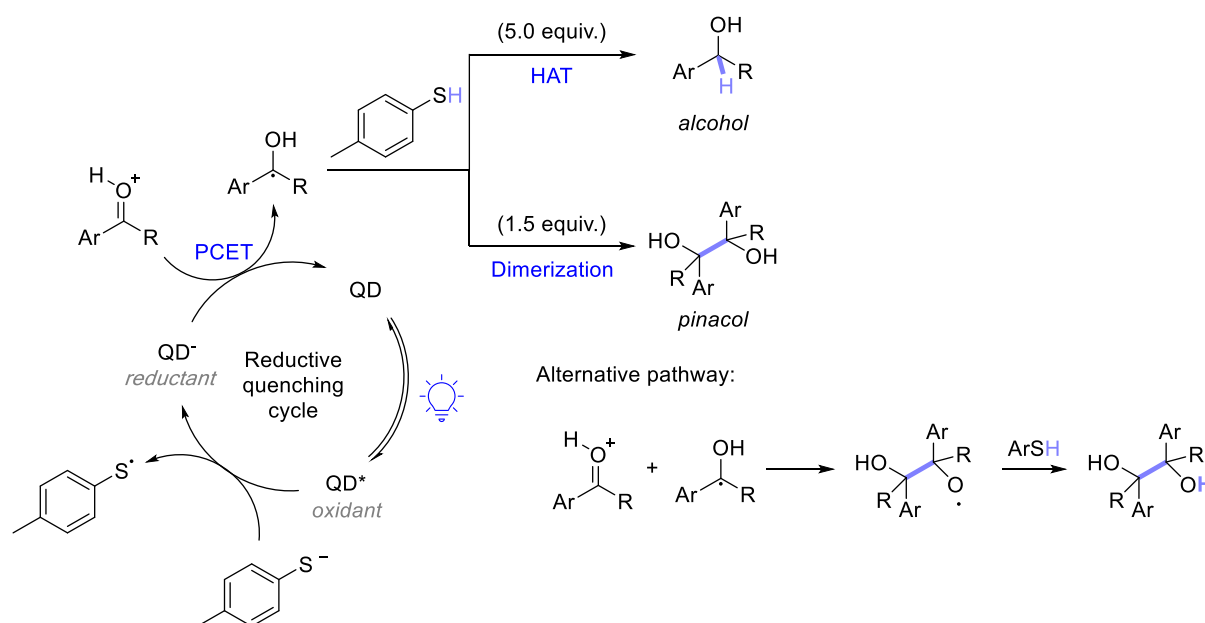
Figure 39. Postulated mechanism for the selective formation of the alcohol or the pinacol products from benzoketone and benzaldehyde derivatives.

Interestingly, the light source needed to be adapted to the substrates. Thus, in the reduction reaction, aldehydes were irradiated with one 3 W green LED while ketones needed two 3 W green LEDs. In the pinacol reaction, two 3 W LEDs were used for all substrates. The irradiation power seemed to be an important parameter in driving an inherently less efficient reaction. In the scale-up reaction to 6 mmol, the irradiation power was also significantly increased (from 2 x 3 W to 40 W). Finally, the authors showed that the quantum dots could be used in 10 consecutive batches with an overall yield of 90% for the picanol coupling of 4,4'-dimethylbenzophenone. Between the first and the last batch, the reaction time only went from 22 hours to 38 hours, a relatively small increase.

1.3.4. Net oxidative reactions

In 2018, Pandey and Mukherjee reported the quantum dot mediated aerobic oxidation of aliphatic and aromatic boronic acids to the corresponding alcohols.[118] The alkyl boronic acids elusive to the same ruthenium mediated protocol[119] were amenable to the quantum dot method using oleyl amine-capped CdSe QDs. Nonetheless the scope mostly features aryl boronic acids, both bearing electron-donating and -withdrawing groups (Figure 40). Oxidizable functional groups such as a formyl and an amine moiety were tolerated with moderate to high yields. It was shown that the standard QD loading

of 0.08 mol% could be reduced to 0.001 mol% with acceptable loss of yield (63% instead of 88%) upon prolonged reaction time. More importantly, the TON was raised from 1100 to 62972, an extremely high value for a photocatalyst. For a scale-up from 0.2 to 2.0 mmol the catalyst loading could also be decreased to 0.005 mol% and after a prolonged reaction time the desired product was obtained with a 20% decrease in yield. Catalyst recycling experiments were also performed. Each run led to a slight decrease in yield and longer reaction time, consistent with a gradual decrease in catalyst loading due to catalyst degradation.
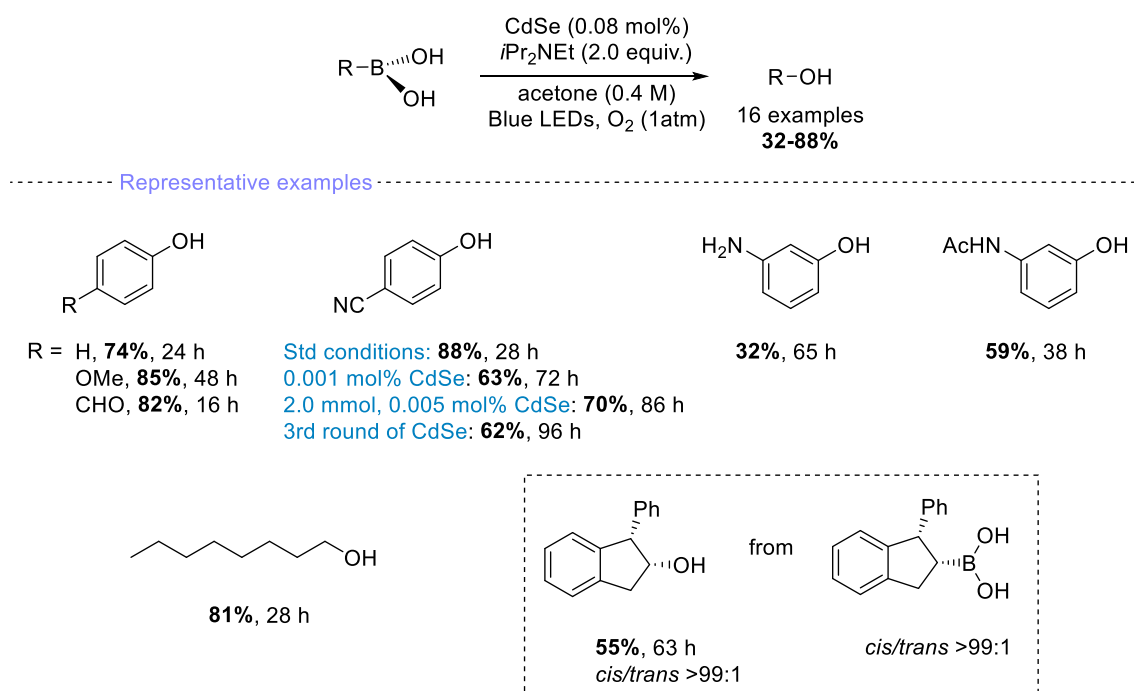
Figure 40. Substrate scope aerobic oxidation of boronic acids mediated by low loadings of CdSe QDs. The generality of the reaction was demonstrated on a wide range of aryl boronic acids and 3 examples of alkyl boronic acids.

The authors performed an optimization based, among other parameters, on the size of the QDs. They could clearly show that the yield was improved with increasing band gap, i.e. with decreasing diameter of the QDs – a parameter that has a strong influence on the position of the conduction band (see Figure 8). Additionally, a drop of yield was obtained upon using type I core-shell CdSe/CdS QDs for which the electrons are located in the core. These results lead the authors to the conclusion that an energy barrier of activation for the electron transfer was at play, suggesting an oxidative quenching catalytic cycle. Additionally, the authors showed that both the boronic acid and the base were necessary for triggering the electron transfer step, however it was not elucidated how. The involvement of a Lewis-base adduct is likely with boronic acids, but has been previously demonstrated by Ley and co-workers to engage in oxidative SET, not reductive.[120] The authors also showed that the boronic acid starting material was responsible for increasing the QD emission lifetime, probably through passivation of the quantum dot. Therefore, it could be hypothesized that the formation of the Lewis-base adduct is necessary to prevent the boronic acid from interacting with the quantum dots, which in turns allows the reaction to start. To summarize these mechanistic studies, it is proposed that electron transfer to molecular oxygen produces the superoxide radical anion that displaces DIPEA to form a boronic acid-superoxide radical anion adduct (Figure 41). Hole transfer from the valence band of the QD to the tertiary amine produces an amminium radical cation and restores the neutral state of the QD. A HAT event from this radical cation by the superoxide radical leads to the peroxyboronate intermediate which delivers the required alcohol after rearrangement and hydrolysis. A similar mechanism has been

described for the same, ruthenium mediated reaction developed by Jorgensen and Xiao in 2012.[119] A reductive quenching by the tertiary amine was proposed in this case, although the possibility of an oxidative quenching pathway had not been ruled out.
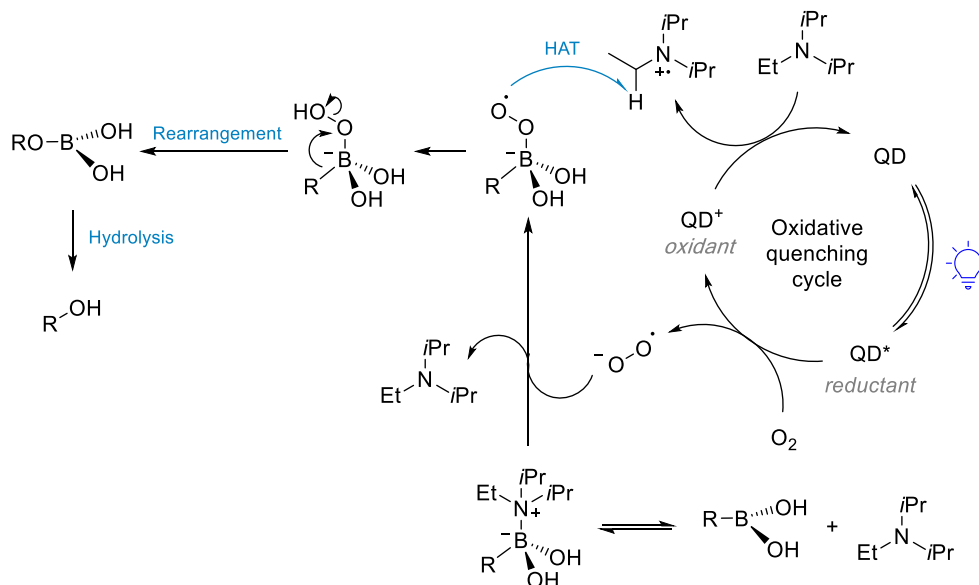
Figure 41. Proposed mechanism for visible light mediated aerobic oxidation of boronic acids. The mechanism is thought to start by an electron transfer to oxygen.

1.3.5. Cyclophotoaddition reactions

Weix and Krauss reported in 2017 that their oleate-capped 3 nm CdSe QDs had not been able to catalyze cyclophotoaddition reactions. This limitation has recently been partially lifted.

When photons of an adequate frequency are absorbed by a quantum dot, electrons are promoted from the valence band to the conduction band. A possible pathway from here, as we have seen, is the transfer of holes or electrons to an organic substrate. Alternatively, a decay to the ground state can lead to the emission of a photon whose frequency is close to the frequency of the corresponding transition. The fluorescence of quantum dots has long been recognized has a powerful tool in imaging and sensing.[121] In these cases, the excited state can be called a "bright" state. In some cases, a decay is observed in a state that is not coupled to any other level, preventing the emission or absorption of light from this state.[122] These states are called "dark" states or, in the specific case of quantum dot photocatalysis, triplet-like excitonic dark states (we will refer to them more simply as triplet excitons). In 2016, Castellano and co-workers showed that CdSe quantum dots were able to transfer their triplet excitons to surface-bound molecular acceptors (Figure 42).[123] Polyaromatic carboxylic acid derivatives, which are able to coordinate QDs, were used as the triplet acceptors. These acceptors can in principle be organic substrates involved in a direct organic transformation, or they can be used as energy transfer shuttles to a substrate in solution. This processus can be described as an interfacial Dexter-like energy transfer.
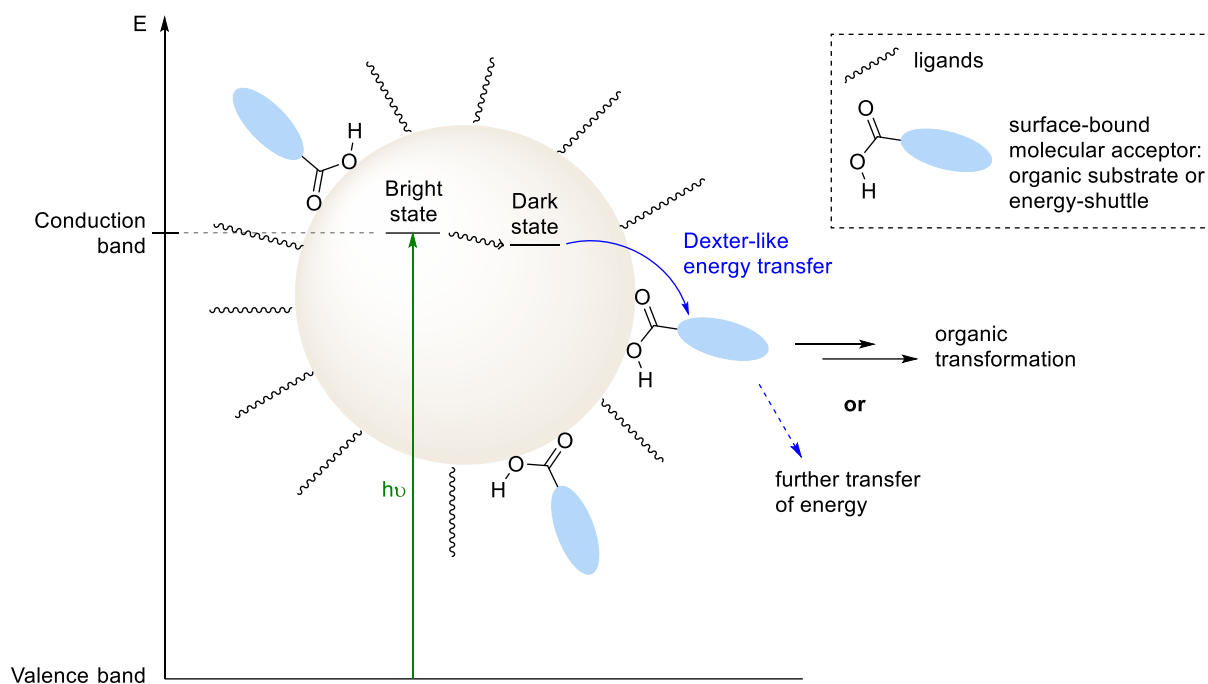
Figure 42. Schematic principle of triplet exciton formation (dark state) in a quantum dot with consecutive Dexter-like energy transfer to a surface-bound molecular acceptor. Inspired and simplified from Castellano et al.[123]

In 2019, Weiss and co-workers built on this discovery to drive the regioselective and diastereoselective, intermolecular [2+2] cycloaddition of 4-vinylbenzoic acid and derivatives by triplet-triplet energy transfer from specifically designed quantum dots.[124] It was found that similarly to hole/electron excitons, triplet state excitons are tunable *via* size adjustment of the QD. It was thus possible to selectively sensitize one olefinic reagent in the reaction mixture by judicious light excitation, thereby achieving high selectivity for the hetero-intermolecular coupling toward cyclobutane synthesis.

The regioselectivity of this reaction can be driven by the template furnished on the quantum dot surface by the anchoring of the carboxylic acid moieties. Therefore, it is possible to reverse it by tuning the carboxylic acid position, although the term of "reversal" is somewhat abusive since different products are obtained (Figure 43A). Nonetheless, it shows that the carboxylic moieties are responsible for the regioselectivity of the reaction. The diastereoselectivity observed in the cycloaddition can also be explained by this anchoring, whereby π-π interactions in the rigid olefinic system at the surface of the QD promotes the *syn*-selectivity. This was mostly demonstrated on homo-coupling transformations, but two hetero-couplings showed to be highly diastereoselective as well (Figure 43B). For each substrate, the corresponding iridium- and ruthenium-photocatalyzed reaction was run as well. The diastereoselectivity in this case was shown to be modest and in favor of the *trans*-products.
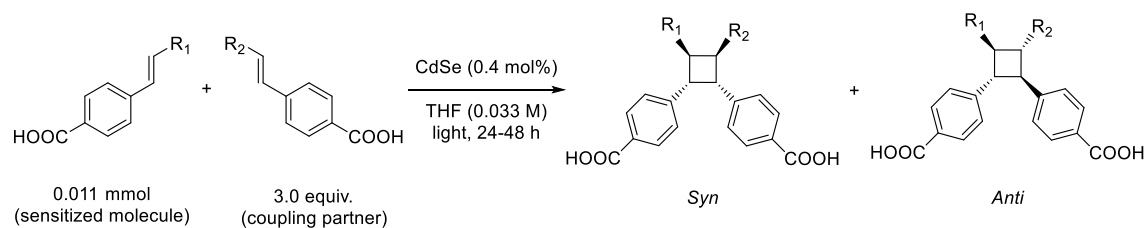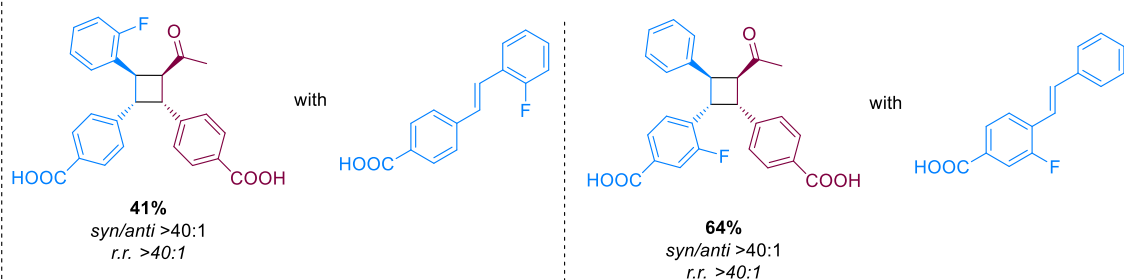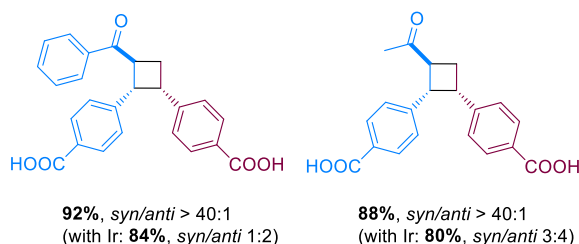
Figure 43. A/ Influence of the position of the carboxylic acid moiety in the product obtained in the [2+2] cycloaddition reaction. B/ Examples of the diastereoselective intermolecular hetero-[2+2] cycloaddition driven by CdSe quantum dots.

Finally, the reversible association of the carboxylates with the Cd^{2+} ions on the QD's surface ensures that coupled products can be displaced by new substrates to allow the reaction to go forward.

Although the observed selectivity is interesting and complementary to the iridium-photocatalyzed reaction, the scalability of this method was not demonstrated. Isolated yields are reported on less than 0.02 mmol scale reactions, which is too low for useful preparative chemistry. Additionally, the scope was limited to alkenes functionalized with carboxylic acid moieties; the use of one coupling partner without the carboxylic acid moiety not only shut down the diastereo- and regioselectivity, but also drastically reduced isolated yields to less than 10%.

In 2021, the Weiss group published an extension of this method using carboxylate-bound polyaromatic "energy shuttles" that were able to act as noncovalent adsorption sites for the substrates of the reaction on the QD surface.[125] As such, no anchoring groups were necessary on the starting materials. The triplet excitons were first transferred to this polyaromatic moiety, which was able to transfer it further to freely diffusing substrates (see Figure 42). The yields obtained were comparable to the iridium-catalyzed reactions run in parallel, but the reaction with QDs has the advantage of catalyst recyclability, lower catalyst loadings, and high stability. Unfortunately, the reaction was not scaled-up above 0.033 mmol.

40

1.3.6. Summary of relevant experimental parameters in the QD catalyzed reactions

Reference	Reaction	Scale	Number of QD cycles	set-up/irradiation
ACIE 2014, 53, 2085 – 2089[71]	Disulfide formation (9 examples)	0.25 mmol. No scale-up.	Max. 4	No details on the reactor, presumably a flask. Irradiation by a mercury lamp with a cutoff filter below 400 nm. 150 mW.cm^{-2} at the flask. Deaeration by bubbling N_2 for 15 min.
Chem 7, 1244–1257[75]	Radical-radical coupling of allylic and alpha-amino radicals, 36 examples	0.1 mmol. One example scaled-up to 5 mmol.	Not investigated.	<u>0.1 mmol scale</u>: 10-mL reaction tube for 3 mL of solvent, deaeration by bubbling Ar for 30 min. Blue LEDs (3W, λ = 450 ±10 nm, 145lm @ 700 mA), not specified how many and what kind of set-up. <u>Gram-scale</u>: 150-mL reaction tube (L=18 cm, diameter = 5 cm) for 100 mL of solvent. No details on the irradiation. Concentration of the reaction increased by 50% compared to 0.1 mmol scale reaction. Reaction time is doubled. Same for all scale-ups by the Li-Whu Zu group.
	Minisci reaction of allylic bonds (35 examples)	0.05 mmol. No scale-up.	Not investigated.	<u>0.05 mmol scale</u>: 10-mL reaction tube for 4 mL of solvent, deaeration by bubbling Ar for 30 min. Blue LEDs, no details.
ACIE 2021, 60, 11779 – 11783[82]	Allylic and vinylic thiolation (28 and 24 examples)	0.05 mmol resp. 0.1 mmol. Scale-up to 2 mmol.	Not investigated.	<u>0.05-0.1 mmol scale</u>: 10-mL reaction tubes for 3-4 mL solvent. Blue LEDs (3W, λ = 450 ±10 nm, 145lm @ 700 mA), not specified how many and what kind of set-up. Deaeration by bubbling Ar for 30 min. <u>2 mmol-scale</u>: 150-mL reaction tube (L=18 cm, diameter = 5 cm) for 80 mL of solvent. Same concentration. Deaeration not specified. 24 h *vs* 12 h.
ACIE 2012, 51, 4062 – 4066[126]	Mannich reaction (4 examples)	0.2 to 0.5 mmol. No scale-up.	Not investigated.	No details given.
JACS 2017, 139, 4250–4253 [91]	C-C bond forming reactions	0.25 to 0.5 mmol. No scale-up.	Not investigated	Two LEDs with collimators for each aluminum cylinder containing a 1-dram vial. Each cylinder is affixed to a small heat sink and attached to an aluminum plate. A fan is employed and T° estimated to reach 35-45 °C. The vial is reached by 520 mW of light.

Reference	Reaction	Scale	Number of QD cycles	set-up/irradiation
CCS Chem. 2022, 10.31635/ccschem.021.2021 01615[89]	C-P bond formation	0.05 to 0.1 mmol. Scale-up to 5 mmol.	Not investigated	0.1 mmol scale: 10-mL reaction tube for 3 mL of solvent, deaeration by bubbling Ar for 30 min. Blue LEDs (3W, λ = 450 ±10 nm, 145lm @ 700 mA), not specified how many and what kind of set-up. Gram-scale: 150-mL reaction tube (L=18 cm, diameter = 5 cm) for 100 mL of solvent. No details on the irradiation. Concentrated by a factor 1.5. 48 h *vs* 16 h.
ACIE 2021, 60, 27201 – 27205[84]	THF activation	0.05 to 0.1 mmol. Scale-up to 5 mmol.	Not investigated	0.1 mmol scale: 10-mL reaction tube for 5 mL of solvent, deaeration by bubbling Ar for 30 min. Blue LEDs (3W, λ = 450 ±10 nm, 145lm @ 700 mA), not specified how many and what kind of set-up. Gram-scale: 150-mL reaction tube (L=18 cm, diameter = 5 cm) for 90 mL of solvent. No details on the irradiation. Concentrated by a factor 2.5. 48 h *vs* 16 h.
ACIE 2017, 56,3020–3024[73]	Alcohol oxidation	0.2 mmol. Scale-up to 10 mmol	Not investigated.	0.2 mmol scale: purple LEDs at 410 nm, no details. 10-mL reaction tubes for 5 mL solvent. Deaeration by bubbling Ar for 30 min. Scale-up: no details on changes in the set-up. 16-24 h irradiation *vs* 6 h. For estradiol scale-up to 3.8 mmol: dilution by 2.2 and increase of QD loading by 4.
ACS Catal. 2018, 8, 5206–5211[118]	Boronic acid oxidation	0.2 mmol. Scale-up to 2 mmol	Max. 3 with overall 20% loss in yield. Each run took longer.	0.2 mmol scale: LED strips (~460 nm, 0.3 mW/cm^2) coiled around in a Dewar, reaction in a Schlenk tube inserted in the Dewar. Anhydrous conditions. 2.0 mmol and low catalyst loading reactions: a 20W blue LED was used
Adv. Synth. Catal. 2019, 361, 708 – 713[105]	Cascade Cyclization of Functionalized Difluoromethyl Chlorides	0.1 mmol. No scale-up.	Not investigated.	36 W blue LEDs; not specified how many and what kind of set-up. A powerful irradiation might be required as the reaction is unusually concentrated and highly loaded in CdS QDs ([QD]=1.0x10^{-3} M in the final reaction solution).
JOC 2018, 83, 11886–11895[107]	Reduction of imines	0.4 mmol. Scale-up to 6 mmol.	Not thoroughly investigated. QDs were	0.4 mmol: 3 W green LEDs. M = 0.05 M. Seal tube. Deaeration by purging Ar for 10 minutes. 8 h.

Reference	Reaction	Scale	Number of QD cycles	set-up/irradiation
			shown to be still active after one reaction cycle.	6 mmol: 20 W green LED. M = 0.05 M. Regular rbf flask (250 ml for 120 ml solvent). Deaeration by purging Ar for 15 minutes. 10 h.
JOC 2021, 86, 2474–2488 [108]	Reduction of carbonyl compounds	0.3 mmol. Scale-up to 6 mmol.	QDs were shown to be active over 10 reaction cycles.	0.3 mmol: 1 or 2 x 3 W green LEDs. M = 0.05 M. Seal tube. Deaeration by purging with Ar for 15 minutes. 6 mmol: 40 W green LED, reaction in a rbf. M = 0.1 M. Deaeration by purging with Ar for 20 minutes.
ACIE 2020, 59, 14091 – 14095 [48]	Aryl sulfonyl deprotection	0.022 mmol. No further scale-up.	Not investigated.	4.5 mW, 532 nm laser diode.
JACS 2022, 144, 12229–12246 [103]	Auger-mediated reduction	0.25 to 0.5 mmol	Reused once after precipitation	0.25-0.5 mmol: see JACS 2017, 139, 4250–4253 [91]. 4 mmol: 20 mL vial for 16 mL of solvent (2.8 mm diameter). Photoreactor Penn PhD M2. Fan cooling. Set-up in the glovebox, irradiation outside the glovebox. Reaction conditions unchanged compared to the small scale.
Nature Chemistry 11, 1034–1040 (2019) [124]	[2+2] cycloaddition	0.011 to 0.033 mmol. No further scale-up.	Not investigated.	16.5 W white-light with a filter for some substrates (to remove the wavelength at which they abosorb).

Table 2. Summary of preparative methodologies using quantum dots as photocatalysts - practical insights.

In most cases, the reaction scopes are performed on 0.1 to 0.3 mmol scale. One reaction is then often scale-up to 2 to 5 mmols, usually without significant changes in reaction conditions. Sometimes the scaled-up reaction is more concentrated, sometimes more diluted; but the quantum dot loading is generally not changed. Importantly, a change in the irradiation power is always observed depending on the scale: a bigger scale requires a more powerful irradiation. Unfortunately, the number of LEDs as well as the exact irradiation set-up are often not described. Finally, it seems that from one method to another, for the same reaction scale, the power of the irradiation can be very different. For example, Li-Zhu Wu uses 3 W LEDs for 0.1 mmol scale reactions. In the oxidation of boronic acids (Figure 40), the authors used 36 W blue LEDs for the same scale. In the absence of a clear description of the irradiation set-up an exact comparison is difficult, however the difference seems significant and very reaction-dependent.

1.4. General goal of the thesis

The reactions developed within this collaboration should tackle unsolved problems in both the organic and physical chemistry communities. As we could see from section 1.3 (Quantum dots as photocatalysts for organic synthesis), several examples of reductive quenching of the QDs are described where sacrificial reductants are used in excess, favoring the hole transfer process. Fewer

examples of redox neutral transformations involving a reductive quenching of the QDs have been reported in preparative methodologies (see section 1.3.2). Therefore, from a quantum dot point of view there is interest in developing redox neutral reactions following a reductive quenching mechanism, that is for which the challenging hole transfer is the first elemental step. The use of core/shell QDs, understudied in these types of transformations, could be a major focus.

From an organic chemist perspective, this could be applied to several transformations. In particular, the visible-light mediated generation of alkoxyl-radicals from simple precursors is desirable and could be achieved *via* the oxidation of relevant boronate complexes. This precursors have been shown to be compatible with quantum dots, as demonstrated by Pandey and Mukherjee (see Figure 41).[118] The developments towards this reaction will be described in Chapter 2.

The ability of tertiary amines to quench holes of quantum dots has already been unambiguously demonstrated. Even more examples are available in the literature when straying away from preparative chemistry, particularly in the context of redox neutral C–C bond formation from tertiary amines. The light-driven alpha-vinylation of tertiary anilines using vinyl sulfones as radical traps, initially developed by MacMillan and co-workers with an iridium photocatalyst,[97] was for example used as model reaction for the development of quantum dots in two independent studies. In 2017, Weiss and co-workers demonstrated that the reaction could be run with CdS quantum dots without the need for sacrificial reagents or co-catalysts.[52] The key discovery was the effects of the quantum dot's ligands on the rate and efficiency of the reaction. In 2019, Pillai and co-workers further demonstrated that InP/ZnS quantum dots were suitable photocatalysts for the reaction.[98] Therefore a similar reaction could be used to develop the quantum dots in Grenoble. In Bern, a cascade reaction involving the photooxidation of tertiary amines was developed and will be presented in Chapter 3. Initial results on the use of quantum dots for this annulation reaction will be detailed in Chapter 4.

The development and characterization of the quantum dots, entirely performed at the CEA in Grenoble, will not be detailed in this thesis.

References

1   K. Kalyanasundaram, *Coordination Chemistry Reviews*, 1982, **46**, 159–244.

2   H. Cano-Yelo and A. Deronzier, *J. Chem. Soc., Perkin Trans. 2*, 1984, 1093–1098.

3   R. C. Young, T. J. Meyer and D. G. Whitten, *J. Am. Chem. Soc.*, 1975, **97**, 4781–4782.

4   C. R. Bock, T. J. Meyer and D. G. Whitten, *J. Am. Chem. Soc.*, 1974, **96**, 4710–4712.

5   *Visible Light Photocatalysis in Organic Chemistry*, John Wiley & Sons, Ltd, 1st edn., 2018.

6   A. Y. Chan, I. B. Perry, N. B. Bissonnette, B. F. Buksh, G. A. Edwards, L. I. Frye, O. L. Garry, M. N. Lavagnino, B. X. Li, Y. Liang, E. Mao, A. Millet, J. V. Oakley, N. L. Reed, H. A. Sakai, C. P. Seath and D. W. C. MacMillan, *Chem. Rev.*, , DOI:10.1021/acs.chemrev.1c00383.

7   K. Ram Bajya and S. Selvakumar, *European Journal of Organic Chemistry*, 2022, **2022**, e202200229.

8   Photochemistry and Photophysics, https://www.wiley.com/en-us/Photochemistry+and+Photophysics%3A+Concepts%2C+Research%2C+Applications-p-9783527334797, (accessed July 14, 2022).

9   K. Kikuchi, C. Sato, M. Watabe, H. Ikeda, Y. Takahashi and T. Miyashi, *J. Am. Chem. Soc.*, 1993, **115**, 5180–5184.

10 R. Tyburski, T. Liu, S. D. Glover and L. Hammarström, *J. Am. Chem. Soc.*, 2021, **143**, 560–576.

11 L. Capaldo, D. Ravelli and M. Fagnoni, *Chem. Rev.*, 2021, acs.chemrev.1c00263.

12 L. Capaldo, D. Ravelli and M. Fagnoni, *Chem. Rev.*, 2022, **122**, 1875–1924.

13 P. R. D. Murray, J. H. Cox, N. D. Chiappini, C. B. Roos, E. A. McLoughlin, B. G. Hejna, S. T. Nguyen, H. H. Ripberger, J. M. Ganley, E. Tsui, N. Y. Shin, B. Koronkiewicz, G. Qiu and R. R. Knowles, *Chem. Rev.*, , DOI:10.1021/acs.chemrev.1c00374.

14 E. Tsui, H. Wang and R. Knowles, *Chem. Sci.*, , DOI:10.1039/D0SC04542J.

15 E. C. Gentry and R. R. Knowles, *Acc. Chem. Res.*, 2016, **49**, 1546–1556.

16 M. H. Shaw, J. Twilton and D. W. C. MacMillan, *The Journal of Organic Chemistry*, 2016, **81**, 6898–6926.

17 J. D. Bell and J. A. Murphy, *Chem. Soc. Rev.*, , DOI:10.1039/D1CS00311A.

18 C. K. Prier, D. A. Rankic and D. W. C. MacMillan, *Chem. Rev.*, 2013, **113**, 5322–5363.

19 K. Teegardin, J. I. Day, J. Chan and J. Weaver, *Organic Process Research & Development*, 2016, **20**, 1156–1163.

20 J. W. Tucker and C. R. J. Stephenson, *J. Org. Chem.*, 2012, **77**, 1617–1622.

21 S. P. Pitre and L. E. Overman, *Chem. Rev.*, 2022, **122**, 1717–1751.

22 K. P. Shing Cheung, S. Sarkar and V. Gevorgyan, *Chem. Rev.*, , DOI:10.1021/acs.chemrev.1c00403.

23 L. Buglioni, F. Raymenants, A. Slattery, S. D. A. Zondag and T. Noël, *Chem. Rev.*, , DOI:10.1021/acs.chemrev.1c00332.

24 A. Tlili and S. Lakhdar, *Angewandte Chemie International Edition*, , DOI:https://doi.org/10.1002/anie.202102262.

25 A. Joshi-Pangu, F. Lévesque, H. G. Roth, S. F. Oliver, L.-C. Campeau, D. Nicewicz and D. A. DiRocco, *J. Org. Chem.*, 2016, **81**, 7244–7249.

26 Xanthene Dye - an overview | ScienceDirect Topics, https://www.sciencedirect.com/topics/chemistry/xanthene-dye, (accessed July 15, 2022).

27 T. Bortolato, S. Cuadros, G. Simionato and L. Dell'Amico, *Chem. Commun.*, , DOI:10.1039/D1CC05850A.

28 J. M. R. Narayanam and C. R. J. Stephenson, *Chem. Soc. Rev.*, 2010, **40**, 102–113.

29 T.-Y. Shang, L.-H. Lu, Z. Cao, Y. Liu, W.-M. He and B. Yu, *Chem. Commun.*, 2019, **55**, 5408–5419.

30 N. A. Romero and D. A. Nicewicz, *Chem. Rev.*, 2016, **116**, 10075–10166.

31 N. Holmberg-Douglas and D. A. Nicewicz, *Chem. Rev.*, , DOI:10.1021/acs.chemrev.1c00311.

32 R. S. Mulliken, *J. Phys. Chem.*, 1952, **56**, 801–822.

33 Y. Sumida and H. Ohmiya, *Chem. Soc. Rev.*, 2021, **50**, 6320–6332.

34 T. Tasnim, M. J. Ayodele and S. P. Pitre, *J. Org. Chem.*, 2022, **87**, 10555–10563.

35 G. E. M. Crisenza, D. Mazzarella and P. Melchiorre, *J. Am. Chem. Soc.*, 2020, **142**, 5461–5476.

36 C. G. S. Lima, T. de M. Lima, M. Duarte, I. D. Jurberg and M. W. Paixão, *ACS Catal.*, 2016, **6**, 1389–1407.

37 Z. Yang, Y. Liu, K. Cao, X. Zhang, H. Jiang and J. Li, *Beilstein J. Org. Chem.*, 2021, **17**, 771–799.

38 M. Tobisu, T. Furukawa and N. Chatani, *Chem. Lett.*, 2013, **42**, 1203–1205.

39 D. Prusty, L. Paramanik and K. Parida, *Energy Fuels*, 2021, **35**, 4670–4686.

40 X.-B. Li, C.-H. Tung and L.-Z. Wu, *Angewandte Chemie International Edition*, 2019, **58**, 10804–10811.

41 H.-L. Wu, X.-B. Li, C.-H. Tung and L.-Z. Wu, *Advanced Materials*, 2019, **31**, 1900709.

42 S. Das and W. M. A. Wan Daud, *RSC Adv.*, 2014, **4**, 20856.

43 Y. H. Park, G. Murali, J. K. R. Modigunta, I. In and S.-I. In, *Frontiers in Chemistry*.

44 V. I. Klimov, *Annual Review of Physical Chemistry*, 2007, **58**, 635–673.

45 R. D. Harris, S. Bettis Homan, M. Kodaimati, C. He, A. B. Nepomnyashchii, N. K. Swenson, S. Lian, R. Calzada and E. A. Weiss, *Chem. Rev.*, 2016, **116**, 12865–12919.

46 J. Zhao, M. A. Holmes and F. E. Osterloh, *ACS Nano*, 2013, **7**, 4316–4325.

47

48 K. A. Perez, C. R. Rogers and E. A. Weiss, *Angewandte Chemie International Edition*, 2020, **59**, 14091–14095.

49 W. W. Yu, L. Qu, W. Guo and X. Peng, *Chem. Mater.*, 2003, **15**, 2854–2860.

50 J. Jasieniak, L. Smith, J. van Embden, P. Mulvaney and M. Califano, *J. Phys. Chem. C*, 2009, **113**, 19468–19474.

51 J. A. Nasir, Z. ur Rehman, S. N. A. Shah, A. Khan, I. S. Butler and C. R. A. Catlow, *J. Mater. Chem. A*, 2020, **8**, 20752–20780.

52 Z. Zhang, K. Edme, S. Lian and E. A. Weiss, *J. Am. Chem. Soc.*, 2017, **139**, 4246–4249.

53 J. Wang, T. Xia, L. Wang, X. Zheng, Z. Qi, C. Gao, J. Zhu, Z. Li, H. Xu and Y. Xiong, *Angewandte Chemie International Edition*, 2018, **57**, 16447–16451.

54 A. Pal, I. Ghosh, S. Sapra and B. König, *Chem. Mater.*, 2017, **29**, 5225–5231.

55 D. A. Hines and P. V. Kamat, *ACS Appl. Mater. Interfaces*, 2014, **6**, 3041–3057.

56 C. Giansante, *Chemistry – A European Journal*, 2021, **27**, 14358–14368.

57 J. J. Calvin, A. S. Brewer and A. P. Alivisatos, *Nat Synth*, 2022, **1**, 127–137.

58 P. Reiss, M. Protière and L. Li, *Small*, 2009, **5**, 154–168.

59 P. Maity, T. Debnath and H. N. Ghosh, *J. Phys. Chem. C*, 2015, **119**, 26202–26211.

60 K. Baba, S. Bulou, M. Quesada-Gonzalez, S. Bonot, D. Collard, N. D. Boscher and P. Choquet, *ACS Appl. Mater. Interfaces*, 2017, **9**, 41200–41209.

61 N. Zhang, S. Liu and Y.-J. Xu, *Nanoscale*, 2012, **4**, 2227–2238.

62 V. Subramanian, E. E. Wolf and P. V. Kamat, *J. Am. Chem. Soc.*, 2004, **126**, 4943–4950.

63 D. M. Adams, L. Brus, C. E. D. Chidsey, S. Creager, C. Creutz, C. R. Kagan, P. V. Kamat, M. Lieberman, S. Lindsay, R. A. Marcus, R. M. Metzger, M. E. Michel-Beyerle, J. R. Miller, M. D. Newton, D. R. Rolison, O. Sankey, K. S. Schanze, J. Yardley and X. Zhu, *J. Phys. Chem. B*, 2003, **107**, 6668–6697.

64 Y. Pu, F. Cai, D. Wang, J.-X. Wang and J.-F. Chen, *Ind. Eng. Chem. Res.*, 2018, **57**, 1790–1802.

65 D.-Y. Wang, Y.-Y. Yin, C.-W. Feng, Rukhsana and Y.-M. Shen, *Catalysts*, 2021, **11**, 275.

66 C. Huang, X.-B. Li, C.-H. Tung and L.-Z. Wu, *Chemistry – A European Journal*, 2018, **24**, 11530–11534.

67 Y. Yuan, N. Jin, P. Saghy, L. Dube, H. Zhu and O. Chen, *J. Phys. Chem. Lett.*, 2021, **12**, 7180–7193.

68 S. Lin, H. Huang, T. Ma and Y. Zhang, *Advanced Science*, 2021, **8**, 2002458.

69 M.-Y. Qi, M. Conte, M. Anpo, Z.-R. Tang and Y.-J. Xu, *Chem. Rev.*, 2021, **121**, 13051–13085.

70 D. Leifert and A. Studer, *Angewandte Chemie International Edition*, 2020, **59**, 74–108.

71 X.-B. Li, Z.-J. Li, Y.-J. Gao, Q.-Y. Meng, S. Yu, R. G. Weiss, C.-H. Tung and L.-Z. Wu, *Angewandte Chemie International Edition*, 2014, **53**, 2085–2089.

72 Robust Photogeneration of H2 in Water Using Semiconductor Nanocrystals and a Nickel Catalyst, https://www.science.org/doi/10.1126/science.1227775, (accessed July 18, 2022).

73 L.-M. Zhao, Q.-Y. Meng, X.-B. Fan, C. Ye, X.-B. Li, B. Chen, V. Ramamurthy, C.-H. Tung and L.-Z. Wu, *Angewandte Chemie International Edition*, 2017, **56**, 3020–3024.

74 K. P. McClelland and E. A. Weiss, *ACS Appl. Energy Mater.*, 2019, **2**, 92–96.

75 C. Huang, J. Qiao, R.-N. Ci, X.-Z. Wang, Y. Wang, J.-H. Wang, B. Chen, C.-H. Tung and L.-Z. Wu, *Chem*, 2021, **7**, 1244–1257.

76 H. Yi, C. Bian, X. Hu, L. Niu and A. Lei, *Chem. Commun.*, 2015, **51**, 14046–14049.

77 K. Ohkubo, K. Mizushima, R. Iwata, K. Souma, N. Suzuki and S. Fukuzumi, *Chemical Communications*, 2010, **46**, 601–603.

78 M. Schmittel and A. Burghart, *Angewandte Chemie International Edition in English*, 1997, **36**, 2550–2589.

79 R. Zhou, H. Liu, H. Tao, X. Yu and J. Wu, *Chemical Science*, 2017, **8**, 4654–4659.

80 M. H. Babu and J. Sim, *European Journal of Organic Chemistry*, , DOI:10.1002/ejoc.202200859.

81 R. S. J. Proctor and R. J. Phipps, *Angewandte Chemie International Edition*, 2019, **58**, 13666–13699.

82 C. Huang, R.-N. Ci, J. Qiao, X.-Z. Wang, K. Feng, B. Chen, C.-H. Tung and L.-Z. Wu, *Angewandte Chemie International Edition*, 2021, **60**, 11779–11783.

83 F. Dénès, M. Pichowicz, G. Povie and P. Renaud, *Chem. Rev.*, 2014, **114**, 2587–2693.

84 J. Qiao, Z.-Q. Song, C. Huang, R.-N. Ci, Z. Liu, B. Chen, C.-H. Tung and L.-Z. Wu, *Angewandte Chemie International Edition*, 2021, **60**, 27201–27205.

85 C. Pu and X. Peng, *J. Am. Chem. Soc.*, 2016, **138**, 8134–8142.

86 K. Yamada, H. Fujihara, Y. Yamamoto, Y. Miwa, T. Taga and K. Tomioka, *Org. Lett.*, 2002, **4**, 3509–3511.

87 B. Giese, *Angew. Chem. Int. Ed. Engl.*, 1983, **22**, 753–764.

88 A. L. Gant Kanegusuku and J. L. Roizen, *Angewandte Chemie International Edition*, 2021, **60**, 21116–21149.

89 R.-N. Ci, C. Huang, L.-M. Zhao, J. Qiao, B. Chen, K. Feng, C.-H. Tung and L.-Z. Wu, *CCS Chemistry*, , DOI:10.31635/ccschem.021.202101615.

90 J. Liu, H.-Z. Xiao, Q. Fu and D.-G. Yu, *Chemical Synthesis*, 2021, **1**, 9.

91 J. A. Caputo, L. C. Frenette, N. Zhao, K. L. Sowers, T. D. Krauss and D. J. Weix, *J. Am. Chem. Soc.*, 2017, **139**, 4250–4253.

92 J. A. Terrett, M. D. Clift and D. W. C. MacMillan, *J. Am. Chem. Soc.*, 2014, **136**, 6858–6861.

93 J. L. Jeffrey, F. R. Petronijević and D. W. C. MacMillan, *J. Am. Chem. Soc.*, 2015, **137**, 8404–8407.

94 E. B. Corcoran, M. T. Pirnot, S. Lin, S. D. Dreher, D. A. DiRocco, I. W. Davies, S. L. Buchwald and D. W. C. MacMillan, *Science*, 2016, **353**, 279–283.

95 Z. Zuo, D. T. Ahneman, L. Chu, J. A. Terrett, A. G. Doyle and D. W. C. MacMillan, *Science*, 2014, **345**, 437–440.

96 M. Durandetti, J. Périchon and J.-Y. Nédélec, *Tetrahedron Letters*, 1997, **38**, 8683–8686.

97 A. Noble and D. W. C. MacMillan, *J. Am. Chem. Soc.*, 2014, **136**, 11602–11605.

98   I. N. Chakraborty, S. Roy, G. Devatha, A. Rao and P. P. Pillai, *Chem. Mater.*, 2019, **31**, 2258–2262.

99   D. Liu, J. Nyakuchena, R. Maity, X. Geng, J. Mahajan, C. C. Hewa-Rahinduwage, Y. Peng, J. Huang and L. Luo, *Chem. Commun.*, , DOI:10.1039/D2CC03872B.

100 A. McNally, C. K. Prier and D. W. C. MacMillan, *Science*, 2011, **334**, 1114–1117.

101 G. Pratsch, G. L. Lackner and L. E. Overman, *J. Org. Chem.*, 2015, **80**, 6025–6036.

102 J. D. Nguyen, E. M. D'Amato, J. M. R. Narayanam and C. R. J. Stephenson, *Nature Chem*, 2012, **4**, 854–859.

103 J. K. Widness, D. G. Enny, K. S. McFarlane-Connelly, M. T. Miedenbauer, T. D. Krauss and D. J. Weix, *J. Am. Chem. Soc.*, 2022, **144**, 12229–12246.

104 A. L. Efros and D. J. Nesbitt, *Nature Nanotech*, 2016, **11**, 661–671.

105 J. Hu, T.-J. Pu, Z.-W. Xu, W.-Y. Xu and Y.-S. Feng, *Advanced Synthesis & Catalysis*, 2019, **361**, 708–713.

106 G. Yin, M. Zhu, G. Yang, X. Wang and W. Fu, *Journal of Fluorine Chemistry*, 2016, **191**, 63–69.

107 Z.-W. Xi, L. Yang, D.-Y. Wang, C.-D. Pu, Y.-M. Shen, C.-D. Wu and X.-G. Peng, *J. Org. Chem.*, 2018, **83**, 11886–11895.

108 Z.-W. Xi, L. Yang, D.-Y. Wang, C.-W. Feng, Y. Qin, Y.-M. Shen, C. Pu and X. Peng, *J. Org. Chem.*, 2021, **86**, 2474–2488.

109 F. G. Bordwell, X.-M. Zhang, A. V. Satish and J.-P. Cheng, *J. Am. Chem. Soc.*, 1994, **116**, 6605–6610.

110 X.-Q. Zhu, Q.-Y. Liu, Q. Chen and L.-R. Mei, *J. Org. Chem.*, 2010, **75**, 789–808.

111 J. A. Leitch; Dixon, T. Rossolini, T. Rogova, J. A. P. Maitland and D. J. Dixon, *ACS Catal.*, 2020, **10**, 2009–2025.

112 B. P. Roberts, *J. Chem. Soc., Perkin Trans. 2*, 1996, 2719–2725.

113 D. J. van As, T. U. Connell, M. Brzozowski, A. D. Scully and A. Polyzos, *Org. Lett.*, 2018, **20**, 905–908.

114 C. Chatgilialoglu, D. Crich, M. Komatsu and I. Ryu, *Chem. Rev.*, 1999, **99**, 1991–2070.

115 Á. Péter, S. Agasti, O. Knowles, E. Pye and D. J. Procter, *Chemical Society Reviews*, 2021, **50**, 5349–5365.

116 T. Wirth, *Angewandte Chemie International Edition in English*, 1996, **35**, 61–63.

117 E. Denisov, C. Chatgilialoglu, A. Shestakov and T. Denisova, *International Journal of Chemical Kinetics*, 2009, **41**, 284–293.

118 A. K. Simlandy, B. Bhattacharyya, A. Pandey and S. Mukherjee, *ACS Catal.*, 2018, **8**, 5206–5211.

119 Y.-Q. Zou, J.-R. Chen, X.-P. Liu, L.-Q. Lu, R. L. Davis, K. A. Jørgensen and W.-J. Xiao, *Angewandte Chemie International Edition*, 2012, **51**, 784–788.

120 F. Lima, U. K. Sharma, L. Grunenberg, D. Saha, S. Johannsen, J. Sedelmeier, E. V. Van der Eycken and S. V. Ley, *Angewandte Chemie International Edition*, 2017, **56**, 15136–15140.

121 U. Resch-Genger, M. Grabolle, S. Cavaliere-Jaricot, R. Nitschke and T. Nann, *Nat Methods*, 2008, **5**, 763–775.

122 P. Lambropoulos and D. Petrosyan, *Fundamentals of quantum optics and quantum information*, Springer, Berlin ; New York, 2007.

123 C. Mongin, S. Garakyaraghi, N. Razgoniaeva, M. Zamkov and F. N. Castellano, *Science*, 2016, **351**, 369–372.

124 Y. Jiang, C. Wang, C. R. Rogers, M. S. Kodaimati and E. A. Weiss, *Nat. Chem.*, 2019, **11**, 1034–1040.

125 Y. Jiang, R. López-Arteaga and E. A. Weiss, *J. Am. Chem. Soc.*, , DOI:10.1021/jacs.2c00833.

126 M. Cherevatskaya, M. Neumann, S. Füldner, C. Harlander, S. Kümmel, S. Dankesreiter, A. Pfitzner, K. Zeitler and B. König, *Angewandte Chemie International Edition*, 2012, **51**, 4062–4066.

Chapter 2

Chapter 2 – Photoredox mediated generation of radicals from boronate complexes

Our first attempt at developing a redox neutral reaction involving a reductive quenching of the photocatalyst focused on the generation of alkoxyl radicals *via* the one-electron oxidation of boronate complexes.

2.1. Literature precedence

Alkoxyl radicals are oxygen-centered radicals that possess, due to the position of the radical center on an electronegative atom, an electrophilic character and an intrinsic high reactivity.[1] In contrast to hydroxyl radicals, the oxygen radical center is linked to an alkyl group. This confers to this highly reactive species a number of interesting reactivity patterns.[2] Oxygen forms strong bonds to hydrogen and carbon atoms. Therefore, elementary reactions of alkoxyl radicals are typically involved in forming these types of bonds (section 2.1.1). On the contrary, oxygen forms relatively weak bonds with heteroelements containing lone pairs (such as nitrogen, oxygen, sulfur, chlorine), and this can and has been used for the selective generation of alkoxyl radicals from a number of precursors (section 2.1.2.1). Additionally, a number of methods have been developed for the direct activation of the strong O-H bond (section 2.1.2.2), in particular light-driven methodologies which will be our focus.

2.1.1. Elementary reactions of alkoxyl radicals

The reactivity of oxygen-centered radicals has been known and studied for a long time. Jens Hartung,[2] Živorad Čeković,[3] and others have been instrumental in understanding and applying this chemistry to organic transformations already more than 30 years ago. Additionally, alkoxyl radicals have long been identified as key intermediates in the tropospheric degradation of alkanes and alkenes,[4–6] as well as in biological processes.[7] For example, the biosynthesis of the prostaglandin PGI$_2$ is thought to proceed *via* an alkoxyl radical intermediate generated by hemethiolate enzyme catalysis.[8]
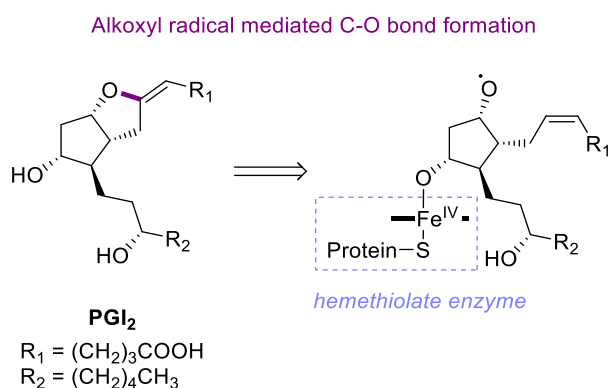
Figure 1. Alkoxyl radical mediated biosynthesis of the prostaglandin PGI$_2$.

A complete review of methodology developments and biological processes involving alkoxyl radicals is outside the scope of the chapter. The description of elementary reactions of alkoxyl radicals will be illustrated with some examples taken from the recent literature on the light-driven generation of alkoxyl radicals.

2.1.1.1. Hydrogen Atom Transfer (HAT)

For the same reason that it is extremely difficult to cleave homolytically a simple O-H bond (the O-H bond has a bond dissociation energy as high as 105 kcal/mol in aliphatic alcohols),[9] the alkoxyl radical is very efficient at abstracting hydrogen from unactivated aliphatic C-H bonds, either intra- or

intermolecularly ($k = 2.7 \times 10^7\,s^{-1}$ and $k = 10^5$–$10^7\,M^{-1}\,s^{-1}$ respectively, 298 K, Figure 2).[3] Since the bond dissociation energy of most C-H bonds is considerably lower than that of the O-H bond, the hydrogen transfer from a C-H bond to an alkoxyl radical is exothermic and the enthalpy of activation will be smaller for more stable carbon radicals. As a matter of fact, structural factors such as steric, conformational, and polar effects will play a key role in the outcome and efficiency of the HAT process.[10]
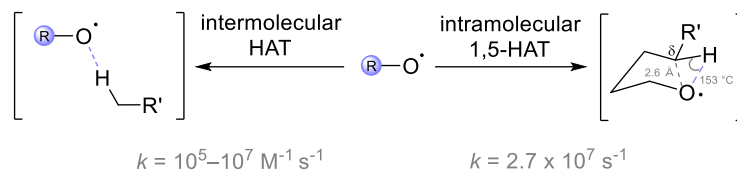
Figure 2. Hydrogen Atom Transfer reactions of alkoxyl radicals.

For example, 1,5-HAT predominates among intramolecular hydrogen atom transfer possibilities because it involves a chair-like transition state in which the orientation between the oxygen centered radical and the δ-H atom results in minimal interactions and distortions.[3] An optimal distance of 2.5-2.7 Å is achieved between the alkoxyl radical and the δ carbon, and this geometry is the lowest in energy. 1,6-HAT can occur if a seven-membered cyclic transition state is conformationally stable and if no hydrogen atom is present at the δ position.[11] Suarez and co-workers reported 1,n-HAT events up to n = 8 in sugars.[12,13] When the resulting C-centered radical is trapped by a suitable radical acceptor, this reactivity allows for the synthesis of δ-functionalized alcohols.[14] In the recent years, photocatalytically generated alkoxyl radicals have been used to this end. For example, Zhu and co-workers reported in 2018 the remote cyanation and azidation of alcohols using alkoxyl radicals.[15] Chen and co-workers developed two different methods for the δ-alkenylation and δ-allylation of alcohols using vinyl- and allylsulfone traps.[16,17] Shortly after, Meggers and co-workers reported an asymmetric alkylation protocol.[18]

2.1.1.2.   Beta-fragmentation

A competitive behavior to the HAT reactivity comes from the propensity of alkoxyl radicals to undergo β-fragmentation to give a carbonyl group and a carbon-centered radical.[19] The efficiency of this process, and therefore the competition with the HAT pathway, will depend on the stability of the generated carbon radical center[20] and, if applicable, on the strain release accompanying the fragmentation of cyclic alkoxyl radicals. This factor also plays a role in the regioselectivity of the fragmentation. Although strain release will result in faster rate of fragmentation,[21] β-fragmentation of alkoxyl radicals can take place without assistance of ring strain (Figure 3). This is probably due to the facile overlap between the half-filled orbital on the oxygen with the σ-orbital of the C-C bond to be cleaved. For example, the fragmentation of a linear, secondary alkoxyl radical such as **I** occurs with a rate of $1.4 \times 10^5\,s^{-1}$.[20] The ring opening of the cyclopentyloxy radical **II** has been studied and was shown to occur at room temperature with a high rate.[22]
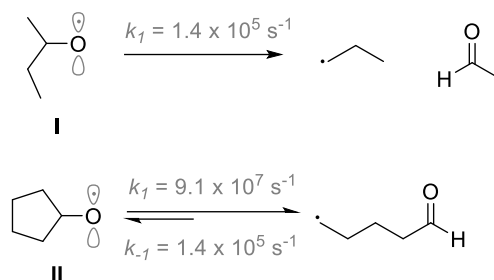
Figure 3. β-fragmentation of acyclic and cyclic alkoxyl radicals.

Notably, this elemental step is reversible, but the addition of the carbon-centered radical to the carbonyl group occurs slowlier (Figure 3). In fact, it is difficult to generate stable alkoxyl radicals from the addition of carbon-centered radicals to ketones or aldehyde, unless the resulting alkoxyl radical is trapped very efficiently. This was for example proposed by Yoshimitsu and co-workers who described the direct intermolecular radical addition of THF rings to aldehydes;[23] the resulting alkoxyl radical was trapped rapidly by triethylborane and expelled the ethyl radical which sustained the radical chain reaction (Scheme 1). Importantly, this reaction exemplifies the ability of alkoxyl radicals to undergo nucleohomolytic substitution reactions at a boron center.[24]
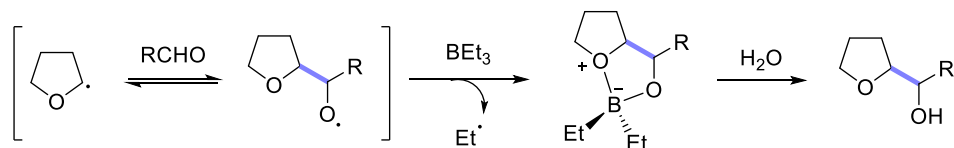
Scheme 1. Nucleohomolytic substitution reaction of the alkoxyl radical on triethylborane prevents the beta-fragmentation reaction.

In a similar strategy, Ryu and co-workers showed that alpha-aminoalkyl radicals could add to ketones or aldehydes and that the resulting alkoxyl radical could be trapped by a chiral oxazaborolidinium ion. Excellent levels of enantioselectivity were obtained.[25,26] Kang and co-workers used a conveniently placed, activated aromatic ring that served as alkoxyl radical acceptor in the synthesis of benzofurans.[27] The Glorius lab reported that simple Lewis or Brønsted acid activation of the carbonyl group could prevent reversibility of the radical addition to the carbonyl center.[28]

This strategy can however be used if the fragmentation of the generated alkoxyl-radical is desired. For example, a recent application of the Dowd-Beckwith[29–31] rearrangement was used as a key step in the total synthesis of (−)-Crinipellins (Scheme 2).[32]
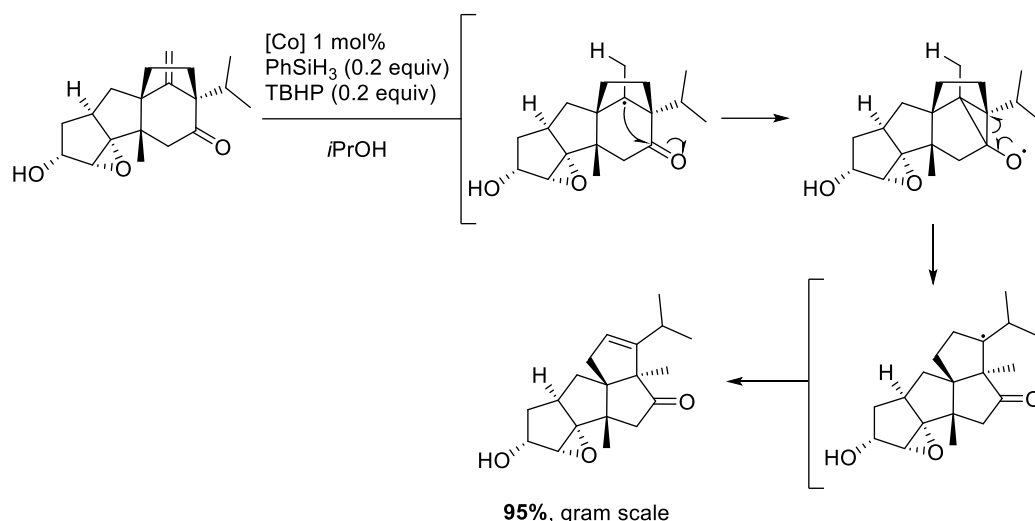
Scheme 2. Application of the Dowd-Beckwith rearrangement in the total synthesis of (−)-Crinipellins.

As visible from the ring opening of the cyclopentyloxy radical **II**, remotely functionalized ketones can be obtained from the β-scission of cyclic alkoxyl-radical. In recent years, this strategy has for example been applied for the asymmetric synthesis of β-aryl ketones[33] or γ-fluorinated ketones.[34]

2.1.1.3.   Addition to double bonds

Since alkoxyl radicals possess a low-lying SOMO (electrophilic character), the interaction with the HOMO of the alkene becomes often predominant. In some cases, the alkoxyl radical showed a borderline reactivity and could be reacted with electron-poor olefins such as ester- and cyano-substituted olefins.[35] Nonetheless, alkoxyl radicals are often trapped intramolecularly by unactivated alkenes so as to render the reaction more effective and competitive. The most studied system in this context has been the 5-*exo*-trig cyclization.[36–38]
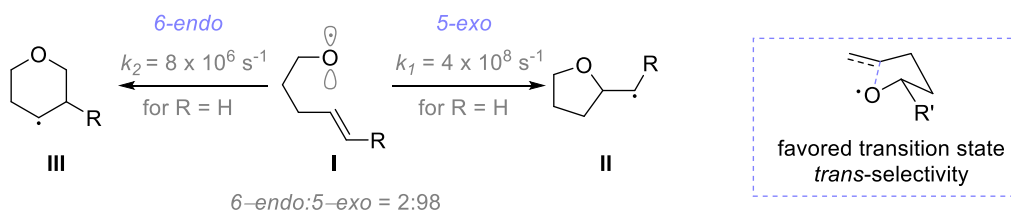
Figure 4. Addition of alkoxyl radicals to olefins — regio- and diastereoselectivity.

The 4-penten-1-oxyl radical **I** cyclizes selectively to form the tetrahydrofuran over the tetrahydropyran in a ratio 98:2 (Figure 4).[2] The rate constant of the 5-*exo* cyclization increases when R ≠ H, i.e. when the resulting carbon radical **II** is more stable and when the olefine is more electron rich. For the same reasons, the ratio of *endo* product can be increased if the alkene is *gem*-disubstituted. The stereoselectivity outcome of this cyclization can be rationalized by a chair-like transition state in which the alpha substituent of the alkoxyl radical adopts a pseudo equatorial position.[39,40] The observed stereoselectivity logically increases with the bulkiness of this substituent.

The formation of C-O bonds under ionic pathway can take place between an alcohol and an alkene under Lewis[41] or Brønsted[42] acidic conditions. In some cases, the regioselectivity outcome can be used to discriminate a radical from an ionic pathway (anti-Markovnikov or Markovnikov adduct). Only few synthetic methods have used this elemental reactivity in the development of alkoxyl radical precursors. Of interest is a photocatalytic method developed by Dagousset and co-workers.[43] They achieved the

intermolecular anti-Markovnikov alkoxylation of styrenes and further functionalization with a nucleophile following radical-polar crossover of the intermediate carbon-centered radical. Knowles and co-workers reported an intramolecular, 5-*exo*-trig cyclization and trapping of the carbon-centered radical with Michael acceptors.[44]

When a model substrate is chosen for the generation of alkoxyl radicals, all the above considerations should be taken into account for the design of the reaction. We shall now look at the existing strategies for the generation of these reactive radical entities, focusing mainly on modern photoredox methodologies. Only the methods based on free alcohols or alkoxide surrogates will be exhaustively discussed.

2.1.2. Methods for the generation of alkoxyl radicals from alcohols

2.1.2.1.   Overview

The generation of alkoxyl radicals can been sorted into 3 categories (Figure 5).[2] These included:

   i)   the conversion of the inert O-H into a weaker (< 70 kcal/mol) O-Y bond, either *in situ* or *via* an isolated intermediate;
   ii)   the introduction of the required oxygen moiety by nucleophilic substitution on the alkyl residue of interest prior to reaction (preparation of *N*-alkoxy compounds);
   iii)   the direct activation of free alcohols (Section 2.1.2.2).

Alkoxyl radicals have also been prepared by the rearrangement of strained carbon-centered radicals such as the epoxymethylene radicals.[45] However, this approach is of limited scope and will not be discussed here.
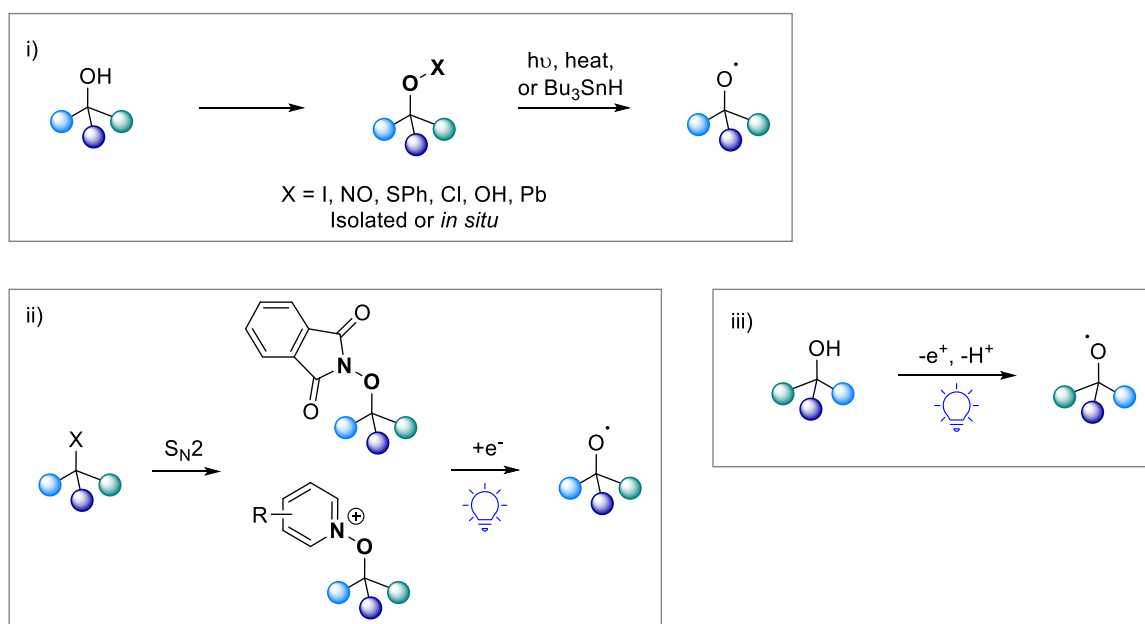
Figure 5. General strategies for the generation of alkoxyl radicals.

The conversion of the O–H bond into an O–X bond (Figure 5, i)) has been developed early on, with the prefunctionalization of alcohols into intermediates containing O-I,[46,47] O-N,[48] O-S,[49] O-Cl,[50] or O-O bonds.[51] These precursors can furnish the desired alkoxyl radical upon light, heat homolysis or treatment with Bu₃SnH. The *in situ* oxidation of alcohols into intermediates of this type is conceptually interesting since no prefunctionalization of the alcohol is necessary, however low functional group

tolerance has been observed due to the use of strong oxidants.[52–54] Stoichiometric transition metal salts have also been used to achieve the single-electron oxidation of strain cyclic alcohols. For example, cyclopropanols or cyclobutanols can be oxidatively opened using stoichiometric Cu(II) and Fe(III) salts.[55] More recently, this chemistry has successfully been extended to the use of transition metal catalysts such as silver salts,[34,56–61] manganese[62] or copper,[63] but is still limited to strained cyclic alcohols. In addition, the chemistry of organohypervalent iodine has been revisited since the development of photoredox catalysis. The use of iodine reagents for the generation of alkoxyl radials under mild conditions has been described with transition-metals such as iridium or ruthenium,[64–69] or only light.[70,71]

The O–N precursors in the second category (Figure 5, ii)) are not directly synthesized from the alcohol, but from the alkyl halide via an S$_N$2 reaction. These precursors have proved useful in the field of photoredox chemistry since the O–N bond can be efficiently reduced using easily available photocatalysts. In particular pyridinium salts have been recognized as versatile redox-active functional groups and have been used not only for the generation of alkoxyl radicals but also N-centered and alkyl radicals.[72,73] From 2016, advances in the field of photocatalytically generated alkoxyl radicals from N-alkoxypyridinium salts have been made by Lakhdar,[74,75] Dagousset,[43,76] and Zhu[15] independently. The precursors were prepared from pyridine N-oxides and the desired alkyl iodides or activated alcohols in gram scale. In 2016, Chen and co-workers were the first to use N-alkoxyphthalimides in combination with visible-light catalysis to generate alkoxyl radicals.[16] A very similar system was published concomitantly by Meggers and co-workers for applications in asymmetric C-C bond formation.[18] In such system the N-alkoxyphthalimide is reduced by a potent Ir^{II} species and a Hantzsch ester is usually used as sacrificial reductant for the catalytic cycle to proceed (Figure 6).[17] In some cases, the Hantzsch ester and the N-alkoxyphthalimide form a donor-acceptor complex so that no transition-metal catalyst is needed.[17,64,77]
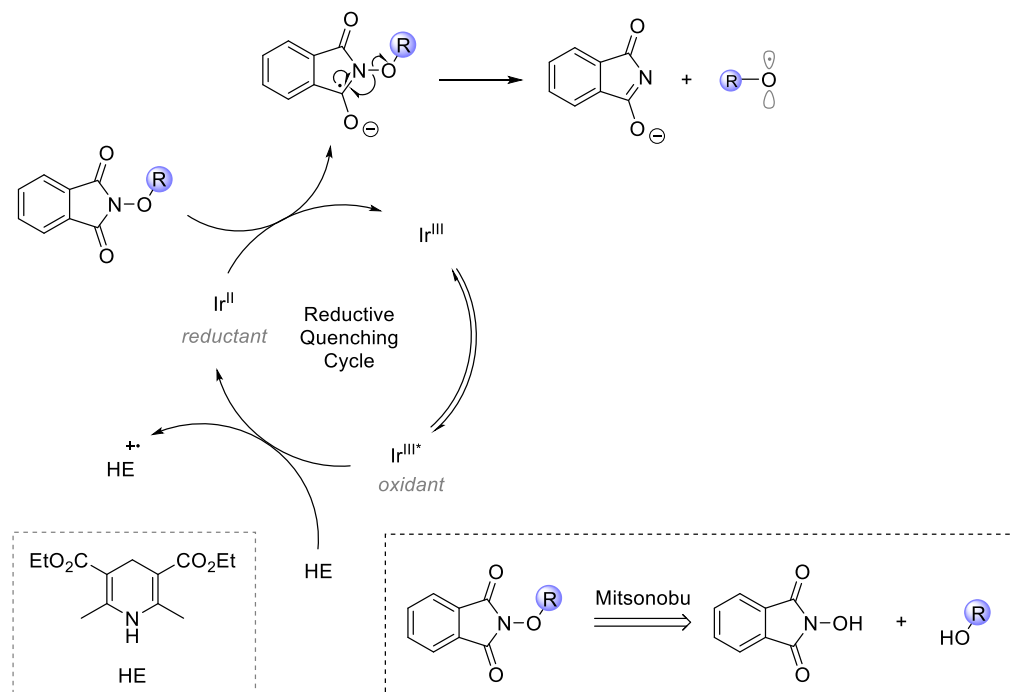
Figure 6. Generation of alkoxyl radicals from N-alkoxyphthalimide precursors – general principle.

This strategy was also successfully applied in more complex structures, as demonstrated by Sorensen and co-workers.[78] They used the ability of alkoxyl-radicals to perform 1,5-HAT for the epimerization a distal unactivated C-H center *en route* to the natural product pleurotin (Scheme 3). They used a N-

alkoxyphthalimide precursor with an iridium photocatalyst, a Hantzsch ester and TRIP thiol (2,4,6-triisopropylbenzenethiol) as final hydrogen donor. The phthalimide precursor was synthesized *via* a Mitsonobu reaction.
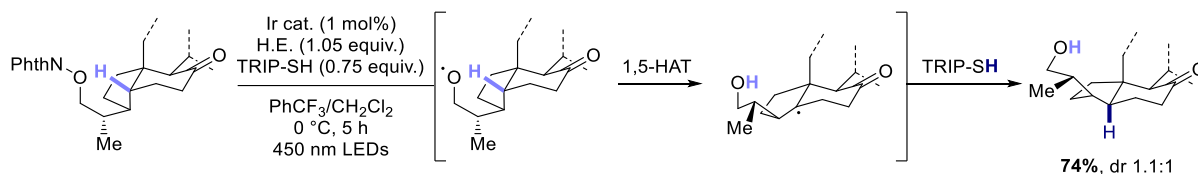
Scheme 3. Radical epimerization of an unactivated C-H bond using alkoxyl-radical initiated 1,5-HAT and a thiol as hydrogen donor.

Although these methods have held their promises in terms of alkoxyl radical generation under mild photocatalytic conditions, the preparation of the radical precursors is not straightforward and limits their synthetic utility.

2.1.2.2. Alkoxyl radicals from in situ generated alkoxide surrogates

Recent work has focused on the direct use of alcohols for the generation of alkoxyl radicals under visible-light catalysis.[79] With the development of highly efficient and targeted photocatalysts, two categories have emerged based on the use of simple alkoxide surrogates: Proton Coupled Electron Transfer (PCET) and Ligand-to-Metal Charge Transfer (LMCT) (Figure 7).
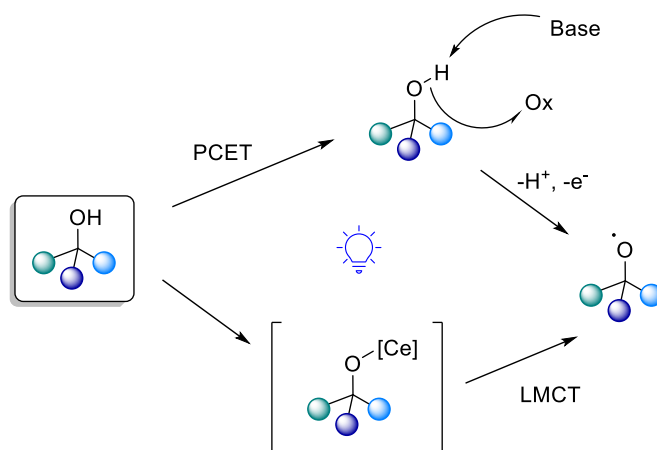
Figure 7. Light-driven generation of alkoxyl radicals from *in situ* formed alkoxide surrogates: proton coupled electron transfer and ligand-to-metal charge transfer.

Ligand-to-Metal-Charge-Transfer (LMCT). Recently, photoinduced charge transfer between a metal center and a ligand has been shown to work well for the *in situ* activation of free alcohols. This general class of mechanism typically occurs with transition metals having an empty valence shell such a cerium.[80,81] In such complexes, photoexcitation results in electron donation from a high-energy ligand orbital to a low-lying metal-centered orbital (LMCT: ligand-to-metal charge transfer).[82] This type of excited complexes is prone to homolysis of the metal-ligand bond and offers a strategy for substrate activation when the substrate plays the role of the ligand. Therefore, in the case of O-H activation, a metal-alkoxide species will selectively generate the desired alkoxyl radical (Figure 8). The process can be made catalytical provided that the reduced metal center [M^{n-1}] is reoxidized by an electron acceptor present in the reaction medium. It can either be a sacrificial electron acceptor or a reaction intermediate. If the metal center [M^{n-1}] is not reducing enough to perform the desired SET (for example for the oxidation of Ce^{IV}, E$_{1/2}$ (Ce^{IV}/Ce^{III}) = 0.40 V *vs.* SCE in MeCN, a low reducing power),[83] a catalyst relay or electron shuttle can be used. Alternatively, the SET event can be necessary not for the metal's

regeneration but for the catalyst's activation (for example if $[M^{n-1}]$ is the pre-catalyst and $[M^n]$ the active catalyst).
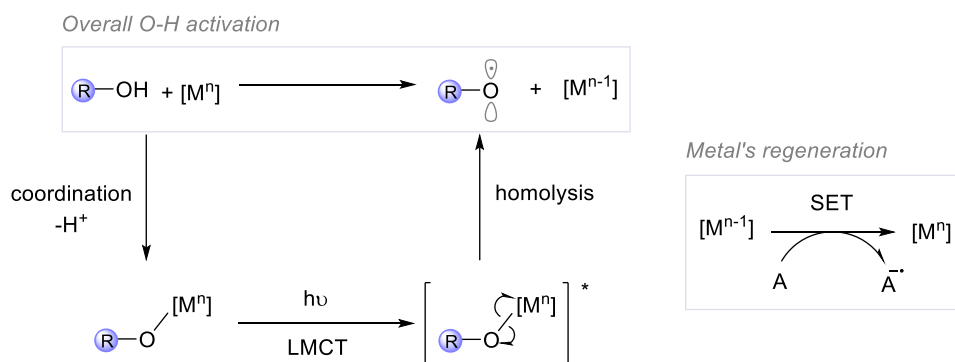
Figure 8. General principle of Ligand-to-Metal Charge Transfer reactivity.

β-scission of alcohols

The Zuo lab has been instrumental in the development of this field for the generation of alkoxyl radicals. In 2016, the group disclosed the LMCT-driven generation of alkoxyl radicals from tertiary and more challenging secondary cycloalkanols and the subsequent amination of the remotely formed carbon-centered radical following β-fragmentation (Scheme 4).[83] They took advantage of the Lewis acidic nature of a Ce^{III} pre-catalyst ($CeCl_3$) and the ability of alcohols to ligate such metal centers. They envisioned that this pre-formed complex **I** could be photoexcited and engage in SET to produce the desired, activ Ce^{IV} complex **II** that could eventually generate the alkoxyl radical **III** *via* LMCT. After beta-fragmentation, the carbon-centered radical **IV** is trapped by di-*tert*-butyl azodicarboxylate (DBAD). The resulting *N*-centered radical **V** is highly oxidizing and is able to perform the SET with Ce^{III}, giving the product and generating the necessary Ce^{IV} species. The initiation of this cycle is not discussed. Using this method, the authors could use catalytic amounts of $CeCl_3$ and *tert*-butylammonium chloride as additive. Under blue LED irradiation in MeCN, remotely aminated aldehydes and ketones could be obtained in very good yields (70-95%), including advanced medicinally relevant scaffolds.
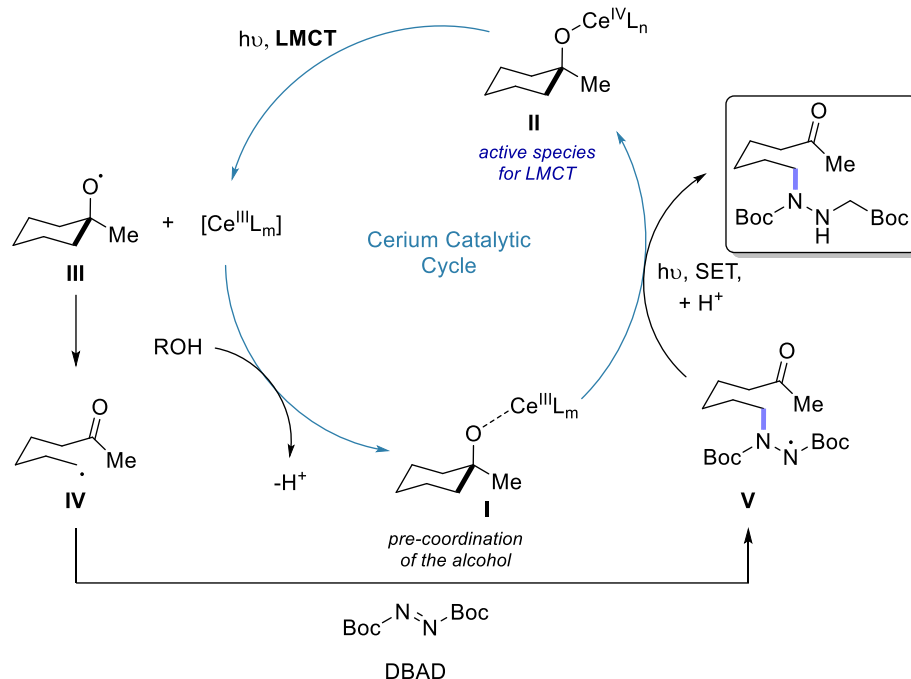
Scheme 4. Ce(III)/Ce(IV) cycle in the alkoxyl radical generation using LMCT.

The group reported in 2020 a follow-up method with alpha-cyano alcohols as starting materials.[84] Additionally, the same reaction was recently disclosed by Zeng and co-workers using a Fe(III) catalyst instead of Ce(III).[85] In these methodologies, a limitation occurs in the type of radical possibly oxidizing the Ce^{III} to Ce^{IV} (*N*-centered radical in this case).

The Zuo lab set to work to accommodate the single-electron reduction of *α*-acyl radicals ($E_{1/2}$ = -0.60 V *vs.* SCE in MeCN).[86] To do so, they investigated the use of a proton shuttle oxidizing enough to generate Ce^{IV} from Ce^{III} and at the same time reducing enough to quench the radical intermediate. They found that 9,10-diphenylanthracene (DPA) was meeting these requirements (Scheme 5). Mechanistically, LMCT event triggers the RO-Ce^{IV} bond homolysis and generates a cyclic alkoxyl radical **I** together with Ce^{III}. This alkoxyl radical fragments to an aldehyde and an alkyl radical **II** that adds to an α,β-unsaturated ester, generating an alpha-ester radical **III**. Reduction of this radical now does not occur *via* Ce^{III} but *via* the reducing excited state of DPA (DPA*). Thus oxidized DPA (DPA•+) is able to generate the Ce^{IV} species from Ce^{III}. As for the enolate **IV**, it can cyclize in an aldol reaction with the pendent carbonyl group and ultimately be converted to bridged lactones upon treatment with *p*-TsOH. A variety of diversely substituted indanols, both on the alkane or on the aromatic ring, were amenable to the reaction conditions. The best substrate proved however to be cyclobutanol that gave nearly quantitative yield in 8 hours. With this substrate, different radical traps could be reacted, however all tri-substituted to favor the reduction event of the alpha-acyl radical **III**.
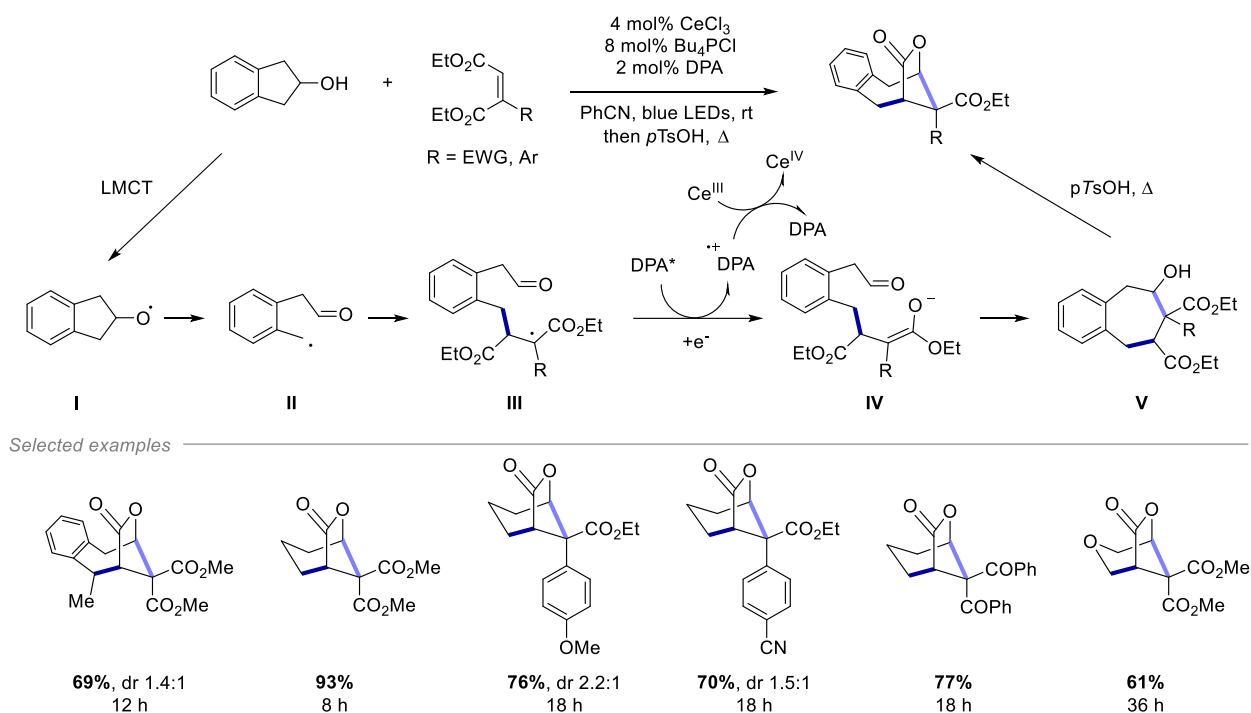
Scheme 5. LMCT method using an electron-shuttle between DPA and cerium.

Zuo an co-workers then showed that occurring on linear primary alkanols, β-fragmentation offers the possibility to generate alkyl radicals by extrusion of formaldehyde.[87] Subsequent addition on a Giese acceptor followed by reduction of the alpha-ester radical enables the dehydroxymethylation of alkenes, this time without the need for an electron shuttle (Scheme 6). Included in this study was a selectivity assessment of β-scission *versus* HAT for a variety of linear primary and secondary alkanols. Complete selectivity for the β-scission was observed when it led to a ketone product, even when the δ-carbon was a secondary center. However, the HAT event was observed when the β-scission gave an aldehyde product, especially in the case of secondary δ-carbons.
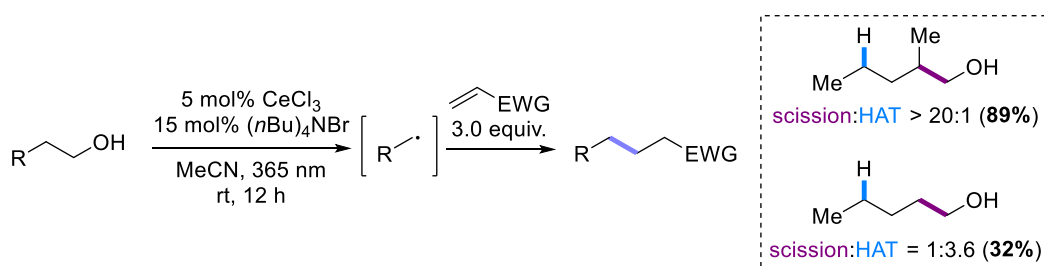
Scheme 6. Beta-scission of linear alcohols and radical addition to electron-deficient olefins. Selectivity assessment of β-scission versus HAT.

Mechanistically, the authors suggested that irradiation of the Ce^{III} alkoxide complex under the right wavelength could promote the complex to its excited state and render it reducing enough for alpha-ester radical reduction, quite similarly as described in Scheme 4. By doing this, the Ce^{IV} complex is formed and can, under irradiation, proceed to LMCT. As an extension of this chemistry, a dual catalysis protocol was developed using cerium-mediated LMCT catalysis with nickel catalysis.[88] The carbon radical obtained after β-scission of a linear alkoxyl radical was trapped by the nickel catalyst to be coupled with an aryl halide. Following this dehydroxymethylative strategy, a variety of alpha-amino radicals, benzylic, allylic and propargylic radicals could be arylated.

A notable addition to the LMCT chemistry of alcohols was very recently disclosed by Huang and Lei.[89] They coupled the LMCT event with electrochemistry, which allowed the easy oxidation of the Ce(III) to the active Ce(IV) species. The generated cycloalkoxyl radical underwent β-scission and the resulting carbon-centered radical was trapped by aryl sulfonyl radical traps diversely functionalized. The sulfonyl radical was further reduced at the cathode. This allowed to significantly extend the scope of available functional group with which the resulting carbon radical could eventually be functionalized, for example cyano groups, oximes, alkynes, alkenes, chlorine and thiols.

Intra– and intermolecular HAT

The understanding of β-scission *versus* 1,5-HAT selectivity was used in a study where the authors further explored the 1,5-HAT reactivity of alkoxyl radicals (Scheme 7A).[90] The method is in all points similar to the remote amination of ketones published earlier (Scheme 4), except that this time linear alcohols are used. After alkoxyl radical generation, 1,5-HAT activates the δ-C-H bond for amination with DBAD. Substrates were chosen so that 1,5-HAT was favored over β-scission.

Next, alkoxyl radicals from simple alcohols such as methanol were used as catalysts in the very challenging hydrogen atom transfer from methane C–H bonds (BDE ~ 97 kcal/mol) and other higher alkanes up to cyclohexane (Scheme 7C).[91] Most examples were based on the use of DBAD as amination agent, but alkylation and arylation of the alkyl radicals have been demonstrated as well.

A/ 1,5-HAT of linear alcohols
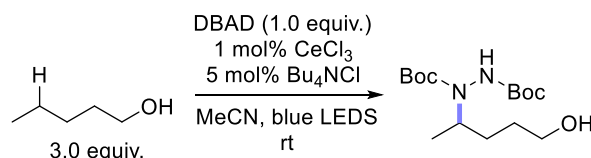
B/ intermolecular HAT on hydrocarbons
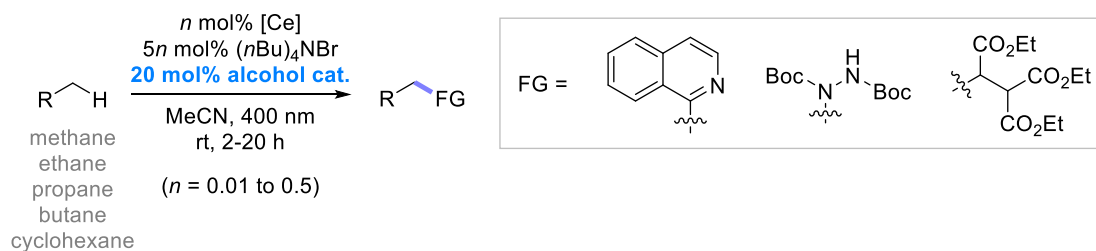
Scheme 7. Further applications of LMCT. A/ 1,5-HAT of linear alcohols. B/ Intermolecular HAT on hydrocarbons.

In a follow-up study, the selectivity of different alcohols for different C–H bonds has been studied for the functionalization of a variety of higher hydrocarbons (cyclic alkanes, aromatic hydrocarbons, bridge bicycloalkanes).[92] The scope of possible olefin coupling partners was as well extended. The reactivity and selectivity of the HAT event were both influenced by the structure of the alcohol catalyst. This experimental study was recently completed by a computational study by Houk and co-workers, confirming the possibility to use different alcohol catalysts for different C–H bonds to be activated.[93] As expected, important parameters were the difference between the BDE's of the C–H bond being abstracted and the O–H bond being formed, and the difference in electronegativity between the alkoxyl radical and the alkyl radical being formed. This indicated that ionic contributions in the transition state were stabilizing. Finally, an important parameter was as anticipated the stability of the carbon-centered radical, e.g., if it was localized (saturated) or delocalized (unsaturated).

Although the great possibilities of this chemistry have been very nicely demonstrated by the Zuo group, the rationalization of the mechanism is not straightforward.[94] Additionally, the reactivity of the cerium complexes is not always foreseeable, with very different behaviors observed under similar conditions. This might explain why this method has not yet been widely adopted by the rest of the scientific community.

Proton Coupled Electron Transfer (PCET). On the contrary, PCET (see Chapter 1, Figure 3) has had a breakthrough after the efforts of the Knowles lab to use this strategy for the generation of reactive radical species from N-H, O-H, S-H and C-H bonds.[95] For alcohols, PCET can virtually be seen as the oxidation of an alkoxide ion or the deprotonation of an oxygen radical cation, although none of these intermediates is actually present in solution since both events are (usually) concerted (Figure 9).[96] It can be seen as a non-traditional mechanism for homolysis of the bond, formally removing a hydrogen atom from the strong O-H bond.
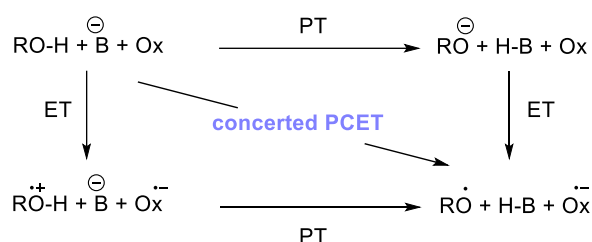
Figure 9. Schematic representation of PCET for the oxidation of an O-H bond.

PCET has been used widely among electrochemical and photochemical methods and has solved a number of problems in the generation of alkoxyl radical from unfunctionalized alkyl alcohols, enols, phenols, oxime, hydroxylamines[97] and hydroxamic acids. For the scope of this chapter, we shall focus on the alkyl alcohols only, keeping in mind that further substrates can be transformed using this strategy.

β-scission of alcohols – Redox relay

In 2016, Knowles and co-workers reported the first example of alkoxyl radical generation using PCET for the ring opening of unstrained cyclic alcohols bearing an electron-rich arene at the alpha-position (Figure 10).[98] The catalytic system encompassed an iridium photocatalyst as the oxidant, collidine as the Brønsted base, and a thiophenol HAT co-catalyst to trap the resulting C-centered radical. Mechanistically, a redox-relay process was proposed. It was postulated that the first oxidation event occurred on the electron-rich arene to give the aromatic radical cation **I**. The "intramolecular" PCET event occurred *via* collidine and this radical cation to afford the alkoxyl radical which underwent β-scission. The resulting C-centered radical **II** was able to abstract a hydrogen from thiophenol. The thiophenol is regenerated by the thiyl radical HAT on protonated collidine **III**, which radical cation **IV** will ultimately regenerate the photocatalyst. The base is theoretically needed in catalytic amounts, but it is used in excess in these reactions. Although largely limited to *para*-methoxyphenyl tertiary carbinols, the method was successful on 4– to 12–membered rings as well as natural-product derived substrates. Additionally, the thiophenol co-catalyst could be replaced with stoichiometric quantities of SelectFluor, CCl_4 or $BrCCl_3$ for distal halogenation of the ring-opened product.
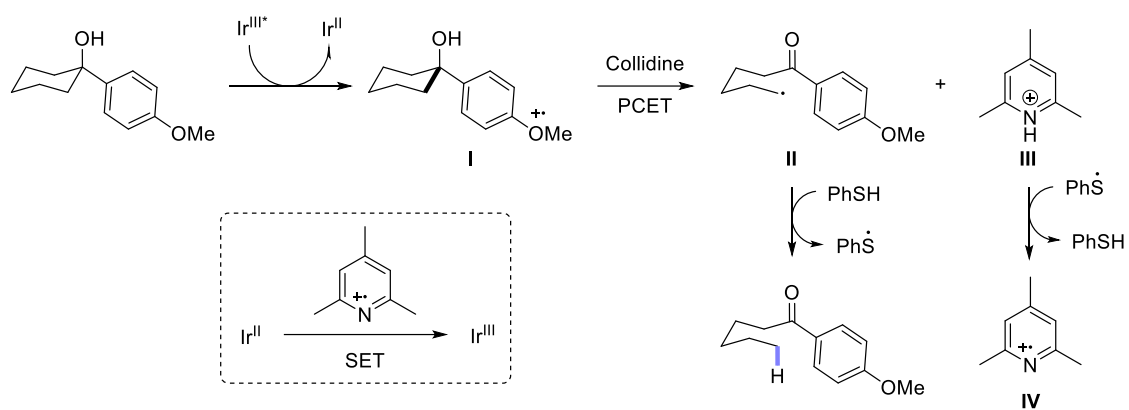
Figure 10. Redox-relay strategy for the PCET of alcohols.

Based on precedents using Bu$_3$SnH/AIBN chemistry,[99,100] the Knowles lab then developed a method for the 1,3-allylic transposition of acyclic allylic alcohols into β-functionalized ketones (Scheme 8).[101] The R$_1$ group could be an acyclic, a mono-cyclic, bi-cyclic, or tri-cyclic aliphatic chain, while the alkene could be di- or tri-substituted without loss of yield. The *para*-methoxyphenyl ketone product was shown to readily engage in Baeyer-Villiger and Schmidt-type rearrangement.
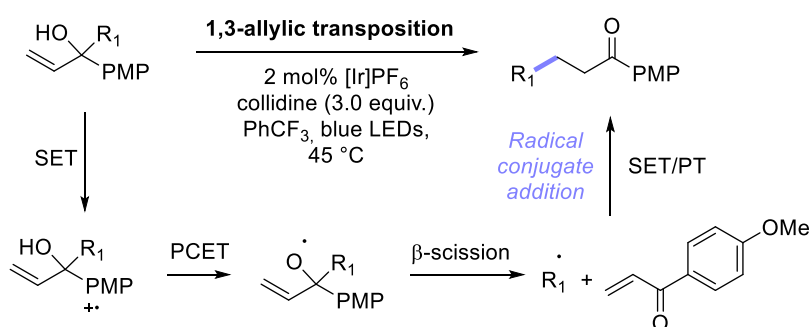
Scheme 8. 1,3-allylic transposition sequence leading to the synthesis of β-functionalized ketones from acyclic allylic alcohols.

This redox-relay chemistry was subsequently applied to a variety of functionalizations. For example, Xia and co-workers reported the formylation and allylation of arylcycloalkanols using air or an allylsulfone respectively.[102] Shortly after, the Rueping lab disclosed a trifluoromethyl thiolation of ketones *via* alkoxyl radical β-fragmentation of the same precursors as in Figure 10.[103] The authors used a Phth-SCF$_3$ reagent that was able to intercept the C-centered radical and to furnish the desired ketone. The resulting phthalimide radical was reduced by the catalyst to close the cycle.

Very recently, Rueping[104] and Wu[105] concomitantly disclosed the use of a cobalt(III) co-catalyst to synthesize distally unsaturated ketones (Scheme 9). The active Co^{II} species **II** was formed concomitantly to the re-oxidation of the photocatalyst following PCET and was thought to intercept the distal carbon-centered radical to give alkyl-Co^{III} intermediate **III**. Beta-hydride elimination would account for the product's formation and liberate a Co^{III}-H species **IV**, whose interaction with a proton leads to H$_2$ evolution.
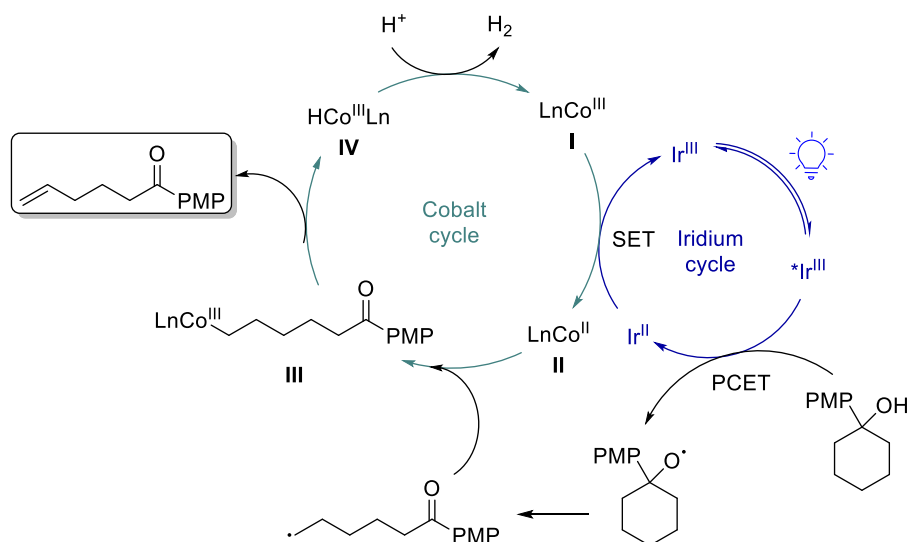
Scheme 9. Mechanistic hypothesis of photoredox and cobalt dual catalysis for the desaturation of alcohols.

The arylation of cycloalkanols[106,107] in particular has attracted much attention. Rueping an co-workers proposed to trap the C-centered radical following β-scission with a Ni catalyst to promote an arylation reaction with an arylbromide, thus allowing for the ring-opening arylation of aryl tertiary carbinols (Scheme 10A).[108] Interestingly, the strategy was not limited to cyclopropanols but to rings of all sizes until 15-membered rings. Additionally, both electron-rich and electron-poor aromatic rings could be introduced. Using a similar strategy, Li and co-workers reported the asymmetric β-arylation of cyclopropanols.[33] Their method could be applied to the late-stage functionalization of bioactive compounds, although the substrates seemed to be limited to -OTIPS containing structures, probably necessary to enhance the enantioselectivity (Scheme 10B). Lu and co-workers disclosed the radical-radical coupling of cyanoarenes with cyclopropanol-derived β-keto radicals under iridium catalysis (Scheme 10C).[109]
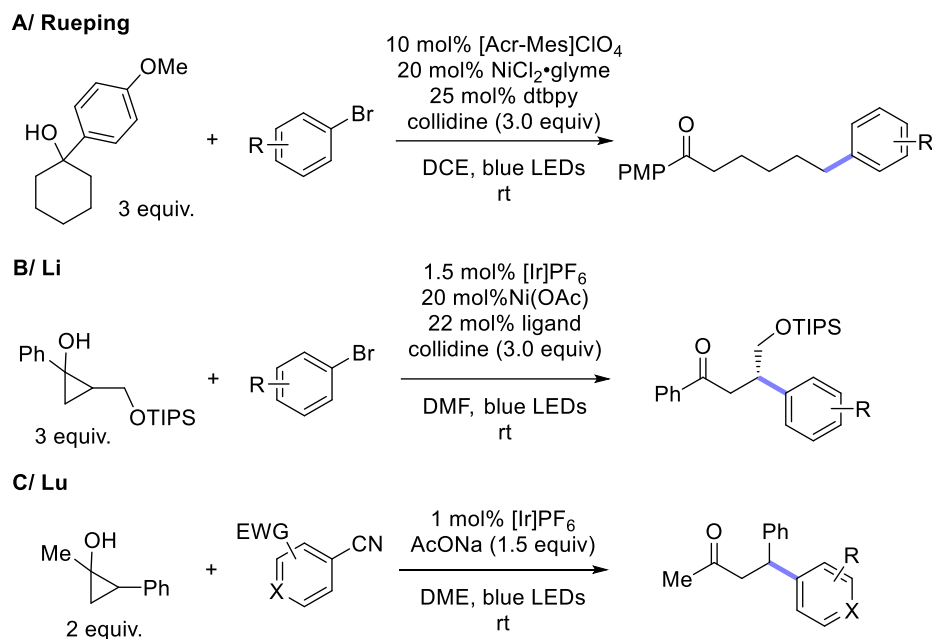
Scheme 10. Strategies for the arylation of cycloalkanols under redox-relay PCET conditions. A/ Metallaphotoredox catalysis on unstrained alcohols. B/ Metallaphotoredox catalysis on strained alcohols. C/ Radical-radical coupling with cyanoarenes.

β-scission of alcohols – Direct PCET

Seeking to enlarge the scope of this transformation, the Knowles lab improved the method towards the use of simple aliphatic alcohols, circumventing the need for an electron-rich arene.[110] The key change was to use the anionic phosphate base nBu$_4$P$^+$(MeO)$_2$P(O)O$^-$ instead of the neutral collidine. The authors proposed that the anionic base could form a more favorable hydrogen bond with the alcohol substrate, thus strongly favoring direct PCET without the need of an intermediate radical cation. The method allowed the isomerization of 1°, 2° and 3° cyclic and acyclic alcohols; as previously described, a thiol co-catalyst was used as HAT agent.

In another application of this chemistry, a similar strategy was applied to cyclic n-membered-ring allylic alcohols (Scheme 11A).[111] Following alkoxyl-radical formation and β-scission, the resulting carbon-centered radical **II** was prone to add to the double-bond present in the substrate, thus giving the ring expanded ketone. In the case of alkyl olefins, cyclization occurred in an *endo*-trig fashion to give the α-acyl radical **III** that could be directly reduced by the iridium catalyst. However, this was limited to aza-cycles, probably because a nucleophilic α-amino radical was necessary for cyclization to occur. In the case of styrenes, *exo*-trig cyclization afforded the benzylic radical **III** which could not be reduced by the iridium catalyst (Scheme 11B). Hence, TRIP-SH was employed as HAT co-catalyst. A variety of aza-cycles, cyclic ethers and carbocycles could be obtained this way. It is to be noted that in this case, the product resulting from HAT prior to cyclization (reduction of intermediate **II**) was observed. Its formation could be reduced by using only 5 mol% of TRIP-SH compared to 20 mol%.
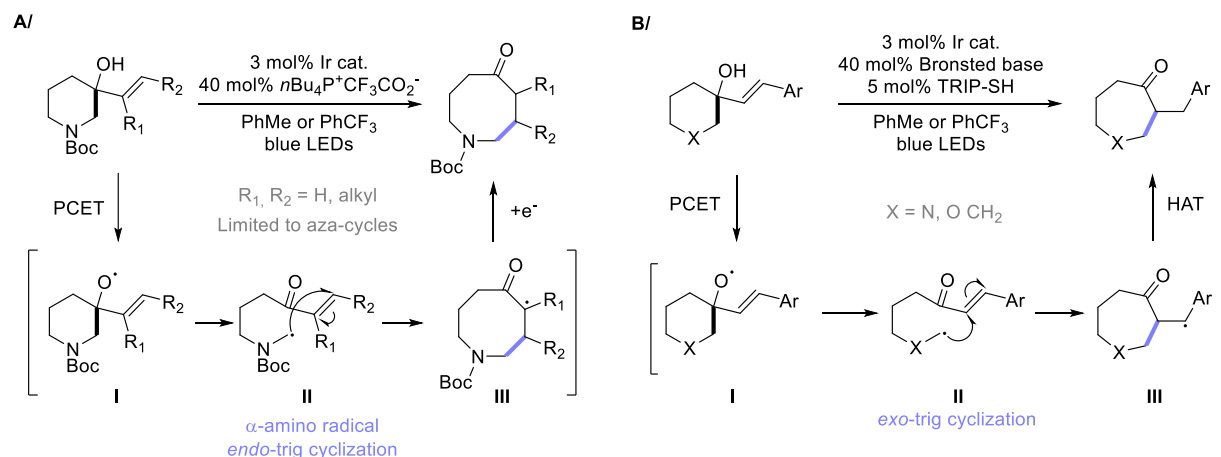
Scheme 11. A/ Ring expansion of azacycles. B/ Ring expansion of carbocycles mediated by a styrene moiety and a HAT catalyst.

Finally, an original application of this chemistry was disclosed by Knowles and co-workers. They used the PCET-driven β-fragmentation of linear alcohols for the depolymerization of hydroxylated polymers.[112] The process allowed for the isolation of well-defined small molecules that could be derivatized and used again as monomers in polymerization.

The special reactivity of strained cyclopropanols

The use of strained cyclopropanols offers the possibility to use a slightly different strategy because these substrates are thought to be oxidized directly to the oxygen radical-cation, undergoing β-scission at the same time as loss of the proton. This circumvents the need for an electron-rich aryl moiety (Figure 11).
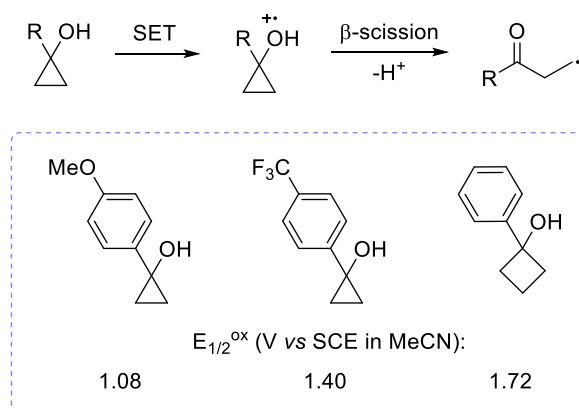
Figure 11. Direct oxidation of strained cycloalkanols and oxidation potential of common starting materials.

Lectka and co-workers reported in 2015 an early example the β-fluorination of ketones from cyclopropanols using 1,2,4,5-tetracyanobenzene (TCB) as photocatalyst and SelectFluor as fluorinating agent and terminal oxidant.[113] Excited TBC is a potent oxidant ($E_{1/2}$ *1TCB/TCB•− = +3.44 V *vs* SCE in MeCN) able to generate the oxygen radical cation. Elongation of the adjacent C–C bond leads to C–C bond fragmentation and accompanying proton loss provides the desired β-carbonyl radical. This intermediate is intercepted by SelectFluor to furnish the desired product and a resulting tertiary aminium radical dication able to regenerate the photocatalyst.[114] This method proved very regioselective and afforded 15 products in good to excellent yields. An example of tandem ring expansion and fluorination was reported as well.

The Zhu group reported the coupling of ring-opened 1-arylcyclopropanols with cyanohydrins using an iridium catalyst with $K_2S_2O_8$ as sacrificial oxidant and BF$_3$.OEt as additive (Scheme 12).[115] Migration of the cyano group and final oxidation afforded unsymmetrical 1,8-diketones. The scope of the method was demonstrated on 32 examples encompassing a variety of electron-rich end electron-poor 1-arylcyclopropanols coupled with aryl and olefin-tethered cyanohydrins.
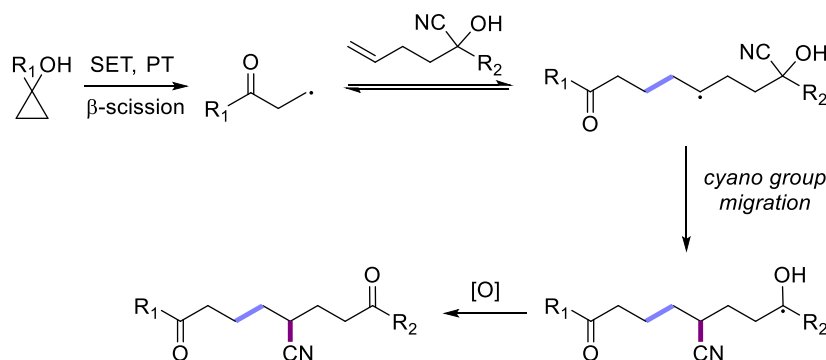
Scheme 12. Synthesis of unsymmetrical 1,8-diketones from 1-arylcyclopropanols.

More recently, Wangelin, Majek, and co-workers[116] as well as the Liu group[117] independently reported the [3+2] cycloaddition of arenediazonium salts and 1-arylcyclopropanols using respectively ruthenium or copper catalysis (Scheme 13). The method allows for the formation of 1,5-diarylpyrazoles with complete regioselectivity but is limited to electron-rich cyclopropanols. The iminium radical cation **II** formed after the addition of the β-keto radical **I** to the arenediazonium salt is thought to undergo SET from the excited Ru(II) to oxidized Ru(III). However, it cannot be excluded that a radical chain process is operative with the nitrogen radical cation quenching the 1-arylcyclopronanol. Initiation is occurring *via* facile reduction of the arenediazonium salt.
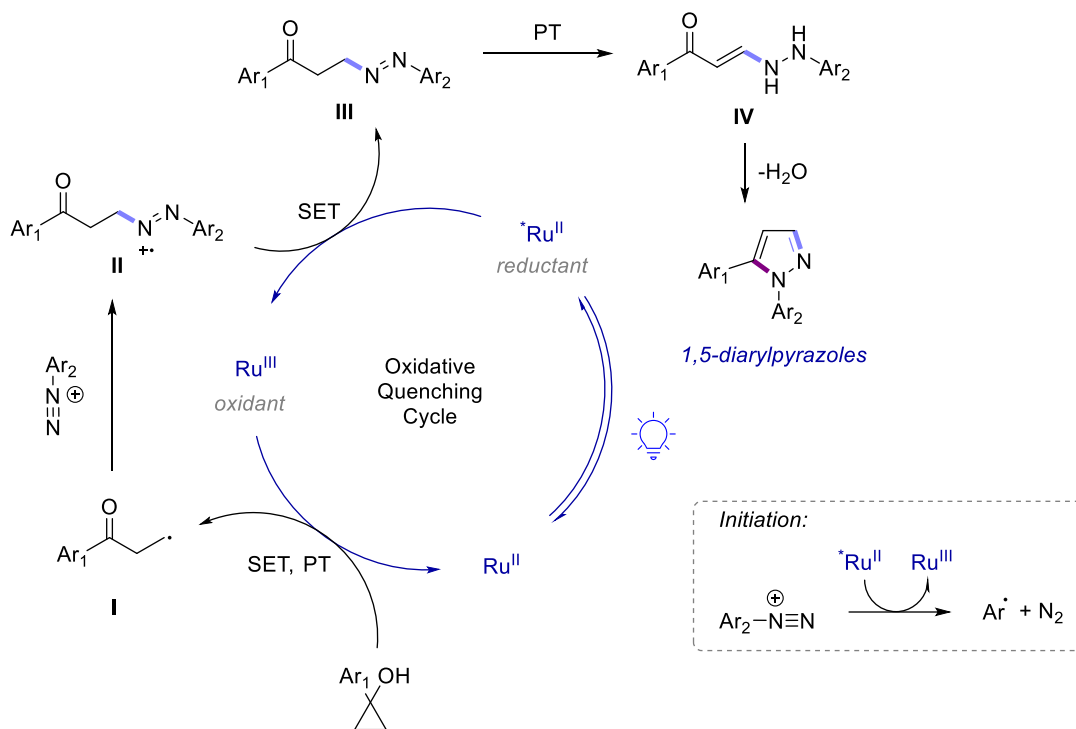
Scheme 13. Synthesis of 1,2-diarylpyrazoles *via* a [3+2] cycloaddition between arenediazonium salts and 1-arylcyclopropanols.

In another recent application, the synthesis of benzo-fused cyclic ketones was obtained *via* the ring expansion of cyclopropanols bearing a pendant styrene moiety.[118] Cyclization of the β-keto radical on this olefin in 6-*exo*-trig or 7-*endo*-trig fashion afforded respectively 6- or 7-membered cyclic ketones.

Remote C–C bond formation through 1,5-HAT

In two consecutive reports by Zhu and co-workers, the photocatalytic heteroarylation[119] and cyanation[120] of remote C-H bonds was achieved using the intermediary of alkoxyl radicals. 1-heteroaryl- and 1-cyanoalkanols bearing a δ-C-H bond were used to generate the alkoxyl radicals that underwent 1,5-HAT to generate the remote carbon-centered radicals (Scheme 14). The mechanism follows an oxidative quenching cycle where $K_2S_2O_8$ plays the role of sacrificial oxidant. The obtained Ir^{IV} species performs the SET in the PCET event leading to the alkoxyl radical. Group migration and final oxidation much like previously described (Scheme 12) afforded the desired products. A variety of alcohols could be used without the need for an easily oxidizable aryl moiety.
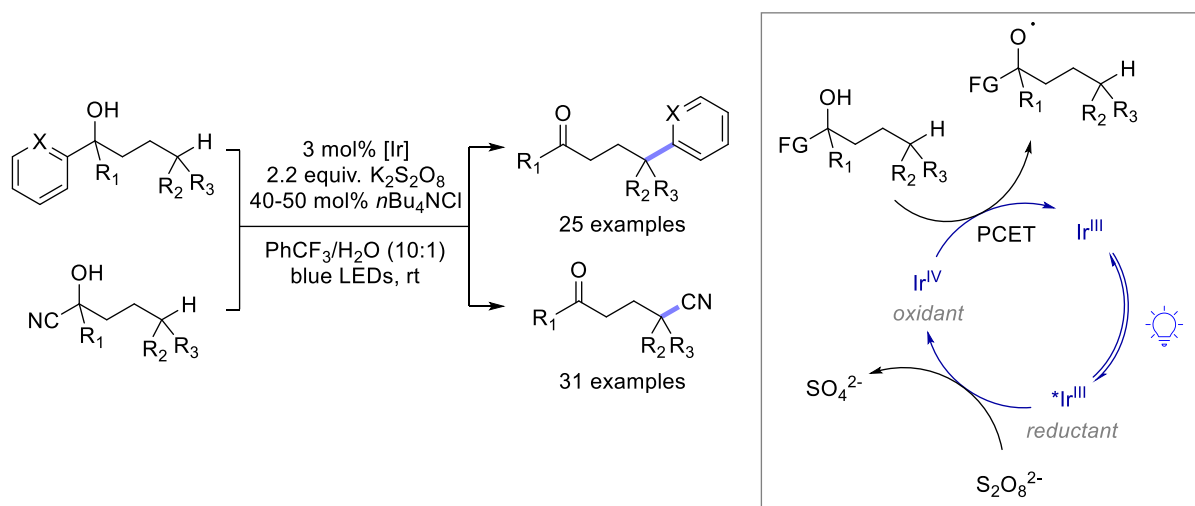
Scheme 14. Remote heteroarylation and cyanation or alcohols using PCET.

Olefin hydroetherification

Finally, the use of alkoxyl radicals for the intramolecular hydroetherification of olefins has only recently been reported by Knowles and co-workers.[44] In line with their previous work, the authors reported the use of an iridium catalyst with the anionic base nBu$_4$P$^+$(PhO)$_2$P(O)O$^-$ to promote the PCET of alcohols tethered with a non-activated olefin. After addition of the electrophilic O-radical to the olefin, the C-centered radical was quenched with a thiol HAT catalyst, which served to regenerate the iridium catalyst (Scheme 15A). Alternatively, the C-centered radical could be intercepted in a conjugate addition with an electron-poor olefin. The catalytic cycle was then closed by reduction of the radical intermediate (Scheme 15B). Interestingly, not only 5-*exo*-trig cyclization was observed but also 6-*endo*-trig and 6-*exo*-trig cyclizations, depending on the substrate.
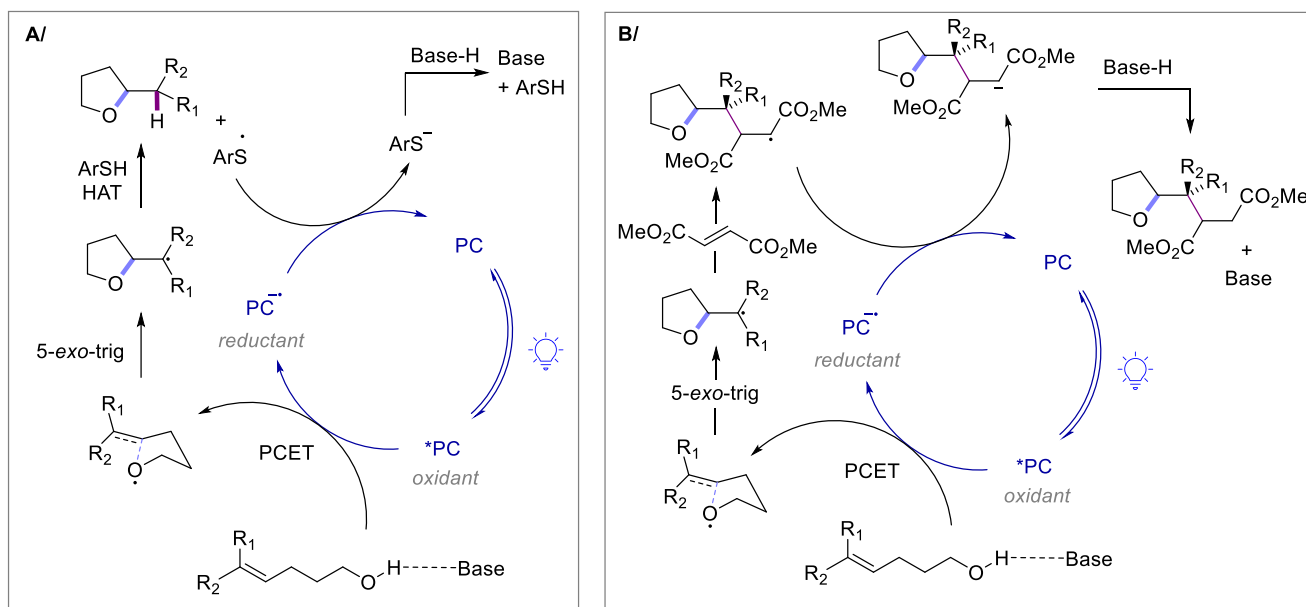
Scheme 15. A/ Hydroetherification of olefins. B/ Carboetherification of olefins.

With this last example, the Knowles lab demonstrated that PCET could be used efficiently to generate alkoxyl-radicals able to engage in the three elemental transformations known to these reactive intermediates: β-fragmentation of the adjacent C–C bond, intramolecular 1,5-HAT, and addition to

olefins. No doubts that further developments involving intermolecular HAT (such as Zuo's chemistry) or chiral thiol catalysis will be reported in the future, either by the Knowles lab or other groups attracted by the simplicity of the protocol.

This chemistry was published by the Knowles group concomitantly to our own efforts in developing reactions for the use of QDs as photocatalysts for alkoxyl radical generation. We had envisioned that it would be possible to engage simple alkoxide anions in the form of boron-ate complexes in a single-electron oxidation pathway under mild conditions.

2.1.3. Boron-ate complexes

The polar reactivity of boronate complexes is well known and has been the subject of intense research.[121–123] They are mild nucleophiles that can react with electrophiles and undergo 1,2-metallate shifts stereospecifically.[124]

The oxidation of the tetraphenyl boron-ate complex is a process that has been studied as early as 1962 by Geske, who showed evidence for the formation of biphenyl by intramolecular dimerization upon electrooxidation of the ate-complex.[125,126] The one-electron oxidation of BPh_4^- was reported to occur at +0.78 V *vs* SCE in acetonitrile.[127] Chemical[128,129] and photochemical[130,131] methods have also been reported to produce the homo-coupled biphenyl product, before this chemistry was extended to the cross-coupling of tetraarylborates using organic oxidants.[132,133]

In 2014, Aggarwal and co-workers demonstrated the possibility to perform the one-electron oxidation of boron-ate complexes using $Mn(OAc)_3$ for the generation of alkyl radicals.[134] In the last decade, there was a surge in the one-electron reactivity of boron-ate complexes due to their use as versatile radical precursor in photoredox chemistry (Figure 12).[135]
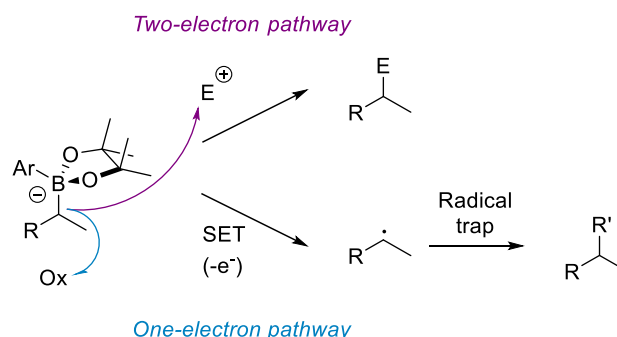
Figure 12. Two- and one-electron chemistry of boronate complexes

2.1.3.1.   *Organotrifluoroborates*

Potassium organotrifluoroborates in particular have been extensively studied.[136,137] Initially, they have been recognized as useful reagents in palladium-catalyzed cross-coupling reactions (two-electron pathway).[121,138] These precursors can be easily prepared from boronic acids, are safe to handle, stable and storable. Numerous alkyl-, alkenyl, and aryltrifluoroborates are nowadays commercially available. More recently, photoredox-catalyzed reactions with organotrifluoroborates have attracted attention and have been developed by Akita and Molander independently.[139] Akita and co-workers demonstrated the possibility to generated alkyl, allyl, benzylic, aryl and alpha-oxy radicals from organotrifluoroborates using photoredox chemistry.[140,141] The one-electron oxidation of these precursors is mediated by an excited iridium catalyst and C-O bond formation is demonstrated with TEMPO, while C-C bond formation could be achieved by employing a Giese-type olefin (Scheme 16). In the case of C-O bond formation, a sacrificial amount of TEMPO was used as final oxidant to regenerate

the iridium catalyst. In the C-C bond formation protocol, the resulting radical alpha to the electron-withdrawing group (ester, cyano, ketone, phosphate) can be reduced by the iridium catalyst. Electron-rich organotrifluoroborates showed to undergo a fast reaction, while electron-poor precursors reacted significantly slowlier. This indicates that the oxidation step of the boron-ate complex is crucial.
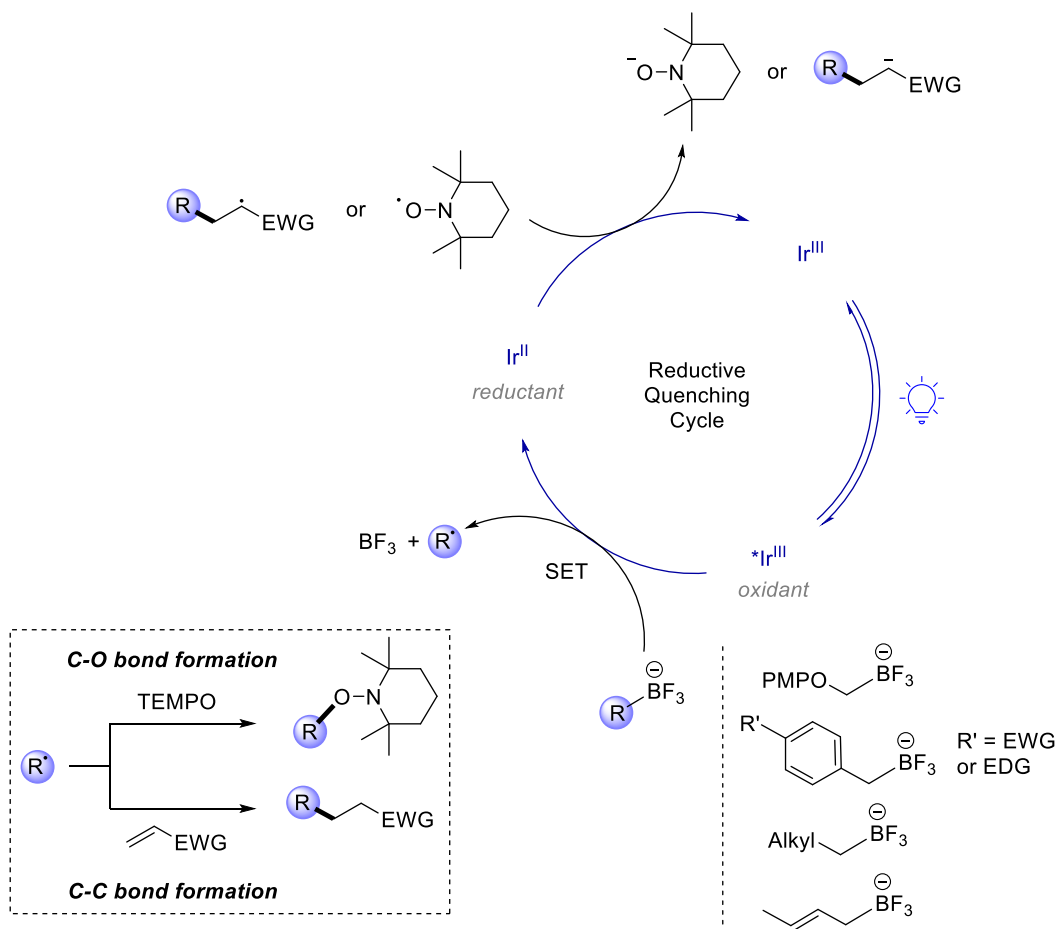
Scheme 16. Organotrifluoroborates as precursors for C-O and C-C bond formation.

Interestingly, it was found that the reduction potential of some precursors (+1.48 V vs SCE in MeCN for a secondary alkyltrifluoroborate) exceeded the oxidation potential of the iridium catalyst (+1.32 V vs SCE in MeCN for Ir(dFCF$_3$ppy)(bpy)PF$_6$).[142] This thermodynamically unfavorable SET is thought to occur because the C-B bond fragmentation is irreversible, thus driving the reaction forward even if only a small portion of the oxidation wave is overlapping. In this work Akita and co-workers also introduced the use of triol boronates. These complexes have a lower oxidation potential and proved essential in the generation of some challenging alkyl radicals (see Figure 15 for a summary of oxidation potentials).

Shortly after this report, Molander and co-workers reported a photoredox cross-coupling reaction employing an organotrifluoroborate precursor, and iridium catalyst, and a nickel catalyst (Scheme 17).[143] The iridium catalytic cycle is responsible for generating the radical from the organotrifluoroborate precursor while the nickel catalytic cycle promotes cross-coupling with an arylhalide. Both catalysts regenerate each other by a SET event. Under this protocol, a variety of electron-poor and electron-rich benzylic trifluoroborates could be coupled with aryl- and heteroaryl moieties.
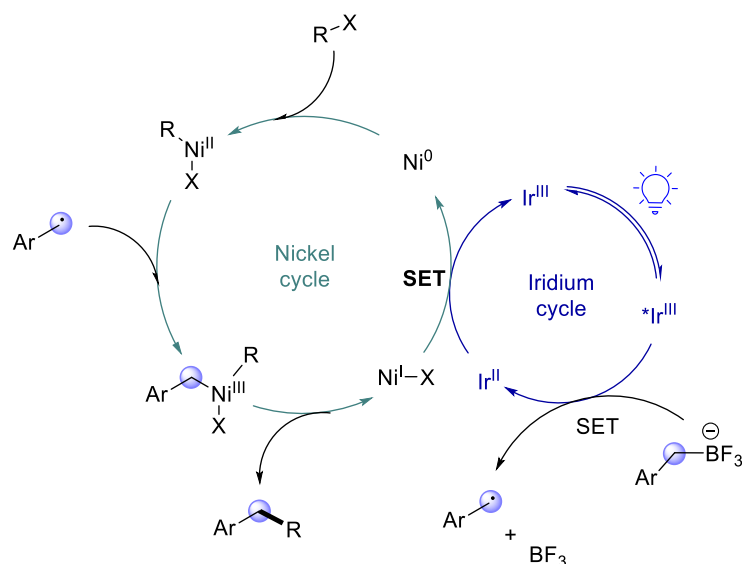
Scheme 17. Photoredox cross-coupling reaction using a Ni/Ir catalytic system.

In a follow-up study, this method was applied to the cross-coupling of more challenging secondary alkyltrifluoroborates.[144] In accordance with previous evidence of thermodynamically unfavorable SET events, the cross-coupling proceeded smoothly between alkyl radicals and an array of aryl halides in presence of Ir(dFCF$_3$ppy)$_2$(bpy)PF$_6$. The use of stoichiometric amounts of cesium carbonate as an additive proved crucial for the efficiency of the reaction, presumably to quench the released BF$_3$ that appeared to inhibit the reaction.

2.1.3.2.   Lewis base catalysis

The above-mentioned studies relied on the use of a pre-formed, isolated boron-ate complex. Ley and co-workers devised another strategy based on the ability of boronic acids, possessing a vacant p orbital, to form adducts with Lewis bases.[145–147] This redox-active complexes can generate the desired radical under SET and offer the possibility to recycle the Lewis base. This allows for the *in situ* formation of the radical precursor without the need for prefunctionalization. The Ley lab was able to perform the conjugate addition of aryl and benzylic radicals generated from BPin- or boronic acid complexes under iridium- or acridium-based catalysis (Scheme 18). Of note, the generation of alpha-amino, alpha-thio and primary alkyl radicals was demonstrated as well. The Lewis base required for the reaction to proceed proved substrate dependent and could be either DMAP, quinuclidine, quinuclidine-3-ol or PPh$_3$. The chemistry was successfully carried out in flow.
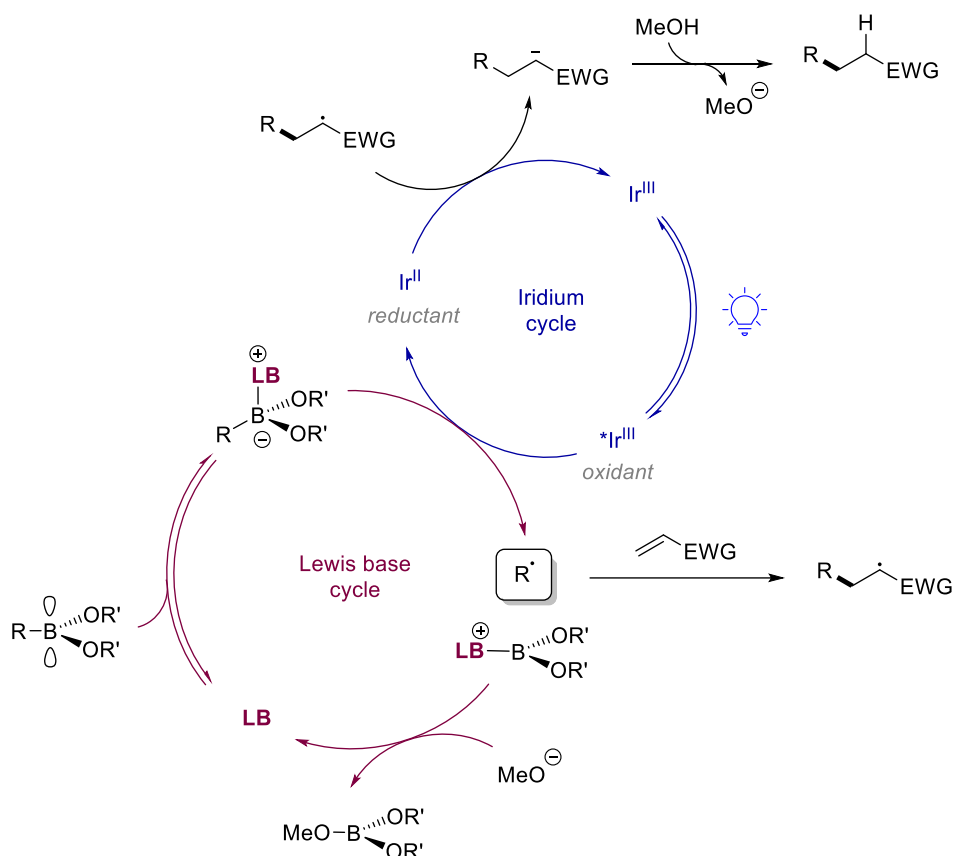
Scheme 18. Lewis base catalysis for the generation of radicals from boronic acids.

Recently, an amine-borane complex $H_3B–NMe_3$ could be oxidized to the boryl-amine radical using an organic dye as photocatalyst.[148] This radical intermediate was used as halogen atom transfer reagent from $ClCF_2H$ for the difluoromethylation of unactivated alkenes.

2.1.3.3.   Arylboronates

Arylboronates for the generation of alkyl radicals

To complete the series of possible boron-ate complexes available for this type of chemistry, Aggarwal and Studer concurrently developed easy oxidizable arylboronates as radical precursors. The desired complex is formed *in vacuo* using an aryl lithium. Aggarwal and co-workers used this method for the generation of 1°, 2° and 3° alkyl radicals with good functional group tolerance.[149] The authors used iodine-containing Giese acceptors for this protocol, allowing after radical-polar crossover the cyclization to cyclobutanes (Scheme 19, pathway a)). Alternatively, it is possible that an homolytic substitution is operative, with final reduction of the iodine radical (Scheme 19, pathway b)).
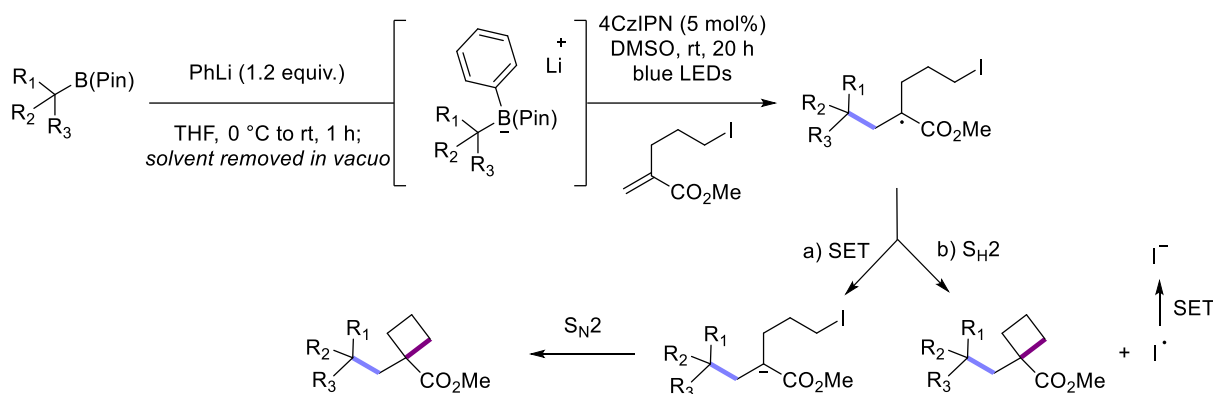
Scheme 19. Arylboron-ate complexes for the generation of alkyl radicals.

Shortly after, the same group showed that 1,2-bis-boronic esters where suitable substrates and that the 1° boron-ate complex was formed selectively over the 2° complex.[150] Light-driven one-electron oxidation affords a β-boryl radical that undergoes 1,2-boron shift (Figure 13). Overall, the method allows for the selective transformation of the more hindered boronic ester. In this publication, the coupling partners were activated olefines.
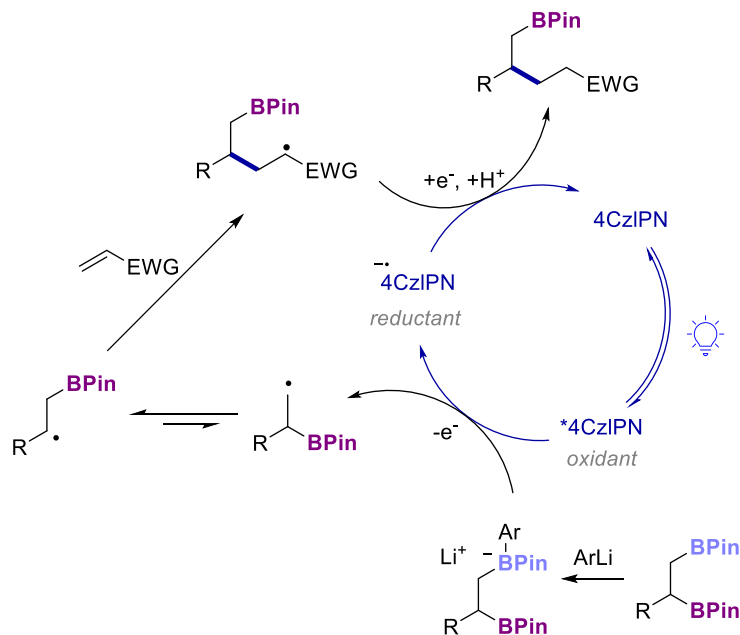
Figure 13. Selective boronate complex formation and following one-electron oxidation on 1,2-bis-boronic esters.

In a follow-up study, the coupling partner was extended to electron-deficient aryl nitriles;[151] this allowed for the formation of an EDA complex between the electron-rich boron-ate complex and the electron-deficient aryl moiety.

Studer and co-workers applied a similar strategy for a protodeboronation protocol reaction using thiophenol as hydrogen donor to intercept the intermediate alkyl radical (Figure 14).[152] The method was amenable to 1°, 2° and 3° alkyl radicals, and was applied to the total synthesis of δ-(R)-coniceine and indolizidine 209B. Additionally, a formal anti-Markovnikov hydromethylation sequence was developed. Hydroboration of the starting alkene gave the boronic ester precursor that was engaged in a Matteson homologation[153] reaction. Boron-ate complex formation followed by catalytic protodeboronation gave the hydromethylated alkene.
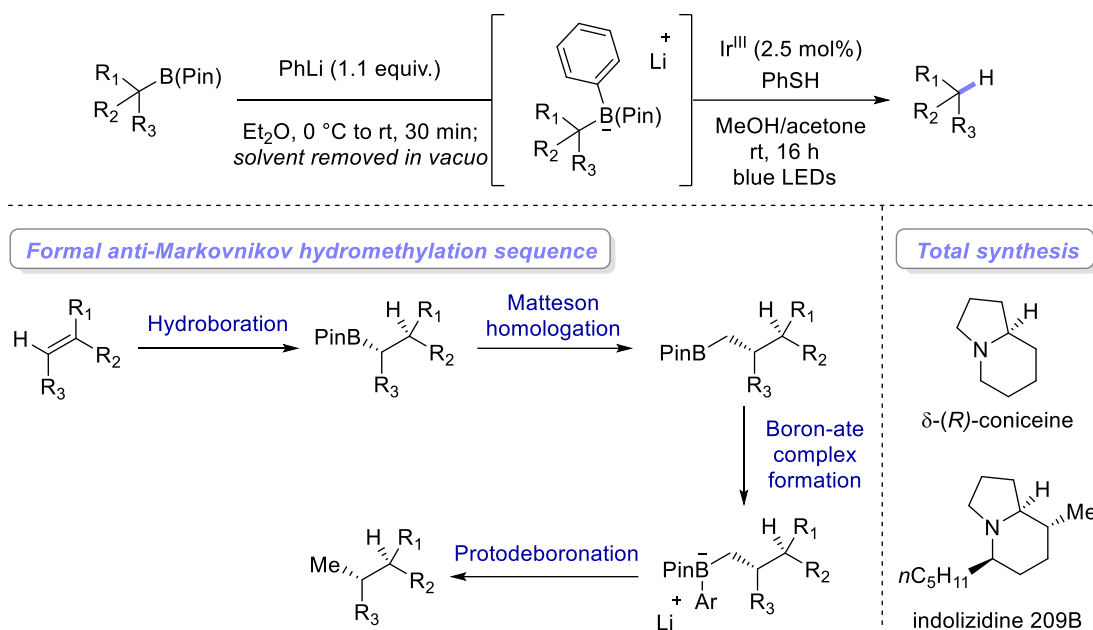
Figure 14. Protodeboronation protocol and application of the method to concise total synthesis and formal hydromethylation reactiona.

Arylboronates for the generation of aryl radicals

These types of boron-ate complexes can also be used to generate not alkyl, but aryl radicals. Notably, two reports by Yoshimi and co-workers[154] and Bloom and co-workers[155] show the use of arylboronic acids in the photoredox mediated generation of aryl radicals and their subsequent addition to electron-deficient alkenes (Meerwein arylation) (Scheme 20).

Scheme 20. Literature precedence on the use of boronic acids for the generation of aryl radicals
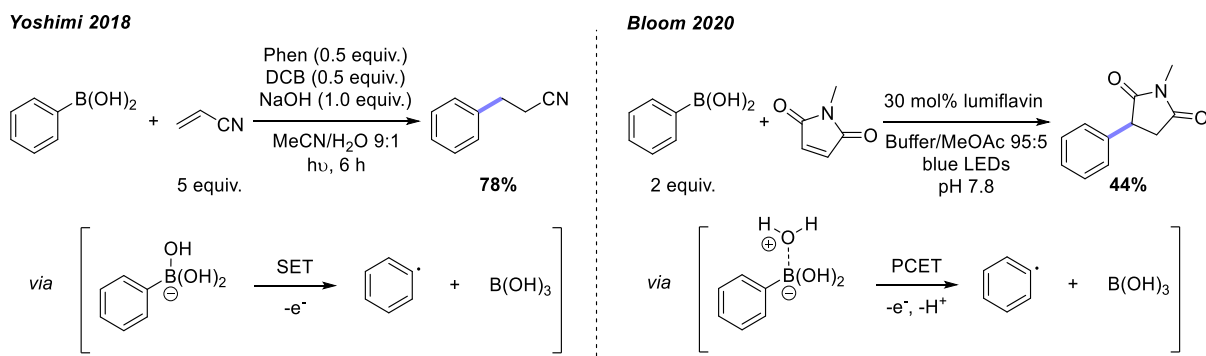
In Yoshimi's reaction design, the arylborate species is formed *in situ* in presence of one equivalent of sodium hydroxide. Oxidation occurs through an organic catalytic system combining phenanthrene (Phen) and 1,4-dicyanobenzene (DCB) under light irradiation. Interestingly, the authors also observed HAT from their solvent MeCN and had to increase the amount of radical trap to 5 equivalents to counter this side reaction. As a side effect, this increased the amount of oligomerization and the catalyst loading had to be increased to 0.5 equivalents. In the work of Bloom and co-workers, the reaction is run in aqueous media and complexation with water is thought to generate a species prone to PCET. Interestingly, this method was not limited to phenyl radicals (14 examples) and allowed the generation of numerous heteroaryl radicals as well (28 examples).

In summary, a variety of boron-ate complexes with different oxidation potentials are described in the literature for photoredox-catalyzed deboronative radical formation. Three main strategies have been developed so far: the prior synthesis and isolation of the boron-ate precursor (for example in the case of organotrifluoroborates), Lewis base catalysis (Ley and co-workers), and *in situ*, stoichiometric formation of the complex (Aggarwal and Studer). Common precursors with their oxidation potentials are compiled in Figure 15.
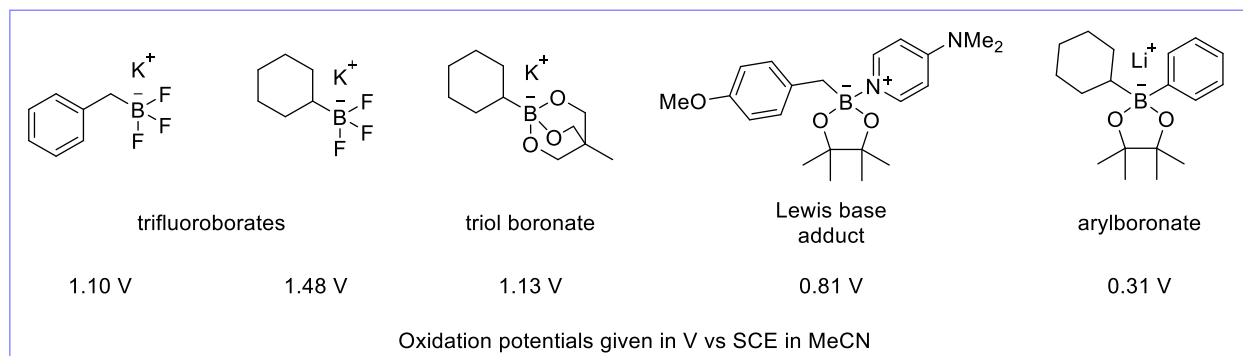
Figure 15. Summary of common boron-ate complexes and their oxidation potentials.

2.1.3.4.   *Previous work in the group*

In line with the presented literature precedence, it should be possible to perform the single-electron oxidation of an alkoxide surrogate in the form of a boron-ate complex. These precursors are easy to synthesize and to handle, they can be formed prior to the reaction or *in situ*. Previous investigations in the group suggested that the fragmentation of the boron-oxygen bond over the boron-carbon bond in such ate-complexes could be favored by using electron poor aromatic rings such as the perfluorophenyl moiety (Scheme 21).[156] A sulfone trap could be used to intercept the radical species.
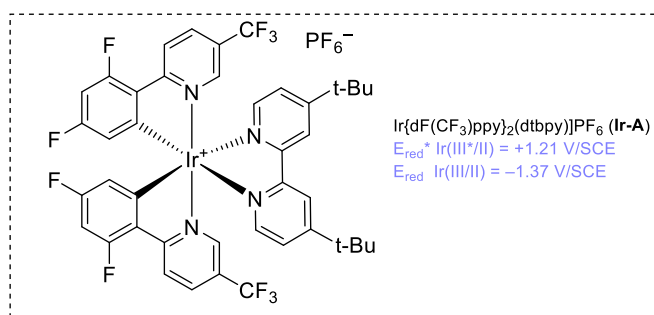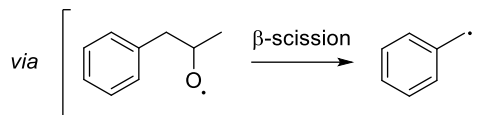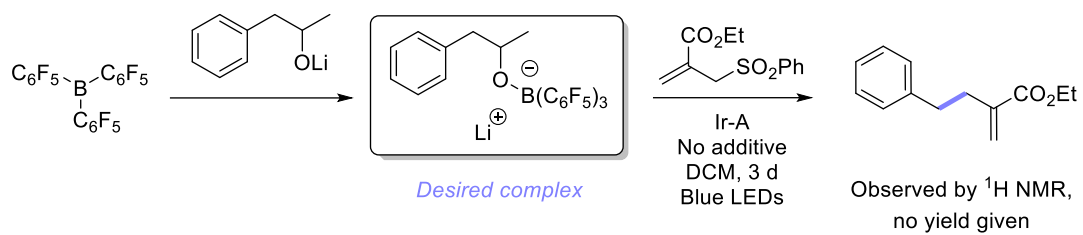
Scheme 21. Model reaction previously investigated in the group and used for future work.

2.2. Results

2.2.1. Alkoxyl radical precursor

2.2.1.1.   Synthesis and characterization

The corresponding tris(perfluorophenyl)borane precursor **1** can be synthesized from bromopentafluorobenzene by lithium-halogen exchange with *n*Butyllithium in hexane, and subsequent quenching with commercially available boron trichloride (Scheme 22). In our hands, the boron NMR value for the obtained compound ranged, depending on the batch, from 0 to 16 ppm. These values have some precedence in the literature.[157] When a preformed toluene solution of a lithium alkoxide salt was added to a solution of the boron precursor, a clear shift of the ^{11}B NMR value was observed from 0 to -5 ppm. This upfield shift seemed consistent with the addition of a Lewis base to the empty *p*-orbital of the boron. The ^{1}H NMR signals of the alcohol residue were shifted as well compared to both the free alcohol and the alkoxide. However, upon closer look at literature values and known general NMR shifts for tricoordinated boron centers, it became clear that the expected and literature reported value for tris(perfluorophenyl)borane was 59 ppm (25 °C, CD$_2$Cl$_2$, 96.3 MHz).[158] This was in sharp contrast to our obtained values which seemed to fit better with water complexes of tris(perfluorophenyl)borane **1•3H$_2$O**.

^{11}B NMR (CD$_2$Cl$_2$) $\delta_{expected}$ 59 ppm

1•3H$_2$O
70%

^{11}B NMR (CD$_2$Cl$_2$) $\delta_{observed}$ -0.7 ppm
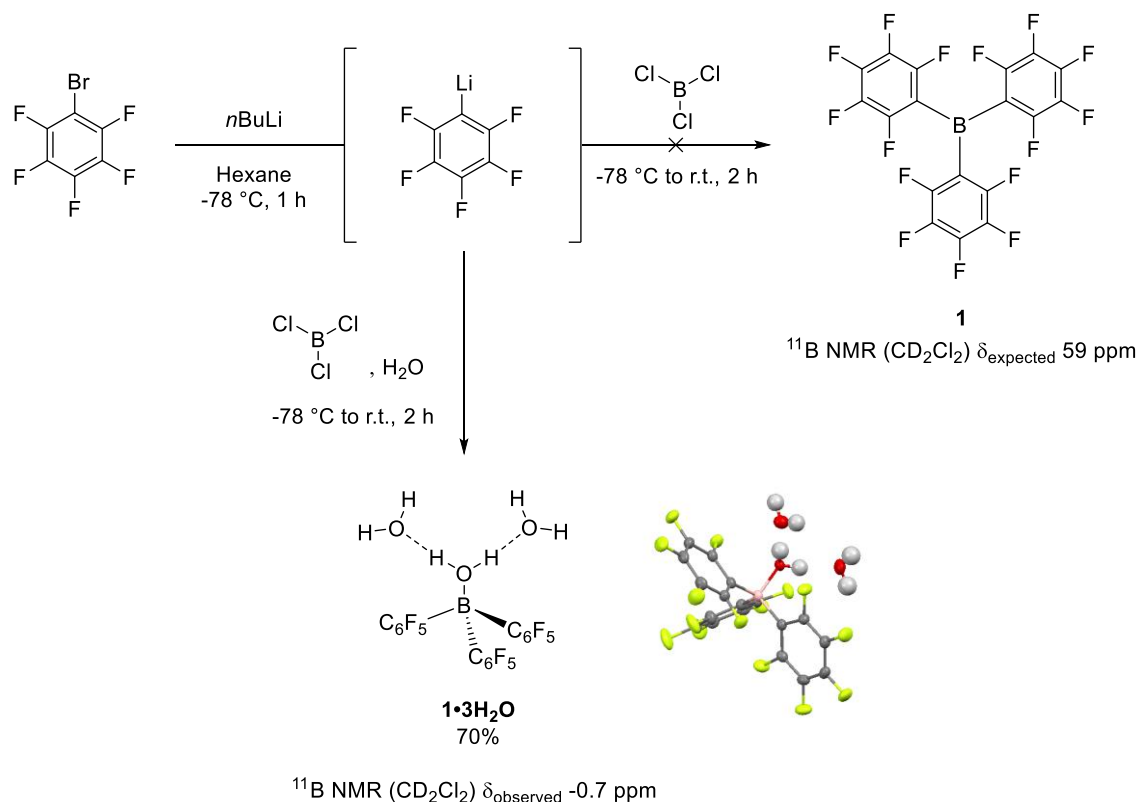
Scheme 22. Precursor synthesis and tri-hydrated adduct.

These water complexes have been previously reported and studied in the literature.[159–161] Beringhelli et al. have titrated B(C$_6$F$_5$)$_3$ with water in a toluene-d$_8$ solution and monitored the results by ^{19}F and ^{1}H NMR at 196 K (-78 °C). They showed that a first adduct was formed with one water molecule coordinated to the boron center in a Lewis acid-Lewis base interaction. A stepwise transformation then occurred into two aqua species containing one or two water molecules hydrogen-bonded to the B-

bound water molecule (Figure 16). However, no ^{11}B NMR values were reported. We were able to crystallize our synthesized boron precursor and to confirm its water-adduct nature, thus attributing a boron NMR value of -0.7 ppm to the most hydrated adduct. The discrepancy observed in the boron NMR value for different batches of the precursor depending on slightly different reaction conditions can likely be attributed to different degrees of hydration. For example, a ^{11}B NMR value of almost 40 ppm was obtained when running the reaction under strictly anhydrous conditions and filtration of the end product with a Schlenk frit device. The most efficient way to obtain reproducible batches of the boron precursor was ultimately to let it in contact with air for several hours after isolation, thus reaching a final ^{11}B NMR value of around 0 ppm for all batches.
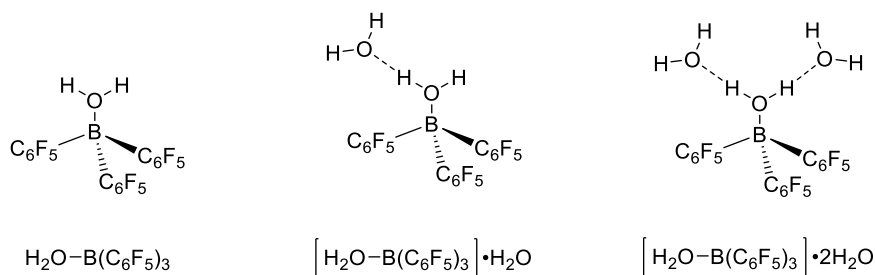
Figure 16. Aqua adducts of B(C$_6$F$_5$)$_3$.

Having this identified water complex in hand, several attempts were made to displace water and to ultimately obtain the desired alcohol-bound complex. Heating the adduct **1•3H$_2$O** at different temperatures under high vacuum led to either small changes in the boron NMR or to degradation, presumably to hydroxybis(pentafluorophenyl)boron and pentafluorobenzene.[162] Sublimation at 70 °C (10^{-2} mmHg) was attempted but did not result in the isolation of the desired water free boron compound, probably because the whole process should be carried out in a glovebox.

The reversibility of adduct formation between B(C$_6$F$_5$)$_3$ and several ligands have been previously investigated. In particular, Bergquist and coworkers have studied the aqua and alcohol adducts of B(C$_6$F$_5$)$_3$.[160] They have shown that upon mixing a stoichiometric amount of water and alcohol (MeOH or BuOH) in presence of B(C$_6$F$_5$)$_3$, the B-bound water complex was isolated and not the B-bound alcohol complex ([(C$_6$F$_5$)$_3$B(OH$_2$)]•HOBu] rather than [(C$_6$F$_5$)$_3$B(HOBu)]•H$_2$O]). This was attributed, after calculations, to the stronger bond energy of the water complex (9.4 kcal.mol^{-1}) compared to the alcohol complex (5.4 kcal.mol^{-1}). Consistent with these findings, our own attempts to replace the water molecule by addition of the free alcohol was met with failure.

Encouragingly, the water molecule could be partially replaced by pyridine in DCM after 36 hours, and the clean B(C$_6$F$_5$)$_3$-pyridine adduct (**1•Py**) was isolated by recrystallization from DCM:Hexanes (Scheme 23A). This exchange could be attributed to the stronger Lewis base nature of the pyridine, explaining why it can replace water while the alcohol cannot. This displacement is probably dissociative with the protonated pyridinium salt as an intermediate, as previously postulated in the literature.[163] The absence of a protic hydrogen in pyridine might as well play a role as it cannot interact through hydrogen bonding with the water adduct. However, replacing the pyridine by the alkoxide did not work. A mixture of the starting complex with two unidentified products was obtained as assessed by ^{11}B and ^{19}F NMR. This mixture was engaged as such in our photoredox protocol and did not promote the desired reaction. It was then attempted to replace the pyridine with the free alcohol (Scheme 23B). The reaction was run in CD$_2$Cl$_2$ in order to follow the reaction by NMR. After several days, no changes were observed.

A/

B/
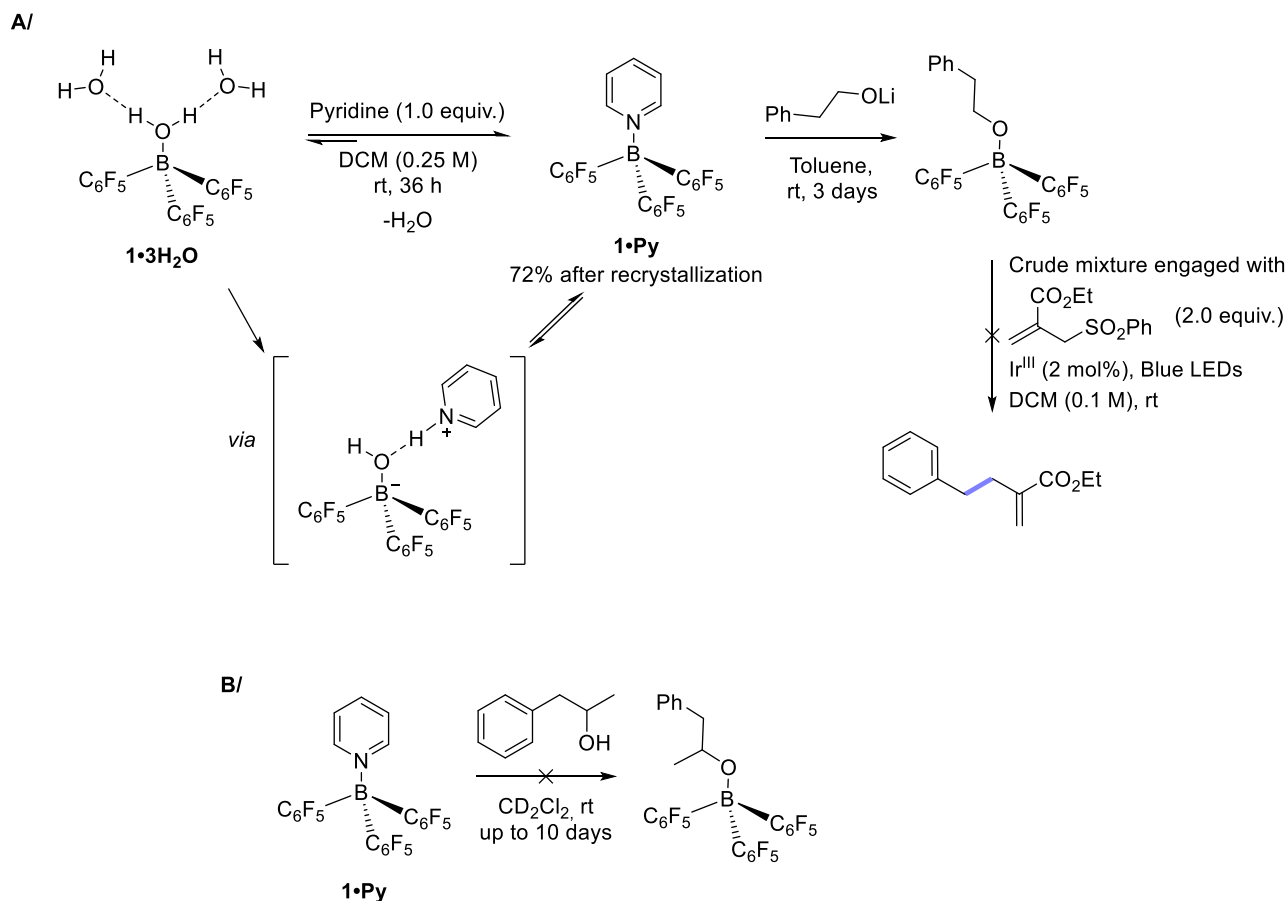
Scheme 23. A/ Displacement of water with pyridine and attempted displacement of pyridine with an alkoxide ion. B/ Attempt at replacing pyridine with a free alcohol.

We have previously mentioned that adding a solution of a lithium alkoxide to the now identified water adduct of $B(C_6F_5)_3$ led to a shift in the ^{11}B NMR and in the ^1H NMR. We wondered if this could be attributed to a replacement of the water by the strongly basic alkoxide, or to an acid-base reaction between the alkoxide and the water adduct (Scheme 24A). Water coordinated to a strong Lewis acid such as $B(C_6F_5)_3$ becomes a strong Brønsted acid, with a pKa estimated at 8.4 in acetonitrile.[160] This can be compared to HCl in acetonitrile. XRay crystallography of our obtained adduct confirmed the deprotonation of the B-bound water and coordination of the thus obtained free alcohol through the lithium ion (pathway b/, **3,** Scheme 24A), explaining the shifts observed in both the ^{11}B and the ^1H NMR spectra even though the desired B-O bond was not formed. This complex exists as a dimer. Deprotonating the aqua complex first with LiH or nBuLi to give **2**, and then adding the free alcohol led to the same complex **3** (Scheme 24B). The advantage of this second approach is that any alcohol could be coordinated without previous treatment from the easily synthesized and stable deprotonated aqua complex **2**.
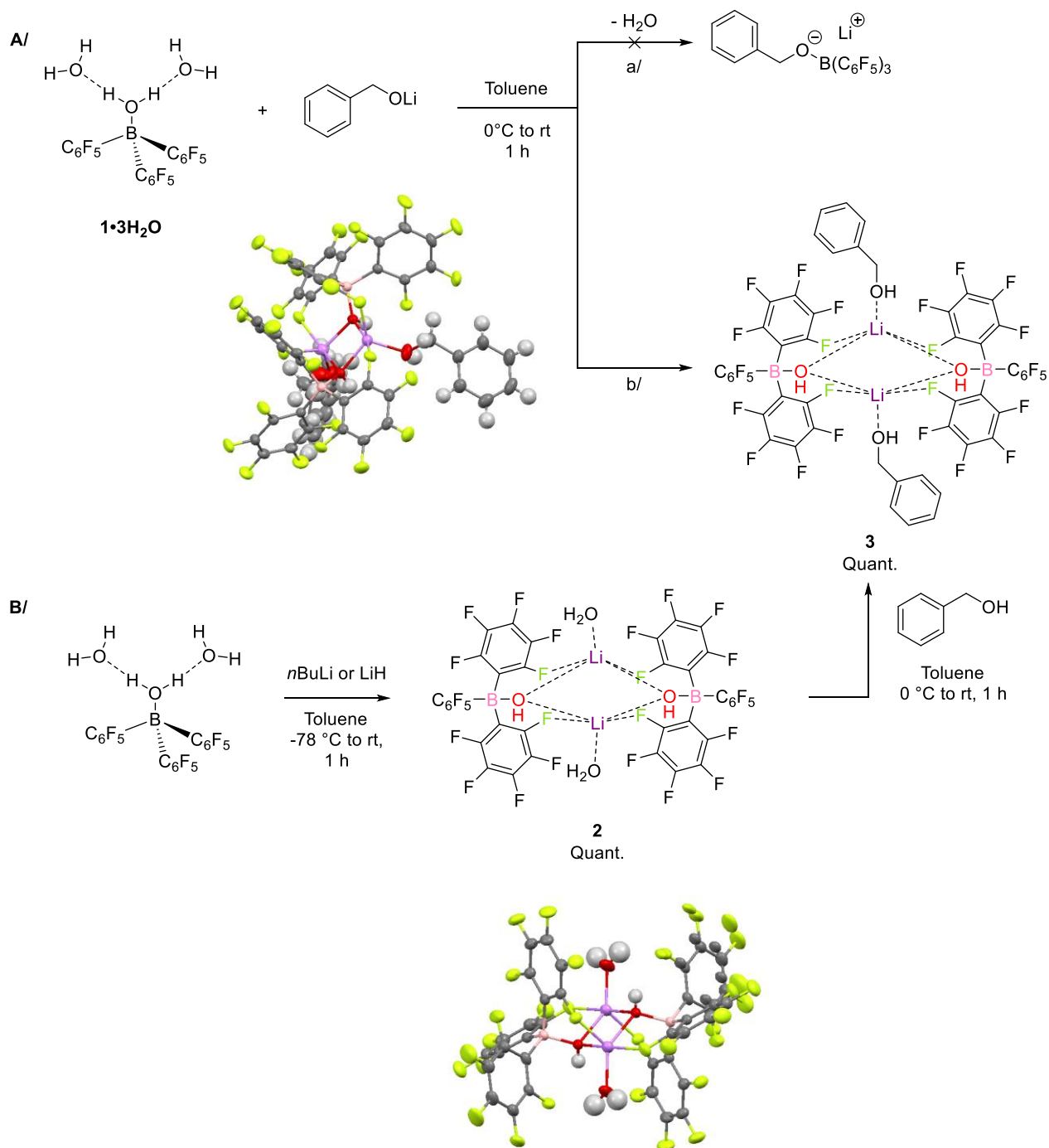
Scheme 24. A/ Possible pathways upon reaction of a lithium alkoxide with **1•3H₂O**. B/ Deprotonation of **1•3H₂O** and subsequent reaction with the free alcohol.

Following this second procedure, **2** was coordinated with 1-phenylpropan-2-ol and the resulting complex was engaged in the model reaction (Scheme 25). After many attempts varying catalyst, solvent, and trap equivalents, no desired product was isolated.
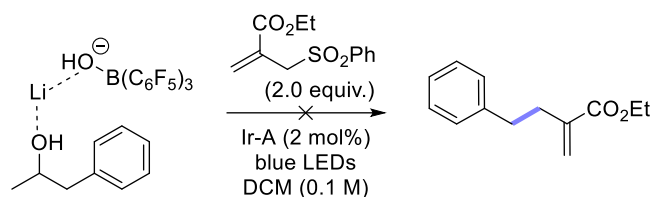
Scheme 25. Model reaction run with the alcohol starting material coordinated to complex **2** via the lithium ion.

2.2.1.2. Oxidation attempts on the hydrated complex

We then wondered whether we could oxidize this deprotonated aqua complex **2**. To this end a series of experiments were carried out. First it was tried to oxidize the complex **2** using electrochemistry. Cyclic voltammograms were recorded in DMSO alone or in MeCN with a solution of $KClO_4$ as electrolyte (working electrode in glassy carbon, counter electrode in cupper, reference electrode trapped hydrogen). After several measurements at different concentrations of the compound, no oxidation/reduction event was observed that could be attributed to the compound. Next, fluorescence quenching experiments were carried out in acetonitrile using the complex **2** as quencher and [Ir{dF(CF$_3$)ppy}$_2$(dtbpy)]PF$_6$ (Ir-A) as the fluorophore. At 20 °C some aggregation of the complex was observed in MeCN so that the measurements had to be repeated at 40 °C. At this temperature no quenching was observed as determined from the flat I_o/I ratio (fluorescence without quencher over fluorescence in presence of the quencher) versus concentration of the quencher. In parallel to these experiments, oxidation of this complex **2** was tried in a preparative manner (Scheme 26). We hypothesized that if the hydroxyl radical was formed, it could abstract a hydrogen from the solvent (THF). The resulting alpha-oxy radical could add to the allylester sulfone radical trap **4** and be detected, since an authentic sample of the expected product **5** was available in the laboratory. Unfortunately, no such product was detected.
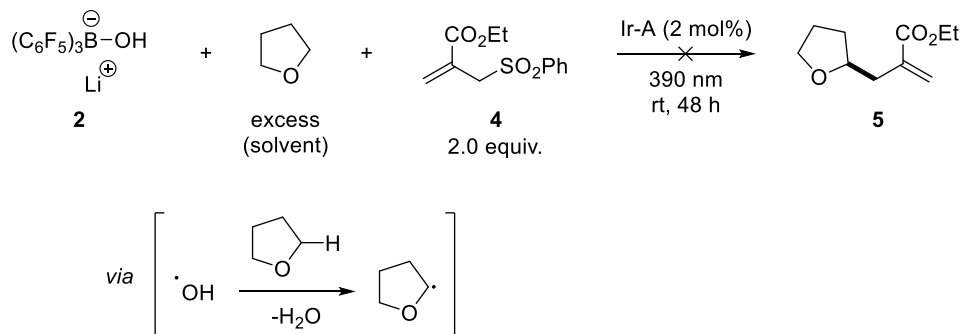
Scheme 26. Oxidation attempt of complex **2** under photoredox catalysis.

2.2.1.3. Synthesis of a radical probe

In order to increase overall reaction efficiency, a radical probe **9** was designed and synthesized containing an internal sulfone moiety (Figure 17). This moiety is known to undergo efficient radical β-fragmentation and could be easily expelled by the carbon radical resulting from β-fragmentation of the alkoxyl radical. Additionally, the sulfonyl radical has been used previously as radical acceptor to close the catalytic cycle of an array of photocatalysts.[164] Hence, we could hope with this probe to have a very efficient substrate.
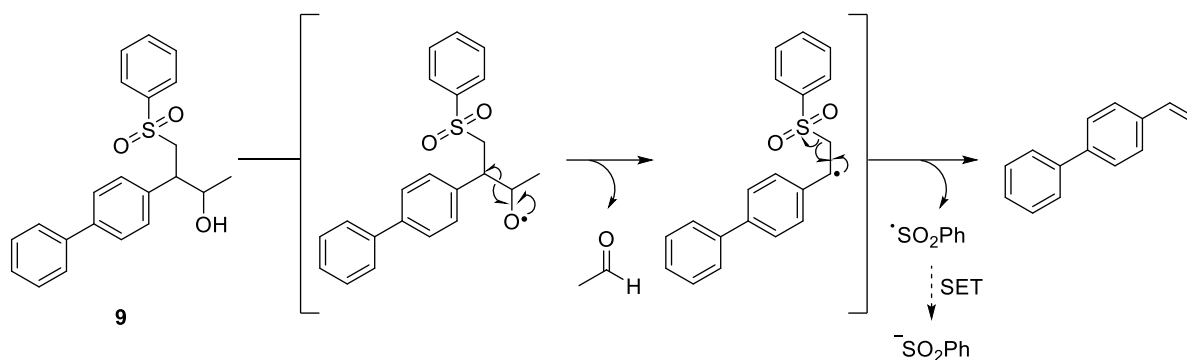
Figure 17. Design and expected reactivity of the sulfone-containing radical probe

Synthetically, the synthesis started with 4-iodophenyl and a copper catalyzed arylation/C-C activation sequence in presence of water.[165] The obtained alpha-aryl ketone **6** can be submitted to a Mannich reaction with *N,N,N',N'*-tetramethylmethanediamine to obtain the alpha-beta unsaturated ketone **7**. Addition of thiophenol to this Michael acceptor delivers the required precursor **8** for oxidation by *m*CPBA. The end sulfone **9** is obtained from this sequence in a good overall yield of 40 % (Scheme 27).
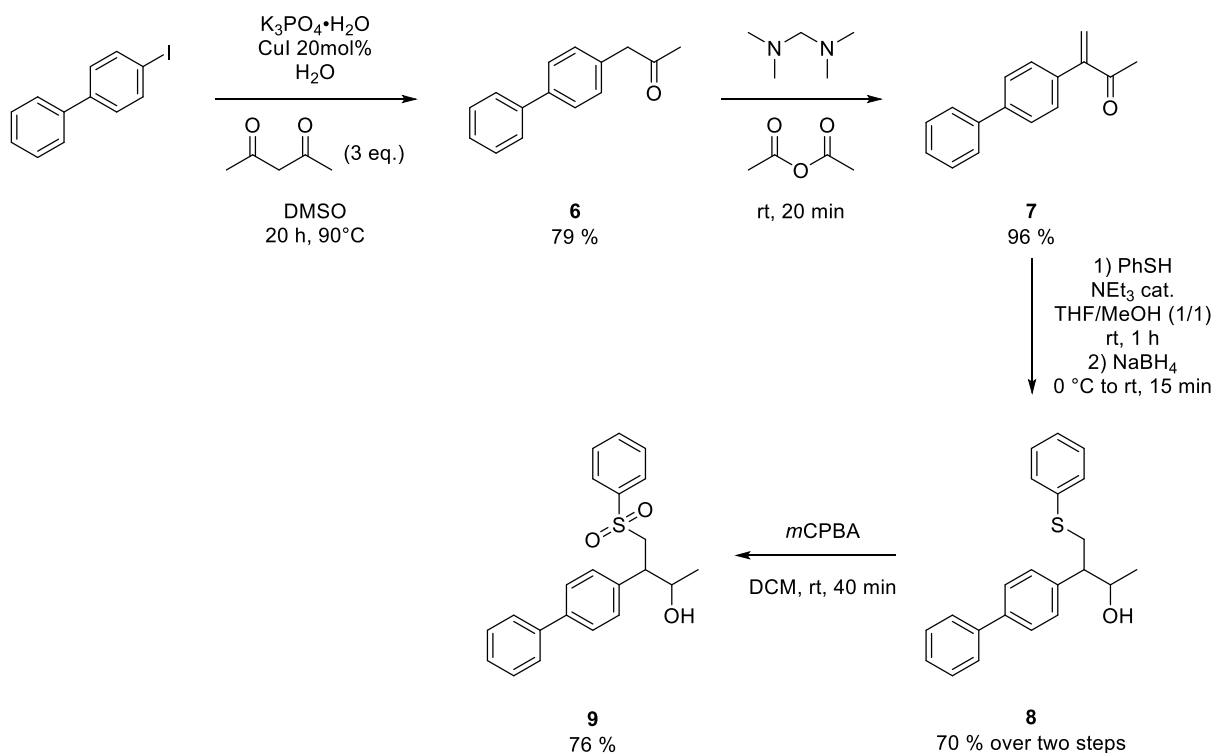
Scheme 27. Synthetic pathway towards a radical probe for alkoxyl radical formation

Unfortunately, since no proof of concept for the oxidation of complexes of type **2** or **3** had been obtained, this radical probe was not tested.

2.2.3. Phenyl radical precursor

2.2.3.1. Investigations

Different boron precursors were investigated, in particular the bench-stable B_2Pin_2 in combination with the influence of the counter ion used in the alkoxide adduct (Li, Na, K).[166] None of them performed the desired reaction. However, the results obtained with triphenylborane are worth discussing. This precursor was initially not chosen because preliminary results using chemical oxidation showed that

the B-C bond was cleaved over the boron-oxygen bond.[156] In a first attempt we sought to reproduce this result using photoredox chemistry. B(Ph)$_3$ is a commercially available and stable starting material that can be easily coordinated with an alkoxide ion. The change in chemical shift for the boron atom from 67.0 ppm (BPh$_3$) to 2.0 ppm (expected product) is consistent with tetra-coordination at the boron atom (Scheme 28). A small survey of solvents showed that among toluene, dichloromethane and tetrahydrofuran, the latter gave the best results with full consumption of BPh$_3$. Attempts to purify the ate-complex by recrystallization failed so the solvent was simply evaporated *in vacuo* prior to the photoredox reactions.
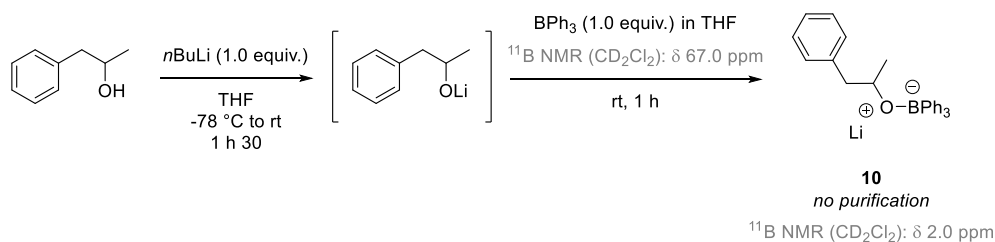
Scheme 28. General protocol for the synthesis of boron-ate complexes from BPh$_3$.

In a first attempt, the photoredox reaction was carried out on ate-complex **10** in presence of the allylsulfone radical trap **4** in MeCN or THF and with [Ir{dF(CF$_3$)ppy}$_2$(dtbpy)]PF$_6$ (Ir-A) as a catalyst. The addition of aryl radicals to double bonds is known and well described[167] ($k = 10^8$ M^{-1} s^{-1} for electron-poor alkenes, $k = 10^7$ M^{-1} s^{-1} for unactivated alkenes, 298 K),[168] so it was anticipated that this model reaction would allow to gain a clear understanding of this boron-ate complex's reactivity by looking at the product's distribution (Scheme 29A). And indeed, the isolated products were a clear proof that the aryl radical had been formed and not the alkoxyl radical which would have fragmented into the benzylic radical (Scheme 29B). At this point, the formation of the biphenyl product was unexpected but can be rationalized based on literature precedence (*vide infra*).
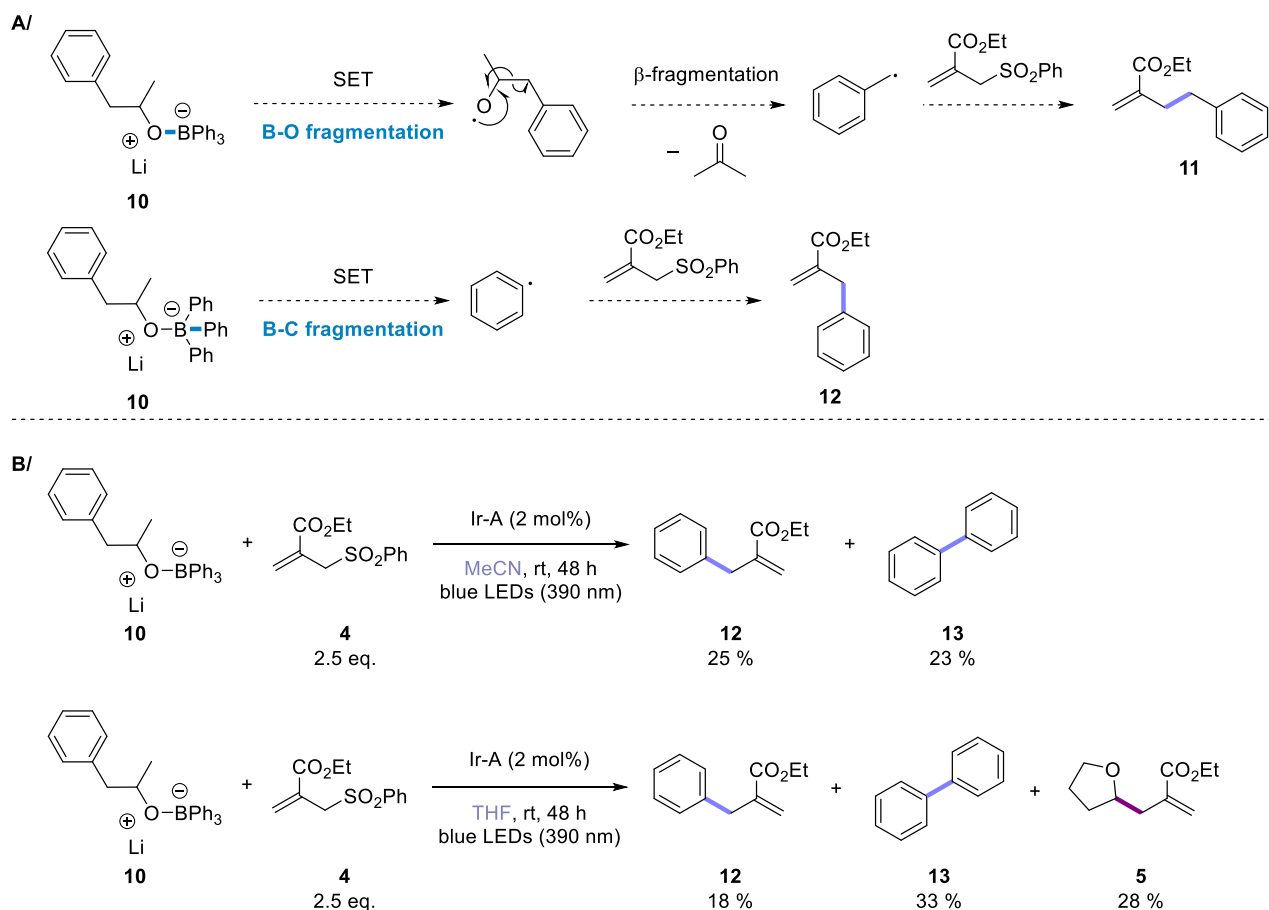
Scheme 29. A/ Expected products depending on the bond fragmentation. B/ Obtained products from the photoredox reaction of complex **10**.

In THF as a solvent, the addition of a THF ring on the radical trap was observed (product **5**); this is in accordance with the ability of aryl radicals to perform efficient HAT from electron-rich C-H bonds (k = 4.8×10^6 M^{-1} s^{-1} for THF, 298 K).[169] The resulting nucleophilic alpha-oxy radical could efficiently add to the electron-deficient double bond of the trap. Overall, the aryl radical seemed to be formed more efficiently in THF than in MeCN, although the HAT pathway is undesired in our case.

It is worth mentioning at this point that aryl radicals are generated, in the vast majority, under light homolysis or reductive conditions (from aryl halides, aryldiazonium salts, aryl carboxylic acids,…).[170] Two notable exceptions have been described in section 2.1.3.3 (Scheme 20). Yoshimi and Bloom both reported the generation of aryl radicals from the oxidation of arylborate starting materials, as discussed in Section 2.1.3.3 (Scheme 20).[154,155] Interestingly, Yoshimi and co-workers explored different borates, including triphenylborane. They observed a decrease in yield by half compared to their arylboronic acid precursor, but do not give a hint on whether they observed the biphenyl byproduct **13**.

The biphenyl product formation is resulting from an undesired pathway, although its formation is not completely clear. A first but rather unlikely possibility would be a radical-radical coupling between two aryl radicals. A more likely pathway would the intermolecular addition of an aryl radical to a phenyl moiety. A very general pathway for this reaction is addition of the aryl radical to a phenyl ring, oxidation of the resulting radical to the cation and loss of a proton to give the rearomatized, biphenyl product (Scheme 30A)[168]. This is usually observed in aromatic solvents, so in presence of a large excess of the phenyl derivative in the reaction mixture. Although not the case here, HAT on THF generates benzene

so this pathway could be effective and explain the higher yield of the biphenyl product observed in THF compared to the reaction run in MeCN (33% versus 23%, see Scheme 29B). A similar reaction could potentially occur on a phenyl group present in the starting material (Scheme 30B).
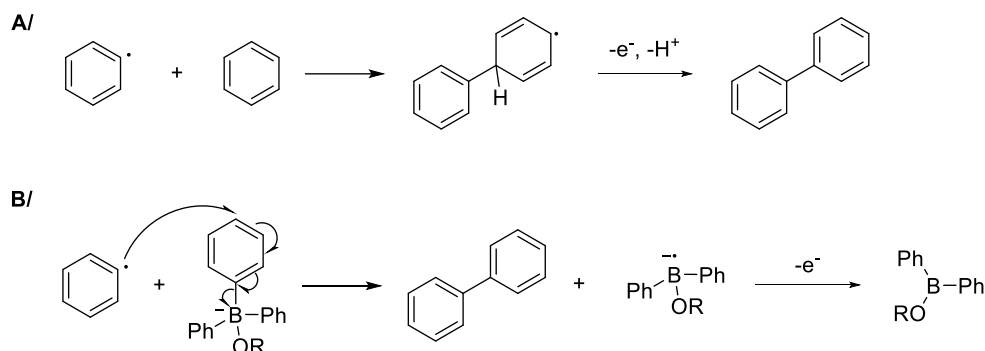
Scheme 30. Possible pathways for the biphenyl formation. A/ Phenyl radical addition to benzene. B/ Intermolecular phenyl radical addition to the starting boron-ate complex.

Based on literature reports, a more likely pathway is however the ligand-ligand coupling of the starting organoborate, more precisely the intramolecular reaction between two phenyl groups attached to the boron atom in presence of an oxidant.[128,132,133] The invoked mechanism is based on single-electron oxidation of the ate-complex followed by 1,2-rearrangement and loss of a second electron to give the biphenyl product (Scheme 31).
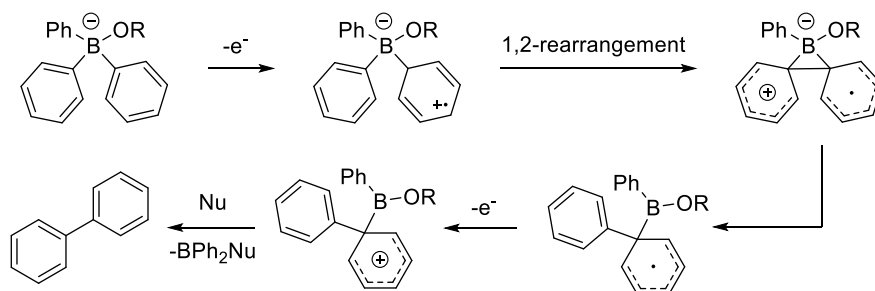
Scheme 31. Ligand-ligand coupling of the starting complex **10**.

This reaction usually requires the presence of stoichiometric amounts of oxidants or the presence of oxygen as terminal oxidant.

This information should be considered in light of our envisioned mechanism for this reaction (Scheme 32). Upon light excitation, the catalyst is promoted to its excited state and reductive quenching occurs to generate the aryl radical from our boron-ate complex **10**. Addition of the aryl radical to the allylsulfone trap gives the product **12** and a sulfonyl radical which is responsible for oxidizing the catalyst back to its ground state (Ir[III]), thus closing the catalytic cycle. In the case of a reaction in THF, the aryl radical first performs a hydrogen atom transfer to the solvent. The generated alpha-oxy radical adds to the allylsulfone trap to give **5**, thus also generating a sulfinyl radical able to close the catalytic cycle. Considering the possibilities discussed for the formation of the biphenyl product **13** and our mechanistic hypothesis, it becomes clear that in our reaction, for each molecule of biphenyl formed, the catalyst cannot be regenerated (no sulfinyl radical is formed). Even more dramatically, an additional oxidation event seems to be necessary, killing further the catalytic activity. Hence the formation of this product should be fully suppressed if a good yield of the desired product is to be obtained.
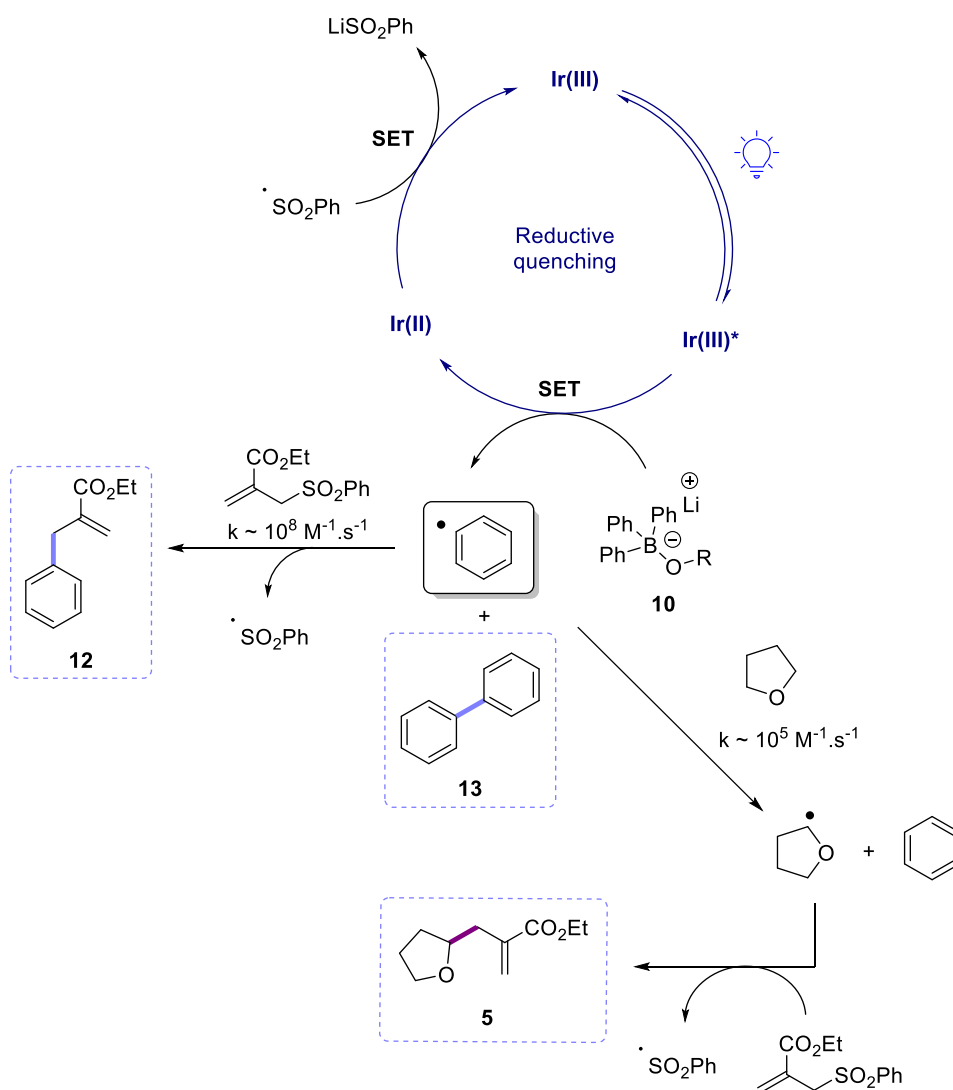
Scheme 32. Envisioned mechanism for the generation and further reactivity of the phenyl radical.

2.2.3.2.   Optimization and reaction design

With these requirements in mind, a small optimization was undertaken (see supporting information). Notably, switching the alcohol to the simpler iPrOH significantly improved the yield of the reaction in acetonitrile. The formation of the biphenyl product was reduced to 11% and 53% of the desired product were obtained (Scheme 33).
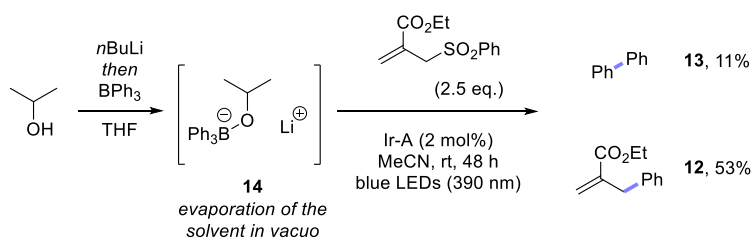
Scheme 33. Generation of the phenyl radical from complex **15**.

Interestingly, a nBuLi complex instead of the usual alkoxide complex gave exclusively the biphenyl product, albeit in low yield (28%). No product resulting from the phenyl radical was observed,

indicating that the alkoxide complex is beneficial for the reaction. It might also suggest that the synthesis of the alkoxide complex might need to be improved, since it cannot be excluded that some nBu-BPPh$_3$Li is formed as well.

With these encouraging results in hand, we turned our attention to a slightly more complex reaction. As mentioned and demonstrated before, aryl radicals are good at hydrogen atom abstraction; the precessus is thermodynamically favored because the newly formed aryl-hydrogen bond is stronger than the starting alkyl-hydrogen bond, even for primary alkyl groups.[9] But aryl radicals are even better at iodine abstraction, for the same reasons, and will abstract iodine atoms faster than hydrogen atoms ($k = 10^9$ M^{-1}s^{-1} for a secondary iodide, $k = 10^5$ M^{-1}s^{-1} for secondary alkyl C-H bonds, 298 K) (Figure 18).[168] Hence the system could be used to efficiently generate alkyl radicals, ideally primary alkyl radicals, from alkyl iodides using our boron-ate complex as radical precursor.
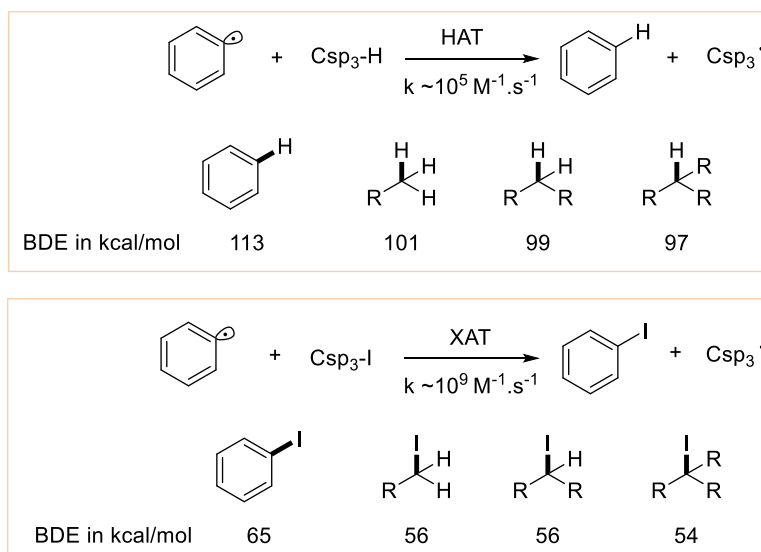
Figure 18. Bond Dissociation Energies of alkyl C-H and alkyl C-I bonds compared to Ar-H and Ar-I bonds.

Such chemistry has been previously explored (Scheme 34). In 2018, Landais and co-workers reported the generation of aryl radicals from arylboronic acids, this time by addition of an alkoxyl radical (resulting from the thermal decomposition of DTBHN) to the boron center.[171] Subsequent iodine abstraction alpha to an electron-withdrawing group formed an electrophilic, carbon-centered radical that was able to add to an alkene. The resulting radical of this cascade was finally trapped by a sulfonyl derived radical trap. In their system the generated sulfonyl radical was unfortunately not able to sustain the chain, so 1.2 equivalents of DTBHN were necessary for the reaction to proceed. In 2019, the same group reported a similar reaction, this time generating the aryl radical *via* single electron transfer from an electron-donor-acceptor (EDA) complex between diaryliodonium salt and triethylamine.[172] This allowed them to somewhat increase the scope of possible alkyl iodides amenable to the reaction, but the aryl precursor still had to be used in stoichiometric amounts.
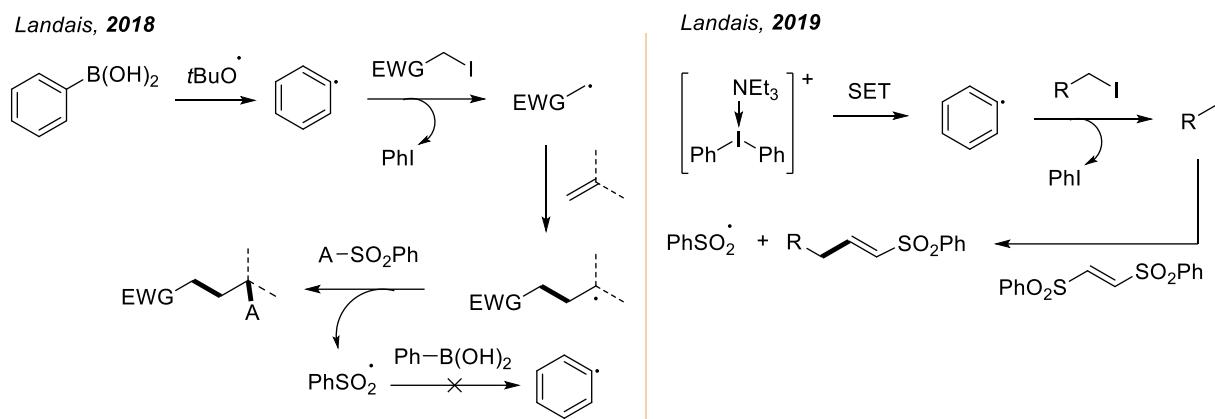
Scheme 34. Literature precedence on the use of aryl radicals for iodine abstraction.

Considering this literature precedence, a cyclic, secondary iodine was chosen in combination with a vinylsulfone trap **15** to test our reaction hypothesis. The vinyl sulfone was chosen instead of the allyl sulfone trap because the corresponding product was known and described in the literature. The mechanism envisioned for this transformation is similar to the one previously shown, but the aryl radical should now perform iodine abstraction before adding to the sulfone trap (Scheme 35).
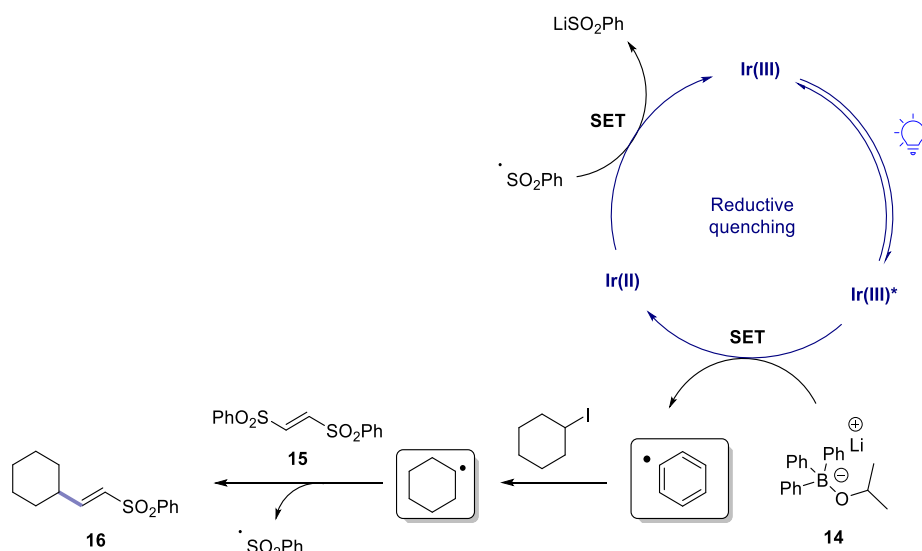
Scheme 35. Envisioned mechanism for the iodine abstraction pathway.

Gratifyingly, using a stoichiometric mixture of the ate-complex **14** and the iodine with 2 equivalents of vinylsulfone trap and 2 mol% of iridium catalyst, the desired product **16** was obtained in 41% yield with 9% yield of the undesired biphenyl product (Scheme 36). No product resulting from phenyl radical addition to the trap was observed. From there, a preliminary optimization was carried out to find the right ratio of reactants and best solvent (Table 1).
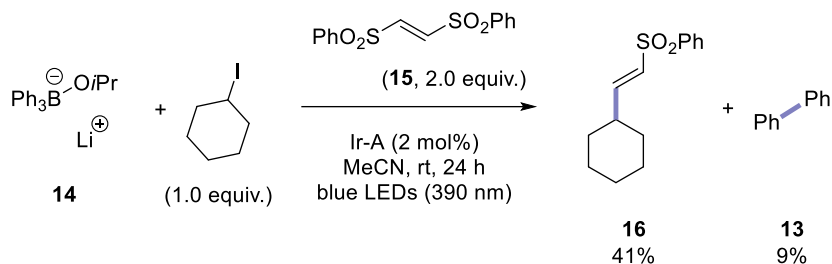
Scheme 36. Proof of concept for the phenyl radical generation under photoredox conditions and subsequent iodine abstraction.

Entry	Solvent	Equiv. trap	Equiv. Iodide	Yield of **16**	Yield of **13**	Other
1 (initial conditions)	MeCN	2	1	41%	9%	
2	DCE	2	1	36%	23%	
3	DCE	2	2	38%	/	
4	MeCN	2	2	44%	6%	
5	MeCN	2	2	31%	/	4 mol% Ir-A

Table 1. Preliminary optimization for the iodine abstraction reaction.

Changing the solvent to DCE proved initially not useful with a sharp increase in the biphenyl formation (entry 2). This was solved by using an excess of iodine, but unfortunately the yield of desired product dropped slightly (although not very significantly, entries 1 and 3). Still, the same reaction in acetonitrile gave the best yield with 44% of desired product despite 6% of biphenyl side product. Increasing the catalyst loading to 4 mol% decreased both the formation of the side and desired products.

2.3. Conclusion and outlook

Although 44% yield is encouraging for this catalytic reaction, the yield should be further increased, and the reaction applied to more challenging primary alkyl iodides. In light of the preliminary results, it seems reasonable to screen more solvents and to investigate the effect of concentration on the reaction. Even THF could be considered, in combination with a higher excess of radical trap to suppress HAT. This would as well allow to generate the complex and run the photoredox reaction in a one pot process. Naturally, different catalysts could be tested for the reaction as well. Finally, a survey of different boron-ate complexes should be carried out, in particular complexes with less phenyl rings such as the arylboronic acid. This boron precursor has literature precedence for the formation of aryl and heteroaryl radicals (Scheme 20). If the biphenyl product is indeed formed by ligand-ligand coupling (Scheme 31), then this would surely be beneficial. Moreover, the effect of additives should be tested, for example the addition of a Lewis base in the reaction mixture to quench the released Lewis acid (BPh$_2$OR) during the course of the reaction.

The desired alkoxyl radical intermediate could not be obtained from a variety of boron-ate complexes. In the case of the B(C$_6$F$_5$)$_3$ precursor, the desired ate-complex could not be synthesized. Instead, a

water adduct was obtained. Upon addition of an alkoxide to this water adduct, a lithium coordinated adduct was isolated and characterized. None of these species showed any sign of oxidation by the iridium catalyst. The electron poor moieties in the boron-ate complex might have increased the overall oxidation potential of the complex. In a continuation of this project, it would be beneficial to calculate the oxidation potential of the water adduct (deprotonated or not).

In the case of the BPh$_3$ precursor, the undesired B-C bond fragmentation was operative. No product arising from the B-O bond fragmentation could ever be observed. It has been previously described that the homolytic fragmentation of a B-O bond is reversible.[173] In a 1985 report, Scaiano reported that the addition of the *tert*-butoxy radical at the boron center of BPh$_3$ occurred at a rate constant of 1.0x10^8 M^{-1}s^{-1} and was followed by a decay to the phenyl radical instead (Scheme 37).[174] A consistent behavior was observed by Landais and co-workers (Scheme 34, first step). The fact that the addition of the alkoxyl radical and generation of the phenyl radical is not reversible at the boron center seems to indicate that generating an alkoxyl radical from our complex **14** was doomed. A similar behavior had been postulated by Wood and co-workers based on ab initio calculations.[175] They showed that complexation of water to a trimethylborane furnished a species activated for O-H bond homolysis and that this resulted in the formation of the methyl radical, rather than the hydroxyl radical.

Scaiano

Wood
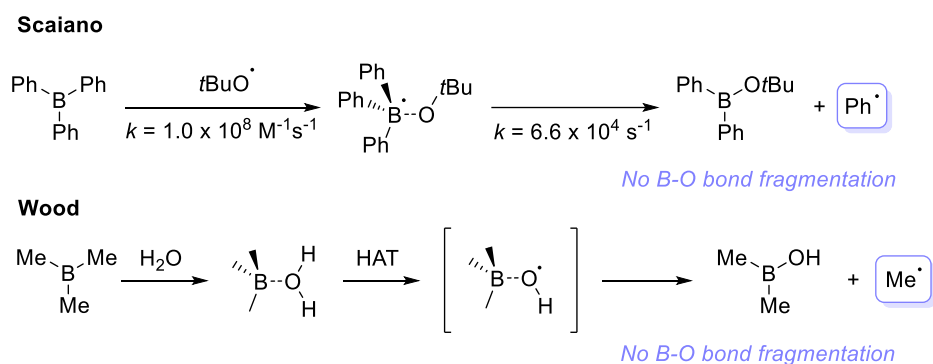
Scheme 37. Literature evidence for preferential B-C bond cleavage over B-O bond cleavage.

This clean boron-phenyl bond fragmentation offered the possibility to generate phenyl radicals under catalytic oxidative conditions and to use these intermediates in an iodine abstraction step. Encouraging preliminary results were obtained towards this direction and would be worth investigating further.

References

1   F. De Vleeschouwer, V. Van Speybroeck, M. Waroquier, P. Geerlings and F. De Proft, *Org. Lett.*, 2007, **9**, 2721–2724.

2   J. Hartung, T. Gottwald and K. Špehar, *Synthesis*, 2002, 1469–1498.

3   Z. Cekovic, *Tetrahedron*, 2003, **59**, 8073–8090.

4   R. Atkinson, E. S. C. Kwok, J. Arey and S. M. Aschmann, *Faraday Discuss.*, 1995, **100**, 23–37.

5   R. Atkinson, *Atmospheric Environment*, 2007, **41**, 8468–8485.

6   R. Atkinson and W. P. L. Carter, *J Atmos Chem*, 1991, **13**, 195–210.

7   W. Herz, R. C. Ligon, J. A. Turner and J. F. Blount, *J. Org. Chem.*, 1977, **42**, 1885–1895.

8   V. Ullrich and R. Brugger, *Angewandte Chemie International Edition in English*, 1994, **33**, 1911–1919.

9   Y.-R. Luo, *Comprehensive Handbook of Chemical Bond Energies*, CRC Press, Boca Raton, 2007.

10   S. Sarkar, K. P. S. Cheung and V. Gevorgyan, *Chem. Sci.*, 2020, **11**, 12974–12993.

11   Y. Zou, X.-S. Xue, Y. Deng, A. B. Smith and K. N. Houk, *Org. Lett.*, 2019, **21**, 5894–5897.

12   E. I. León, A. Martín, I. Pérez-Martín and E. Suárez, *Org. Lett.*, 2018, **20**, 3385–3389.

13   C. G. Francisco, A. J. Herrera, A. R. Kennedy, A. Martín, D. Melián, I. Pérez-Martín, L. M. Quintanal and E. Suárez, *Chemistry – A European Journal*, 2008, **14**, 10369–10381.

14   S. K. Sinha, S. Guin, S. Maiti, J. P. Biswas, S. Porey and D. Maiti, *Chem. Rev.*, , DOI:10.1021/acs.chemrev.1c00220.

15   X. Bao, Q. Wang and J. Zhu, *Angewandte Chemie International Edition*, 2019, **58**, 2139–2143.

16   J. Zhang, Y. Li, F. Zhang, C. Hu and Y. Chen, *Angewandte Chemie International Edition*, 2016, **55**, 1872–1875.

17   J. Zhang, Y. Li, R. Xu and Y. Chen, *Angewandte Chemie International Edition*, 2017, **56**, 12619–12623.

18   C. Wang, K. Harms and E. Meggers, *Angewandte Chemie*, 2016, **128**, 13693–13696.

19   M. Murakami and N. Ishida, *Chem. Lett.*, 2017, **46**, 1692–1700.

20   D. Johnson, P. Cassanelli and R. Anthony Cox, *Atmospheric Environment*, 2004, **38**, 1755–1765.

21   S. Wilsey, P. Dowd and K. N. Houk, *J. Org. Chem.*, 1999, **64**, 8801–8811.

22   A. L. J. Beckwith and B. P. Hay, *J. Am. Chem. Soc.*, 1989, **111**, 230–234.

23   T. Yoshimitsu, Y. Arano and H. Nagaoka, *J. Org. Chem.*, 2003, **68**, 625–627.

24   C. Carra and J. C. Scaiano, *European Journal of Organic Chemistry*, 2008, 4454–4459.

25   S. M. Cho, J. Y. Kim, S. Han and D. H. Ryu, *J. Org. Chem.*, 2022, **87**, 11196–11203.

26   J. Y. Kim, Y. S. Lee, Y. Choi and D. H. Ryu, *ACS Catal.*, 2020, **10**, 10585–10591.

27   H.-X. Zheng, X.-H. Shan, J.-P. Qu and Y.-B. Kang, *Org. Lett.*, 2018, **20**, 3310–3313.

28   L. Pitzer, F. Sandfort, F. Strieth-Kalthoff and F. Glorius, *J. Am. Chem. Soc.*, 2017, **139**, 13652–13655.

29   P. Dowd and S. C. Choi, *J. Am. Chem. Soc.*, 1987, **109**, 3493–3494.

30   A. L. J. Beckwith, R. Kazlauskas and M. R. Syner-Lyons, *J. Org. Chem.*, 1983, **48**, 4718–4722.

31   T. Singha, A. R. S. Mondal, S. Midya and D. P. Hari, *Chemistry – A European Journal*, , DOI:10.1002/chem.202202025.

32   Y. Zhao, J. Hu, R. Chen, F. Xiong, H. Xie and H. Ding, *J. Am. Chem. Soc.*, , DOI:10.1021/jacs.1c13370.

33   J. Wang and X. Li, *Chem. Sci.*, , DOI:10.1039/D1SC07237D.

34   H. Zhao, X. Fan, J. Yu and C. Zhu, *J. Am. Chem. Soc.*, 2015, **137**, 3490–3493.

35   I. Kempter, A. Groß and J. Hartung, *Tetrahedron*, 2012, **68**, 10378–10390.

36   J. Hartung and R. Kneuer, *Tetrahedron: Asymmetry*, 2003, **14**, 3019–3031.

37   J. Hartung, *European Journal of Organic Chemistry*, 2001, **2001**, 619–632.

38   J. Hartung, in *Radicals in Organic Synthesis*, Wiley-Blackwell, 2008, pp. 427–439.

39   D. C. Spellmeyer and K. N. Houk, *J. Org. Chem.*, 1987, **52**, 959–974.

40   A. L. J. Beckwith and C. H. Schiesser, *Tetrahedron*, 1985, **41**, 3925–3941.

41   L. Coulombel, I. Favier and E. Duñach, *Chem. Commun.*, 2005, 2286–2288.

42   L. Coulombel and E. Duñach, *Green Chem.*, 2004, **6**, 499–501.

43   C. Banoun, F. Bourdreux, E. Magnier and G. Dagousset, *Org. Lett.*, , DOI:10.1021/acs.orglett.1c03444.

44   E. Tsui, A. J. Metrano, Y. Tsuchiya and R. R. Knowles, *Angewandte Chemie International Edition*, 2020, **59**, 11845–11849.

45   D. Crich and X.-S. Mo, *J. Org. Chem.*, 1997, **62**, 8624–8625.

46   J. I. Concepcion, C. G. Francisco, R. Freire, R. Hernandez, J. A. Salazar and E. Suarez, *The Journal of Organic Chemistry*, 1986, **51**, 402–404.

47   J. I. Concepción, C. G. Francisco, R. Hernández, J. A. Salazar and E. Suárez, *Tetrahedron Letters*, 1984, **25**, 1953–1956.

48   D. H. R. Barton, J. M. Beaton, L. E. Geller and M. M. Pechet, 1961, **83**, 8.

49   D. J. Pasto and F. Cottard, *Tetrahedron Letters*, 1994, **35**, 4303–4306.

50   C. Walling, 1963, **85**, 5.

51   J. E. Leffler, *Chem. Rev.*, 1949, **45**, 385–417.

52   V. M. Mićović, R. I. Mamuzić, D. Jeremić and M. Lj. Mihailović, *Tetrahedron*, 1964, **20**, 2279–2287.

53   A. Clerici, F. Minisci, K. Ogawa and J.-M. Surzur, *Tetrahedron Letters*, 1978, **19**, 1149–1152.

54   K. Heusler, *Tetrahedron Letters*, 1964, **5**, 3975–3982.

55   S. E. Schaafsma, R. Jorritsma, H. Steinberg and Th. J. de Boer, *Tetrahedron Letters*, 1973, **14**, 827–830.

56 Y. Zhou, M. Wu, Y. Liu, C. Cheng and G. Zhu, *Org. Lett.*, , DOI:10.1021/acs.orglett.0c02735.

57 Y. Zhu, Z. Zhang, R. Jin, J. Liu, G. Liu, B. Han and N. Jiao, *Angewandte Chemie*, , DOI:10.1002/ange.202007187.

58 S. Ren, C. Feng and T.-P. Loh, *Organic & Biomolecular Chemistry*, 2015, **13**, 5105–5109.

59 N. Ishida, S. Okumura, Y. Nakanishi and M. Murakami, *Chem. Lett.*, 2015, **44**, 821–823.

60 R.-C. Raclea, P. Natho, L. A. T. Allen, A. J. P. White and P. J. Parsons, *J. Org. Chem.*, 2020, **85**, 9375–9385.

61 Y. Zhu, K. Huang, J. Pan, X. Qiu, X. Luo, Q. Qin, J. Wei, X. Wen, L. Zhang and N. Jiao, *Nat Commun*, 2018, **9**, 2625.

62 R. Ren, H. Zhao, L. Huan and C. Zhu, *Angewandte Chemie International Edition*, 2015, **54**, 12692–12696.

63 H. Ren, J.-R. Song, Z.-Y. Li and W.-D. Pan, *Org. Lett.*, 2019, **21**, 6774–6778.

64 J.-L. Shi, Z. Wang, R. Zhang, Y. Wang and J. Wang, *Chemistry – A European Journal*, 2019, **25**, 8992–8995.

65 K. Jia, F. Zhang, H. Huang and Y. Chen, *J. Am. Chem. Soc.*, 2016, **138**, 1514–1517.

66 K. Jia, Y. Pan and Y. Chen, *Angewandte Chemie*, 2017, **129**, 2518–2521.

67 K. Jia, J. Li and Y. Chen, *Chemistry – A European Journal*, 2018, **24**, 3174–3177.

68 D. Wang, J. Mao and C. Zhu, *Chem. Sci.*, 2018, **9**, 5805–5809.

69 X. Hu, G.-X. Li, G. He and G. Chen, *Organic Chemistry Frontiers*, 2019, **6**, 3205–3209.

70 X. Wu, H. Zhang, N. Tang, Z. Wu, D. Wang, M. Ji, Y. Xu, M. Wang and C. Zhu, *Nat Commun*, 2018, **9**, 3343.

71 G.-X. Li, X. Hu, G. He and G. Chen, *Chem. Sci.*, 2019, **10**, 688–693.

72 Y. Wang, Y. Bao, M. Tang, Z. Ye, Z. Yuan and G. Zhu, *Chem. Commun.*, , DOI:10.1039/D2CC00369D.

73 S. L. Rössler, B. J. Jelier, E. Magnier, G. Dagousset, E. M. Carreira and A. Togni, *Angewandte Chemie International Edition*, , DOI:10.1002/anie.201911660.

74 V. Quint, F. Morlet-Savary, J.-F. Lohier, J. Lalevée, A.-C. Gaumont and S. Lakhdar, *J. Am. Chem. Soc.*, 2016, **138**, 7436–7441.

75 A. Inial, F. Morlet-Savary, J. Lalevée, A. Gaumont and S. Lakhdar, *Org. Lett.*, , DOI:10.1021/acs.orglett.0c01409.

76 A.-L. Barthelemy, B. Tuccio, E. Magnier and G. Dagousset, *Angewandte Chemie International Edition*, 2018, **57**, 13790–13794.

77 C. Shu, R. Madhavachary, A. Noble and V. K. Aggarwal, *Org. Lett.*, 2020, **22**, 7213–7218.

78 J. F. Hoskin and E. J. Sorensen, *J. Am. Chem. Soc.*, , DOI:10.1021/jacs.2c06504.

79 E. Tsui, H. Wang and R. Knowles, *Chem. Sci.*, , DOI:10.1039/D0SC04542J.

80 H. Yin, P. J. Carroll, J. M. Anna and E. J. Schelter, *J. Am. Chem. Soc.*, 2015, **137**, 9234–9237.

81 H. Yin, P. J. Carroll, B. C. Manor, J. M. Anna and E. J. Schelter, *J. Am. Chem. Soc.*, 2016, **138**, 5984–5993.

82

83 J.-J. Guo, A. Hu, Y. Chen, J. Sun, H. Tang and Z. Zuo, *Angewandte Chemie International Edition*, 2016, **55**, 15319–15322.

84 Y. Chen, J. Du and Z. Zuo, *Chem*, 2020, **6**, 266–279.

85 T. Xue, Z. Zhang and R. Zeng, *Org. Lett.*, , DOI:10.1021/acs.orglett.1c04365.

86 A. Hu, Y. Chen, J.-J. Guo, N. Yu, Q. An and Z. Zuo, *J. Am. Chem. Soc.*, 2018, **140**, 13580–13585.

87 K. Zhang, L. Chang, Q. An, X. Wang and Z. Zuo, *J. Am. Chem. Soc.*, 2019, **141**, 10556–10564.

88 Y. Chen, X. Wang, X. He, Q. An and Z. Zuo, *J. Am. Chem. Soc.*, , DOI:10.1021/jacs.1c00618.

89 Z. Yang, D. Yang, J. Zhang, C. Tan, J. Li, S. Wang, H. Zhang, Z. Huang and A. Lei, *J. Am. Chem. Soc.*, , DOI:10.1021/jacs.2c05520.

90 A. Hu, J.-J. Guo, H. Pan, H. Tang, Z. Gao and Z. Zuo, *J. Am. Chem. Soc.*, 2018, **140**, 1612–1616.

91 A. Hu, J.-J. Guo, H. Pan and Z. Zuo, *Science*, 2018, **361**, 668–672.

92 Q. An, Z. Wang, Y. Chen, X. Wang, K. Zhang, H. Pan, W. Liu and Z. Zuo, *J. Am. Chem. Soc.*, 2020, **142**, 6216–6226.

93 F. Liu, S. Ma, Z. Lu, A. Nangia, M. Duan, Y. Yu, G. Xu, Y. Mei, M. Bietti and K. N. Houk, *J. Am. Chem. Soc.*, 2022, **144**, 6802–6812.

94 Q. Yang, Y.-H. Wang, Y. Qiao, M. Gau, P. J. Carroll, P. J. Walsh and E. J. Schelter, *Science*, 2021, **372**, 847–852.

95 P. R. D. Murray, J. H. Cox, N. D. Chiappini, C. B. Roos, E. A. McLoughlin, B. G. Hejna, S. T. Nguyen, H. H. Ripberger, J. M. Ganley, E. Tsui, N. Y. Shin, B. Koronkiewicz, G. Qiu and R. R. Knowles, *Chem. Rev.*, , DOI:10.1021/acs.chemrev.1c00374.

96 J. W. Darcy, B. Koronkiewicz, G. A. Parada and J. M. Mayer, *Acc. Chem. Res.*, 2018, **51**, 2391–2399.

97 J. E. Nutting, M. Rafiee and S. S. Stahl, *Chem. Rev.*, 2018, **118**, 4834–4885.

98 H. G. Yayla, H. Wang, K. T. Tarantino, H. S. Orbe and R. R. Knowles, *J. Am. Chem. Soc.*, 2016, **138**, 10794–10797.

99 R. Chuard, A. Giraud and P. Renaud, *Angewandte Chemie International Edition*, 2002, **41**, 4321–4323.

100 R. Chuard, A. Giraud and P. Renaud, *Angewandte Chemie International Edition*, 2002, **41**, 4323–4325.

101 K. Zhao, G. Seidler and R. R. Knowles, *Angewandte Chemie International Edition*, , DOI:10.1002/anie.202105285.

102 J. Wang, B. Huang, C. Shi, C. Yang and W. Xia, *J. Org. Chem.*, 2018, **83**, 9696–9706.

103 T. Ji, X.-Y. Chen, L. Huang and M. Rueping, *Org. Lett.*, 2020, **22**, 2579–2583.

104 L. Huang, T. Ji, C. Zhu, H. Yue, N. Zhumabay and M. Rueping, *Nat Commun*, 2022, **13**, 809.

105 X. Wang, Y. Li and X. Wu, *ACS Catal.*, 2022, 3710–3718.

106 T. R. McDonald, L. R. Mills, M. S. West and S. A. L. Rousseaux, *Chem. Rev.*, 2021, **121**, 3–79.

107 A. Nikolaev and A. Orellana, *Synthesis*, 2016, **48**, 1741–1768.

108 L. Huang, T. Ji and M. Rueping, *J. Am. Chem. Soc.*, 2020, **142**, 3532–3539.

109 J. Lu, Y. Tong, N. Hao, L. Zhang, J. Wei, Z. Zhang, Q. Fu, D. Yi, J. Wang, Y. Mu, X. Pan, L. Yang, S. Wei and L. Zhong, *Org. Chem. Front.*, , DOI:10.1039/D1QO01844B.

110 E. Ota, H. Wang, N. L. Frye and R. R. Knowles, *Journal of the American Chemical Society*, , DOI:10.1021/jacs.8b12552.

111 K. Zhao, K. Yamashita, J. E. Carpenter, T. C. Sherwood, W. R. Ewing, P. T. W. Cheng and R. R. Knowles, *Journal of the American Chemical Society*, , DOI:10.1021/jacs.9b03973.

112 S. T. Nguyen, E. A. McLoughlin, J. H. Cox, B. P. Fors and R. R. Knowles, *J. Am. Chem. Soc.*, , DOI:10.1021/jacs.1c05330.

113 S. Bloom, D. D. Bume, C. R. Pitts and T. Lectka, *Chemistry – A European Journal*, 2015, **21**, 8060–8063.

114 F. J. Aguilar Troyano, K. Merkens and A. Gómez-Suárez, *Asian Journal of Organic Chemistry*, 2020, **9**, 992–1007.

115 M. Ji, Z. Wu and C. Zhu, *Chem. Commun.*, 2019, **55**, 2368–2371.

116 L. Cardinale, M. Neumeier, M. Majek and A. Jacobi von Wangelin, *Org. Lett.*, 2020, **22**, 7219–7224.

117 J. Liu, E. Xu, J. Jiang, Z. Huang, L. Zheng and Z.-Q. Liu, *Chem. Commun.*, 2020, **56**, 2202–2205.

118 T. Kikuchi, K. Yamada, T. Yasui and Y. Yamamoto, *Org. Lett.*, , DOI:10.1021/acs.orglett.1c01436.

119 X. Wu, M. Wang, L. Huan, D. Wang, J. Wang and C. Zhu, *Angewandte Chemie International Edition*, 2018, **57**, 1640–1644.

120 M. Wang, L. Huan and C. Zhu, *Org. Lett.*, 2019, **21**, 821–825.

121 G. A. Molander and N. Ellis, *Acc. Chem. Res.*, 2007, **40**, 275–286.

122 K. K. Das and S. Panda, *Chemistry – A European Journal*, 2020, **26**, 14270–14282.

123 H. Wang, C. Jing, A. Noble and V. K. Aggarwal, *Angewandte Chemie International Edition*, 2020, **59**, 16859–16872.

124 C. Sandford and V. K. Aggarwal, *Chem. Commun.*, 2017, **53**, 5481–5494.

125 D. H. Geske, *J. Phys. Chem.*, 1962, **66**, 1743–1744.

126 S. B. Beil, S. Möhle, P. Enders and S. R. Waldvogel, *Chem. Commun.*, 2018, **54**, 6128–6131.

127 P. K. Pal, S. Chowdhury, M. G. B. Drew and D. Datta, *New J. Chem.*, 2002, **26**, 367–371.

128 P. Abley and J. Halpern, *J. Chem. Soc. D*, 1971, 1238–1239.

129 H. Mizuno, H. Sakurai, T. Amaya and T. Hirao, *Chemical Communications*, 2006, **0**, 5042–5044.

130 J. D. Wilkey and G. B. Schuster, *J. Org. Chem.*, 1987, **52**, 2117–2122.

131 A. Pelter, R. T. Pardasani and P. Pardasani, *Tetrahedron*, 2000, **56**, 7339–7369.

132 R. N. Dhital and H. Sakurai, *Asian Journal of Organic Chemistry*, 2014, **3**, 668–684.

133 C. Gerleve and A. Studer, *Angewandte Chemie International Edition*, 2020, **59**, 15468–15473.

134 R. Rasappan and V. K. Aggarwal, *Nature Chemistry*, 2014, **6**, 810–814.

135 J.-P. Goddard, C. Ollivier and L. Fensterbank, *Acc. Chem. Res.*, 2016, **49**, 1924–1936.

136 S. Darses and J.-P. Genet, *Chem. Rev.*, 2008, **108**, 288–325.

137 G. A. Molander, *J. Org. Chem.*, 2015, **80**, 7837–7848.

138 S. Darses, J.-P. Genêt, J.-L. Brayer and J.-P. Demoute, *Tetrahedron Letters*, 1997, **38**, 4393–4396.

139 T. Koike and M. Akita, *Org. Biomol. Chem.*, 2016, **14**, 6886–6890.

140 Y. Yasu, T. Koike and M. Akita, *Advanced Synthesis & Catalysis*, 2012, **354**, 3414–3420.

141 K. Miyazawa, Y. Yasu, T. Koike and M. Akita, *Chem. Commun.*, 2013, **49**, 7249–7251.

142 D. Hanss, J. C. Freys, G. Bernardinelli and O. S. Wenger, *European Journal of Inorganic Chemistry*, 2009, **2009**, 4850–4859.

143 J. C. Tellis, D. N. Primer and G. A. Molander, *Science*, 2014, **345**, 433–436.

144 D. N. Primer, I. Karakaya, J. C. Tellis and G. A. Molander, *J. Am. Chem. Soc.*, 2015, **137**, 2195–2198.

145 F. Lima, U. K. Sharma, L. Grunenberg, D. Saha, S. Johannsen, J. Sedelmeier, E. V. Van der Eycken and S. V. Ley, *Angewandte Chemie International Edition*, 2017, **56**, 15136–15140.

146 F. Lima, M. A. Kabeshov, D. N. Tran, C. Battilocchio, J. Sedelmeier, G. Sedelmeier, B. Schenkel and S. V. Ley, *Angewandte Chemie International Edition*, 2016, **55**, 14085–14089.

147 F. Lima, L. Grunenberg, H. B. A. Rahman, R. Labes, J. Sedelmeier and S. V. Ley, *Chem. Commun.*, 2018, **54**, 5606–5609.

148 Z.-Q. Zhang, Y.-Q. Sang, C.-Q. Wang, P. Dai, X.-S. Xue, J. L. Piper, Z.-H. Peng, J.-A. Ma, F.-G. Zhang and J. Wu, *J. Am. Chem. Soc.*, , DOI:10.1021/jacs.2c05356.

149 C. Shu, A. Noble and V. K. Aggarwal, *Angewandte Chemie International Edition*, 2019, **58**, 3870–3874.

150 D. Kaiser, A. Noble, V. Fasano and V. K. Aggarwal, *J. Am. Chem. Soc.*, 2019, **141**, 14104–14109.

151 H. Wang, J. Wu, A. Noble and V. K. Aggarwal, *Angewandte Chemie International Edition*, 2022, **61**, e202202061.

152 F. Clausen, M. Kischkewitz, K. Bergander and A. Studer, *Chemical Science*, 2019, **10**, 6210–6214.

153 D. S. Matteson, *Journal of Organometallic Chemistry*, 1999, **581**, 51–65.

154 Y. Iwata, Y. Tanaka, S. Kubosaki, T. Morita and Y. Yoshimi, *Chem. Commun.*, 2018, **54**, 1257–1260.

155 M. Chilamari, J. R. Immel and S. Bloom, *ACS Catal.*, 2020, 12727–12737.

156 S. Rieder, Thesis manuscript, University of Bern, 2017.

157 Z. Yu, Y. Li, J. Shi, B. Ma, L. Liu and J. Zhang, *Angewandte Chemie International Edition*, 2016, **55**, 14807–14811.

158 K. Bläsing, J. Bresien, R. Labbow, A. Schulz and A. Villinger, *Angewandte Chemie International Edition*, 2018, **57**, 9170–9175.

159 T. Beringhelli, D. Maggioni and G. D'Alfonso, *Organometallics*, 2001, **20**, 4927–4938.

160 C. Bergquist, B. M. Bridgewater, C. J. Harlan, J. R. Norton, R. A. Friesner and G. Parkin, *J. Am. Chem. Soc.*, 2000, **122**, 10581–10590.

161 A. A. Danopoulos, J. R. Galsworthy, M. L. H. Green, L. H. Doerrer, S. Cafferkey and M. B. Hursthouse, *Chem. Commun.*, 1998, **0**, 2529–2560.

162 D. C. Bradley, I. S. Harding, A. D. Keefe, M. Motevalli and D. H. Zheng, *Journal of the Chemical Society, Dalton Transactions*, 1996, 3931.

163 F. Focante, I. Camurati, L. Resconi, S. Guidotti, T. Beringhelli, G. D'Alfonso, D. Donghi, D. Maggioni, P. Mercandelli and A. Sironi, *Inorg. Chem.*, 2006, **45**, 1683–1692.

164 A. Noble and D. W. C. MacMillan, *J. Am. Chem. Soc.*, 2014, **136**, 11602–11605.

165 C. He, S. Guo, L. Huang and A. Lei, *J. Am. Chem. Soc.*, 2010, **132**, 8273–8275.

166 S. Pietsch, E. C. Neeve, D. C. Apperley, R. Bertermann, F. Mo, D. Qiu, M. S. Cheung, L. Dang, J. Wang, U. Radius, Z. Lin, C. Kleeberg and T. B. Marder, *Chemistry – A European Journal*, 2015, **21**, 7082–7098.

167 M. R. Heinrich, *Chemistry – A European Journal*, 2009, **15**, 820–833.

168 C. Galli, *Chem. Rev.*, 1988, **88**, 765–792.

169 J. C. Scaiano and L. C. Stewart, *J. Am. Chem. Soc.*, 1983, **105**, 3609–3614.

170 N. Kvasovs and V. Gevorgyan, *Chem. Soc. Rev.*, 2021, **50**, 2244–2259.

171 R. Hara, C. Khiar, N. S. Dange, P. Bouillac, F. Robert and Y. Landais, *European Journal of Organic Chemistry*, 2018, **2018**, 4058–4063.

172 A. Chaambi, G. Kurtay, R. Abderrahim, F. Robert and Y. Landais, *Helvetica Chimica Acta*, 2019, **102**, e1900140.

173 A.-P. Schaffner and P. Renaud, *European Journal of Organic Chemistry*, 2004, **2004**, 2291–2298.

174 D. Griller, K. U. Ingold, L. K. Patterson, J. C. Scaiano and R. D. Small, *J. Am. Chem. Soc.*, 1979, **101**, 3780–3785.

175 D. A. Spiegel, K. B. Wiberg, L. N. Schacherer, M. R. Medeiros and J. L. Wood, *J. Am. Chem. Soc.*, 2005, **127**, 12513–12515.

Supporting information

Table of content

General information

All the glassware was oven-dried at 160 °C or flame-dried under vacuum, assembled hot and allowed to cool under a positive pressure of nitrogen. Unless otherwise stated, all reactions were performed under nitrogen atmosphere. Non-aqueous reagents were transferred under nitrogen *via* syringe or cannula. Silica gel 60 Å (230–400 mesh particle size, SiliCycle) and aluminum oxide neutral (40–160 µm) were used for flash column chromatography. Thin layer chromatography (TLC) was performed on 0.25 mm silica gel 60 with fluorescent indicator UV 254; visualization under UV light (254 nm) or by staining with a solution of potassium permanganate [KMnO$_4$ (3 g), K$_2$CO$_3$ (20 g) and NaOH 5% (3 mL) in H$_2$O (300 mL)] and subsequent heating.

Instrumentation

^{1}H, ^{13}C, ^{11}B and ^{19}F NMR spectra were recorded on a 300 MHz spectrometer (^{1}H: 300 MHz, ^{13}C: 75 MHz, ^{11}B: 96 MHz, ^{19}F: 282 MHz) and on a 400 MHz spectrometer (^{1}H: 400 MHz, ^{13}C: 101 MHz) operating at 22 °C, unless otherwise stated. Chemical shifts (δ) were reported in parts per million with the residual solvent peak used as an internal standard (CDCl$_3$: δ = 7.26 ppm and CD$_2$Cl$_2$: δ = 5.32 ppm for ^{1}H NMR spectra and CDCl$_3$: δ = 77.0 ppm and CD$_2$Cl$_2$: δ = 53.84 ppm for ^{13}C NMR spectra). The following

abbreviations were used to explain the multiplicities: s (singlet), d (doublet), t (triplet), q (quadruplet), p (pentuplet), hx (hexuplet), hp (heptuplet), m (multiplet), br (broad). The prefix app (apparent) was added when different coupling constants appeared accidentally equal. Coupling constants *J* are reported in Hz and with an accuracy of one unit of the last digit. HRMS analyses were recorded on a hybrid quadrupole time-of-flight mass spectrometer using positive electrospray and on a double-focusing magnetic sector mass spectrometer using electron impact (70 eV). Mass spectra were measured in electron impact (EI) mode at 70 eV, with solid probe inlet, source temperature of 200 °C, acceleration voltage of 5 kV, and resolution of 2'500. The instrument was scanned between m/z 50 and 1000 at scan rate of 2 s / decade in the magnetic scan mode. Perfluorokerosene served for calibration. Infrared spectra were recorded neat on an FT-IR spectrometer equipped with a Golden Gate Single Reflection Diamond ATR System and are reported in wave numbers (cm^{-1}). Kessil lamps were used for photoredox reactions and were run at maximum power (100 W) 5 cm away from reaction vessel with a cooling fan.

Materials

Unless otherwise stated, all reagents were obtained from commercial sources and used without further purification. Solvents for reactions (THF, Et_2O, CH_2Cl_2, n-hexane) were first distilled then filtered over two columns of dried alumina under a positive pressure of argon. Commercial benzene and toluene were filtered over two columns of dried alumina under a positive pressure of argon. Solvents for extraction and flash column chromatography were of technical grade and were distilled prior to use. Commercial photocatalysts (Strem or Aldrich) were used without purification.

Experimental procedures

Model reaction
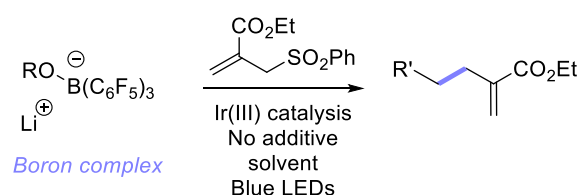
General procedure 1 – Model reaction for probing alkoxyl radical generation

To a seal-tube were added the radical trap ethyl 2-(benzenesulfonylmethyl)prop-2-enoate (104 mg, 0.40 mmol, 2.0 equiv.) and [Ir{dF(CF_3)ppy}$_2$(dtbpy)]PF$_6$ (4.5 mg, 0.004 mmol, 2 mol%). The tube was sealed and evacuated/refilled with N_2 (3 x). A 0.1 M solution of the appropriate boron complex in the reaction solvent was added *via* syringe (2 mL, 0.20 mmol, 1.0 equiv.). The tube was placed in front of

a 390 nm blue light for 24 hours. The reaction mixture was evaporated under reduced pressure to give the crude product. Purification by fcc on silica gel afforded pure product.

B(C$_6$F$_5$)$_3$ complexes

B(C$_6$F$_5$)$_3$•3H$_2$O (1•3H$_2$O)

To a flame-dried, three-neck, 1-L round-bottom flask equipped with a dropping funnel, an argon inlet and a thermometer was added bromo(pentafluoro)benzene (9.35 mL, 75.0 mmol) and dry hexanes (300 mL). The mixture was cooled down to -78 °C and *n*-Butyllithium (2.50 M, 30 mL, 75.0 mmol) was added dropwise *via* the dropping funnel, keeping the temperature below -70 °C. A white precipitate formed (caution: this ArLi salt can detonate above -30°C, so the temperature needs to be strictly monitored). Upon completion of the addition, the mixture was further stirred at -78 °C for one hour. Then, BCl$_3$ (1.00 M, 25.0 mL, 25.0 mmol) was added in one portion and a heavy white precipitate formed. The cold bath was removed, and the reaction mixture was further stirred for 2 hours while reaching room temperature. The reaction mixture was diluted with cold hexanes (50 mL) and the precipitated LiCl was filtered off, rinsing with hexanes. The clear filtrate was concentrated under reduced pressure until precipitation started, then placed in a cold bath at -78 °C. The white precipitate was filtered, washed with cold hexanes, and dried under high vacuum. The flask was then open to air for 72 h to give the expected hydrated product as a white powder (8.65 g, 16.3 mmol, 65%). The yield can fluctuate between 50-70% depending on the scale. Best yields are usually obtained on bigger scale.

^{1}H NMR (300 MHz, CD$_2$Cl$_2$): δ no signals. ^{11}B NMR (96 MHz, CD$_2$Cl$_2$): δ 0.08. ^{19}F NMR (282 MHz, CD$_2$Cl$_2$): δ -135.49 (dd, J = 23.0, 8.4 Hz, 6F), -156.50 (t, J = 20.3 Hz, 3F), -163.80 (td, J = 22.3, 8.7 Hz, 6F). ^{13}C NMR (101 MHz, CD$_2$Cl$_2$): δ 148.3 (dm, $^1J_{FC}$ = 240 Hz), 140.8 (dm, $^1J_{FC}$ = 250 Hz), 137.6 (dm, $^1J_{FC}$ = 248 Hz), 116.9 (br). FT-IR (neat, cm^{-1}): 3668, 3599, 1648, 1520, 1457, 1377, 1284, 1098, 967, 676. mp = 108.3 – 111.9 °C.

The physical and spectral data are in accordance with the reported literature data.[1]

Crystals suitable for XRay analysis can be grown from DCM/hexanes.
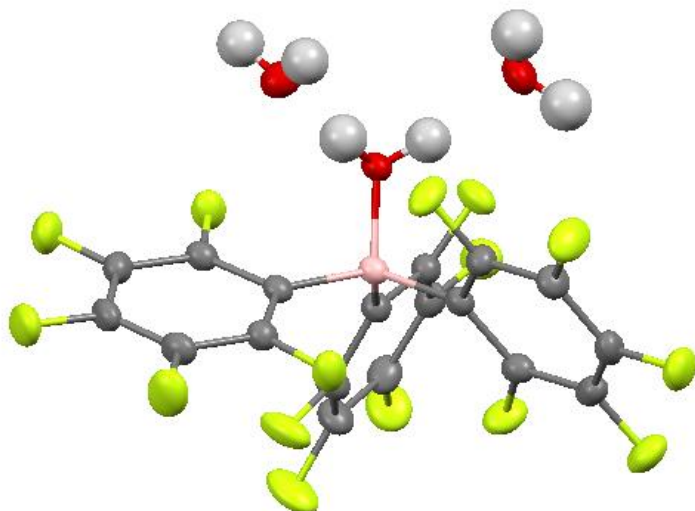
B(C$_6$F$_5$)$_3$-OH.Li (2)

B(C$_6$F$_5$)$_3$•3H$_2$O (1.70 g, 3.0 mmol) was dissolved in dry toluene (40 mL) and cooled down to -78 °C. *n-*Butyllithium (2.69 M, 1.12 mL, 3.0 mmol) was added dropwise while the temperature was carefully monitored. The reaction mixture was stirred for 30 minutes at this temperature, then allowed to warm up to room temperature and evaporated (the product doesn't precipitate). The product is not further purified (1.61 g, 3.0 mmol, quantitative yield).

^{1}H NMR (300 MHz, CDCl$_3$): δ 2.71 (brs, disappears upon addition of D$_2$O). ^{11}B NMR (96 MHz, CD$_2$Cl$_2$): δ -4.0. ^{19}F NMR (282 MHz, CD$_2$Cl$_2$): δ -139.65 (dd, *J* = 21.5, 8.4 Hz, 6F), -158.77 (t, *J* = 20.0 Hz, 3F), -163.85 (td, *J* = 18.7 Hz, 6F). ^{13}C NMR (101 MHz, CD$_2$Cl$_2$): δ 148.3 (dm, $^1J_{FC}$ = 232 Hz), 139.9 (dm, $^1J_{FC}$ = 239 Hz), 137.6 (dm, $^1J_{FC}$ = 217 Hz), 122.0 (br). FT-IR (neat, cm^{-1}): 1647, 1516, 1453, 1364, 1277, 1080, 957. mp = 196–198 °C.

Crystals suitable for XRay analysis can be grown from DCM/hexanes.
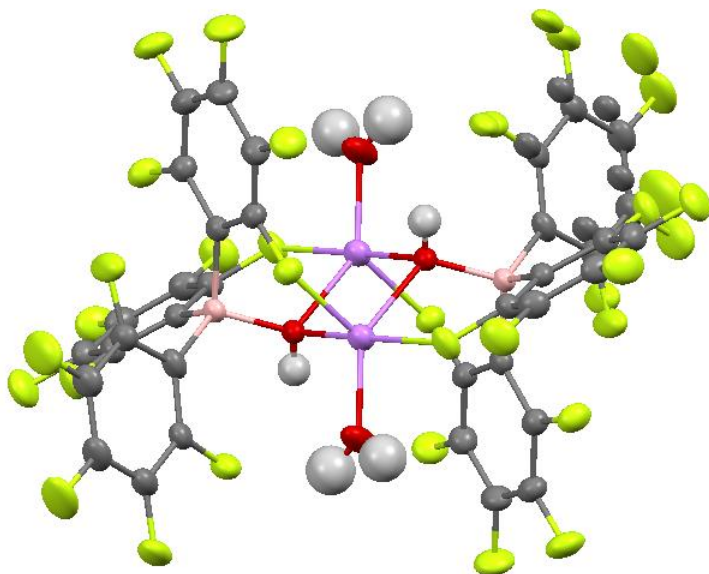
B(C₆F₅)₃•Py 1-115

Pyridine (0.40 mL, 5.00 mmol) was added at room temperature to a solution of B(C₆F₅)3•3H₂O (2.74 g, 5.00 mmol) in DCM (20.0 mL). A better solubilization of the reaction mixture occurred upon addition of the pyridine (a clear colorless solution was obtained). The displacement of water was followed by ^{19}F NMR and after 36 hours, no more changes in the ratio were observed (1:8.4 in favor of the desired product). The reaction mixture was evaporated to give the crude product as a beige solid. Purification was carried out *via* recrystallization at room temperature in DCM/hexanes 3:8. The crude mixture was suspended in enough DCM so that complete solubilization occurs at room temperature (17 mL), and 45 mL of hexanes were added. The mixture was let at room temperature for two days and white crystals were obtained. They were filtrated and washed several times with hexane, then dried under high vacuum. More product can be obtained from the mother liquor after standing one night at room temperature. The product is obtained as a stable, white crystalline solid (2.13 g, 3.60 mmol, 72%).

^{1}H NMR (300 MHz, CD₂Cl₂): δ 8.61 (d, *J* = 5.2 Hz, 2H), 8.21 (tt, *J* = 7.7, 1.5 Hz, 1H), 7.71 (t, *J* = 7.1 Hz, 2H). ^{11}B NMR (96 MHz, CD₂Cl₂): δ -3.5. ^{19}F NMR (282 MHz, CD₂Cl₂): δ -131.8 (d, *J* = 21.4 Hz, 6F), -157.5 (t, *J* = 20.2 Hz, 3F), -164.0 (m, 6F). ^{13}C NMR (101 MHz, CD₂Cl₂): δ 148.2 (d, $^{1}J_{FC}$ ~ 238 Hz, C₆F₅), 147.2 (*o*-pyr), 143.3 (*p*-pyr), 140.7 (d, $^{1}J_{FC}$ = 248.8 Hz, C₆F₅), 137.7 (d, $^{1}J_{FC}$ = 242.2 Hz, C₆F₅), 126.3 (*m*-pyr), 118.7 (br, *i*-C₆F₅).

The physical and spectral data are in accordance with the reported literature data.[2]

The structure was confirmed by XRay crystallography analysis of a single crystal. No bonded water was present. Crystals suitable for XRay analysis can be grown from DCM/hexanes.
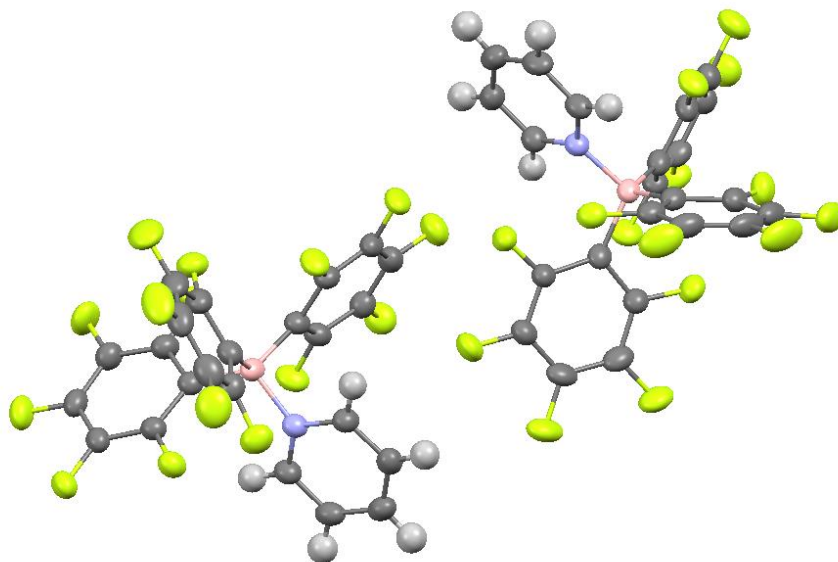
Displacement of pyridine by an alkoxide.
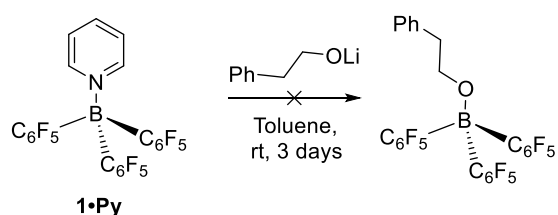
A solution of 1•Py (296 mg, 0.50 mmol) in dry toluene (8 mL) was added *via* syringe at room temperature to a solution of 2-phenylethoxylithium (64.0 mg, 0.50 mmol) in dry toluene (2 mL). The mixture was stirred at room temperature for 3 days and reaction's progress was followed by ^{1}H, ^{11}B and ^{19}F NMR. Remaining starting material as well as two unidentified products were observed. The solvent was evaporated under high vacuum and the oily residue was suspended in MeCN.

The model reaction was run with this mixture according to **GP1** in MeCN. No desired product was obtained.

Synthesis of 3.
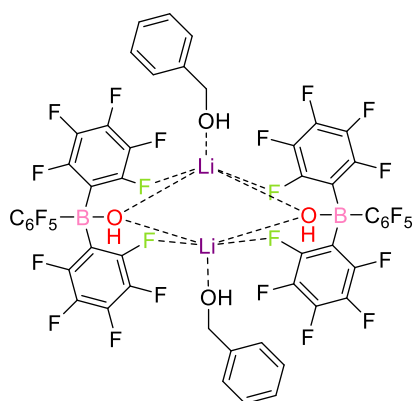
Via **1•3H₂O** and the alkoxide.

Alkoxyde preparation. To a solution of benzylic alcohol (0.62 mL, 6.0 mmol) in dry hexane (36 mL) at -10 °C was added *n*BuLi (2.50 M in hexanes, 2.4 mL, 6 mmol) dropwise, while the temperature was carefully monitored. A white precipitate immediately formed. The reaction mixture was stirred 30 minutes at -10°C, then allowed to warm up to 0 °C and stirred 30 more minutes. Filtration and washing of the white powder with cold hexane gave the desired alkoxide. After careful drying under high vacuum, the alkoxide was directly used for the complex's synthesis. **Complex preparation.** Benzyloxylithium (0.114 g, 1.00 mmol) was suspended in toluene (5 mL) and the mixture was cooled down to -78 °C. 1•3H₂O in toluene (5 mL) was added dropwise *via* syringe. After the addition was complete, the reaction mixture was stirred for 1 hour at 0 °C and 1 hour at room temperature. The volatiles were evaporated under reduced pressure to give crude product. Purification by recrystallization (DCM/hexanes) afforded the desired product as a beige crystalline solid (282 mg, 0.45 mmol, 45%).

Via **2** and the free alcohol.

Benzylic alcohol (0.10 mL, 1.0 mmol) was added to a solution of **2** (536 mg, 1.0 mmol) in dry toluene (10 mL) at 0°C under a nitrogen atmosphere. The reaction mixture was stirred at this temperature for 1 h, then allowed to warm up to room temperature. Evaporation of the volatiles under reduced pressure gave the desired product. No further purification was necessary (644 mg, 1.0 mmol, quantitative yield).

^{1}H NMR (300 MHz, CD₂Cl₂): δ 7.45–7.31 (m, 3H), 7.29–7.19 (m, 2H), 4.61 (d, *J* = 4.5 Hz, 2H), 2.52 (s, 1H), 2.46 (t, *J* = 5.1 Hz, 1H). ^{11}B NMR (96 MHz, CD₂Cl₂): δ -4.2. ^{19}F NMR (282 MHz, CD₂Cl₂): δ -138.2 (d, *J* = 23.7 Hz, 6F), -160.6 (t, *J* = 20.2 Hz, 3F), -165.2 (td, *J* = 24.4, 7.6 Hz, 6F). ^{13}C NMR (101 MHz, CD₂Cl₂): δ 148.28 (dm, $^1J_{FC}$ ~ 234 Hz, C₆F₅), 139.43 (dm, $^1J_{FC}$ ~ 228 Hz, C₆F₅), 138.51 (dm, $^1J_{FC}$ ~ 228 Hz, C₆F₅), 138.0 (Cq), 129.5 (2x CH Ar), 129.4 (CH Ar), 128.1 (2x CH Ar), 122.8 (br, *i*-C₆F₅), 66.7 (CH₂). FT-IR (neat, cm⁻¹): 1647, 1516, 1456, 1282, 1077, 962, 685. mp = 123.4 – 125.6 °C.

Crystals suitable for XRay analysis can be grown from DCM/hexanes.
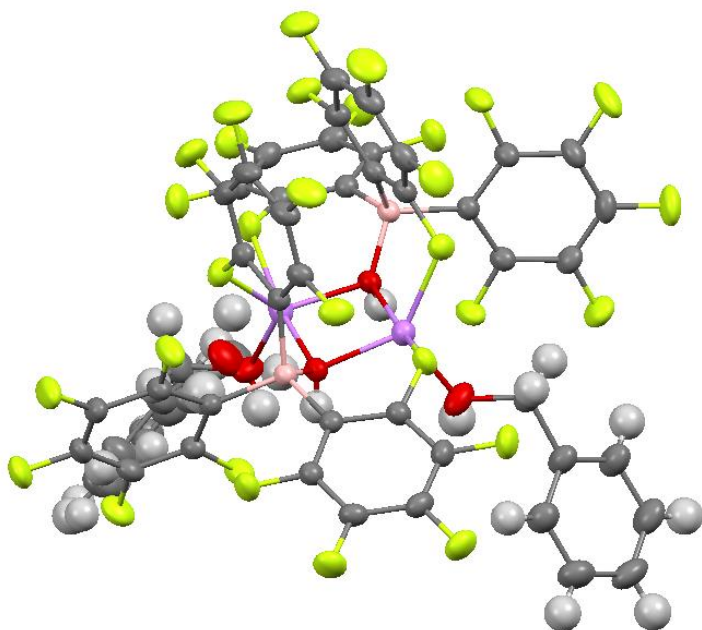
This complex was used as starting material in the model reaction following **GP1** (in MeCN). No desired product was observed.

BPh₃ complexes

General Procedure 2 – **Synthesis of the BPh₃ complexes**

To an oven-dried 25 mL round-bottomed flask was added THF (5 mL) and the appropriate alcohol (1.00 mmol). The reaction mixture was cooled down to -78 °C and *n*-BuLi (2.69 M, 0.37 mL, 1.00 mmol) was added dropwise. Stirring was continued at this temperature for 30 minutes, then at room temperature for 1 h. The reaction mixture is a clear, pale-yellow solution. Then, a solution of triphenylborane (242 mg, 1.00 mmol) in THF (5 mL) was added in one portion at room temperature. After 15 minutes, a ^{11}B NMR monitoring is carried out to assess the consumption of BPh₃. Upon completion of the reaction, the solvent is evaporated on the Schlenk and the solid complex is kept under a nitrogen atmosphere until solubilization in the appropriate solvent for photoredox reaction.

The complexes are used as starting material in the photoredox reaction following **GP1** in MeCN or THF.
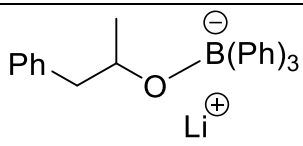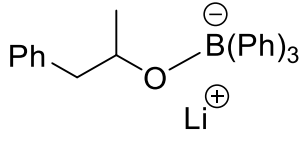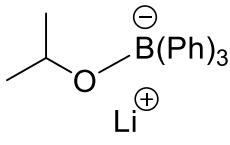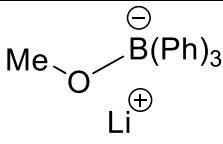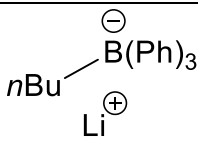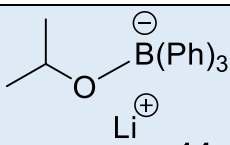
Complex	Solvent	Yield of **12**	Yield of **13**	Yield of **14**	ELN
Ph OB(Ph)$_3$ Li	MeCN	23%	25%	N.A.	ECO-2-040
Ph OB(Ph)$_3$ Li	THF	33%	18%	28%	ECO-2-046
OB(Ph)$_3$ Li	THF	13%	Traces	21%	ECO-2-079
MeOB(Ph)$_3$ Li	THF	8%	Traces	19%	ECO-2-078
*n*BuB(Ph)$_3$ Li	THF	28%	Traces	Traces	ECO-2-075
OB(Ph)$_3$ Li **14**	MeCN	11%	**53%**	N.A.	ECO-2-102

Table 1: Outcome of the reaction following GP1 with different boronate complexes

Characterization of the products:

Biphenyl (12).

$C_{12}H_{10}$
MW: 154,2120
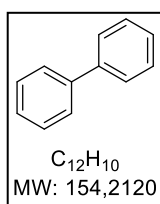
^{1}H NMR (300 MHz, CDCl$_3$): δ 7.64 – 7.56 (m, 4H), 7.49 – 7.40 (m, 4H), 7.39 – 7.31 (m, 2H).

The physical and spectral data are in accordance with the reported literature data[3] and can be compared with an authentic sample (commercially available).
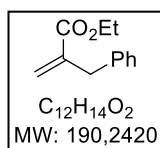
Ethyl 2-benzylacrylate (13).

$C_{12}H_{14}O_2$
MW: 190,2420

^{1}H NMR (300 MHz, CDCl$_3$): δ 7.33–7.16 (m, 5H), 6.23 (q, *J* = 1.0 Hz, 1H), 5.44 (q, *J* = 1.5 Hz, 1H), 4.18 (q, *J* = 7.1 Hz, 2H), 3.62 (s, 2H), 1.25 (t, *J* = 7.1 Hz, 3H).

The physical and spectral data are in accordance with the reported literature data.[4]
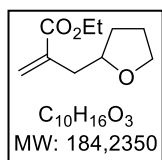
Ethyl 2-((tetrahydrofuran-2-yl)methyl)acrylate (5).

$C_{10}H_{16}O_3$
MW: 184,2350

^{1}H NMR (300 MHz, CDCl$_3$): δ 6.22 (d, J = 1.5 Hz, 1H), 5.66 (q, J = 1.3 Hz, 1H), 4.20 (q, J = 7.1 Hz, 2H), 4.08–3.98 (m, 1H), 3.91–3.82 (m, 1H), 3.77–3.66 (m, 1H), 2.51 (dd, J = 6.4, 1.2 Hz, 2H), 2.04–1.77 (m, 3H), 1.58–1.44 (m, 1H), 1.29 (t, J = 7.1 Hz, 3H).

The physical and spectral data are in accordance with the reported literature data.[5]

Iodine atom abstraction

General Procedure 3 – Photoredox reaction with the alkyl iodides (ECO-2-101)

To an oven dried seal-tube were successively added [Ir{dF(CF$_3$)ppy}$_2$(dtbpy)]PF$_6$ (4.5 mg, 2 mol%, 0.004 mmol) and the sulfone trap [(E)-2-(benzenesulfonyl)vinyl]sulfonylbenzene (123 mg, 0.40 mmol). The tube was evacuated and filled with N$_2$ three times, and a solution of the boronate complex **14** (**GP2**) in the appropriate solvent (0.1 M, 2.0 mL, 0.20 mmol) was added. Then, iodocyclohexane (0.026 mL, 0.20 mmol) was added *via* syringe. The mixture was degassed by three freeze-and-thaw cycles, the tube was sealed and placed in front of a 390 nm blue LED for 24 h. After reaction, the end mixture was dissolved in EtOAc, filtered over Celite, and evaporated to give crude product as an orange solid. Purification by flash column chromatography on silica gel (heptanes/EtOAc 95:5) afforded the desired products.

The best yield for compound **16** was obtained in ECO-2-113 following **GP3** in MeCN (Entry 4, 22.0 mg, 0.088 mmol, 44%).

Entry	Solvent	Equiv. trap	Equiv. Iodide	Yield of 16	Yield of 13	Other
1 (initial conditions)	MeCN	2	1	41%	9%	
2	DCE	2	1	36%	23%	
3	DCE	2	2	38%	/	
4	MeCN	2	2	44%	6%	
5	MeCN	2	2	31%	/	4 mol% Ir-A

Table 2: Outcome of the iodine abstraction reaction using boronate complex **14** following **GP3**
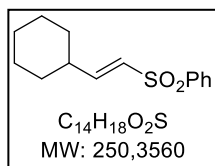
(E)-((2-cyclohexylvinyl)sulfonyl)benzene (16).

$C_{14}H_{18}O_2S$
MW: 250,3560

^{1}H NMR (300 MHz, CDCl$_3$): δ 7.92–7.83 (m, 2H), 7.65–7.47 (m, 3H), 6.95 (dd, J = 15.2, 6.4 Hz, 1H), 6.24 (dd, J = 15.2, 1.5 Hz, 1H), 2.26–2.09 (m, 1H), 1.88–1.56 (m, 5H), 1.39–1.02 (m, 5H).

The physical and spectral data are in accordance with the reported literature data.[6]

Radical probe

K$_3$PO$_4$•H$_2$O (3.0 equiv)
CuI 20mol%
H$_2$O (10 equiv.)

(3 eq.)

DMSO
20 h, 90°C

79 %

6
$C_{15}H_{14}O$
MW: 210,2760
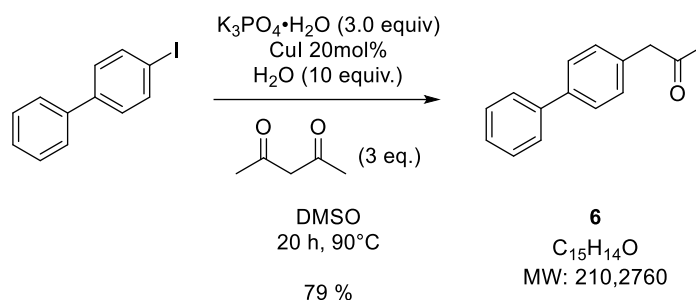
1-biphenyl-propan-2-one (6) was synthesized following a protocol adapted from the literature.[7]

A mixture of 1-iodo-4-phenyl-benzene (97.0 %, 2.9 g, 10.0 mmol), iodocopper (381 mg, 2.00 mmol), K$_3$PO$_4$.1H$_2$O (95.0 %, 7.3 g, 30.0 mmol), acetylacetone (redistilled, 3.1 mL, 30.00 mmol) and water (1.80 mL, 100 mmol) in DMSO (30 mL) was stirred under nitrogen at 90°C. After stirring for 20 h, the reaction mixture was cooled down to room temperature and quenched with 2 M aqueous HCl (30 mL). Water (100 mL) was added, and the aqueous phase was extracted with EtOAc (6 x 100 mL). The combined organic layers were dried (Na$_2$SO$_4$), filtered, and evaporated under reduced pressure to give crude product. Purification by flash column chromatography on silica gel (heptanes/EtOAc 100:0 to 99:1) afforded the desired product as a pale-yellow solid (1.65 g, 7.87 mmol, 79%).

^{1}H NMR (300 MHz, CDCl$_3$): δ 7.63–7.52 (m, 4H), 7.49–7.40 (m, 2H), 7.39–7.31 (m, 1H), 7.31–7.23 (m, 2H), 3.75 (s, 2H), 2.20 (s, 3H). ^{13}C NMR (75 MHz, CDCl$_3$): δ 206.5, 140.9, 140.2, 133.4, 130.0, 128.9, 127.6, 127.4, 127.2, 50.8, 29.5. The physical and spectral data are in accordance with the reported literature data.[7]
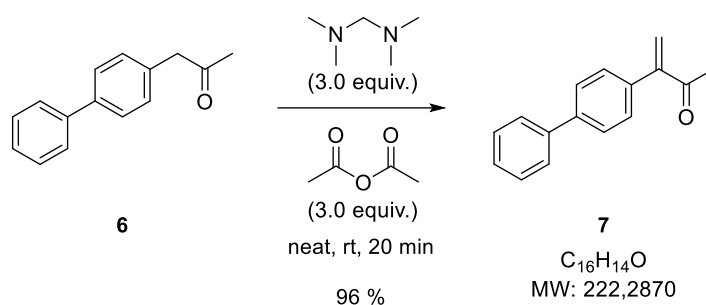
3-biphenyl-but-3-en-2-one (7).

Acetic anhydride (1.30 mL, 13.3 mmol) was slowly added to solution of 1-(4-phenylphenyl)propan-2-one **6** (933 mg, 4.44 mmol) in N,N,N',N'-tetramethylmethanediamine (1.84 mL, 13.3 mmol) at 0 °C. After complete addition the reaction mixture was allowed to warm up to room temperature and was further stirred 20 minutes at this temperature. After completion of the reaction, the reaction mixture diluted with water (10 mL) and extracted with EtOAc (3 x 20 mL). The combined organic layers were washed with sat. aq. NaHCO$_3$ (1 x 20 mL) and brine (1 x 20 mL), dried over Na$_2$SO$_4$, filtered and evaporated under reduced pressure to give crude product. Purification by flash column chromatography on silica gel (pentane/Et$_2$O 92:8) afforded the desired product as a white solid (950 mg, 4.27 mmol, 96%).

^{1}H NMR (300 MHz, CDCl$_3$): δ 7.65–7.56 (m, 4H), 7.50–7.32 (m, 5H), 6.21 (s, 1H), 6.05 (s, 1H), 2.49 (s, 3H). ^{13}C NMR (75 MHz, CDCl$_3$): δ 199.6 (C=O), 149.2 (Cq), 141.2 (Cq), 140.8 (Cq), 136.0 (Cq), 129.1 (2x CH Ar), 128.9 (2x CH Ar), 127.6 (CH Ar), 127.2 (2x CH Ar), 127.1 (2x CH Ar), 126.0 (=CH$_2$), 27.6 (CH$_3$). FT-IR (cm^{-1}, neat): 1661, 1485, 1358, 1322, 1172, 1075. HRMS (ESI) m/z: [M+Na]$^+$ Calcd for C$_{16}$H$_{14}$ONa 245.0937; Found 245.0927. mp 100.7–102.1 °C. R$_f$ = 0.41 (pentane/Et$_2$O 92:8).
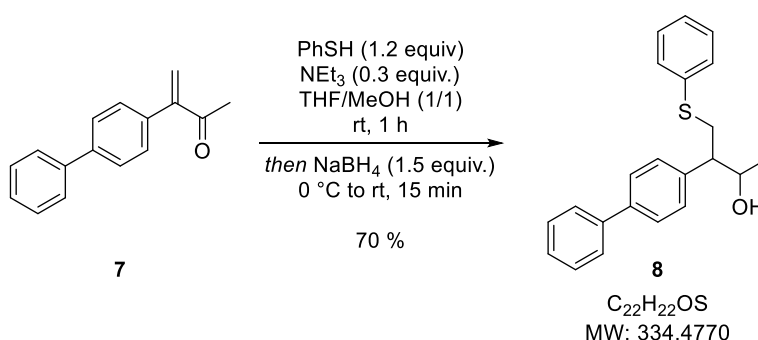
1-(4-phenylphenyl)-1-phenylsulfanyl-propan-2-ol (8).

To a solution of 3-(4-phenylphenyl)but-3-en-2-one **7** (1.1 g, 4.97 mmol) in THF/MeOH (20 mL, 1/1) was added NEt$_3$ (0.21 mL, 1.49 mmol) followed by thiophenol (97.0 %, 0.63 mL, 5.97 mmol) at room

temperature. Upon completion of the reaction (1 h), the solution was cooled to 0°C and NaBH$_4$ (96.0 %, 294 mg, 7.46 mmol) was added to reduce the intermediate ketone. The reaction mixture was stirred at room temperature until TLC indicated complete reduction (15 minutes). The reaction mixture was diluted with DCM (50 mL), and washed with saturated aqueous NH$_4$Cl (2 x 20 mL), saturated aqueous NaHCO$_3$ (1 x 20 mL), water (1 x 20 mL) and brine (1 x 20 mL). The organic phase was dried (Na$_2$SO$_4$), filtered and concentrated under reduced pressure to give crude product. Purification by flash column chromatography on silica gel (toluene/EtOAc 100:0 to 95:5) afforded the desired product as a thick oil (1.17 g, 3.50 mmol, 70%).

^{1}H NMR (300 MHz, CDCl$_3$): δ 7.64–7.54 (m, 4H), 7.50–7.41 (m, 2H), 7.39–7.24 (m, 7H), 7.23–7.15 (m, 1H), 4.26 (qd, J = 6.3, 4.6 Hz, 1H), 3.54–3.28 (m, 2H), 2.87 (td, J = 7.5, 4.6 Hz, 1H), 1.17 (d, J = 6.4 Hz, 3H). ^{13}C NMR (75 MHz, CDCl$_3$): δ 140.9 (Cq), 140.2 (Cq), 138.7 (Cq), 136.6 (Cq), 129.6 (2x CH Ar), 129.4 (2x CH Ar), 129.1 (2x CH Ar), 128.9 (2x CH Ar), 127.4 (CH Ar), 127.3 (2x CH Ar), 127.2 (2x CH Ar), 126.1 (CH Ar), 69.2 (CH), 51.9 (CH), 36.3 (CH$_2$), 21.7 (CH$_3$). FT-IR (cm^{-1}, neat): 3433, 1581, 1480, 1438, 1372, 1241, 734, 690. HRMS (ESI) m/z: [M+Na]$^+$ Calcd for C$_{22}$H$_{22}$ONaS 357.1282; Found 357.1284. R$_f$ = 0.49 (toluene/EtOAc 90:10).
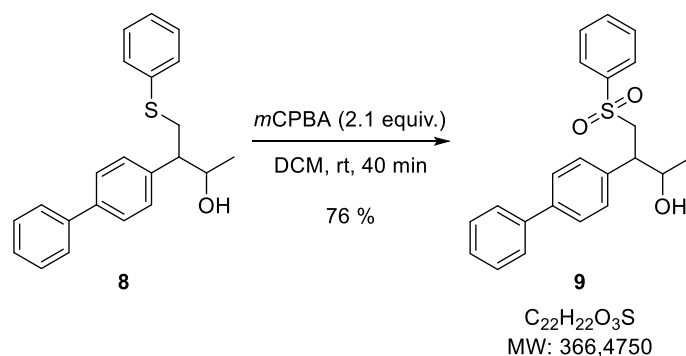
4-(benzenesulfonyl)-3-(4-phenylphenyl)butan-2-ol (9).

A solution of *m*CPBA (77.0 %, 1.65 g, 7.35 mmol) in DCM (10 mL) was added dropwise to a stirred solution of 3-(4-phenylphenyl)-4-phenylsulfanyl-butan-2-ol **8** (1.17 g, 3.50 mmol) in DCM (20 ml). The reaction mixture was stirred at room temperature until completion of the reaction (40 minutes). The reaction was cooled to 0 °C and sat. aq. NaHCO$_3$ (20 mL) was added. The mixture was stirred vigorously for 20 min at room temperature. The organic phase was separated, and the aqueous phase was extracted with DCM (2 x 20 mL). The combined organic phases were washed with 10% aq. Na$_2$S$_2$O$_4$ (2 x 20 mL), water (1 x 20 mL) and brine (1 x 20 mL), dried over Na$_2$SO$_4$, filtered, and concentrated under reduced pressure. The crude product was pure and did not require further purification (968 mg, 2.64

mmol, 76%). If necessary, the product can be purified by flash column chromatography on silica gel (heptane/EtOAc 1:1).

^{1}H NMR (300 MHz, CDCl$_3$): δ 7.80–7.70 (m, 2H), 7.60–7.48 (m, 3H), 7.48–7.30 (m, 7H), 7.21–7.10 (m, 2H), 4.29 (qd, J = 6.4, 3.8 Hz, 1H), 3.85–3.50 (m, 2H), 3.37 (td, J = 6.8, 3.8 Hz, 1H), 1.08 (d, J = 6.3 Hz, 3H). ^{13}C NMR (75 MHz, CDCl$_3$): δ 140.7 (Cq), 140.4 (Cq), 139.9 (Cq), 136.5 (Cq), 133.5 (CH Ar), 129.6 (2x CH Ar), 129.2 (2x CH Ar), 128.9 (2x CH Ar), 128.0 (2x CH Ar), 127.5 (CH Ar), 127.2 (2x CH Ar), 127.1 (2x CH Ar), 69.4 (CH), 58.8 (CH$_2$), 46.9 (CH), 21.2 (CH). FT-IR (cm^{-1}, neat): 3531, 2969, 1489, 1446, 1285, 1138, 1080, 747, 684, 564. HRMS (ESI) m/z: [M+Na]$^{+}$ Calcd for C$_{22}$H$_{22}$O$_3$NaS 389.1182; Found 389.1181. mp 153.2–154.1 °C. R$_f$ = 0.40 (heptane/EtOAc 1:1)

C$_{14}$H$_{12}$
MW: 180,2500
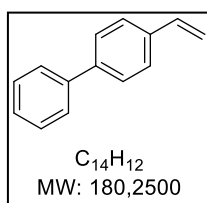
4-vinyl-1,1'-biphenyl (reference product of the radical probe fragmentation). ECO-1-178

4-phenylbenzaldehyde (97.0 %, 0.34 mL, 2.0 mmol) was added to a stirred solution of methyltriphenylphosphonium bromide (98.0 %, 875 mg, 2.40 mmol) and K$_2$CO$_3$ (442 mg, 3.20 mmol) in THF (3 mL). The resultant mixture was stirred at 75 °C overnight to give a white slurry. The reaction mixture was cooled down to room temperature and THF was removed under reduced pressure. Pentane (20 mL) was added to the residue, the resultant suspension was filtered through Celite and the solvent was evaporated under reduced pressure to give crude product as a white solid. Purification by flash column chromatography on silica gel (100% pentane) afforded the desired product as a white solid (199 mg, 1.10 mmol, 55%).

^{1}H NMR (300 MHz, CDCl$_3$): δ 7.65–7.55 (m, 4H), 7.53–7.41 (m, 4H), 7.39–7.32 (m, 1H), 6.78 (dd, J = 17.6, 10.9 Hz, 1H), 5.81 (dd, J = 17.6, 0.9 Hz, 1H), 5.29 (dd, J = 10.8, 0.9 Hz, 1H). ^{13}C NMR (75 MHz, CDCl$_3$): δ 140.9, 140.7, 136.7, 136.5, 128.9, 127.46, 127.37, 127.1, 126.8, 114.0.

The physical and spectral data are in accordance with the reported literature data.[8]

GC-1 fast: RT = 8.35 min

Fluorescence quenching experiments

General protocol:

1. Solutions are prepared in acetonitrile. [Fluorophore] = $4.10.10^{-5}$ M (Abs between 0.3 and 0.5).

    [Quencher] = 0.5 M
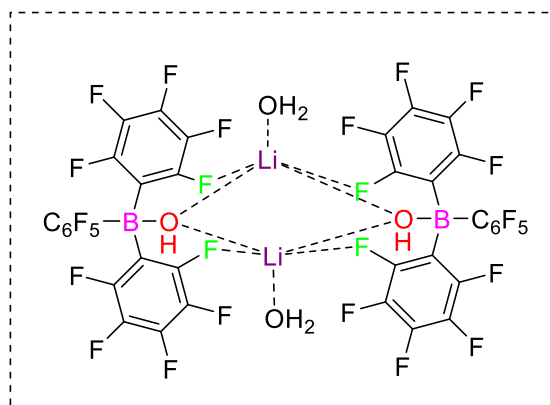
    Quencher: **Fluorophore:**
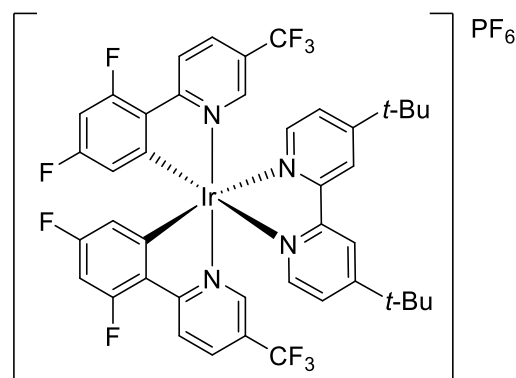
Ir-A
Ir{dF(CF$_3$)ppy}$_2$(dtbpy)]PF$_6$

CAS: 870987-63-6

Quencher negative control:
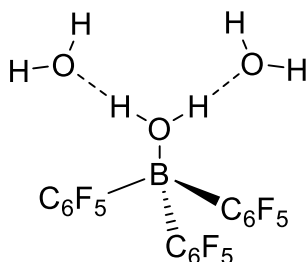
2. The absorbance of the fluorophore and of the quencher are measured to make sure that there is no overlap.

3. The initial emission intensity of the fluorophore (I_0) is measured in absence of the quencher. Then, aliquots of the quencher are added to the cuvette, and the emission I is measured each time. The ratio I_0/I is plotted versus the concentration of the quencher <u>in the cuvette</u>. A I_0/I ratio close to 1 indicates that the quencher does not reduce strongly or at all the intensity of emission of the fluorophore (no quenching).

	Measured intensities	I_0/I_i	Added volume (µl) of the quencher	Total volume (µl) of the quencher in the cuvette	Total volume (µl) in the cuvette	[Q]$_{corrected}$ (M) (concentration of the quencher in the cuvette)
I0	21540,1476	1,000	0	0	1000	0,00E+00
I1	19748,593	1,091	5	5	1005	2,49E-03
I2	18731,6226	1,150	5	10	1010	4,95E-03
I3	18022,7423	1,195	10	20	1020	9,80E-03
I4	17694,1565	1,217	20	40	1040	1,92E-02
I5	17449,0552	1,234	20	60	1060	2,83E-02
I6	17172,1963	1,254	20	80	1080	3,70E-02
I7	16429,1746	1,311	80	160	1160	6,90E-02
I8	15385,8904	1,400	80	240	1240	9,68E-02

Table 3: Fluorescence quenching experiment at 20 °C with **2** as the quencher
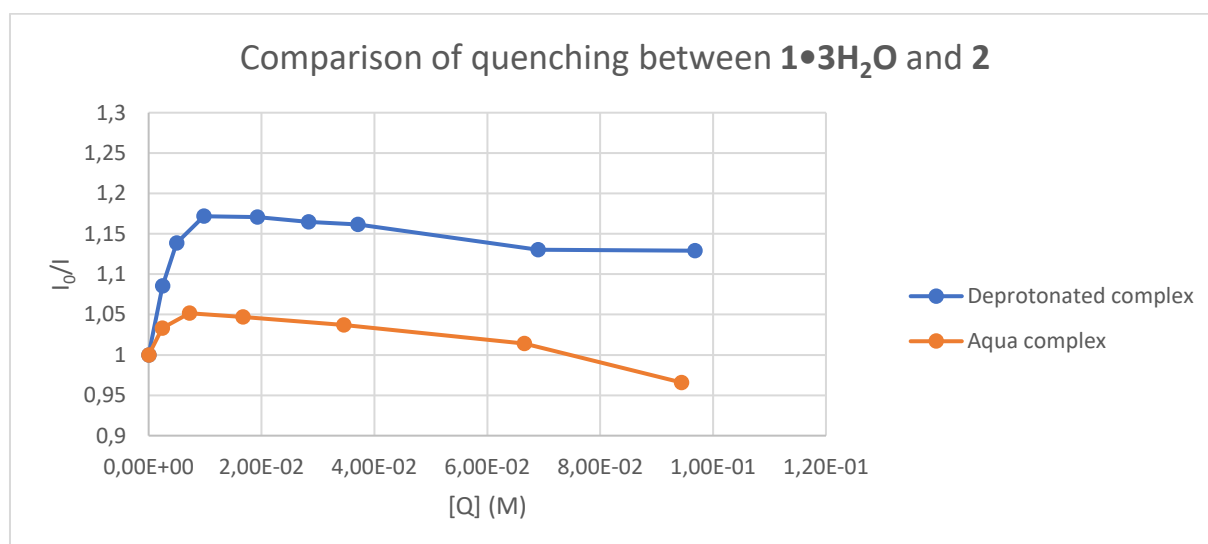
Scheme 1: quenching of the deprotonated complex **2** compared to the negative control 1•3H$_2$O (aqua complex) at 20 °C

The slight quenching observed in the case of **2** is probably an artefact due to problems of solubilization (**1•3H₂O** is much more soluble in organic solvents than **2**). The same experiment was run at 40 °C to favor solubilization.

	Intensities	I_0/I_i	Added volume (µl) of the quencher	Total volume (µl) of the quencher in the cuvette	Total volume (µl) in the cuvette	$[Q]_{corrected}$ (M) (concentration of the quencher in the cuvette)
I0	21892,0412	1,00	0	0	1000	0,00E+00
I1	20375,5786	1,07	5	5	1005	2,49E-03
I2	20522,4407	1,07	10	15	1015	7,39E-03
I3	19580,4808	1,12	20	35	1035	1,69E-02
I4	19208,6923	1,14	40	75	1075	3,49E-02
I5	18329,8957	1,19	80	155	1155	6,71E-02
I6	17451,721	1,25	80	235	1235	9,51E-02

Table 4: Fluorescence quenching experiment at 40 °C with 2 as the quencher
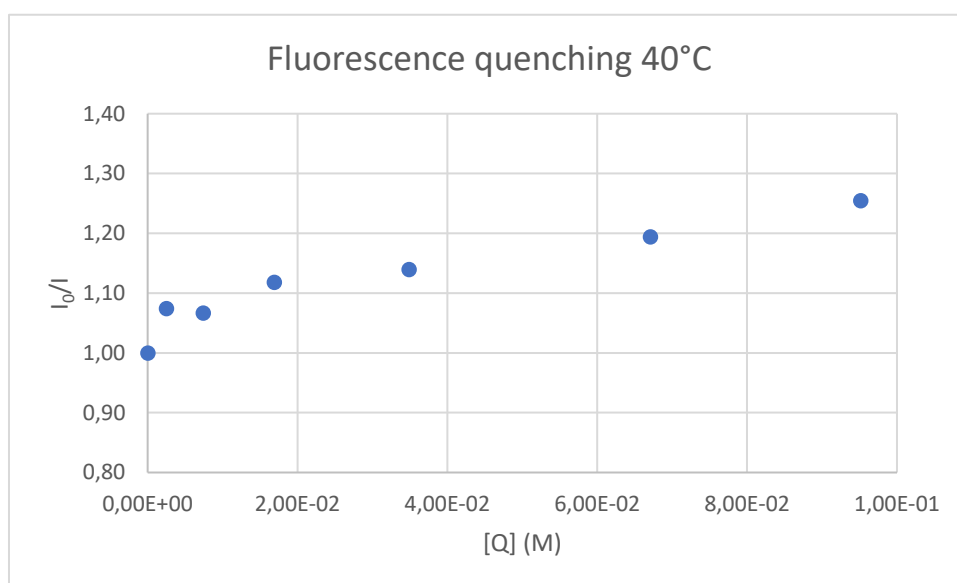
Scheme 2: quenching of the deprotonated complex **2** at 40 °C

At 40 °C we can observe a lower I_0/I ratio, meaning that quenching was lower at 40 °C than at 20 °C. This could be explained by a better solubility of the quencher in solution, better reflecting the behavior of the system (no artefact due to light scattering for example).

References

1 C. Bergquist, B. M. Bridgewater, C. J. Harlan, J. R. Norton, R. A. Friesner and G. Parkin, *J. Am. Chem. Soc.*, 2000, **122**, 10581–10590.

2 Q. Sun, C. G. Daniliuc, C. Mück-Lichtenfeld, K. Bergander, G. Kehr and G. Erker, *J. Am. Chem. Soc.*, 2020, **142**, 17260–17264.

3 R. Arundhathi, D. Damodara, K. V. Mohan, M. L. Kantam and P. R. Likhar, *Advanced Synthesis & Catalysis*, 2013, **355**, 751–756.

4 A. N. Matralis, D. Xanthopoulos, G. Huot, S. Lopes-Paciencia, C. Cole, H. de Vries, G. Ferbeyre and Y. S. Tsantrizos, *Bioorganic & Medicinal Chemistry*, 2018, **26**, 5547–5554.

5 S. V. Patil and J. M. Tanko, *Tetrahedron*, 2016, **72**, 7849–7858.

6 A. Chaambi, G. Kurtay, R. Abderrahim, F. Robert and Y. Landais, *Helvetica Chimica Acta*, 2019, **102**, e1900140.

7 C. He, S. Guo, L. Huang and A. Lei, *J. Am. Chem. Soc.*, 2010, **132**, 8273–8275.

8 S.-D. Cho, H.-K. Kim, H. Yim, M.-R. Kim, J.-K. Lee, J.-J. Kim and Y.-J. Yoon, *Tetrahedron*, 2007, **63**, 1345–1352.

Chapter 3

Chapter 3 – Tropane and related alkaloid skeletons *via* a radical [3+3]-annulation reaction

3.1. Literature precedence

Alpha-amino radicals have long been used as versatile intermediates for the synthesis of *N*-heterocycles and in particular alkaloids *via* intramolecular radical cyclizations.[1]

3.1.1. General characteristics of α-aminoalkyl radicals

Alpha-amino- and alpha-amidoalkyl radicals are differentiated by the functional group Z present on the nitrogen atom (Figure 1). When Z is an alkyl, aryl, or benzyl group, the nitrogen is part of an amine moiety, and the term α-aminoalkyl radical applies. When Z is a carbonyl group, the nitrogen atom is part of an amide or sometimes also a carbamate moiety, and the term α-amidoalkyl radical is appropriate.

Z = H, alkyl, aryl, benzyl: α-aminoalkyl radical
Z = carbonyl group: α-amidoalkyl radical

Figure 1: Terminology of α-amino- and α-amidoalkyl radicals.

These two radicals located alpha to a nitrogen have a slightly different reactivity due to the electron-withdrawing character of the carbonyl group in the case of the α-amidoalkyl radical, absent for α-aminoalkyl radicals. However, they are intimately related to one another, being often generated following similar protocols. In this preliminary overview, they will be presented together but we shall focus primarily on α-aminoalkyl radicals.

Alpha-aminoalkyl radicals are stabilized species due to the conjugative delocalization with the unpaired electrons of the nitrogen atom.[2] This stability increases with substitution at the nitrogen atom and at the carbon atom bearing the radical center. At the same time, the low ionization potentials observed for these radical species decreases even further with increasing C– or N–alkylation, reaching values close to those of lithium and sodium (around 5-6 eV).[3] Consequently, α-aminoalkyl radicals are powerful reducing agents ($E_{1/2}^{red} = -1.03\ V\ vs\ SCE\ in\ MeCN$ for the α-aminoalkyl radical of NMe$_3$)[4] and are considered as electron-rich, nucleophilic radicals that will react efficiently with electron-deficient alkenes.[5] On the contrary, α-amidoalkyl radicals are less reducing ($E_{1/2}^{red} = -0.12\ V\ vs\ SCE\ in\ MeCN$)[6] and less nucleophilic – they have been shown to add intramolecularly to unactivated alkenes.[7] Additionally, α-aminoalkyl radicals abstract halogen atoms with high rate constants[8,9] and have increasingly been used as halogen atom transfer reagents from alkyl and aryl halides.[10–14]

3.1.2. Available methods for the generation of α-aminoalkyl radicals

There exist several methods to generate α-amino radicals (Figure 2),[15] based on different radical precursors. Some methods can be said reductive when an electron is given to the radical precursor in the step leading to the α-aminoalkyl radical. These include the radical addition to enamines (Figure 2A), and the reduction of N-X acetals (Figure 2B), imines (Figure 2C), and α-amino redox esters (Figure 2D). In oxidative methods, an electron is removed from the radical precursor in the step leading to the α-aminoalkyl radical. This can be done during an HAT event (which formally removes an electron and a proton, Figure 2E), or *via* the one-electron oxidation of α-silylamines, α-amino acids, or tertiary amines (Figure 2F).
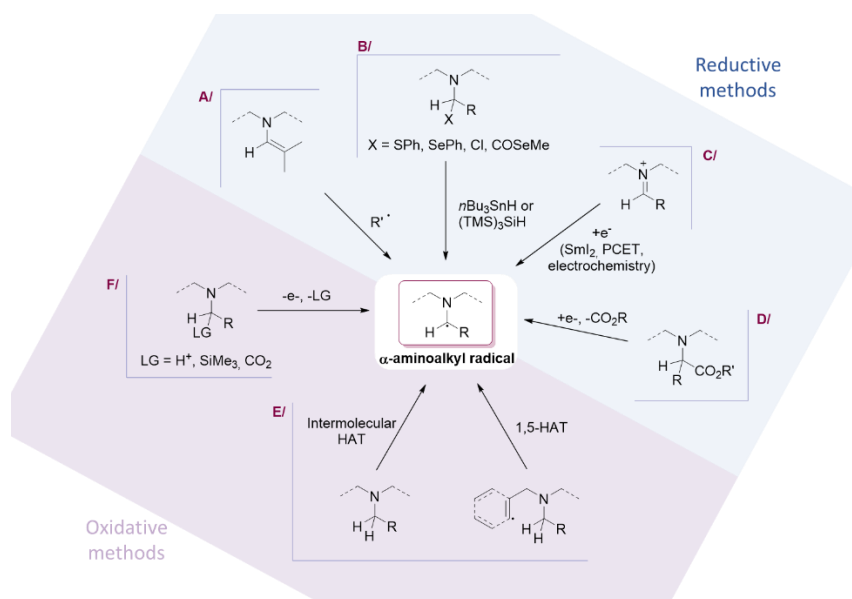
Figure 2. General overview of the strategies available for the generation of α-aminoalkyl radicals. A/ Via radical addition to enamines. B/ From N-X acetal precursors. C/ Via one-electron reduction of imine derivatives. D/ Via the reduction of redox active esters. E/ Via intra- or intermolecular HAT events. F/ Via one-electron oxidation of amine precursors.

3.1.2.1.   Radical addition to enamines

The radical addition at the beta position of enamines results in the formation of α-amino radicals (Figure 2A). Intramolecular additions are particularly interesting in the context of alkaloid synthesis. When an enamine is present in the substrate, radical cyclization occurs to give the α-amino- or α-amidoalkyl radical, which can abstract a hydrogen to give isoquinoline derivatives. Several examples have been reported following this methodology, including 6-endo[16,17] and 7-endo ring closures (Scheme 1).[18]
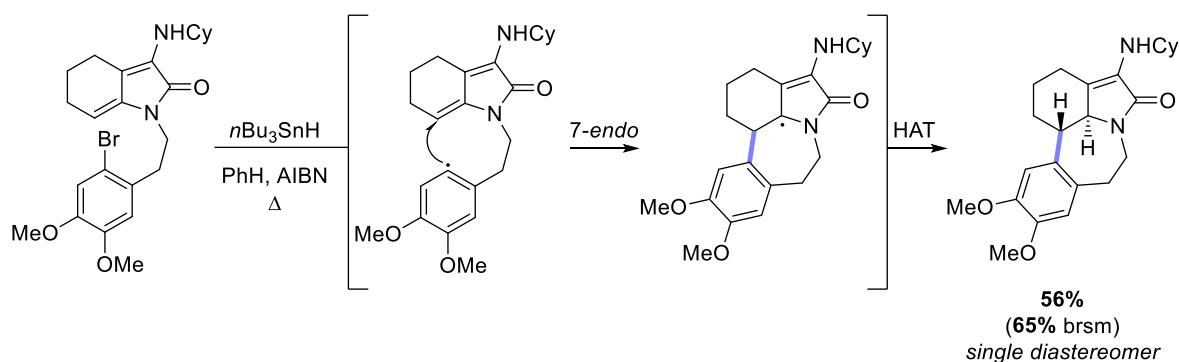
Scheme 1. Aryl radical addition to enamides leading to an α-amidoalkyl radical. Example of a 7-endo cyclization process by Rigby and co-workers.

In recent years, photoredox protocols have emerged that leveraged this reactivity for the α-functionalization of aldehydes *via* transient enamine intermediates.[19] When employing an optically active organocatalyst for the formation of the enamine, enantioselectivity can be achieved. The α-aminoalkyl radical resulting from radical addition to the enamine is often oxidized to the iminium ion *via* SET to the photoredox catalyst. Hydrolysis of this iminium ion gives the desired product along with the regenerated organocatalyst. Following this strategy, the MacMillan group reported the

enantioselective α-trifluoromethylation,[20] -benzylation,[21] -alkylation,[22] and -amination[23] of aldehydes. The Melchiorre group also made significant advances in this field by directly photoexciting the *in situ* formed enamine, thus avoiding the use of a photoredox catalyst.[24–26] Very recently, Molander and coworkers reported the organophotoredox-mediated addition of α-bromocarbonyls to *N*-alkenyl amides.[27] The resulting α-amidoalkyl radical was oxidized by the photocatalyst and the resulting cationic species was trapped by nucleophilic reagents (alcohols, water, thiols, azides).

3.1.2.2.   N-X acetals

N-X acetal precursors can be reduced to α-amino- and α-amidoalkyl radicals *via* C-X bond homolysis (Figure 2B). These precursors have been routinely used in the synthesis of pyrrolizidine alkaloids but also tropane derivatives.[28] For example, Hart and co-workers reported several syntheses of pyrrolizidine alkaloids using specifically designed α-amidoalkyl radical precursors. The olefin component of the substrates ranged from electron-deficient olefins to electron-rich vinylsilanes, alkynes, and allenes (Scheme 2). More complex structures could be cyclized as well, as demonstrated by the synthesis of gelsemine, for which the radical precursor was however lengthy to prepare (12 steps). A common by-product in these reactions is the direct reduction of the α-aminoalkyl radical prior to cyclization. This can be avoided by tuning the electronic properties of the olefinic partner. The lactam can be reduced to the desired amine by reduction with LiAlH$_4$.
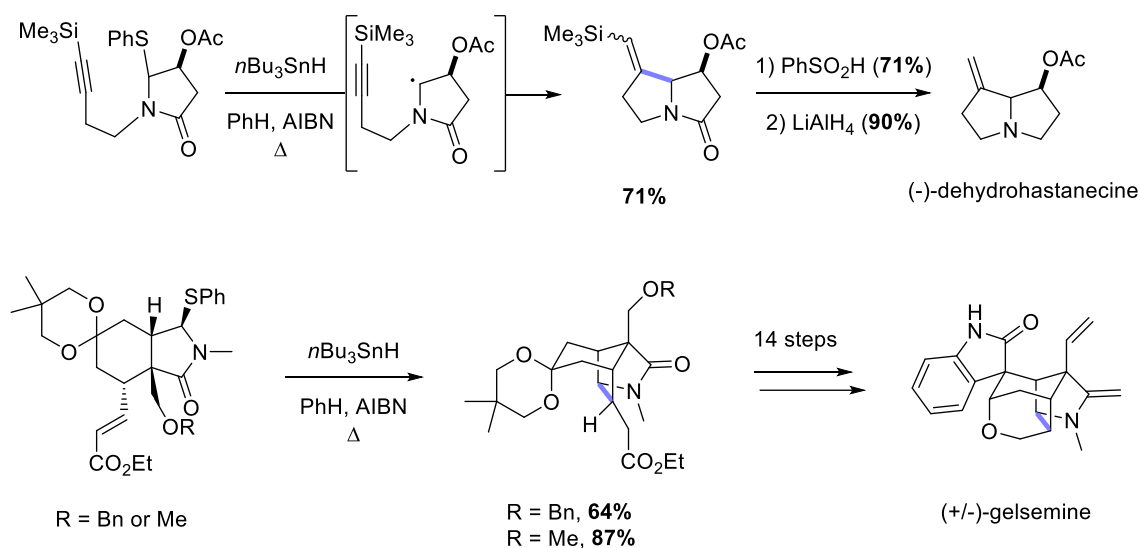
Scheme 2. Leveraging N-S acetals for the synthesis of complex alkaloids.

Clive and co-workers reported a similar strategy for the synthesis of the azabicyclo[2.2.1] alkaloid (–)-epibatidine (Scheme 3).[29] The optically active precursor for cyclization was prepared in 9 steps from commercially available pyroglutamic acid. *n*-Bu₃SnH mediated homolysis of the carbon-sulfur bond afforded the α-amidoalkyl radical that cyclized on the pendant alkyne moiety, giving the key intermediate to (–)-epibatidine in 76% yield.
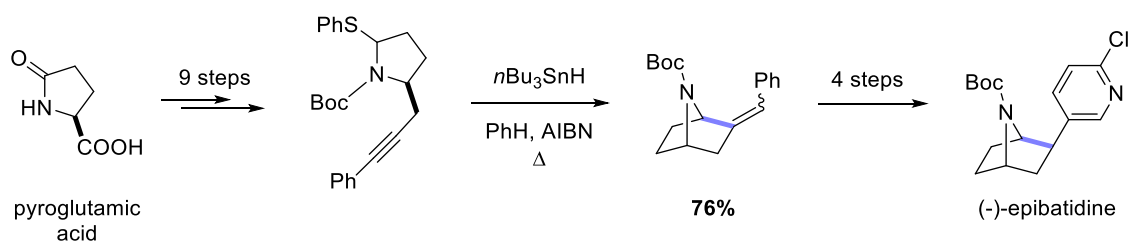
Scheme 3. Clive's synthesis of toxin epibatidine.

Bonjoc described the generation of α-amino radicals by treatment of α-amino selenoesters using hydride reagents such as *n*Bu₃SnH or (TMS)₃SiH with AIBN.[30] The method is based on the decarbonylation of acyl radicals occurring when more stable radicals can be obtained.[31] While the previous methods using N-S acetals were mostly limited to deactivated nitrogen moiety, this methodology was amenable to tertiary benzylamines and afforded azabicyclo[3.2.1] alkaloids in good yield (Scheme 4). No side product resulting from the addition of the acyl radical was observed for either activated or unactivated olefins. However, reduction of the α-aminoalkyl radical took place exclusively when unactivated olefins were used.
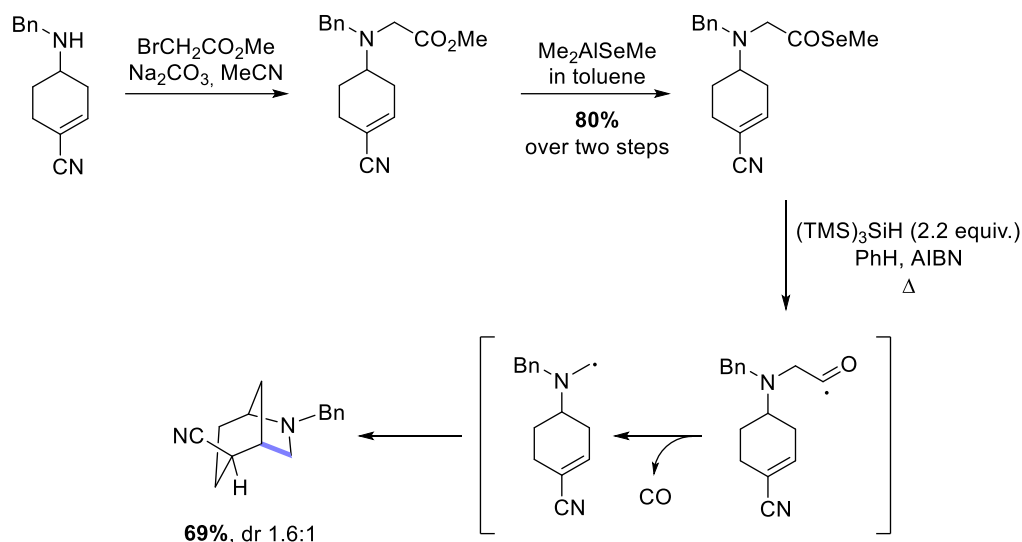
Scheme 4. Bonjoc synthesis of azabicyclo[3.2.1]octanes using α-amino selenoester precursors.

3.1.2.3.   Reduction of imines

The reduction of imines has been extensively studied for the generation of α-amino radicals (Figure 2C). Early reports described the SmI₂-promoted reduction of iminium ions formed *in situ* from aldehydes and secondary amines.[32–34] This strategy was also used recently for the reduction of iminium ions generated from N,O-acetal precursors in presence of a Lewis acid.[35] This type of chemistry has gained more interest in the context of photoredox chemistry, as the reduction of imines has been shown to occur readily under mild PCET conditions (Figure 3; see Chapter 1 for more details on PCET). This strategy offers an opportunity for umpolung from an electrophilic, two-electron acceptor to a nucleophilic, one-electron donor and can now be applied on a broad scope of starting materials. This topic has been extensively reviewed by Dixon and co-workers in 2020[36] and will not be discussed in detail in this chapter.
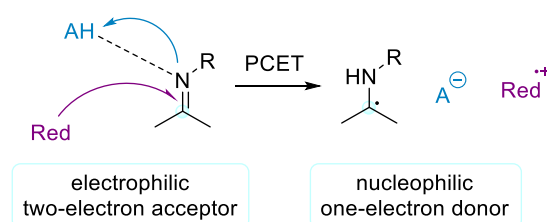
Figure 3. Reductive PCET on imines for the generation of α-aminoalkyl radicals.

Of note is a methodology published by the same authors in 2022 showcasing the use of electrophile-tethered imines for intramolecular C–C bond formation (Figure 4).[37] Under two different sets of

reaction conditions, product A or product B was obtained by single or dual cyclization, respectively, from aryl imines decorated with an α,β-unsaturated olefin. The Hantzsch ester used as sacrificial reductant in the catalytic cycle proved to be crucial in determining the reaction's selectivity. When R was a hydrogen, facile HAT event or sequential transfer of an electron and a proton from the oxidized Hantzsch ester **I** to the radical intermediate **III** occurred to give product **A**. In the case of the ethyl substituted Hantzsch ester, the more difficult oxidation of this species compared to the unsubstituted derivative may result in lower concentration of species **I** in solution, leading to product **B**. Both products A and B were obtained in excellent diastereomeric ratio.
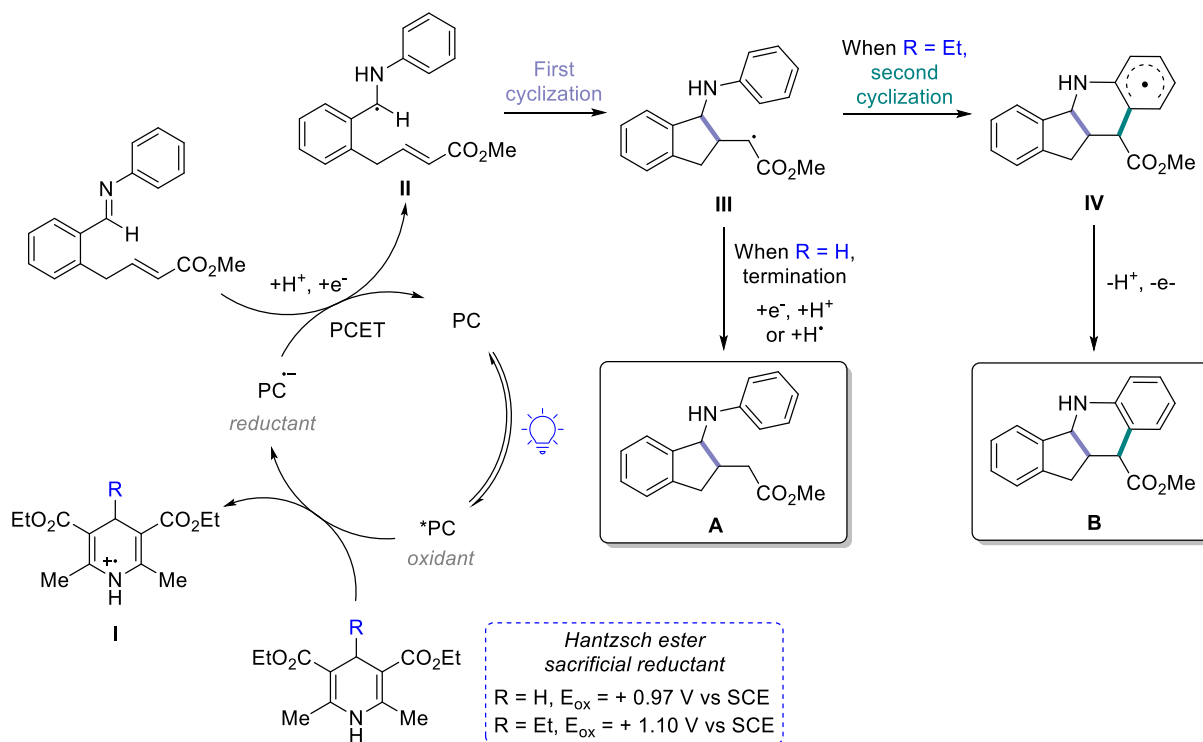
Figure 4. Intramolecular C-C bond formation under PCET conditions from imines – mechanism and product distribution.

The electrochemical reduction of iminium ions was also demonstrated by Rovis and co-workers.[38] The methodology was used to generate otherwise elusive α-tertiary primary and secondary amines.

3.1.2.4.   Redox active esters

Alpha-amino ester derivatives where the ester moiety possesses a low reduction potential can be used to generate α-aminoalkyl radicals by reduction of the ester moiety and loss of CO_2 (Scheme 5). This is the case for the *N*-(acyloxy)phthalimide moiety for which the reduction potential lies between −1.28 and −1.37 V *vs* SCE in MeCN.[39]

amino ester derivative

Y = redox
active moiety

N-(acyloxy)phthalimide
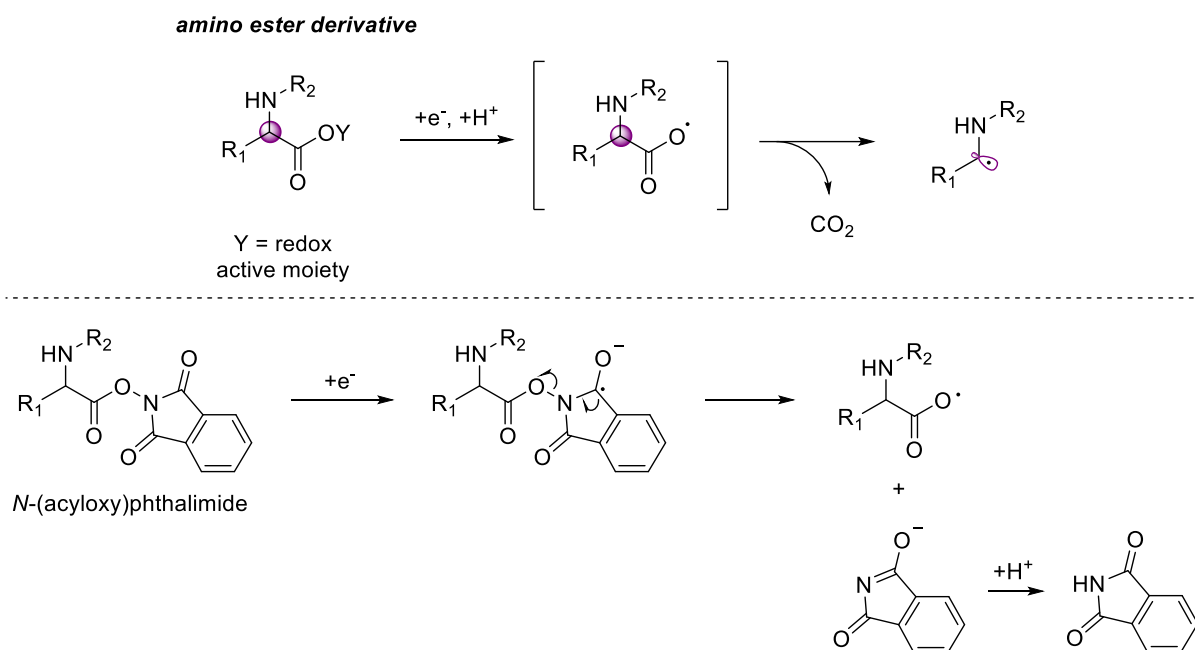
Scheme 5. Redox active esters in the formation of α-aminoalkyl radicals. Example of the N-(acyloxy)phthalimide moiety.

This strategy was used repeatedly under photoredox conditions for the functionalization of amino acids and peptides *via* the α-aminoalkyl radical intermediate,[40–42] including for enantioselective protocols.[43–45]

In sections 3.1.2.1 to 3.1.2.4, the α-aminoalkyl radicals were generated under reducing conditions. The low oxidation potential of these radicals have sometimes limited their use under oxidative conditions due to their fast conversion to iminium ions.[46–50] However, there exist precursors that can be efficiently used for α-aminoalkyl radical generation under mild oxidative conditions, including photocatalytic protocols.

3.1.2.5.   Hydrogen Atom Abstraction alpha to the nitrogen

Alpha-aminoalkyl radicals can be generated by hydrogen atom abstraction at the α-amino carbon, either intramolecularly or intermolecularly (Figure 2B). A HAT event corresponds to the simultaneous removal of an electron and a proton. This is favorable when the resulting bond has a higher bond dissociation energy than the α-amino C-H bond (89-94 kcal/mol).[51] Additionally, the HAT agent should be sufficiently electron poor to abstract the most hydridic hydrogen in the molecule, if there are several α-amino C−H bonds. Direct intermolecular HAT events have been reported using the ethyl radical generated from the Et₃B/O₂ system,[52,53] or the *tert*-butoxyl radical generated from *tert*-butyl hydroperoxide.[54–56] Problems of regioselectivities have been observed in all these studies when using unsymmetrical substrates, in addition to over-oxidation.

Already in 1990, Curran reported the generation of α-amidoalkyl radicals following 1,5-hydrogen atom transfer and subsequent cyclization on an electron-poor olefin (translocation-cyclization process, Scheme 6A).[57] Undheim and co-workers extended this chemistry to a limited scope of cyclic tertiary amines whose α-aminoalkyl radicals were reacted intermolecularly with electron-poor olefins (Scheme 6B).[58] In 2002, Ikeda and co-workers reported the racemic synthesis of the Cbz-protected (±) − euphococcinine alkaloid using a similar methodology (Scheme 6C).[59] The radical cyclization from the iodophenyl precursor **1** furnished the 9-azabicyclo[3.3.1]nonane scaffold **2** in 95% yield. Removal of the silyl group and ozonolysis afforded the beta-ketoamine **4** in good overall yield. The ketone was

converted to the vinyl triflate and subsequent reductive removal of the triflate under palladium catalysis gave the allylamine **5** in 61% yield over two steps. The hydroboration step proved not regioselective, and the desired alcohol **6** was obtained in a modest 39% yield. Oxidation using the TPAP/NMO system gave the desired Cbz-protected alkaloid **7** in quantitative yield. The main drawback in this synthesis was the preparation of **1**, obtained in 13 steps from methyl *N*-Boc-pipecolinate.

A/ Curran - 1990

B/ Undheim - 1994

X = O, **55%**
CH₂, **65%**
NCHO, **41%**
S, **23%**
NMe, **29%**

C/ Ikeda - 2002 *Translocation Cyclization sequence*
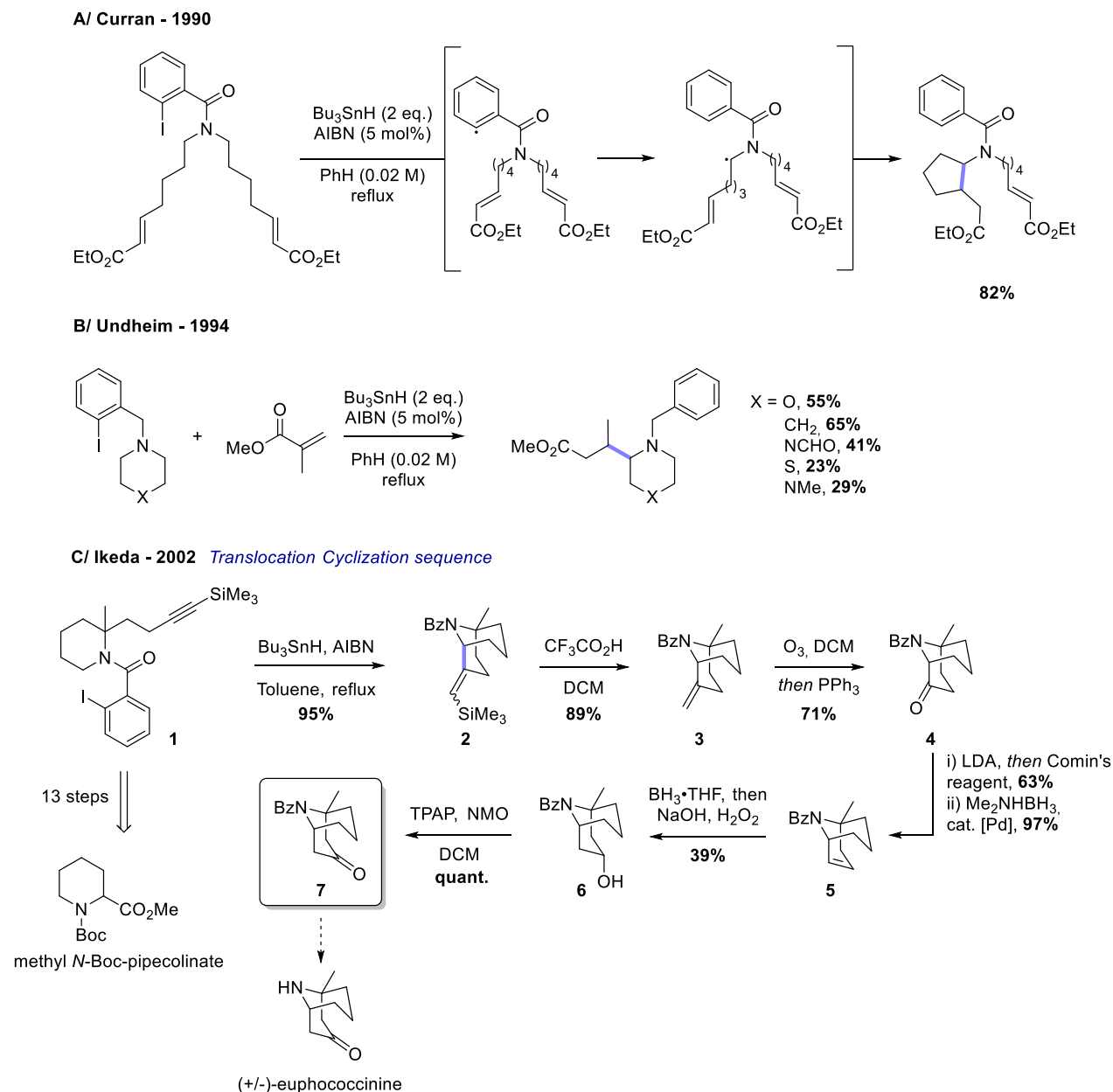
Scheme 6. Examples of α-amino- and α-amidoalkyl radicals generated via 1,5-hydrogen atom transfer. A/ Curran, α-amidoalkyl radicals. B/ Undheim, extension to α-aminoalkyl radicals. C/ Ikeda, application to the synthesis of an advanced precursor of euphococcinine.

A similar strategy is also possible using the intermediacy of vinyl radicals instead of aryl radicals, obtained either from a vinyl iodide precursor,[60] or from radical addition to an alkyne moiety (Radical Addition-Translocation-Cyclization process, RATC). For example, Renaud and co-workers reported the sequential addition of thiyl radicals to *N*-homopropargylic amines such as **8**, 1,5-HAT to generate the α-aminoalkyl radical, and cyclization of this radical on the newly formed olefin moiety to synthesize 1-azabicyclic compounds like **9** (Scheme 7A).[61] A similar process was recently published using sulfonyl

radicals obtained *via* photoredox-mediated oxidation of sulfinate salts (Scheme 7B).[62] While in Renaud's work the transformation was a radical chain transfer reaction initiated by AIBN, the photoredox mediated reaction was proposed to follow an iridium catalytic cycle.

A/ Renaud, 2007

Radical Addition Translocation Cyclization sequence

B/ Cai and Ji, 2022
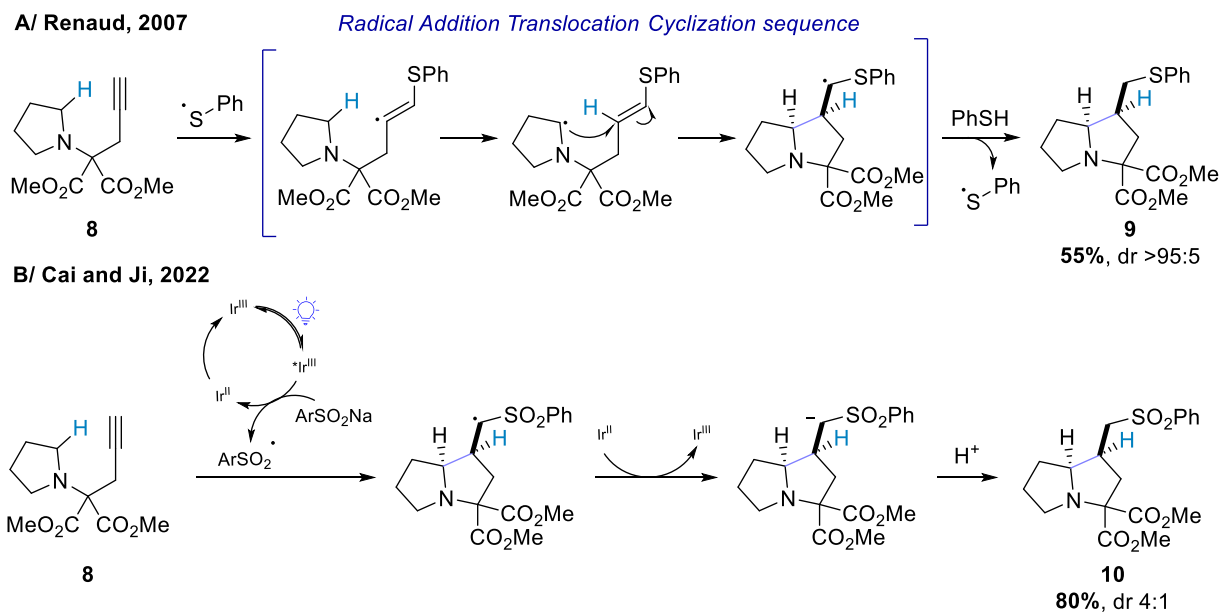
Scheme 7. Radical Addition Translocation Cyclization sequences for the synthesis of 1-azabicyclic derivatives. A/ Radical chain transfer reaction proposed by Renaud and co-workers. B/ Photoredox protocol proposed by Cai and Ji.

More recently, photoredox chemistry has also been used to generate direct HAT catalysts from quinuclidine,[63–65] thiols,[66,67] azides,[68] or phosphate salts.[69] The strategy is to use easily oxidizable reagents in order to generate the reactive HAT intermediate *via* photoredox catalysis (Scheme 8, intermediate **I** in the case of quinuclidine). Upon hydrogen atom abstraction from the starting material, the α-aminoalkyl radical **II** is generated and reacted with an appropriate coupling partner to give the corresponding radical intermediate **III**. The reduced photocatalyst can give an electron to this intermediate, closing the photoredox cycle and generate an anion **IV** prone to be protonated by the HAT agent, thereby closing the HAT catalytic cycle.
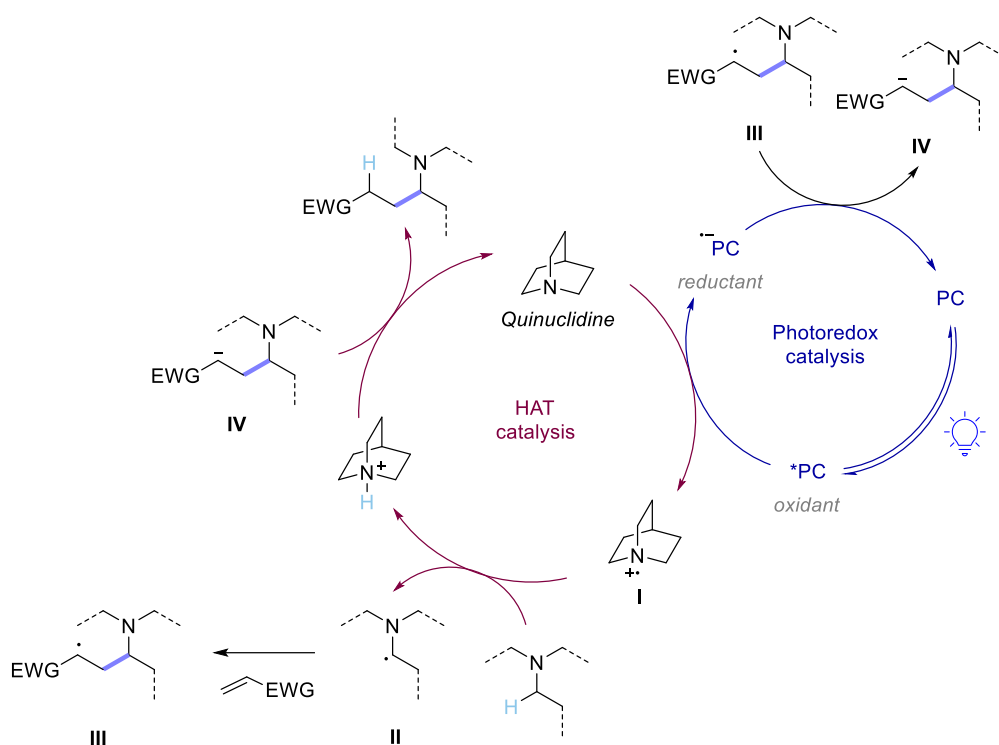
Scheme 8. General mechanism for a dual HAT/photoredox catalysis reaction.

Under these conditions, a large scope of α-aminoalkyl radicals can be generated from primary, secondary and tertiary amines. The possibility to use primary amines allows for a subsequent ionic cyclization as demonstrated by Cresswell and co-workers.[68] Interestingly in this methodology, switching the catalyst from an organic to an iridium photocatalyst in combination with an excess of trap led to the formation of bis-alkylated, mono-cyclized products **11** and **12** (Scheme 9A). Zhu and co-workers described a radical cyclization reaction on a pre-installed ester substituted olefin (Scheme 9B).[70]

A/ Cresswell - 2020. Radical addition, ionic cyclization.
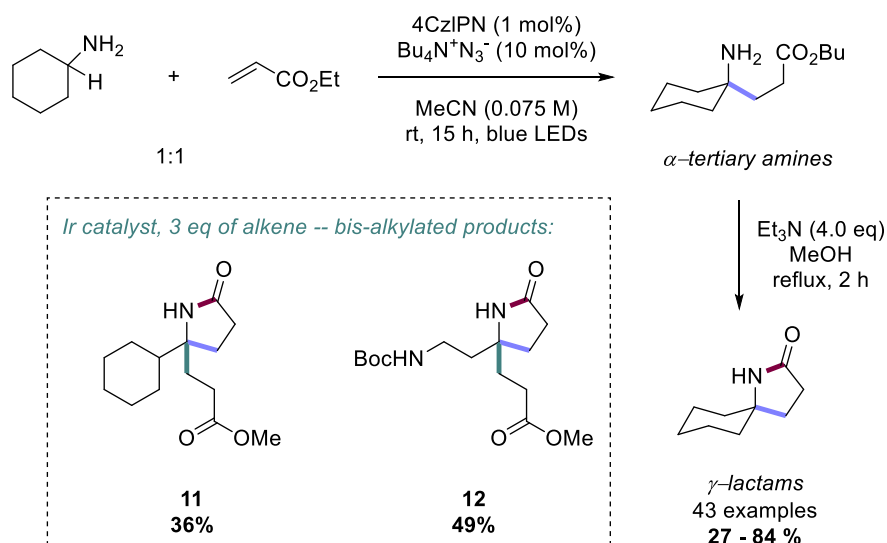
B/ Zhu - 2017. Radical cyclization.
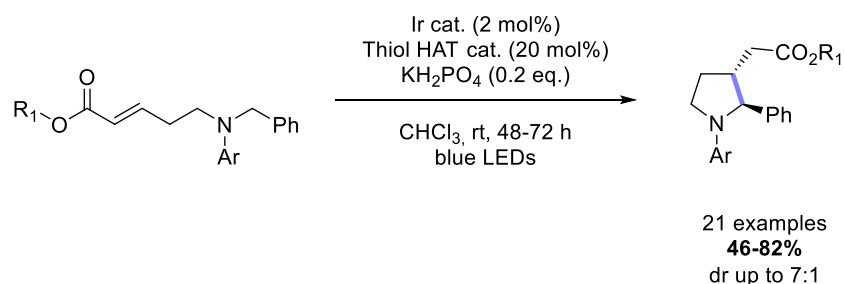
Scheme 9. Applications of the dual HAT/photoredox catalysis protocols. A/ Synthesis of γ-lactams by ionic cyclization of a primary amine. B/ Synthesis of pyrrolidine derivatives by radical cyclization.

3.1.2.6. *One-electron oxidation of amine derivatives*

Alpha-amino carboxylic acid precursors

It is also possible, under mild oxidation conditions, to perform decarboxylation reactions directly on carboxylic acids, or more precisely on the carboxylate salts (as opposed to the use of redox esters, see section 3.1.2.4). After single-electron oxidation of the carboxylate moiety, decarboxylation affords the corresponding α-aminoalkyl radical (Figure 5A).

A/

amino acid derivative

B/

13 (*N*-Boc-proline)
E_{ox} = + 0.95 V *vs* SCE in MeCN

No exact value in the literature. Similar reactivity as the proline derivative.

14 (*N*-phenyl glycine)
E_{ox} = + 0.42 V *vs* SCE in MeCN
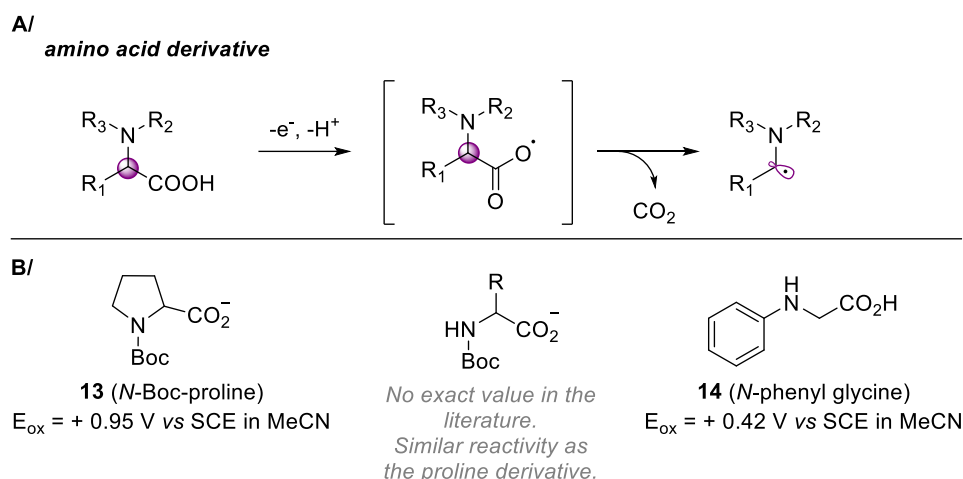
Figure 5. Alpha-amino-and alpha-amidoalkyl radicals from the oxidation of the carboxylic acid precursors. A/ General mechanism. B/ Oxidation potentials of common precursors.

Typical oxidation potentials for Boc-protected α-amino acids such as Boc-Proline (Figure 5B, precursor **13**) have been measured to reach + 0.95 V *vs* SCE in acetonitrile.[71] No values are known for secondary derivatives, but the oxidation potentials should be relatively close since these precursors can be reacted under the same reaction conditions as **13**, with the same photocatalysts.[71,72] *N*-aryl glycine derivatives such as **14** are also common precursors with very low oxidation potentials (+ 0.42 V *vs* SCE in MeCN for *N*-phenyl glycine). These precursors have typically been used in photoredox protocols since their oxidation potential is in the range of common iridium-based photocatalysts. They allow for the direct α-functionalization of amino-acid precursors by radical addition to Michael acceptors,[71–77] and are compatible with metallaphotoredox catalysis protocols.[78–82]

Following a very similar mechanism and concept, Akita and co-workers reported in 2014 the use of aminomethyltrifluoroborates as precursors for α-aminoalkyl radical synthesis.[83] One-electron oxidation of the trifluoroborate moiety was reported to be in the range of the [Ir(dF(CF₃)ppy)₂(bpy)](PF₆) photocatalyst (Ir$_{III*/II}$ = + 0.97 V vs SCE in MeCN).[84]

Aminium radical cation intermediates

Other precursors of α-aminoalkyl radicals by one electron oxidation of amines go through the aminium radical cation intermediates. Loss of the silyl group in silylamines (Scheme 10A), or of a proton in non-silylated tertiary amines (Scheme 10B), gives rise to the thought-after α-aminoalkyl radical.

A/ *α–silylamine*   **B/** *tertiary amine*
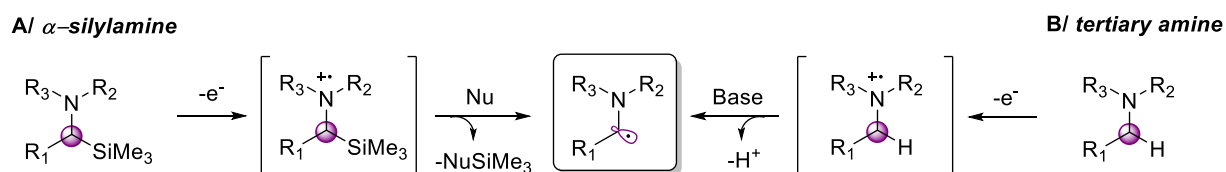
Scheme 10. Alpha-aminoalkyl radical formation through the radical cation intermediates from α-silylamines (A) and tertiary amines (B).

Alpha-silylated amines

Silyl substitution at the α-carbon of the amine induces a significant drop in the oxidation potential as demonstrated by Cooper and Owen with compounds **15** and **16** (Figure 6).[85] When the silyl group is

placed one carbon further away from the nitrogen, the oxidation potential increases again (compare **17** and **18**, Figure 6).
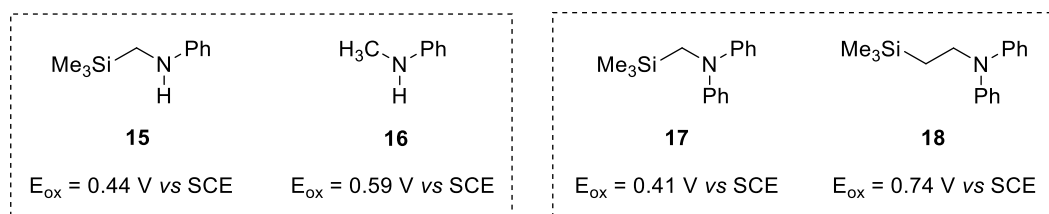
Figure 6. Comparison of some α-silylamines and non-silylated counterparts. Influence of the position of the silyl group on the oxidation potential.

This beta-silicon effect was attributed to a rise of the HOMO level in the neutral molecule due to the overlap between the 2p orbital of the nitrogen and the filled C–Si bond, which favors electron transfer. In addition, but less dominant, the filled C–Si bond overlaps with the half-vacant 2p orbital of the radical cation intermediate, which has a stabilizing effect. Consequently, the beta-silicon effect is the strongest when the molecule's geometry allows for the C-Si bond and the p orbital on the nitrogen to be coplanar.[86] Moreover, the rate of radical cation decay, that is the rate of desilylation, was shown to be related to the concentration of silophile in the reaction medium. Hence nucleophilic solvents (H_2O, MeOH) or the addition of salts such as *n*Bu$_4$NF strongly favor the formation of the α-aminoalkyl radical from the silyl radical cation. In the absence of an efficient desilylation process, back electron transfer (BET) to the catalyst occurs.[87]

Yoon and Mariano reported in the late 1980s the photoinduced single electron transfer between α,β-unsaturated cyclohexenones and α-silyl tertiary amine donors.[88] They showed that the aminium radical cation derived from one-electron oxidation of α-silylamines underwent α-C–Si bond rupture to produce α-aminoalkyl radicals (Figure 7A). In 1991, the same authors demonstrated that the intramolecular photoaddition of silylamines **19** to α,β-unsaturated olefins could be promoted by a SET photosensitizer, for example 9,10-dicyanoanthracene **21** (Figure 7B).[89] After addition of the photogenerated α-aminoalkyl radical, 6-endo cyclization on the pendant olefin generated an α-keto radical that was reduced by the sensitizer, giving the fused 6-membered ring **20** in 54% NMR yield.
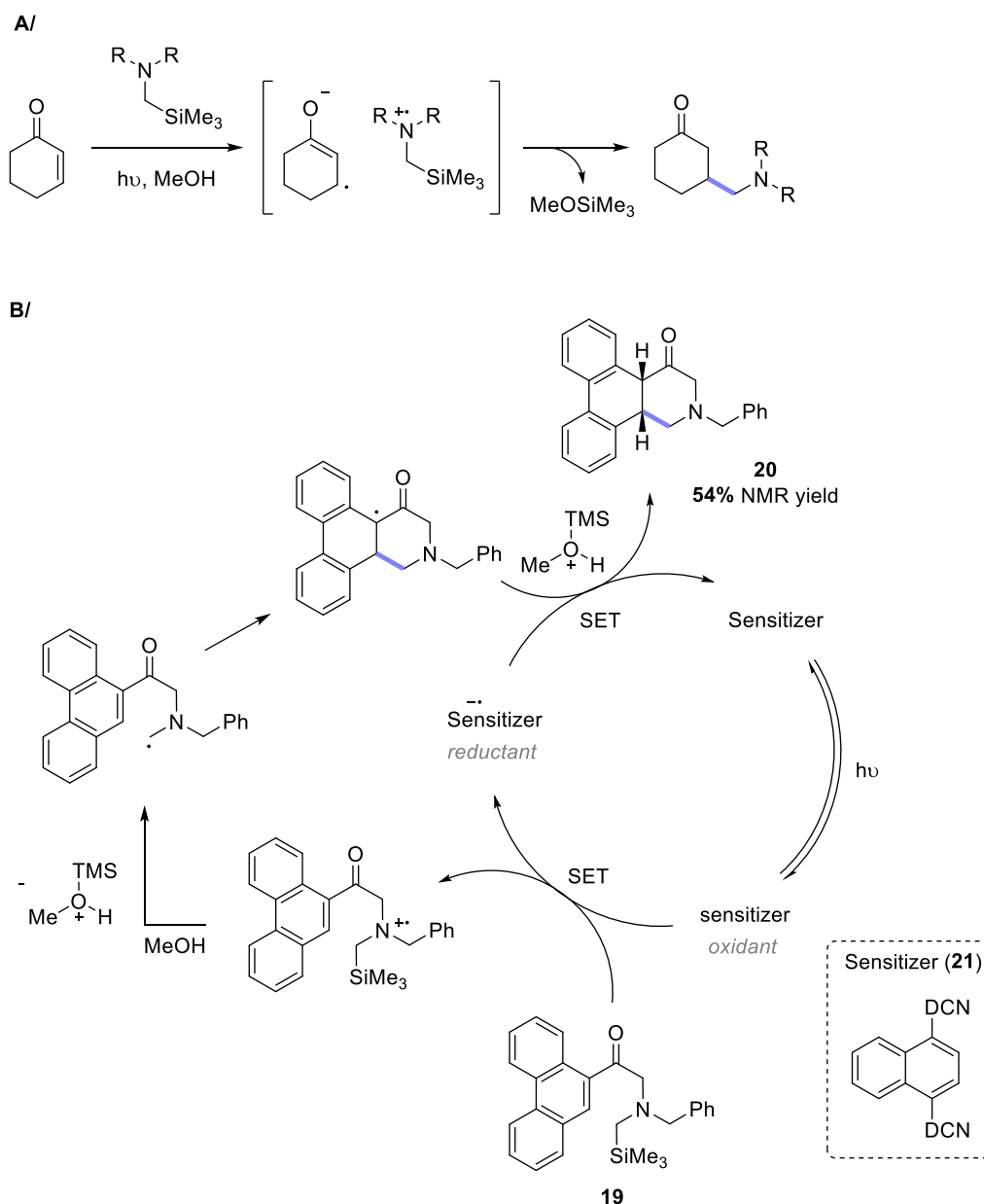
Figure 7. Early reports on the photogeneration of α-aminoalkyl radicals from α-silylamines. A/ SET between an enone and the tertiary amine. B/ Catalytic cycle of the sensitized reaction.

Pandey and co-workers reported the synthesis of the pyrrolizidine ring system **23** using this strategy and precursor **22**.[90] Interestingly they reported an excellent yield of 88% for the radical addition of the α-aminoalkyl radical to the unactivated olefin (Scheme 11A). The authors demonstrated as well the possibility to use an allylchloride **24** as intramolecular radical acceptor for the synthesis of (±) − epilupinine, presumably *via* a radical addition-elimination sequence leading to intermediate **25** (Scheme 11B).

A/

22 → **23**
88%, dr >20:1

B/

24 → **25** → (+/-)-epilupinine

via
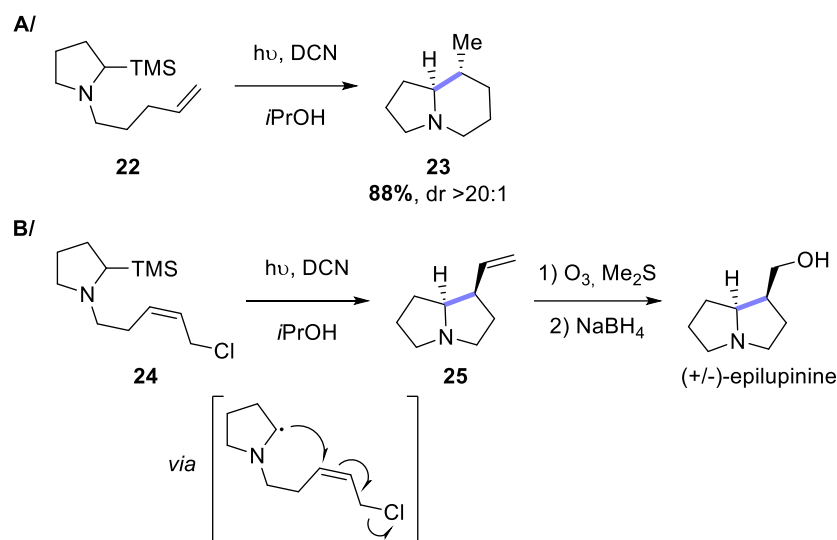
Scheme 11. A/ General synthesis of the pyrrolizidine ring system. B/ Small total synthesis of racemic epilupinine by Pandey.

After the initial reports by Pandey and Mariano, the same type of chemistry was carried out with transition metal polypyridyl complexes by Nishibayashi.[91,92] In 2015, Yoon and co-workers reported the enantioselective radical addition of siliylated amines to Michael acceptors using a chiral ligand.[93] Metallaphotoredox protocols proved successful for arylation[94,95] and conjunctive cross-coupling reactions.[96] The report by Molander and co-workers describing the α-arylation of α-silylamines under dual Ru/Ni catalysis (Scheme 12) deserves to be discussed.[94]

Ru(bpy)$_3$(PF$_6$)$_2$ (2 mol%)
[Ni(dtbbpy)(H$_2$O)$_4$]Cl$_2$ (5 mol%)
DMF, rt, 24 h
blue LEDs

1.2 eq.

25 examples
41-83% yield

26 → **27**
54%
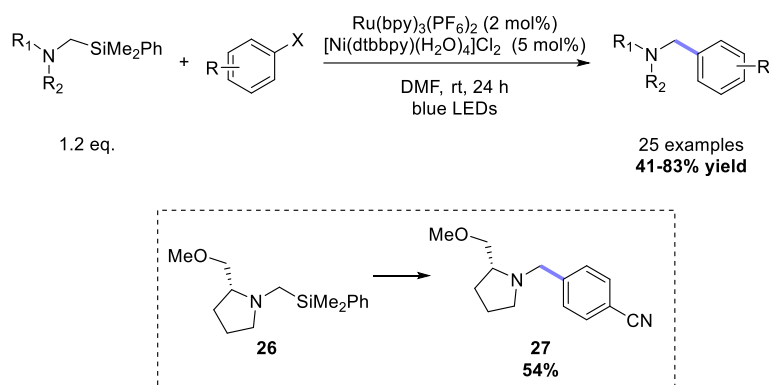
Scheme 12. Alpha-arylation of silylated amines under metallaphotoredox catalysis by Molander.

The authors measured the oxidation potential of selected α-silylamines and their corresponding arylated products. They observed that the oxidation potentials of the products were around 0.3 V greater than that of their precursors. By carefully choosing the photocatalyst, no bis-arylated product was observed. Additionally, an optically active substrate **26** was used to give the corresponding product **27** with retained optical activity, ruling out a radical formation at this substituted position.

The advantage of pre-functionalized precursors such as α-silylated or -carboxylated amines is that the regioselectivity of the α-aminoalkyl radical formation is dictated by the position of the functional group. Additionally, the significant difference in oxidation potential between the starting material and the product prevents further reactivity of the product under mild oxidative conditions. Finally, α-aminoalkyl radicals on secondary amines can be easily generated in this way (see Figure 5 and Figure

6). The disadvantage is the necessary pre-functionalization of the starting materials. While α-amino acids are abundant, this is a non-negligeable problem for α-silylamines.

As a result, methods for the direct one-electron oxidation of non-functionalized amines have been developed.

One-electron oxidation of tertiary amines

Upon one-electron oxidation of tertiary amines, the acidity of the α-C—H bond is significantly increased. For example for triethylamine (Scheme 13), the *p*Ka of the alpha proton decreases from around 40 to 15 (in acetonitrile),[97] making a deprotonation by common organic and inorganic bases possible.

E_{ox} = +0.78 V vs SCE in MeCN
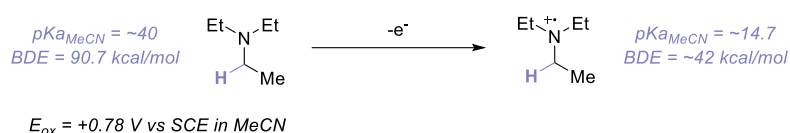
Scheme 13. Comparison of pKa and BDE of the α-C-H bond in the neutral triethylamine and in the radical cation.

One of the challenges in the formation of α-aminoalkyl radicals from tertiary amines is the regioselectivity of the deprotonation alpha to the radical cation when several C–H bonds are available, as in the example of *N*-ethyl,*N*-isopropylaniline radical cation depicted in Figure 8. In such example, literature precedence has shown that the least hindered position was deprotonated to give exclusively the least substituted, secondary radical over the tertiary radical (**I** over **II**).[98] This is attributed to the overlap between the half-vacant p orbital of the radical cation and the C—H bond to be broken. Steric interactions as depicted by a Newman projection are greater in **RCII** than in **RCI**. In some cases, the radical stability also plays the role. Thus in the case of tetrahydroisoquinolines, a common starting material for α-aminoalkyl generation, the radical is exclusively formed at the benzylic position and not at the other secondary position.
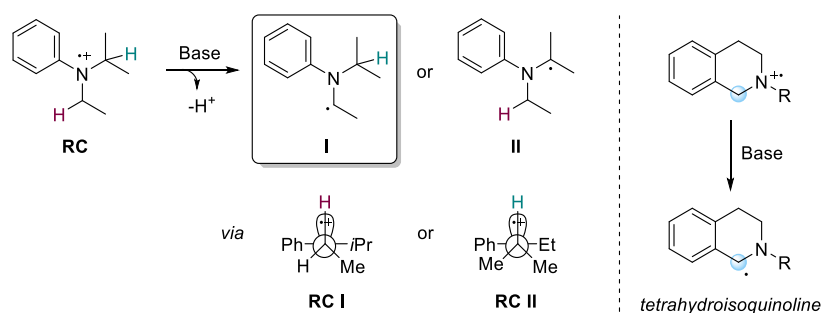
Figure 8. Regioselectivity considerations in the deprotonation of asymmetric amine radical cations (RC).

Mariano and co-workers have extensively studied the dynamics of α-CH deprotonation in tertiary amine radical cations.[87] In addition to the steric effects induced by α-substituents discussed above (Figure 8), they have shown that remote electronic effects were predominant in the rate of decay of the radical cation. Hence in the aniline series, the electron-rich, *para*-methoxyphenyl derivative **29** is easier to oxidize than the non-substituted aniline **28**. However, its deprotonation leading to the α-aminoalkyl radical is 15 times slowlier (Figure 9).
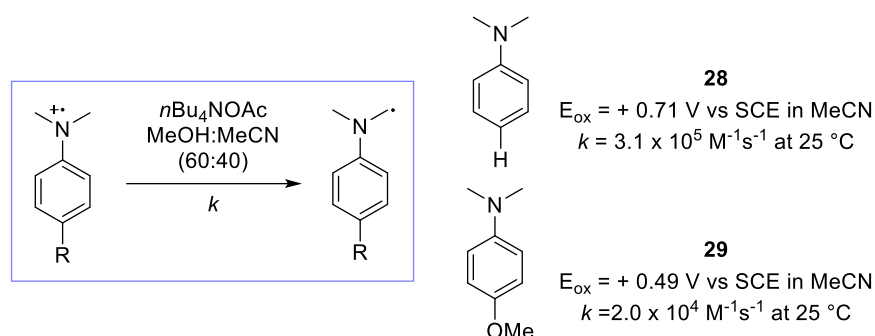
Figure 9. Comparison of oxidation potentials and rates of radical cation decay for diversely substituted N,N-dimethylanilines.

There exist systems in which the deprotonation of the α-proton is not feasible due the impossible orbital overlap, for example in bridged, azabicyclic systems.[99] Quinuclidine, which was encountered earlier (Scheme 8), is easily oxidized to the radical cation, but the α-aminoalkyl radical cannot be formed. Instead, the radical cation will act as a hydrogen abstraction agent. Additionally, Wei and Shi recently reported the addition of the quinuclidinium radical cation to unactivated olefins, thus enabling the formation of Morita-Baylis-Hillman products from non-electron-deficient olefins.[100,101] For the *n*-hexene olefin, they observed that the radical addition was more favorable than a potential HAT event leading to an allylic radical. Other reactivity pathways of the aminium radical cation include back electron transfer (BET) to the catalyst,[87] the removal of a hydrogen to give the iminium ion[102,103] and fragmentation reactions largely limited to aminocyclopropanes.[104,105] Furthermore, aminium radical-cations have been shown to be one-electron oxidants of amines, leading to new radical cation products.[106–108] These reactivity pathways are described in Figure 10 and are important to keep in mind, but they will not be discussed further in this chapter.
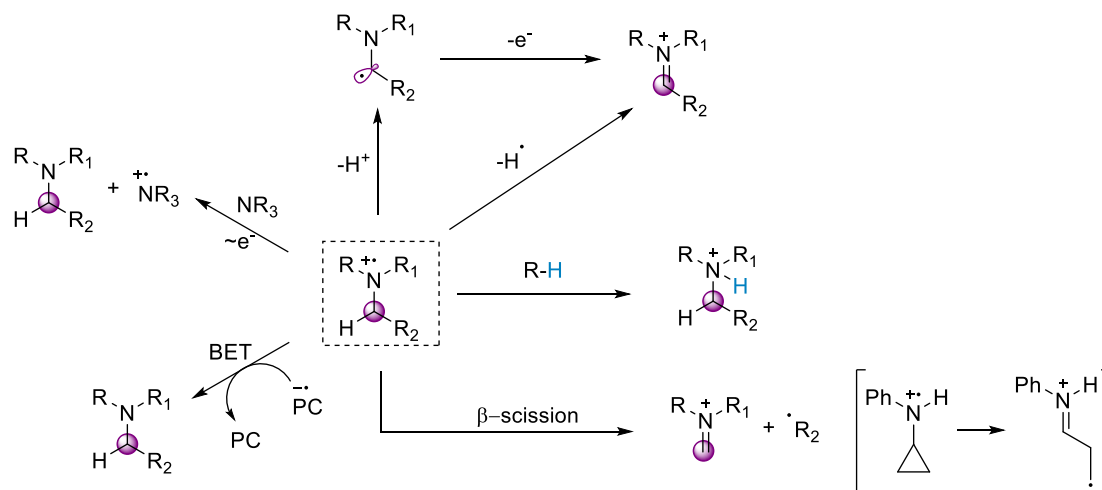
Figure 10. The chemistry of aminium radical cations.

Bertrand, Hoffmann and Pete investigated early-on the photoinduced electron-transfer between tertiary amines and a photosensitizer.[109,110] They optimized in particular the intermolecular addition of tertiary amines to alkenes, so far limited by oligomerization processes and undesired reactions involving the sensitizer. The authors focused on the addition of tertiary alkyl amines **30** on optically active menthyloxyfuranone **31** (Figure 11A). The reaction was amenable to *N*-methyl, *N*-ethyl, and *N*-*tert*-butyl pyrrolidines (**30a** to **30c**). The high regioselectivity observed for *N*-ethylpyrrolidine **30b** is probably due to stereoelectronic effects. Indeed, the specific geometry induced by the pyrrolidine ring is considered to allow for a perfect and low-energy alignment of the p orbital on the nitrogen atom

with the C-H bond of the pyrrolidine ring. This could also explain the lowered efficiency observed with *N*-methylpiperidine **30h**, which gave the desired product **32h** in increased diastereoselectivity but moderate yield of 46%. Interestingly, bulky silyl-*N*-protected amine **30d** was well tolerated (77% yield). However, *N*-allylpyrrolidine **30g** only resulted in a Michael addition product **33** in 53% yield. The mechanism of this dealkylation reaction was not deciphered (radical fragmentation of the allyl radical or overoxidation to the iminium ion). Additionally, the authors described the enantioselective synthesis of the pyrrolizidine alkaloid (+)-laburnine from **32a** (single diastereomer) (Figure 11B). The menthyloxy moiety was removed using NaBH$_4$, followed by a light driven dealkylation reaction at the nitrogen center[111,112] and lactamization to give **35**. Reduction of the lactam gave the desired product in 22% overall yield from radical acceptor **31**.
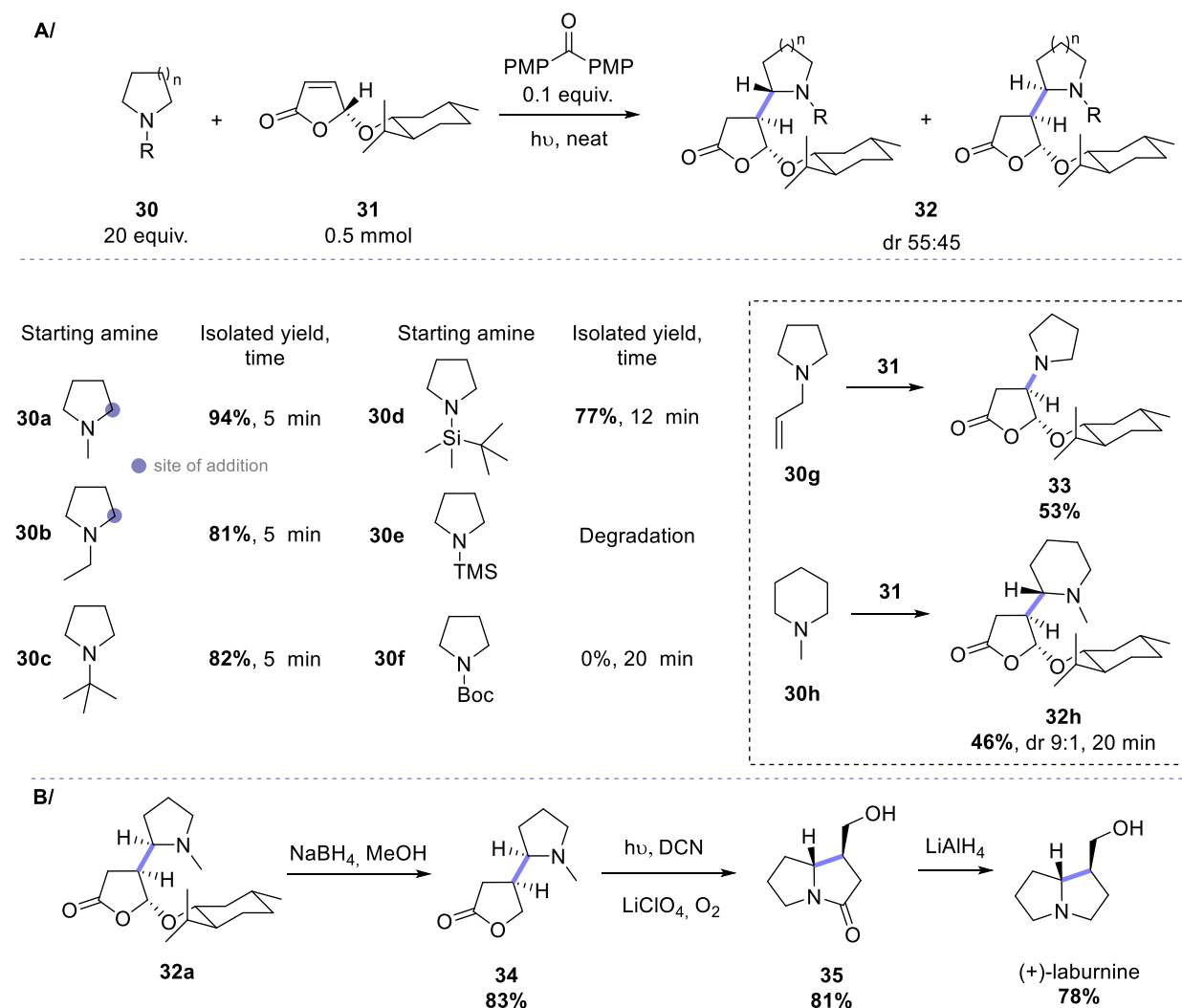
Figure 11. A/ Diastereoselectivity in the radical addition of tertiary amines to (5R)-5-Menthyloxy-2-(5H)-furanone and selected substrate scope. B/ Application to the enantioselective synthesis of necine bases.

Mechanistically, the authors proposed that an electron-rich benzophenone sensitizer was able to initiate the reaction and that a chain-transfer reaction was operative in the presence of a large excess of amine (Figure 12). They suggested that a polarity-matched HAT between the radical intermediate **V** and the starting amine **30a** was kinetically favored in the presence of the excess amine. Additionally, they observed the recovery of the photosensitizer, from which they concluded that an HAT event was also possible between the ketyl radical **III** and **V**, leading to the same addition product **32**. The apparent regioselectivity observed in the initiation step for the formation of the secondary α-aminoalkyl radical

IV over the primary radical was not accounted for. It is possible that the other regioisomer was formed during the initiation step, but the corresponding product formed in too small quantity to be detected. The attack of the α-aminoalkyl radical was stereoselective and *anti* with respect to the installed menthyloxy substituent. However, the configuration of the asymmetric center alpha to the nitrogen was not controlled and diastereomeric ratios close to 1:1 were obtained for starting materials with a 5-membered ring.
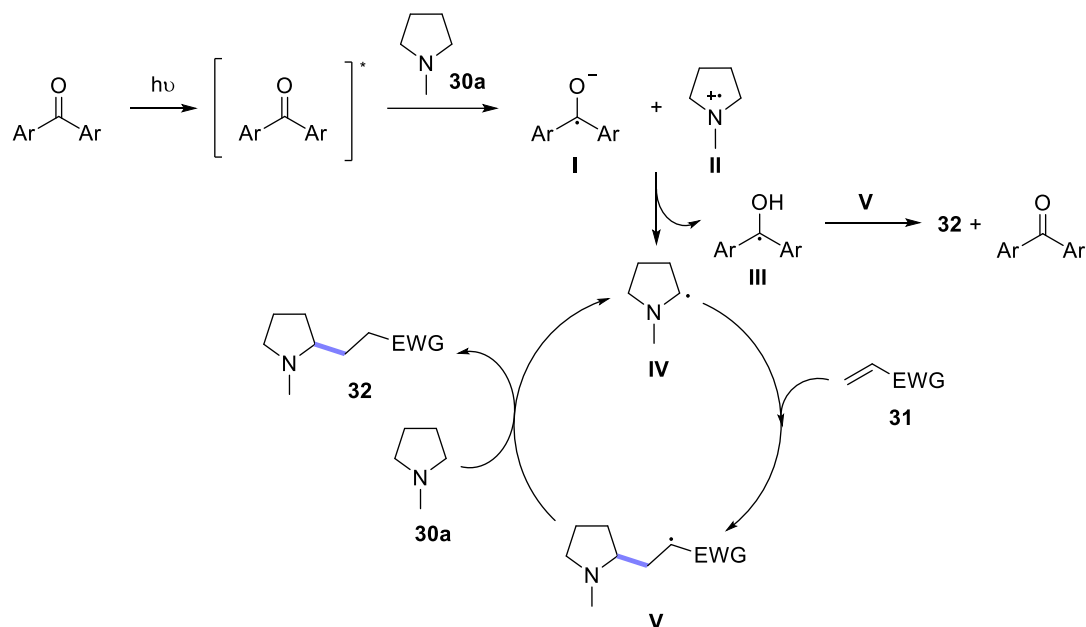
Figure 12. Mechanistic proposal for a photo-initiated chain transfer reaction between tertiary amines and activate olefins.

Interestingly, the authors reported the same reaction using bulk semiconductors as photocatalysts (TiO$_2$, ZnS).[113] The amine was again used in high excess (40 equivalents) to favor hydrogen abstraction in the chain propagation. The choice of the semiconductors was driven by the necessity to avoid overoxidation of the α-aminoalkyl radical.

The one-electron oxidation tertiary amines followed by radical addition to electron-deficient olefins has been used in the very first modern photoredox protocols involving iridium and ruthenium catalysis, as demonstrated by MacMillan in 2011[114], Nishibayashi,[91,115] and Pandey and Reiser[116] in 2012. Since then, an extensive number of papers have been published varying starting materials (amine precursor and coupling partner), merging photoredox with metal-catalyzed cross-couplings, or proposing enantioselective protocols. A general mechanism for the generation of α-aminoalkyl radical and subsequent addition to an electron-deficient olefin is presented in Figure 13. The resulting carbon-centered radical, located alpha to an electron-withdrawing group, is reduced by the catalyst to close the catalytic cycle and give the desired product after protonation. Hence for a redox-neutral protocol, the photocatalyst should both be able to oxidize the starting material and reduce the radical adduct. The product in this case, in contrary to reactions involving α-amino acid or α-silylated amine precursors, looks relatively similar to the starting material. It is indeed a tertiary amine, usually containing at least one α-C–H bond that could be involved in a second α-aminoalkyl radical formation.

133
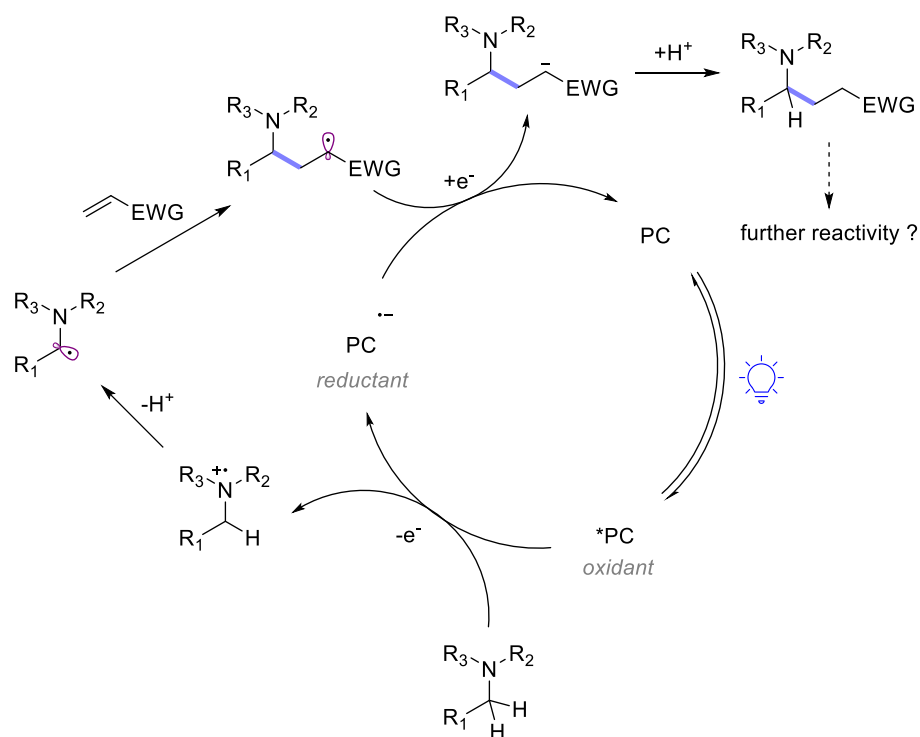
Figure 13. General mechanism for the redox-neutral photocatalyzed generation of α-aminoalkyl radicals and subsequent addition to activated olefins.

Nishibayashi and co-workers published a review on this topic in 2016,[117] but this field has grown tremendously between 2016 and 2022, so much that an exhaustive review of the literature is not relevant in the context of this chapter. Instead, we are particularly interested in protocols describing further reactivity of the obtained α-functionalized products, either towards bis-functionalization of the starting materials or for cyclization reactions. The next section will solely focus on the corresponding studies.

In their 2012 publication, Nishibayashi and co-workers described the photoredox mediated single electron oxidation of tertiary amines for the generation of α-aminoalkyl radicals.[91,115] Addition of this radical was demonstrated on electron-deficient alkenes following a mechanism presented in Figure 13, using a 1.2 to 1.5 excess of amine in NMP at room temperature. The radical trap scope was limited to *beta*-substituted diethyl methylidenemalonate derivatives such as **36**. The unsubstituted analogue, bearing a terminal alkene moiety, did not lead to the formation of the desired product; this was attributed to rapid polymerization of the radical trap under the reaction conditions. The introduction of two electron-withdrawing groups at the alkene was also necessary to drive the reaction, possibly to facilitate the radical addition, but also to favor the terminal reduction event. The amine scope featured mostly easily oxidizable methyldiarylamines for which no regioselectivity issues were present. Dialkylaniline derivatives bearing bulky alkyl groups such as *iso*-propyl or *tert*-butyl chains were amenable to the reaction conditions as well. However, *N,N*-dimethylaniline **37** gave a mixture of mono- and bis-alkylated products **38** and **39** in a 3.6 to 1 ratio in the presence of 1.5 equivalents of the amine precursor (Scheme 14). The authors did not specify whether they tried to run this reaction with a higher excess of amine to prevent bis-alkylation.

CO₂Et / CO₂Et (36, 0.25 mmol) + H–N(Ph)–H (37, 1.5 equiv.) →[Ir^III (1 mol%); NMP (0.1 M), White LEDs, rt, 18 h]→ **38** + **39** **97% (38:39 = 3.6:1)**

Scheme 14. Evidence for bis-functionalization in the case of symmetrical, sterically unencumbered N,N-dimethylaniline.

This "high-excess" strategy was for example used by MacMillan and co-workers who reported in 2014 the α-vinylation of tertiary amines and α-amino acid derivatives using a vinyl sulfone radical trap **40** (Figure 14).[72] A 5-fold excess of the amine **37** was used, and the authors did not report the formation of any bis-functionalized product under these conditions. They did not report either if using a lower excess of amine resulted in the formation of such by-product. Nonetheless, the necessity to use such an excess greatly impaired the purification of the α-vinylated products, which turned out to have a similar polarity as the starting amine. As a result, the products had to be purified by preparative TLC on 0.5 mmol scale. Mechanistically, it was proposed that the addition of the α-aminoalkyl radical to the vinyl sulfone proceeded *via* a radical addition-elimination sequence expelling a sulfinyl radical that could be reduced by the photocatalyst to close the catalytic cycle ($E^{red}_{1/2}(PhSO_2^{\bullet}/PhSO_2Na) = +0.50$ V vs SCE and $E_{1/2}(Ir^{III}/Ir^{II}) = -1.37$ V vs SCE).

40 (0.5 mmol) + **37** (5.0 equiv.) →[Ir^III (1 mol%), CsOAc (3.0 equiv.); DCE (0.1 M), 26 W CFL, rt, 24 h]→ **41** **80%, *E/Z* >98:2** *No bis-vinylated product observed*

Figure 14. Alpha-vinylation reaction proposed by MacMillan and co-workers. No bis-vinylated products were observed using 5.0 equivalents of amine. The mechanism was proposed to go through an addition-elimination sequence expelling the sulfonyl radical, which is easily reduced.

In 2014, Li and co-workers reported the use of Baylis-Morita-Hillman allylic radical traps **42** for the α-allylation of *N*-aryl tertiary amines using a ruthenium photocatalyst.[118] Using two equivalents of amine in the presence of a base in DMSO, the authors obtained the desired products in moderate to good yields and products arising from bis-allylation were not observed. Mechanistically, the reaction proceeded as described in Figure 13, except that the α-ester anion is prone to beta-elimination of the acetate group instead of being protonated. This led to a product bearing an activated olefin moiety

(Figure 15). When the trap was initially substituted (R = Ph), the resulting beta-substituted olefin moiety was less reactive than the radical trap, and the product **43** not further consumed. When R = H, the terminal alkene moiety in **44** was prone to react with the amine present in slight excess, giving the addition product **45** in 18% yield. The authors mentioned that extensive screening of reaction conditions had been performed to optimize this reaction, without results. Unfortunately, this screening was not made available, and it was not mentioned if intramolecular cyclization on the pendant olefin moiety had been observed as well. No bis-allylated product was reported neither.
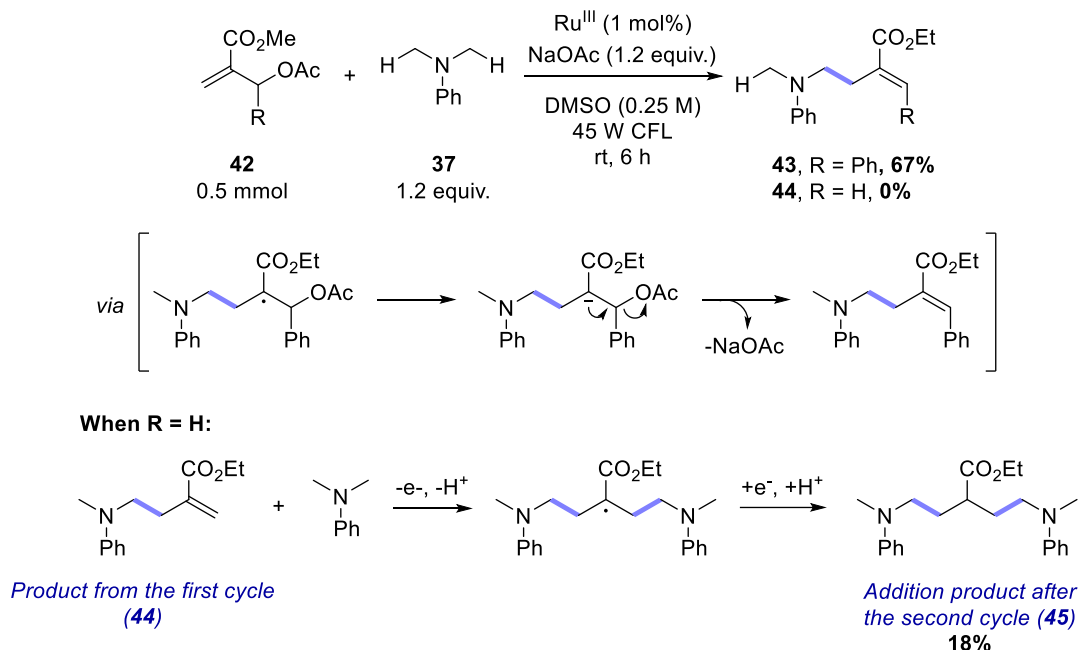
Figure 15. Alpha-allylation of N-aryl tertiary amines using an allyl acetate trap. Different outcome when R = Ph or R = H.

In 2020, Ready and co-workers reported the controlled bis-alkylation of *N*-aryl tertiary amines, in particular *N*-benzyl-*N*-methylaniline **46** (Scheme 15).[119] Experimentally, the starting amine was firstly reacted with 1.1 equivalents of methyl vinyl ketone **47** (MVK) in the presence of substoichiometric amounts of DBU and 5 mol% of photocatalyst, under 24 hours of irradiation in MeCN. Then, 2.0 equivalents of another α,β-unsaturated olefin **49a-d** were added to the reaction mixture and the initially formed α-alkylated product **48** could be further functionalized at the aliphatic position over the benzylic position, giving products **50a-d**. The scope of electron-withdrawing groups present on the second acceptor was broad, including ketones, nitriles, sulfones, amides and esters.
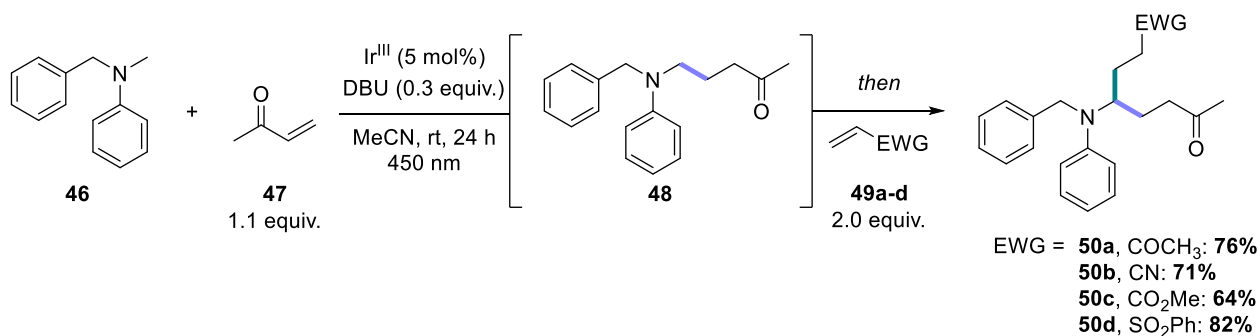
Scheme 15. Regioselective and unsymmetrical bis-alkylation of *N*-benzyl,*N*-methylaniline by Ready and co-workers.

While the addition of α-aminoalkyl radical to electron-poor olefins is undoubtedly one of the most studied transformations in the context of α-aminoalkyl radical utilization under photoredox conditions, the α-arylation of tertiary amines has also attracted much interest. Mechanistically, it is usually proposed that the amine is oxidized by the photoexcited catalyst Ir[III]*, while the coupling arene partner is reduced to the radical anion by the Ir[II] species, thus closing the catalytic cycle. Radical-radical coupling is alleged to account for product formation. The MacMillan lab has been pioneer in developing this chemistry using iridium-based photocatalysts. [71,114,120,121]

In 2017, Hashmi and co-workers reported the controlled mono- and di-perfluoroarylation of *N*-aryl tertiary amines by precisely tuning the equivalents of the perfluoroarene precursor.[122] Hence when using 1.5 equivalents of the aryl fluoride **51**, the mono-arylated product **52** was obtained. When the excess of aryl fluoride was increased to 4 equivalents, the bis-arylated product **53** was obtained (Scheme 16). The authors reported a hetero-diarylation protocol as well, sequentially adding 1.5 equivalents of two different aryl fluoride coupling partners **51** and **54**, leading to product **55**. Interestingly, the bis-arylation protocol was limited to *N*,*N*-dimethylaniline and *N*-phenylpyrrolidine derivatives. Engaging piperidine and azepane derivatives in the bis-arylation sequence resulted in little to no product at all, which the authors attributed to stereo-electronic factors.
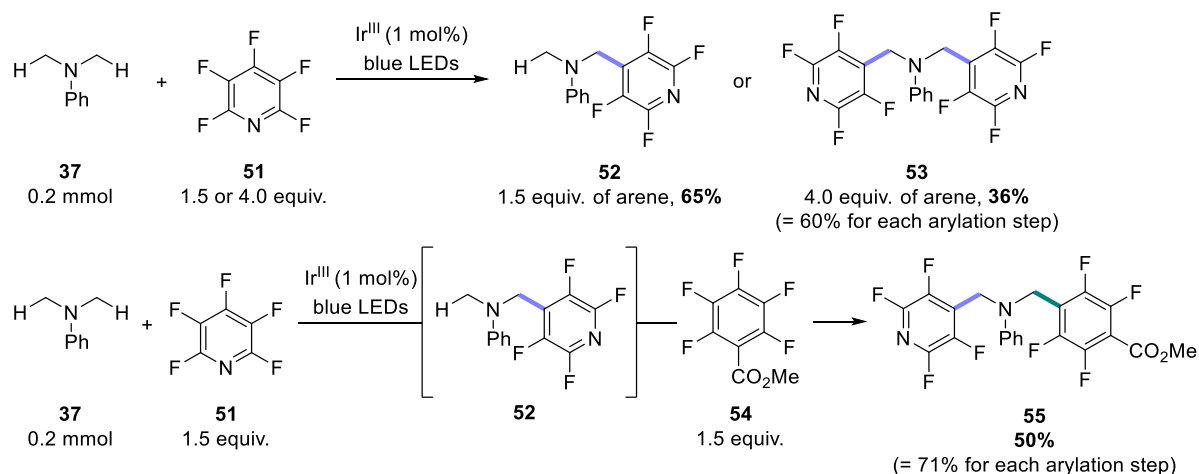
Scheme 16. Mono- and di-multifluoroarylation of N-aryl tertiary amines by Hashmi and co-workers.

Mechanistically, it was proposed as previously mentioned that the arene precursor was reduced by an Ir[II] species, giving a fluoroaryl radical anion. Radical-radical coupling of the α-aminoalkyl radical with this radical anion would be followed by fluoride extrusion to give the mono-arylated product. While this first catalytic cycle proceeds through reductive quenching due to the ease of oxidation of the starting tertiary amine, the second catalytic cycle is thought to undergo an oxidative quenching event. Indeed, the mono-arylated product **52** has a much higher oxidation potential than the starting amine **37** due to the electron-withdrawing character of the perfluoroaryl moiety. Hence it was suggested that in the second cycle, the prefluoroarene precursor was reduced by the photoexcited photocatalyst first, giving a potent Ir[IV] oxidant. One-electron oxidation of the α-arylated product could finally occur through this species, and radical-radical coupling accounts for the di-arylated product formation. The authors supported this mechanistic hypothesis with radical trapping, DFT calculations, fluorescence quenching experiments and cyclic voltammetry.

As exemplified from the previous studies, aniline derivatives are common substrates for the generation of α-aminoalkyl radicals and their addition to activated olefins. Some of their advantages include ease of handling and of purification in comparison with their trialkyl amine analogues, tunable redox potential through functionalization of the aromatic ring (see Figure 9), as well as the blocking of one

α-nitrogen position for increased regioselectivity in the α-aminoalkyl radical generation (compare for example trimethylamine and *N,N*-dimethylaniline). These substrates also offer the possibility for a slightly different strategy than previously described, in that the aromatic ring can play the role of a radical acceptor.[123,124] Combined with a first addition step as previously described, the overall sequence can lead to formally [4+2] annulated products **57**. Maleimides **56** have typically been used as olefins for these transformations,[56,125,126] and the reaction necessitates a sacrificial oxidant for the final rearomatization step, usually oxygen (reactions run under air) (Figure 16).
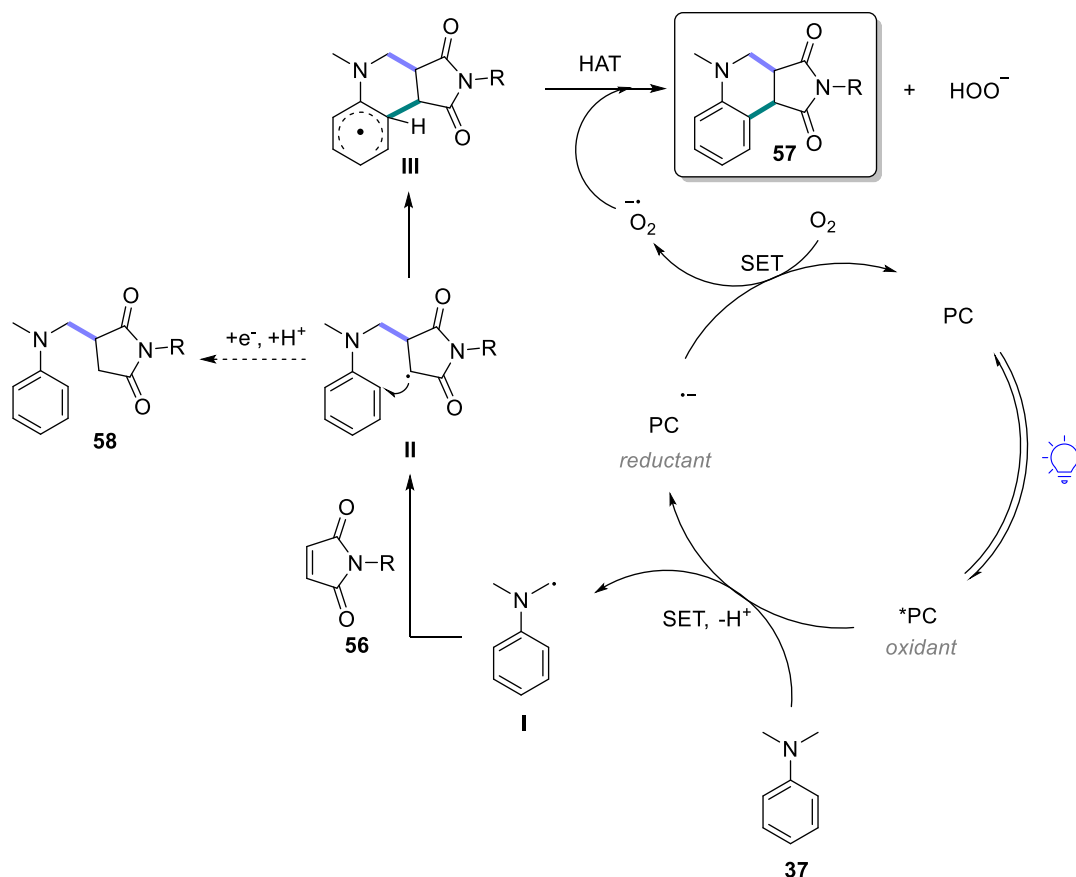
Figure 16. Typical mechanism for the radical addition/cyclization sequence with aniline derivatives.

In addition to the reduction potential of radical intermediate **II**, the presence of air was found to be a crucial factor in determining whether **II** will evolve to the reduced (**58**) or the cyclized product (**57**). Curran and Rueping reported that the radical addition to the aromatic ring was a reversible process and that in the absence of oxygen or a suitable oxidant in the reaction mixture, the equilibrium was in favor of the reduced product.[127] Only in the presence of oxygen became the tetrahydroquinoline derivative **62** the main product, as very clearly exemplified in their study with **59** and **60** (Scheme 17).
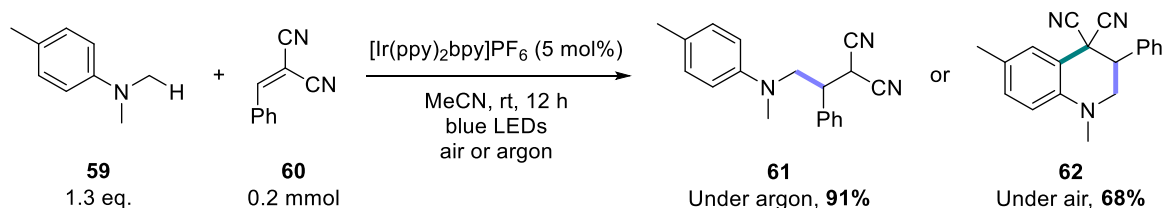
Scheme 17. Reactivity switch in presence or absence of oxygen. Under argon the addition product is obtained. In presence of oxygen, the addition/cyclization adduct is formed.

In this publication the radical scope was not investigated, but this reactivity does not seem to be limited to maleimides or to alkenes gem-disubstituted with electron withdrawing groups. Examples involving α,β-unsaturated ketones[128] or amides[129] have been reported as well.

Finally in one notable example by Pandey and co-workers,[130] the addition/cyclization product was obtained under oxygen-free conditions. It was hypothesized that the α,β-unsaturated ketone used as the radical trap and present in excess (2.5 equivalents) could be reduced by the photocatalyst. The obtained radical anion was protonated, and the resulting radical was able to perform the HAT event leading to the rearomatized product (instead of the superoxide radical anion, see Figure 16). The resulting desaturated ketone was observed in the reaction mixture.

This addition/cyclization sequence proved efficient for the synthesis of the tetrahydroquinoline scaffold. However no application towards the synthesis of complex tetrahydroquinoline alkaloids[131] was reported so far.

3.1.3. Tropane alkaloids

Tropane alkaloids are defined by their bicyclic structure possessing a nitrogen at the bridge position, namely a 8-azabicyclo[3.2.1]octane skeleton for the tropanes and a 9-azabicyclo[3.3.1]nonane skeleton for the nortropanes (Figure 17). These alkaloids are secondary plant metabolites found in the Solanaceae (or "nightshades", e.g. mandrake, belladonna, datura) and Erythroxylaceae (the "coca family") plants. The most famous natural occurring tropane alkaloids are cocaine and scopolamine, both able to pass the blood-brain barrier and cause dose-dependent psychoactive effects. Polyhydroxylated congeners of this large family like Calystegine A_3 are too hydrophilic to pass the blood-brain barrier and exhibit therefore minimal pharmacological activity or toxicity; they are for example present in tomatoes, potatoes, eggplants and chili peppers, all Solanaceae plants we consume on a daily basis.[132] Homotropane family members such as euphococcinine and adaline are less known from the general public but have attracted interest from the organic chemistry community due to the possibility to synthesize them as single enantiomers.[133,134]

Figure 17. Structures of relevant naturally occurring tropanes and nortropanes.

Natural products isolated from the Solanaceae family, such as scopolamine, are muscarinic antagonists.[i] It means that they prevent the binding of the physiological neurotransmitter acetylcholine and disable completely its receptor. These muscarinic receptors are responsible for controlling smooth and cardiac muscles; hence an anticholinergic poisoning can affect heart rate, respiration, and central nervous system functions.[135,136] But as says the adage credited to Paracelsus, "the dose makes the poison" and scopolamine is in fact one of the most used pharmaceutical agents. Under the proper dosage, it is used in the treatment of nausea and motion sickness, internal cramping, and for ophthalmic purposes.[137] The use and application of cocaine however is largely restricted, and therefore the research is limited. Nonetheless, the psychoactive effects have been proven and are attributed to the inhibition of the reuptake of dopamine, norepinephrine, and serotonin in the central nervous system.[138] A high concentration of these species in the limbic system leads to the psychoactive effects. Cocaine has also been shown to exhibit local anaesthetic properties and has served as lead substance for different local anaesthetics and painkillers.

Whether these compounds are toxic, healing, or psychoactive, it proves that they have a biological effect on the human body. As such, they are of interest for the scientific community. Their biological synthesis has been studied in depth; the pharmaceutical sciences have tried to design analogues of these compounds to design marketable drugs; and the synthetic chemists have developed methods to synthesize and produce these compounds. After briefly going over all these endeavors, we will describe our own efforts towards the synthesis of tropane derivatives.

3.1.3.1.   *Medicinally relevant scaffolds*

Given the biological activity exerted by tropane derivatives, medicinal chemists have been interested in developing advanced analogues of these alkaloids. Some examples are depicted in Figure 18.

YZJ-1139 is an orexin receptor antagonist. Since orexin is a neuropeptide involved in maintaining wakefulness, YZJ-1139 is currently being tested for the treatment of insomnia. It has already completed phase II clinical trials.[139] In 2019, Novartis AG disclosed the pharmaceutical composition of Tropifexor,[140] whose active ingredient is also a *N*-arylated tropane derivative that was found to be a potent agonist of a nuclear hormone receptor. Tropifexor is currently in clinical studies for the treatment of non-alcoholic steatohepatitis.[141] Researchers at the University of Gothenburg identified a *N*-arylated tropanol derivative ACP-105 as an effective agonist of the androgen receptor in the human body.[142] In a follow-up work, structure-activity-relationship study revealed that the aryl substitution pattern had strong effects on the potency.[143] For example, while the methylated ACP-105 compound is an agonist[ii] of the androgen receptor, the demethylated compound was found to be an antagonist. Some compounds are also being investigated for the treatment of cancer tumors.[144,145]

---

[i] Antagonist : A drug which binds to a receptor without activating it, and which prevents a natural messenger from binding.[135]

[ii] Agonist : A drug that produces the same response at a receptor as the natural messenger.[135]

YZJ-1139   **Tropifexor**   R = Me (**ACP-105**), antagonist
                                              R = H, agonist

Figure 18. Examples of tropane-derived drugs already on the market or undergoing clinical trials.

These examples illustrate well the versatility and promises of tropane derivatives as pharmaceutical agents. In this context, it appears that *N*-arylated tropane derivatives are promising candidates and we shall now look at some synthetic strategies to obtain these compounds.

3.1.3.2.   Bio- and biomimetic synthesis

The biosynthesis of tropinone, and from there of a large number of tropane derivatives, goes through a key *N*-methyl-pyrrolinium intermediate (Scheme 18).[146] The biosynthesis of this intermediate starts with α-amino acid ornithine, which is decarboxylated to give the linear diamine putrescine. After mono-*N*-methylation by putrescine *N*-methyltransferase, oxidation of the remaining primary amine **63** affords the γ-aminoaldehyde **64** that cyclizes spontaneously to *N*-methyl-pyrrolinium. Pyrrolidine ketide synthase is an enzyme that catalyzes the formation of acetonedicarboxylic acid.[147] The Mannich condensation of this precursor with the pyrrolinium is a non-enzymatic, spontaneous process leading to **65**. Finally, tropinone synthase (or cytochrome P450 monooxygenase CYP82M3) is postulated to catalyze the hydroxylation of the heterocyclic ring at the α' position leading to **66**, followed by dehydration, Mannich condensation, and decarboxylation to give tropinone.

Scheme 18. Biosynthesis of tropinone.

In 1917, Robinson published the biomimetic synthesis of tropinone following a one-step protocol making use of a double Mannich condensation.[148] The methodology relied on the same acetondicarboxylic acid intermediate as in the biosynthetic pathway, but the *N*-methyl-pyrrolinium equivalent was formed from succinaldehyde and *N*-methylamine. Following this protocol, tropinone was obtained in 42% yield. In 1935, Schöpf showed that the reaction could be run and the yield increased under physiological pH.[149] This reaction is nowadays known as the Robinson tropinone synthesis, or as the Robinson-Schöpf annulation.
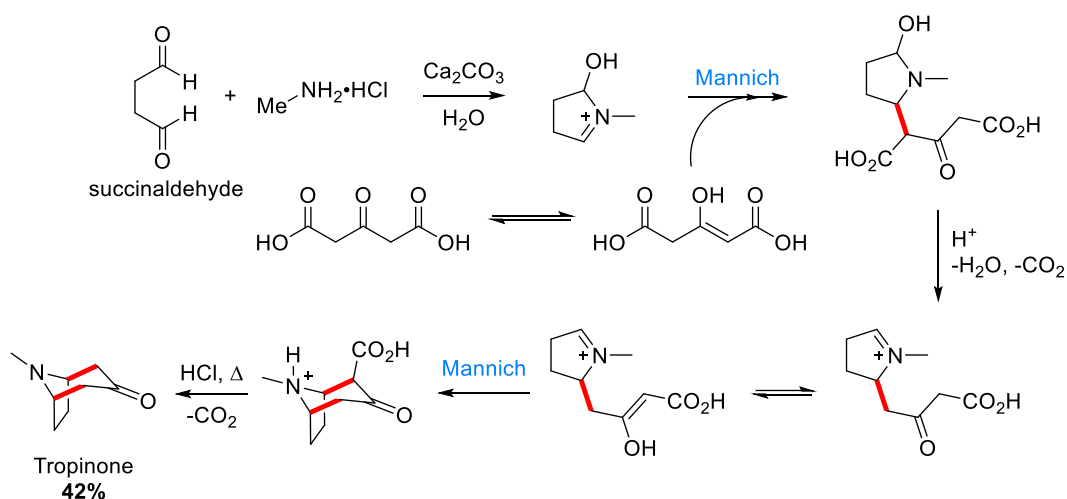
Scheme 19. Robinson's biomimetic synthesis of tropinone.

The synthesis can be applied to unsymmetrical starting material. Process chemists of the Yangtze River Pharmaceutical Group reported the use of ester derivatives instead of acetondicarboxylic acid (Scheme 20A).[139] The reaction was carried out on 0.65 mol scale and afforded the desired product **67** in an excellent 98% yield but poor diastereomeric ratio of 3 to 2. The diastereomers were later separated by recrystallization. Compound **67** is an advanced intermediate of YZJ-1139 (Figure 18). Paton and

Hodgson synthesized the 1-methyltropane derivative **68** by using 4-oxopentanal instead of succinaldehyde (Scheme 20B).[150] The reaction afforded the product in 56% on 23 mmol scale. After further synthetic transformation and chiral resolution, a tropane-derived enamine was used for asymmetric induction in alkylation reactions. Finally, a decorated succinaldehyde derivative **69** was used in the synthesis of a benzylsulfinyl substituted tropinone derivative **70**,[151] proving the feasibility of such a methodology albeit a low overall yield of 10% from the dialdehyde precursor (Scheme 20C).
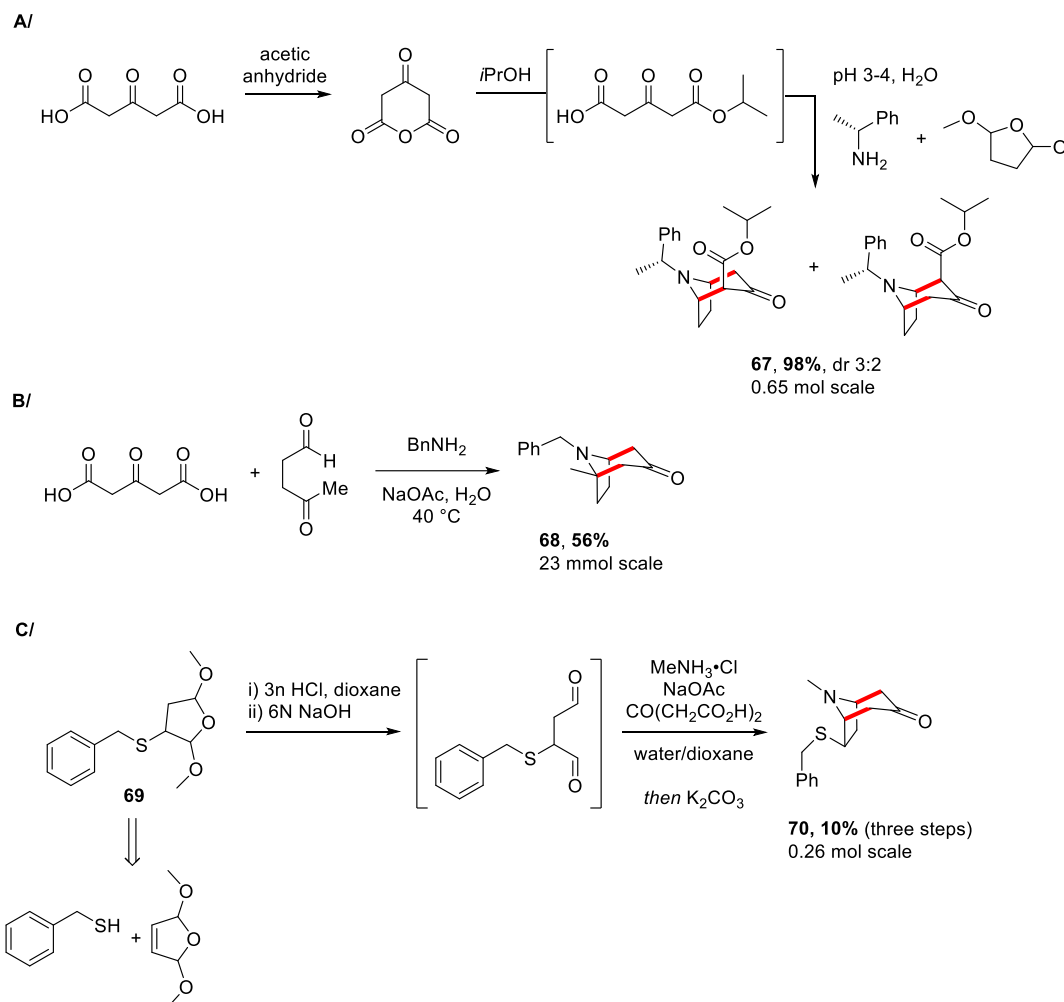
Scheme 20. Applications of the Robinson-Schöpf synthesis. A/ Use of an ester derivative of acetondicarboxylic acid. B/ Use of a ketoaldehyde. C/ Use of a substituted succinaldehyde derivative.

3.1.3.3. Synthetic pathways towards N-arylated tropane derivatives

Examples using *N*-arylated amines in the Robinson-Schöpf annulation are limited. De Ridder and co-workers reported that aniline, *para*-toluidine and 3,5-dimethylaniline gave the corresponding *N*-aryltropinone derivatives in respectively 43%, 49% and 39% under Robinson's conditions.[152] Researchers at the Campbell Family Institute for Breast Cancer Research synthesized nortropinone derivatives using these conditions, but reported low yields of 15 to 31% for the annulated products **71** and **72** (Scheme 21A).[145] Jung and co-workers discovered that using acetone instead of acetondicarboxylic acid resulted in slightly higher yields of the annulated products **73**.[153] Additionally, they extended the scope to both electron-rich and electron-poor aromatic systems, however only *para*-substituted (Scheme 21B).

A/ Robinson annulation for the synthesis of *N*-arylated nortropane derivatives

71, X= CH$_2$, **31%**
72, X = O, **15%**

X = CH$_2$ or O
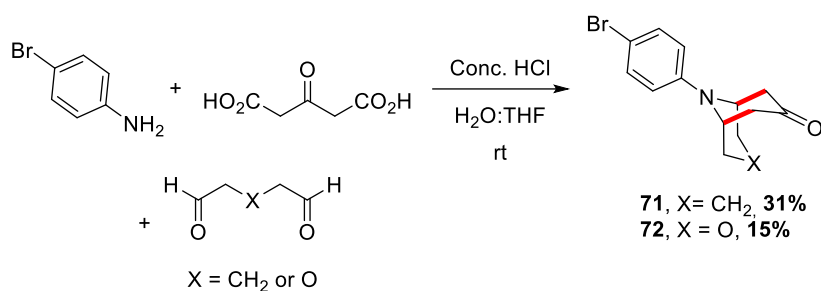
B/ Modified Robinson annulation for the synthesis of *N*-arylated tropane derivatives

6 examples

73

R = H, **55%** (**73a**)
OMe, **84%** (**73b**)
COMe, **79%** (**73c**)
F, **83 %** (**73d**)
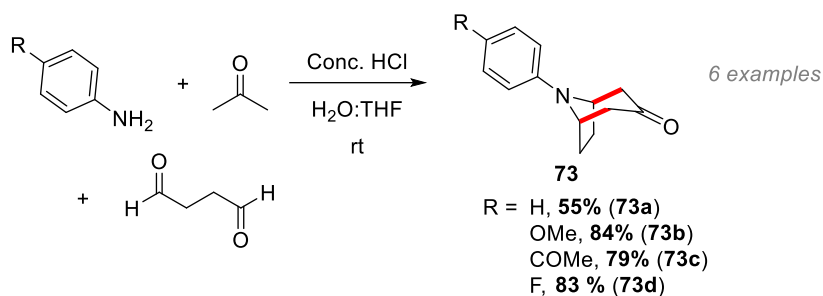
Scheme 21. Reported examples of Robinson annulation protocols with aniline derivatives.

The Robinson biomimetic synthesis is an ionic [3+3] annulation based on 1,3-bis-electrophile and 1,3-bis-nucleophile synthons. Based on a similar concept, distinct methods have emerged in the literature. A double Michael condensation was described between primary amines and 2,6-cycloheptadienone **75**.[154] The latter can be synthesized from cycloheptanone **74** *via* a protection-bromination-elimination-deprotection sequence,[155,156] but its isolation proved tedious and the yields of cyclized product were low with aniline derivatives (typically 20%).[157] In 2002, Nicolaou and co-workers reported an improved synthesis of 2,6-cycloheptadienone from cycloheptanone using IBX (Scheme 22).[158] As a result, the subsequent addition of *N*-methylamine gave tropinone in 72% yield. The one-pot synthesis of tropinone from cycloheptanone was also possible (59% yield).
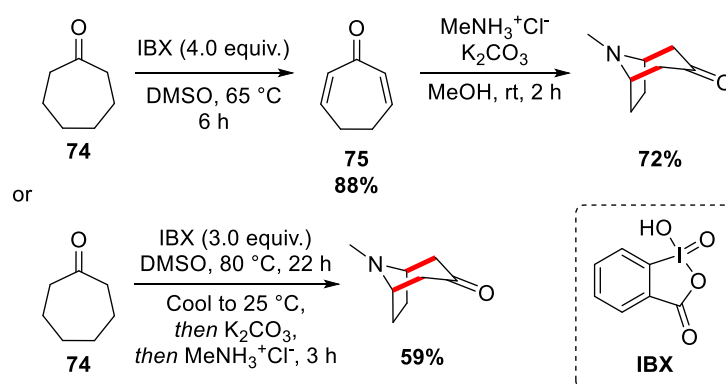
Scheme 22. Improved synthesis of 2,6-cycloheptadienone using IBX, and double Michael condensation with methylamine.

Most protocols encountered in the synthesis of complex *N*-arylated tropane derivatives are however based on the transformation of the common tropinone core *via* the free amine. *N*-Boc-nortropinone is for example commercially available (CAS number 185099-67-6, price range 200-300 CHF/100 g) or

can be obtained *via* demethylation of tropinone with chloroformate reagents,[159] then protection. This is a stable compound that can be transformed to the free amine on demand.

Compounds such as ACP-105 and Tropifexor (Figure 18) were synthesized *via* a nucleophilic aromatic substitution step, as were all the analogues tested in the course of these studies[142,160], and others.[144] Messouadi and co-workers developed a palladium-catalyzed cross-coupling procedure for the synthesis of *N*-(hetero)arylconvolvine derivatives **76** (Figure 19).[161] Their protocol could be used to couple convolvine with electron-poor and electron-rich aromatics, as well as heteroaryl groups, in good to excellent yields. The method was not tested on other tropane cores. Convolvine was synthesized in 3 steps from tropine, which can be obtained *via* the conventional Robinson route.

Representative examples

76a, R = F, **70%**
76b, R = OMe, **88%**

76c, *ortho*, **30%**
76d, *para*, **76%**
76e, *meta*, **44%**

76f, **70%**
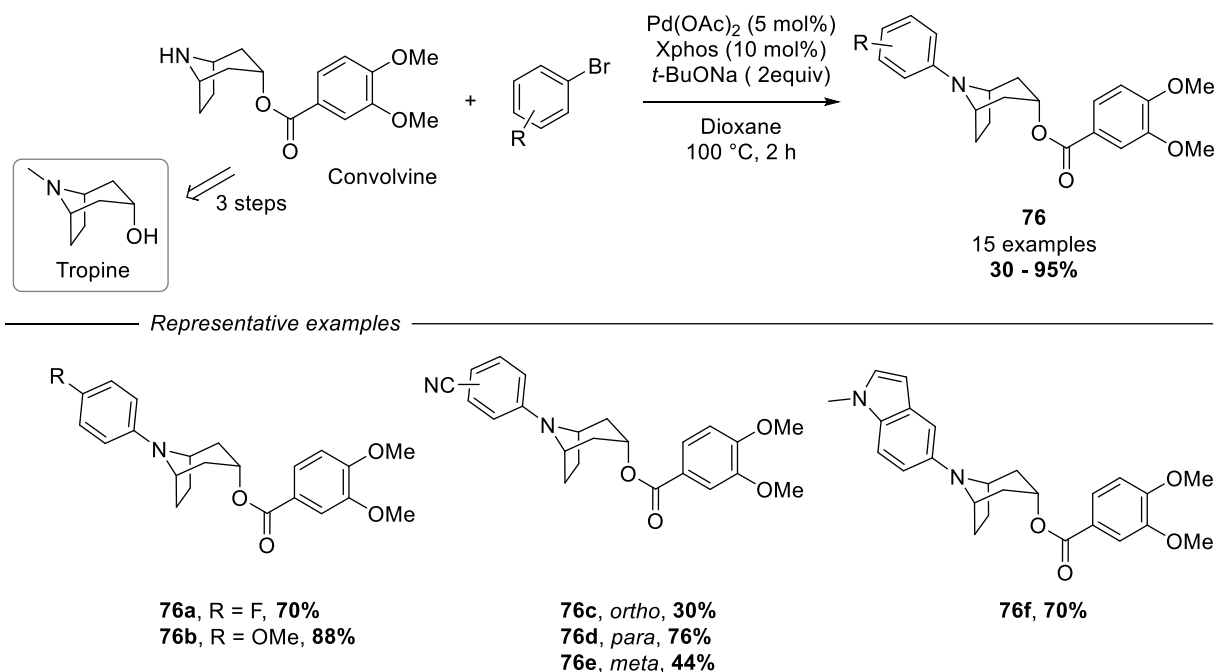
Figure 19. Buchwald-Hartwig-type cross-coupling of convolvine with (hetero)aryls.

Another known strategy for the synthesis of tropane derivatives is to quaternarize the nitrogen of tropinone. Refluxing this intermediate under basic conditions in presence of a primary amine yields the *N*-alkylated nortropinone derivatives in moderate to good yields (Scheme 23).[162] However only one example was successful with an aniline, giving the *N*-arylated nortropinone in a low 30% yield.
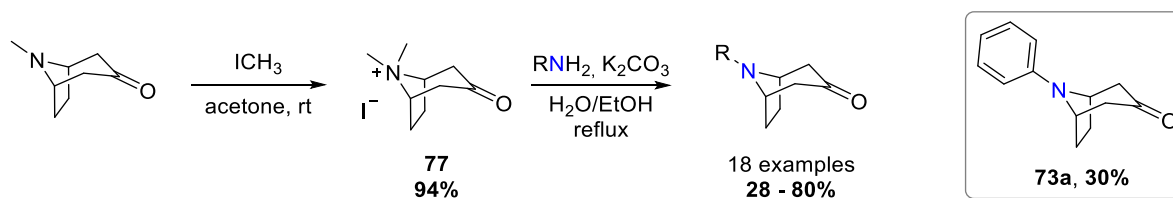
Scheme 23. Two-step synthesis of N-substituted nortropinone derivatives starting from tropinone.

These strategies are routinely used and have proven their value; however, they focus on varying the nitrogen substituent and do not allow the straightforward modulation of the bicyclic core, since tropinone is always the starting point. As a result, homotropane derivatives or higher analogues have for example been understudied, as well as the introduction of a different functional group than a ketone or an alcohol at position 4 of the tropane core. Given the promises of *N*-arylated tropane derivatives as biologically active compounds and the craze for 3D shaped molecules in medicinal

chemistry ,[163] a method that modulates both the tropane core and the nitrogen aryl substituent is still desirable.

3.2. Results

Our investigations in the radical-mediated alpha functionalization of tertiary amines using quantum dots started with an allylation reaction based on the protocol proposed by MacMillan and co-workers for their vinylation reaction (see Figure 14). Instead of a vinyl sulfone radical trap, we proposed to use an allyl sulfone trap which would deliver the sulfinyl radical required to close the catalytic cycle (Scheme 24).
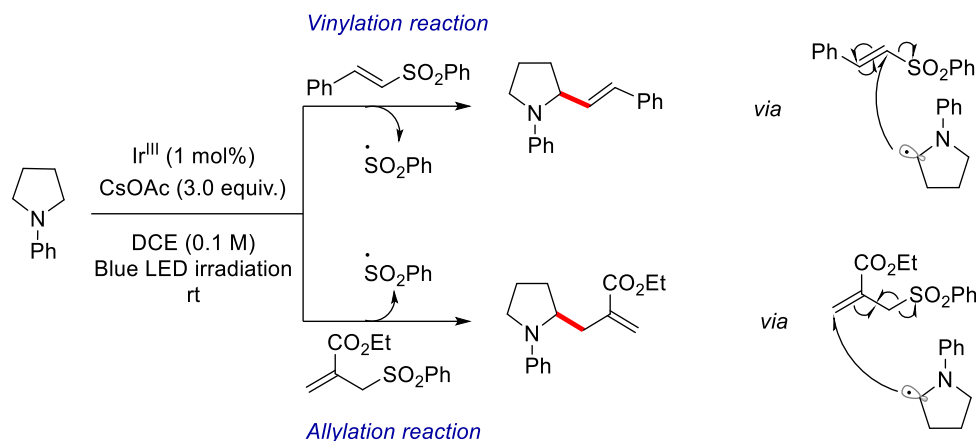
Scheme 24. Alpha-vinylation and -allylation of *N*-phenylpyrrolydine using sulfone-based radical traps under iridium photocatalysis.

Aware of the possibility to obtain addition products in presence of an excess amine, as described by Li and co-workers (see Figure 15), MacMillan's conditions were adapted, and a slight excess of radical trap was used (1.4 equivalents, Scheme 25). We hoped that under these conditions, both the addition product and the bis-allylated product would be suppressed. Indeed, an addition product as described by Li and co-workers was not isolated. However, no desired mono-allylated product **2a** was obtained either after 8 hours of reaction. Instead, we identified a cyclized product **3a** as the main product of the reaction, albeit in a low 12% yield. When reducing the reaction time to two hours, the mono-allylated product was isolated in 35% yield. Engaging this intermediate product in presence of a base and the iridium catalyst provided the cyclized product, as assessed by comparison with an authentic sample of the cyclized product.
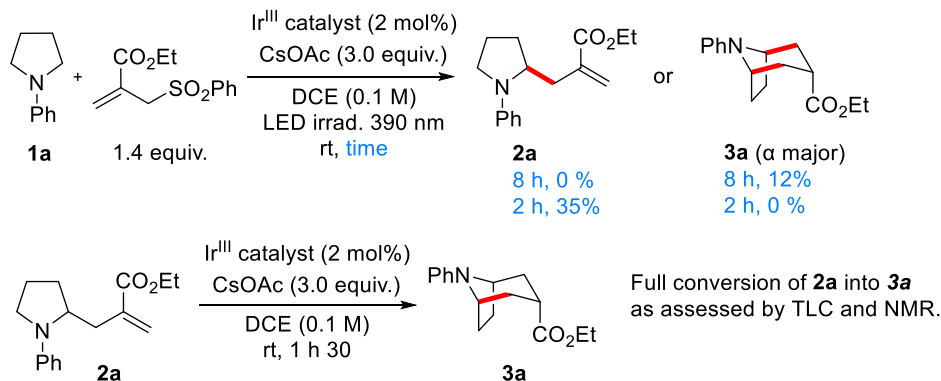
Scheme 25: Discovery of an intramolecular addition reaction of mono-allylated product **2a**.

These findings led us to investigated this unprecedented radical [3+3]-annulation process for the synthesis of tropane and related alkaloid skeletons. This work was published in Communications Chemistry in 2021.[164]

3.2.1. Published results

The following results have been the subject of a publication:

Eloïse Colson, Julie Andrez, Ali Dabbous, Fabrice Dénès, Vincent Maurel, Jean-Marie Mouesca & Philippe Renaud. Tropane and related alkaloid skeletons via a radical [3+3]-annulation process. *Commun Chem* **5**, 57 (2022).

3.2.1.1.   Abstract

Tropanes and related bicyclic alkaloids are highly attractive compounds possessing a broad biological activity. Here we report a mild and simple protocol for the synthesis of N-arylated 8-azabicyclo[3.2.1]octane and 9-azabicyclo[3.3.1]nonane derivatives. It provides these valuable bicyclic alkaloid skeletons in good yields and high levels of diastereoselectivity from simple and readily available starting materials using visible-light photoredox catalysis. These bicyclic aniline derivatives are hardly accessible via the classical Robinson tropane synthesis and represent a particularly attractive scaffold for medicinal chemistry. This unprecedented annulation process takes advantage of the unique reactivity of ethyl 2-(acetoxymethyl)acrylate as a 1,3-bis radical acceptor and of cyclic N,N-dialkylanilines as radical 1,3-bis radical donors. The success of this process relies on efficient electron transfer processes and highly selective deprotonation of aminium radical cations leading to the key α-amino radical intermediates.

3.2.1.2.   Introduction

Nitrogen-containing moieties are omnipresent in natural products, biologically active compounds and agricultural chemicals. In particular, the 8-azabicyclo[3.2.1]octane and 9-azabicyclo[3.3.1]nonane skeletons constitute the core of many natural tropane[132] and homotropane alkaloids,[165] respectively, and analogues presenting a wide range of biological activities. For instance, tropinone, cocaine and scopolamine (Figure 20) are amongst the most popular representative examples of natural alkaloids presenting a 8-azabicyclo[3.2.1]octane (tropane) skeleton as their base structure. Unlike its natural enantiomer, unnatural (−)-ferruginine (Figure 20), is a good agonist for nicotinic acetylcholine receptor (nAchR). The 9-azabicyclo[3.3.1]nonane (homotropane) skeleton can be found in the structure of (−)-adaline, and (+)-euphococcinine (Figure 20),[165] two important defensive alkaloids from, respectively, the European ladybug *Adalia bipunctata* and the Australian ladybug *Cryptolaemis montrouzieri*. Moreover, *N*-arylated tropanes and related bicyclic aniline derivatives[166] represent a particularly attractive scaffold for medicinal chemistry as illustrated by ACP 105,[143,167] an orally available and potent selective androgen receptor modulator (SARM), and CFI-401870,[168] a single-digit nanomolar tyrosine threonine kinase (TTK) inhibitor (Figure 20).
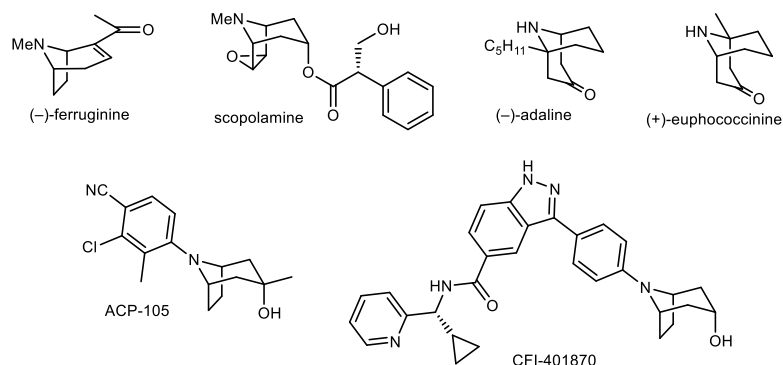
Figure 20. Tropanes and homotropanes. Selected example of tropane and homotropane alkaloids as well as *N*-arylated tropane derivatives of biological interest.

Since the report by Robinson of the multicomponent synthesis of tropinone based on a cascade Mannich reaction,[148,169] access to tropanes and related alkaloids has been the object of intense activity.[170] Strategies based on ionic reactions, cycloadditions and transition metal mediated processes have been reported. The preparation of *N*-arylated tropane derivatives via Robinson synthesis is a knotty process[171] with limited scope[172–174] and they are mostly prepared via *N*-demethylation followed by a dubious *N*-arylation step.[175] Despite their attractiveness to build cycles, radical processes have only been scarcely used in tropane synthesis.[176] The development of a general and flexible access to tropane related heterocycles using a mild radical-based approach is expected to complement nicely the existing methods by allowing a direct preparation of *N*-arylated derivatives and by modifying the substitution pattern at position 3 of the tropane skeleton. To gain in efficiency, a cascade processes involving consecutive formation of C–C bonds is particularly sought. The biosynthesis of tropane alkaloids[177] as well as Robinson biomimetic synthesis[148,169] are both based on an ionic [3+3]-annulation processes involving 1,3-bis-iminium ions and 1,3-bis-enolates synthons (Figure 21a). Inspired by this observation, we hypothesized that a radical version might be possible by using 1,3-bis-α-amino radical donor and 1,3-bis radical acceptor (Figure 21b), radical donor and acceptor being defined and represented according to Curran's proposal in his seminal article on retrosynthetic planning of radical reactions.[178] To the best of our knowledge, this type of radical [3+3]-annulation has not yet been reported.[179–185]
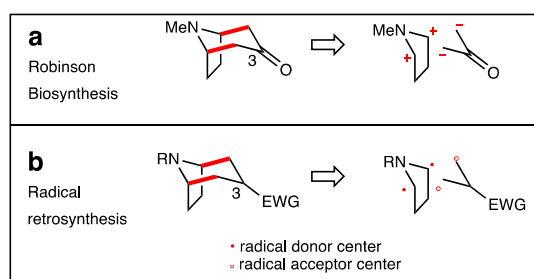
Figure 21. Retrosynthetic analysis. Retrosynthetic analysis of tropane alkaloids according to their biosynthesis and to Robinson synthesis (**a**) as a source of inspiration for a radical retrosynthetic analysis (**b**). New C–C bonds are indicated in red, radical donor as red dot and radical acceptor as red circle.

The α-functionalization of tertiary amines has attracted much interest in the past and methods involving one- and two-electron oxidation pathway have been reported (Figure 22). One-electron oxidation of the amine affords a nitrogen-centered radical cation. The oxidation leads to a massive increase of the acidity of the α-C–H bond relative to the starting amine.[186] Rapid deprotonation of the radical cation gives the α-aminoalkyl radical that can be used for a variety of radical processes, such as

for instance addition to alkenes leading to C–C bond formation (one-electron pathway).[187] On the other hand, the α-aminoalkyl radical is more easily oxidized than the starting amine and therefore further oxidation to the corresponding iminium ion can take place (two-electron pathway).[188] The iminium intermediate can be used for a variety of useful ionic transformations.[189,190] As a consequence, the use of stoichiometric oxidants to perform radical reaction via the one-electron pathway is very challenging due to rapid overoxidation of the intermediate α-aminoalkyl radical to the corresponding iminium ion.[191]
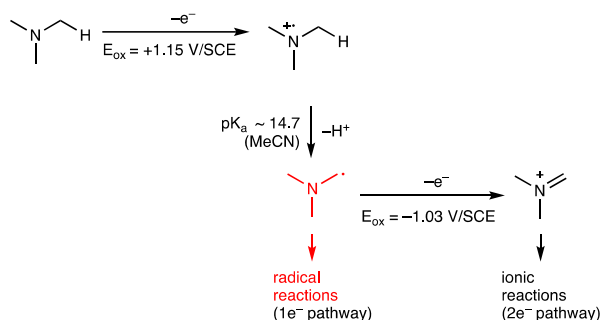
Figure 22. Oxidation of trimethylamine. One- vs. two-electron pathways. Desired radical process indicated in red.

In this context, the single electron oxidation of amines *via* photoinduced electron transfer has been shown to be a suitable method to suppress this overoxidation. Mariano and co-workers reported in 1992 the photosensitized generation of α-aminoalkyl radicals from easily oxidized α-silylamines and their subsequent intra- and intermolecular addition to electron-poor olefins. Interestingly, they reported a 6-*endo*-trig cyclization process (Figure 23a).[192] Pandey took also advantage of the oxidation of a bis-α-silylamine to generate an azomethine ylide that can be used in 1,3-dipolar cycloaddition.[193] Pandey, Reiser and co-workers[194] and Nishibayashi[187,195] independently extended this chemistry to photoredox-mediated protocols not only on α-silylated amines but also respectively on *N*-aryl-tetrahydroisoquinolines[194] and on cyclic and acyclic amines. Nishibayashi and co-workers reported the formation of bis-alkylated product starting from symmetrical starting materials, demonstrating that the intermediate mono-alkylated product has a similar reactivity as the starting amine under specific reaction conditions (Figure 23b).[195] In 2014, MacMillan and co-workers reported the α-vinylation of aniline derivatives and *N*-Boc-protected amino acids using vinyl sulfones as coupling partners (Figure 23c).[196] In this case, no bis-vinylation was reported presumably due to the excess of the starting amine used under their conditions. The same year, Li and co-workers reported the first α-allylation of *N*-aryl tertiary amines using an allylic radical trap.[197] Double addition to the radical trap was observed in one case albeit in very moderate yield (Figure 23d). In 2020, Ready and co-workers reported a method for the regioselective α-functionalization of tertiary amines. Interestingly, the initially formed α-alkylation product could be further alkylated in a one-pot sequence (Figure 23e).[198] The second alkylation takes place in a regioselective manner at the aliphatic position over the benzylic position. In one example, they observed the formation of a remarkable [3+3] adduct (Figure 23e). In this reaction, the initial radical adduct is presumably abstracting a hydrogen from the benzylic position. Reduction of the benzylic radical followed by nucleophilic displacement of the Evans auxiliary account for product formation. All these results incited us to examine annulation reactions based on the double activation of tertiary amines. We described here a tandem process for the synthesis of tropane and homotropane alkaloid skeletons (Figure 23f). The reaction is based on the activation of cyclic tertiary *N*-arylamines to generate 1,3-bis radical donors that react with ester activated allylic radical traps acting as 1,3-bis radical acceptors. This formal [3+3] annulation reaction relies on the regioselective radical formation

at the α and α' positions of the amine, on a rapid 6-*endo*-cyclization that outcompetes intermolecular processes, and on the fact that the final azabicycles are not undergoing further oxidation.
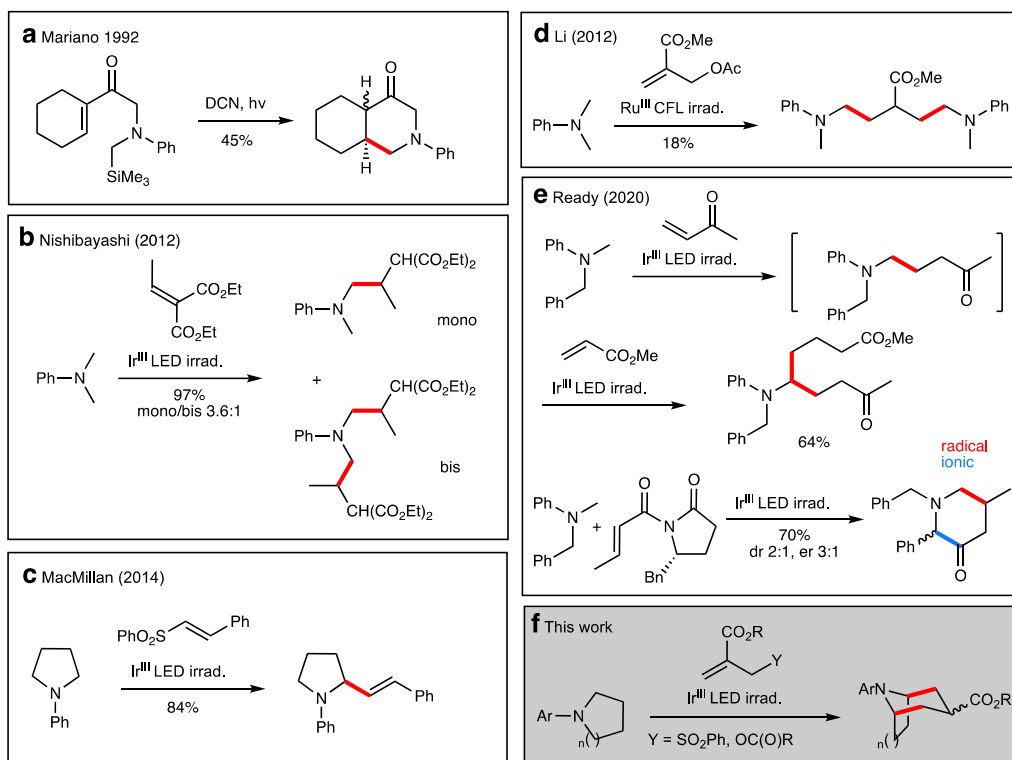
Figure 23. Photoredox catalyzed α-functionalization of tertiary amines. Selected leading contributions in the field (**a**–**e**) and proposed annulation strategy (**f**). New C–C bonds are indicated in red (radical process) and in blue (ionic process).

3.2.1.3.   *Results and discussion*

Proof of concept and optimization. To prove the validity of the annulation approach, *N*-phenylpyrrolidine **1a** was reacted in 1,2-dichloroethane with a series of allyl radical traps possessing different leaving groups Y in the presence of different catalysts and base additives. The results are collected in Table 1 (more entries are available in the supporting information). Three side products were identified during this optimization phase: the mono-allylated product **2a** (an intermediate in the reaction leading to **3a**), the α,α'-bis-allylated product **4a** and the bis-addition product **5a**. Since all these side products are difficult to separate from the desired tropane **3a**, conditions were sought to minimize their formation. We started the optimization by using ethyl 2-((phenylsulfonyl)methyl)acrylate (Y = SO$_2$Ph, 1.2 equivalents) as a trap under conditions similar to the one reported in the literature for reactions with vinyl sulfones (see Figure 23C),[196] i.e. by using [Ir{dF(CF$_3$)ppy}$_2$(dtbpy)]PF$_6$ (Ir-A) as a catalyst, CsOAc (3 equivalents) as a base and irradiating with 390 nm LEDs in 1,2-dichloroethane (DCE) (Table 1, entry 1). Gratifyingly, the reaction afforded the desired tropane **3a** in 45% yield (all yields determined by ^{1}H-NMR analysis using an internal standard). Decreasing the base loading to 1.2 equivalents and slightly increasing the amount of the allylsulfone to 1.4 equivalents proved to be beneficial and the product was formed in 65% yield (Table 1, entry 3). However, under these conditions, the product was contaminated with **4a** and **5a** leading to difficult isolation (isolated yield of 43%). The readily available catalyst [Ir(dtbbpy)(ppy)$_2$]PF$_6$ (Ir-B) proved to be a suitable catalyst for the reaction, yielding the cyclized product in 47% yield (Table 1, entry 4). A screening of bases revealed that CsOAc was the optimal base. The use of NaOAc and Cs$_2$CO$_3$ gave low yields of mono-allylated

pyrrolidine **2a** (Table 1 Entries 5 and 6). The use of [Ir(dFppy)₂(dtbbpy)]PF₆ (Ir-C) afforded the cyclic product **3a** in 50% yield (Table 1, entry 7). Other catalysts presenting suitable redox properties were also tested (for redox properties of the tested catalysts, see supporting information). Ru(bpy)₃(PF₆)₂ (Ru-A) and 2,4,5,6-tetrakis(9*H*-carbazol-9-yl) isophthalonitrile (4CzIPN) afforded the bicycle **3a**, together with significant amounts of mono-allylated intermediate **2a** (Table 1, entries 8–9). Eosin Y provide only the mono-allylated product **2a** (51% yield, Table 1, entry 10). The influence of the radical trap was investigated next. Pleasingly, ethyl 2-(acetoxymethyl)acrylate[197] (Y = OAc) gave the desired product in shorter reaction time (Table 1, entry 11) and similar yield than that with the sulfone trap (Table 1, entries 3). The corresponding sulfide trap (Y = S-*tert*-docedyl) provided also the desired cyclized product in satisfactory yield (Table 1, Entry 12). However, product isolation was more difficult and the release of one equivalent of a smelly thiol makes the reaction less attractive. Finally, the allyl bromide (Y = Br) was tested and only intermediate **2a** was obtained, with no further conversion to the tropane skeleton **3a** (Table 1, Entry 13). Other catalysts (organic photocatalysts), bases (Na₂CO₃, K₂CO₃) and solvents (DMF, DME, EtOAc, DCM or MeCN) were tested but were all detrimental to the formation of **3a** (see supporting information). Due to shorter reaction time and cleaner product formation, the reaction was further optimized using the allyl acetate trap and catalyst Ir-A. The formation of the bis-allylated product **4a** and the bis-addition product **5a** could be minimized by working under higher dilution (0.05 M) and a much shorter reaction time of 20 minutes (Table 1, entry 14). Reducing the catalyst loading to 1 mol% proved beneficial to the reaction (Table 1, entry 15) and using a smaller excess of the allyl acetate radical trap (1.1 equivalents) did not affect the reaction yield (Table 1, entry 16). Finally, the optimized conditions were used with the corresponding pivalate (Y = OPiv) and trifluoroacetate (Y = OTFA) radical traps (Table 1, entries 17 and 18) but the yields were lower, particularly with the trifluoroacetate.

Table 1: Optimization of the reaction conditions.
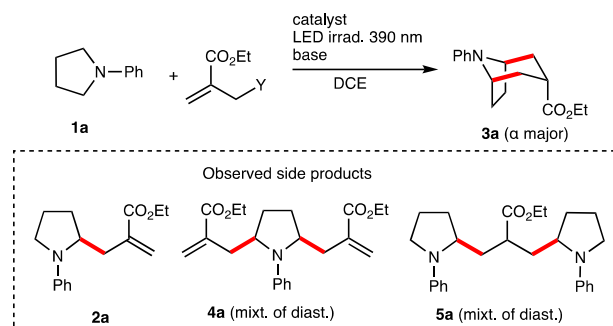
Entry	Cat (mol%)	Base (equiv)	Y (equiv)	Time	[1a]	Yield[a]	Side product
1	Ir-A (2)	CsOAc (3.0)	SO₂Ph (1.2)	16 h	0.1 M	45%[b]	4a, 5a
2	Ir-A (2)	CsOAc (1.2	SO₂Ph (1.2)	16 h	0.1 M	59%[b]	4a, 5a
3	Ir-A (2)	CsOAc (1.2)	SO₂Ph (1.4)	16 h	0.1 M	65%[b] 43%[c,d]	4a, 5a
4	Ir-B (2)	CsOAc (1.2)	SO₂Ph (1.4)	16 h	0.1 M	47%[b]	4a, 5a
5	Ir-B (2)	NaOAc (1.2)	SO₂Ph (1.4)	16 h	0.1 M	–	2a (26%)[b]
6	Ir-B (2)	Cs₂CO₃ (1.2)	SO₂Ph (1.4)	16 h	0.1 M	–	2a (31%)[b]
7	Ir-C (2)	CsOAc (1.2)	SO₂Ph (1.4)	16 h	0.1 M	50%[b]	4a, 5a
8	Ru-A (2)	CsOAc (1.2)	SO₂Ph (1.4)	16 h	0.1 M	30%[b]	2a (30%)[b]
9	4CzIPN (2)	CsOAc (1.2)	SO₂Ph (1.4)	16 h	0.1 M	21%[b]	2a (31%)[b]

10	Eosin Y[f] (2)	CsOAc (1.2)	SO$_2$Ph (1.4)	16 h	0.1 M	–	2a (51%)[b]
11	Ir-A (2)	CsOAc (1.2)	OAc (1.4)	8 h	0.1 M	46%[b]	none
12	Ir-A (2)	CsOAc (1.2)	S*t*-Do (1.4)	8 h	0.1 M	51%[b]	none
13	Ir-A (2)	CsOAc (1.2)	Br (1.4)	8 h	0.1 M	–	2a (66%)[b]
14	Ir-A (2)	CsOAc (1.2)	OAc (1.4)	20 min	0.05	52%[d]	4a
15	Ir-A (1)	CsOAc (1.2)	OAc (1.4)	20 min	0.05	58%[c,d]	4a
16	Ir-A (1)	CsOAc (1.2)	OAc (1.1)	20 min	0.05	57%[d]	–
17	Ir-A (1)	CsOAc (1.2)	OPiv (1.1)	20 min	0.05	45%[d]	–
18	Ir-A (1)	CsOAc (1.2)	OTFA (1.1)	2 h	0.05	27%[d]	–

New C–C bonds are indicated in red. a) Reactions run on 0.2 mmol scale. b) Yield for the major diastereomer determined on the crude product by ^{1}H-NMR analysis using ethylene carbonate as a standard. Levels of diastereoselectivity ranging from 5:1 to 7:1. c) Average of 3 runs. d) Isolated yield. f) Irradiation at 325 nm in DMF as a solvent.

To gain more understanding on the reaction efficiency, cyclization of the pure mono-allylated **2a** product was examined (Figure 24). The reaction was run in deuterated dichloromethane under identical conditions (catalyst and base) than the annulation process and was monitored by ^{1}H-NMR. Full conversion of **2a** was achieved after 3 hours of irradiation and the bicyclic product **3a** resulting from a 6-*endo* cyclization was obtained in 72% yield. The long reaction time necessary to reach full conversion was puzzling since the overall one-pot annulation process was complete within less than 20 minutes. Since acetic acid (one equivalent) is generated during the allylation step leading to **2a**, the reaction was repeated in the presence of one equivalent of acetic acid. Remarkably, the cyclization was finished in 3 minutes and an improved yield of 91% was obtained. Running the reaction with CsOPiv (1.2 equiv) and acetic acid (1.0 equiv) afforded the cyclized product in nearly quantitative yield within 2 minutes. This is in accordance with findings reported by Yoon and co-workers where their photocatalytic addition of α-aminoalkyl radicals on Michael acceptors was improved by the addition of a Brønsted acids such as TFA.[199]

base	react. time	additive	yield
CsOAc	180 min	–	72%
CsOAc	3 min	AcOH	91%
CsOPiv	2 min	AcOH	>95%
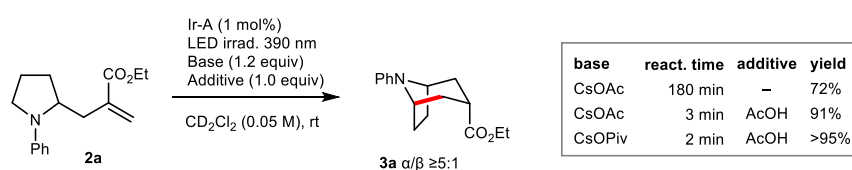
Figure 24. Cyclization of the mono-allylated pyrrolidine **2a**. Influence of acid additives on the cyclization step. New C–C bonds are indicated in red.

Adding acetic acid (1 equiv) to the one-pot annulation reaction either at the beginning or during the reaction did not improve the yield indicating that the in situ generated acetic acid was sufficient for the whole process to occur. Running the reaction with CsOPiv (1.2 equivalents) as a base gave results very similar to CsOAc. Overall, these findings show that the optimized conditions for the annulation reaction (Table 1, entry 16) do not need to be modified.

Reaction scope. The scope of the reaction was examined using the optimized reaction conditions. At first, different *N*-arylpyrrolidines **1a**–**f** were examined (Figure 25). The reaction works well with p-substituted *N*-arylpyrrolidines leading to **3a**–**3d** in 42–57% yield and good levels of diastereoselectivity in favor of the α isomer (α/β ≥5:1). The relative configuration of the **3a** was determined by single crystal

152

X-ray diffraction crystallography. Interestingly, the electron rich *N-p*-methoxyphenylpyrrolidine required longer reaction time despite the fact that this compound is more easily oxidizable, indicating that the critical step of the reaction is probably the deprotonation of the radical cations leading to the α-aminoalkyl radicals as discussed by Mariano in his early work (see a discussion of the mechanism, *vide infra*).[200,201] In this particular case, the use of the slightly more basic CsOPiv instead of CsOAc provided **3d** in a good 56% yield. The presence of *ortho*-substituent proved to be more problematic as shown by the long reaction time and low yield (20%) observed for the formation of **3e**.
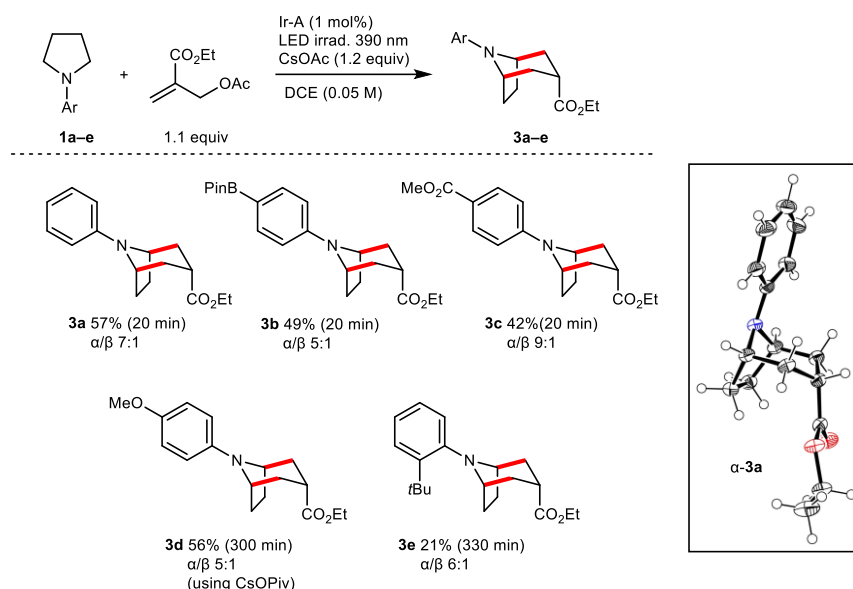
Figure 25. Tropane skeletons via radical annulation. Scope of the *N*-aryl moiety. New C–C bonds are indicated in red. X-ray crystal structure of **3a** (ellipsoids drawn at 50% probability).

Next, the use of a 2-substituted pyrrolidine was examined. For this purpose, the 2-methyl substituted *N*-phenylpyrrolidine **1f** was prepared and submitted to our standard reaction conditions (Figure 26). It afforded the desired bicyclic **3f** containing a quaternary carbon at the bridgehead position in 40% yield. This result was surpassing our expectation since a difficult regioselectivity control was expected for the second step of the process, i.e. the conversion of **2f** to **3f** via 6-*endo*-trig cyclization. A study of this cyclization showed that **3f** could be obtained from **2f** in 66% isolated yield indicating that the desired α-amino-α-methyl radical **R2f** was preferentially formed over **R2f'**. This cyclization yield compared well with the non-methylated substrate **2a** that afforded **3a** in 77% isolated yield.
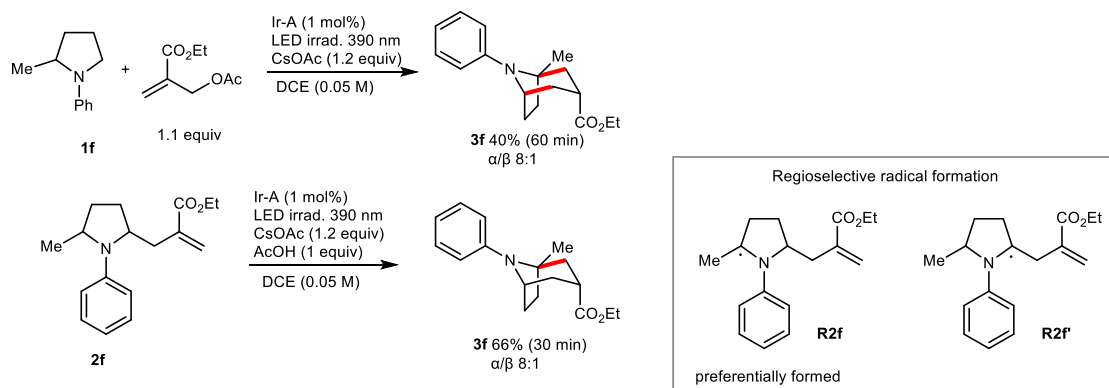
Figure 26. Annulation reaction of *N*-phenyl-2-methylpyrrolidine. New C–C are indicated in red. The reaction involves the regioselective activation of 2,5-disubstituted pyrrolidine to form preferentially **R2f** over **R2f'**.

Encouraged by these results, we then turned our attention to the preparation of the homotropane 9-azabicyclo[3.3.1]nonane skeleton as well as higher [4.3.1]-analogues (Figure 27). Piperidine derivatives proved in general to react slightly better than pyrrolidine derivatives. *N*-Phenylpiperidine **6a** gave the cyclized product **8a** in 67% yield (57% on 3 mmol scale) with an excellent level of diastereoselectivity (α/β > 20:1). The *N*-toluyl derivatives **8b**–**8d** were obtained in similar yields and levels of diastereoselectivity. The electron rich *N*-*p*-anisyl derivatives in the presence of CsOPiv as a base required longer reaction time and afforded **8e** in lower yield (32%). Aromatic rings substituted by electron withdrawing groups afforded the homotropanes **8f**–**8j** in good yields and shorter reaction times in most cases. The *p*-ester substituted homotropane **8g** was prepared 63% yield on 1 mmol scale and the *p*-pinacolboryl derivative **8j** in 56% yield on 3 mmol scale. Gratifyingly, in all the scale-up experiments for **8a**, **8g** and **8j**, the catalyst loading could be decreased to 0.5 mol%. The relative α-configuration of **8g** was confirmed by single crystal X-ray diffraction crystallography. Annulations starting from *N*-phenylmorpholine, *N*-phenylpiperazine and *N*-phenylthiomorpholine derivatives **6k**–**m** provided the bicyclic amines **8k**–**m** in good yields. Remarkably, no products arising from the ring-opening of the piperazine[202] and thiomorpholine[203,204] were observed. Finally, the reactivity of azepane derivatives were investigated. The *N*-phenyl derivative **6n** gave the bicylic amine **8n** in a modest 25% yield after 14h. When the reaction was stopped after 10 minutes, the allylated product **7n** was obtained in 65% yield together with some cyclized product indicating that the 6-*endo* cyclization was probably the yield limiting step. This was confirmed by an independent cyclization attempt starting from **7n** that afforded **8n** in 24% yield after two hours, along with 9% unreacted **7n** and some unidentified side products. The *N*-(*p*-methoxycarbonylphenyl) derivative **6o** was also examined. After 9 h of reaction, only the allylated product **7o** was formed in a low 25% yield and incomplete conversion.
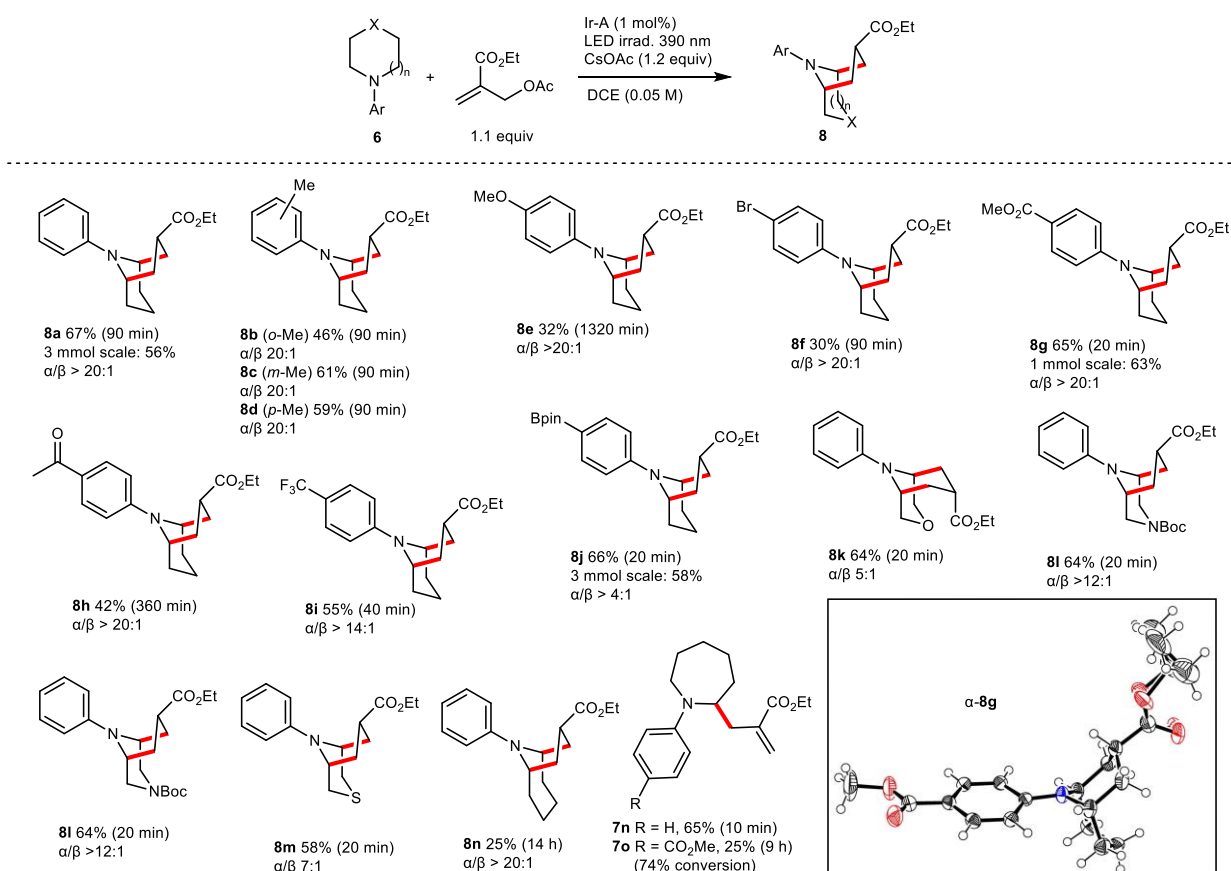
Figure 27. Homotropane [3.3.1] and extended tropane [4.3.1] skeletons. New C–C bonds are indicated in Red. Product are drawn it their major conformations attributed from ^{1}H-NMR spectra analysis. X-ray crystal

structures of α-**8g,** ellipsoids drawn at 50% probability (oxygen and nitrogen atom are represented in red and blue, respectively).

2-Alkyl-3-ethoxycarbonyl substituted tropanes and homotropanes skeletons are expected to be accessible by using easily available acetylated Baylis-Hillman adducts. In order to test this hypothesis, ethyl 2-(1-acetoxyethyl)acrylate was prepared from the ethyl acrylate and acetaldehyde and reacted with *N*-(*p*-methoxycarbonylphenyl)piperidine **6g** (Figure 28). When 1.1 equivalent of the trap was employed under our standard reaction conditions, prolongated irradiation afforded a mixture of the desired tropane skeleton **10** together with mono-allylated piperidine **9** and the bis-allylated product. Using a 2.5 fold excess of the amine allowed for the formation of the bis-allylated product to be suppressed and, after 10 minutes of irradiation, the intermediate **9** was obtained in 73% yield and with a good *E*-stereoselectivity (*E/Z* 7:1). Recrystallization of **9** afforded a virtually diastereomerically pure product (*E/Z* > 20:1). Gratifyingly, under our optimized cyclization conditions the major *E*-**9** afforded **10** in 66% yield and as a single diastereomer (dr > 20:1). However, despite the good results obtained for both steps separately, the one-pot process provided a mixture of **9** and **10**. This mixture can be treated under the cyclization conditions to ultimately give the cyclized product **10** in 71% yield contaminated with a by-product, presumably a diastereomer. The diester **10** was converted to corresponding diol **11** whose relative configuration could be determined by single crystal X-ray diffraction crystallography (Figure 28). The formation of the major diastereomers results presumably from a chair-like transition state as depicted in Figure 28.
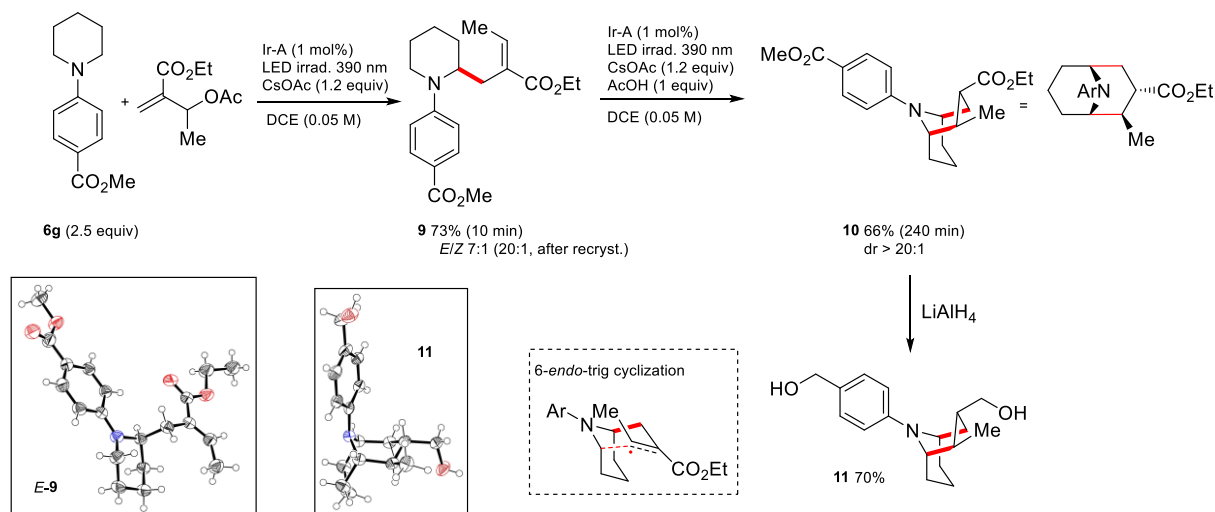
Figure 28. 2,3-Disubsituted [4.4.1]-homotropane. Diastereoselective preparation of a 2,3-disubsituted [4.4.1]-homotropane. New C–C are indicated in red. X-Ray crystal structure of *E*-**9** and **11**, ellipsoids drawn at 50% probability.

Since most of the bicyclic alkaloids are either secondary amines (nortropanes, homotropanes) or *N*-methylated tertiary amines (tropanes), it is important to achieve the deprotection of the *N*-aryl moiety. Methoxyphenyl substituents can be removed under oxidative conditions using chemical oxidants such as cerium ammonium nitrate (CAN) or electrochemical methods.[205] The cleavage of the *N*-*p*-MeOPh group of **3c** and **8e** was investigated first and proved to be problematic when an aqueous CAN solution was used[206] as the quinone liberated during the process reacted with the liberated secondary amines. Gratifyingly, the deprotections were successfully achieved using CAN in CH$_3$CN/water followed by subsequent treatment of the reaction mixture with sodium borohydride to reduce the quinone, then with benzyl chloroformate to prepare their *N*-Cbz-protected form.[207] Under these conditions, the desired Cbz-protected nortropane **12** and homotropane **13** were obtained in 90% and 80% yields,

respectively, without erosion of the diastereomeric ratio (Figure 29a). The Cbz-protecting group was introduced to facilitate product purification but also for both its facile deprotection and conversion to the corresponding *N*-methyl derivative.[208] Since annulation reactions with the *N*-*p*-MeOPh substituted cyclic amines were slow and moderately efficient, we also investigated the deprotection of the *N*-(*p*-pinacolboryl)phenyl derivative **8j** that was formed in good yield. The dearylation of **8j** to **13** (Figure 29b) was conveniently performed in 71% yield by perboric acid treatment, affording after simple extraction the crude phenol, followed by CAN and CbzCl treatment according to the optimized procedure developed for the *para*-methoxy derivatives **3c** and **8e**.
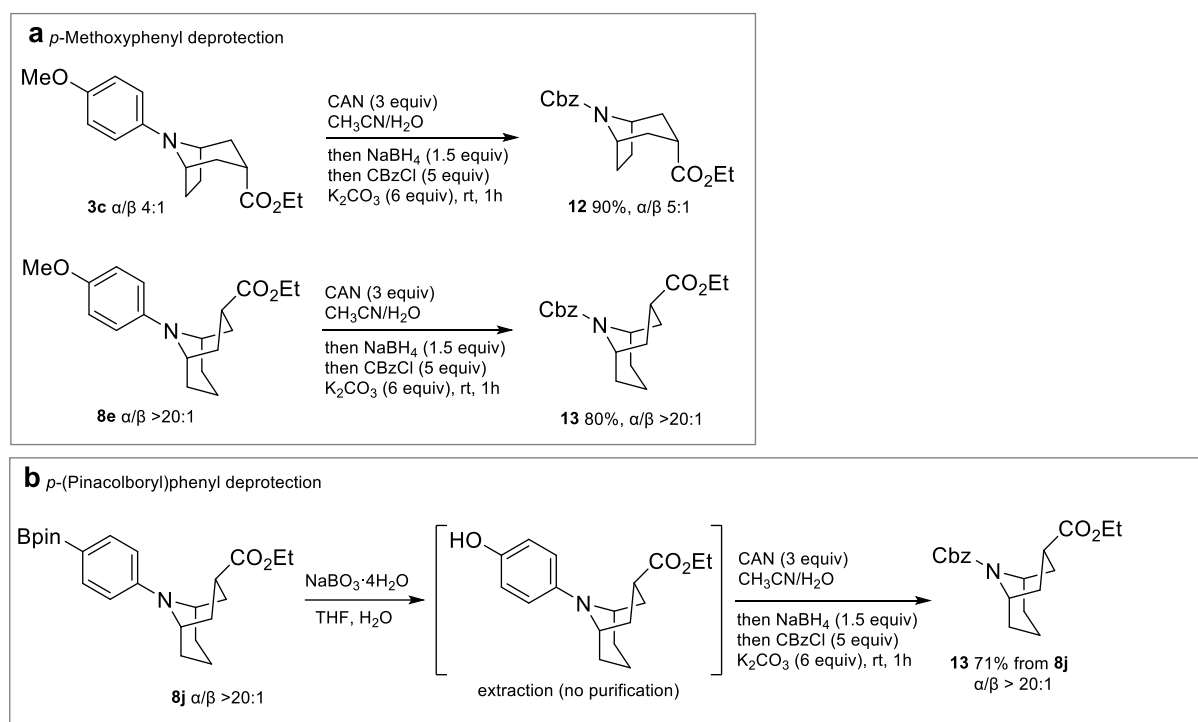
Figure 29. *N*-Dearylation. Dearylation of (a) the *N*-MeOPh derivative **3c** and **8e**, and (b) the *N*-*p*-pinBPh derivative **8j**.

Finally, we hypothesized that the major α-ethoxycarbonyl substituted tropanes and homotropanes were formed by kinetic protonation of the intermediate enolate from the less hindered *exo*-face (see mechanism, *vide infra*). Epimerization of α-stereoisomers to the more stable β-products was therefore examined. Heating the ester **3a** and **8a** at 40 °C in ethanol in the presence of sodium ethoxide afforded the β isomers in good to excellent levels of diastereoselectivity (Figure 30). This strategy is expected to be useful for the stereocontrolled synthesis of tropanes and homotropane alkaloids.
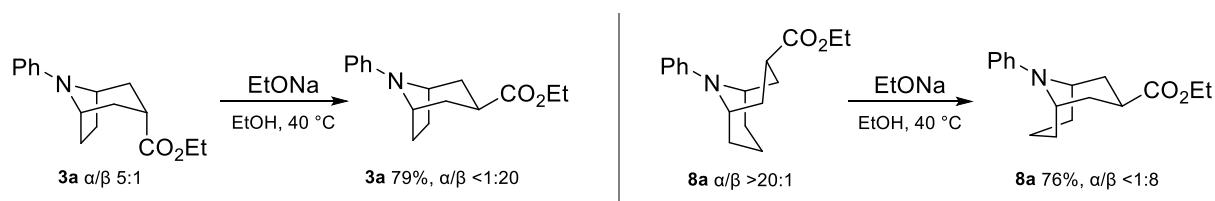
Figure 30. Epimerization. Base promoted thermodynamic epimerization of tropane and homotropane derivatives.

Mechanism. As mentioned in the introduction, the photocatalytic generation of α-aminoalkyl radicals from cyclic anilines and their subsequent intermolecular addition to Michael acceptors are well-

established processes. However, the selectivity of the reaction sequence responsible for the annulation process is quite unique and deserves to be discussed (Figure 31). Upon blue light irradiation the catalyst Ir-A reaches its excited state Ir(III)*(E_{ox*} Ir (III*/II) = +1.21 V SCE in MeCN)[209] and is able to oxidize *N*-phenylpyrrolidine **1a** to its aminium radical cation **RC1a** (E_{red} = +0.62 V/SCE in MeCN), which generates the α-aminoalkyl radical **R1a** upon deprotonation. This nucleophilic radical adds to the electron-poor double bond of the allylic trap, leading to an intermediate α-ester radical **RE2a**. The reduction potential of the tertiary radical **RE2a** is estimated to be E_{red} > –0.29 V SCE (see supporting information for details). Such a radical is expected to be readily reduced by the Ir(II) species (E_{red} Ir (III/II) = –1.37 V/SCE),[209] thus closing the first catalytic cycle and providing a transient enolate intermediate that produces the mono-allylated pyrrolidine **2a** upon β-fragmentation. The intermediate **2a** is now able to enter the second catalytic cycle. After oxidation of **2a** and subsequent deprotonation, the α-aminoalkyl radical **R2a** is formed selectively. The latter undergoes a 6-*endo*-trig cyclization, leading to the bicyclic α-ester radical **RE3a** whose calculated reduction potential (Er_{ed} = –0.77 V SCE, see supporting information for details) is in good agreement with the experimental value of E_{red} = –0.66 V SCE reported for the secondary α-ester radical $CH_3CH(\bullet)CO_2Me$.[210] This allows for its facile reduction by the Ir(II) species, thus closing the second catalytic cycle. *exo*-Selective protonation of the transient enolate ultimately delivers the desired bicyclic product **3a**.

The success of this approach relies on three key features. Firstly, the radical cation **RC2a** needs to be regioselectively deprotonated to form the radical **R2a**. No product results resulting from **R2a'** has been identified but we cannot exclude that such products are formed in small amount (Figure 31a). The calculated pK_a values for the C(2)–H and C(3)–H bond (see scheme 11A) are very close and cannot be used to rationalize this result. Nevertheless, this type of selectivity for the less substituted position is well-established and can be rationalized by both steric and stereoelectronic effects.[211–216] Secondly, in principle all three amines **1a**, **2a** and **3a** present in solution can be easily oxidized by the Ir(III)* catalyst excited state. However, only **RC1a** and **RC2a** (calculated pK_a 51.4 and 52.7 in DCE) are undergoing deprotonation to generate α-aminoalkyl radicals. The deprotonation of the bicyclic radical **RC3a** (pK_a 58.4) is much less favorable and no product resulting from the bicyclic radical **R3a** has been observed (Figure 31b). A separate attempt to achieve allylation of pure **3a** under our standard reaction conditions led only to partial decomposition of the starting material without formation of an allylated product. Since the oxidation potentials of all three amines **1a**, **2a** and **3a** are close and well below the oxidation potential of the excited Ir(III)* catalyst, we believe that the efficacy of the whole process is due to the fact that oxidation of **3a**, which is becoming increasingly important as the reaction proceeds, is not leading to its decomposition as long as **1a** and **2a** are present in solution due to rapid electron transfers between the different amines in solution (Figure 31c). Such rapid electron transfers involving radical cations are well-documented in the literature[107,217,218] and have led to the use of triarylaminium radical cation as organic mediator in electro-organic synthesis.[219–222]
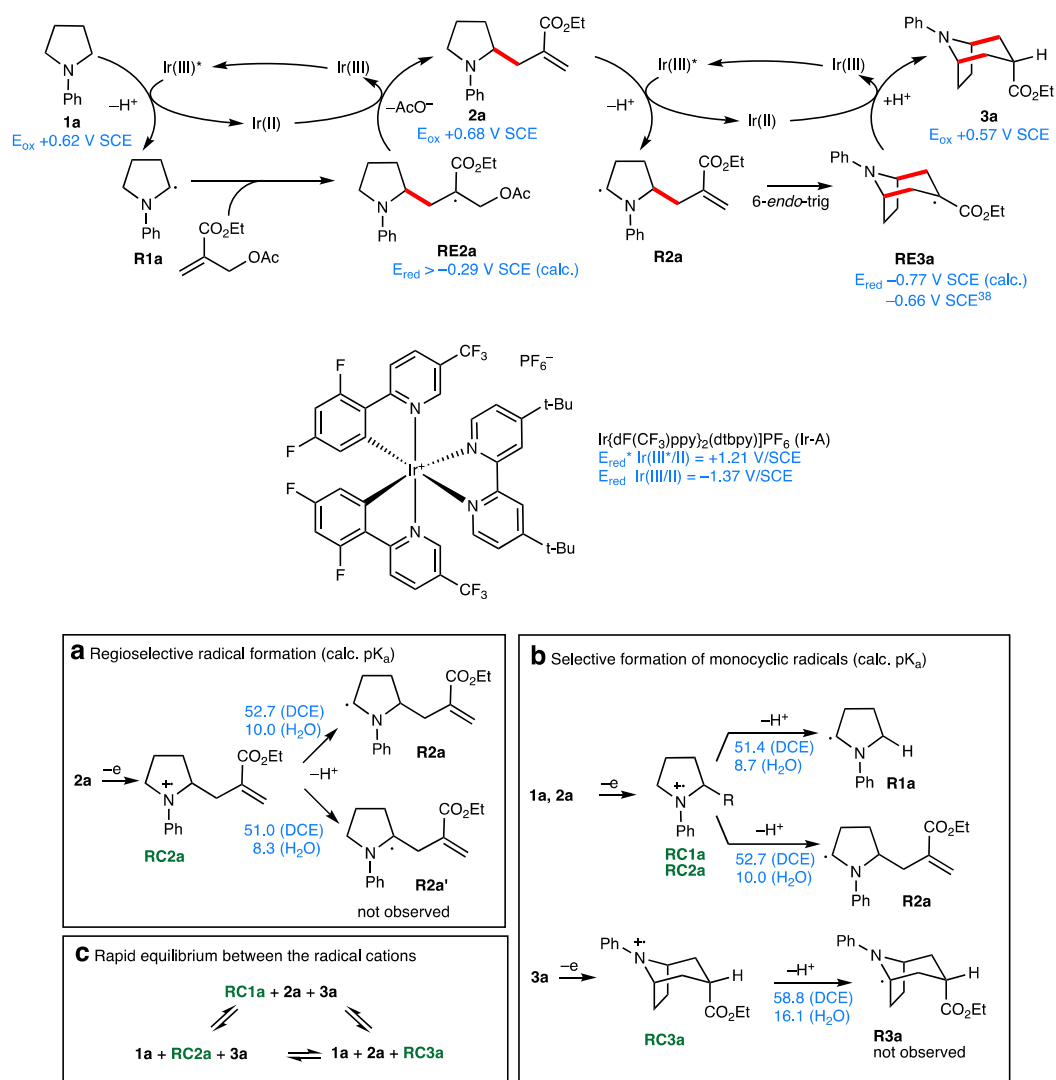
Figure 31. Mechanism. Possible mechanism for the [3+3] radical annulation and analysis of (a) the regioselectivity of radical formation, (b) the selective formation of bicyclic radicals, and (c) the equilibrium between the different radical cations formed during the reaction. New C–C bonds are indicated in red. Redox potentials and pKₐs are indicated in blue. Radical cations are labeled in green.

The proposed mechanism suggests that the efficiency of the annulation process is dictated by the formation of a final product that cannot deliver efficiently an α-aminoakyl radical due to an unfavorable (or less favorable) deprotonation step. This may explain the difficulties and low yield observed in the annulation of azepanes leading to [4.3.1] bicycles (see formation of **8n** in Figure 27), for which the larger bicyclic systems are expected to favor deprotonation due to an increase of conformational flexibility leading to product and catalyst degradation. This assumption is supported by calculations, the oxidation potential of **8n** (E_{ox} +0.66 V/SCE) lying within the range of our catalyst and the pKₐ of the corresponding radical cation **RC8n** (pKₐ 49.5 (DCE), 6.8 (H_2O)) being far below the ones of the less flexible **RC3a** (pKₐ 58.8 (DCE), 16.1 (H_2O)) and **RC8a** (pKₐ 57.1 (DCE), 14.4 (H_2O)) and similar to the one of the monocyclic amines.

Counter-intuitively, the reactions with electron-enriched aniline systems such as *N*-(para-methoxyphenyl)pyrrolidine **1d** (to form **3d**, see Figure 25) and *N*-(para-methoxyphenyl)piperidine **6e** (to form **8e**, Figure 27) were more difficult than those with electron-poorer systems. They required much longer reaction times and, in the case of **1d**, the use of a slightly stronger base. This indicates

that the critical step of the process is probably not the amine oxidation but rather the deprotonation of the radical cation. Calculations showed that the more stable *para*-methoxyphenyl substituted radical cation **RC1d** is also much less acidic (pK$_a$ = +57.1 (DCE)/+14.4 (H$_2$O)) than **RC1a** (pK$_a$ = +51.4 (DCE)/+8.7 (H$_2$O)). The electrochemical investigation of **1d** by cyclic voltammetry provided a quasi-reversible oxidation wave in the absence of added base (Figure 32a) whilst the simple *N*-phenylpyrrolidine **1a** produced irreversible oxidation event (see supporting information).[223,224] The addition of cesium pivalate drastically changed the cyclic voltammogram of **1d** and two oxidation waves were observed (Figure 32b). A first irreversible oxidation wave appeared at a slightly lower oxidation potential than the oxidation event of the amine alone. This shift of potential relative to the cyclic voltammogram in the absence of base is attributed to an oxidation event of the amine interacting with cesium pivalate, possibly a proton-coupled electron transfer (PCET) process.[225,226] The second wave, whose potential corresponds to the oxidation event observed in the absence of base, becomes less reversible in presence of cesium pivalate. The voltammogram of the tropane **3d** (Figure 32c) indicates as anticipated a reversible oxidation process. Interestingly, it is almost not affected by the presence of cesium pivalate indicating that the bicyclic cation radical of **3d** is not deprotonated by the base during the measurement (Figure 32d). This observation supports the proposed mechanism and the fact that the photoredox annulation process stops at the bicyclic stage.
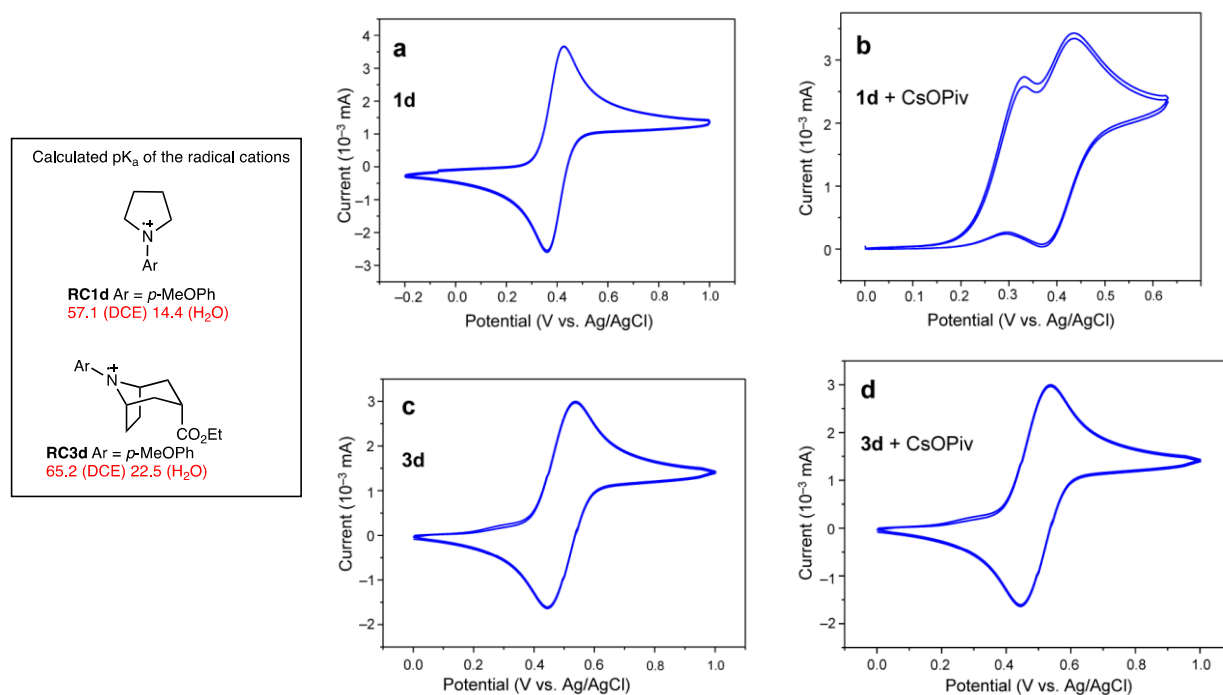
Figure 32. Electrochemical study performed in Grenoble. Cyclic voltammograms of *N-p*-methoxyphenylamines **1d** and **3d** (1 mM) in the absence (a and c) and in the presence of cesium pivalate (1.2 mM) (b and d). Voltammograms were recorded at 100 mV/s in acetonitrile containing [Bu$_4$N][PF$_6$] (0.1 M) as a supporting electrolyte. pK$_a$s are indicated in red. Voltammogram traces are depicted in blue.

The hypothesis that the reactions stop at the bicyclic stage due to inefficient deprotonation of the bicyclic radical cation offers the opportunity to run a more complex reaction process involving a bis-annulation process starting from a tertiary acyclic aniline derivative and ending with an oxidation-resistant bicyclic system. This assumption was tested with *N,N*-dimethyl aniline. In the presence of 2.2 equivalents of the allylic acetate radical trap added in two portions (at the beginning of the reaction and after 15 minutes), the product of bis-annulation product **14** was isolated in 13% yield with good stereocontrol. By starting from *N*-methyl-*N*-trimethylsilylmethylaniline, the yield for the formation of

14 could be improved to 22%. In this process, the product of the first annulation (Figure 33, blue bond formation) leads to a piperidine derivative that can further react via a second annulation process (Figure 33, red bond formation) to produce **14**. All attempts to stop at the piperidine stage gave complex inseparable mixture of products.
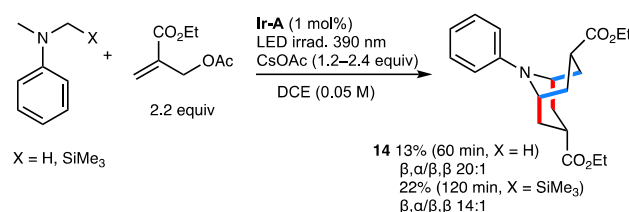
Figure 33. Double annulation process. Synthesis of a homotropane skeleton via a double [3+3] annulation reaction. C–C Bonds formed during the first annulation process are indicated in red, C–C Bonds formed during the second annulation process are indicated in blue.

3.2.1.4. Conclusion

In summary, we have developed a new annulation strategy for the synthesis of bicyclic alkaloid skeletons. The reactions take place under mild conditions and afford *N*-arylated tropane and homotropane frameworks in good yields and good to excellent levels of diastereoselectivity starting from simple and readily available starting materials using visible-light photoredox catalysis. This annulation process takes advantage of the unique reactivity of ethyl 2-(acetoxymethyl)acrylate as a 1,3-bis radical acceptor and of cyclic *N,N*-dialkylanilines as radical 1,3-bis radical donor. This method complements nicely the classical Robinson synthesis by allowing to prepare directly the biologically relevant *N*-arylated skeletons and by introducing an ester group at position 3 suitable for further derivatization towards application in medicinal chemistry. Preliminary results with differently 2-substituted allyl acetates indicate that the ester group can be substituted by other electron withdrawing groups such as a nitrile, a sulfone and a boronic ester. Details will be reported in due time together with the synthesis of optically pure biologically relevant compounds.

3.2.1.5. Author contributions

In Bern

E.C. F.D. and P.R. designed the synthetic experiments. E.C. executed all the synthetic work and analyzed the data. E.C., F.D. and P.R. co-wrote the manuscript.

In Grenoble

J.-M.M. performed the calculations in collaboration with V.M.. J.A., A.D and V.M. designed and run the electrochemical studies and analyzed the data.

All the authors discussed the results and commented on the manuscript.

3.2.2. Towards the synthesis of optically active tropane and homotropane alkaloids using the radical [3+3]-annulation – Unpublished results

3.2.2.1. *Retention of chiral information throughout the radical process*

In collaboration with Walter Le Goas

We envisioned that applying our radical [3+3]-annulation reaction to a 2-substituted, optically active substrate would provide the opportunity to synthesize optically active tropane alkaloids substituted at the bridgehead position. We observed during the substrate scope that the cyclization of the methyl-substituted, mono-allylated intermediate **2f** proceeded with a good 66% yield, indicating that α-aminoalkyl radical formation occurred preferentially on the methyl side rather than on the allylated side, despite similar substitution pattern (Scheme 26, compared H_a and H_b). We wondered whether a reversibility of the α-aminoalkyl radical formation was involved in this selectivity, as proposed in Scheme 26.
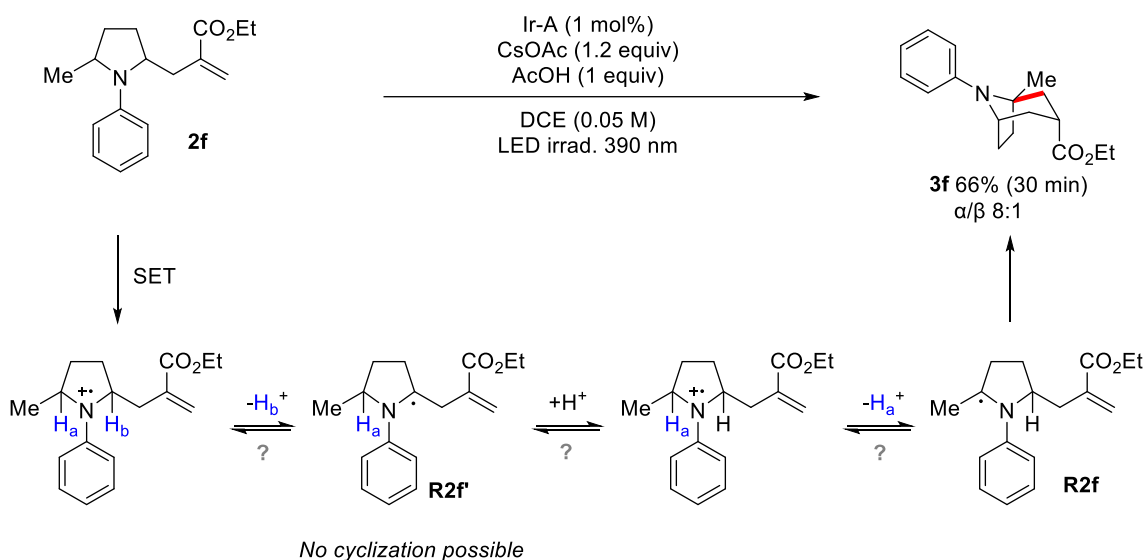
Scheme 26. Possible intermediates in the cyclization of methyl-substituted intermediate **2f**.

Such a process has been proposed by Houk, Mayer and Ellman who reported the α-amino arylation reaction of substituted piperidines with electron-deficient cyano(hetero)arenes (Figure 34A).[222] The authors reported a slow thermodynamic epimerization of the product to an equilibrium mixture of diastereomers, eventually controlling the diastereomeric ratio *via* a light-driven process (Figure 34B).

A/ Alpha-arylation of substituted piperidines

2.0 equiv.
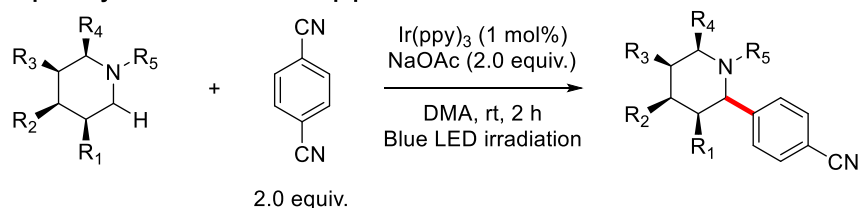
B/ Thermodynamic equilibration

(+/-)-*anti*
dr > 95:5

(+/-)-*syn*
dr 78:22
94% recovery
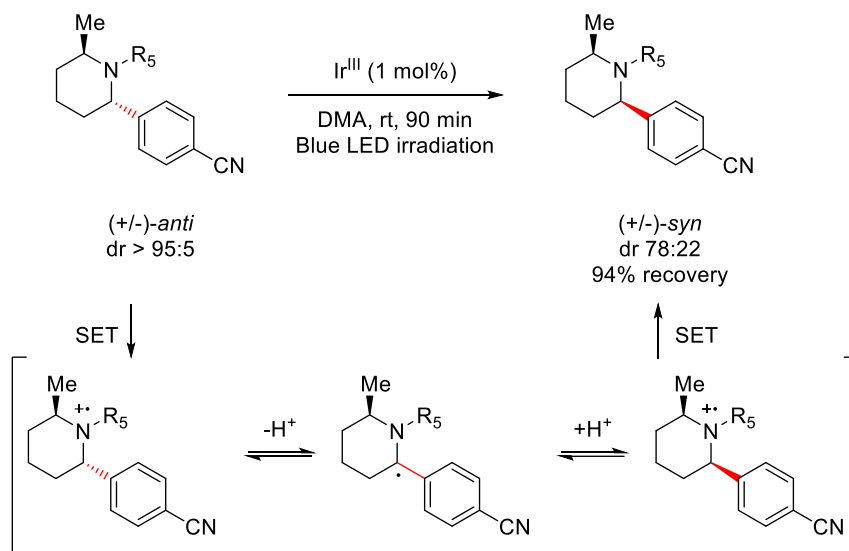
Figure 34. Reversible α-aminoalkyl radical formation invoked in the thermodynamic epimerization of α-aryl, α-methyl bis-functionalized piperidine derivatives (Houk, Mayer and Ellman).

We identified 2-(methoxymethyl)-phenylpyrrolidine **1g** as a model substrate to rule out such a reactivity in our system (Figure 35). We expected the stereochemistry to be fixed at position 5 of the pyrrolidine ring upon formation of the mono-allylated intermediate **2g**. Both the *trans* and *cis* diastereomers are expected be optically active at this stage since no issue in the regioselectivity of the α-aminoalkyl radical formation is expected (**R1g**). After separation of the *trans* and *cis* isomers, each intermediate would give rise to a single enantiomer of the cyclized product, provided that no reversibility occurred in **R2g-*trans*** and **R2g-*cis***.
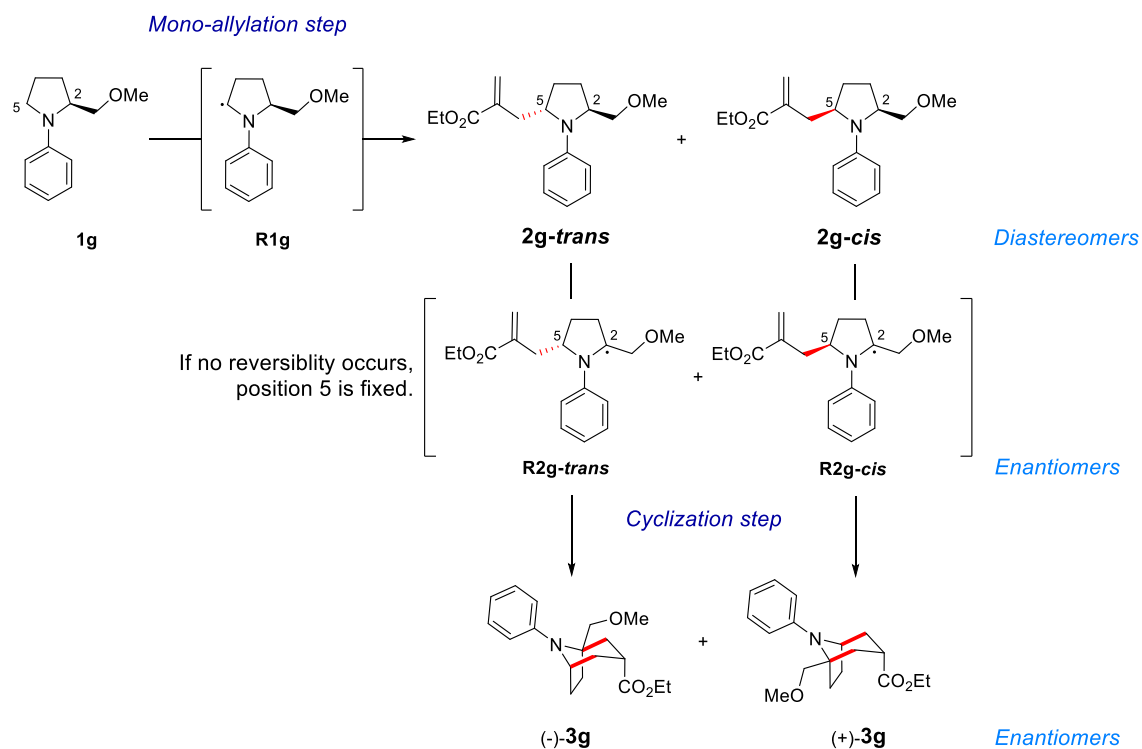
Figure 35. Expected transmission of the chiral information between **1g**, **2g** and **3g** if no reversibility occurs in the radical formation.

The racemic and enantiopure versions of the precursor **1g** were successfully synthesized following a reported procedure.[227] The sequence started with an *N*-arylation between bromobenzene and commercially available DL-proline (respectively L-proline), directly followed by the formation of the methyl ester derivative. The desired precursor was obtained after two straightforward steps of reduction and methylation (Figure 36). The *N*-arylation step, although described on a multigram scale in the literature, proved challenging in our hands and only delivered the methyl ester in poor yield. An alternative way for the synthesis of racemic methyl 1-phenylpyrrolidine-2-carboxylate, instead of repeating the low yielding C-N coupling, was to deprotonate alpha to the ester group in the optically active methyl ester intermediate using freshly prepared LDA (76% yield).
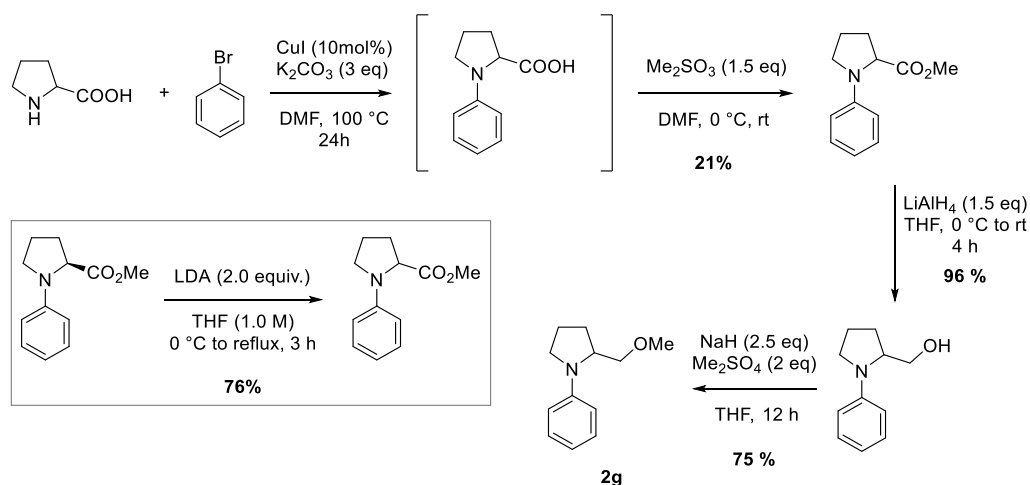
Figure 36. Synthetic sequence for the formation of 2-(methoxymethyl)-1-phenyl-pyrrolidine **2g** from proline

With the model substrate in hand, the optimized photoredox conditions were applied. Gratifyingly, the mono-allylated product **2g** could be obtained in 42% yield along with 25% recovered starting

163

material, and in a *trans/cis* ratio of 77:23 (Figure 37A). The reaction had to be interrupted before full conversion of the starting material in order to prevent the cyclization of the desired mono-allylated intermediate **2g**. The diastereomers of **2g** had first to be separated in order to obtain the optically active **3g**. Gratifyingly, this could be done on a reverse phase semi-preparative HPLC system and the relative configuration of the major diastereomer was assessed by XRay crystallography analysis of a single crystal. HPLC analysis on chiral stationary phase was used to demonstrate that the optical purity had been retained in both the *trans* and *cis* isomers as well as in the recovered starting material, excluding any racemization during this first mono-allylation step. The *trans* isomer was then subjected to the standard cyclization conditions. The cyclized product was obtained in 64% yield (α/β 9:1) and its enantiopurity was controlled by HPLC analysis on chiral stationary phase, excluding any racemization at this step as well (Figure 37B). For practical reasons, the same reaction could not be run on the *cis* isomer (-)-**2g**-*cis*, as too little product was obtained from the allylation reaction. However, an enantiopure mix of **2g** in a *trans/cis* ration of 77:23 was engaged in the cyclization reaction and resulted in the expected ratio of enantiomers withing a 5% error (71% ee, see supporting information for details). This proved that both **2g**-*trans* and **2g**-*cis* were cyclizing in a similar fashion and with retention of the chiral information.

A/ Mono-allylation step
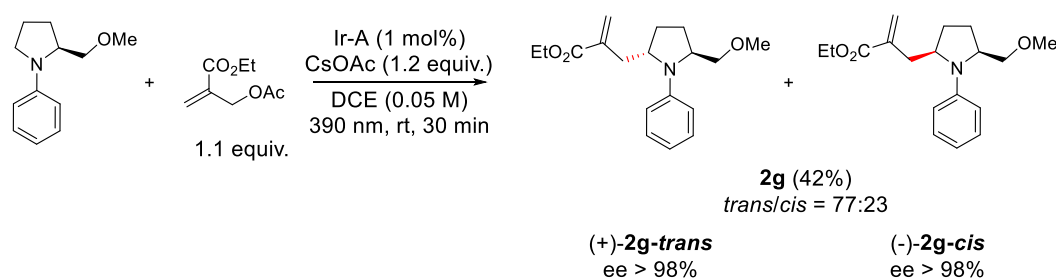
A/ Cyclization step
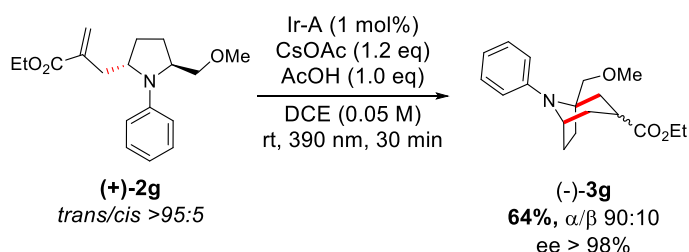
Figure 37: Retention of chiral information through A/ the mono-allylation step and B/ the cyclization step.

Overall, this study set the stage for the synthesis of optically active natural products *via* our method. In the next section, our investigations towards the synthesis of (+)–euphococcinine will be reported.
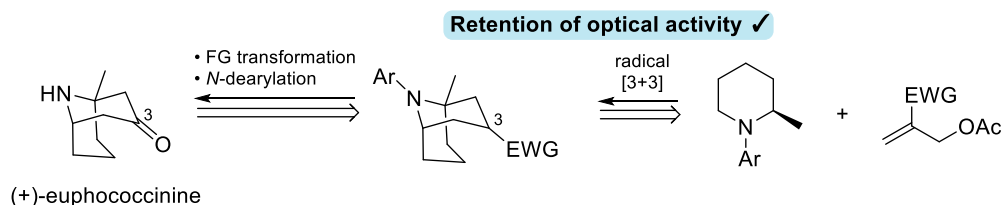
Figure 38. Radical [3+3]-annulation as the key step in the synthesis of (+)-euphococcinine.

3.2.2.2.   *Towards the synthesis of (+)–euphococcinine*

In collaboration with Anja Baumann and Lukas Bader

The synthesis of (+)–euphococcinine has attracted much interest in the past and several methods have been reported based on the Mannich reaction, double Michael addition sequences, and intramolecular cycloadditions.[165,228]

In order to use our radical [3+3]-annulation reaction as key step in the synthesis of (+)–euphococcinine, suitable precursors should be designed. As part of her Master thesis, Anja Bauman investigated the possibility of diversifying the scope of radical traps in order to incorporate different functional groups at position 3 of the tropane core,[229] allowing a straightforward conversion into the ketone group present in the natural product (see Figure 38). Among sulfone-, cyano-, and BPin-functionalized olefins, the latter proved to be the more promising. Phenylpyrrolidine **1a** could be converted to BPin-functionalized **3aa** in 38% yield and excellent diastereoselectivity (Figure 39). In addition, the high-yielding oxidation of the BPin to the alcohol **3ab** was demonstrated. Unfortunately, the performance of the BPin radical trap proved to be very substrate-dependent. Hence the phenylpiperidine **6a** was only converted to **8aa** in a low 8% isolated yield along with 30% recovered starting material and unidentified side products. This reaction could not be further optimized.
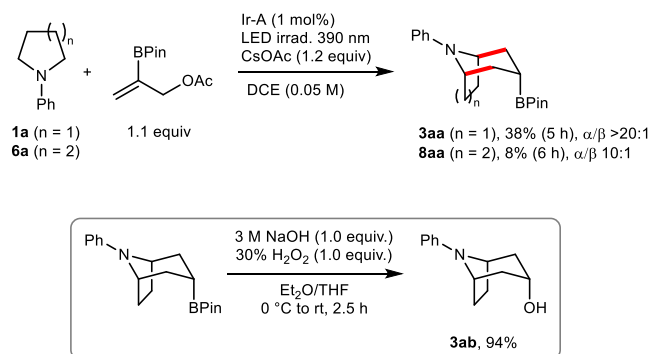
Figure 39. Synthesis of BPin-functionalized tropane cores and subsequent oxidation to the alcohol.

Considering the low reliability of this radical trap, and despite the straightforward access to the required C–O bond connection at position 3, this trap was not further investigated for the synthesis of (+)–euphococcinine. In a preliminary approach, it should be feasible to use the ester-functionalized radical trap and to perform a α-hydroxylation using for example the Davis oxaziridine,[230,231] followed by reduction of the ester moiety and oxidative cleavage of the resulting diol (Figure 40).
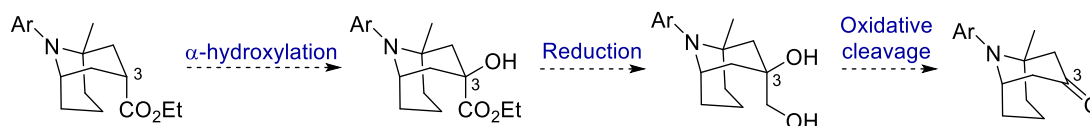
Figure 40. Envisioned synthetic transformations towards the ketone moiety in (+)–euphococcinine.

Since we have demonstrated the possibility of a *N*-dearylation protocol from the *para*-BPin-phenyl derivative, this moiety has to be present in our starting material. This led us to investigate the aniline derivative **6p** as possible precursor for the photoredox reaction towards (+)–euphococcinine (Figure 41). Retrosynthetically, the desired starting *N*-aryl piperidine could be obtained *via* an annulation reaction with the commercially available *p*-BPin-aniline and a 1, 5-disubstituted hexane derivative such as a 1,5-bis-tosylate, -mesylate, or- triflate derived from 1,5-hexanediol. A disconnection between

carbons 3 and 4 would give two 3-carbon synthons tracing back to the commercially available propargyl alcohol and methylated epoxide,[232] following a sequence of epoxide opening and hydrogenation.
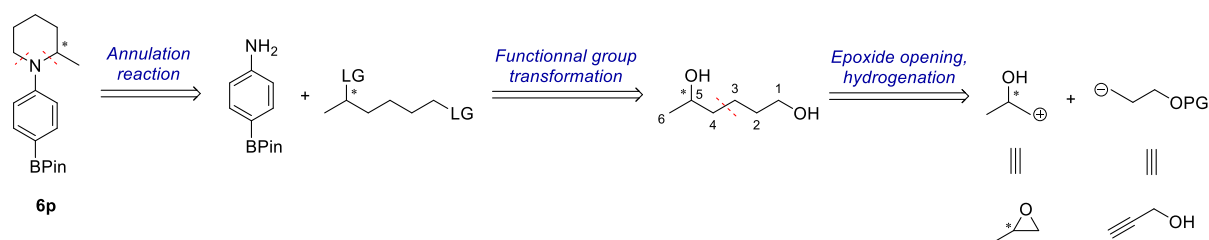
Figure 41. Retrosynthesis analysis towards **6p**.

This retrosynthetic planning has the advantage of avoiding an *N*-arylamination step, usually not efficient with alpha-substituted amines[233] and poorly compatible with a BPin moiety. More importantly, the synthetic pathway could be used for both the racemic and enantioselective synthesis depending on the starting epoxide. The alkyl chain could also easily be modulated. All the steps are known and reported reactions on large scale; only the annulation reaction on a *p*-BPin-aniline was not reported.

The envisioned sequence was carried out starting with a simple protection of the propargyl alcohol as a tetrahydropyranyl (THP) ether, followed by a deprotonation of the terminal alkyne and epoxide opening sequence first reported by Yamaguchi in presence of boron trifluoride etherate (Figure 44).[234] The protocol favored the opening of the epoxide at the least hindered position with exquisite regioselectivity and good yield. Hydrogenation of the resulting alkyne under atmospheric pressure of hydrogen proved to be a fast reaction but gave a disappointing yield of 68% in EtOAc with Pd/C, the rest of the mass accounting for the formation of un undesired ketone by-product. Switching the solvent to methanol or the catalyst to the Pearlman's catalyst only degraded the yield further. Deprotecting the alcohol before running the hydrogenation was also not beneficial. Finally, increasing the pressure of H_2 proved to be the optimal solution, giving yields above 85% in very short reaction times for reactions below 5 mmol scales. Upon scale-up of the reaction, the formation of the ketone increased again, limiting the scale of the reaction to 20 mmol. However, the product could be obtained in a synthetically useful yield of 79% and the ketone could easily be converted to the desired alcohol by reduction with sodium borohydride. The deprotection of the THP protecting group under acidic conditions in refluxing methanol afforded the 1,5-hexanediol in 81% yield. Next the nature of the leaving group was investigated for the annulation reaction. First attempts with tosyl chloride afforded the mono-tosylated product at the primary alcohol position in low yield, the rest of the mass presumably lost as the volatile 2-methyltetrahydropyran derivative resulting from intramolecular cyclization of the mono-tosylated product. The same problem seemed to occur with the triflate derivative, even when running the reaction at very low temperature. Finally, the mesylation worked well and the desired bis-mesylated alcohol was obtained in nearly quantitative yield.
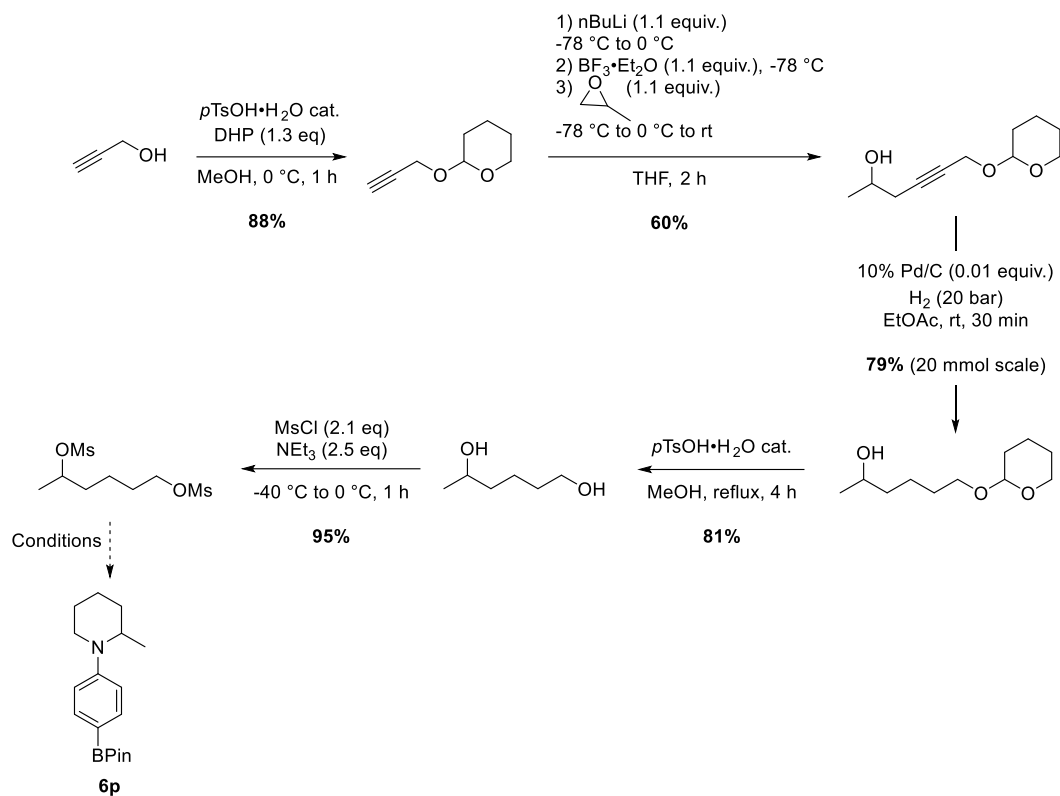
Figure 42. Synthesis of the 1,5-substituted hexane derivative leading to **6p**.

Finally, the cyclization step of the activated alcohol with the *p*-BPin-aniline was investigated. The Hünigh's base needed to be used for this transformation, as K_2CO_3 led to complete protodeboronation of the product, presumably due to a too slow quenching of the released HBr. Still the product was obtained in a low 18% yield in a first attempt. This was attributed to both the substitution on a secondary carbon instead of a primary carbon (Figure 43A), and the use of a mesylate instead of a bromide as a leaving group (Figure 43A). Furthermore, the bis-mesylated substrate seemed to be consumed much faster than the aniline under these reaction conditions, indicating that bis-alkylation was likely to occur, or even oligomerization. Although no such by-products were isolated, and although no increase in the yield was observed upon dilution of the reaction medium, we cannot exclude that this type of reactivity is operative in our system. In accordance with these findings, adding tetrabutylammonium bromide in the reaction mixture to *in situ* substitute the mesylate group by a bromide increased the reaction yield to a synthetically useful 50% (Figure 43C).

A/ Influence of the substitution

DIPEA (3.0 equiv.)
DMF
80 °C, 16 h

1.1 equiv.

R = CH$_3$ (**6p**), **18%**
R = H, (**6j**), **35%**

B/ Influence of the leaving group

DIPEA (3.0 equiv.)
DMF
80 °C, 16 h

1.1 equiv.

LG = leaving group

LG = OMs, **35%**
LG = Br, **76%**

C/ Final conditions for the racemic synthesis

DIPEA (3.0 equiv.)
*n*Bu$_4$NBr (2.2 equiv.)
DMF
80 °C, 16 h

1.1 equiv.

6p
50%
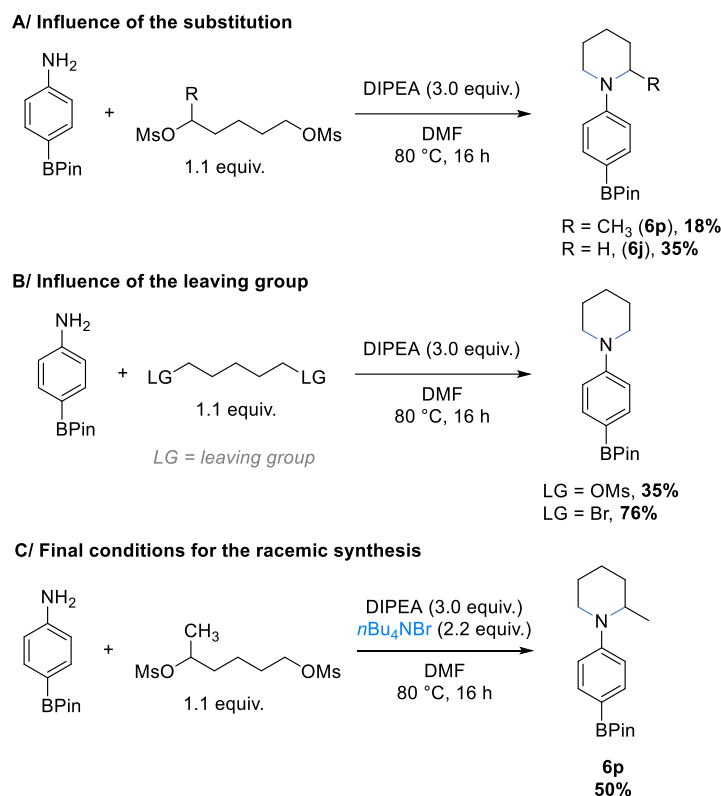
Figure 43: Annulation of the para-BPin-aniline with a 1,5-substituted hexane derivative. Influence of the substitution at the leaving group and of the leaving group nature (LG).

With a sample of the racemic substrate **6p** in hand, we turned our attention to the photoredox reaction (Figure 44). Under the optimized conditions, the one-pot sequence gave after 7 hours of irradiation a mixture of mono-allylated intermediate **7p** in 11% yield and of cyclized product **8p** in 13% yield. Complete conversion of the starting material was observed. Reducing the reaction time to 40 minutes afforded, on 1 mmol scale, 40% of **7p** in a good diastereomeric ratio of 1:5.5, along with 9% recovered starting material and traces of cyclized product. The relative configuration of the major diastereomer could not yet be determined. Although the isolated yield of the mono-allylated intermediate was acceptable in this case, the amount of starting material and cyclized product recovered did not account for the loss of mass. Hoping to gain a better understanding of the reaction, the diastereomers of **7p** were separated and the major diastereomer was engaged in an independent cyclization reaction. The reaction proved to be slow and after some cyclized product was formed, the reaction seemed to stumble. Adding one more portion of catalyst and letting the reaction overnight finally allowed a full conversion of the starting material. The cyclized product **8p** was only formed in 35% yield but with excellent diastereoselectivity. It is possible that with this substrate the regioselectivity of the radical formation is low. An over oxidation of the unreactive α-aminoalkyl radical to the iminium ion would account for both the loss of catalyst activity and the loss of mass.
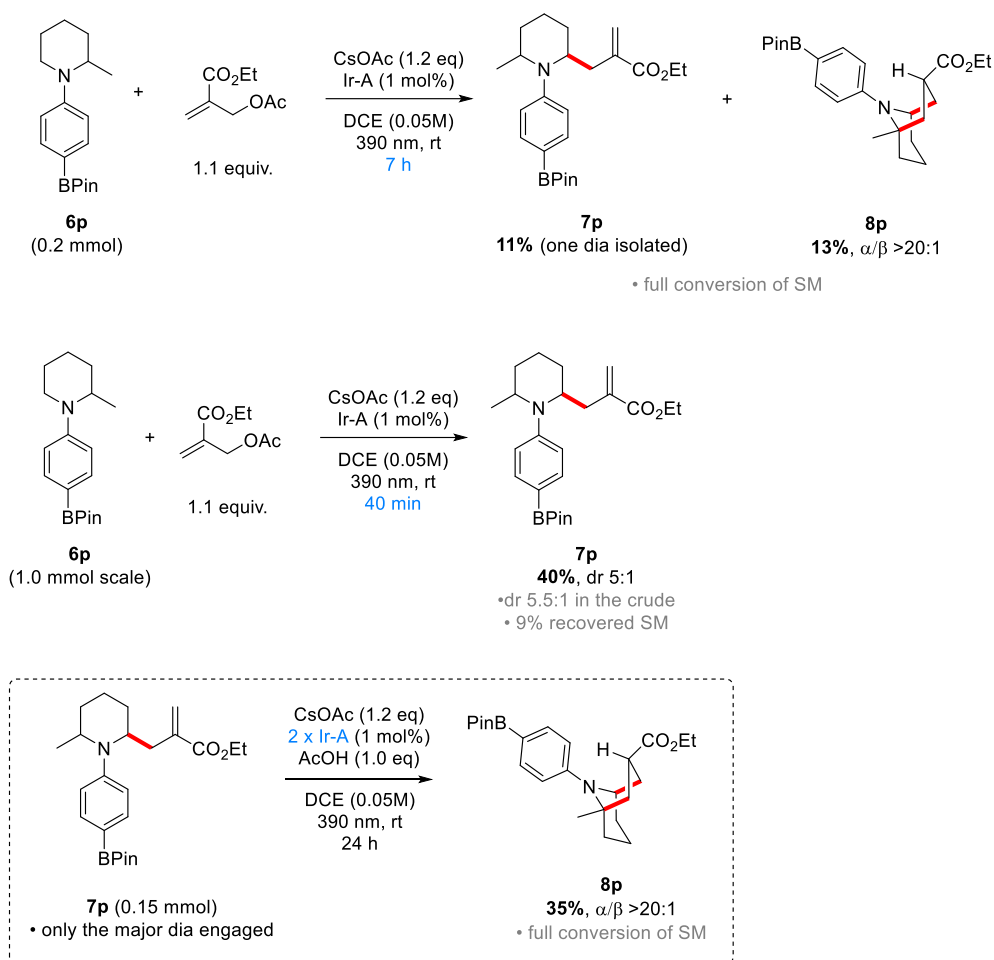
Figure 44: Preliminary investigations on the reactivity of the substrate under standard photoredox conditions

In parallel to these investigations, the possibility to use other protecting groups than a *para*-BPin-aryl moiety was evaluated. This could potentially facilitate the synthesis of the starting material, but also increase the efficiency of the cyclization reaction and/or increase the diastereomeric ratio of product **7p**, which is desirable since only one diastereomer should be engaged in the cyclization reaction.

Cbz-protected piperidine

In 2018, Nicewicz and co-workers reported that acridinium photoredox catalysts were able to perform the one-electron oxidation of carbamate-protected amines with oxidation potentials as high as + 1.96 V *vs* SCE (for Boc-protected piperidine).[235,236] The reaction conditions were amenable to Boc-, Cbz-, and Fmoc-protected amines (Figure 45). Interestingly, a 2-methylated piperidine derivative was alkylated with retention of optical activity. The scope of radical traps was mostly limited to α,β-unsaturated ketones, but the use of acrylates was reported as well, indicating that the reduction of alpha-ester radicals should be feasible.
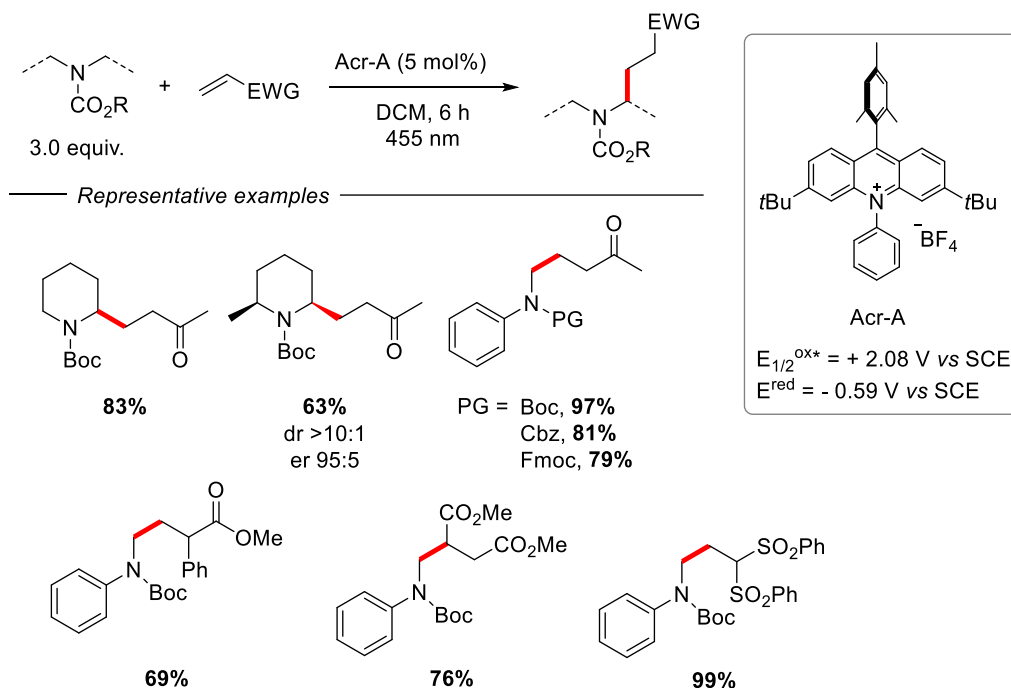
Figure 45. Alpha-alkylation of carbamate-protected amines using an acridinium photocatalyst (Nicewicz).

Similar conditions were applied to our system using Cbz-protected piperidine as starting material, since the expected product had been previously isolated (product **13**, Figure 29). Unfortunately, none of the screened acridinium-based catalysts promoted the formation of **13**, presumably due to a too low reduction potential of the catalysts (Figure 46). In addition, witching the solvent to DCM and removing the base as in Nicewicz's conditions did not afford any product with either photocatalyst Acr-A, -B, or -C.
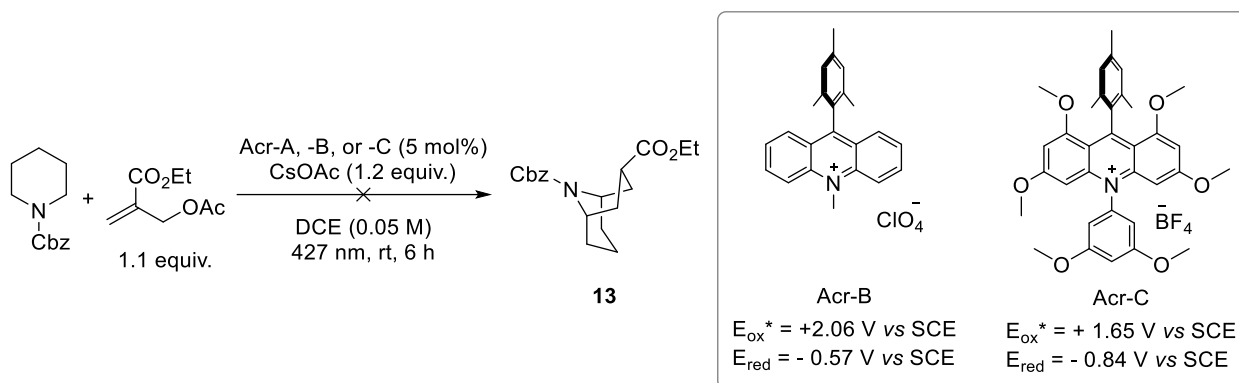
Figure 46. Screened acridinium photocatalysts for the radical [3+3]-annulation of Cbz-protected piperidine.

Benzaldehyde moiety

The *para*-aldehyde functionality was investigated in lieu of the *para*-BPin for the *N*-dearylation sequence because the starting material could potentially be made *via* a nucleophilic aromatic substitution of the free amine on 4-fluorobenzaldehyde in presence of a base in refluxing DMF.[237] Engaging the benzaldehyde functionality in a Baeyer-Villiger oxidation would lead to the required phenol moiety for the dearylation procedure.[238]
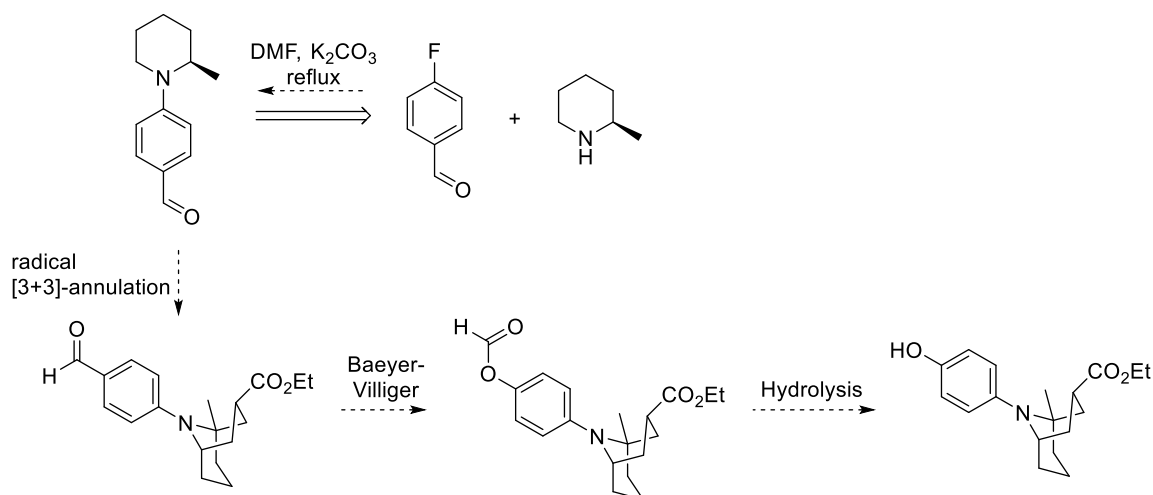
Figure 47. Envisioned strategy for starting material preparation and *N*-dearylation with a benzaldehyde moiety.

Preliminary investigations towards this strategy started by testing the compatibility of the photoredox protocol with the (protected) benzaldehyde derivative. While the free aldehyde **6q** was not amenable to the reaction conditions, the acetal **P-6q** afforded the cyclized product **P-8q** in 56% yield. Deprotection under acidic deprotection furnished the free aldehyde **8q** in 94% yield (53% over two steps, α/β >20:1). Applying this strategy to the methyl ketone derivative allowed to increase the yield of product **8h** to 57% over two steps (42% with the unprotected ketone starting material).
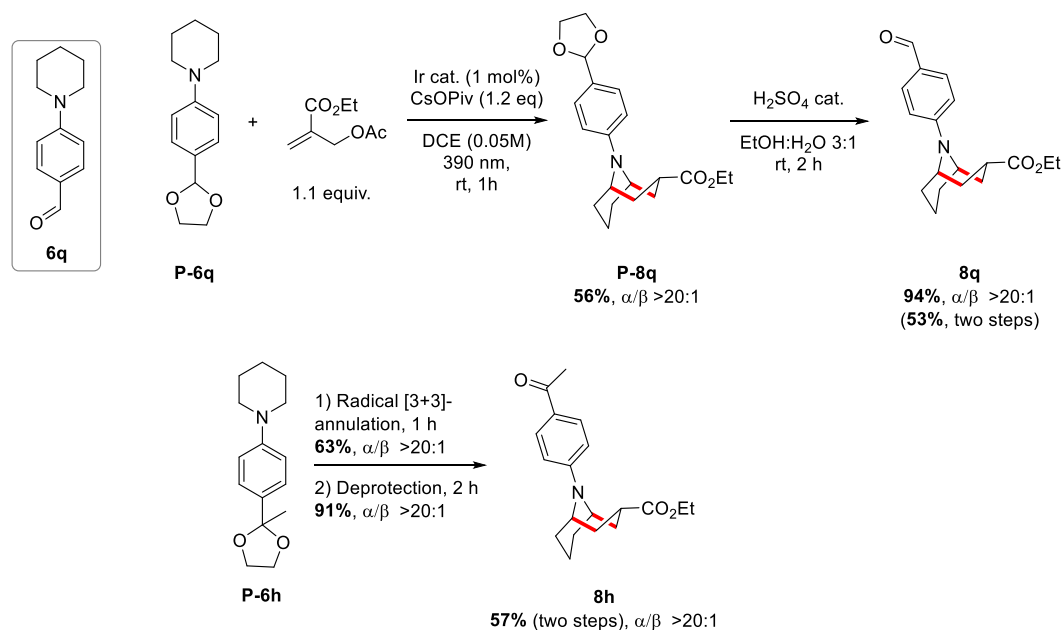
Next, the Baeyer-Villiger oxidation was tested on **6q**. There are only scarce examples of Baeyer-Villiger oxidations on aniline derivatives,[239] presumably due to the competitive oxidation of the nitrogen. Nonetheless, we envisaged that acidic conditions could protected the sensitive nitrogen under the oxidative conditions. Unfortunately, our efforts were not fruitful, and the chloride salt of the starting material could not be converted to the desired product.
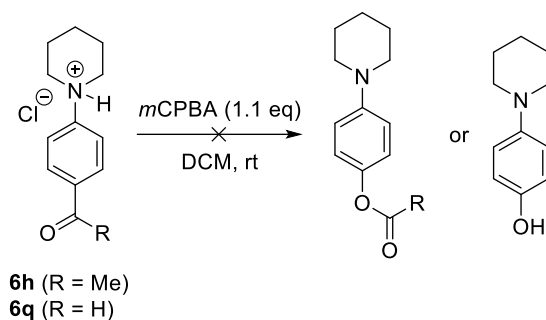
Figure 48. Unsuccessful Bayer-Villiger oxidation attempts.

Hence this strategy was not pushed further. Nonetheless, product **8q** is a nice addition to the reaction scope and provides an interesting handle for further derivatization of the tropane derivative.

Continuation of this work is now being performed by Lukas Bader as part of a master thesis in the Renaud group, including the synthesis of optically pure **6p** and the investigation of further protecting groups. These endeavors will be reported in due course and will not be discussed in this manuscript.

3.3. Outlook

3.3.1. Easy access to *N*-arylated 2-tropinone derivatives

2-tropinone is a very useful precursor in the preparation of compounds with biological activity[240–243] but is not as easily available as its *meso* isomer 3-tropinone (Figure 49).
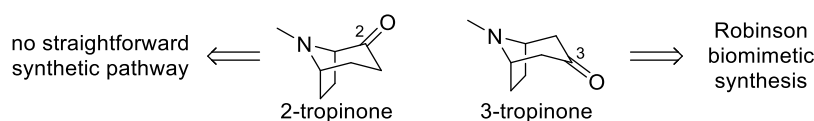
Figure 49. Structures of 2-tropinone versus 3-tropinone.

The most used method to date is still by degradation of cocaine under strongly acidic and refluxing conditions (Figure 50A).[244] The resulting α,β-unsaturated carboxylic acid can be converted to the acyl azide using diphenylphosphoryl azide under basic conditions. Curtius rearrangement finally leads to the desired compound. Starting from optically pure cocaine leads to optically pure 2-tropinone. This strategy has the advantage of being high-yielding and scalable, but the major drawback is the necessity to start with the more complex precursor cocaine, moreover a restricted substance. Davies and co-workers reported a synthesis of the racemic alpha-ketoester derivative in 6 steps from ethyl pyrrole-2-carboxylate (Figure 50B).[245] Decarboxylation of this intermediate under mild acidic conditions and heat afforded 2-tropinone. The authors demonstrated the possibility to resolve the racemic compound as a chiral salt.

A/ Synthesis of (+)-2-tropinone from (-)-cocaine by Trudell, 1997
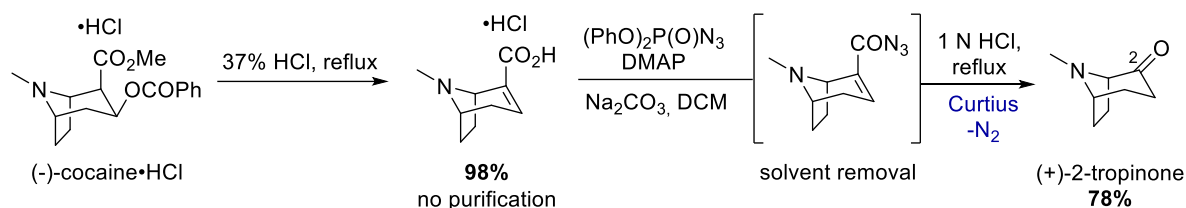
B/ Racemic synthesis and resolution of 2-tropinone by Davies, 1961
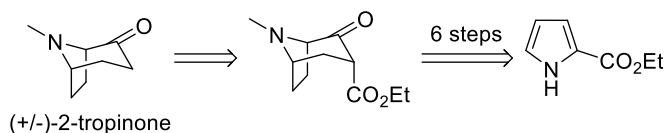
Figure 50. Reported synthesis of 2-tropinone from A/ cocaine; B/ ethyl pyrrole-2-carboxylate.

In these two strategies, the scope is strictly restricted to the formation of the tropane core and the synthesis cannot be easily modulated. Using our previously reported radical [3+3]-annulation with an allenic trap would allow a facile access to a library of *N*-arylated tropane and homotropane derivatives substituted at position 2 with an alkene moiety (Figure 51). This key intermediate could be cleaved to give the alpha-ketoester, which has already been reported to undergo the desired decarboxylation readily.[245,246]
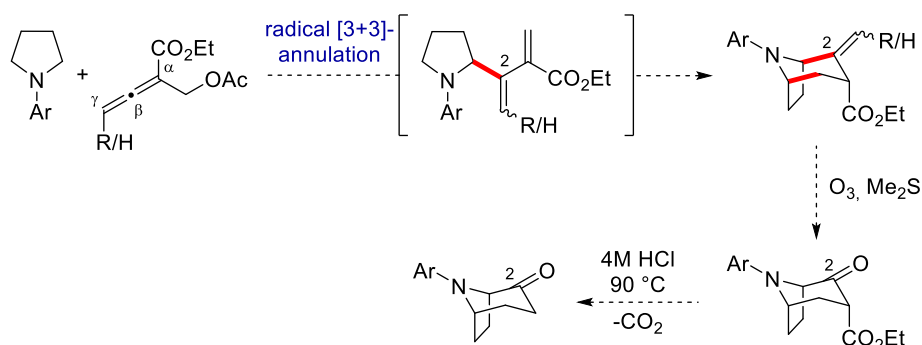
Figure 51. Easy access to N-arylated 2-tropinone derivatives using a radical [3+3]-annulation step.

The required allenic radical trap is a known product and can be accessed *via* the allenylic alcohol.[247] Kwon and co-workers recently reported 13 examples of such precursors.[248] In addition, its electrophilic reactivity at position β over position γ has been previously demonstrated.[249] If problems of regioselectivity do arise, substituting position γ with one or two substituents should slow down undesired radical addition at this position.[5]

3.3.2. Enantioselectivity

In order to render this reaction enantioselective, the stereochemistry of the newly formed center at the alpha-position of the nitrogen should be controlled in the mono-allylated intermediate.[250] Such an intermediate would be forced to cyclize from one side of the pyrrolidine ring only, a strategy that would be interesting as well for the enantioselective synthesis of unsymmetrical products such as **10** (Figure 52).

optically activ

9

10
optically activ

● Controled during the radical addition step *via* a chiral induction
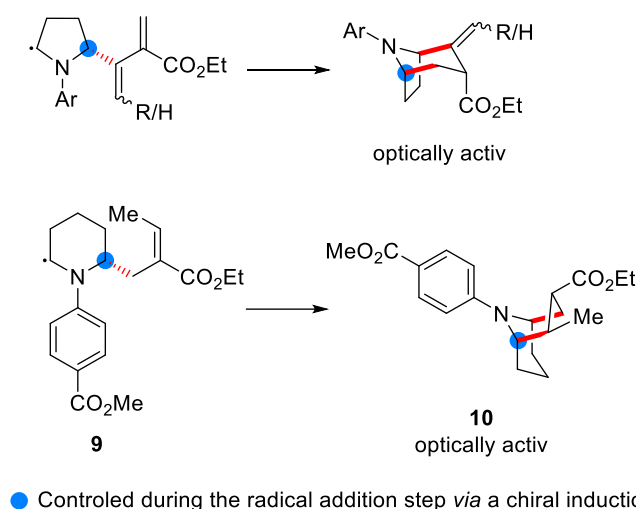
Figure 52. Necessity to control the stereochemistry of the newly-formed center in the alpha-aminoalkyl radical addition to the radical trap in order to obtain optically active cyclized products.

To do so we envisioned to use a phosphate-based achiral base in combination with a chiral phosphoric acid catalyst which would provide the non-covalent interactions necessary to exert stereochemical control.[43,251] To this end K_3PO_4 was found to be a suitable base for our radical [3+3]-annulation and provided the model compound **3a** in 47% yield. Concomitantly to these investigations, the Phipps group disclosed an advanced study towards the enantioselective addition of α-aminoalkyl radicals to Giese acceptor electrophiles.[252] They reported that *N,N*-dimethylpyridin-2-amine derivatives could be enantioselectively α-alkylated in presence of an iridium photocatalyst, 2 equivalents of K_3PO_4, 5 mol% of a chiral phosphoric acid, and a thiol as sacrificial hydrogen atom donor (Figure 53). This was necessary to suppress any background racemic reaction occurring upon escaping of the α-aminoalkyl radical outside the catalytic pocket. The methodology was limited to radical traps able to engage in hydrogen bonding with the chiral catalyst, such as α,β-unsaturated secondary amides. Interestingly, the authors reported that the pyridyl ring could be easily removed from the product. This would be an interesting protecting groups for our investigations towards a natural product and should facilitate starting material synthesis.

Phipps, 2022
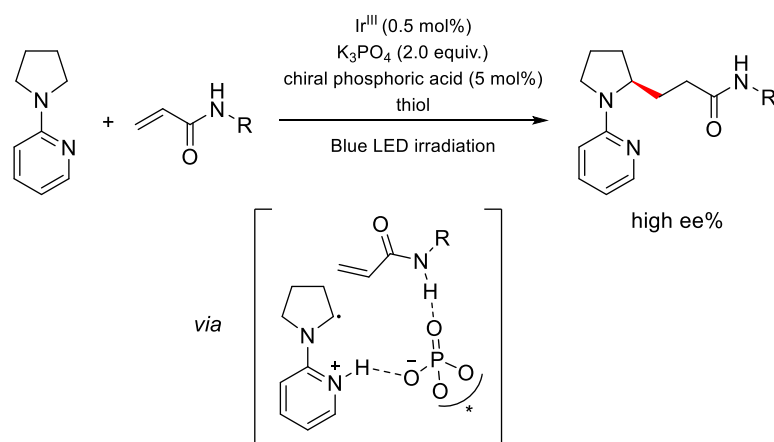
Figure 53. Enantioselective alpha-alkylation of *N*-(hetero)aryl pyrrolidine in development in the Phipps group.

3.3.3. Diastereoselectivity

The high diastereoselectivity observed in the formation of bis-annulated product **14** (Figure 33) is best explained by applying the Fürst-Plattner rule favoring a *trans*-diaxial attack.[253] The chair-like transition state leads to the *trans*-piperidine intermediate (Figure 54).
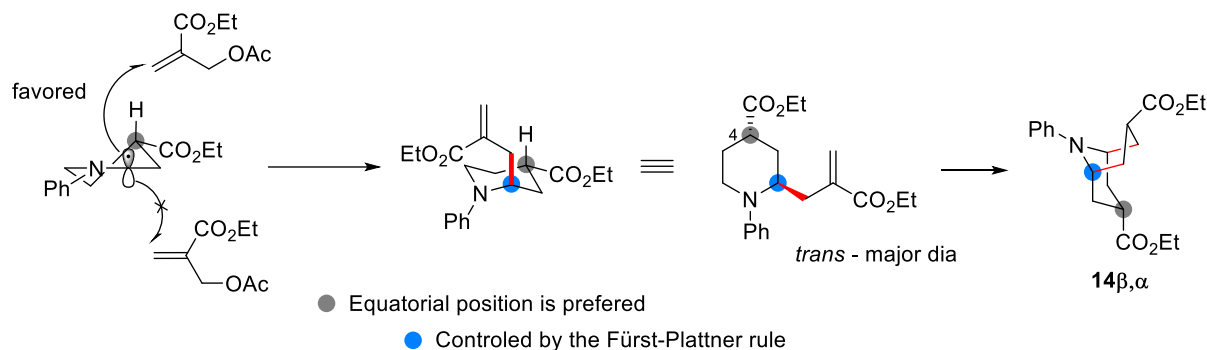
Figure 54. Diastereoselective α-functionalization of 4-substituted piperidines.

In order to further investigate this diastereoselective reaction and to assess its generality, it should be tested on a series of piperidine precursors decorated at position 4 with substituents such as ethyl ester, methyl, benzyl and *tert*-butyl. These compounds can be obtained *via* palladium couplings of the corresponding piperidines with bromo- or iodobenzene.[254] While some 4-substituted piperidines are commercially available, 4-alkylpiperidines can typically be obtained by hydrogenation of the pyridine precursors.[255,256] In the case of a methyl group, 4-piperidone can be used as a precursor in a Wittig olefination, hydrogenation sequence.[257]
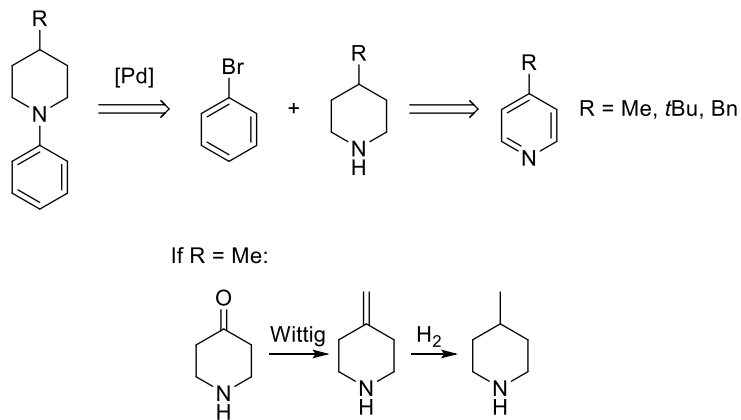
Figure 55. Synthetic pathway to 4-substituted *N*-arylated piperidines.

References

1   J. M. Aurrecoechea and R. Suero, *Arkivoc*, 2004, **2004**, 10–35.

2   D. Griller and F. P. Lossing, *J. Am. Chem. Soc.*, 1981, **103**, 1586–1587.

3   T. J. Burkey, A. L. Castelhano, D. Griller and F. P. Lossing, *J. Am. Chem. Soc.*, 1983, **105**, 4701–4703.

4   D. D. M. Wayner, J. J. Dannenberg and D. Griller, *Chemical Physics Letters*, 1986, **131**, 189–191.

5   B. Giese, *Angew. Chem. Int. Ed. Engl.*, 1983, **22**, 753–764.

6   Y. Fu, L. Liu, H.-Z. Yu, Y.-M. Wang and Q.-X. Guo, *J. Am. Chem. Soc.*, 2005, **127**, 7227–7234.

7   D. J. Hart and Y. M. Tsai, *J. Am. Chem. Soc.*, 1984, **106**, 8209–8217.

8   J. Lalevée, X. Allonas and J. P. Fouassier, *Chemical Physics Letters*, 2008, **454**, 415–418.

9   N. Sanosa, B. Peñin, D. Sampedro and I. Funes-Ardoiz, *European Journal of Organic Chemistry*, , DOI:10.1002/ejoc.202200420.

10 T. Constantin, M. Zanini, A. Regni, N. S. Sheikh, F. Juliá and D. Leonori, *Science*, 2020, **367**, 1021–1026.

11 Y.-L. Su and M. P. Doyle, *Synthesis*, 2022, **54**, 545–554.

12 G. S. Yedase, A. K. Jha and V. R. Yatham, *J. Org. Chem.*, , DOI:10.1021/acs.joc.2c00251.

13 R. K. Neff, Y.-L. Su, S. Liu, M. Rosado, X. Zhang and M. P. Doyle, *J. Am. Chem. Soc.*, 2019, **141**, 16643–16650.

14 F. Yue, J. Dong, Y. Liu and Q. Wang, *Org. Lett.*, , DOI:10.1021/acs.orglett.1c02905.

15 P. Renaud and L. Giraud, *Synthesis*, 1996, **1996**, 913–926.

16 S. Takano, M. Suzuki, A. Kijima and K. Ogasawara, *Tetrahedron Letters*, 1990, **31**, 2315–2318.

17 S. A. Glover and J. Warkentin, *J. Org. Chem.*, 1993, **58**, 2115–2121.

18 J. H. Rigby and M. N. Qabar, *J. Org. Chem.*, 1993, **58**, 4473–4475.

19 M. Silvi and P. Melchiorre, *Nature*, 2018, **554**, 41–49.

20 D. A. Nagib, M. E. Scott and D. W. C. MacMillan, *J. Am. Chem. Soc.*, 2009, **131**, 10875–10877.

21 H.-W. Shih, M. N. Vander Wal, R. L. Grange and D. W. C. MacMillan, *J. Am. Chem. Soc.*, 2010, **132**, 13600–13603.

22 D. A. Nicewicz and D. W. C. MacMillan, *Science*, 2008, **322**, 77–80.

23 G. Cecere, C. M. König, J. L. Alleva and D. W. C. MacMillan, *J. Am. Chem. Soc.*, 2013, **135**, 11521–11524.

24 G. Filippini, M. Silvi and P. Melchiorre, *Angewandte Chemie International Edition*, 2017, **56**, 4447–4451.

25 A. Bahamonde and P. Melchiorre, *J. Am. Chem. Soc.*, 2016, **138**, 8019–8030.

26 M. Silvi, E. Arceo, I. D. Jurberg, C. Cassani and P. Melchiorre, *J. Am. Chem. Soc.*, 2015, **137**, 6120–6123.

27 R. K. Dhungana, A. Granados, M. Sharique, J. Majhi and G. A. Molander, *Chem. Commun.*, , DOI:10.1039/D2CC04101D.

28 D. J. Hart, in *Radicals in Organic Synthesis*, Wiley-Blackwell, 2008, pp. 279–302.

29 D. L. J. Clive and V. S. C. Yeh, *Tetrahedron Letters*, 1998, **39**, 4789–4792.

30 J. Quirante, C. Escolano and J. Bonjoch, *Synlett*, 1997, **1997**, 179–180.

31 C. Chatgilialoglu, D. Crich, M. Komatsu and I. Ryu, *Chem. Rev.*, 1999, **99**, 1991–2070.

32 J. M. Aurrecoechea, B. López, A. Fernández, A. Arrieta and F. P. Cossío, *J. Org. Chem.*, 1997, **62**, 1125–1135.

33 J. Aurrecoechea, A. Fernández, J. Gorgojo and C. Saornil, *Tetrahedron*, 1999, **55**, 7345–7362.

34 JoséM. Aurrecoechea and A. Fernández-Acebes, *Tetrahedron Letters*, 1993, **34**, 549–552.

35 C.-H. Liu, J.-M. Guo, X. Li, J.-T. Sun, B.-G. Wei and C.-M. Si, *Chem. Commun.*, , DOI:10.1039/D2CC03984B.

36 J. A. Leitch; Dixon, T. Rossolini, T. Rogova, J. A. P. Maitland and D. J. Dixon, *ACS Catal.*, 2020, **10**, 2009–2025.

37 J. A. P. Maitland, J. A. Leitch, K. Yamazaki, K. E. Christensen, D. J. Cassar, T. A. Hamlin and D. J. Dixon, *Angewandte Chemie International Edition*, , DOI:10.1002/anie.202107253.

38 D. Lehnherr; Rovis, Y. Lam, M. C. Nicastri, J. Liu, J. A. Newman, E. L. Regalado, D. A. DiRocco and T. Rovis, *J. Am. Chem. Soc.*, 2020, **142**, 468–478.

39 Keiji. Okada, Kazushige. Okamoto and Masaji. Oda, *J. Am. Chem. Soc.*, 1988, **110**, 8736–8738.

40 Y. Jin, M. Jiang, H. Wang and H. Fu, *Sci Rep*, 2016, **6**, 20068.

41 J. Schwarz and B. König, *Green Chem.*, 2016, **18**, 4743–4749.

42 W.-M. Cheng, R. Shang and Y. Fu, *ACS Catal.*, 2017, **7**, 907–911.

43 R. S. J. Proctor, H. J. Davis and R. J. Phipps, *Science*, 2018, **360**, 419–422.

44 X. Liu, Y. Liu, G. Chai, B. Qiao, X. Zhao and Z. Jiang, *Org. Lett.*, 2018, **20**, 6298–6301.

45 M.-C. Fu, R. Shang, B. Zhao, B. Wang and Y. Fu, *Science*, 2019, **363**, 1429–1434.

46 R. Kumar and P. Banerjee, *J. Org. Chem.*, , DOI:10.1021/acs.joc.1c02069.

47 L. F. T. Novaes, J. S. K. Ho, K. Mao, K. Liu, M. Tanwar, M. Neurock, E. Villemure, J. A. Terrett and S. Lin, *J. Am. Chem. Soc.*, , DOI:10.1021/jacs.1c09412.

48 R. S. J. Proctor and R. J. Phipps, *Angewandte Chemie International Edition*, 2019, **58**, 13666–13699.

49 P. Renaud and D. Seebach, *Synthesis*, 1986, **1986**, 424–426.

50 G. S. Kumar, P. S. Shinde, H. Chen, K. Muralirajan, R. Kancherla and M. Rueping, *Org. Lett.*, 2022, **24**, 6357–6363.

51 D. D. M. Wayner, K. B. Clark, A. Rauk, D. Yu and D. A. Armstrong, *J. Am. Chem. Soc.*, 1997, **119**, 8925–8932.

52 T. Yoshimitsu, Y. Arano and H. Nagaoka, *J. Org. Chem.*, 2003, **68**, 625–627.

53 T. Yoshimitsu, K. Matsuda, H. Nagaoka, K. Tsukamoto and T. Tanaka, *Org. Lett.*, 2007, **9**, 5115–5118.

54 C. Zhang, C. Liu, Y. Shao, X. Bao and X. Wan, *Chemistry – A European Journal*, 2013, **19**, 17917–17925.

55 J. Zhang, J. Jiang, D. Xu, Q. Luo, H. Wang, J. Chen, H. Li, Y. Wang and X. Wan, *Angewandte Chemie International Edition*, 2015, **54**, 1231–1235.

56 Z. Song and A. P. Antonchick, *Tetrahedron*, 2016, **72**, 7715–7721.

57 V. Snieckus, J. C. Cuevas, C. P. Sloan, H. Liu and D. P. Curran, *Journal of the American Chemical Society*, 1990, **112**, 896–898.

58 L. Williams, S. E. Booth and K. Undheim, *Tetrahedron*, 1994, **50**, 13697–13708.

59 T. Sato, T. Yamazaki, Y. Nakanishi, J. Uenishi and M. Ikeda, *J. Chem. Soc., Perkin Trans. 1*, 2002, 1438–1443.

60 J. Robertson, M. A. Peplow and J. Pillai, *Tetrahedron Letters*, 1996, **37**, 5825–5828.

61 F. Dénès, F. Beaufils and P. Renaud, *Org. Lett.*, 2007, **9**, 4375–4378.

62 Y. Liang, Y.-X. Xu, Z.-J. Cai and S.-J. Ji, *Chem. Commun.*, , DOI:10.1039/D2CC03799H.

63 M. H. Shaw, V. W. Shurtleff, J. A. Terrett, J. D. Cuthbertson and D. W. C. MacMillan, *Science*, 2016, **352**, 1304–1308.

64 M. A. Ashley, C. Yamauchi, J. C. K. Chu, S. Otsuka, H. Yorimitsu and T. Rovis, *Angewandte Chemie International Edition*, 2019, **58**, 4002–4006.

65 J. Ye, I. Kalvet, F. Schoenebeck and T. Rovis, *Nature Chemistry*, 2018, **10**, 1037–1041.

66 T. Ide, J. P. Barham, M. Fujita, Y. Kawato, H. Egami and Y. Hamashima, *Chem. Sci.*, 2018, **9**, 8453–8460.

67 Y. Shen, I. Funez-Ardoiz, F. Schoenebeck and T. Rovis, *J. Am. Chem. Soc.*, , DOI:10.1021/jacs.1c07144.

68 A. S. H. Ryder, W. B. Cunningham, G. Ballantyne, T. Mules, A. G. Kinsella, J. Turner-Dore, C. M. Alder, L. J. Edwards, B. S. J. McKay, M. N. Grayson and A. J. Cresswell, *Angewandte Chemie International Edition*, , DOI:10.1002/anie.202005294.

69 T. Wakaki, K. Sakai, T. Enomoto, M. Kondo, S. Masaoka, K. Oisaki and M. Kanai, *Chemistry – A European Journal*, 2018, **24**, 8051–8055.

70 J. Liu, J. Xie and C. Zhu, *Org. Chem. Front.*, 2017, **4**, 2433–2436.

71 Z. Zuo and D. W. C. MacMillan, *J. Am. Chem. Soc.*, 2014, **136**, 5257–5260.

72 A. Noble and D. W. C. MacMillan, *J. Am. Chem. Soc.*, 2014, **136**, 11602–11605.

73 L. Chu, C. Ohta, Z. Zuo and D. W. C. MacMillan, *J. Am. Chem. Soc.*, 2014, **136**, 10886–10889.

74 Y. Miyake, K. Nakajima and Y. Nishibayashi, *Chem. Commun.*, 2013, **49**, 7854–7856.

75 H. Yang, G. Wei and Z. Jiang, *ACS Catal.*, 2019, **9**, 9599–9605.

76 L. Gingipalli, J. Boerth, D. Emmons, T. Grebe, H. Hatoum-Mokdad, B. Peng, L. Sha, S. Tentarelli, H. Wang, Y. Wu, X. Zheng, S. Edmondson and A. Gopalsamy, *Org. Lett.*, , DOI:10.1021/acs.orglett.0c00873.

77 C. Shu, R. S. Mega, B. J. Andreassen, A. Noble and V. K. Aggarwal, *Angewandte Chemie International Edition*, 2018, **57**, 15430–15434.

78 Z. Zuo, D. T. Ahneman, L. Chu, J. A. Terrett, A. G. Doyle and D. W. C. MacMillan, *Science*, 2014, **345**, 437–440.

79 S. B. Lang, K. M. O'Nele and J. A. Tunge, *J. Am. Chem. Soc.*, 2014, **136**, 13606–13609.

80 Z. Zuo, H. Cong, W. Li, J. Choi, G. C. Fu and D. W. C. MacMillan, *J. Am. Chem. Soc.*, 2016, **138**, 1832–1835.

81 R. S. Mega, V. K. Duong, A. Noble and V. K. Aggarwal, *Angewandte Chemie International Edition*, 2020, **59**, 4375–4379.

82 H. Yue, C. Zhu, R. Kancherla, F. Liu and M. Rueping, *Angewandte Chemie International Edition*, 2020, **59**, 5738–5746.

83 K. Miyazawa, T. Koike and M. Akita, *Advanced Synthesis & Catalysis*, 2014, **356**, 2749–2755.

84 D. Hanss, J. C. Freys, G. Bernardinelli and O. S. Wenger, *European Journal of Inorganic Chemistry*, 2009, **2009**, 4850–4859.

85 B. E. Cooper and W. J. Owen, *Journal of Organometallic Chemistry*, 1971, **29**, 33–40.

86 J. Yoshida, T. Maekawa, T. Murata, S. Matsunaga and S. Isoe, *J. Am. Chem. Soc.*, 1990, **112**, 1962–1970.

87 X. Zhang, S.-R. Yeh, S. Hong, M. Freccero, A. Albini, D. E. Falvey and P. S. Mariano, *J. Am. Chem. Soc.*, 1994, **116**, 4211–4220.

88 U. C. Yoon, J. U. Kim, E. Hasegawa and P. S. Mariano, *J. Am. Chem. Soc.*, 1987, **109**, 4421–4423.

89 Yoon T. Jeon; Mariano, C. P. Lee and P. S. Mariano, *J. Am. Chem. Soc.*, 1991, **113**, 8847–8863.

90 G. Pandey and G. D. Reddy, *Tetrahedron Letters*, 1992, **33**, 6533–6536.

91 Y. Miyake, Y. Ashida, K. Nakajima and Y. Nishibayashi, *Chemical Communications*, 2012, **48**, 6966.

92 K. Nakajima, M. Kitagawa, Y. Ashida, Y. Miyake and Y. Nishibayashi, *Chem. Commun.*, 2014, **50**, 8900–8903.

93 L. Ruiz Espelt, I. S. McPherson, E. M. Wiensch and T. P. Yoon, *J. Am. Chem. Soc.*, 2015, **137**, 2452–2455.

94 C. Remeur, C. B. Kelly, N. R. Patel and G. A. Molander, *ACS Catal.*, 2017, **7**, 6065–6069.

95 W. Dong, S. O. Badir, X. Zhang and G. A. Molander, *Org. Lett.*, , DOI:10.1021/acs.orglett.1c01207.

96 S. Zheng, Z. Chen, Y. Hu, X. Xi, Z. Liao, W. Li and W. Yuan, *Angewandte Chemie International Edition*, 2020, **59**, 17910–17916.

97 S. F. Nelsen and J. Thomas. Ippoliti, *Journal of the American Chemical Society*, 1986, **108**, 4879–4881.

98 F. D. Lewis and T.-I. Ho, *J. Am. Chem. Soc.*, 1980, **102**, 1751–1752.

99 S. F. Nelsen, C. R. Kessel and D. J. Brien, *J. Am. Chem. Soc.*, 1980, **102**, 702–711.

100 L.-H. Li, H.-Z. Wei, Y. Wei and M. Shi, *Chem. Sci.*, 2022, **13**, 1478–1483.

101 X.-T. Gu, L.-H. Li, Y. Wei and M. Shi, *Chem. Commun.*, , DOI:10.1039/D2CC03694K.

102 J. W. Beatty and C. R. J. Stephenson, *Acc. Chem. Res.*, 2015, **48**, 1474–1484.

103 A. G. Condie, J. C. González-Gómez and C. R. J. Stephenson, *J. Am. Chem. Soc.*, 2010, **132**, 1464–1465.

104 Y. L. Chow, W. C. Danen, S. F. Nelsen and D. H. Rosenblatt, *Chem. Rev.*, 1978, **78**, 243–274.

105 M.-M. Wang, T. V. T. Nguyen and J. Waser, *Chem. Soc. Rev.*, , DOI:10.1039/D2CS00090C.

106 Y. Cai, J. Wang, Y. Zhang, Z. Li, D. Hu, N. Zheng and H. Chen, *J. Am. Chem. Soc.*, 2017, **139**, 12259–12266.

107 M. S. Workentin, L. J. Johnston, D. D. M. Wayner and V. D. Parker, *J. Am. Chem. Soc.*, 1994, **116**, 8279–8287.

108 J. L. Jeffrey, F. R. Petronijević and D. W. C. MacMillan, *J. Am. Chem. Soc.*, 2015, **137**, 8404–8407.

109 S. Bertrand, N. Hoffmann, S. Humbel and J. P. Pete, *J. Org. Chem.*, 2000, **65**, 8690–8703.

110 S. Bertrand, N. Hoffmann and J.-P. Pete, *European Journal of Organic Chemistry*, 2000, **2000**, 2227–2238.

111 F. P. Guengerich, O. Okazaki, Y. Seto and T. L. Macdonald, *Xenobiotica*, 1995, **25**, 689–709.

112 H. Zhao and D. Leonori, *Angewandte Chemie International Edition*, 2021, **60**, 7669–7674.

113 S. Marinković and N. Hoffmann, *Chemical Communications*, 2001, **0**, 1576–1578.

114 A. McNally, C. K. Prier and D. W. C. MacMillan, *Science*, 2011, **334**, 1114–1117.

115 Y. Miyake, K. Nakajima and Y. Nishibayashi, *J. Am. Chem. Soc.*, 2012, **134**, 3338–3341.

116 P. Kohls, D. Jadhav, G. Pandey and O. Reiser, *Org. Lett.*, 2012, **14**, 672–675.

117 K. Nakajima, Y. Miyake and Y. Nishibayashi, *Acc. Chem. Res.*, 2016, **49**, 1946–1956.

118 X. Dai, D. Cheng, B. Guan, W. Mao, X. Xu and X. Li, *J. Org. Chem.*, 2014, **79**, 7212–7219.

119 L. Leng, Y. Fu, P. Liu and J. M. Ready, *J. Am. Chem. Soc.*, 2020, **142**, 11972–11977.

120 C. K. Prier and D. W. C. MacMillan, *Chem. Sci.*, 2014, **5**, 4173–4178.

121 X. Sun and T. Ritter, *Angewandte Chemie International Edition*, 2021, **60**, 10557–10562.

122 J. Xie, M. Rudolph, F. Rominger and A. S. K. Hashmi, *Angewandte Chemie International Edition*, 2017, **56**, 7266–7270.

123 A. Citterio, D. Fancelli, C. Finzi, L. Pesce and R. Santi, *J. Org. Chem.*, 1989, **54**, 2713–2718.

124 B. B. Snider, *Chem. Rev.*, 1996, **96**, 339–364.

125 M. Nishino, K. Hirano, T. Satoh and M. Miura, *J. Org. Chem.*, 2011, **76**, 6447–6451.

126 X. Ju, D. Li, W. Li, W. Yu and F. Bian, *Advanced Synthesis & Catalysis*, 2012, **354**, 3561–3567.

127 S. Zhu, A. Das, L. Bui, H. Zhou, D. P. Curran and M. Rueping, *J. Am. Chem. Soc.*, 2013, **135**, 1823–1829.

128 A. Runemark, S. C. Zacharias and H. Sundén, *J. Org. Chem.*, , DOI:10.1021/acs.joc.0c02819.

129 K. Itoh, S. Nagao, K. Tokunaga, S. Hirayama, F. Karaki, T. Mizuguchi, K. Nagai, N. Sato, M. Suzuki, M. Hashimoto and H. Fujii, *Chemistry – A European Journal*, , DOI:https://doi.org/10.1002/chem.202004186.

130 G. Pandey, D. Jadhav, S. K. Tiwari and B. Singh, *Advanced Synthesis & Catalysis*, 2014, **356**, 2813–2818.

131 G. D. Muñoz and G. B. Dudley, *Organic Preparations and Procedures International*, 2015, **47**, 179–206.

132 K. L. Kohnen-Johannsen and O. Kayser, *Molecules*, 2019, **24**, 796.

133 D. J. P. Lima, A. E. G. Santana, M. A. Birkett and R. S. Porto, *Beilstein J. Org. Chem.*, 2021, **17**, 28–41.

134 J. N. Tawara, A. Blokhin, T. A. Foderaro, F. R. Stermitz and H. Hope, *J. Org. Chem.*, 1993, **58**, 4813–4818.

135 G. L. Patrick, *An Introduction to Medicinal Chemistry, Fifth Edition- Graham L. Patrick*, Oxford University Press., 2017.

136 I. Izquierdo, *Trends in Pharmacological Sciences*, 1989, **10**, 175–177.

137 U. D. Renner, R. Oertel and W. Kirch, *Therapeutic Drug Monitoring*, 2005, **27**, 655–665.

138 N. E. Goeders, *Psychoneuroendocrinology*, 1997, **22**, 237–259.

139 Z. Zeng, J. Zhang, M. Jia, B. Wu, X. Cai, X. Zhang, Y. Feng, Y. Ma, Q. Gao and Z. Fei, *Org. Process Res. Dev.*, , DOI:10.1021/acs.oprd.1c00457.

140 World Intellectual Property Organization, WO2019053581A1, 2019.

141 D. C. Tully, P. V. Rucker, D. Chianelli, J. Williams, A. Vidal, P. B. Alper, D. Mutnick, B. Bursulaya, J. Schmeits, X. Wu, D. Bao, J. Zoll, Y. Kim, T. Groessl, P. McNamara, H. M. Seidel, V. Molteni, B. Liu, A. Phimister, S. B. Joseph and B. Laffitte, *J. Med. Chem.*, 2017, **60**, 9960–9973.

142 N. Schlienger, B. W. Lund, J. Pawlas, F. Badalassi, F. Bertozzi, R. Lewinsky, A. Fejzic, M. B. Thygesen, A. Tabatabaei, S. R. Bradley, L. R. Gardell, F. Piu and R. Olsson, *J. Med. Chem.*, 2009, **52**, 7186–7191.

143 H. Sundén, M. C. Holland, P. K. Poutiainen, T. Jääskeläinen, J. T. Pulkkinen, J. J. Palvimo and R. Olsson, *J. Med. Chem.*, 2015, **58**, 1569–1574.

144 World Intellectual Property Organization, WO2009055077A1, 2009.

145 Y. Liu, Y. Lang, N. K. Patel, G. Ng, R. Laufer, S.-W. Li, L. Edwards, B. Forrest, P. B. Sampson, M. Feher, F. Ban, D. E. Awrey, I. Beletskaya, G. Mao, R. Hodgson, O. Plotnikova, W. Qiu, N. Y. Chirgadze, J. M. Mason, X. Wei, D. C.-C. Lin, Y. Che, R. Kiarash, B. Madeira, G. C. Fletcher, T. W. Mak, M. R. Bray and H. W. Pauls, *J. Med. Chem.*, 2015, **58**, 3366–3392.

146 J.-P. Huang, Y.-J. Wang, T. Tian, L. Wang, Y. Yan and S.-X. Huang, *Nat. Prod. Rep.*, , DOI:10.1039/D0NP00076K.

147 M. A. Bedewitz, A. D. Jones, J. C. D'Auria and C. S. Barry, *Nat Commun*, 2018, **9**, 5281.

148 R. Robinson, *J. Chem. Soc., Trans.*, 1917, **111**, 762–768.

149 C. Schöpf, *Angew. Chem.*, 1937, **50**, 779–787.

150 Y. Li, K. E. Jackson, A. Charlton, B. Le Neve-Foster, A. Khurshid, H.-K. A. Rudy, A. L. Thompson, R. S. Paton and David. M. Hodgson, *J. Org. Chem.*, 2017, **82**, 10479–10488.

151 F. Masri, F. Riche, A. Durif, C. Philouze and Y. Vallée, *Journal of Sulfur Chemistry*, 2004, **25**, 259–268.

152 D. J. A. De Ridder, K. Goubitz, H. Schenk, B. Krijnen and J. W. Verhoeven, *Helvetica Chimica Acta*, 2003, **86**, 812–826.

153 J. H. Song, S. M. Bae and D. I. Jung, *Asian Journal of Chemistry*, 2020, **32**, 1145–1150.

154 R. K. Hill and L. A. Renbaum, *Tetrahedron*, 1982, **38**, 1959–1963.

155 E. W. Garbisch, *J. Org. Chem.*, 1965, **30**, 2109–2120.

156 H. O. Krabbenhoft, *J. Org. Chem.*, 1979, **44**, 4285–4294.

157 B. Krijnen, H. B. Beverloo, J. W. Verhoeven, C. A. Reiss, K. Goubitz and D. Heijdenrijk, *J. Am. Chem. Soc.*, 1989, **111**, 4433–4440.

158 K. C. Nicolaou, T. Montagnon, P. S. Baran and Y.-L. Zhong, *J. Am. Chem. Soc.*, 2002, **124**, 2245–2258.

159 S. Thavaneswaran, K. McCamley and P. J. Scammells, *Natural Product Communications*, 2006, **1**, 1934578X0600101008.

160 World Intellectual Property Organization, WO 2012/087519 A1, 2012.

161 M. Hassine, H. B. Jannet, N. Ghermani, M. Alami and S. Messaoudi, *Synthesis*, 2020, **52**, 450–458.

162 N. Willand, B. Folléas, C. Boutillon, L. Verbraeken, J.-C. Gesquière, A. Tartar and B. Deprez, *Tetrahedron Letters*, 2007, **48**, 5007–5011.

163 F. Lovering, J. Bikker and C. Humblet, *J. Med. Chem.*, 2009, **52**, 6752–6756.

164 E. Colson, J. Andrez, A. Dabbous, F. Dénès, V. Maurel, J.-M. Mouesca and P. Renaud, , DOI:10.26434/chemrxiv-2021-gq1jb-v2.

165 D. J. P. Lima, A. E. G. Santana, M. A. Birkett and R. S. Porto, *Beilstein J. Org. Chem.*, 2021, **17**, 28–41.

166 D. L. Goanvic and M. A. Tius, *J. Org. Chem.*, 2006, **71**, 7800–7804.

167 N. Schlienger, B. W. Lund, J. Pawlas, F. Badalassi, F. Bertozzi, R. Lewinsky, A. Fejzic, M. B. Thygesen, A. Tabatabaei, S. R. Bradley, L. R. Gardell, F. Piu and R. Olsson, *J. Med. Chem.*, 2009, **52**, 7186–7191.

168 Y. Liu, Y. Lang, N. K. Patel, G. Ng, R. Laufer, S.-W. Li, L. Edwards, B. Forrest, P. B. Sampson, M. Feher, F. Ban, D. E. Awrey, I. Beletskaya, G. Mao, R. Hodgson, O. Plotnikova, W. Qiu, N. Y. Chirgadze, J. M. Mason, X. Wei, D. C.-C. Lin, Y. Che, R. Kiarash, B. Madeira, G. C. Fletcher, T. W. Mak, M. R. Bray and H. W. Pauls, *J. Med. Chem.*, 2015, **58**, 3366–3392.

169 J. W. Medley and M. Movassaghi, *Chem. Commun.*, 2013, **49**, 10775–10777.

170 S. Afewerki, J.-X. Wang, W.-W. Liao and A. Córdova, in *The Alkaloids: Chemistry and Biology*, ed. H.-J. Knölker, Academic Press, 2019, vol. 81, pp. 151–233.

171 N. Willand, B. Folléas, C. Boutillon, L. Verbraeken, J.-C. Gesquière, A. Tartar and B. Deprez, *Tetrahedron Letters*, 2007, **48**, 5007–5011.

172 D. Jung, J. Park, S. Roh, Y. Lee, Y. Park, I. Kim, I. Jeong and M. Park, *J. Korean Chem. Soc.*, 1997, **41**, 414–419.

173 D. J. A. De Ridder, K. Goubitz, H. Schenk, B. Krijnen and J. W. Verhoeven, *Helvetica Chimica Acta*, 2003, **86**, 812–826.

174 J. H. Song, S. M. Bae, S. K. Cho, J. H. Cho and D. I. Jung, *Asian J. Chem.*, 2020, **32**, 1145–1150.

175 M. Hassine, H. B. Jannet, N. Ghermani, M. Alami and S. Messaoudi, *Synthesis*, 2020, **52**, 450–458.

176 M. Ikeda, Y. Kugo, Y. Kondo, T. Yamazaki and T. Sato, *J. Chem. Soc., Perkin Trans. 1*, 1997, 3339–3344.

177 J.-P. Huang, Y.-J. Wang, T. Tian, L. Wang, Y. Yan and S.-X. Huang, *Nat. Prod. Rep.*, 2021, **38**, 1634–1658.

178 D. P. Curran, *Synlett*, 1991, **1991**, 63–72.

179 Paul. Dowd and Wei. Zhang, *Chem. Rev.*, 1993, **93**, 2091–2115.

180 A. J. McCarroll and J. C. Walton, *J. Chem. Soc., Perkin Trans. 1*, 2001, 3215–3229.

181 T. R. Rheault and M. P. Sibi, *Synthesis*, 2003, **2003**, 803–819.

182 J. Feng and B. Liu, *Tetrahedron Letters*, 2015, **56**, 1474–1485.

183 J.-R. Chen, D.-M. Yan, Q. Wei and W.-J. Xiao, *ChemPhotoChem*, 2017, **1**, 148–158.

184 J. Xuan, L.-Q. Lu, J.-R. Chen and W.-J. Xiao, *European Journal of Organic Chemistry*, 2013, **2013**, 6755–6770.

185 V. Srivastava, P. K. Singh, S. Tivari and P. P. Singh, *Org. Chem. Front.*, , DOI:10.1039/D1QO01602D.

186 F. D. Lewis, *Acc. Chem. Res.*, 1986, **19**, 401–405.

187 K. Nakajima, Y. Miyake and Y. Nishibayashi, *Acc. Chem. Res.*, 2016, **49**, 1946–1956.

188 D. D. M. Wayner, J. J. Dannenberg and D. Griller, *Chemical Physics Letters*, 1986, **131**, 189–191.

189 A. G. Condie, J. C. González-Gómez and C. R. J. Stephenson, *J. Am. Chem. Soc.*, 2010, **132**, 1464–1465.

190 D. B. Freeman, L. Furst, A. G. Condie and C. R. J. Stephenson, *Org. Lett.*, 2012, **14**, 94–97.

191 J. Hu, J. Wang, T. H. Nguyen and N. Zheng, *Beilstein J. Org. Chem.*, 2013, **9**, 1977–2001.

192 Y. T. Jeon, C. P. Lee and P. S. Mariano, *J. Am. Chem. Soc.*, 1991, **113**, 8847–8863.

193 G. Pandey, G. Lakshmaiah and G. Kumaraswamy, *J. Chem. Soc., Chem. Commun.*, 1992, 1313–1314.

194 P. Kohls, D. Jadhav, G. Pandey and O. Reiser, *Org. Lett.*, 2012, **14**, 672–675.

195 Y. Miyake, K. Nakajima and Y. Nishibayashi, *J. Am. Chem. Soc.*, 2012, **134**, 3338–3341.

196 A. Noble and D. W. C. MacMillan, *J. Am. Chem. Soc.*, 2014, **136**, 11602–11605.

197 X. Dai, D. Cheng, B. Guan, W. Mao, X. Xu and X. Li, *J. Org. Chem.*, 2014, **79**, 7212–7219.

198 L. Leng, Y. Fu, P. Liu and J. M. Ready, *J. Am. Chem. Soc.*, 2020, **142**, 11972–11977.

199 L. Ruiz Espelt, E. M. Wiensch and T. P. Yoon, *J. Org. Chem.*, 2013, **78**, 4107–4114.

200 X. Zhang, S.-R. Yeh, S. Hong, M. Freccero, A. Albini, D. E. Falvey and P. S. Mariano, *J. Am. Chem. Soc.*, 1994, **116**, 4211–4220.

201 G. W. Dombrowski, J. P. Dinnocenzo, P. A. Zielinski, S. Farid, Z. M. Wosinska and I. R. Gould, *J. Org. Chem.*, 2005, **70**, 3791–3800.

202 S. Cai, X. Zhao, X. Wang, Q. Liu, Z. Li and D. Z. Wang, *Angewandte Chemie International Edition*, 2012, **51**, 8050–8053.

203 J.-M. Surzur, M.-P. Crozet and C. Dupuy, *Tetrahedron Letters*, 1971, **12**, 2025–2028.

204 R. McCourt and E. M. Scanlan, *Helvetica Chimica Acta*, 2019, **102**, e1900162.

205 S. De Lamo Marin, T. Martens, C. Mioskowski and J. Royer, *J. Org. Chem.*, 2005, **70**, 10592–10595.

206 G.-Q. Xu, T.-F. Xiao, G.-X. Feng, C. Liu, B. Zhang and P.-F. Xu, *Org. Lett.*, 2021, **23**, 2846–2852.

207 D. Taniyama, M. Hasegawa and K. Tomioka, *Tetrahedron Letters*, 2000, **41**, 5533–5536.

208 F. J. Sardina, M. H. Howard, A. M. P. Koskinen and H. Rapoport, *J. Org. Chem.*, 1989, **54**, 4654–4660.

209 K. Teegardin, J. I. Day, J. Chan and J. Weaver, *Org. Process Res. Dev.*, 2016, **20**, 1156–1163.

210 N. Bortolamei, A. A. Isse and A. Gennaro, *Electrochimica Acta*, 2010, **55**, 8312–8318.

211 F. D. Lewis, *Acc. Chem. Res.*, 1986, **19**, 401–405.

212 F. D. Lewis, T.-I. Ho and J. T. Simpson, *J. Org. Chem.*, 1981, **46**, 1077–1082.

213 J. E. Barry, M. Finkelstein, E. A. Mayeda and S. D. Ross, *J. Org. Chem.*, 1974, **39**, 2695–2699.

214 L. Eberson, B. Helgée, A.-C. Wiehager, S. Liaaen-Jensen, G. Schroll and C. Altona, *Acta Chem. Scand.*, 1975, **29b**, 451–456.

215 J. R. L. Smith and D. Masheder, *J. Chem. Soc., Perkin Trans. 2*, 1976, 47–51.

216 J. Xie, M. Rudolph, F. Rominger and A. S. K. Hashmi, *Angewandte Chemie International Edition*, 2017, **56**, 7266–7270.

217 A. Ledwith, *Acc. Chem. Res.*, 1972, **5**, 133–139.

218 P. Beresford, M. C. Lambert and A. Ledwith, *J. Chem. Soc. C*, 1970, 2508–2510.

219 N. G. Connelly and W. E. Geiger, *Chem. Rev.*, 1996, **96**, 877–910.

220 E. Steckhan, *Angewandte Chemie International Edition in English*, 1986, **25**, 683–701.

221 E. Steckhan, in *Electrochemistry I*, ed. E. Steckhan, Springer, Berlin, Heidelberg, 1987, pp. 1–69.

222 M. Quiroz-Guzman and S. N. Brown, *Acta Cryst C*, 2010, **66**, m171–m173.

223 E. T. Seo, R. F. Nelson, J. M. Fritsch, L. S. Marcoux, D. W. Leedy and R. N. Adams, *J. Am. Chem. Soc.*, 1966, **88**, 3498–3503.

224 R. N. Adams, *Acc. Chem. Res.*, 1969, **2**, 175–180.

225 A. Nakamura, M. A. Latif, P. A. Deck, N. Castagnoli Jr. and J. M. Tanko, *Chemistry – A European Journal*, 2020, **26**, 823–829.

226 C. Costentin, M. Robert and J.-M. Savéant, *Chem. Rev.*, 2010, **110**, PR1–PR40.

227 B. Jiang, Z.-G. Huang and K.-J. Cheng, *Tetrahedron: Asymmetry*, 2006, **17**, 942–951.

228 S. P. Khandare and K. R. Prasad, *J. Org. Chem.*, 2021, **86**, 12285–12291.

229 A. Baumann, *Radical annulation involving N-Arylamines*, University of Bern, 2021.

230 J. J. Li, *Name reactions for functional group transformations*, John Wiley & Sons, Hoboken, N.J, 2007.

231 R. D. Bach, J. L. Andres and F. A. Davis, *J. Org. Chem.*, 1992, **57**, 613–618.

232 S. E. Schaus, B. D. Brandes, J. F. Larrow, M. Tokunaga, K. B. Hansen, A. E. Gould, M. E. Furrow and E. N. Jacobsen, *J. Am. Chem. Soc.*, 2002, **124**, 1307–1315.

233 Q. Yang, Y. Zhao and D. Ma, *Org. Process Res. Dev.*, 2022, **26**, 1690–1750.

234 M. Yamaguchi and I. Hirao, *Tetrahedron Letters*, 1983, **24**, 391–394.

235 J. B. McManus, N. P. R. Onuska and D. A. Nicewicz, *J. Am. Chem. Soc.*, 2018, **140**, 9056–9060.

236 A. Joshi-Pangu, F. Lévesque, H. G. Roth, S. F. Oliver, L.-C. Campeau, D. Nicewicz and D. A. DiRocco, *J. Org. Chem.*, 2016, **81**, 7244–7249.

237 B. K. Çavuşoğlu, B. N. Sağlık, D. Osmaniye, S. Levent, U. Acar Çevik, A. B. Karaduman, Y. Özkay and Z. A. Kaplancıklı, *Molecules*, 2018, **23**, 60.

238 G. R. Krow, in *Organic Reactions*, John Wiley & Sons, Ltd, 2004, pp. 251–798.

239 EP3976185A1, 2022.

240 E. R. Atkinson, D. D. McRitchie-Ticknor, L. S. Harris, S. Archer, M. D. Aceto, J. Pearl and F. P. Luduena, *J. Med. Chem.*, 1983, **26**, 1772–1775.

241 E. R. Atkinson, D. D. McRitchie, L. F. Shoer, L. S. Harris, S. Archer, M. D. Aceto, J. Pearl and F. P. Luduena, *J. Med. Chem.*, 1977, **20**, 1612–1617.

242 C. Zhang, L. Gyermek and M. L. Trudell, *Tetrahedron Letters*, 1997, **38**, 5619–5622.

243 20160229869, A1.

244 C. Zhang, S. A. Lomenzo, C. J. Ballay and M. L. Trudell, *J. Org. Chem.*, 1997, **62**, 7888–7889.

245 W. A. M. Davies, A. R. Pinder and I. G. Morris, *Tetrahedron*, 1962, **18**, 405–412.

246 S. E. Denmark and H. Matsuhashi, *J. Org. Chem.*, 2002, **67**, 3479–3486.

247 C. Park and P. H. Lee, *Org. Lett.*, 2008, **10**, 3359–3362.

248 B. R. Blank, I. P. Andrews and O. Kwon, *ChemCatChem*, 2020, **12**, 4352–4372.

249 X. Dai, R. Mao, B. Guan, X. Xu and X. Li, *RSC Adv.*, 2015, **5**, 55290–55294.

250 R. S. J. Proctor, A. C. Colgan and R. J. Phipps, *Nat. Chem.*, 2020, **12**, 990–1004.

251 D. Parmar, E. Sugiono, S. Raja and M. Rueping, *Chem. Rev.*, 2014, **114**, 9047–9153.

252 D. Bacos, A. Lahdenperä and R. J. Phipps, in Book of Abstracts, 17th Belgian Organic Synthesis Symposium (Namur), 2022, p. 192.

253 G. Bellucci, G. Berti, G. Ingrosso, A. Vatteroni, G. Conti and R. Ambrosetti, *J. Chem. Soc., Perkin Trans. 2*, 1978, 627–632.

254 M. M. Walker, B. Koronkiewicz, S. Chen, K. N. Houk, J. M. Mayer and J. A. Ellman, *J. Am. Chem. Soc.*, 2020, **142**, 8194–8202.

255 C. Cheng, J. Xu, R. Zhu, L. Xing, X. Wang and Y. Hu, *Tetrahedron*, 2009, **65**, 8538–8541.

256 G. Chambournier and R. E. Gawley, *Org. Lett.*, 2000, **2**, 1561–1564.

257 WO2016202253A1, 2016.

Supporting information

Table of Contents

General information

All the glassware was oven-dried at 160 °C or flame-dried under vacuum, assembled hot and allowed to cool under a positive pressure of nitrogen. Unless otherwise stated, all reactions were performed under nitrogen atmosphere. Non-aqueous reagents were transferred under nitrogen *via* syringe or cannula. Silica gel 60 Å (230–400 mesh particle size, SiliCycle) and aluminum oxide neutral (40–160 μm) were used for flash column chromatography. Thin layer chromatography (TLC) was performed on 0.25 mm silica gel 60 with fluorescent indicator UV 254; visualization under UV light (254 nm) or by staining with a solution of potassium permanganate [$KMnO_4$ (3 g), K_2CO_3 (20 g) and NaOH 5% (3 mL) in H_2O (300 mL)] and subsequent heating.

Instrumentation

NMR. ^{1}H, ^{13}C, ^{11}B and ^{19}F NMR spectra were recorded on a 300 MHz spectrometer ([1]H: 300 MHz, [13]C: 75 MHz, [11]B: 96 MHz, [19]F: 282 MHz) and on a 400 MHz spectrometer ([1]H: 400 MHz, [13]C: 101 MHz) operating at 22 °C, unless otherwise stated. Chemical shifts (δ) were reported in parts per million with the residual solvent peak used as an internal standard ($CHCl_3$: δ = 7.26 ppm and C_6H_6: δ = 7.16 ppm for ^{1}H NMR spectra and $CDCl_3$: δ = 77.0 ppm and C_6D_6: δ = 128.0 ppm for ^{13}C NMR spectra). The following abbreviations were used to explain the multiplicities: s (singlet), d (doublet), t (triplet), q (quadruplet), p (pentuplet), hx (hexuplet), hp (heptuplet), m (multiplet), br (broad). The prefix app (apparent) was added when different coupling constants appeared accidentally equal. Coupling constants *J* are reported in Hz and with an accuracy of one unit of the last digit. *HRMS* analyses were recorded on a

hybrid quadrupole time-of-flight mass spectrometer using positive electrospray and on a double-focusing magnetic sector mass spectrometer using electron impact (70 eV). Mass spectra were measured in electron impact (EI) mode at 70 eV, with solid probe inlet, source temperature of 200 °C, acceleration voltage of 5 kV, and resolution of 2'500. The instrument was scanned between m/z 50 and 1000 at scan rate of 2 s / decade in the magnetic scan mode. Perfluorokerosene served for calibration. *Infrared* spectra were recorded neat on an FT-IR spectrometer equipped with a Golden Gate Single Reflection Diamond ATR System and are reported in wave numbers (cm^{-1}). *GC* analyses were carried out on a Thermo Electron Trace GC ULTRA instrument fitted with a Macherey-Nagel Optima delta-3-0.25 μm capillary column (20 m, 0.25 mm). Gas carrier: He 1.4 mL/min; injector: 220 °C split mode; detector: FID 280 °C, H_2 35 mL/min, air 350 mL/min. *Blue LED irradiation*: Kessil lamps were used for photoredox reactions and were run at maximum power (100 W) 5 cm away from reaction vessel with a cooling fan.

Materials

Unless otherwise stated, all reagents were obtained from commercial sources and used without further purification. Aniline and *N,N*-dimethylaniline were redistilled prior to use. Solvents for reactions (THF, Et_2O, CH_2Cl_2, *n*-hexane) were first distilled then filtered over two columns of dried alumina under a positive pressure of argon. Commercial benzene and toluene were filtered over two columns of dried alumina under a positive pressure of argon. Commercial 1,2-dichloroethane was dried over a short column of activated neutral alumina under a positive pressure of nitrogen, stored on activated 3Å molecular sieve and used within less than a month; it was degassed by bubbling nitrogen for 15 minutes prior to reaction. Solvents for extraction and flash column chromatography were of technical grade and were distilled prior to use. Commercial photocatalysts (Strem or Aldrich) were used without purification.

Preparation of starting materials

Amine precursors

General procedure A

In a two-neck, oven-dried flask equipped with a magnetic stirring bar and a reflux condenser, was introduced K_2CO_3 (27.5 mmol, 1.1 equiv.), N,N-dimethylformamide (25 mL) and the appropriate aniline (25 mmol, 1 equiv.). The resulting mixture was degassed by bubbling N_2 for 15 min, and then the dibromoalkane (27.5 mmol, 1.1 equiv.) was added to the suspension *via* a syringe. The reaction mixture was heated to 80 °C and stirred overnight at the same temperature. Upon completion (TLC monitoring), the reaction mixture was diluted with Et_2O (100 mL). Water (100 mL) was added and the phases were separated. The organic phase was extracted with 1 M HCl (3 x 50 mL). The pH of the aqueous phase was adjusted to pH = 8 with 1 M NaOH and extracted with Et_2O (3 x 100 mL). The combined organic phases were dried with Na_2SO_4, filtered and concentrated under reduced pressure to give crude product. Purification by flash column chromatography on silica gel afforded the desired products.

The purity of the reagents was taken into account in most cases, hence some discrepancy can be observed between the indicated mass and the number of mmols. The purity of the reagent was only indicated if lower than 97%.
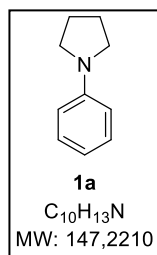
1-phenylpyrrolidine (1a). Following **General Procedure A** with aniline (4.6 mL, 50.0 mmol) and 1,4-dibromobutane (6.6 mL, 55.0 mmol). Purification by flash column chromatography on silica gel (heptanes/EtOAc 1:30 to 1:10) afforded 1-phenylpyrrolidine as a pale-yellow oil (6.27 g, 42.6 mmol, 85%). The product was stored at −18 °C, protected from light and under N_2.

1a
$C_{10}H_{13}N$
MW: 147,2210

^{1}H NMR (300 MHz, $CDCl_3$): δ 7.24 (m, 2H), 6.67 (m, 1H), 6.58 (m, 2H), 3.37–3.22 (m, 4H), 2.02 (m, 4H). The physical and spectral data are in accordance with the reported literature data.[1]
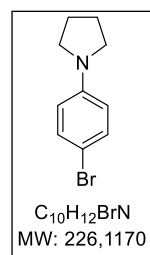
1-(4-bromophenyl)pyrrolidine. Following **general procedure A** with 4-bromoaniline (869 mg, 5.00 mmol) and 1,4-dibromobutane (0.66 mL, 5.50 mmol). Purification by silica gel column chromatography (heptanes/EtOAc 1:9) afforded 1-(4-bromophenyl)pyrrolidine as an off-white solid (148 mg, **13%**).

$C_{10}H_{12}BrN$
MW: 226,1170

^{1}H NMR (300 MHz, $CDCl_3$): δ 7.28 (m, 2H), 6.46 – 6.38 (m, 2H), 3.33 – 3.18 (m, 4H), 2.08 – 1.91 (m, 4H). The physical and spectral data are in accordance with the reported literature data.[2]
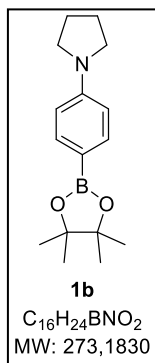
1-[4-(3,3,4,4-tetramethyl-1lambda3,2,5-bromadioxolan-1-yl)phenyl]pyrrolidine (1b). Synthesized following a reported procedure.[3]

1b
C$_{16}$H$_{24}$BNO$_2$
MW: 273,1830

In a two-neck round-bottomed flask equipped with a reflux condenser was added 1-(4-bromophenyl)pyrrolidine (150 mg, 0.663 mmol) and degassed 1,4-dioxane (5 mL). To the solution was then added Bis(pinacolato)diboron (B$_2$Pin$_2$) (253 mg, 0.995 mmol), KOAc (195 mg, 1.99 mmol) and PdCl$_2$(dppf)-CH$_2$Cl$_2$ (12.0 mg, 0.0164 mmol). The reaction was stirred at 90 °C for 16 h. The reaction mixture was allowed to cool down to rt and was filtered through a pad of celite (washing with EtOAc). Volatile organic solvents were evaporated *in vacuo* to give crude product. Purification by flash column chromatography on silica gel (heptanes/EtOAc 98:2) afforded the title compound as an off-white solid (87 mg, 0.25 mmol, 38%).

Alternative procedure:

In a two-neck flask equipped with a magnetic stirring bar and a reflux condenser were introduced 4-(4,4,5,5-tetramethyl-1,3,2-dioxaborolan-2-yl)aniline (1.11 g, 5.00 mmol), N,N-dimethylformamide (5 mL), diisopropylethylamine (DIPEA) (2.56 mL, 15.0 mmol), and 1,4-dibromobutane (0.67 mL, 5.50 mmol). The reaction mixture was heated to 80 °C and stirred overnight at the same temperature. Upon completion (TLC monitoring), the reaction mixture was diluted with Et$_2$O (20 mL). Water (10 mL) was added and the phases were separated. The organic phase was washed with water (3 x 10 mL). The organic phase was dried with Na$_2$SO$_4$, filtered and concentrated under reduced pressure to give crude product. Purification by flash column chromatography on silica gel (pentane:Et$_2$O 90:10) afforded the desired product as a white crystalline solid (1.15 g, 4.2 mmol, 84%).

^{1}H NMR (300 MHz, C$_6$D$_6$): δ 8.34–8.23 (m, 2H), 6.58–6.48 (m, 2H), 2.86–2.74 (m, 4H), 1.41–1.27 (m, 4H), 1.20 (s, 12H). ^{11}B NMR (96 MHz, C$_6$D$_6$): δ 31.7. The physical and spectral data are in accordance with the reported literature data.[4]
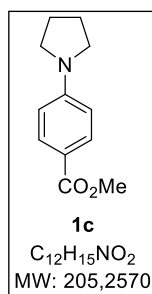
Methyl 4-pyrrolidin-1-ylbenzoate (1c). Following **General Procedure A** with methyl 4-aminobenzoate (2.29 g, 15.0 mmol) and 1,4-dibromobutane (2.0 mL, 16.5 mmol). Purification by flash column chromatography on silica gel (heptanes/EtOAc 1:10) afforded methyl 4-pyrrolidin-1-ylbenzoate as a white solid (334 mg, 1.65 mmol, 11%).

1c
C$_{12}$H$_{15}$NO$_2$
MW: 205,2570

^{1}H NMR (300 MHz, CDCl$_3$): δ 7.94–7.86 (m, 2H), 6.56–6.47 (m, 2H), 3.85 (s, 3H), 3.40–3.31 (m, 4H), 2.10–1.96 (m, 4H). The physical and spectral data are in accordance with the reported literature data.[5]
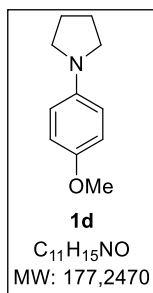
1-(4-methoxyphenyl)pyrrolidine (1d). Following **General Procedure A** with 4-methoxyaniline (6.16 g, 50.0 mmol) and 1,4-dibromobutane (6.6 mL, 55.0 mmol). Purification by flash column chromatography on silica gel (pentane/Et$_2$O 90:10) afforded 1-(4-methoxyphenyl)pyrrolidine as a white solid (7.36 g, 41.5 mmol, 83%). The product was stored at −18 °C, protected from light and under N$_2$.

1d
C$_{11}$H$_{15}$NO
MW: 177,2470

^{1}H NMR (300 MHz, CDCl$_3$): δ 6.89–6.81 (m, 2H), 6.58–6.50 (m, 2H), 3.76 (s, 3H), 3.28–3.18 (m, 4H), 2.03–1.95 (m, 4H). The physical and spectral data are in accordance with the reported literature data.[5]
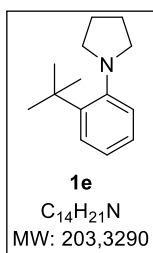
1-(2-*tert*-butylphenyl)pyrrolidine (1e) Following **General Procedure A** with 2-*tert*-butylaniline (1.56 mL, 10.0 mmol) and 1,4-dibromobutane (1.3 mL, 11.0 mmol). Purification by flash column chromatography on silica gel (heptanes/EtOAc 20:1) afforded 1-(2-*tert*-butylphenyl)pyrrolidine as a colorless oil (879 mg, 4.3 mmol, 43%).

1e
C$_{14}$H$_{21}$N
MW: 203,3290

^{1}H NMR (300 MHz, CDCl$_3$): δ 7.39–7.35 (m, 2H), 7.23 (td, J = 7.6, 1.7 Hz, 1H), 7.12 (td, J = 7.8, 1.6 Hz, 1H), 3.07–2.90 (m, 4H), 2.00–1.85 (m, 4H), 1.43 (s, 9H). ^{13}C NMR (75 MHz, CDCl$_3$): δ 151.8 (Cq), 149.3 (Cq), 127.1 (CH$_{Ar}$), 126.8 (CH$_{Ar}$), 126.7 (CH$_{Ar}$), 125.6 (CH$_{Ar}$), 56.3 (2xCH$_2$), 35.6 (Cq), 31.2 (3xCH$_3$), 24.8 (2xCH$_2$). FT-IR (neat, cm^{-1}): 2949, 2907, 2872, 2805, 1485, 1440, 1121, 1088, 1054, 753, 532. HRMS (ESI) m/z: [M+H]$^+$ Calcd for C$_{14}$H$_{22}$N 204.1747. Found 204.1738. R$_f$ = 0.75 (heptanes/EtOAc 40:1).
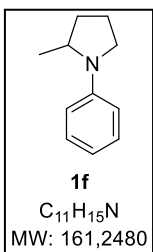
2-methyl-1-phenyl-pyrrolidine (1f). In a two-neck oven-dried flask equipped with a magnetic stirring bar and a reflux condenser, was introduced K$_2$CO$_3$ (1.54 g, 11.0 mmol), N,N-dimethylformamide (10 mL) and aniline (1.0 mL, 11.0 mmol). The resulting mixture was degassed by bubbling N$_2$ for 15 min, and then 1,4-dibromopentane (1.4 mL, 10.0 mmol) was added to the suspension *via* a syringe. The reaction mixture was heated to

1f
C$_{11}$H$_{15}$N
MW: 161,2480

80 °C and stirred overnight at the same temperature. Upon completion (TLC monitoring), the mixture was diluted with EtOAc (40 mL). Water (40 mL) was added and the phases were separated. The organic phase was extracted with 1 M HCl (3 x 25 mL). The water phase was adjusted to pH = 8 with 1 M NaOH and extracted with EtOAc (3 x 25 mL). The combined organic phases were dried with Na$_2$SO$_4$, filtered and concentrated to give crude product. Purification by flash column chromatography on silica gel (heptanes/EtOAc 20:1 to 10:1) afforded 2-methyl-1-phenyl-pyrrolidine as a yellow oil (1.07 g, 6.7 mmol, 67%).

^{1}H NMR (300 MHz, CDCl$_3$): δ 7.29–7.14 (m, 2H), 6.63 (m, 3H), 3.89 (m, 1H), 3.48–3.38 (m, 1H), 3.17 (m, 1H), 2.17–1.92 (m, 3H), 1.78–1.66 (m, 1H), 1.19 (d, J = 6.2 Hz, 3H). The physical and spectral data are in accordance with the reported literature data.[1]
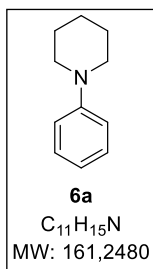
1-phenylpiperidine (6a). Following **General Procedure A** with aniline (4.6 mL, 50.0 mmol) and 1,5-dibromopentane (7.5 mL, 55.0 mmol). Purification by flash column chromatography on silica gel (pentane/Et$_2$O 20:1) afforded 1-phenylpiperidine as a colorless oil (6.12 g, 38 mmol, 76%).

6a
C$_{11}$H$_{15}$N
MW: 161,2480

^{1}H NMR (300 MHz, CDCl$_3$): δ 7.30–7.19 (m, 2H), 6.99–6.89 (m, 2H), 6.86–6.78 (m, 1H), 3.20–3.10 (m, 4H), 1.77–1.65 (m, 4H), 1.63–1.52 (m, 2H). The physical and spectral data are in accordance with the reported literature data.[6]
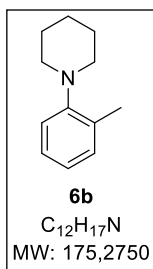
1-(o-tolyl)piperidine (6b). Following **General Procedure A** with 2-methylaniline (1.06 mL, 10.0 mmol) and 1,5-dibromopentane (1.5 mL, 11.0 mmol). Purification by flash column chromatography on silica gel (heptanes/EtOAc 20:1) afforded 1-(o-tolyl)piperidine as a light yellow oil (1.32 g, 7.5 mmol, 75%).

6b
C$_{12}$H$_{17}$N
MW: 175,2750

^{1}H NMR (300 MHz, CDCl$_3$): δ 7.21–710 (m, 2H), 7.01 (d, J = 7.5 Hz, 1H), 6.95 (td, J = 7.3, 1.4 Hz, 1H), 2.89–2.80 (m, 4H), 2.31 (s, 3H), 1.78–1.65 (m, 4H), 1.64–1.51 (m, 2H). The physical and spectral data are in accordance with the reported literature data.[7]
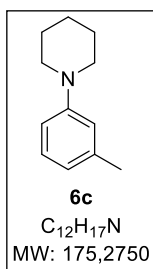
1-(m-tolyl)piperidine (6c). Following **General Procedure A** with 3-methylaniline (1.1 mL, 10.0 mmol) and 1,5-dibromopentane (1.5 mL, 11.0 mmol). Purification by flash column chromatography on silica gel (heptanes/EtOAc 20:1 to 15:1) afforded 1-(m-tolyl)piperidine as a light yellow oil (941 mg, 5.4 mmol, 54%).

6c
C$_{12}$H$_{17}$N
MW: 175,2750

^{1}H NMR (300 MHz, CDCl$_3$): δ 7.20–7.08 (m, 1H), 6.83–6.71 (m, 2H), 6.65 (d, J = 7.4 Hz, 1H), 3.18–3.10 (m, 4H), 2.31 (s, 3H), 1.78–1.64 (m, 4H), 1.64–1.50 (m, 2H). The physical and spectral data are in accordance with the reported literature data.[8]
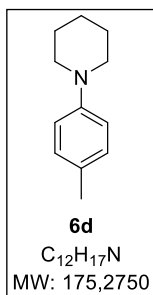
1-(p-tolyl)piperidine (6d). Following **General Procedure A** with 4-methylaniline (2.71 g, 25.0 mmol) and 1,5-dibromopentane (3.8 mL, 27.5 mmol). Purification by flash column chromatography on silica gel (heptanes/EtOAc 20:1 to 15:1) afforded 1-(p-tolyl)piperidine as a pale-yellow oil (3.48 g, 19.25 mmol, 77%).

6d
C$_{12}$H$_{17}$N
MW: 175,2750

^{1}H NMR (300 MHz, CDCl$_3$): δ 7.06 (d, J = 8.3 Hz, 2H), 6.87 (d, J = 8.4 Hz, 2H), 3.14–3.05 (m, 4H), 2.27 (s, 3H), 1.79–1.65 (m, 4H), 1.63–1.49 (m, 2H). The physical and spectral data are in accordance with the reported literature data.[9]
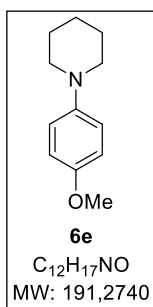
1-(4-methoxyphenyl)piperidine (6e). Following **General Procedure A** with 4-methoxyaniline (6.28 g, 50.0 mmol) and 1,5-dibromopentane (7.6 mL, 55.0 mmol). Purification by flash column chromatography on silica gel (heptanes/EtOAc 85:15 to 80:20) afforded 1-phenylpiperidine as a pale-yellow oil (8.58 g, 45 mmol, 90%).

6e
$C_{12}H_{17}NO$
MW: 191,2740

^{1}H NMR (300 MHz, CDCl$_3$): δ 6.95–6.88 (m, 2H), 6.86–6.79 (m, 2H), 3.77 (s, 3H), 3.02 (t, J = 5.5, 4H), 1.72 (p, J = 5.7 Hz, 4H), 1.60–1.49 (m, 2H). The physical and spectral data are in accordance with the reported literature data.[10]
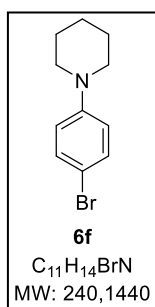
1-(4-bromophenyl)piperidine (6f). Following **General Procedure A** with 4-bromoaniline (8.6 g, 50.0 mmol) and 1,5-dibromopentane (7.6 mL, 55.0 mmol). Purification by flash column chromatography on silica gel (pentane/Et$_2$O 20:1) afforded 1-(4-bromophenyl)piperidine as a crystalline white solid (6.68 g, 28 mmol, 56%).

6f
$C_{11}H_{14}BrN$
MW: 240,1440

^{1}H NMR (300 MHz, CDCl$_3$): δ 7.35–7.28 (m, 2H), 6.83–6.75 (m, 2H), 3.17–3.07 (m, 4H), 1.74–1.64 (m, 4H), 1.65–1.50 (m, 2H). The physical and spectral data are in accordance with the reported literature data.[11]
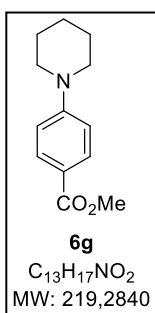
Methyl 4-(1-piperidyl)benzoate (6g). Following **General Procedure A** with methyl 4-aminobenzoate (3.86 g, 25.0 mmol) and 1,5-dibromopentane (3.8 mL, 27.5 mmol). Purification by flash column chromatography on silica gel (heptanes/EtOAc 95:5) afforded methyl 4-(1-piperidyl)benzoate as a shiny white solid (1.20 g, 9.5 mmol, 38%).

6g
$C_{13}H_{17}NO_2$
MW: 219,2840

^{1}H NMR (300 MHz, CDCl$_3$): δ 7.95–7.86 (m, 2H), 6.88 (m, 2H), 3.86 (s, 3H), 3.33 (t, J = 5.2 Hz, 4H), 1.77–1.55 (m, 6H). The physical and spectral data are in accordance with the reported literature data.[9]
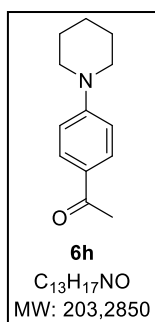
1-[4-(1-piperidyl)phenyl]ethanone) (6h). Following **General Procedure A** with 1-(4-aminophenyl)ethanone (3.4 g, 25.0 mmol) and 1,5-dibromopentane (3.8 mL, 27.5 mmol). Purification by flash column chromatography on silica gel (heptanes/EtOAc 90:10 to 80:20) followed by trituration in pentane afforded 1-[4-(1-piperidyl)phenyl]ethenone) as a crystalline pale-yellow solid (1.51 g, 7.5 mmol, 30%).

6h
$C_{13}H_{17}NO$
MW: 203,2850

^{1}H NMR (300 MHz, CDCl$_3$): δ 7.91–7.80 (m, 2H), 6.91–6.79 (m, 2H), 3.36 (m, 4H), 2.51 (s, 3H), 1.74–1.61 (m, 6H). The physical and spectral data are in accordance with the reported literature data.[9]
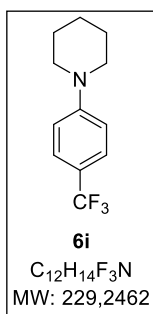
1-[4-(trifluoromethyl)phenyl]piperidine (6i). Following **General Procedure A** with 4-(trifluoromethyl)aniline (3.2 mL, 25.0 mmol) and 1,5-dibromopentane (3.8 mL, 27.5 mmol). Purification by flash column chromatography on silica gel (pentane/Et$_2$O 20:1) afforded 1-[4-(trifluoromethyl)phenyl]piperidine as a colorless oil (602 mg, 2.63 mmol, 11%).

6i
C$_{12}$H$_{14}$F$_3$N
MW: 229,2462

^{1}H NMR (300 MHz, CDCl$_3$): δ 7.45 (d, J = 8.8 Hz, 2H), 6.91 (d, J = 8.7 Hz, 2H), 3.27 (t, J = 5.6 Hz, 4H), 1.76–1.54 (m, 6H). ^{19}F NMR (282 MHz, CDCl$_3$): δ –61.2. The physical and spectral data are in accordance with the reported literature data.[9]
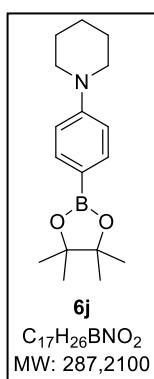
1-[4-(3,3,4,4-tetramethyl-1lambda3,2,5-bromadioxolan-1-yl)phenyl]piperidine (6j). Synthesized following a reported procedure.[3]

In a two-neck round-bottomed flask equipped with a reflux condenser was added 1-(4-bromophenyl)piperidine **6f** (3.60 g, 15.0 mmol) and degassed 1,4-dioxane (120 mL). Bis(pinacolato)diboron (B$_2$Pin$_2$) (5.71 g, 22.5 mmol), KOAc (4.42 g, 45 mmol) and PdCl$_2$(dppf)-CH$_2$Cl$_2$ (549 mg, 5 mol%, 0.75 mmol) were added to the solution and the reaction mixture was stirred at 90 °C for 14 h. The reaction mixture was allowed to cool down to rt and was filtered through a pad of celite (washing with EtOAc). Volatile organic solvents were evaporated *in vacuo* to give crude product. Purification by flash column chromatography on silica gel (pentane/Et$_2$O 20:1) afforded title compound as a white crystalline solid (1.82 g, 6.3 mmol, 42%).

6j
C$_{17}$H$_{26}$BNO$_2$
MW: 287,2100

Alternative procedure:

In a two-neck flask equipped with a magnetic stirring bar and a reflux condenser were introduced 4-(4,4,5,5-tetramethyl-1,3,2-dioxaborolan-2-yl)aniline (1.11 g, 5.00 mmol), N,N-dimethylformamide (5 mL), diisopropylethylamine (DIPEA) (2.56 mL, 15.0 mmol), and 1,4-dibromopentane (0.77 mL, 5.50 mmol). The reaction mixture was heated to 80 °C and stirred overnight at the same temperature. Upon completion (TLC monitoring), the reaction mixture was diluted with Et$_2$O (20 mL). Water (10 mL) was added and the phases were separated. The organic phase was washed with water (3 x 10 mL). The organic phase was dried with Na$_2$SO$_4$, filtered and concentrated under reduced pressure to give crude product. Purification by flash column chromatography on silica gel (pentane:Et$_2$O 90:10) afforded the desired product as a white crystalline solid (1.09 g, 3.8 mmol, 76%).

^{1}H NMR (300 MHz, CDCl$_3$): δ 7.73–7.64 (m, 2H), 6.94–6.83 (m, 2H), 3.30–3.20 (m, 4H), 1.74–1.56 (m, 6H), 1.32 (s, 12H). ^{11}B NMR (96 MHz, CDCl$_3$): δ 30.6. ^{13}C NMR (75 MHz, CDCl$_3$): δ 154.1 (Cq), 136.2 (2xCH$_{Ar}$), 114.7 (2xCH$_{Ar}$), 83.4 (2xCq), 49.6 (2xCH$_2$), 25.7 (2xCH$_2$), 25.0 (4xCH$_3$), 24.6 (CH$_2$). Due to coupling to the quadrupolar ^{11}B and ^{10}B nuclei, the aromatic carbon atom bearing the BPin was not detected. FT-IR (neat, cm^{-1}): 2976, 2934, 2846, 1604, 1360, 1238, 1141, 1127, 1090, 860, 819, 654.

HRMS (ESI) m/z: [M+H]$^+$ Calcd for $C_{17}H_{27}O_2NB$ 288.2129; found 288.2125. mp 96.2–97.1 °C. R_f = 0.43 (pentane/Et$_2$O 99:1).

***tert*-Butyl 4-phenylpiperazine-1-carboxylate (6l)**.

6l
$C_{15}H_{22}N_2O_2$
MW: 262,3530
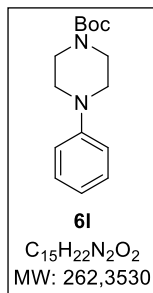
To a solution of Boc$_2$O (1.6 mL, 7.00 mmol) and DMAP (122 mg, 1.00 mmol) in DCM (15 mL) were added dropwise 1-phenylpiperazine (0.8 mL, 5.00 mmol) and triethylamine (0.73 mL, 5.25 mmol). The resulting reaction mixture was stirred at rt for 2 h. Water (15 mL) was added. The phases were separated and the aqueous layer was extracted with DCM (3 x 20 mL). The combined organic layers were dried with Na$_2$SO$_4$ and concentrated under reduced pressure to give crude product as a yellow solid. The residue was purified by flash column chromatography on silica gel (heptanes/EtOAc 90:10) to give product as a white solid (1.17 g, 4.45 mmol, 89%).

^{1}H NMR (300 MHz, CDCl$_3$): δ 7.32–7.23 (m, 2H), 6.90 (m, 3H), 3.58 (t, *J* = 5.0 Hz, 4H), 3.13 (t, *J* = 5.3 Hz, 4H), 1.48 (s, 9H). The physical and spectral data are in accordance with reported the literature data.[12]

4-Phenylthiomorpholine (6m).

6f
$C_{10}H_{13}NS$
MW: 179,2810
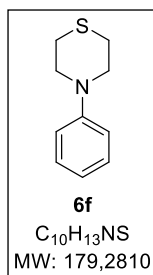
In a flame-dried two-neck flask equipped with a reflux condenser was added K$_2$CO$_3$ (2.76 g, 20.0 mmol), CuI (190 mg, 1.00 mmol), L-proline (230 mg, 2.00 mmol) and dry DMSO (22 mL). Then, iodobenzene (1.12 mL, 10.0 mmol) and thiomorpholine (1.56 mL, 15.0 mmol) were added *via* a syringe. The reaction mixture was vigorously stirred at 100 °C for 5 hours, before being allowed to cool down to rt. Water (60 mL) and EtOAc (60 mL) were added. The phases were separated and aqueous phase was extracted with EtOAc (2 x 30 mL). The combined organic phases were washed with brine (1 x 50 mL), dried over Na$_2$SO$_4$, and concentrated under reduced pressure to give crude product as a brown oil. Purification by flash column chromatography on silica gel (pentane/Et$_2$O 95:5) afforded the title compound as a pale-yellow oil that became a white solid upon storage at 4 °C (912 mg, 5.1 mmol, 51%).

^{1}H NMR (300 MHz, CDCl$_3$): δ 7.34–7.21 (m, 2H), 6.92–6.84 (m, 3H), 3.59–3.50 (m, 4H), 2.81–2.70 (m, 4H). The physical and spectral data are in accordance with the reported literature data.[13]
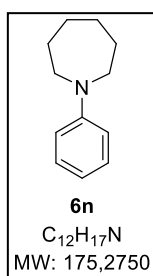
1-phenylazepane (6n). Following **General Procedure A** with aniline (2.3 mL, 25.0 mmol) and 1,6-dibromohexane (4.3 mL, 27.5 mmol). Purification by flash column chromatography on silica gel (heptanes/EtOAc 97:3 to 95:5) afforded 1-phenylazepane as a colorless oil (608 mg, 3.25 mmol, 13%). The product is suspected to decompose upon prolonged reaction time.

6n
$C_{12}H_{17}N$
MW: 175,2750

^{1}H NMR (300 MHz, CDCl$_3$): δ 7.25–7.15 (m, 2H), 6.69 (d, J = 8.2 Hz, 2H), 6.63 (t, J = 7.3 Hz, 1H), 3.48 (t, J = 5.9 Hz, 4H), 1.94–1.73 (m, 4H), 1.67–1.46 (m, 4H). The physical and spectral data are in accordance with the reported literature data.[5]
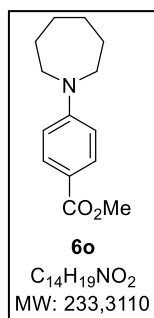
Methyl 4-(azepan-1-yl)benzoate (6o). Following **General Procedure A** with methyl 4-aminobenzoate (1.53 g, 10.0 mmol) and 1,6-dibromohexane (1.7 mL, 11.0 mmol) for 2h45 (Caution: the product decomposes upon prolonged reaction time and reaction must be stopped before complete conversion of starting aniline). Purification by flash column chromatography on silica gel (heptanes/EtOAc 90:10 to 70:30) afforded 1-phenylazepane as a shiny white solid (587 mg, 2.4 mmol, 24%).

6o
C$_{14}$H$_{19}$NO$_2$
MW: 233,3110

^{1}H NMR (300 MHz, CDCl$_3$) δ 7.90–7.81 (m, 2H), 6.62–6.51 (m, 2H), 3.85 (s, 3H), 3.41 (t, J = 6.7 Hz, 2H), 3.17 (t, J = 7.1 Hz, 2H), 1.95–1.80 (m, 2H), 1.71–1.60 (m, 2H), 1.57–1.36 (m, 4H). The physical and spectral data are in accordance with the reported literature data.[14]
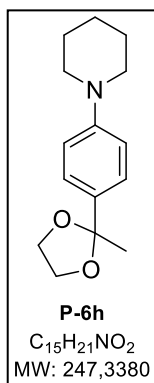
1-[4-(2-methyl-1,3-dioxolan-2-yl)phenyl]piperidine (P-6h). In a 50-ml round-bottom flask equipped with a Dean-Stark was added 1-[4-(1-piperidyl)phenyl]ethenone **6h** (407 mg, 2.00 mmol), ethylene glycol (3.4 mL, 60 mmol), toluene (16 mL), and pTsOH•H$_2$O (190 mg, 1.00 mmol). The reaction mixture was stirred at 110 °C for 16 h. Upon completion of the reaction, the mixture was cooled down to room temperature and poured into cold water. The aqueous phase was extracted with EtOAc (3 x 50 ml). The organic layer was washed with brine (70 mL), dried over Na$_2$SO$_4$, filtered and evaporated under reduced pressure to give crude as a very oily, pinkish residue. Purification by silica gel column chromatography (pentane/Et$_2$O 90:10 to 80:20) afforded 1-[4-(2-methyl-1,3-dioxolan-2-yl)phenyl]piperidine as a crystalline white solid (265 mg, 1.1 mmol, 54%).

P-6h
C$_{15}$H$_{21}$NO$_2$
MW: 247,3380

^{1}H NMR (400 MHz, CDCl$_3$): δ 7.40–7.28 (m, 2H), 6.89 (d, J = 8.4 Hz, 2H), 4.09–3.93 (m, 2H), 3.86–3.70 (m, 2H), 3.23–3.08 (m, 4H), 1.76–1.66 (m, 3H), 1.64 (s, 3H), 1.62–1.51 (m, 2H). ^{13}C NMR (101 MHz, CDCl$_3$): δ 151.8 (Cq$_{Ar}$), 133.7 (Cq$_{Ar}$), 126.2 (2x CH$_{Ar}$), 115.9 (2xCH$_{Ar}$), 109.0 (Cq$_{aliph.}$), 64.5 (2xCH$_2$), 50.6 (2xCH$_2$), 27.7 (CH$_3$), 25.9 (2xCH$_2$), 24.4 (CH$_2$). FT-IR (cm^{-1}, neat): 2932, 1608, 1510, 1218, 1187, 1029, 865, 816. HRMS (ESI) m/z: [M+Na]$^+$ Calcd for C$_{15}$H$_{22}$O$_2$N 248.1645; Found 248.1654. mp = 71.8 – 72.6 °C. R$_f$ = 0.28 (pentane/Et$_2$O 90:10).
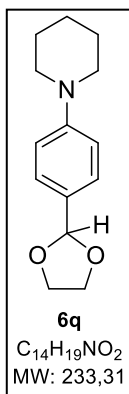
1-[4-(2-methyl-1,3-dioxolan-2-yl)phenyl]piperidine (6q). In a 100-ml round-bottom flask was added 4-(1-piperidyl)benzaldehyde (946 mg, 5.00 mmol), ethylene glycol (8.4 mL, 150 mmol), toluene (40 mL), and pTsOH•H_2O (476 mg, 2.50 mmol). A Dean Stark apparatus was fitted to the flask and the reaction mixture was stirred at 110 °C overnight. Upon completion of the reaction, the mixture was cooled down to 0 °C and quenched by addition of sat. aq. $NaHCO_3$. The aqueous phase was extracted with EtOAc (3 x 70 ml). The organic layer was washed with brine (100 mL), dried over Na_2SO_4, filtered and evaporated under reduced pressure to give crude as a very oily, pinkish residue. Purification by silica gel column chromatography (pentane/Et_2O 70:30) afforded 1-[4-(2-methyl-1,3-dioxolan-2-yl)phenyl]piperidine as an off-white solid (543 mg, 2.3 mmol, 47%).

6q
$C_{14}H_{19}NO_2$
MW: 233,31

^{1}H NMR (400 MHz, CDCl$_3$): δ 7.40–7.30 (m, 2H), 6.93 (d, J = 8.3 Hz, 2H), 5.74 (s, 1H), 4.21–3.92 (m, 4H), 3.24–3.12 (m, 4H), 1.77–1.64 (m, 4H), 1.63–1.52 (m, 2H). ^{13}C NMR (101 MHz, CDCl$_3$): δ 153.0 (CqAr), 128.0 (CqAr), 127.5 (2xCHAr), 116.1 (2xCHAr), 104.2 (CH), 65.3 (2xCH$_2$), 50.5 (2xCH$_2$), 25.8 (2xCH$_2$), 24.5 (CH$_2$). FT-IR (cm^{-1}, neat): 2931, 1612, 1517, 1384, 1217, 1066, 914, 819. HRMS (ESI) m/z: [M+Na]$^+$ Calcd for $C_{14}H_{19}O_2N$ 233.1416; Found 233.1414. mp = 42.5 – 43.4 °C. R_f = 0.44 (pentane/Et_2O 70:30)
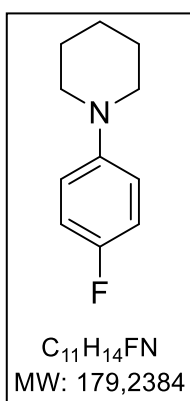
1-(4-fluorophenyl)piperidine. In a flame-dried round-bottom flask was added under a nitrogen flow K_2CO_3 (2.7 g, 19.8 mmol), NaI (3.0 g, 19.8 mmol), MeCN (30 mL), 1,5-dibromopentane (1.2 mL, 9.00 mmol), and 4-fluoroaniline (1.0 mL, 10.8 mmol). The reaction mixture was refluxed under stirring for 4 hours and allowed to cool down. It was taken in water (50 mL) and EtOAc (50 mL). The phases were separated and the organic phase was extracted with 1M HCl (3 x 50 mL). The combined aq. phases were made basic by addition of 2M NaOH (pH > 10) and extracted with EtOAc (3 x 50 mL).

$C_{11}H_{14}FN$
MW: 179,2384

The combined organic phases were dried over Na_2SO_4, filtered and evaporated in vacuo. Purification by silica gel column chromatography (pentane/Et_2O 95:5) afforded the title compound as a pale-yellow oil (1.07 g, 6.0 mmol, 66%).

^{1}H NMR (300 MHz, CDCl$_3$): δ 7.01–6.82 (m, 4H), 3.14–2.97 (m, 4H), 1.72 (p, J = 5.7 Hz, 4H), 1.62–1.50 (m, 2H). ^{13}C NMR (75 MHz, CDCl$_3$): δ 157.1 (d, J = 238.2 Hz), 149.2, 118.5 (d, J = 7.5 Hz), 115.5 (d, J = 22.0 Hz), 51.9, 26.1, 24.3. ^{19}F NMR (282 MHz, CDCl$_3$): δ -125.08 – -125.28 (m). The physical and spectral data are in accordance with the reported literature data.[15]

Radical traps

CO₂Et
SO₂Ph
$C_{12}H_{14}O_4S$
MW: 254,3000
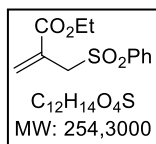
Ethyl 2-(benzenesulfonylmethyl)prop-2-enoate was synthesized following a known literature procedure.[16]

Ethyl 2-methylprop-2-enoate (5.02 mL, 40.0 mmol) and absolute ethanol (80 mL) were added to a 250-mL, three-necked, round-bottomed flask equipped with a thermometer, a nitrogen inlet, and a septum. The mixture was cooled to 0 °C and I_2 (12.0 g, 47.3 mmol) and benzenesulfinic acid sodium salt (13.8 g, 84.1 mmol) were then added. The reaction mixture was stirred at 0 °C for 5 h, then allowed to warm-up to room temperature. The reaction mixture was partitioned between DCM (120 mL) and water (100 mL). The phases were separated (use a flashlight to see the phase separation) and the organic phase was washed with water (2 x 100 mL). The combined aqueous layers were extracted with DCM (2 x 25 mL). The combined organic phases were washed with saturated $NaHCO_3$ (2 x 100 mL) and with 5% $Na_2S_2O_3$ (2 x 100 mL) then dried over Na_2SO_4, filtered and concentrated to give crude intermediate as a thick orange oil. The crude intermediate was diluted with DCM (50 mL). Freshly distilled triethylamine (11.0 mL, 78.9 mmol) was added dropwise over 10 minutes and the reaction mixture was stirred overnight at rt. The reaction mixture was concentrated *in vacuo* until half volume, then directly loaded on the column including precipitated solids. Elution with heptanes/TBME (80:20 to 40:60) afforded the title compound as a pale-yellow thick oil (8.00 g, 31.6 mmol, 79%).

^{1}H NMR (300 MHz, CDCl₃): δ 7.90–7.80 (m, 2H), 7.64 (m, 1H), 7.59–7.47 (m, 2H), 6.50 (d, J = 0.6 Hz, 1H), 5.90 (q, J = 0.8, 0.6 Hz, 1H), 4.15 (d, J = 0.8 Hz, 2H), 4.00 (q, J = 7.1 Hz, 2H), 1.16 (t, J = 7.1 Hz, 3H). The physical and spectral data are in accordance with the reported literature data.[16]

CO₂Et
OH
$C_6H_{10}O_3$
MW: 130,1430
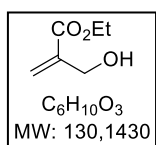
Ethyl 2-(hydroxymethyl)prop-2-enoate

To a solution of paraformaldehyde (95.0 %, 4.1 g, 130 mmol) and ethyl prop-2-enoate (11.0 mL, 100 mmol) in 80 mL dioxane-water (1:1, v/v) was added DABCO (1.49 g, 130 mmol) and the reaction was stirred at room temperature overnight. The reaction mixture was partitioned between EtOAc (400 mL) and water (200 mL). The organic layer was separated and washed with brine (1 x 200 mL), dried over anhydrous Na_2SO_4 and concentrated under reduced pressure to give crude product. Purification by flash column chromatography on silica gel (heptanes/EtOAc 70:30 to 50:50) afforded the title compound as a pale-yellow oil (6.1 g, 47 mmol, 47%). The compound can be stored in the fridge at +4 °C for several months.

^{1}H NMR (300 MHz, CDCl₃): δ 6.23 (q, J = 1.0 Hz, 1H), 5.81 (q, J = 1.4 Hz, 1H), 4.30 (m, 2H), 4.22 (q, J = 7.1 Hz, 2H), 2.56 (bs, 1H), 1.29 (t, J = 7.1 Hz, 3H). The physical and spectral data are in accordance with the reported literature data.[17]

Benzyl 2-(hydroxymethyl)prop-2-enoate

CO₂Bn
OH
C₁₁H₁₂O₃
MW: 192,2140

To a solution of formaldehyde (95.0 %, 2.05 g, 65.0 mmol) and benzyl prop-2-enoate (99.0 %, 7.50 mL, 48.1 mmol) in 40 mL dioxane-water (1:1, v/v) was added DABCO (98.0 %, 7.44 g, 65.0 mmol) and the reaction was let to react at room temperature for 15 hours. The reaction mixture was partitioned between EtOAc (200 mL) and water (100 mL). The organic layer was separated and washed with brine (100 mL), dried over anhydrous Na_2SO_4 and concentrated under reduced pressure to give crude product. Purification by column chromatography on silica gel (EtOAc/heptanes 3:7) afforded the title compound as a colorless oil (3.88 g, 20.2 mmol, 42%).

^{1}H NMR (300 MHz, $CDCl_3$): δ 7.45–7.28 (m, 5H), 6.32 (q, J = 0.9 Hz, 1H), 5.87 (q, J = 1.4 Hz, 1H), 5.23 (s, 2H), 4.39–4.32 (m, 2H), 2.19 (bs, 1H). The physical and spectral data are in accordance with the reported literature data.[18]

Ethyl 3-hydroxy-2-methylene-butanoate

CO₂Et
OH
C₇H₁₂O₃
MW: 144,1700
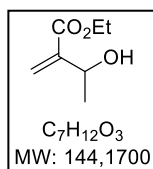
In a seal tube were successively added DABCO (3.37 g, 30 mmol), ethyl prop-2-enoate (16.0 mL, 150 mmol) and acetaldehyde (4.2 mL, 75 mmol). The neat reaction mixture was stirred at room temperature for 4 days and was then diluted with Et_2O (300 mL). The organic phase was washed with water (2x 150 mL), brine (1 x 100 mL), dried over anhydrous Na_2SO_4 and concentrated under reduced pressure to give crude product as a yellow liquid (8.43 g, 58.5 mmol, 78%) which was sufficiently pure for the acetylation step.

^{1}H NMR (300 MHz, $CDCl_3$): δ 6.24–6.18 (m, 1H), 5.84–5.76 (m, 1H), 4.67–4.56 (m, 1H), 4.25 (q, J = 7.1 Hz, 2H), 2.70 (bs, 1H, hydroxyl proton), 1.39 (d, J = 6.4 Hz, 3H), 1.32 (t, J = 7.2 Hz, 3H). The physical and spectral data are in accordance with the reported literature data.[19]
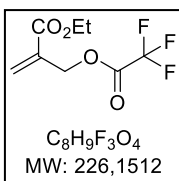
Ethyl 2-[(2,2,2-trifluoroacetyl)oxymethyl]prop-2-enoate

CO₂Et   F
O   F
‖   F
O
C₈H₉F₃O₄
MW: 226,1512

To a stirred solution of ethyl 2-(hydroxymethyl)prop-2-enoate (1.32 g, 10.0 mmol) and 2,6-lutidine (1.28 mL, 11.0 mmol) at 0 °C and under N_2 was added dropwise trifluoroacetic anhydride (1.39 mL, 10.0 mmol). Upon completion of the reaction (TLC monitoring), the reaction mixture was directly subjected to a distillation which afforded unclean product. Further purification by flash column chromatography on silica gel (heptanes/EtOAc 90:10) afforded clean title compound as a colorless oil (966 mg, 4.7 mmol, 47%).

^{1}H NMR (300 MHz, $CDCl_3$): δ 6.48 (d, J = 0.8 Hz, 1H, C=C<u>H</u>₂), 5.93 (q, J = 1.2 Hz, 1H, C=C<u>H</u>₂), 5.06 (m, 2H, C<u>H</u>₂OCOCF₃), 4.26 (q, J = 7.1 Hz, 2H, CO₂C<u>H</u>₂CH₃), 1.31 (t, J = 7.1 Hz, 3H, CO₂CH₂C<u>H</u>₃). ^{13}C NMR (75 MHz, $CDCl_3$): δ 164.6 (<u>C</u>O₂Et), 157.1 (q, $^2J_{C–F}$ = 42.7 Hz, F₃C-<u>C</u>=O), 133.8 (<u>C</u>=CH₂), 129.5 (C=<u>C</u>H₂), 114.6 (q, $^1J_{C–F}$ = 285.8 Hz, F₃<u>C</u>), 65.7 (<u>C</u>H₂OCOCF₃), 61.5 (CO₂<u>C</u>H₂CH₃), 14.2 (CO₂CH₂<u>C</u>H₃). ^{19}F NMR (282 MHz, $CDCl_3$): δ

−75.0. FT-IR (cm^{-1}, neat): 1787, 1718, 1220, 1132, 1025, 774, 732, 522. HRMS (ESI) m/z: [M+Na]$^+$ Calcd for $C_8H_8O_4F_3Na$ 249.0345; Found 249.0346. R_f = 0.37 (heptanes/EtOAc 90:10).

Ethyl 2-(bromomethyl)prop-2-enoate

$C_6H_9BrO_2$
MW: 193,0400
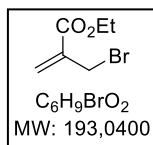
Phosphorus tribromide (0.72 mL, 7.53 mmol) was added dropwise to a solution of ethyl 2-(hydroxymethyl)prop-2-enoate (2.80 g, 21.5 mmol) in dry Et_2O (20 mL) at −10°C and under N_2,. The reaction mixture was allowed to warm up to rt and stirred at this temperature for 1h30. Water (10 mL) was added and the mixture was extracted with Et_2O (3 x 50 mL). The organic phase was washed with brine (1 x 50 mL), dried over Na_2SO_4 and concentrated under reduced pressure to give crude product. Purification by flash column chromatography on silica gel (heptanes/EtOAc 90:10) afforded the title compound as a pale-yellow oil (3.44 g, 17.85 mmol, 83%).

^{1}H NMR (300 MHz, CDCl$_3$): δ 6.33 (d, J = 0.8 Hz, 1H), 5.94 (q, J = 0.9 Hz, 1H), 4.27 (q, J = 7.1 Hz, 2H), 4.18 (d, J = 0.9 Hz, 2H), 1.33 (t, J = 7.1 Hz, 3H). The physical and spectral data are in accordance with the reported literature data.[17]
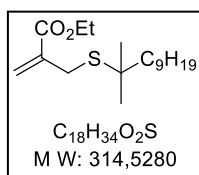
Ethyl 2-(1,1-dimethyldecylsulfanylmethyl)prop-2-enoate

$C_{18}H_{34}O_2S$
M W: 314,5280

In a 50-mL oven-dried flask under N_2 was added sodium methoxide (341 mg, 6.00 mmol) and dry methanol (25 mL). 2-Methylundecane-2-thiol (mixture of isomers, 1.19 mL, 5.00 mmol) was then added dropwise and the mixture was stirred at rt for 1h. Then, ethyl 2-(bromomethyl)prop-2-enoate (1.06 g, 5.50 mmol) was added and the mixture was stirred 6 hour at rt. At this point a second more polar spot appeared and the reaction was stopped before completion. Water (25 mL) was added and the mixture was extracted with Et_2O (3 x 50 mL) The combined organic phases were dried over anhydrous Na_2SO_4, filtered and concentrated to give crude product. Purification by flash column chromatography on silica gel (heptanes/EtOAc 98:2) afforded the title compound as a pale-yellow oil (mixture of isomers, 0.55 g, 1.75 mmol, 35%).

^{1}H NMR (300 MHz, CDCl$_3$): δ 6.18 (m, 1H), 5.76 (m, 1H), 4.19 (q, J = 7.1 Hz, 2H), 3.42–3.21 (m, 2H), 1.58–1.02 (m, 17H), 0.94–0.76 (m, 12H). ^{13}C NMR (75 MHz, CDCl$_3$): δ 166.4, 138.1, 126.6, 61.0, 32.6, 29.5, 28.8, 22.8, 14.3, 8.8. FT-IR (neat, cm^{-1}): 2957, 2929, 2871, 1716, 1632, 1462, 1323, 1182, 1126, 1026, 942, 810. HRMS (ESI) m/z: [M+H]$^+$ Calcd for $C_{18}H_{35}O_2S$ 315.2352; Found 315.2347. R_f = 0.32 (heptanes/EtOAc 94:6).

General Procedure B: acetylation of allylester-alcohols

To a solution of allylester-alcohol (10 mmol, 1 equiv.) in dry DCM (40 mL) cooled to 0 °C was added pyridine (1.6 mL, 20 mmol, 2 equiv.) and then slowly the acyl chloride derivative (20 mmol, 2 equiv.). The reaction mixture was stirred at rt until completion (TLC monitoring). The reaction mixture was

taken up in Et$_2$O (200 mL) and successively washed with 2M HCl (2 x 100 mL), sat. NaHCO$_3$ (2 x 100 mL) and brine (1 x 100 mL). The organic layer was dried over anhydrous Na$_2$SO$_4$ and concentrated under reduced pressure to give crude product as a yellow liquid essentially analytically clean. A short purification by flash column chromatography on silica gel afforded pure product.
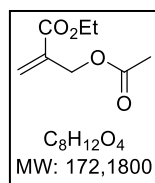
CO$_2$Et

O

O

C$_8$H$_{12}$O$_4$
MW: 172,1800

Ethyl 2-(acetoxymethyl)prop-2-enoate was synthesized following **General Procedure B** with ethyl 2-(hydroxymethyl)prop-2-enoate (6.10 g, 46.9 mmol) and acetyl chloride (6.80 mL, 93.7 mmol) reacting for 1h30. Purification by flash column chromatography on silica gel (heptanes/EtOAc 80:20) afforded the title compound as a colorless liquid (7.03 g, 40.8 mmol, 87%).

^{1}H NMR (300 MHz, CDCl$_3$): δ 6.35 (q, J = 1.0 Hz, 1H), 5.83 (q, J = 1.4 Hz, 1H), 4.81 (m, 2H), 4.24 (q, J = 7.1 Hz, 2H), 2.10 (s, 3H), 1.30 (t, J = 7.1 Hz, 3H). The physical and spectral data are in accordance with the reported literature data.[20]

CO$_2$Bn

O

O

C$_{13}$H$_{14}$O$_4$
MW: 234,2510
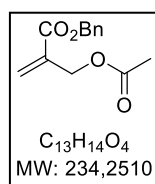
Benzyl 2-(acetoxymethyl)prop-2-enoate was synthesized following **General Procedure B** with benzyl 2-(hydroxymethyl)prop-2-enoate (1.92 g, 10.0 mmol) and acetyl chloride (98.0 %, 1.45 mL, 20.0 mmol) reacting for 20 minutes. Purification by silica gel column chromatography (heptanes/EtOAc 80:20) afforded the title compound as a colorless oil (2.02 g, 8.60 mmol, 86 %).

^{1}H NMR (300 MHz, CDCl$_3$): δ 7.41–7.31 (m, 5H), 6.41 (q, J = 1.0 Hz, 1H), 5.87 (q, J = 1.4 Hz, 1H), 5.23 (s, 2H), 4.83 (t, J = 1.2 Hz, 2H), 2.08 (s, 3H). ^{13}C NMR (75 MHz, CDCl$_3$): δ 170.5, 165.2, 135.8, 135.4, 128.7, 128.5, 128.3, 128.1, 66.8, 62.6, 21.0. FT-IR (neat, cm^{-1}): 1717, 1225, 1149, 1046, 1030, 954, 736, 696, 602, 458. HRMS (ESI) m/z: [M+H]$^+$ Calcd for C$_{13}$H$_{15}$O$_4$ 235.0965; Found 235.0964. R$_f$ = 0.45 (heptanes/EtOAc 80:20).

CO$_2$Et

O

O

C$_{11}$H$_{18}$O$_4$
MW: 214,2610
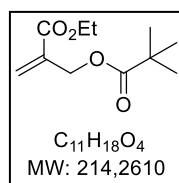
2-ethoxycarbonylallyl 2,2-dimethylpropanoate was synthesized following **General Procedure B** with ethyl 2-(hydroxymethyl)prop-2-enoate (0.65 g, 5.00 mmol) and pivaloyl chloride (0.73 mL, 10.0 mmol) reacting for 16 h. Purification by flash column chromatography on silica gel (pentane/Et$_2$O 90:10) afforded the title compound as a colorless liquid (912 mg, 4.25 mmol, 85%).

^{1}H NMR (300 MHz, CDCl$_3$): δ 6.34 (q, J = 1.1 Hz, 1H), 5.79 (q, J = 1.5 Hz, 1H), 4.79 (dd, J = 1.6, 1.1 Hz, 2H), 4.23 (q, J = 7.1 Hz, 2H), 1.30 (t, J = 7.1 Hz, 3H), 1.22 (s, 9H). ^{13}C NMR (75 MHz, CDCl$_3$): δ 178.0 (C=O), 165.4 (C=O), 136.0 (Cq), 126.6 (CH$_2$), 62.5 (CH$_2$), 61.1 (CH$_2$), 39.0 (Cq), 27.3 (3xCH$_3$), 14.3 (CH$_3$). FT-IR

(neat, cm^{-1}): 2976, 2874, 1725, 1304, 1270, 1132, 1031. HRMS (ESI) m/z: [M+H]$^+$ Calcd for C$_{11}$H$_{19}$O$_4$ 215.1278; Found 215.1276. R$_f$ = 0.63 (pentane/Et$_2$O 90:10).
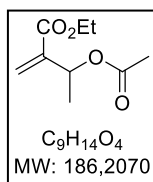
Ethyl 3-acetoxy-2-methylene-butanoate was synthesized following **General Procedure B** with ethyl 3-hydroxy-2-methylene-butanoate (1.84 g, 12.8 mmol) and acetyl chloride (1.1 mL, 15.3 mmol; Comment: 1.2 eq were used instead of the usual 2.0 eq) reacting for 60 minutes. Purification by flash column chromatography on silica gel (heptanes/EtOAc 90:10) afforded the title compound as a colorless oil (1.89 g, 10.2 mmol, 80%).

^{1}H NMR (300 MHz, CDCl$_3$): δ 6.28–6.25 (br s, 1H), 5.79 (t, J = 1.2 Hz, 1H), 5.70 (br q, J = 6.6 Hz, 1H), 4.22 (q, J = 7.1 Hz, 2H), 2.06 (s, 3H), 1.39 (d, J = 6.5 Hz, 3H), 1.29 (t, J = 7.1 Hz, 3H). ^{13}C NMR (75 MHz, CDCl$_3$): δ 169.9 (C=O), 165.4 (C=O), 141.5 (Cq), 124.5 (CH$_2$), 68.3 (CH), 61.0 (CH$_2$), 21.3 (CH$_3$), 20.3 (CH$_3$), 14.3 (CH$_3$). FT-IR (neat, cm^{-1}): 2984, 1715, 1635, 1369, 1232, 1174, 1079, 1040, 952, 814. HRMS (ESI) m/z: [M+Na]$^+$ Calcd for C$_9$H$_{14}$O$_4$Na 208.0784; Found 209.0781. R$_f$ = 0.33 (heptanes/EtOAc 90:10).

Optimization of the one-pot procedure

All reactions were performed on 0.2 mmol scale. NMR yields were measured using 0.5 equivalent of ethylene carbonate as internal standard. 2,5-Bis-allylated product **4a** and dimer **5a** were identified as the major undesired products of the reaction and it was sought to suppress their formation.

4a   **5a**
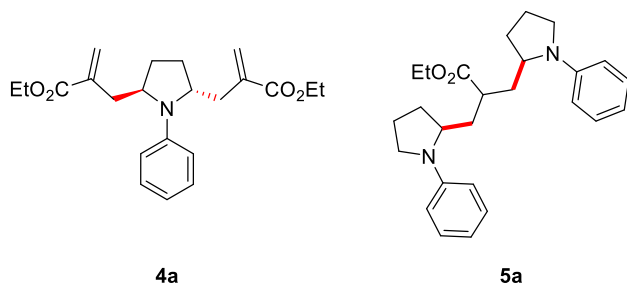
Table 1. Allyl sulfone trap and [Ir{dF(CF$_3$)ppy}$_2$(dtbpy)]PF$_6$: screening of equivalents and preliminary solvent screening
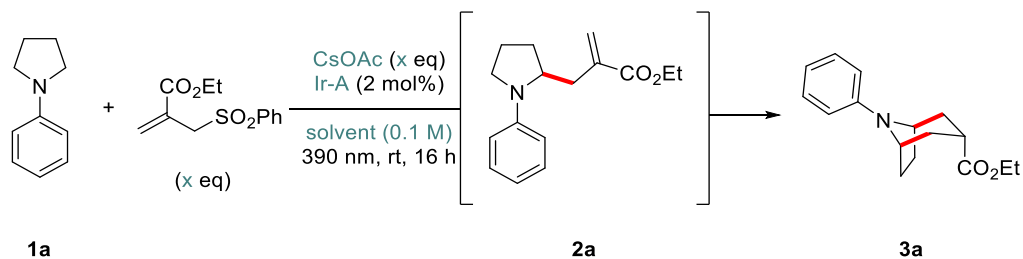
Ir-A = [Ir{dF(CF$_3$)ppy}$_2$(dtbpy)]PF$_6$

Entry	Solvent	Eq. CsOAc	Eq. trap	Cat. loading	NMR yield	Isolated yield
1	DCE	3.0	1.2	2 mol%	45%	
2	MeCN	3.0	1.2	2 mol%	15%	
3	DCE	2.0	1.2	2 mol%	55%	
4	DCE	2.0	3.0	2 mol%	Traces[a]	
5	DCE	1.2	1.2	2 mol%	59%	51%
6	Acetone	1.2	1.2	2 mol%	33%	
7	MeCN	1.2	1.2	2 mol%	29%	
8	EtOAc	1.2	1.2	2 mol%	41%	
9	**DCE**	**1.2**	**1.4**	**2 mol%**	**75%**	**40%**
10	**DCE**	**1.2**	**1.4**	**2 mol%**	**61%**	**42%**
11	**DCE**	**1.2**	**1.4**	**2 mol%**	**59%**	**47%**
12	DCE	1.2 (wet)	1.4	2 mol%	46%	
13	DCE	1.2	1.4	2 mol%	51%	
14	DCE	1.2	1.4	2 mol%	54%	
15	DCE	1.0	1.0	2 mol%	31%	
16	DCE	1.0	1.0	1 mol%	n.d.	

[a] 30% of **4a** was observed

Table 2. Catalyst screening

1a   **2a**   **3a**
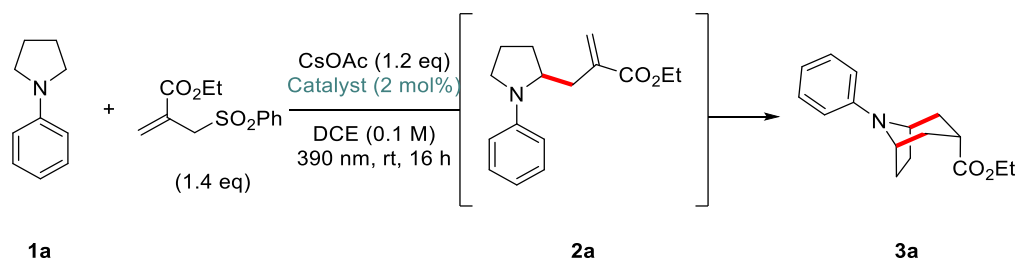
Entry	Catalyst (CAS)	Ir(III*/II) (V vs SCE in MeCN)	Ir(III/II) (V vs SCE in MeCN)	NMR yield of 2a	NMR yield of 3a
1	870987-63-6 (Ir-A)	+1.21	−1.37	–	65%
2	1072067-44-7 (Ir-C)	+1.10	−1.74	–	50%
3	676525-77-2 (Ir-B)	+0.66	−1.51	–	47%
4	1092775-62-6	+0.97	−1.23	–	43%
5	1335047-34-1	+0.97	−1.43	–	42%
6	60804-74-2 (Ru-A)	Ru(II*/I) = +0.77	Ru(II/I) = −1.33	30%	30%
7	1416881-51-1	+1.35	−1.21	31%	21%
8	387859-70-3	+0.36	−1.87	45%	–
9[a]	Eosin Y	+0.83	−1.06	15%[b]	–
10[a]	Fluorescein	+0.78	−1.27	6%	–

[a] Reactions performed under 525 nm Kessil lamps. [b] 51% for the reaction carried out in DMF

Ir-A
Ir{dF(CF$_3$)ppy}$_2$(dtbpy)]PF$_6$

CAS: 870987-63-6

Ir-B
[Ir(dtbbpy)(ppy)$_2$]PF$_6$

CAS: 676525-77-2

Ir-C
[Ir(dFppy)$_2$(dtbbpy)]PF$_6$

CAS: 1072067-44-7

Ru-A
Ru(bpy)$_3$(PF$_6$)$_2$

CAS: 60804-74-2

Ir(dFppy)$_3$

CAS: 387859-70-3

[Ir(dF(Me)ppy)$_2$(dtbbpy)]PF$_6$

CAS: 1335047-34-1

[Ir{dFCF$_3$ppy}$_2$(bpy)]PF$_6$

CAS: 1092775-62-6

Fluorescein
CAS: 2321:07-5

Eosin Y
CAS: 15086-94-9

4CzIPN
1,2,3,5-Tetrakis(carbazol-9-yl)-4,6-dicyanobenzene
CAS: 1416881-51-1
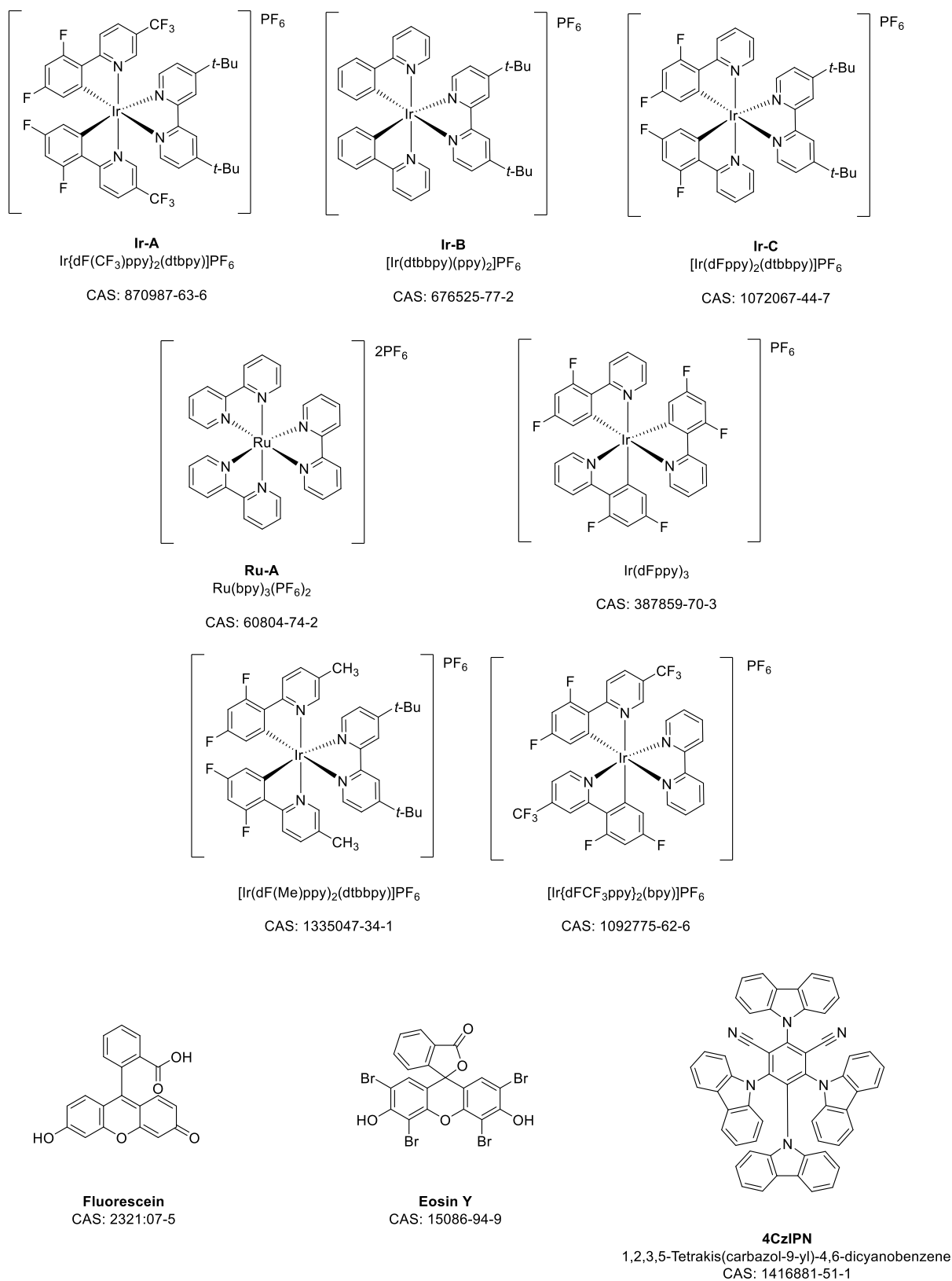
Figure 1: structures of the screened catalysts

Table 3. Allyl sulfone trap and [Ir(dtbbpy)(ppy)$_2$]PF$_6$. Base and solvent screening
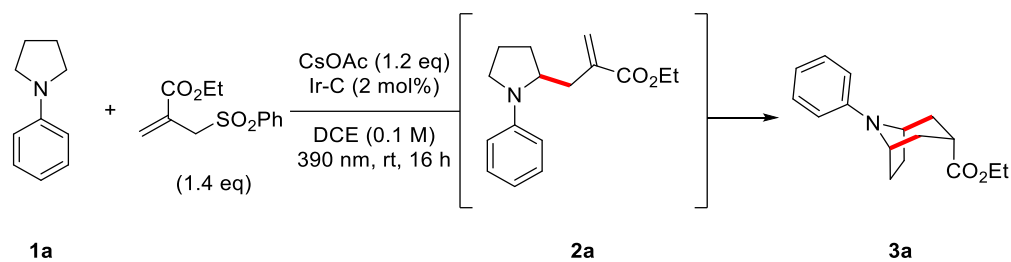
Entry	Deviation to standard conditions	NMR yield of **3a**	other
1	**None**	**47±3%**[a]	
2	1h45	–	37% of **2a**[b]
3	CsOAc (2.0 equiv)	47%	
4	DCE passed over SiO$_2$	51%	
5	DCE not dried	49%	
6	0.05 M	47%	
7	0.5 M	38%	
8	NaOAc (1.2 equiv)	-	15–26% of **2a**
11	K$_2$CO$_3$ (1.2 equiv)	30±15%[c]	
12	Na$_2$CO$_3$ (1.2 equiv)	12%[b]	
14	Cs$_2$CO$_3$ (1.2 equiv)	-	31% of **2a**
15	CsOAc (0.5 equiv)	39%	
16	DMSO	-	-
18	DMF	-	14% of **5a**[b]
19	DMA	-	-
20	**DCM**	**50%**	
21	CHCl$_3$	-	-
22	**1a** (2.0 equiv), Allylsulfone (1.0 equiv)	14% (isolated yield)	28% of **5a**[b]

[a] Average of 3 runs. [b] Isolated yield. [c] Not reproducible.

Table 4. Allyl acetate trap and [Ir{dF(CF₃)ppy}₂(dtbpy)]PF₆: Final optimization

Ir-A = [Ir{dF(CF₃)ppy}₂(dtbpy)]PF₆
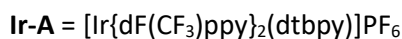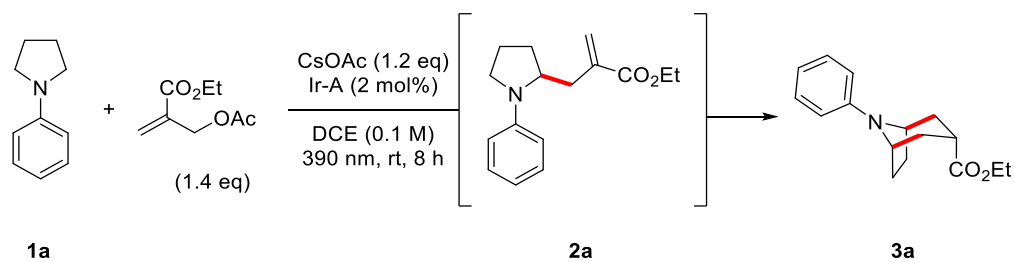
Entry	Deviation to standard conditions	NMR yield of **3a**	Isolated yield of **3a**	Other remarks
1	Allylsulfone trap	65%		
2	None	-	46±2%, dr 7:1[b]	**4a** not detected[a]
3	Allylbromide trap	-		66% NMR yield of **2a**
4	Allylsulfide	77%	~51% isolated, dr 5:1	Difficult separation
5	Eosin Y (5 mol%, 525 nm)	-		Traces of **2a**
6	2 h		41%, dr 7:1	
7	20 min	44%		Full conversion within 20 min
8	5 min	-	-	50% NMR yield of **2a**
9	20 min, Ir cat. 1 mol%	49%	37%, dr 7:1	**4a** (10%, isolated yield)[a]
10	15 min, 1.0 eq trap	44%	36%, dr 8:1	
11	10 min	52%	43%, dr 7:1	9% (isolated yield) of **4a**[a]
	In further experiments, reaction time was lowered to 20 min for all reactions			
12	1.0 eq trap, 0.5 eq base		14%	4% of **5a**
13	0.5 eq base	51%	39%	5% of **5a**
14	0.05 M	67%	52%, dr 9:1	
15	0.025 M	64%	58%, dr 8:1	
16	0.05 M, 1 mol% cat	-	58±4 %, dr 7:1[b]	
17	0.05 M, 0.5 mol% cat	-	55%, dr 8:1	

Entry	Deviation to standard conditions	NMR yield of **3a**	Isolated yield of **3a**	Other remarks
In further experiments, reaction molarity was set to 0.05 M and catalyst loading to 1 mol%				
18	DCM	-	59%, dr 10:1	
19	CF$_3$-C$_6$H$_5$	-	50%, dr 7:1	
20	AcOH 1.0 eq	-	51%, dr 9:1	
21	AcOH 0.5 eq at t0	-	52%, dr 7:1	
22	AcOH 0. 5eq at t+5min	-	52%, dr 7:1	
23	Trap 1.0 eq, AcOH 1.0 eq	-	41%, dr 7:1	
24	CsPiv	-	51%, dr 5:1	
25	AcOH 1.0 eq at t0, then 0.5 eq over 10 min	56%	49%, dr 10:1	
26	AcOH 1.0 eq, trap 3.0 eq	-	31%	18% of **4a**
27	**Trap 1.1 eq**	**-**	**57%, dr 7:1**	No **4a** detected
28	Trap 1.2 eq	-	56%, dr 7:1	No **4a** detected
29	Trap 1.3 eq	-	52%, dr 7:1	**4a** detected
30	Trap 1.5 eq	-	-	Messy crude
31	Trap 1.1 eq, 0.025 M	-	56%, dr 7:1	
32	Trap 1.1 eq, 0.01 M	-	54%, dr 7:1	
33	Trap 1.1 eq, 2.0 eq. CsOAc	-	53%, dr 7:1	
34	Trap 1.1 eq, 3.0 eq. CsOAc	-	49%, dr 7:1	
35	Trap 1.1 eq., Y = OTFA	-	27%, dr 7:1	2h20 reaction time
36	Trap 1.1 eq., Y = OPiv	-	45%, dr 5:1	
37	K$_3$PO$_4$ (0.4 equiv.) as a base	-	47%, dr 7:1	
Control experiments				
38	No catalyst	–	–	20 min reaction time
39	No catalyst	–	–	6 h reaction time
40	No light	–	–	
41	No base	–	–	

[a] It was showed that under the reaction conditions, undesired product **4a** is able to cyclize. This explains why **4a** was observed after 20 minutes, but not after 8 hours of reaction. [b] average of three runs.

One-pot synthesis of the bicyclic products

General Procedure C (0.2 mmol scale)

In an oven-dried 10 mL-vial were successively added the radical trap (0.22 mmol, 1.1 equiv.), the aniline derivative, if solid or oily (0.20 mmol, 1 equiv.), [Ir{dF(CF$_3$)ppy}$_2$(dtbpy)]PF$_6$ (2.2 mg, 0.02 mmol, 1 mol%) and cesium acetate (46 mg, 0.24 mmol, 1.2 equiv.). The vial was closed with a rubber septum and evacuated/refilled with N$_2$ (x 3). If liquid, the aniline starting material (0.20 mmol, 1 equiv.) was then added *via* a Hamilton syringe. Finally, dry and degassed 1,2-dichloroethane (4.00 mL, 0.05 M) was added. The resulting yellow mixture was placed in front of a 390 nm blue LED (5 cm distance) and stirred until completion of the reaction (TLC monitoring). Reactions usually turned orange and a fine white precipitate was observed. The reaction mixture was diluted with sat. NaHCO$_3$ (3 mL). The aqueous phase was extracted with DCM (3 x 5 mL) and the combined organic phases were dried over Na$_2$SO$_4$, filtered, and concentrated under reduced pressure to give crude product as an orange oil. Purification by flash column chromatography on neutral Alox or SiO$_2$ afforded the bicyclic product.

Modified general procedure C for the synthesis of electron-rich derivatives (0.2 mmol):

Cesium acetate was replaced by the slightly more basic cesium pivalate (56.2 mg, 0.24 mmol, 1.2 equiv.). All other parameters unchanged.

Note: for most characterized compounds, the major (α) diastereoisomer is slightly more apolar than the minor (β) diastereoisomer. It is usually possible, with great care, to partially or fully separate them; this was done only if characterization of the mix was difficult. Unless otherwise stated, FT-IR and HRMS were measured on the mixture of diastereoisomers.

Pyrrolidine derivatives

Ethyl 8-phenyl-8-azabicyclo[3.2.1]octane-3-carboxylate (3a)

Following **General Procedure C** with *N*-phenylpyrrolidine **1a** (0.029 mL, 0.200 mmol) and ethyl 2-(acetoxymethyl)prop-2-enoate (37.9 mg, 0.220 mmol), reacting for 20 minutes. Purification by flash column chromatography (SiO$_2$, heptanes/EtOAc 99:1 or pentane/Et$_2$O 96:4) afforded the major diastereoisomer as a white crystalline solid, closely followed by the minor diastereoisomer as a white solid (29.6 mg, 0.114 mmol, 57%, α/β 7:1).
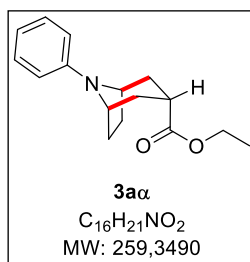
Characterization of the α diastereoisomer:

3aα
C$_{16}$H$_{21}$NO$_2$
MW: 259,3490

^{1}H NMR (400 MHz, CDCl$_3$): δ 7.29–7.20 (m, 2H), 6.78 (d, J = 8.1 Hz, 2H), 6.71 (t, J = 7.2 Hz, 1H), 4.21 (q, J = 7.2 Hz, 2H), 4.17–4.15 (m, 2H), 2.48 (tt, J = 7.7, 1.8 Hz, 1H, -CH-CO$_2$Et), 2.28–2.17 (m, 2H), 2.17–2.09 (m, 2H), 2.04–1.96 (m, 2H), 1.88–1.78 (m, 2H), 1.31 (t, J = 7.1 Hz, 3H). ^{13}C NMR (101 MHz, CDCl$_3$): δ 176.1 (C=O), 146.4 (Cq), 129.7 (2xCH$_{Ar}$), 116.9 (CH$_{Ar}$), 115.2 (2CH$_{Ar}$), 61.0 (CH$_2$), 53.2 (2xCH), 34.6 (CH-CO$_2$Et), 27.1 (2xCH$_2$), 26.4 (2xCH$_2$), 14.4 (CH$_3$). FT-IR (cm^{-1}, neat): 2926, 1721, 1596, 1494, 1368, 1330, 1292, 1173, 1047, 748, 693. HRMS (ESI) m/z: [M+H]$^+$ Calcd for C$_{16}$H$_{22}$NO$_2$ 260.1645; Found 260.1639. Mp 83.0–84.2 °C. R$_f$ = 0.34 (pentane/Et$_2$O 96:4).

Coupling constant compatible with an equatorial proton (CH-CO$_2$Et) on a chair conformation (J_{ax-eq} = 7.7 Hz, J_{eq-eq} = 1.8 Hz). Structure confirmed by single-crystal X-ray diffraction.

Crystallization from DCM upon slow evaporation affords colorless crystals suitable for X-Ray analysis.
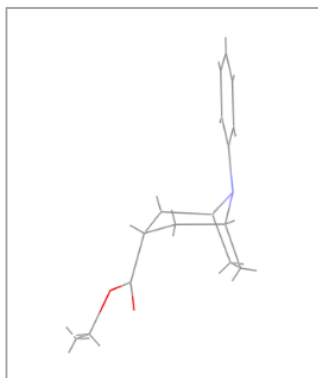
Characterization of the β diastereoisomer:

3aβ
C$_{16}$H$_{21}$NO$_2$
MW: 259,3490

^{1}H NMR (300 MHz, CDCl$_3$): δ 7.25–7.19 (m, 2H), 6.77 (d, J = 8.1 Hz, 2H), 6.70 (tt, J = 7.3, 1.1 Hz, 1H), 4.32–4.25 (m, 2H), 4.05 (q, J = 7.1 Hz, 2H), 2.89 (tt, J_{ax-ax} = 12.3, J_{ax-eq} = 5.3 Hz, 1H, -CH-CO$_2$Et), 2.16–2.07 (m, 2H), 2.07–1.97 (m, 2H), 1.85–1.75 (m, 2H), 1.64 (ddd, J = 13.8, 6.0, 2.9 Hz, 2H), 1.20 (t, J = 7.2 Hz, 3H).

Coupling constants of CH-CO$_2$Et compatible with an axial proton on a chair conformation (J_{ax-ax} = 12.3 Hz, J_{ax-eq} = 5.3 Hz).

^{13}C NMR (75 MHz, CDCl$_3$): δ 175.1 (C=O), 146.2 (Cq), 129.7 (2xCH$_{Ar}$), 117.2 (CH$_{Ar}$), 115.2 (2xCH$_{Ar}$), 60.5 (CH$_2$), 53.7 (2xCH), 35.5 (CH-CO$_2$Et), 29.3 (2xCH$_2$), 28.3 (2xCH$_2$), 14.3 (CH$_3$). FT-IR (cm^{-1}, neat): 2957, 1722, 1597, 1501, 1365, 1179, 1045, 937, 754, 694, 583. HRMS (ESI) m/z: [M+H]$^+$ Calcd for C$_{16}$H$_{22}$NO$_2$ 260.1645; Found 260.1642. Mp 71.5–73.1 °C. R$_f$ = 0.22 (pentane/Et$_2$O 96:4).

3b
C$_{22}$H$_{32}$BNO$_4$
MW: 385,3110
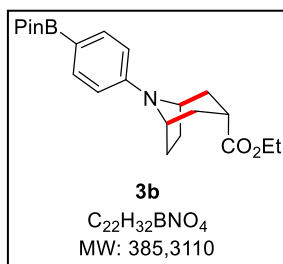
Ethyl 8-[4-(4,4,5,5-tetramethyl-1,3,2-dioxaborolan-2-yl)phenyl]-8-azabicyclo[3.2.1]octane-3-carboxylate (3b)

Following **General Procedure C** with 1-[4-(4,4,5,5-tetramethyl-1,3,2-dioxaborolan-2-yl)phenyl]pyrrolidine **1b** (54.6 mg, 0.20 mmol) and ethyl 2-(acetoxymethyl)prop-2-enoate (37.9 mg, 0.220 mmol) reacting for 20 minutes. Purification by flash column chromatography (SiO$_2$, heptanes/EtOAc 95:5) afforded the major diastereoisomer as a crystalline white solid (30.3 mg), followed by a mixture of both diastereoisomers as a white solid (7.5 mg, α/β 0.59/1) (m$_{tot}$ = 37.8 mg, 0.10 mmol, 49%, α/β 5:1 (from crude NMR)).

Characterization of the α diastereoisomer:

^{1}H NMR (300 MHz, CDCl$_3$): δ 7.74–7.64 (m, 2H), 6.78–6.69 (m, 2H), 4.20 (m, 4H, overlapping -N-C<u>H</u> and -CO$_2$C<u>H$_2$</u>CH$_3$), 2.46 (tt, J_{ax-eq} = 7.0, J_{eq-eq} = 2.5 Hz, 1H, -C<u>H</u>-CO$_2$Et), 2.26–2.07 (m, 4H), 2.06–1.89 (m, 2H), 1.84 (m, 2H), 1.32 (s, 12H), 1.30 (t, J = 7.2 Hz, 3H). ^{13}C NMR (101 MHz, CDCl$_3$): δ 176.1 (C=O), 148.7 (Cq), 136.7 (2xCH$_{Ar}$), 114.11 (2xCH$_{Ar}$), 83.3 (2xCq), 61.0 (CH$_2$), 53.0 (2xCH), 34.6 (CH), 27.0 (2xCH$_2$), 26.7 (2xCH$_2$), 25.0 (4xCH$_3$), 14.4 (CH$_3$). Due to coupling to the quadrupolar ^{11}B and ^{10}B nuclei, the aromatic carbon atom bearing the BPin was not detected. ^{11}B NMR (96 MHz, CDCl$_3$): δ 30.9. FT-IR (cm^{-1}, neat): 2982, 2956, 2927, 1716, 1596, 1353, 1295, 1140, 1090, 1041, 825, 654. HRMS (ESI) m/z: [M+H]$^+$ Calcd for C$_{22}$H$_{33}$O$_4$NB 386.2497; Found 386.2492. Mp 152.9–153.9 °C. R$_f$ = 0.19 (heptanes/EtOAc 90:10)

Characteristic peaks of the β diastereoisomer extracted from the mixture:

^{1}H NMR (300 MHz, CDCl$_3$): δ 4.37–4.29 (m, 2H, 2xN-C<u>H</u>), 4.03 (q, J = 7.1 Hz, 2H, -CO$_2$C<u>H$_2$</u>CH$_3$), 2.89 (tt, J_{ax-ax} = 11.7, J_{ax-eq} = 5.3 Hz, 1H, -C<u>H</u>-CO$_2$Et), 1.18 (t, J = 7.1 Hz, 3H, -CO$_2$CH$_2$C<u>H$_3$</u>). ^{13}C NMR (101 MHz, CDCl$_3$): δ 174.9 (C=O), 148.6 (Cq), 114.09 (2xCH$_{Ar}$), 60.5 (CH$_2$), 53.5 (2xCH), 35.4 (CH), 29.7 (2xCH$_2$), 28.2 (2xCH$_2$), 14.3 (CH$_3$). ^{11}B NMR (96 MHz, CDCl$_3$): δ 30.9.

3c
C$_{18}$H$_{23}$NO$_4$
MW: 317,3850
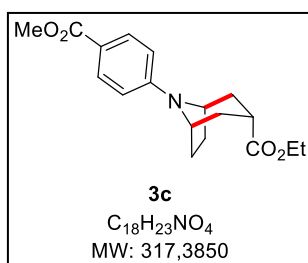
8-(4-methoxycarbonylphenyl)-8-azabicyclo[3.2.1]octane-3-carboxylate (3c)

Following **General Procedure C** with methyl 4-pyrrolidin-1-ylbenzoate (41.1 mg, 0.20 mmol) and ethyl 2-(acetoxymethyl)prop-2-enoate **1c** (37.9 mg, 0.220 mmol) reacting for 40 minutes. Purification by flash column chromatography (SiO$_2$, heptanes/EtOAc 95:5) afforded the product as a white solid (26.6 mg, 0.084 mmol, 42%, α/β 9:1).

Characterization of the α diastereoisomer:

^{1}H NMR (400 MHz, CDCl$_3$): δ 7.95–7.87 (m, 2H), 6.72 (d, J = 8.3 Hz, 2H), 4.28–4.21 (m, 2H), 4.21 (q, J = 7.1 Hz, 2H), 3.85 (s, 3H), 2.51 (tt, $J_{ax\text{-}eq}$ = 7.2, $J_{eq\text{-}eq}$ = 2.0 Hz, 1H, -CH-CO$_2$Et), 2.28–2.10 (m, 4H), 2.06–1.96 (m, 2H), 1.90–1.82 (m, 2H), 1.31 (t, J = 7.1 Hz, 3H). ^{13}C NMR (101 MHz, CDCl$_3$): δ 175.8 (C=O), 167.4 (C=O), 149.6 (Cq), 131.9 (2xCH$_{Ar}$), 117.9 (Cq), 113.8 (2xCH$_{Ar}$), 61.1 (CH$_2$), 53.5 (2xCH), 51.7 (O-CH$_3$), 34.5 (CH), 27.3 (2xCH$_2$), 27.0 (2xCH$_2$), 14.3 (CH$_3$). FT-IR (cm^{-1}, neat): 2949, 1717, 1695, 1603, 1516, 1434, 1382, 1279, 1176, 1110, 1044, 769. HRMS (ESI) m/z: [M+H]$^+$ Calcd for C$_{18}$H$_{24}$NO$_4$ 318.1700; Found 318.1688. Mp 104–106 °C. R$_f$ = 0.25 (heptanes/EtOAc 80:20).

Characteristic peaks of the β diastereoisomer extracted from a mixed fraction:

^{1}H NMR (400 MHz, CDCl$_3$): δ 4.35 (dq, J = 5.3, 2.8 Hz, 2H), 4.05 (q, J = 7.1 Hz, 2H), 2.92 (tt, $J_{ax\text{-}ax}$ = 12.2, $J_{ax\text{-}eq}$ = 5.4 Hz, 1H, -CH-CO$_2$Et), 1.94 (dd, J = 12.7, 2.7 Hz, 2H), 1.70 (ddd, J = 13.8, 5.6, 2.5 Hz, 2H), 1.19 (t, J = 7.1 Hz, 3H). ^{13}C NMR (101 MHz, CDCl$_3$): δ 174.7 (C=O), 149.7 (Cq), 131.3 (2xCH$_{Ar}$), 117.7 (Cq), 60.7 (CH$_2$), 53.7 (2xCH), 35.4 (CH), 29.9 (CH$_2$), 28.2 (CH$_2$), 14.3 (CH$_3$).

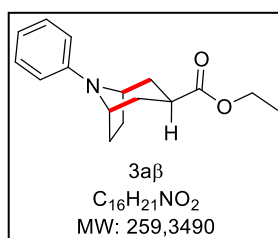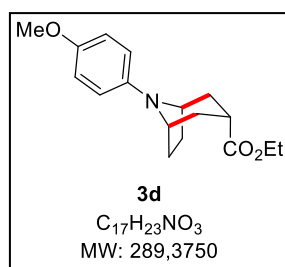**Ethyl 8-(4-methoxyphenyl)-8-azabicyclo[3.2.1]octane-3-carboxylate (3d)**

Following **modified General Procedure C** with 1-(4-methoxyphenyl)pyrrolidine **1d** (35.4 mg, 0.20 mmol) and ethyl 2-(acetoxymethyl)prop-2-enoate (37.9 mg, 0.22 mmol), reacting for 5h30. Purification by flash column chromatography (SiO$_2$, heptanes/EtOAc 92:8) afforded the product as a white solid (32.1 mg, 0.11 mmol, 56%, α/β 5:1). Under the same purification conditions, the diastereoisomers can be partially separated to give a pure sample of the major diastereoisomer.

Characterization of the α diastereoisomer:

^{1}H NMR (300 MHz, CDCl$_3$): δ 6.87–6.80 (m, 2H), 6.76–6.69 (m, 2H), 4.20 (q, J = 7.1 Hz, 2H), 4.11–4.04 (m, 2H), 3.76 (s, 3H), 2.48 (tt, $J_{ax\text{-}eq}$ = 7.8, $J_{eq\text{-}eq}$ = 1.6 Hz, 1H, -CH-CO$_2$Et), 2.21 (ddd, J = 14.4, 7.8, 3.2 Hz, 2H), 2.21 (ddd, J = 14.5, 3.2, 1.5 Hz, 2H), 2.00–1.95 (m, 2H), 1.85–1.75 (m, 2H), 1.30 (t, J = 7.1 Hz, 3H). ^{13}C NMR (101 MHz, CDCl$_3$): δ 176.2 (C=O), 151.6 (Cq), 141.0 (Cq), 116.4 (2xCH$_{Ar}$), 115.2 (2xCH$_{Ar}$), 60.9 (CH$_2$), 55.8 (O-CH$_3$), 53.8 (2xCH), 34.6 (CH), 27.1 (2xCH$_2$), 26.3 (2xCH$_2$), 14.4 (CH$_3$). Mp 74.8–75.9 °C. R$_f$ $_{\text{major dia}}$: 0.43 (heptanes/EtOAc 80:20)

Characteristic peaks of the β diastereoisomer extracted from the mixed fraction:

^{1}H NMR (300 MHz, CDCl$_3$): δ 4.05 (q, J = 7.0 Hz, 2H), 3.76 (s, 3H), 2.86 (tt, $J_{ax\text{-}ax}$ = 12.3, $J_{ax\text{-}eq}$ = 5.2 Hz, 1H, -CH-CO$_2$Et), 2.07–1.97 (m, 2H), 1.64–1.58 (m, 2H), 1.20 (t, J = 7.1 Hz, 3H). ^{13}C NMR (101 MHz, CDCl$_3$): δ

175.2 (C=O), 151.8 (Cq), 140.7 (Cq), 116.43 (2xCH$_{Ar}$), 60.5 (CH$_2$), 55.85 (O-CH$_3$), 54.4 (2xCH), 35.4 (CH), 29.2 (2xCH$_2$), 28.3 (2xCH$_2$), 14.32 (CH$_3$). R$_{f\ minor\ dia}$: 0.34 (heptanes/EtOAc 80:20).

FT-IR (cm^{-1}, neat): 2985, 2952, 1719, 1510, 1446, 1372, 1244, 1176, 1163, 1079, 1048, 1032, 820. HRMS (ESI) m/z: [M-H]$^-$ Calcd for C$_{17}$H$_{22}$NO$_3$ 288.1594; Found 288.1586.
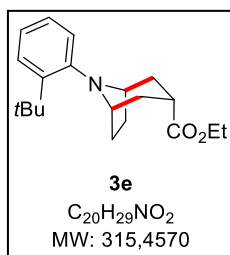
Ethyl 8-(2-tert-butylphenyl)-8-azabicyclo[3.2.1]octane-3-carboxylate (3e)

Following **General Procedure C** with 1-(2-*tert*-butylphenyl)pyrrolidine **1e** (40.7 mg, 0.20 mmol) and ethyl 2-(acetoxymethyl)prop-2-enoate (37.9 mg, 0.22 mmol) reacting for 6 hours. Purification by flash column chromatography (SiO$_2$, heptanes/EtOAc 99.25:0.75) afforded unclean product (contaminated with traces mono-allylated intermediate having the same Rf), from which a dr of 6:1 could be determined. Second purification afforded clean product as a colorless oil (13.0 mg, 0.042 mmol, 21%). Only the major diastereoisomer was characterized.

Characterization of the α diastereoisomer:

^{1}H NMR (300 MHz, CDCl$_3$): δ 7.40 (dd, *J* = 7.4, 2.3 Hz, 1H), 7.12 (td, *J* = 7.6, 2.1 Hz, 1H), 7.07 (td, *J* = 7.4, 1.8 Hz, 1H), 6.99 (dd, *J* = 7.4, 2.1 Hz, 1H), 4.21 (q, *J* = 7.1 Hz, 2H), 3.43 (pent, *J* = 3.0 Hz, 2H), 2.72 (tt, *J*$_{ax-eq}$ = 8.4, *J*$_{eq-eq}$ = 2.4 Hz, 1H, -CH-CO$_2$Et), 2.41 (ddd, *J* = 13.8, 8.6, 4.1 Hz, 2H), 2.25 (dt, *J* = 14.0, 2.4 Hz, 2H), 2.12 (dd, *J* = 8.9, 4.5 Hz, 2H), 1.86–1.71 (m, 2H), 1.52 (s, 9H), 1.31 (t, *J* = 7.1 Hz, 3H). ^{13}C NMR (75 MHz, CDCl$_3$): δ 176.6 (C=O), 152.2 (Cq), 147.7 (Cq), 127.1 (CH$_{Ar}$), 126.5 (CH$_{Ar}$), 126.3 (CH$_{Ar}$), 124.8 (CH$_{Ar}$), 61.5 (2xCH), 60.7 (CH$_2$), 35.7 (Cq), 33.8 (CH), 33.2 (2xCH$_2$), 31.6 (3xCH$_3$), 28.7 (2xCH$_2$), 14.2 (CH$_3$). FT-IR (cm^{-1}, neat): 2949, 1717, 1695, 1603, 1516, 1434, 1382, 1279, 1176, 1110, 1044, 769. HRMS (ESI) m/z: [M+H]$^+$ Calcd for C$_{20}$H$_{30}$NO$_2$ 316.2271; Found 318.2266. Mp 104–106 °C. R$_f$ = 0.41 (heptanes/EtOAc 90:10).
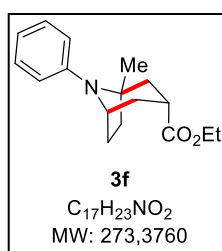
Ethyl 1-methyl-8-phenyl-8-azabicyclo[3.2.1]octane-3-carboxylate (3f)

Following **General Procedure C** with 2-methyl-1-phenyl-pyrrolidine **1f** (32.2 mg, 0.20 mmol) and ethyl 2-(acetoxymethyl)prop-2-enoate (37.9 mg, 0.220 mmol) reacting for 60 minutes. Purification by flash column chromatography (SiO$_2$, pentane/Et$_2$O 95:5) afforded the product as a colorless oil (22.0 mg, 0.08 mmol, 40%, α/β 8:1).

Characterization of the α diastereoisomer:

^{1}H NMR (400 MHz, CDCl$_3$): δ 7.25–7.17 (m, 2H), 7.06–6.99 (m, 2H), 6.80 (tt, J = 7.3, 1.1 Hz, 1H), 4.28–4.14 (m, 3H), 2.65–2.57 (m, 1H, -CH-CO$_2$Et), 2.30 (ddd, J = 14.2, 8.0, 1.8 Hz, 1H), 2.22 (dd, J = 14.1, 1.8 Hz, 1H), 2.14–2.06 (m, 2H), 2.06–1.90 (m, 2H), 1.74–1.60 (m, 2H), 1.48 (s, 3H), 1.31 (t, J = 7.1 Hz, 3H). ^{13}C NMR (101 MHz, CDCl$_3$): δ 176.2 (C=O), 147.5 (Cq), 129.0 (2xCH$_{Ar}$), 119.5 (2xCH$_{Ar}$), 118.9 (CH$_{Ar}$), 60.9 (Cq + CH$_2$), 59.6 (CH), 38.1 (CH$_2$), 35.7 (CH), 33.6 (CH$_2$), 27.7 (CH$_2$), 27.4 (CH$_3$), 25.7 (CH$_2$), 14.2 (CH$_3$). R$_f$ $_{major\ dia}$= 0.31 (heptanes/EtOAc 90:10).

Characteristic peaks of the β diastereoisomer:

^{1}H NMR (400 MHz, CDCl$_3$): δ 4.33–4.29 (m, 1H), 4.08 (q, J = 7.2 Hz, 2H), 2.89 (tt, $J_{ax\text{-}ax}$ = 12.3, $J_{ax\text{-}eq}$ = 5.4 Hz, 1H, -CH-CO$_2$Et), 1.89–1.82 (m, 2H), 1.49 (s, 3H), 1.22 (t, J = 7.1 Hz, 3H). ^{13}C NMR (101 MHz, CDCl$_3$): δ 175.2 (C=O), 147.2 (Cq), 129.0 (2xCH$_{Ar}$), 119.9 (2xCH$_{Ar}$), 119.2 (CH$_{Ar}$), 60.5 (CH$_2$), 60.2 (CH), 39.2 (CH$_2$), 36.6 (CH-CO$_2$Et), 36.0 (CH$_2$), 30.1 (CH$_2$), 26.8 (CH$_3$), 26.7 (CH$_2$), 14.2 (CH$_3$). R$_f$ $_{minor\ dia}$= 0.22 (heptanes/EtOAc 90:10).

FT-IR (cm^{-1}, neat): 2927, 1723, 1596, 1494, 1368, 1184, 1106, 1028, 861, 751, 692. HRMS (ESI) m/z: [M+H]$^+$ Calcd for C$_{17}$H$_{24}$NO$_2$ 274.1802; Found 274.1793.

Piperidine derivatives
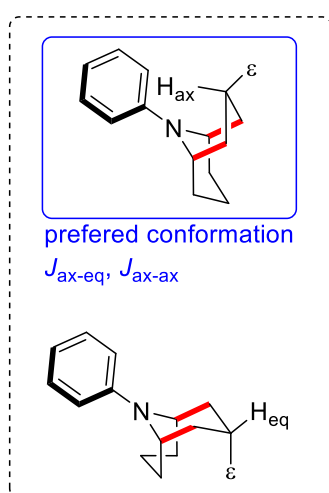
major (α) diastereoisomer   minor (β) diastereoisomer
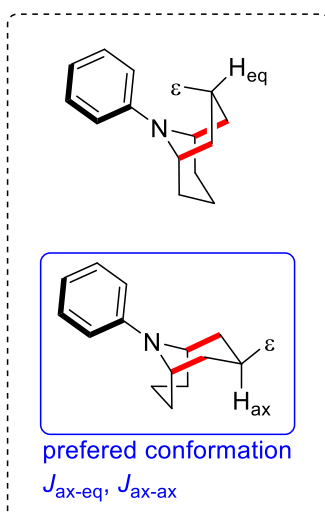
The configuration of the major diastereoisomer was confirmed by single crystal X-ray crystallography of **8g**. In the solid state, the ring containing the ester moiety adopts a boat conformation with the ester group lying in the bowsprit position, which is in agreement with the ^3J coupling constants observed in the ^{1}H NMR spectrum. As similar coupling constants were observed for the proton alpha to the ester group in the two diastereoisomers, it can be concluded that the minor diastereoisomer adopts in solution a chair conformation for the 6-membered ring containing the ester group, with the latter adopting an equatorial position as well. In agreement with these finding, the CH-CO$_2$Et proton of the major diastereoisomer is systematically observed at higher field (shielding effect

of the aromatic ring) compared to the minor diastereoisomer, as it was the case for the pyrrolidine derivatives.
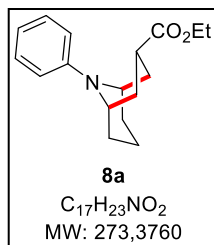
Ethyl 9-phenyl-9-azabicyclo[3.3.1]nonane-3-carboxylate (8a)

0.2 mmol scale synthesis:

Following **General Procedure C** with freshly purified 1-phenylpiperidine **6a** (32.2 mg, 0.20 mmol) and ethyl 2-(acetoxymethyl)prop-2-enoate (37.9 mg, 0.22 mmol) reacting for 1h30. Purification by flash column chromatography (SiO$_2$, heptanes/EtOAc 90:10) afforded the product as a colorless oil (37.3 mg, 0.13 mmol, 67%, α/β >20:1 on this scale). Erosion of the yield of up to 20% was observed when using not fresh 1-phenylpiperidine.

3 mmol scale synthesis:

Into a flame-dried Schlenck tube under N$_2$ were added ethyl 2-(acetoxymethyl)prop-2-enoate (568 mg, 3.30 mmol), freshly purified 1-phenylpiperidine **6a** (484 mg, 3.00 mmol), [Ir{dF(CF$_3$)ppy}$_2$(dtbpy)]PF$_6$ (16.8 mg, **0.5 mol%**) and cesium acetate (692 mg, 3.61 mmol). The vial was evacuated and filled with nitrogen (x 3). Dry 1,2-dichloroethane (60 mL) was added. The resulting yellow solution was was degassed by freeze-pump-thaw cycles (x 3). The mixture was placed between two 390 nm LEDs and stirred for 1h30. The reaction mixture was diluted with sat. NaHCO$_3$ (40 mL). The aqueous phase was extracted with DCM (3 x 60 mL) and the combined organic phases were dried over Na$_2$SO$_4$, filtered, and concentrated under reduced pressure to give crude product as an orange oil. Purification by flash column chromatography (SiO$_2$, heptanes/EtOAc 95:5) afforded the product as a colorless oil (462 mg, 1.68 mmol, 56%, α/β 92:8 on this scale). The diastereoisomers can be separated by flash column chromatography (SiO$_2$, pentane/Et$_2$O 95:5).

Characterization of the α diastereoisomer:

^{1}H NMR (300 MHz, CDCl$_3$): δ 7.25–7.17 (m, 2H), 6.88–6.82 (m, 2H), 6.68 (tt, *J* = 7.3, 1.0 Hz, 1H), 4.29–4.18 (m, 2H), 4.11 (q, *J* = 7.1 Hz, 2H), 2.48–2.31 (m, 3H), 2.02 (qt, *J* = 13.3, 4.5 Hz, 1H), 1.78 (tt, *J* = 13.2, 4.3 Hz, 2H), 1.73–1.63 (m, 2H), 1.63–1.50 (m, 1H), 1.50–1.43 (m, 2H), 1.23 (t, *J* = 7.1 Hz, 3H). ^{13}C NMR (101 MHz, CDCl$_3$): δ 176.0 (C=O), 150.7 (Cq), 129.6 (2xCH$_{Ar}$), 117.1 (CH$_{Ar}$), 114.3 (2xCH$_{Ar}$), 60.4 (CH$_2$), 47.2 (2xCH), 34.9 (CH), 30.5 (2xCH$_2$), 28.5 (2xCH$_2$), 14.4 (CH$_3$), 14.3 (CH$_2$). FT-IR (cm^{-1}, neat): 2928, 1726, 1594, 1498, 1280, 1244, 1174, 1033, 909, 747, 688. HRMS (ESI) m/z: [M+H]$^+$ Calcd for C$_{17}$H$_{24}$NO$_2$ 274.1802; Found 274.1803. R$_f$ = 0.40 (heptanes/EtOAc 90:10).

Characterization of the β diastereoisomer:

^{1}H NMR (300 MHz, CDCl$_3$): δ 7.29–7.17 (m, 2H), 6.84 (d, J = 8.3 Hz, 2H), 6.68 (t, J = 7.2 Hz, 1H), 4.18–4.03 (m, 4H), 3.32 (tt, J_{ax-ax} = 12.1, J_{ax-eq} = 5.7 Hz, 1H, -CH-CO$_2$Et), 2.20–1.98 (m, 5H), 1.93 (ddd, J = 13.9, 5.7, 2.0 Hz, 2H), 1.76–1.62 (m, 3H), 1.23 (t, J = 7.1 Hz, 3H). ^{13}C NMR (75 MHz, CDCl$_3$): δ 175.5 (C=O), 148.7 (Cq), 129.6 (2xCH$_{Ar}$), 116.9 (CH$_{Ar}$), 114.0 (2xCH$_{Ar}$), 60.5 (CH$_2$), 48.0 (2xCH), 37.8 (CH-CO$_2$Et), 31.0 (2xCH$_2$), 27.9 (2xCH$_2$), 20.4 (CH$_2$), 14.4 (CH$_3$). FT-IR (cm^{-1}, neat): 2935, 1725, 1592, 1500, 1189, 1111, 1036, 908, 746, 689. HRMS (ESI) m/z: [M+H]$^+$ Calcd for C$_{17}$H$_{24}$NO$_2$ 274.1802; Found 274.1800. Mp 74.4–75.0 °C. R$_f$ = 0.25 (pentane/Et$_2$O 94:6).

8b
C$_{18}$H$_{25}$NO$_2$
MW: 287,4030

Ethyl 9-(o-tolyl)-9-azabicyclo[3.3.1]nonane-3-carboxylate (8b)

Following **General Procedure C** with 1-(o-tolyl)piperidine **6b** (35.1 mg, 0.20 mmol) and ethyl 2-(acetoxymethyl)prop-2-enoate (37.9 mg, 0.22 mmol), reacting for 1h30. Purification by flash column chromatography (SiO$_2$, pentane/Et$_2$O 98:2) afforded the product as a colorless oil (26.2 mg, 0.09 mmol, 46%, α/β 20:1).

Characterization of the α diastereoisomer:

^{1}H NMR (400 MHz, CDCl$_3$): δ 7.16–7.07 (m, 2H), 6.95 (dd, J = 8.5, 1.2 Hz, 1H), 6.82 (td, J = 7.4, 1.2 Hz, 1H), 4.13 (q, J = 7.2 Hz, 2H), 3.84–3.74 (m, 2H), 2.73 (tt, J_{ax-ax} = 12.8, J_{ax-eq} = 6.0 Hz, 1H, -CH-CO$_2$Et), 2.41–2.30 (m, 2H), 2.27 (s, 3H), 2.06 (qt, J = 13.2, 4.4 Hz, 1H), 1.89 (tt, J = 13.1, 4.2 Hz, 2H), 1.69 (td, J = 13.6, 3.5 Hz, 2H), 1.64–1.53 (m, 1H), 1.51–1.41 (m, 2H), 1.25 (t, J = 7.2 Hz, 3H). ^{13}C NMR (101 MHz, CDCl$_3$): δ 176.2 (C=O), 151.8 (Cq), 131.9 (CH$_{Ar}$), 129.9 (Cq), 126.7 (CH$_{Ar}$), 120.4 (CH$_{Ar}$), 118.7 (CH$_{Ar}$), 60.4 (CH$_2$), 49.4 (2xCH), 34.9 (CH), 31.67 (2xCH$_2$), 29.1 (2xCH$_2$), 19.9 (CH$_3$), 14.4 (CH$_3$), 14.1 (CH$_2$). FT-IR (cm^{-1}, neat): 2927, 1727, 1595, 1488, 1277, 1241, 1173, 1049, 751. HRMS (ESI) m/z: [M+H]$^+$ Calcd for C$_{18}$H$_{26}$NO$_2$ 288.1958; Found 288.1970. R$_f$ = 0.21 (pentane/Et$_2$O 95:5)

Characteristic peaks of the β diastereoisomer:

^{1}H NMR (400 MHz, CDCl$_3$): δ 3.62–3.55 (m, 2H, 2xN-CH), 3.39–3.29 (m, 1H, -CH-CO$_2$Et). ^{13}C NMR (101 MHz, CDCl$_3$): δ 176.0 (C=O), 131.8 (CH$_{Ar}$), 126.5 (CH$_{Ar}$), 120.8 (CH$_{Ar}$), 119.4 (CH$_{Ar}$), 60.5 (CH$_2$), 50.6 (2xCH), 37.5 (CH), 31.72 (2xCH$_2$), 28.6 (2xCH$_2$).

Ethyl 9-(m-tolyl)-9-azabicyclo[3.3.1]nonane-3-carboxylate (8c)

Following **modified General Procedure C** with 1-(m-tolyl)piperidine **6c** (35.1 mg, 0.20 mmol) and ethyl 2-(acetoxymethyl)prop-2-enoate (37.9 mg, 0.22 mmol), reacting for 1h30. Purification by flash column chromatography (SiO$_2$, pentane/Et$_2$O 97:3) afforded the product as a colorless oil (35.2 mg, 0.12 mmol, 61%, α/β > 20:1).

^{1}H NMR (300 MHz, CDCl$_3$): δ 7.10 (t, J = 7.7 Hz, 1H), 6.71–6.61 (m, 2H), 6.51 (d, J = 7.4 Hz, 1H), 4.28–4.19 (m, 2H), 4.10 (q, J = 7.1 Hz, 2H), 2.49–2.31 (m, 3H), 2.29 (s, 3H), 2.01 (qt, J = 13.3, 4.4 Hz, 1H), 1.78 (tt, J = 13.1, 4.3 Hz, 2H), 1.71–1.63 (m, 2H), 1.60–1.50 (m, 1H), 1.50–1.40 (m, 2H), 1.23 (t, J = 7.2 Hz, 3H). ^{13}C NMR (75 MHz, CDCl$_3$): δ 176.0 (C=O), 150.7 (Cq), 139.3 (Cq), 129.5 (CH$_{Ar}$), 118.1 (CH$_{Ar}$), 115.1 (CH$_{Ar}$), 111.3 (CH$_{Ar}$), 60.4 (CH$_2$), 47.2 (2xCH), 34.9 (CH), 30.5 (2xCH$_2$), 28.5 (2xCH$_2$), 22.1 (CH$_3$), 14.4 (CH$_3$), 14.3 (CH$_2$). FT-IR (cm^{-1}, neat): 2925, 1726, 1597, 1492, 1282, 1245, 1174, 764, 729, 690. HRMS (ESI) m/z: [M+H]$^+$ Calcd for C$_{18}$H$_{26}$NO$_2$ 288.1958; Found 288.1967. R$_f$ = 0.28 (pentane/Et$_2$O 95:5).
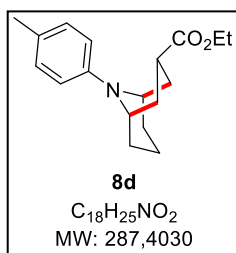
Ethyl 9-(p-tolyl)-9-azabicyclo[3.3.1]nonane-3-carboxylate (8d)

Following **modified General Procedure C** with 1-(p-tolyl)piperidine **6d** (35.1 mg, 0.20 mmol) and ethyl 2-(acetoxymethyl)prop-2-enoate (37.9 mg, 0.22 mmol), reacting for 1h30. Purification by flash column chromatography (SiO$_2$, heptanes/EtOAc 96:4) afforded the product as a colorless oil (33.9 mg, 0.12 mmol, 59%, α/β 20:1).

Characterization of the α diastereoisomer:

^{1}H NMR (400 MHz, CDCl$_3$): δ 7.07–6.98 (m, 2H), 6.82–6.73 (m, 2H), 4.23–4.15 (m, 2H), 4.10 (q, J = 7.1 Hz, 2H), 2.50–2.30 (m, 3H, overlapping signals containing -C<u>H</u>-CO$_2$Et), 2.24 (s, 3H), 2.01 (qt, J = 13.4, 4.6 Hz, 1H), 1.78 (tt, J = 13.2, 4.3 Hz, 2H), 1.66 (ddd, J = 13.8, 12.1, 3.5 Hz, 2H), 1.58–1.49 (m, 1H), 1.49–1.40 (m, 2H), 1.23 (t, J = 7.1 Hz, 3H). ^{13}C NMR (101 MHz, CDCl$_3$): δ 176.0 (C=O), 148.6 (Cq), 130.1 (2xCH$_{Ar}$), 126.3 (Cq), 114.4 (2xCH$_{Ar}$), 60.4 (CH$_2$), 47.4 (2xCH), 34.8 (CH), 30.4 (2xCH$_2$), 28.4 (2xCH$_2$), 20.4 (CH$_3$), 14.4 (CH$_3$), 14.3 (CH$_2$). FT-IR (cm^{-1}, neat): 2923, 1726, 1615, 1511, 1279, 1246, 1173, 801. HRMS (ESI) m/z: [M+H]$^+$ Calcd for C$_{18}$H$_{26}$NO$_2$ 288.1958; Found 288.1968. R$_f$ = 0.29 (heptanes/EtOAc 90:10).

Characteristic peaks of the β diastereoisomer:

^{1}H NMR (400 MHz, CDCl$_3$): δ 3.31 (tt, J_{ax-ax} = 12.2, J_{ax-eq} = 5.7 Hz, 1H, C<u>H</u>-CO$_2$Et). ^{13}C NMR (101 MHz, CDCl$_3$): δ 48.1 (2xCH), 37.8 (CH$_3$), 30.9 (2xCH$_2$), 27.8 (2xCH$_2$).

8e
$C_{18}H_{25}NO_3$
MW: 303,4020
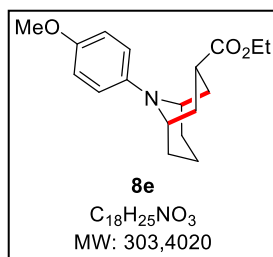
Ethyl 9-(4-methoxyphenyl)-9-azabicyclo[3.3.1]nonane-3-carboxylate (8e)

Following **modified General Procedure C** with 1-(4-methoxyphenyl)piperidine **6e** (38.3 mg, 0.20 mmol) and ethyl 2-(acetoxymethyl)prop-2-enoate (37.9 mg, 0.22 mmol), reacting for 22h. Purification by flash column chromatography (SiO$_2$, pentane/Et$_2$O 96:4) afforded the product as a colorless oil that crystallizes slowly to a white solid upon storage at 4 °C (19.2 mg, 0.064 mmol, 32%, α/β >20:1).

Characterization of the α diastereoisomer:

^{1}H NMR (300 MHz, CDCl$_3$): δ 6.80 (s, 4H), 4.17–4.10 (m, 2H), 4.10 (q, *J* = 7.1 Hz, 2H), 3.75 (s, 3H), 2.47 (tt, *J* = 12.4, 5.9 Hz, 1H), 2.42–2.26 (m, 2H), 2.00 (qt, *J* = 13.3, 4.4 Hz, 1H), 1.79 (tt, *J* = 13.2, 4.3 Hz, 2H), 1.65 (ddd, *J* = 14.0, 12.3, 3.5 Hz, 2H), 1.58–1.49 (m, 1H), 1.49–1.39 (m, 2H), 1.23 (t, *J* = 7.1 Hz, 3H). ^{13}C NMR (101 MHz, CDCl$_3$): δ 176.1 (C=O), 151.6 (Cq), 145.3 (Cq), 115.7 (2xCH$_{Ar}$), 115.1 (2xCH$_{Ar}$), 60.4 (CH$_2$), 55.9 (CH$_3$), 47.8 (2xCH), 34.7 (CH), 30.6 (2xCH$_2$), 28.4 (2xCH$_2$), 14.4 (CH$_3$), 14.3 (CH$_2$). FT-IR (cm^{-1}, neat): 2870, 1726, 1507, 1241, 1177, 1039, 910, 812, 731, 616. HRMS (ESI) m/z: [M+H]$^+$ Calcd for $C_{18}H_{26}NO_3$ 304.1907; Found 304.1899. Mp 42.5–43.7 °C. R$_f$ = 0.31 (pentane/Et$_2$O 90:10).

8f
$C_{17}H_{22}BrNO_2$
MW: 352,2720

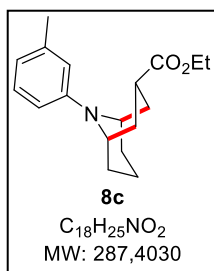### Ethyl 9-(4-bromophenyl)-9-azabicyclo[3.3.1]nonane-3-carboxylate (8f)

Following **General Procedure C** with 1-(4-bromophenyl)piperidine **6f** (49.0 mg, 0.20 mmol) and ethyl 2-(acetoxymethyl)prop-2-enoate (37.9 mg, 0.22 mmol) reacting for 1h30. Purification by flash column chromatography (SiO$_2$, heptanes/EtOAc 97:3) afforded the product as a colorless oil (21.2 mg, 0.06 mmol, 30%, α/β >20:1).

Characterization of the α diastereoisomer:

^{1}H NMR (300 MHz, CDCl$_3$): δ 7.32–7.21 (m, 2H), 6.76–6.67 (m, 2H), 4.22–4.12 (m, 2H), 4.11 (q, *J* = 7.1 Hz, 2H), 2.45–2.27 (m, 3H), 2.01 (qt, *J* = 13.4, 4.1 Hz, 1H), 1.82–1.64 (m, 4H), 1.64–1.50 (m, 1H), 1.50–1.38 (m, 2H), 1.23 (t, *J* = 7.1 Hz, 3H). ^{13}C NMR (75 MHz, CDCl$_3$): δ 175.7 (C=O), 149.7 (Cq), 132.3 (2xCH$_{Ar}$), 115.9 (2xCH$_{Ar}$), 108.6 (Cq), 60.5 (CH$_2$), 47.4 (2xCH), 34.9 (CH), 30.2 (2xCH$_2$), 28.4 (2xCH$_2$), 14.4 (CH$_3$), 14.2 (CH$_2$). FT-IR (cm^{-1}, neat): 2927, 2868, 1724, 1586, 1490, 1282, 1246, 1174, 1043, 908, 804, 732. HRMS (ESI) m/z: [M+H]$^+$ Calcd for $C_{17}H_{23}BrNO_2$ 352.0907; Found 352.0914. R$_f$ = 0.30 (heptanes/EtOAc 90:10).

8g
C$_{19}$H$_{25}$NO$_4$
MW: 331,4120

Ethyl 9-(4-methoxycarbonylphenyl)-9-azabicyclo[3.3.1]nonane-3-carboxylate (8g).

0.2 mmol synthesis

Following **General Procedure C** with methyl 4-(1-piperidyl)benzoate **6g** (43.9 mg, 0.20 mmol) and ethyl 2-(acetoxymethyl)prop-2-enoate (37.9 mg, 0.22 mmol) reacting for 20 minutes. Purification by flash column chromatography (SiO$_2$, heptanes/EtOAc 90:10) afforded the product as a white solid (43.1 mg, 0.13 mmol, 65%, α/β >20:1). Recrystallization from Et$_2$O/hexane at rt afforded single-crystals suitable for X-Ray diffraction analysis.

1 mmol synthesis

Into an oven-dried seal tube were added under N$_2$ ethyl 2-(acetoxymethyl)prop-2-enoate (189 mg, 1.1 mmol), methyl 4-(1-piperidyl)benzoate (219 mg, 1.0 mmol), [Ir{dF(CF$_3$)ppy}$_2$(dtbpy)]PF$_6$ (5.6 mg, **0.5 mol%**) and cesium acetate (231 mg, 1.2 mmol). The vial was evacuated and filled with nitrogen (x 3). Dry and degassed 1,2-dichloroethane (20 mL) was added. The resulting yellow solution was placed in front of a 390 nm LED and stirred for 1h. Purification by flash column chromatography (SiO$_2$, heptanes/EtOAc 90:10) afforded the product a white solid (209 mg, 0.63 mmol, 63%, α/β >20:1).

Characterization of the α diastereoisomer:

^{1}H NMR (300 MHz, CDCl$_3$): δ 7.91–7.82 (m, 2H), 6.83–6.74 (m, 2H), 4.38–4.28 (m, 2H), 4.10 (q, *J* = 7.1 Hz, 2H), 3.84 (s, 3H), 2.45–2.23 (m, 3H, including -CH-CO$_2$Et), 2.14–1.89 (m, 1H), 1.82–1.63 (m, 4H), 1.63–1.42 (m, 3H), 1.22 (t, *J* = 7.2 Hz, 3H). ^{13}C NMR (75 MHz, CDCl$_3$): δ 175.5 (C=O), 167.2 (C=O), 153.7 (Cq), 131.8 (2xCH$_{Ar}$), 117.7 (Cq), 112.5 (2xCH$_{Ar}$), 60.6 (CH$_2$), 51.6 (CH$_3$), 47.2 (2xCH), 35.1 (CH), 30.2 (2xCH$_2$), 28.5 (2xCH$_2$), 14.3 (CH$_3$), 14.1 (CH$_2$). FT-IR (cm^{-1}, neat): 2929, 1729, 1694, 1599, 1517, 1282, 1247, 1170, 1107, 836, 768. HRMS (ESI) m/z: [M+H]$^+$ Calcd for C$_{19}$H$_{26}$NO$_4$ 332.1856; Found 332.1862. Mp 85.9–86.5 °C. R$_f$ = 0.31 (heptanes/EtOAc 80:20).

Characteristic peaks of the β diastereoisomer:

^{1}H NMR (400 MHz, CDCl$_3$): δ 3.31 (tt, J$_{ax-ax}$ = 11.8, J$_{ax-eq}$ = 5.7 Hz, 1H, -CH-CO$_2$Et).
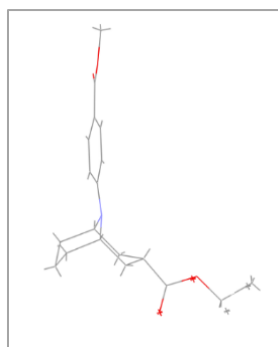
X-Ray diffraction analysis confirmed the configuration of the major diastereoisomer.
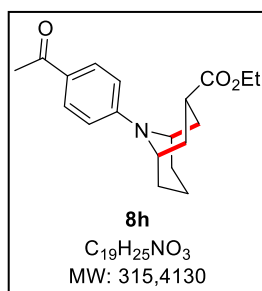
Ethyl 9-(4-acetylphenyl)-9-azabicyclo[3.3.1]nonane-3-carboxylate (8h)

Following **General Procedure C** with 1-[4-(1-piperidyl)phenyl]ethanone **6h** (40.7 mg, 0.20 mmol) and ethyl 2-(acetoxymethyl)prop-2-enoate (37.9 mg, 0.22 mmol) reacting for 3h. Purification by flash column chromatography (SiO$_2$, heptanes/EtOAc 95:5 to 88:12) afforded the product as a colorless oil (27.1 mg, 0.08 mmol, 42%, α/β >20:1) along with mono-allylated intermediate (3.7 mg, 6%; R$_f$ = 0.24 (heptanes/EtOAc 80:20)).

Characterization of the α diastereoisomer:

^{1}H NMR (400 MHz, CDCl$_3$): δ 7.87–7.81 (m, 2H), 6.83–6.76 (m, 2H), 4.40–4.32 (m, 2H), 4.11 (q, *J* = 7.2 Hz, 2H), 2.49 (s, 3H), 2.45–2.25 (m, 3H), 2.04 (qt, *J* = 12.5, 4.2 Hz, 1H), 1.80–1.67 (m, 4H), 1.62–1.46 (m, 3H), 1.23 (t, *J* = 7.2 Hz, 3H).^{13}C NMR (75 MHz, CDCl$_3$): δ 196.2 (C=O), 175.4 (C=O), 153.8 (Cq), 131.1 (2xCH$_{Ar}$), 126.1 (Cq), 112.3 (2xCH$_{Ar}$), 60.6 (CH$_2$), 47.2 (2xCH), 35.1 (CH), 30.3 (2xCH$_2$), 28.6 (2xCH$_2$), 26.1 (CH$_3$), 14.3 (CH$_3$), 14.2 (CH$_2$). FT-IR (cm^{-1}, neat): 2927, 2870, 1725, 1661, 1591, 1278, 1253, 1188, 1044, 908, 813, 727, 588. HRMS (ESI) m/z: [M+H]$^+$ Calcd for C$_{19}$H$_{26}$NO$_3$ 316.1907; Found 316.1880. R$_f$ = 0.21 (heptanes/EtOAc 80:20).

Characteristic peak of the β diastereoisomer:

^{1}H NMR (400 MHz, CDCl$_3$): δ 3.32 (tt, *J*$_{ax-ax}$ = 12.0, *J*$_{ax-eq}$ = 5.8 Hz, 1H, -C<u>H</u>-CO$_2$Et).

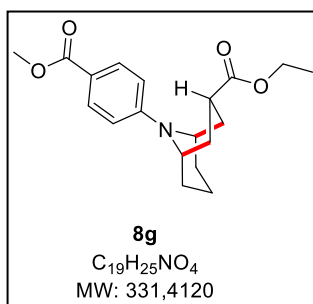**Ethyl 9-[4-(trifluoromethyl)phenyl]-9-azabicyclo[3.3.1]nonane-3-carboxylate (8i)**

Following **General Procedure C** with 1-[4-(trifluoromethyl)phenyl]piperidine **6i** (45.8 mg, 0.20 mmol) and ethyl 2-(acetoxymethyl)prop-2-enoate (37.9 mg, 0.22 mmol) reacting for 40 minutes. Purification by flash column chromatography (SiO$_2$, pentane/Et$_2$O 95:5) afforded the product as a colorless oil (37.5 mg, 0.11 mmol, 55%, α/β >14:1).

Characterization of the α diastereoisomer:

^{1}H NMR (400 MHz, CDCl$_3$): δ 7.42 (d, *J* = 8.9 Hz, 2H), 6.84 (d, *J* = 8.8 Hz, 2H), 4.33–4.24 (m, 2H), 4.12 (q, *J* = 7.1 Hz, 2H), 2.46–2.24 (m, 3H), 2.04 (qt, *J* = 13.3, 4.3 Hz, 1H), 1.82–1.64 (m, 4H), 1.60–1.53 (m, 1H), 1.53–1.42 (m, 2H), 1.24 (t, *J* = 7.1 Hz, 3H). ^{13}C NMR (101 MHz, CDCl$_3$): δ 175.4 (C=O), 152.5 (Cq), 126.8 (q, $^3J_{C-F}$ = 3.7 Hz, 2xCH$_{Ar}$), 124.9 (q, $^1J_{C-F}$ = 270.1 Hz, CF$_3$), 118.1 (q, $^2J_{C-F}$ = 32.8 Hz, Cq), 113.0 (2xCH$_{Ar}$), 60.4 (CH$_2$), 47.1 (2xCH), 34.9 (CH), 30.1 (2xCH$_2$), 28.4 (2xCH$_2$), 14.2 (CH$_3$), 14.0 (CH$_2$). ^{19}F NMR (282 MHz,

CDCl$_3$): δ –61.1. FT-IR (cm^{-1}, neat): 2931, 1726, 1610, 1521, 1401, 1320, 1302, 1286, 1257, 1103, 1067, 813, 588. HRMS (ESI) m/z: [M+H]$^+$ Calcd for C$_{18}$H$_{23}$F$_3$NO$_2$ 342.1675; Found 342.1674. R$_f$ = 0.28 (pentane/Et$_2$O 90:10).

Characteristic peaks of the β diastereoisomer:

^{1}H NMR (400 MHz, CDCl$_3$): δ 4.19 (br m, 2H), 3.32 (tt, $J_{ax\text{-}ax}$ = 12.0, $J_{ax\text{-}eq}$ = 5.7 Hz, 1H, -CH-CO$_2$Et), 1.23 (t, 3H, J = 7.1 Hz). ^{13}C NMR (101 MHz, CDCl$_3$): δ 175.0 (C=O), 112.8 (2xCH$_{Ar}$), 60.5 (CH$_2$), 47.9 (2xCH), 37.5 (CH), 31.0 (2xCH$_2$), 28.0 (2xCH$_2$).
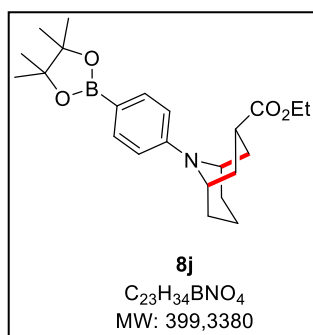
8j
C$_{23}$H$_{34}$BNO$_4$
MW: 399,3380

Ethyl 9-[4-(4,4,5,5-tetramethyl-1,3,2-dioxaborolan-2-yl)phenyl]-9-azabicyclo[3.3.1]nonane-3-carboxylate (8j)

0.2 mmol scale synthesis:

Following **General Procedure C** with 1-[4-(4,4,5,5-tetramethyl-1,3,2-dioxaborolan-2-yl)phenyl]piperidine **6j** (58.6 mg, 0.20 mmol) and ethyl 2-(acetoxymethyl)prop-2-enoate (37.9 mg, 0.22 mmol) reacting for 40 minutes. Purification by flash column chromatography (SiO$_2$, heptanes/EtOAc 90:10) afforded the product as a colorless oil (52.4 mg, 0.13 mmol, 66%, α/β >20:1). Upon evaporation from pentane the oil became a crystalline solid.

3 mmol scale synthesis:

Into a flame-dried Schlenck tube were added under nitrogen ethyl 2-(acetoxymethyl)prop-2-enoate (568 mg, 3.30 mmol), 1-[4-(4,4,5,5-tetramethyl-1,3,2-dioxaborolan-2-yl)phenyl]piperidine **6j** (862 mg, 3.00 mmol), [Ir{dF(CF$_3$)ppy}$_2$(dtbpy)]PF$_6$ (16.8 mg, **0.5 mol%**) and cesium acetate (692 mg, 3.61 mmol). The vial was evacuated and filled with nitrogen (x 3). Dry 1,2-dichloroethane (60 mL) was canuled into the vial, a yellow solution was obtained that was degassed by 3 freeze-and-thaw cycles. The mixture was placed between two 390 nm LED and stirred for 1h. Purification by flash column chromatography (SiO$_2$, heptanes/EtOAc 90:10) afforded the product as a white solid (694 mg, 1.74 mmol, 58%, α/β >20:1).

Characterization of the α diastereoisomer:

^{1}H NMR (300 MHz, CDCl$_3$): δ 7.72–7.61 (m, 2H), 6.85–6.77 (m, 2H), 4.37–4.25 (m, 2H), 4.09 (q, J = 7.1 Hz, 2H), 2.45–2.25 (m, 3H), 2.02 (qt, J = 11.7, 3.6 Hz, 1H), 1.82–1.59 (m, 4H), 1.59–1.40 (m, 3H), 1.32 (s, 12H), 1.22 (t, J = 7.1 Hz, 3H). ^{13}C NMR (101 MHz, CDCl$_3$): δ 175.8 (C=O), 152.8 (Cq), 136.8 (2xCH$_{Ar}$), 113.0 (2xCH$_{Ar}$), 83.4 (2xCq), 60.5 (CH$_2$), 47.0 (2xCH), 35.0 (CH), 30.3 (2xCH$_2$), 28.5 (2xCH$_2$), 25.0 (4xCH$_3$),

14.4 (CH_3), 14.3 (CH_2). Due to coupling to the quadrupolar ^{11}B and ^{10}B nuclei, the aromatic carbon atom bearing the BPin was not detected. ^{11}B NMR (96 MHz, $CDCl_3$): δ +31.6. FT-IR (cm^{-1}, neat): 2975, 2928, 1726, 1600, 1399, 1359, 1141, 1091, 961, 908, 860, 731, 653. HRMS (ESI) m/z: $[M+H]^+$ Calcd for $C_{23}H_{34}BNO_2$ 400.2654; Found 400.2663. Mp 86.7–88.0 °C. R_f = 0.31 (heptanes/EtOAc 90:10).

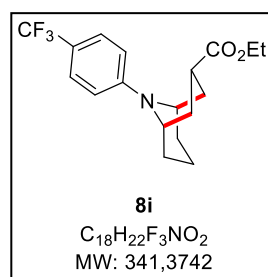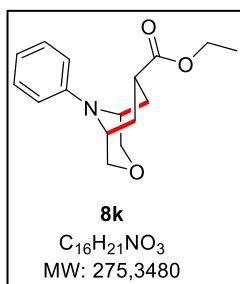**Ethyl 9-phenyl-3-oxa-9-azabicyclo[3.3.1]nonane-7-carboxylate (8k)**

8k
$C_{16}H_{21}NO_3$
MW: 275,3480

Following **General Procedure C** with 4-phenylmorpholine (32.6 mg, 0.20 mmol) and ethyl 2-(acetoxymethyl)prop-2-enoate (37.9 mg, 0.22 mmol) reacting for 20 minutes. Purification by flash column chromatography (SiO_2, heptanes/EtOAc 92:8) afforded an inseparable mixture of diastereoisomers as a colorless oil (35.4 mg, 0.13 mmol, 64%, α/β 5:1). The oil became a white solid after a few days at 4 °C.

Characterization of the α diastereoisomer:

1H NMR (400 MHz, $CDCl_3$) δ 7.28–7.25 (m, 2H), 6.82–6.80 (m, 2H), 6.77–7.73 (m, 1H), 4.18 (q, J = 7.2 Hz, 2H), 3.92 (br d, J = 11.3, 2H), 3.83 (dt, J = 11.0, 2.3 Hz, 2H), 3.77–3.73 (m, 2H), 2.60 (tt, J = 7.5, 1.9 Hz, 1H), 2.42 (dq, J = 14.2, 1.8 Hz, 2H), 2.17 (dddd, J = 14.7, 7.3, 5.2, 2.0 Hz, 2H), 1.29 (t, J = 7.1, 7.1 Hz, 3H). ^{13}C NMR (101 MHz, $CDCl_3$): δ 173.7 (C=O), 147.7 (Cq), 129.8 (2xCH_{Ar}), 117.9 (CH_{Ar}), 113.66 (2xCH_{Ar}), 70.8 (2xCH_2), 60.5 (CH_2), 48.9 (2xCH), 37.0 (CH), 25.3 (2xCH_2), 14.3 (CH_3). R_f = 0.35 (heptanes/EtOAc 80:20).

Characteristic peaks of the β diastereoisomer:

^1H NMR (400 MHz, $CDCl_3$): δ 7.28–7.25 (m, 2H), 6.82–6.80 (m, 2H), 6.77–7.73 (m, 1H), 4.07 (q, J = 7.1 Hz, 2H), 4.02–3.95 (m, 4H), 3.87–3.84 (m, 3H), 2.08 (ddt, J = 14.0, 12.3, 3.9 Hz, 2H), 1.96 (ddd, J = 14.0, 5.6, 2.7 Hz, 2H), 1.21 (t, J = 7.1 Hz, 3H). ^{13}C NMR (101 MHz, $CDCl_3$): δ 175.3 (C=O), 147.4 (Cq), 129.7 (2xCH_{Ar}), 118.0 (CH_{Ar}), 113.71 (2xCH_{Ar}), 71.4 (2xCH_2), 60.4 (CH_2), 49.5 (2xCH), 37.6 (<u>CH</u>-CO_2Et), 28.1 (2xCH_2), 14.3 (CH_3).

FT-IR (cm^{-1}, neat): 2958, 2851, 1721, 1595, 1497, 1258, 1112, 1187, 1033, 920, 748, 688. HRMS (ESI) m/z: $[M+H]^+$ Calcd for $C_{16}H_{22}NO_3$ 275.1516; Found 275.1512. Mp 54.5–55.6 °C (measured on the mixture).
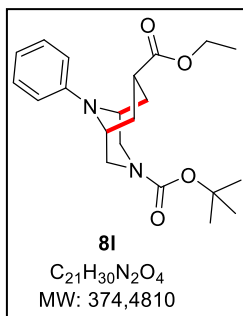
O3-tert-butyl O7-ethyl 9-phenyl-3,9-diazabicyclo[3.3.1]nonane-3,7-dicarboxylate (8l)

Following **General Procedure C** with *tert*-butyl 4-phenylpiperazine-1-carboxylate **6l** (52.5 mg, 0.20 mmol) and ethyl 2-(acetoxymethyl)prop-2-enoate (37.9 mg, 0.22 mmol) reacting for 20 minutes. Purification by flash column chromatography (SiO$_2$, heptanes/EtOAc 90:10) afforded the product as a colorless oil (48.2 mg, 0.13 mmol, 64%, α/β >12:1).

Characterization of the α diastereoisomer:

^{1}H NMR (400 MHz, CDCl$_3$): δ 7.29–7.21 (m, 2H), 6.89–6.80 (m, 2H), 6.76 (tt, *J* = 7.2, 1.1 Hz, 1H), 4.16–4.00 (m, 2H), 4.10 (q, *J* = 7.1 Hz, 2H), 4.00–3.75 (br s, 2H), 3.09 (br d, *J* = 12.4 Hz, 2H), 2.46 (pent, *J* = 6.7 Hz, 1H, -C<u>H</u>-CO$_2$Et), 2.27 (pent, *J* = 7.4, 2H), 2.09 (ddd, *J* = 14.2, 6.5, 2.7 Hz, 2H), 1.49 (s, 9H), 1.24 (t, *J* = 7.2 Hz, 3H). ^{13}C NMR (101 MHz, CDCl$_3$): δ 175.0 (C=O), 156.2 (C=O), 148.6 (Cq), 129.79 (2xCH$_{Ar}$), 118.3 (CH$_{Ar}$), 114.4 (2xCH$_{Ar}$), 80.1 (Cq), 60.56 (CH$_2$), 48.4 (CH$_2$), 47.8 (2xCH), 47.4 (CH$_2$), 35.4 (<u>C</u>H-CO$_2$Et), 28.5 (3xCH$_3$), 27.1 (2xCH$_2$), 14.25 (CH$_3$). FT-IR (cm^{-1}, neat): 2976, 2928, 2859, 1723, 1693, 1596, 1500, 1388, 1365, 1277, 1172, 1123, 1075, 1035, 918, 749, 729, 689. HRMS (ESI) m/z: [M+H]$^+$ Calcd for C$_{21}$H$_{31}$N$_2$O$_4$ 375.2278; Found 375.2269. R$_f$ = 0.34 (heptanes/EtOAc 80:20).

Characteristic peaks of the β diastereoisomer:

^{1}H NMR (400 MHz, CDCl$_3$): δ 3.38–3.20 (m, 2H), 1.48 (s, 9H), 1.20 (t, *J* = 7.2 Hz, 3H). ^{13}C NMR (101 MHz, CDCl$_3$): δ 174.0 (C=O), 155.1 (C=O), 147.5 (Cq), 129.75 (2xCH$_{Ar}$), 80.3 (Cq), 60.5 (CH$_2$), 36.1 (<u>C</u>H-CO$_2$Et), 28.6 (3xCH$_3$), 14.27 (CH$_3$).
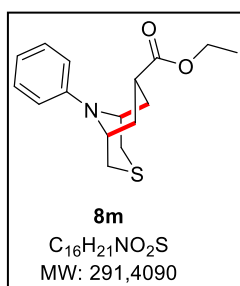
Ethyl 9-phenyl-3-thia-9-azabicyclo[3.3.1]nonane-7-carboxylate (8m)

Following **General Procedure C** with 4-phenylthiomorpholine **6m** (35.9 mg, 0.20 mmol) and ethyl 2-(acetoxymethyl)prop-2-enoate (37.9 mg, 0.22 mmol) reacting for 20 minutes. Purification by flash column chromatography (SiO$_2$, pentane/Et$_2$O 90:10) afforded the product as a colorless oil (33.7 mg, 0.12 mmol, 58%, α/β 7:1).

Characterization of the α diastereoisomer:

^{1}H NMR (400 MHz, CDCl$_3$): δ 7.24 (dd, *J* = 8.9, 7.3 Hz, 2H), 6.84 (d, *J* = 8.3 Hz, 2H), 6.74 (t, *J* = 7.2 Hz, 1H), 4.43–4.33 (m, 2H), 4.15 (q, *J* = 7.1 Hz, 2H), 3.20 (dd, *J* = 13.2, 3.0 Hz, 2H), 2.49 (tt, *J*$_{ax-ax}$ = 11.4, *J*$_{ax-eq}$ = 5.4 Hz, 1H, -C<u>H</u>-CO$_2$Et), 2.44–2.32 (m, 2H), 2.32–2.15 (m, 2H), 2.12–2.02 (m, 2H), 1.26 (t, *J* = 7.2 Hz, 3H). ^{13}C

NMR (101 MHz, CDCl$_3$): δ 175.2 (C=O), 150.0 (Cq), 129.7 (2xCH$_{Ar}$), 118.0 (CH$_{Ar}$), 115.0 (2xCH$_{Ar}$), 60.5 (CH$_2$), 47.4 (2xCH), 35.5 (CH), 31.0 (2xCH$_2$), 28.2 (2xCH$_2$), 14.4 (CH$_3$). FT-IR (cm^{-1}, neat): 2924, 2866, 1723, 1594, 1497, 1392, 1272, 1173, 1034, 748, 689. HRMS (ESI) m/z: [M+H]$^+$ Calcd for C$_{16}$H$_{22}$NO$_2$S 292.1366; Found 292.1363. R$_f$ = 0.25 (pentane/Et$_2$O 90:10).

Characteristic peaks of the β diastereoisomer:

^{1}H NMR (400 MHz, CDCl$_3$): δ 4.57 (tt, J_{ax-ax} = 11.3, J_{ax-eq} = 5.9 Hz, 1H, -CH-CO$_2$Et), 4.33–4.27 (m, 2H), 4.10 (q, J = 7.0 Hz, 2H), 3.40 (ddd, J = 13.5, 3.8, 1.5 Hz, 2H), 2.32–2.15 (m, 2H), 1.21 (t, J = 7.2 Hz, 3H). ^{13}C NMR (101 MHz, CDCl$_3$): δ 175.2 (C=O), 148.1 (Cq), 117.9 (CH$_{Ar}$), 114.6 (2xCH$_{Ar}$), 60.4 (CH$_2$), 47.2 (2xCH), 36.6 (CH-CO$_2$Et), 28.3 (2xCH$_2$), 14.4 (CH$_3$).
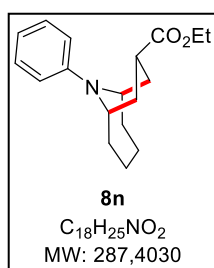
Ethyl 10-phenyl-10-azabicyclo[4.3.1]decane-8-carboxylate (8n)

Following **General Procedure C** with 1-phenylazepane **6n** (35.1 mg, 0.20 mmol) and ethyl 2-(acetoxymethyl)prop-2-enoate (37.9 mg, 0.22 mmol) reacting for 14 hours. Purification by flash column chromatography (SiO$_2$, heptanes/AcOEt 98:2) afforded the product as a pale-yellow oil (14.6 mg, 0.05 mmol, 25%, α/β >20:1).

8n
C$_{18}$H$_{25}$NO$_2$
MW: 287,4030

The yield could not be increased by using a two-step procedure. The chemical shifts (^{1}H NMR) and coupling constants are compatible with depicted configuration and conformation.

Characterization of the α diastereoisomer:

^{1}H NMR (300 MHz, CDCl$_3$): δ 7.19 (dd, J = 8.7, 7.1 Hz, 2H), 6.78 (d, J = 8.4 Hz, 2H), 6.62 (t, J = 7.2 Hz, 1H), 4.27–4.18 (m, 2H), 4.13 (q, J = 7.1 Hz, 2H), 2.49 (tt, J_{ax-ax} = 11.9, J_{ax-eq} = 5.7 Hz, 1H, -CH-CO$_2$Et), 2.29–2.15 (m, 4H), 1.82 (td, J = 12.8, 6.0 Hz, 2H), 1.63–1.47 (m, 6H), 1.25 (t, J = 7.1 Hz, 3H). ^{13}C NMR (75 MHz, CDCl$_3$): δ 176.2 (C=O), 149.9 (Cq), 129.5 (2xCH$_{Ar}$), 115.7 (CH$_{Ar}$), 111.9 (2xCH$_{Ar}$), 60.6 (CH$_2$), 50.5 (2xCH), 36.9 (CH, CH-CO$_2$Et), 34.9 (2xCH$_2$), 29.7 (2xCH$_2$), 25.9 (2xCH$_2$), 14.4 (CH$_3$). FT-IR (cm^{-1}, neat): 2924, 2858, 1728, 1594, 1501, 1178, 1155, 1039, 744, 690. HRMS (ESI) m/z: [M+H]$^+$ Calcd for C$_{18}$H$_{26}$NO$_2$ 288.1958; Found 288.1966. R$_f$ = 0.50 (heptanes/EtOAc 90:10)

Bis-annulation of *N,N*-dimethylaniline

14 β,α
(major dia)

14 β,β
(minor dia)

C$_{20}$H$_{27}$NO$_4$
MW: 345,4390

Diethyl 9-phenyl-9-azabicyclo[3.3.1]nonane-3,7-dicarboxylate (14).

Protocol 1 from *N,N*-dimethyl aniline (0.5 mmol scale)

In an oven-dried vial were added under N_2 ethyl 2-(acetoxymethyl)prop-2-enoate (94.7 mg, 0.55 mmol), [Ir{dF(CF$_3$)ppy}$_2$(dtbpy)]PF$_6$ (5.6 mg, 0.005 mmol), and cesium acetate (230 mg, 1.20 mmol, 2.4 equiv.). The vial was evacuated and filled with nitrogen (x 3). *N,N*-dimethylaniline (63 µL, 0.50 mmol) and degassed 1,2-dichloroethane (10.0 mL) were added. The resulting yellow solution was placed in front of a 390 nm LED and stirred for 15 min. At this point a solution of ethyl 2-(acetoxymethyl)prop-2-enoate (94.7 mg, 0.55 mmol) in degassed DCE (0.5 mL) was added and the reaction mixture was stirred for one more hour. Upon completion of reaction the reaction mixture was diluted with sat. NaHCO$_3$ (15 mL). The aqueous phase was extracted with DCM (3 x 15 mL). The combined organic phases were washed once with brine, dried over Na$_2$SO$_4$, filtered and concentrated. Flash column chromatography (Si$_2$O, pentane/Et$_2$O 90:10 to 80:20) afforded the desired product as a colorless oil (22.5 mg, 0.065 mmol, 13%, β,α/β,β 20:1).

Protocol 2 from N-methyl-N-(trimethylsilylmethyl)aniline (0.5 mmol scale)

Identical as protocol 1 except for the base: cesium acetate (115 mg, 0.60 mmol, 1.2 equiv.) is used. The desired product was obtained as a colorless oil (38.1 mg, 0.11 mmol, 22 %, β,α/β,β 14:1).

Characterization of the β,α diastereoisomer:

^{1}H NMR (400 MHz, CDCl$_3$): δ 7.22 (dd, J = 8.9, 7.2 Hz, 2H), 6.85 (d, J = 7.9 Hz, 2H), 6.71 (tt, J = 7.2, 1.1 Hz, 1H), 4.37–4.27 (m, 2H), 4.13 (q, J = 7.1 Hz, 2H), 4.10 (q, J = 7.2 Hz, 2H), 3.03 (tt, J_{ax-ax} = 12.5, J_{ax-eq} = 4.6 Hz, 1H, 1x -<u>CH</u>-CO$_2$Et), 2.51–2.37 (m, 3H), 1.89 (td, J = 12.9, 4.0 Hz, 2H), 1.83–1.74 (m, 2H), 1.71–1.56 (m, 2H), 1.25 (t, J = 7.1 Hz, 3H), 1.23 (t, J = 7.1 Hz, 3H). ^{13}C NMR (101 MHz, CDCl$_3$): δ 175.6 (C=O), 175.5 (C=O), 150.0 (Cq), 129.7 (2xCH$_{Ar}$), 117.8 (CH$_{Ar}$), 114.5 (2xCH$_{Ar}$), 60.64 (CH$_2$), 60.59 (CH$_2$), 46.7 (2xCH), 34.6 (CH), 33.0 (2xCH$_2$), 32.6 (CH), 28.7 (2xCH$_2$), 14.4 (2xCH$_3$). FT-IR (neat, cm^{-1}): 2978, 2950, 1724, 1594, 1498, 1256, 1176, 1032, 749, 731, 690. HRMS (ESI) m/z: [M+H]$^+$ Calcd for C$_{20}$H$_{28}$NO$_4$ 346.2013; Found 346.2006. [M+Na]$^+$ Calcd for C$_{20}$H$_{27}$NO$_4$Na 368.1832; Found 368.1826. R$_f$ = 0.29 (pentane/Et$_2$O 84:16).

Characteristic peaks of the β,β diastereoisomer:

^{1}H NMR (400 MHz, CDCl$_3$): δ 4.25–4.19 (m, 4H), 3.16 (tt, J_{ax-ax} = 12.2, J_{ax-eq} = 5.8 Hz, 2H, 2x -<u>CH</u>-CO$_2$Et), 2.14 (td, J = 13.0, 5.4 Hz, 4H). ^{13}C NMR (101 MHz, CDCl$_3$): δ 175.0 (C=O), 148.0 (Cq), 129.6 (CH$_{Ar}$), 117.5 (2xCH$_{Ar}$), 114.2 (2xCH$_{Ar}$), 47.6 (CH), 37.5 (CH), 30.4 (CH$_2$).

Unsuccessful substrates
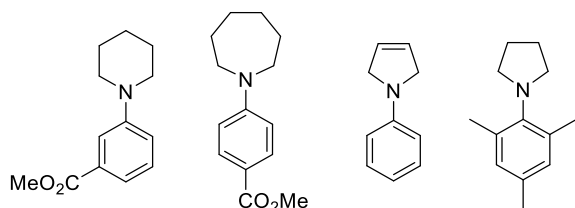
Additional substrate scope

C$_{24}$H$_{27}$NO$_4$
MW: 393,4830
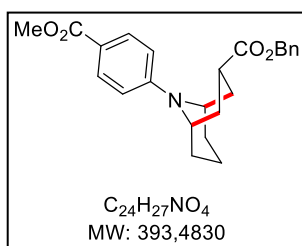
Benzyl 9-(4-methoxycarbonylphenyl)-9-azabicyclo[3.3.1]nonane-3-carboxylate

Following **General Procedure C** with benzyl 2-(acetoxymethyl)prop-2-enoate (51.5 mg, 0.22 mmol) and methyl 4-(1-piperidyl)benzoate (43.9 mg, 0.20 mmol) reacting for 40 minutes. Purification by column chromatography (SiO$_2$, EtOAc/heptanes 1:9) afforded the product as a pale-yellow oil (38.7 mg, 0.11 mmol, 55%, α/β >20:1).

^{1}H NMR (400 MHz, CDCl$_3$): δ 7.92–7.83 (m, 2H), 7.40–7.27 (m, 5H), 6.82–6.74 (m, 2H), 5.10 (s, 2H), 4.37–4.29 (m, 2H), 3.85 (s, 3H), 2.47–2.33 (m, 3H), 2.02 (qt, *J* = 13.1, 3.7 Hz, 1H), 1.81–1.68 (m, 4H), 1.60–1.53 (m, 1H), 1.53–1.45 (m, 2H). ^{13}C NMR (101 MHz, CDCl$_3$): δ 175.3 (C=O), 167.2 (C=O), 153.6 (Cq), 136.1 (Cq), 131.9 (2x CH Ar), 128.7 (2x CH Ar), 128.3 (CH Ar), 128.2 (2x CH Ar), 117.8 (Cq), 112.5 (2x CH Ar), 66.4 (CH$_2$), 51.6 (CH$_3$), 47.2 (2x CH), 35.1 (CH), 30.2 (2x CH$_2$), 28.5 (2x CH$_2$), 14.2 (CH$_2$). FT-IR (cm^{-1}, neat) 2926, 2850, 1729, 1705, 1516, 1434, 1280, 1255, 1183, 1109, 770, 697. HRMS (ESI) m/z: [M+H]$^+$ Calcd for C$_{24}$H$_{28}$NO$_4$ 394.2013; Found 394.2004. Rf = 0.32 (EtOAc/heptane 2:8).

C$_{17}$H$_{22}$FNO$_2$
MW: 291,3664

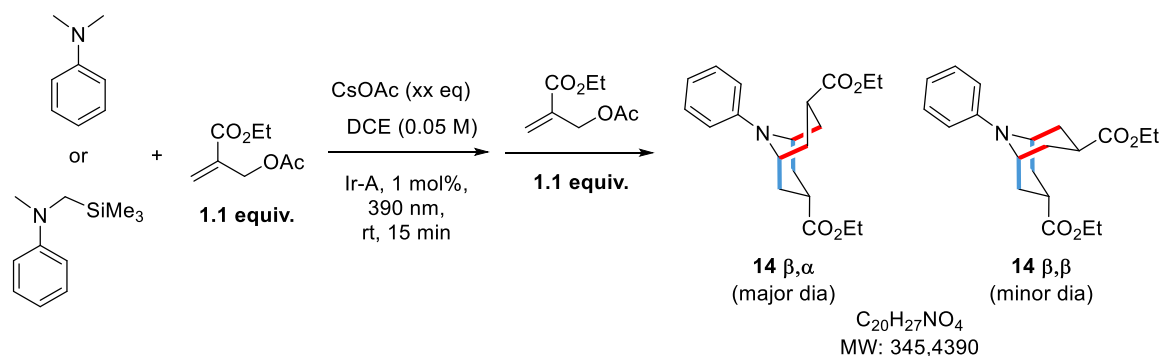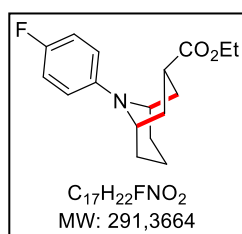**Ethyl 9-(4-fluorophenyl)-9-azabicyclo[3.3.1]nonane-3-carboxylate**

Following **General Procedure C** with 1-(4-fluorophenyl)piperidine (35.8 mg, 0.20 mmol) and ethyl 2-(acetoxymethyl)prop-2-enoate (37.9 mg, 0.22 mmol) reacting for 40 minutes. Purification by column chromatography (SiO$_2$, pentane/Et$_2$O 95:5) afforded the product as a colorless oil (23.6 mg, 0.08 mmol, 41%, α/β >20:1).

Characterization of the major diastereoisomer:

^{1}H NMR (400 MHz, CDCl$_3$): δ 6.95–6.86 (m, 2H), 6.81–6.72 (m, 2H), 4.19–4.05 (m, 2H), 4.11 (q, J = 7.1 Hz, 2H), 2.49–2.29 (m, 3H), 2.00 (qt, J = 13.4, 4.6 Hz, 1H), 1.77 (tt, J = 13.2, 4.2 Hz, 2H), 1.67 (ddd, J = 13.7, 12.0, 3.4 Hz, 2H), 1.58–1.49 (m, 1H), 1.49–1.41 (m, 2H), 1.23 (t, J = 7.2 Hz, 3H). ^{19}F NMR (376 MHz, CDCl$_3$): δ -128.23 (tt, apparent sept., J_{F-H} = 8.3, 4.7 Hz). ^{13}C NMR (101 MHz, CDCl$_3$): δ 175.9 (C=O), 155.3 (Cq Ar, d, $^1J_{C-F}$ = 236.2 Hz), 147.3 (Cq Ar, d, $^4J_{C-F}$ = 2.1 Hz), 115.9 (2x CH Ar, d, $^2J_{C-F}$ = 22.0 Hz), 115.4 (2x CH Ar, d, $^3J_{C-F}$ = 7.3 Hz), 60.5 (CH$_2$), 47.8 (2x CH), 34.8 (CH), 30.4 (2x CH$_2$), 28.4 (2x CH$_2$), 14.4 (CH$_3$), 14.2 (CH$_2$). FT-IR (cm^{-1}, neat): 2927, 1725, 1504, 1281, 1247, 1225, 1175, 809, 614, 522. HRMS (ESI) m/z: [M+H]$^+$ Calcd for C$_{17}$H$_{23}$FNO$_2$ 292.1707; Found 292.1709. R$_f$ = 0.28 (pentane/Et$_2$O 95:5).

Characteristic peaks of the minor diastereoisomer:

^{1}H NMR (400 MHz, CDCl$_3$): δ 4.02 (bs, 2H), 3.29 (tt, J = 12.4, 5.6 Hz, 1H). ^{13}C NMR (101 MHz, CDCl$_3$): δ 48.6, 37.7. ^{19}F NMR (376 MHz, CDCl$_3$): δ -128.53 (tt, J = 8.3, 4.3 Hz).

Characterization of the mono-allylated intermediates

Ethyl 2-[(1-phenylpyrrolidin-2-yl)methyl]prop-2-enoate (2a)
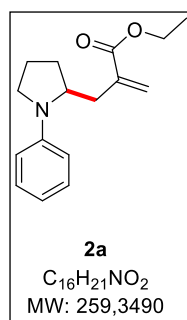
In a 10 mL oven-dried vial were added under N$_2$ ethyl 2-(acetoxymethyl)prop-2-enoate (72.4 mg, 0.42 mmol), [Ir{dF(CF$_3$)ppy}$_2$(dtbpy)]PF$_6$ (3.4 mg, 0.030 mmol), and cesium acetate (69 mg, 0.36 mmol). The vial was evacuated and filled with N$_2$ (x 3), and 1-phenylpyrrolidine **1a** (0.043 mL, 0.30 mmol) was added *via* a Hamilton syringe. Degassed 1,2-dichloroethane (6.00 mL) was added. The resulting yellow solution was placed in front of a 390 nm LED and stirred for 15 minutes. The reaction mixture was diluted with sat. NaHCO$_3$ (5 mL) and the aqueous phase was extracted with DCM (3 x 7 mL). The combined organic phases were dried over Na$_2$SO$_4$, filtered, and concentrated under reduced pressure to give crude product as an orange oil. Purification by flash column chromatography (SiO$_2$, heptanes/EtOAc 99.5:0.5) afforded the mono-allylated product as a colorless oil (33.0 mg, 0.13 mmol, 42%).

2a
C$_{16}$H$_{21}$NO$_2$
MW: 259,3490

^{1}H NMR (300 MHz, CDCl$_3$): *δ* 7.25 (t, J = 7.8 Hz, 2H), 6.78 (d, J = 8.1 Hz, 2H), 6.68 (t, J = 7.3 Hz, 1H), 6.27 (d, J = 1.5 Hz, 1H), 5.60 (br s, 1H), 4.33–4.21 (m, 2H), 4.01–3.91 (m, 1H), 3.47–3.32 (m, 1H), 3.19 (td, J = 9.2, 7.2 Hz, 1H), 2.93 (dd, J = 13.7, 2.3 Hz, 1H), 2.12 (m, J = 13.7, 10.4 Hz, 1H), 2.08–1.94 (m, 2H), 1.91–1.81 (m, 2H), 1.37 (t, J = 7.1 Hz, 3H). ^{13}C NMR (101 MHz, CDCl$_3$): *δ* 167.3 (C=O), 147.2 (Cq), 138.7 (Cq), 129.4 (2xCH$_{Ar}$), 127.7 (=CH$_2$), 115.6 (CH$_{Ar}$), 112.1 (2xCH$_{Ar}$), 61.1 (CH$_2$), 57.4 (CH), 48.4 (CH$_2$), 35.5 (CH$_2$), 29.1 (CH$_2$), 23.2 (CH$_2$), 14.4 (CH$_3$). FT-IR (cm^{-1}, neat): 2967, 1709, 1596, 1504, 1363, 1177, 1159, 1139, 991, 743, 692, 512. HRMS (ESI) m/z: [M+H]$^+$ Calcd for C$_{16}$H$_{22}$O$_2$N 260.1643; Found 260.1645. R$_f$ = 0.23 (heptanes/EtOAc 95:5).
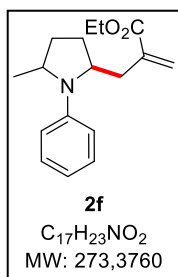
Ethyl 2-[(5-methyl-1-phenyl-pyrrolidin-2-yl)methyl]prop-2-enoate (2f)

2f
$C_{17}H_{23}NO_2$
MW: 273,3760

In an oven-dried vial were added under N_2 2-methyl-1-phenyl-pyrrolidine **1f** (161 mg, 1.00 mmol), ethyl 2-(acetoxymethyl)prop-2-enoate (207 mg, 1.20 mmol), [Ir{dF(CF$_3$)ppy}$_2$(dtbpy)]PF$_6$ (5.6 mg, 0.005 mmol) and cesium acetate (231 mg, 1.20 mmol). The vial was evacuated and filled with nitrogen (x 3). Degassed 1,2-dichloroethane (20 mL) was added. The mixture was placed in front of a 390 nm LED and stirred for 10 minutes. The reaction mixture was diluted with sat. NaHCO$_3$ (15 mL) and the aqueous phase was extracted with DCM (3 x 20 mL). The combined organic phases were dried over Na$_2$SO$_4$, filtered, and concentrated under reduced pressure to give crude product as an orange oil. Purification by flash column chromatography (SiO$_2$, pentane/Et$_2$O 40:1) afforded the mono-allylated product as a colorless oil and inseparable mixture of diastereoisomers (130 mg, 0.48 mmol, 48%, *trans*/*cis* = 2.8:1).

R$_f$ = 0.33 (pentane/Et$_2$O 40:1)

The diastereoisomers were separated on a <u>reverse phase preparative system</u> (acidic conditions).

The mixture of diastereoisomers (130 mg) was dissolved in a mix of solution D [100% MeCN + 1% TFA] and solution A [100% H$_2$O + 1% TFA]. The 15-mL solution was centrifugated and loaded on a Waters PrepLC System (15% D in A to 65% D in A over 50 minutes at a flow rate of 20 mL/min). The minor diastereoisomer was recovered with 28% D in A. The major diastereoisomer was recovered with 47% D in A. The solvent was evaporated on a lyophilisation system overnight and the TFA-salt was taken in EtOAc (10 mL) and aq. sat. NaHCO$_3$ (10 mL). The phases were separated and the aqueous phase extracted with EtOAc (2 x 10 mL). A short filtration on silica gel afforded the clean fractions.

Description of the trans diastereoisomer:

Appearance: white solid

^{1}H NMR (400 MHz, CDCl$_3$): δ 7.24 (td, *J* = 7.8, 7.3, 1.5 Hz, 2H), 6.78 (d, *J* = 7.9 Hz, 2H), 6.63 (tt, *J* = 7.3, 1.1 Hz, 1H), 6.27 (d, *J* = 1.5 Hz, 1H), 5.58 (br s, 1H), 4.33–4.21 (m, 2H), 4.11–4.01 (m, 2H, including N-C*H*Me), 2.97 (br dd, *J* = 13.8, 3.2 Hz, 1H), 2.20 (tt, *J* = 11.9, 7.2 Hz, 1H), 2.11–2.00 (m, 1H), 1.98 (dd, *J* = 13.8, 10.5 Hz, 1H), 1.82 (dd, *J* = 12.4, 6.7 Hz, 1H), 1.64 (dd, *J* = 12.0, 6.6 Hz, 1H), 1.38 (t, *J* = 7.2 Hz, 3H), 1.12 (d, *J* = 6.1 Hz, 3H, N-CH*Me*). ^{13}C NMR (101 MHz, CDCl$_3$): δ 167.3 (C=O), 145.1 (Cq), 138.9 (Cq), 129.3 (2xCH$_{Ar}$), 127.6 (=CH$_2$), 115.1 (CH$_{Ar}$), 113.7 (2xCH$_{Ar}$), 61.0 (CH$_2$), 56.5 (CH), 53.0 (CH), 33.9 (CH$_2$), 30.2 (CH$_2$), 26.3 (CH$_2$), 18.2 (CH$_3$), 14.4 (CH$_3$). FT-IR (cm^{-1}, neat): 2960, 2927, 1709, 1596, 1502, 1359, 1181, 1147, 744, 694. HRMS (ESI) m/z: [M+H]$^+$ Calcd for C$_{17}$H$_{24}$O$_2$N 274.1802; Found 274.1794. Mp 36.9–37.7 °C. R$_f$ = 0.33 (pentane/Et$_2$O 40:1).

Description of the cis diastereoisomer:

Appearance: colorless oil

^{1}H NMR (400 MHz, CDCl$_3$): δ 7.29–7.19 (dd, J = 8.9, 7.2 Hz, 2H), 6.80 (d, J = 7.6 Hz, 2H), 6.67 (tt, J = 7.3, 1.1 Hz, 1H), 6.26 (d, J = 1.5 Hz, 1H), 5.62 (br s, 1H), 4.35–4.19 (m, 2H), 3.90 (ddt, J = 10.8, 7.6, 4.0 Hz, 1H), 3.80 (hx, J = 6.2 Hz, 1H, N-C_H_Me), 3.05 (ddd, J = 13.7, 3.5, 1.4 Hz, 1H), 2.16 (dd, J = 13.7, 10.3 Hz, 1H), 2.07 (dtd, J = 12.0, 7.2, 6.0 Hz, 1H), 1.92–1.75 (m, 2H), 1.70 (ddt, J = 12.3, 8.2, Hz, 1H), 1.37 (t, J = 7.2 Hz, 3H), 1.29 (d, J = 6.1 Hz, 3H, N-CH-_Me_). ^{13}C NMR (101 MHz, CDCl$_3$): δ 167.3 (C=O), 147.5 (Cq), 138.6 (Cq), 129.3 (2xCH$_{Ar}$), 127.6 (=CH$_2$), 115.8 (CH$_{Ar}$), 112.3 (2xCH$_{Ar}$), 61.1 (CH$_2$), 59.8 (CH), 55.9 (CH), 38.11 (CH$_2$), 32.4 (CH$_2$), 28.8 (CH$_2$), 21.9 (CH$_3$), 14.4 (CH$_3$). FT-IR (cm^{-1}, neat): 2962, 1709, 1595, 1501, 1354, 1147, 744, 694. HRMS (ESI) m/z: [M+H]$^+$ Calcd for C$_{17}$H$_{24}$O$_2$N 274.1802; Found 274.1793. R$_f$ = 0.33 (pentane/Et$_2$O 40:1).

Attribution of the relative configuration:

Literature reports: with respect to the *cis* isomer, the ring proton α to the nitrogen and the methyl group in the *trans* product will appear at lower field (higher ppm), and the methyl group will appear at higher field (lower ppm). No exceptions to this rule are known.[21,22]

	1-Phenyl-2,5-dimethylpyrrolidine *trans*	1-Phenyl-2,5-dimethylpyrrolidine *cis*	Product Major dia	Product Minor dia
N-C_H_Me	m, 3.98 (lower field)	m, 3.75	m, 4.06 (lower field)	m, 3.79
N-CH_Me_	d, 1.08 (higher field)	d, 1.27	d, 1.12 (higher field)	d, 1.29

Hence it can be concluded that, in our case, the major diastereoisomer is the *trans* product and the minor diastereoisomer the *cis* product.
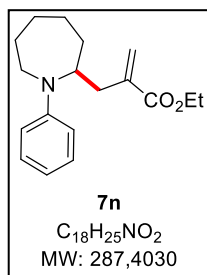
Ethyl 2-[(1-phenylazepan-2-yl)methyl]prop-2-enoate (7n)

In an oven-dry vial were added under N_2 1-phenylazepane **6n** (87.6 mg, 0.50 mmol), ethyl 2-(acetoxymethyl)prop-2-enoate (94.7 mg, 0.55 mmol), [Ir{dF(CF$_3$)ppy}$_2$(dtbpy)]PF$_6$ (5.6 mg, 0.005 mmol), and cesium acetate (115 mg, 0.6 mmol). The vial was evacuated and filled with nitrogen (x 3). Degassed 1,2-dichloroethane (10 mL) was added. The resulting yellow solution was placed in front of a 390 nm LED and stirred for 10 min. The reaction mixture was diluted with sat. $NaHCO_3$ (10 mL) and the aqueous phase was extracted with DCM (3 x 10 mL); combined organic phases were dried over Na_2SO_4, filtered, and concentrated under reduced pressure to give crude product as an orange oil. Purification by flash column chromatography (SiO$_2$, pentane/Et$_2$O 99:1 to 98:2) afforded the mono-allylated product as a colorless oil (93.1 mg, 0.33 mmol, 65%). Some cyclized product was also recovered at this point (2.6 mg, 2%), hence the necessity to control very closely the reaction.

^{1}H NMR (300 MHz, CDCl$_3$): δ 7.29–7.16 (m, 2H), 6.83 (d, J = 8.1 Hz, 2H), 6.62 (tt, J = 7.2, 1.0 Hz, 1H), 6.19 (d, J = 1.6 Hz, 1H), 5.60 (br s, 1H), 4.31–4.19 (m, 2H), 3.95 (dq, J = 15.1, 5.2 Hz, 1H), 3.54–3.41 (m, 1H), 3.31–3.12 (m, 1H), 2.77 (ddd, J = 13.5, 5.0, 1.4 Hz, 1H), 2.29 (dd, J = 13.4, 9.3 Hz, 1H), 2.07 (ddd, J = 14.4, 8.3, 6.2 Hz, 1H), 1.92–1.79 (m, 1H), 1.79–1.71 (m, 1H), 1.71–1.60 (m, 2H), 1.42–1.15 (m, 3H), 1.35 (t, J = 7.1 Hz, 3H). ^{13}C NMR (75 MHz, CDCl$_3$): δ 167.4 (C=O), 148.5 (Cq), 138.2 (Cq), 129.4 (2xCH$_{Ar}$), 127.3 (=CH$_2$), 114.8 (CH$_{Ar}$), 110.6 (2xCH$_{Ar}$), 61.0 (CH$_2$), 55.6 (CH), 43.0 (CH$_2$), 36.2 (CH$_2$), 34.8 (CH$_2$), 30.2 (CH$_2$), 27.2 (CH$_2$), 25.2 (CH$_2$), 14.3 (CH$_3$). FT-IR (cm^{-1}, neat): 2925, 2851, 1708, 1594, 1400, 1164, 1135, 908, 729, 692. HRMS (ESI) m/z: [M+H]$^+$ Calcd for C$_{18}$H$_{26}$O$_2$N 288.1958. Found 288.1956. [M+Na]$^+$ Calcd for C$_{18}$H$_{25}$O$_2$NNa 310.1778; Found 310.1775. R$_f$ = 0.34 (heptanes/EtOAc 95:5).
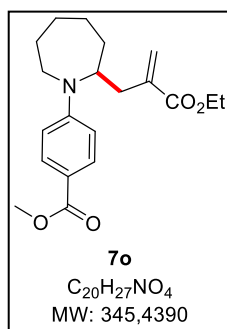
Methyl 4-[2-(2-ethoxycarbonylallyl)azepan-1-yl]benzoate (7o)

In an oven-dry vial were added under N_2 methyl 4-(azepan-1-yl)benzoate **6o** (93.3 mg, 0.40 mmol), ethyl 2-(acetoxymethyl)prop-2-enoate (75.8 mg, 0.44 mmol), [Ir{dF(CF$_3$)ppy}$_2$(dtbpy)]PF$_6$ (4.5 mg, 0.04 mmol), and cesium acetate (92.3 mg, 0.48 mmol). The vial was evacuated and filled with nitrogen (x 3). Degassed 1,2-dichloroethane (8.00 mL) was added. The resulting yellow solution was placed in front of a 390 nm LED and stirred for 9 h. The reaction mixture was diluted with sat. $NaHCO_3$ (10 mL) and the aqueous phase was extracted with DCM (3 x 8 mL). The combined organic phases were dried over Na_2SO_4, filtered, and concentrated under reduced pressure to give crude product as an orange oil. Purification by flash column chromatography (SiO$_2$, pentane/Et$_2$O 80:20) afforded the mono-

allylated product as a colorless oil (34.4 mg, 0.10 mmol, 25%) along with 26% unreacted starting material.

^{1}H NMR (300 MHz, CDCl$_3$): δ 7.85–7.80 (m, 2H), 6.57–6.51 (m, 2H), 6.20 (d, J = 1.4 Hz, 1H), 5.58 (q, J = 1.2 Hz, 1H), 4.24–4.17 (m, 2H), 3.84 (s, 3H), 3.71–3.61 (m, 1H), 3.38 (t, J = 6.7 Hz, 2H), 2.60 (ddd, J = 13.9, 7.3, 1.0 Hz, 1H), 2.45 (ddd, J = 13.8, 6.1, 0.9 Hz, 1H), 1.89–1.78 (m, 2H), 1.68–1.56 (m, 1H), 1.53–1.33 (m, 5H), 1.29 (t, J = 7.2 Hz, 3H). ^{13}C NMR (101 MHz, CDCl$_3$): δ 167.5 (C=O), 151.7 (Cq), 137.8 (Cq), 131.8 (2xCH$_{Ar}$), 127.8 (=CH$_2$), 118.1 (Cq), 111.7 (2xCH$_{Ar}$), 61.2 (CH$_2$), 52.4 (CH), 51.6 (CH$_3$), 37.8 (CH$_2$), 34.8 (CH$_2$), 33.9 (CH$_2$), 32.7 (CH$_2$), 28.2 (CH$_2$), 25.3 (CH$_2$), 14.3 (CH$_3$). FT-IR (cm^{-1}, neat): 3367, 2935, 1703, 1600, 1525, 1432, 1271, 1171, 1106, 769. HRMS (ESI) m/z: [M+H]$^+$ Calcd for C$_{20}$H$_{28}$O$_4$N 346.2013; Found 346.2014. R$_f$ = 0.36 (pentane/Et$_2$O 60:40).

C$_{20}$H$_{27}$NO$_4$

MW: 345,4390
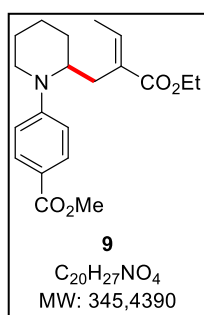
Methyl 4-[2-[(E)-2-ethoxycarbonylbut-2-enyl]-1-piperidyl]benzoate (9)

In an oven-dry vial were added under N$_2$ methyl 4-(1-piperidyl)benzoate **6g** (110 mg, 0.50 mmol), ethyl 3-acetoxy-2-methylene-butanoate (37.2 mg, 0.20 mmol), [Ir{dF(CF$_3$)ppy}$_2$(dtbpy)]PF$_6$ (2.2 mg, 0.002 mmol), and CsOAc (46.1 mg, 0.24 mmol). The vial was evacuated and filled with nitrogen (x 3). Degassed 1,2-dichloroethane (4.0 mL) was added. The resulting yellow solution was placed in front of a 390 nm LED and stirred for **10 min**. The reaction mixture was diluted with sat. NaHCO$_3$ (5 mL) and the aqueous phase was extracted with DCM (3 x 5 mL). The combined organic phases were dried over Na$_2$SO$_4$, filtered, and concentrated under reduced pressure to give crude product as an orange oil. Purification by flash column chromatography (SiO$_2$, pentane/Et$_2$O 90:10) afforded the mono-allylated product as a colorless oil (49.9 mg, 0.14 mmol, 73%, E/Z = 7:1). Crystallization from pentane at 4 °C afforded the product as a white solid, enriched in the E isomer (E/Z = 20/1).

^{1}H NMR (300 MHz, CDCl$_3$): δ 7.90–7.82 (m, 2H), 6.90–6.72 (m, 3H), 4.35–4.27 (m, 1H), 4.18 (q, J = 7.1 Hz, 2H), 3.84 (s, 3H), 3.65–3.56 (m, 1H), 3.11 (td, J = 12.6, 3.1 Hz, 1H), 2.67 (dd, J = 13.6, 9.0 Hz, 1H), 2.52 (dd, J = 13.5, 5.9 Hz, 1H), 1.79 (d, J = 7.2 Hz, 3H), 1.78–1.48 (m, 6H), 1.28 (t, J = 7.1 Hz, 3H). ^{13}C NMR (101 MHz, CDCl$_3$): δ 167.8 (C=O), 167.4 (C=O), 154.0 (Cq), 139.3 (=CH), 131.8 (2xCH$_{Ar}$), 130.9 (Cq), 118.1 (Cq), 113.5 (2xCH$_{Ar}$), 60.7 (CH$_2$), 53.8 (CH), 51.6 (CH$_3$), 42.1 (CH$_2$), 27.7 (CH$_2$), 25.5 (CH$_2$), 25.3 (CH$_2$), 19.3 (CH$_2$), 14.8 (CH$_3$), 14.4 (CH$_3$). FT-IR (cm^{-1}, neat): 2932, 2850, 1700, 1599, 1515, 1432, 1247, 1185, 1163, 1106, 768. HRMS (ESI) m/z: [M+H]$^+$ Calcd for C$_{20}$H$_{28}$O$_4$N 346.2013. Found 346.2016. Calcd for C$_{20}$H$_{27}$O$_4$NNa [M+Na]$^+$ 368.1832; Found 368.1835. Mp 52.3–54.1 °C. R$_f$ = 0.33 (pentane/Et$_2$O 80:20).

RXay
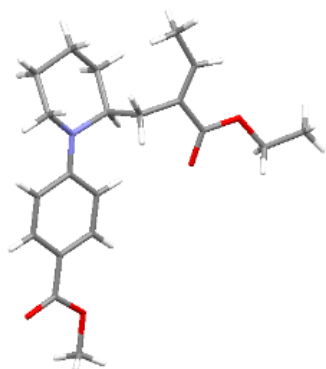
A sample was dissolved in the minimum amount of pentane with gentle heating, and the solution was then placed at 4 °C overnight to afford single crystals suitable for X-Ray diffraction analysis.

Study of the cyclization step

NMR experiments
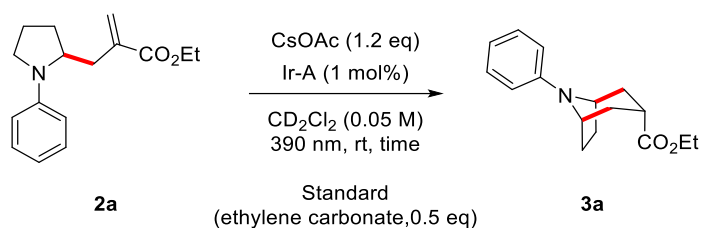
General Procedure D

In a dry NMR tube were added ethyl 2-[(1-phenylpyrrolidin-2-yl)methyl]prop-2-enoate **2a** (6.5 mg, 0.025 mmol), [Ir{dF(CF$_3$)ppy}$_2$(dtbpy)]PF$_6$ (0.3 mg, 0.27 x 10^{-3} mmol), 1,3-dioxolan-2-one (1.1 mg, 0.0125 mmol, standard) and cesium acetate (5.8 mg, 0.03 mmol). The tube was evacuated and filled with N$_2$ (x 3), and dry CD$_2$Cl$_2$ (0.5 mL) was added. The resulting yellow solution was degassed by freeze-pump-thaw cycles (x 3) and a first NMR measurement was made before irradiation to determine the exact standard-to-starting material ratio. The tube was then placed in front of a 390 nm LED and measurements were taken regularly (see Table 5 and Image 1).

	% conversion of **2a**	% yield of **3a**
t1: 3min	15	7
t2: 10min	24	18
t3: 20 min	41	26
t4: 40min	56	41
t5: 60min	65	48
t6: 90min	80	53
t7: 120min	87	58
t8: 150 min	94	66
t9: 180 min	100	72

Table 5. NMR follow-up of the cyclization step. Comparison of starting material conversion and yield of product.
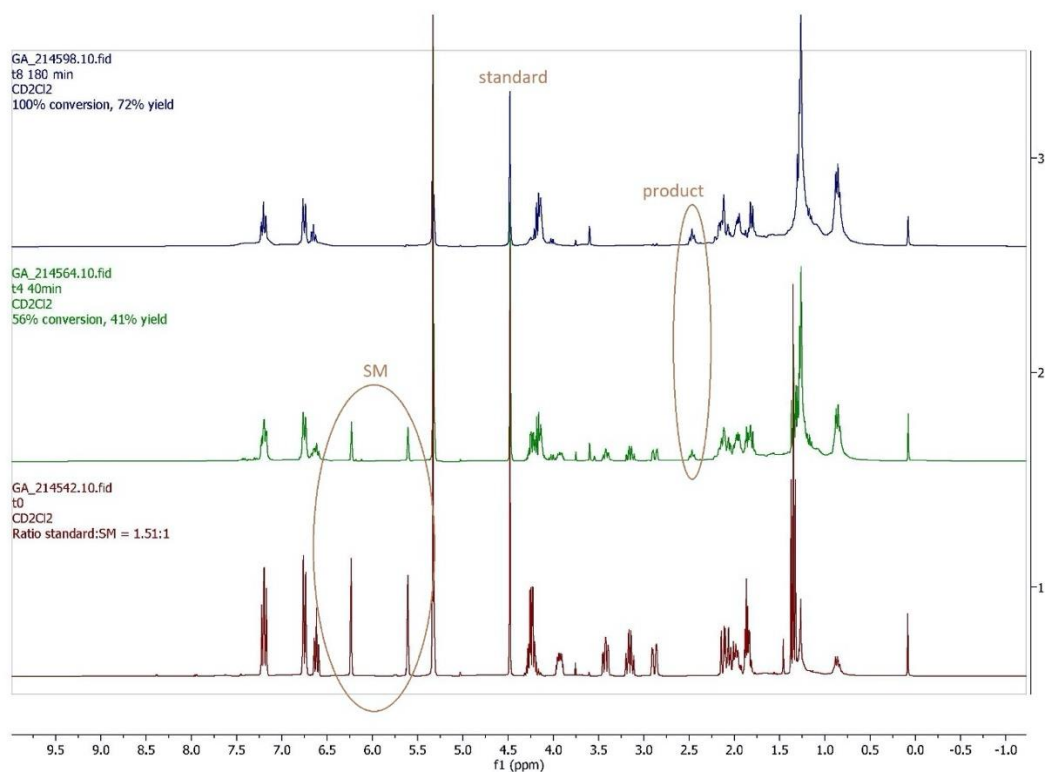
Image 1. Characteristic signals of **2a** (SM), **3a** (product), and standard (ethylene carbonate).

The ratio conversion/yield was not satisfying, and the reaction was very slow compared to the one-pot process, in which acetic acid is generated from the OAc-trap. The investigated reaction conditions are summarized in Table 6.

Entry	Deviation to general procedure D	NMR yield	Time	remarks
1	None	72%	3 h	Much slower than the one-pot process[a]
2	No catalyst	--	24 h	No product visible, degradation
4	AcOH (1.0 eq)	**91%**	**3 min**	dr 9:1[b]
5	CsPiv instead of CsOAc	Quant.	25 min	dr 5:1
6	CsPiv, AcOH (1.0 eq)	Quant.	< 2 min	dr 5:1

Table 6. NMR follow-up of the cyclization step. Optimization. [a] Major diastereoisomer only. [b] The stability of product under the reaction conditions was studied (stable, not reacting).

Batch reactions and synthesis of bicyclic compounds

The previously optimized conditions (see above) were applied on a substituted pyrrolidine derivative to study the influence of an alpha-substituent on the cyclization reaction.

R = H, 5 min, **77%**, α/β 88:12
R = Me, 30 min, **66%**, α/β 82:18
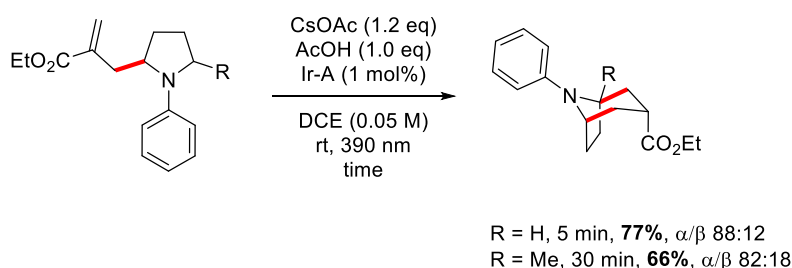
Modified General Procedure D

In an oven-dry vial were added under N_2 the mono-allylated starting material (0.20 mmol, 1.0 equiv.), [Ir{dF(CF$_3$)ppy}$_2$(dtbpy)]PF$_6$ (2.2 mg, 0.02 mmol, 1 mol%), and cesium acetate (46 mg, 0.24 mmol, 1.2 equiv.). The vial was evacuated and filled with N_2 (x 3), then CH_3CO_2H (11.4 µL, 0.20 mmol, 1.0 equiv.) and degassed 1,2-dichloroethane (4 mL, 0.05 M) were successively added. The resulting yellow solution was placed in front of a 390 nm LED and stirred until consumption of the starting material (TLC or NMR monitoring). The reaction mixture was diluted with sat. NaHCO$_3$ (3 mL). The aqueous phase was extracted with DCM (3 x 5 mL) and the combined organic phases were dried over Na$_2$SO$_4$, filtered, and concentrated under reduced pressure to give crude product as an orange oil. Purification by flash column chromatography on silica gel afforded the bicyclic product.
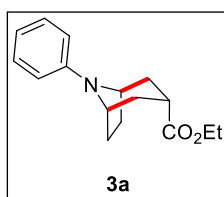
Ethyl 8-phenyl-8-azabicyclo[3.2.1]octane-3-carboxylate (3a)

Following **modified General Procedure D** with ethyl 2-[(1-phenylpyrrolidin-2-yl)methyl]prop-2-enoate **2a** (19.2 mg, 0.07 mmol), reacting for 5 minutes. Purification by flash column chromatography (SiO$_2$, heptanes/EtOAc 98:2) afforded the title compound as a white solid (14.0 mg, 0.054 mmol, 77%, α/β 88:12). Spectra in accordance with previously described product.
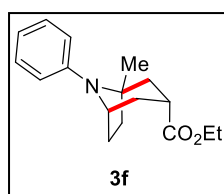
Ethyl 1-methyl-8-phenyl-8-azabicyclo[3.2.1]octane-3-carboxylate (3f)

Following **modified General Procedure D** with ethyl 2-[(5-methyl-1-phenyl-pyrrolidin-2-yl)methyl]prop-2-enoate **2f** (54.7 mg, 0.20 mmol, dr 3:1), reacting for 30 minutes. Purification by flash column chromatography (SiO$_2$, pentane/Et$_2$O 95:5) afforded the title compound as a white solid (35.8 mg, 0.13 mmol, 66%, α/β 82:18). Spectra in accordance with previously described product.
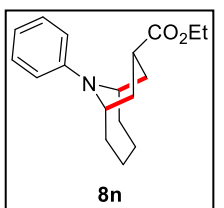
Ethyl 10-phenyl-10-azabicyclo[4.3.1]decane-8-carboxylate (8n)

Following **modified General Procedure D** with ethyl 2-[(1-phenylazepan-2-yl)methyl]prop-2-enoate **7n** (57.5 mg, 0.20 mmol), reacting for 30 minutes. Purification by flash column chromatography (SiO$_2$, pentane/Et$_2$O 99:1 to 98:2) afforded the product as a colorless oil (13.8 mg, 0.048 mmol, 24%, α/β >20:1) along with recovered starting material (5.2 mg, 9% recovered SM). Spectra in accordance with previously described product.
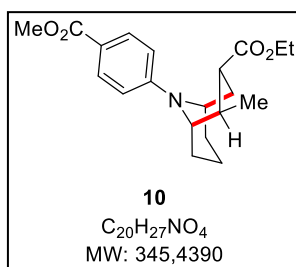
Ethyl 9-(4-methoxycarbonylphenyl)-2-methyl-9-azabicyclo[3.3.1]nonane-3-carboxylate (10)

10
C$_{20}$H$_{27}$NO$_4$
MW: 345,4390

Following **modified General Procedure D** with methyl 4-[2-[(E)-2-ethoxycarbonylbut-2-enyl]-1-piperidyl]benzoate **9** (69.1 mg, 0.20 mmol), reacting for 4 hours (NMR follow-up). Purification by flash column chromatography (SiO$_2$, pentane/Et$_2$O 80:20) afforded the product as a colorless oil (45.4 mg, 0.13 mmol, 66%, dr >20:1).

^{1}H NMR (400 MHz, CDCl$_3$): δ 7.90–7.83 (m, 2H), 6.81–6.75 (m, 2H), 4.36–4.25 (m, 1H), 4.17–4.09 (m, 2H), 3.86–3.83 (m, 1H), 3.85 (s, 3H), 2.35 (ddd, J = 13.3, 10.9, 4.3 Hz, 1H), 2.14–1.95 (m, 3H), 1.77–1.64 (m, 3H), 1.64–1.49 (m, 2H), 1.45 (ddd, J = 13.9, 4.6, 2.1 Hz, 1H), 1.24 (t, J = 7.1 Hz, 3H), 1.07 (d, J = 6.1 Hz, 3H). ^{13}C NMR (75 MHz, CDCl$_3$): δ 175.8 (C=O), 167.3 (C=O), 153.5 (Cq), 131.9 (2xCH$_{Ar}$), 117.5 (Cq), 112.4 (2xCH$_{Ar}$), 60.5 (CH$_2$), 56.5 (CH), 51.6 (CH$_3$), 46.5 (CH), 43.4 (CH), 35.9 (CH), 29.8 (CH$_2$), 29.4 (CH$_2$), 28.9 (CH$_2$), 21.8 (CH$_3$), 14.8 (CH$_2$), 14.4 (CH$_3$). FT-IR (cm^{-1}, neat): 2932, 1705, 1599, 1514, 1433, 1279, 1253, 1182, 1107, 1060, 768, 729, 697. HRMS (ESI) m/z: Calcd for C$_{19}$H$_{28}$NO$_4$ 346.2013; Found 346.2004. R$_f$ = 0.33 (pentane/Et$_2$O 80:20).

*Derivatization of **10** for crystallization:*
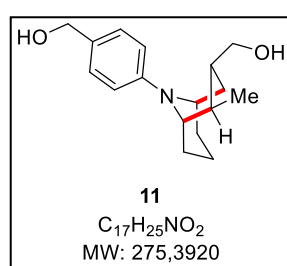
[4-[3-(hydroxymethyl)-2-methyl-9-azabicyclo[3.3.1]nonan-9-yl]phenyl]methanol (11)

11
C$_{17}$H$_{25}$NO$_2$
MW: 275,3920

In a 25 mL two-neck round-bottom flask equipped with a reflux condenser and a rubber septum were added THF (3 mL) and LiAlH$_4$ (58 mg, 1.5 mmol). A solution of **10** (0.5 mmol, 173 mg, dr > 95:5) in THF (2 mL) was added dropwise at room temperature and the reaction mixture was stirred for 1 h. Upon completion of the reaction (TLC monitoring), the reaction mixture was cooled to 0 °C and 2 M aqueous NaOH was added to the mixture dropwise until a thick white precipitate was obtained (around 1 mL was necessary). The mixture was refluxed for 1 h, allowed to cool down to room temperature and filtered, rinsing with Et$_2$O. The mother liquor was dried over Na$_2$SO$_4$, filtered and concentrated under reduced pressure. The crude residue was purified by flash column chromatography (SiO$_2$, pentane/Et$_2$O 20:80) to afford the product as a thick colorless oil (97.0 mg, 0.35 mmol, 70%). The product was crystallized by slow evaporation from a heptanes/EtOAc or pentane/Et$_2$O mixture to give a white crystalline solid suitable for X-Ray analysis. Note that the product is not stable in CDCl$_3$.

^{1}H NMR (400 MHz, C$_6$D$_6$): 7.19 (d, J = 8.7 Hz, 2H), 6.75 (d, J = 8.7 Hz, 2H), 4.43 (s, 2H), 4.02–3.92 (m, 1H), 3.59–3.54 (m, 1H), 3.32–3.22 (m, 2H), 1.98 (ddd, J = 12.2, 10.8, 4.3 Hz, 1H), 1.78 (qt, J = 13.1, 4.3 Hz, 1H), 1.64–1.56 (m, 2H), 1.45–1.08 (m, 6H), 0.90 (d, J = 6.8 Hz, 3H). ^{13}C NMR (101 MHz, C$_6$D$_6$): δ 150.8 (Cq), 129.8 (Cq), 129.1 (2xCH$_{Ar}$), 114.3 (2xCH$_{Ar}$), 65.3 (CH$_2$), 64.6 (CH$_2$), 57.8 (CH), 47.2 (CH), 38.4 (CH), 34.9 (CH), 30.28 (CH$_2$), 29.4 (CH$_2$), 29.3 (CH$_2$), 21.6 (CH$_3$), 15.2 (CH$_2$). FT-IR (cm^{-1}, neat): 3319, 2916, 2865, 1611, 1512, 1398, 1287, 1256, 1187, 999, 793. HRMS (ESI) m/z: [M+H]$^+$ Calcd for C$_{17}$H$_{26}$NO$_2$ 276.1958. Found 276.1932. Mp 101.5–103.2 °C. R$_f$ = 0.29 (heptanes/EtOAc 55:45).

X-Ray:
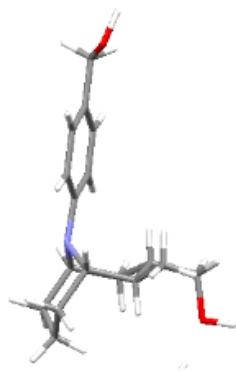
Synthetic utility of the bicyclic derivatives

Oxidation of the BPin derivative

8j
α/β > 20:1

NaBO$_2$.H$_2$O$_2$.3H$_2$O (5 eq)

THF:H$_2$O (v/v 1:1)
rt, 1 h

C$_{17}$H$_{23}$NO$_3$
289,3750

NaH (1.2 eq)
MeI (2x 1.2 eq)
THF, rt, 4 h

8e
64%, 2 steps,
α/β > 20:1
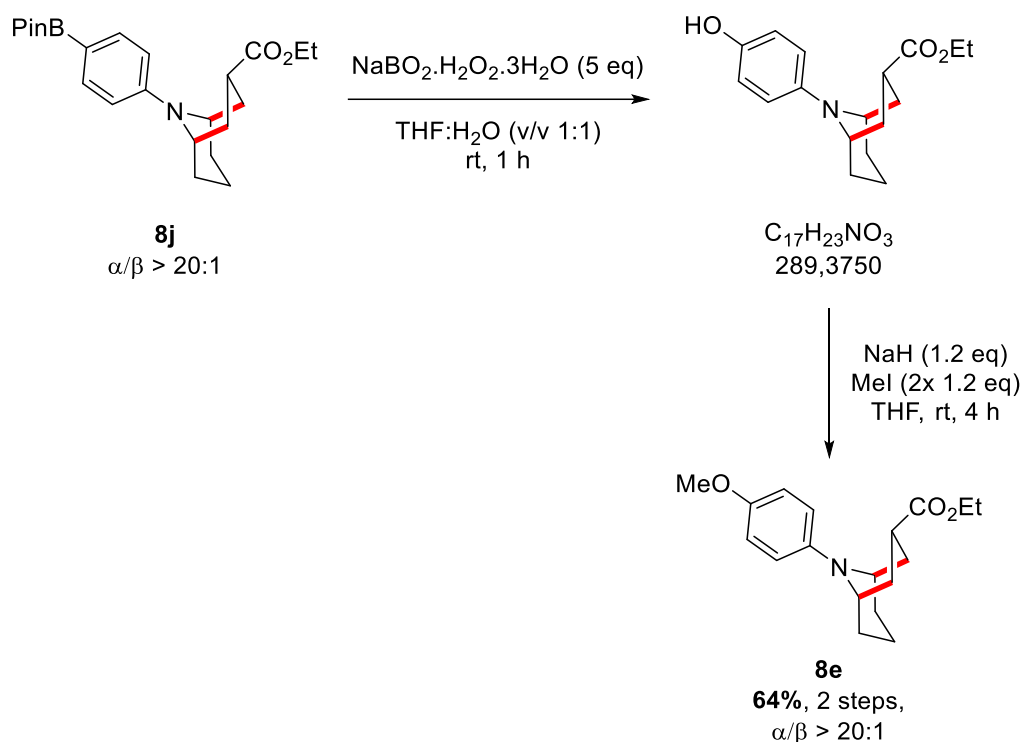
Ethyl 9-(4-hydroxyphenyl)-9-azabicyclo[3.3.1]nonane-3-carboxylate.

To a suspension of ethyl 9-[4-(4,4,5,5-tetramethyl-1,3,2-dioxaborolan-2-yl)phenyl]-9-azabicyclo[3.3.1]nonane-3-carboxylate **8j** (120 mg, 0.30 mmol) in THF/H$_2$O (2.5 mL, v/v 1:1) was added sodium perborate (231 mg, 1.50 mmol) in one portion. The reaction mixture gradually turned bright pink. Upon completion (TLC monitoring, approx. 1h), the reaction mixture was quenched by addition of saturated aq. NH$_4$Cl (10 mL). The aqueous layer was extracted with Et$_2$O (3 x 10 mL) and the combined organic extracts were dried over Na$_2$SO$_4$, filtered and concentrated in vacuo. The crude

residue was purified by flash column chromatography (SiO$_2$, pentane/Et$_2$O 70:30) to afford the ethyl 9-(4-hydroxyphenyl)-9-azabicyclo[3.3.1]nonane-3-carboxylate intermediate as a pink sticky oil, from which the residual solvents proved to be difficult to remove. Additionally, extreme broadening of the signals was observed in the NMR spectra (^{1}H and ^{13}C), hence it could not be directly characterized, and solvent could not be quantified.

Partial characterization of ethyl 9-(4-hydroxyphenyl)-9-azabicyclo[3.3.1]nonane-3-carboxylate:

FT-IR (neat, cm^{-1}): 3388, 2927, 1725, 1701, 1507, 1246, 1178, 908, 811, 729. HRMS (ESI) m/z: [M+H]$^+$ Calcd for C$_{17}$H$_{24}$O$_3$N 290.1751; Found 290.1746.

The structure of this compound was assessed after methylation to form known compound **8e** according to the following procedure:

Ethyl 9-(4-methoxyphenyl)-9-azabicyclo[3.3.1]nonane-3-carboxylate (8e). In an oven-dried seal tube was added THF (4 mL) followed by NaH (12.9 mg, 0.34 mmol, 55–60 % in mineral oil). Then, a solution of ethyl 9-(4-hydroxyphenyl)-9-azabicyclo[3.3.1]nonane-3-carboxylate previously obtained (estimated quantitative yield, 0.3 mmol engaged) in THF (4 mL, pink solution) was added dropwise. The mixture became dark green/blue and was stirred at rt for 20 minutes before addition of iodomethane (21 µL, 0.34 mmol). The reaction mixture was stirred at rt for 3 hours without reaching completion, hence another portion of iodomethane (21 µL, 0.34 mmol) was added. Approximately 2 hours after the second addition, the starting material was fully converted. The reaction mixture was quenched with water (5 mL) and extracted with EtOAc (2 x 10 mL). The organic extract was washed with brine (10 mL), dried over Na$_2$SO$_4$, and concentrated in vacuo. Purification by flash column chromatography (SiO$_2$, pentane/Et$_2$O 90:10) afforded the product as a crystalline white solid (57.9 mg, 0.19 mmol, 64% over two steps. α/β >20:1). Spectral data are in accordance with previously described product.

^{1}H NMR (300 MHz, CDCl$_3$): δ 6.80 (s, 4H), 4.17–4.10 (m, 2H), 4.10 (q, J = 7.1 Hz, 2H), 3.75 (s, 3H), 2.47 (tt, J = 12.4, 5.9 Hz, 1H), 2.42–2.26 (m, 2H), 2.00 (qt, J = 13.3, 4.4 Hz, 1H), 1.79 (tt, J = 13.2, 4.3 Hz, 2H), 1.65 (ddd, J = 14.0, 12.3, 3.5 Hz, 2H), 1.58–1.49 (m, 1H), 1.49–1.39 (m, 2H), 1.23 (t, J = 7.1 Hz, 3H). ^{13}C NMR (101 MHz, CDCl$_3$): δ 176.1 (C=O), 151.6 (Cq), 145.3 (Cq), 115.7 (2xCH$_{Ar}$), 115.1 (2xCH$_{Ar}$), 60.4 (CH$_2$), 55.9 (CH$_3$), 47.8 (2xCH), 34.7 (CH), 30.6 (2xCH$_2$), 28.4 (2xCH$_2$), 14.4 (CH$_3$), 14.3 (CH$_2$). FT-IR (cm^{-1}, neat): 2870, 1726, 1507, 1241, 1177, 1039, 910, 812, 731, 616. HRMS (ESI) m/z: [M+H]$^+$ Calcd for C$_{18}$H$_{26}$NO$_3$ 304.1907; Found 304.1899. Mp 42.5–43.7 °C. R$_f$ = 0.31 (pentane/Et$_2$O 90:10).

Epimerization (from the α to the β diastereoisomer)
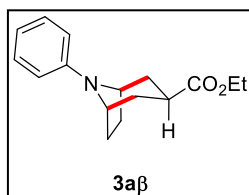
Ethyl 8-phenyl-8-azabicyclo[3.2.1]octane-3-carboxylate (3aβ, *exo* product):

To a solution of ethyl 8-phenyl-8-azabicyclo[3.2.1]octane-3-carboxylate **3aα** (α/β 5:1, 130 mg, 0.50 mmol) in absolute ethanol (4 mL) was added dropwise a solution of NaOEt in EtOH (2.7 M, 0.20 mL, 0.54 mmol).The reaction mixture was heated at 40 °C for 3 hours. TLC indicated complete epimerization and volatiles were evaporated under reduced pressure. The crude residue was purified by flash column chromatography (SiO$_2$, heptanes/EtOAc 90:10) to afford the desired product as a light yellow crystalline solid (61.7 mg, 0.40 mmol, 79%, α/β 1:20).

^{1}H NMR (300 MHz, CDCl$_3$): δ 7.25–7.19 (m, 2H), 6.77 (d, J = 8.1 Hz, 2H), 6.70 (tt, J = 7.3, 1.1 Hz, 1H), 4.32–4.25 (m, 2H), 4.05 (q, J = 7.1 Hz, 2H), 2.89 (tt, $J_{ax\text{-}ax}$ = 12.3, $J_{ax\text{-}eq}$ = 5.3 Hz, 1H, -CH-CO$_2$Et), 2.16–2.07 (m, 2H), 2.07–1.97 (m, 2H), 1.85–1.75 (m, 2H), 1.64 (ddd, J = 13.8, 6.0, 2.9 Hz, 2H), 1.20 (t, J = 7.2 Hz, 3H). ^{13}C NMR (75 MHz, CDCl$_3$): δ 175.1 (C=O), 146.2 (Cq), 129.7 (2xCH$_{Ar}$), 117.2 (CH$_{Ar}$), 115.2 (2xCH$_{Ar}$), 60.5 (CH$_2$), 53.7 (2xCH), 35.5 (CH-CO$_2$Et), 29.3 (2xCH$_2$), 28.3 (2xCH$_2$), 14.3 (CH$_3$). FT-IR (cm^{-1}, neat): 2957, 1722, 1597, 1501, 1365, 1179, 1045, 937, 754, 694, 583. HRMS (ESI) m/z: [M+H]$^+$ Calcd for C$_{16}$H$_{22}$NO$_2$ 260.1645; Found 260.1642. Mp 71.5–73.1 °C. R$_f$ = 0.22 (pentane/Et$_2$O 96:4).

Ethyl 9-phenyl-9-azabicyclo[3.3.1]nonane-3-carboxylate (8aβ, exo product)

To a solution of ethyl 9-phenyl-9-azabicyclo[3.3.1]nonane-3-carboxylate **8aα** (α/β >20:1, 122 mg, 0.45 mmol) in absolute ethanol (4 mL) was added dropwise a solution of NaOEt in EtOH (2.7 M, 0.17 mL, 0.46 mmol). The reaction mixture was stirred at rt for 1 hour and, in absence of epimerization, for 3 hours at 40 °C. TLC indicated complete epimerization and volatiles were evaporated under reduced pressure. The crude residue was purified by flash column chromatography (SiO$_2$, pentane/Et$_2$O 94:6) to afford the desired product as a white crystalline solid (92.7 mg, 0.34 mmol, 76%, α/β 1:8). For easier characterization of the β product, the diastereoisomers were separated by flash column chromatography (SiO$_2$, pentane/Et$_2$O 95:5).

Characterization of the β diastereoisomer:

^{1}H NMR (300 MHz, CDCl$_3$): δ 7.29–7.17 (m, 2H), 6.84 (d, J = 8.3 Hz, 2H), 6.68 (t, J = 7.2 Hz, 1H), 4.18–4.03 (m, 4H), 3.32 (tt, $J_{ax\text{-}ax}$ = 12.1, $J_{ax\text{-}eq}$ = 5.7 Hz, 1H, -CH-CO$_2$Et), 2.20–1.98 (m, 5H), 1.93 (ddd, J = 13.9, 5.7, 2.0 Hz, 2H), 1.76–1.62 (m, 3H), 1.23 (t, J = 7.1 Hz, 3H). ^{13}C NMR (75 MHz, CDCl$_3$): δ 175.5 (C=O),

148.7 (C$_q$), 129.6 (2xCH$_{Ar}$), 116.9 (CH$_{Ar}$), 114.0 (2xCH$_{Ar}$), 60.5 (CH$_2$), 48.0 (2xCH), 37.8 ($\underline{C}$H-CO$_2$Et), 31.0 (2xCH$_2$), 27.9 (2xCH$_2$), 20.4 (CH$_2$), 14.4 (CH$_3$). FT-IR (cm^{-1}, neat): 2935, 1725, 1592, 1500, 1189, 1111, 1036, 908, 746, 689. HRMS (ESI) m/z: [M+H]$^+$ Calcd for C$_{17}$H$_{24}$NO$_2$ 274.1802; Found 274.1800. Mp 74.4–75.0 °C. R$_f$ = 0.25 (pentane/Et$_2$O 94:6).

Deprotection of the aryl moiety

General procedure E: deprotection of the aryl moiety[23]

To a solution of *N*-aryl precursor (0.20 mmol) in MeCN/H$_2$O (12 mL, v/v 3:1) was added cerium ammonium nitrate (329 mg, 0.60 mmol) at 0 °C. The resulting clear yellow solution was stirred at rt overnight. Upon completion of the reaction, NaBH$_4$ (11.3 mg, 0.30 mmol) was added in one portion at 0 °C. *This should be done carefully as NaBH$_4$ can react violently under the aqueous acidic conditions of the reaction mixture*. After addition, the reaction mixture was stirred at rt for 30 min and TLC indicated full reduction of the quinone by-product. K$_2$CO$_3$ (powder, ~800 mg, 6.00 mmol) was added to the reaction mixture until pH = 11. At this point the reaction mixture was a dark red solution with a white precipitate on the bottom of the flask, however stirring was not prevented. An excess of benzyl chloroformate (Cbz-Cl) (0.14 mL, 1.0 mmol) was then added and the reaction mixture was stirred at rt for 2 h. The reaction mixture was transferred to a separatory funnel filtrating the white precipitate over cotton and rinsing with Et$_2$O. Water (15 mL) was added and the mixture extracted with Et$_2$O (3 x 15 mL). The combined organic phases were washed with aq. sat. Na$_2$CO$_3$ (1 x 15 mL) and brine (1 x 15 mL), dried over anhydrous Na$_2$SO$_4$ and the solvent was removed in vacuo to give a dark red liquid. Flash column chromatography on silica gel afforded the desired products.
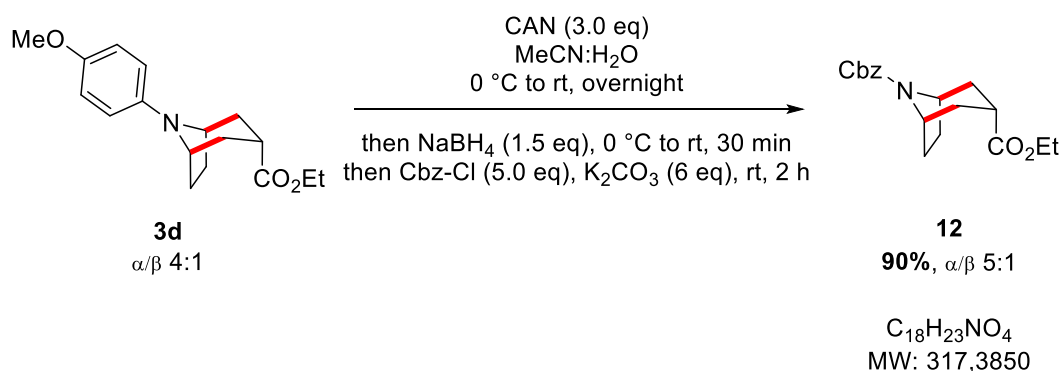
O8-benzyl O3-ethyl 8-azabicyclo[3.2.1]octane-3,8-dicarboxylate (12)

The title product was prepared following **General Procedure E** with ethyl 8-(4-methoxyphenyl)-8-azabicyclo[3.2.1]octane-3-carboxylate **3d** (57.9 mg, 0.20 mmol, α/β 4:1). Flash column

chromatography (SiO$_2$, pentane/Et$_2$O 90:10 to 80:20) afforded the desired product as a pale-yellow oil (57.0 mg, 0.18 mmol, 90%, α/β 5:1).

Characterization of the α diastereoisomer at 25 °C:

^{1}H NMR (300 MHz, CDCl$_3$, **25 °C**): δ 7.43–7.27 (m, 5H), 5.14 (s, 2H), 4.26 (br m, 2H), 4.19 (q, *J* = 7.1 Hz, 2H), 2.61 (tt, *J*$_{ax–eq}$ = 8.1, *J*$_{eq–eq}$ = 1.4 Hz, 1H, -C$\underline{H}$-CO$_2$Et), 2.29 (dq, J = 14.6, 1.4 Hz, 2H), 2.21–1.58 (m, 6H, br signals), 1.28 (t, *J* = 7.1 Hz, 3H). ^{13}C NMR (75 MHz, CDCl$_3$, **25 °C**): δ 175.7 (C=O), 153.5 (C=O), 137.1 (Cq), 128.6 (2xCH$_{Ar}$), 128.03 (CH$_{Ar}$), 127.94 (2xCH$_{Ar}$), 66.7 (CH$_2$), 61.1 (CH$_2$), 53.0 (2xCH), 34.2 (CH), 31.3 (CH$_2$, br signal), 30.7 (CH$_2$, br signal), 27.4 (CH$_2$, br signal), 26.6 (CH$_2$, br signal), 14.3 (CH$_3$).

Characteristic peaks of the β diastereoisomer at 25 °C:

^{1}H NMR (300 MHz, CDCl$_3$, **25 °C**): δ 7.43–7.27 (m, 5H), 5.14 (s, 2H), 4.37 (br m, 2H), 4.11 (q, *J* = 7.2 Hz, 2H), 2.81 (tt, *J*$_{ax–ax}$ = 11.8, *J*$_{ax–eq}$ = 5.6 Hz, 1H, -C$\underline{H}$-CO$_2$Et), 1.22 (t, *J* = 7.1 Hz, 3H). ^{13}C NMR (75 MHz, CDCl$_3$, **25 °C**): δ 174.8 (C=O), 137.0 (Cq), 66.9 (CH$_2$), 60.7 (CH$_2$), 53.2 (CH), 34.9 (CH).

FT-IR (neat, cm^{-1}): 2961, 1723, 1695, 1414, 1300, 1183, 1095, 1068, 1044, 729, 696. HRMS (ESI) m/z: [M+Na]$^+$ Calcd for C$_{18}$H$_{23}$O$_4$NNa 340.1519; Found 340.1514. R$_f$ = 0.33 (pentane/Et$_2$O 3:1).

Note: an NMR measured in C$_6$D$_6$ at 70 °C showed that free rotation around the C-N bond was still not fully achieved, hence extreme broadening of the signals was observed.

In order to obtain well defined signals, several measurements were made from 25 °C to –45 °C in CDCl$_3$. At –45 °C the rotation around the C-N bond was fully impaired and well-defined NMR spectra could be recorded (^{1}H, ^{13}C, HSQC, COSY):

Characterization of the α diastereoisomer at –45 °C:

^{1}H NMR (400 MHz, CDCl$_3$, **–45 °C**): δ 7.48–7.28 (m, 5H), 5.27–5.02 (m, 2H), 4.28–4.24 (m, 1H), 4.24–4.20 (m, 1H), 4.17 (q, *J* = 7.2 Hz, 2H), 2.63 (t, *J*$_{ax-eq}$ = 7.8 Hz, 1H, -C$\underline{H}$-CO$_2$Et), 2.30 (ddd, *J* = 14.1, 7.0, 2.3 Hz, 2H), 2.07 (ddd, *J* = 14.3, 8.0, 3.3 Hz, 1H), 2.03–1.53 (m, 5H), 1.28 (t, *J* = 7.1 Hz, 3H). ^{13}C NMR (101 MHz, CDCl$_3$, **–45 °C**): δ 175.7 (C=O), 153.1 (C=O), 136.5 (Cq), 128.5 (2xCH$_{Ar}$), 128.0 (CH$_{Ar}$), 127.9 (2xCH$_{Ar}$), 66.6 (CH$_2$), 61.2 (CH$_2$), 52.6 (CH), 52.5 (CH), 33.8 (CH), 30.8 (CH$_2$), 30.3 (CH$_2$), 27.0 (CH$_2$), 26.2 (CH$_2$), 14.20 (CH$_3$).

Characteristic peaks of the β diastereoisomer at –45 °C:

^{1}H NMR (400 MHz, CDCl$_3$, **–45 °C**): δ 7.48–7.28 (m, 5H), 4.39–4.35 (m, 1H), 4.34–4.29 (m, 1H), 4.08 (q, *J* = 7.2 Hz, 2H), 2.81 (tt, *J*$_{ax-ax}$ = 11.9, *J*$_{ax-eq}$ = 5.5 Hz, 1H, -C$\underline{H}$-CO$_2$Et), 1.23 (t, *J* = 7.2 Hz, 3H). ^{13}C NMR (101 MHz, CDCl$_3$, **–45 °C**): δ 175.1 (C=O), 136.4, 127.94, 66.7 (CH$_2$), 60.8 (CH$_2$), 52.8 (CH), 52.7 (CH), 34.5 (CH), 33.4 (CH$_2$), 32.9 (CH$_2$), 28.2 (CH$_2$), 27.4 (CH$_2$), 14.18 (CH$_3$).

8e
α/β > 20:1

CAN (3.0 eq)
MeCN:H₂O
0 °C to rt, overnight

then NaBH₄ (1.5 eq), 0 °C to rt, 30 min
then Cbz-Cl (5.0 eq), K₂CO₃ (6 eq), rt, 1 h

13
80%, α/β > 20:1

$C_{19}H_{25}NO_4$
MW: 331,4120

8j
α/β > 20:1

$NaBO_2 \cdot H_2O_2 \cdot 3H_2O$ (5 eq)

THF:H₂O (v/v 1:1)
rt, 1 h

CAN (3.0 eq), MeCN:H₂O
then NaBH₄ (1.5 eq)
then Cbz-Cl (5.0 eq), K₂CO₃ (6 eq)

13
71%, 2 steps,
α/β > 20:1

O9-benzyl O3-ethyl 9-azabicyclo[3.3.1]nonane-3,9-dicarboxylate (13) from the PMP-derivative (8e)

The title compound was prepared following **General Procedure E** with ethyl 9-(4-methoxyphenyl)-9-azabicyclo[3.3.1]nonane-3-carboxylate **8e** (60.7 mg, 0.20 mmol, α/β >20:1). Flash column chromatography (SiO₂, pentane/Et₂O 90:10 to 80:20) afforded the desired product as a pale-yellow oil (53.1 mg, 0.16 mmol, 80%, α/β >20:1).

O9-benzyl O3-ethyl 9-azabicyclo[3.3.1]nonane-3,9-dicarboxylate (13) from the BPin-derivative (8j)

To a suspension of ethyl-9-[4-(4,4,5,5-tetramethyl-1,3,2-dioxaborolan-2-yl)phenyl]-9-azabicyclo[3.3.1]nonane-3-carboxylate **8j** (79.9 mg, 0.20 mmol, α/β >20:1) in THF/H$_2$O (2 mL, v/v 1:1) was added sodium perborate (154 mg, 1.0 mmol) in 1 portion. The reaction mixture gradually turned bright pink. Upon completion (TLC monitoring, ca. 1h), the mixture was quenched by addition of sat. aq. NH$_4$Cl (10 mL). The aqueous layer was extracted with Et$_2$O (3 x 10 mL) and the combined organic extracts were dried over Na$_2$SO$_4$, filtered and concentrated in vacuo. The crude residue was engaged in the deprotection sequence following **General Procedure E**. Flash column chromatography (SiO$_2$, pentane/Et$_2$O 90:10 to 80:20) afforded the desired product as a pale-yellow oil (47.0 mg, 0.14 mmol, 71%, α/β >20:1).

Characterization of the α diastereoisomer (fully impaired rotation at 25 °C):

^{1}H NMR (400 MHz, CDCl$_3$): δ 7.42–7.27 (m, 5H), 5.19–5.07 (m, 2H), 4.59–4.51 (m, 1H), 4.51–4.44 (m, 1H), 4.12 (q, J = 7.1 Hz, 2H), 2.35–2.19 (m, 3H), 1.92 (qt, J = 13.2, 4.4 Hz, 1H), 1.73–1.52 (m, 5H), 1.52–1.38 (m, 2H), 1.24 (t, J = 7.1 Hz, 3H). ^{13}C NMR (75 MHz, CDCl$_3$): δ 175.3 (C=O), 155.3 (C=O), 137.1 (Cq), 128.6 (2xCH$_{Ar}$), 128.1 (CH$_{Ar}$), 127.8 (2xCH$_{Ar}$), 67.1 (CH$_2$), 60.6 (CH$_2$), 45.2 (CH), 44.7 (CH), 35.6 (CH), 30.9 (CH$_2$), 30.5 (CH$_2$), 28.5 (CH$_2$), 28.3 (CH$_2$), 14.3 (CH$_3$), 13.9 (CH$_2$). FT-IR (neat, cm^{-1}): 2931, 1728, 1689, 1423, 1323, 1300, 1248, 1176, 1087, 1048, 696. HRMS (ESI) m/z: [M+H]$^+$ Calcd for C$_{19}$H$_{26}$NO$_4$ 332.1856; Found 332.1854. R$_f$ = 0.30 (heptanes/EtOAc 80:20).

Characteristic peak of the β diastereoisomer:

^{1}H NMR (400 MHz, CDCl$_3$): δ 3.23 (tt, J$_{ax\text{-}ax}$ = 11.8, J$_{ax\text{-}eq}$ = 6.4 Hz, 1H, -CH-CO$_2$Et).

Note: an NMR measured in C$_6$D$_6$ at 70 °C showed that free rotation around the C-N bond was still not fully achieved and peak broadening of the signals was observed. Hence the product was characterized at room temperature in CDCl$_3$.
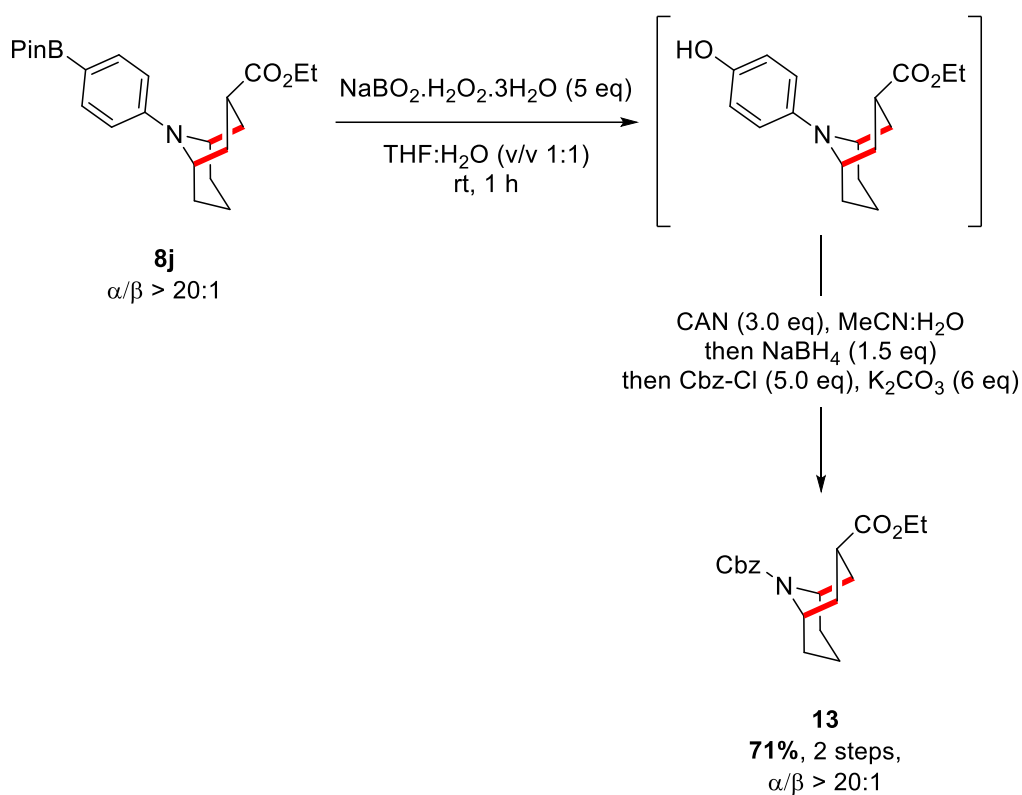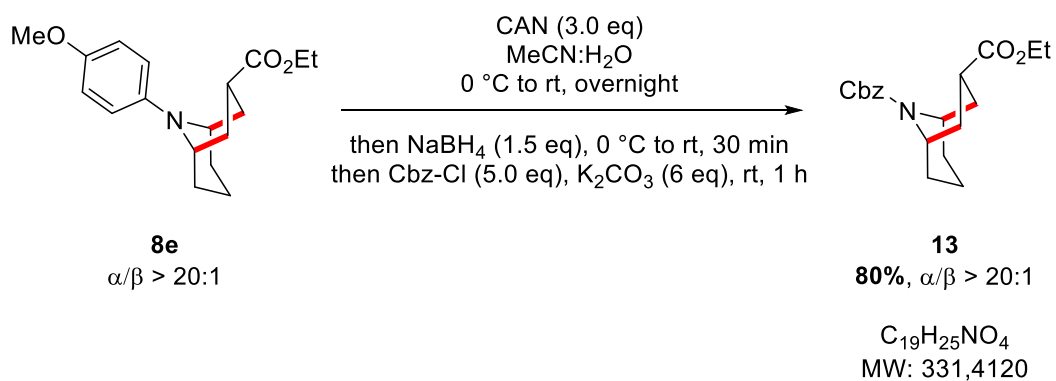
Characterization of side-products

Note that these procedures are not optimized procedures. The goal of these experiments was to characterize possible non-desired products for a better optimization of the desired pathway for the model reaction.

Bis-allylated product

4a
$C_{22}H_{29}NO_4$
MW: 371,4770
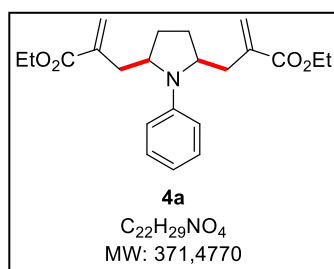
Ethyl 2-[[5-(2-ethoxycarbonylallyl)-1-phenyl-pyrrolidin-2-yl]methyl]prop-2-enoate (4a)

In an oven-dried vial were added under N_2 ethyl 2-(benzenesulfonylmethyl)prop-2-enoate (153 mg, 0.60 mmol. 3.0 eq.), [Ir{dF(CF$_3$)ppy}$_2$(dtbpy)]PF$_6$ (4.5 mg, 0.04 mmol), and cesium acetate (76.8 mg, 0.400 mmol). The vial was evacuated and refilled with nitrogen (x 3), and 1-phenylpyrrolidine **1a** (0.029 mL, 0.20 mmol) was added *via* a Hamilton syringe. Degassed 1,2-dichloroethane (2.00 mL) was added and the mixture was placed in front of a 390 nm LED and stirred for 2h30. The reaction mixture was diluted with sat. NaHCO$_3$ (3 mL). The aqueous phase was extracted with DCM (3 x 5 mL) and the combined organic phases were dried over Na$_2$SO$_4$, filtered, and concentrated under reduced pressure to give crude product as an orange oil. Purification by flash column chromatography (SiO$_2$, heptanes/EtOAc 95:5) afforded the title compound as a colorless oil (22.4 mg, 0.06 mmol, 30%, dr 4:1, *cis*/*trans* relationship not assigned).

^{1}H NMR (300 MHz, CDCl$_3$): δ 7.32–7.21 (m, 2H, major+minor), 7.02–6.92 (m, 2H, major), 6.80–6.62 (m, 1H, major+minor, and 2H, minor), 6.29–6.23 (m, 2H, major+minor), 5.66–5.62 (m, 2H, minor), 5.56 (q, *J* = 1.1 Hz, 2H, major), 4.32–4.20 (m, 4H, major+minor), 4.09 (ddt, *J* = 10.0, 6.8, 3.6 Hz, 2H, major), 3.97–3.87 (m, 2H, minor), 3.08 (ddd, *J* = 13.3, 3.4, 1.1 Hz, 2H, minor), 2.98 (d, *J* = 13.7 Hz, 2H, major), 2.15 (dd, *J* = 13.6, 10.3 Hz, 2H, minor), 2.06–1.75 (m, 6H, major+minor), 1.375 (t, *J* = 7.2 Hz, 6H, major), 1.370 (t, *J* = 7.2 Hz, 6H, minor). ^{13}C NMR (75 MHz, CDCl$_3$): δ 167.3 (major+minor), 147.5 (minor), 144.8 (major), 138.8 (major), 138.5 (minor), 129.4 (major), 129.3 (minor), 127.7 (major), 127.6 (minor), 116.2 (minor), 115.6 (major), 114.0 (major), 112.5 (minor), 61.08 (minor), 61.05 (major), 59.4 (minor), 56.7 (major), 38.1 (minor), 33.9 (major), 28.3 (minor), 26.0 (major), 14.4 (major+minor). FT-IR (cm^{-1}, neat): 2972, 2900, 1708, 1596, 1503, 1360, 1179, 1151, 745, 698. HRMS (ESI) m/z: [M+H]$^+$ Calcd for $C_{22}H_{30}NO_4$ 372.2169; Found 372.2159. R$_f$ = 0.37 (heptanes/EtOAc 80:20).

Cyclized bis-allylated product
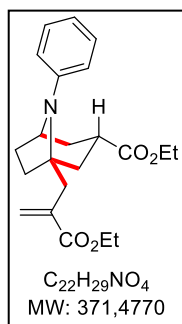
Ethyl 1-(2-ethoxycarbonylallyl)-8-phenyl-8-azabicyclo[3.2.1]octane-3-carboxylate

$C_{22}H_{29}NO_4$
MW: 371,4770

Into an oven-dry vial were added under N_2 ethyl 2-[[5-(2-ethoxycarbonylallyl)-1-phenyl-pyrrolidin-2-yl]methyl]prop-2-enoate **4a** (23 mg, 0.06 mmol), [Ir{dF(CF$_3$)ppy}$_2$(dtbpy)]PF$_6$ (1.4 mg, 2 mol%), and cesium acetate (23 mg, 0.12 mmol). The vial was evacuated and filled with nitrogen (x 3). Degassed 1,2-dichloroethane (1.00 mL) was added. The resulting yellow solution was placed in front of a 390 nm LED and stirred for 40 min. The reaction mixture was diluted with sat. NaHCO$_3$ (3 mL). The aqueous phase was extracted with DCM (3 x 3 mL) and the combined organic phases were dried over Na$_2$SO$_4$, filtered, and concentrated under reduced pressure to give crude product as an orange oil. Purification by flash column chromatography (neutral Alox, 100% heptanes to heptanes/EtOAc 99:1–97:3) afforded a first fraction containing the major diastereoisomer (3.0 mg) and a second fraction containing both diastereoisomers (5.4 mg, α/β 4:1), both as colorless oils (m$_{tot}$ = 8.4 mg, 0.022 mmol, 37%, α/β 85:15). Only the major diastereoisomer was characterized.

^{1}H NMR (300 MHz, CDCl$_3$): δ 7.22 (t, *J* = 7.8 Hz, 2H), 7.07 (d, *J* = 8.1 Hz, 2H), 6.82 (t, *J* = 7.2 Hz, 1H), 6.22 (d, *J* = 1.6 Hz, 1H), 5.72 (d, *J* = 1.6 Hz, 1H), 4.26–4.12 (m, 5H), 3.13 (d, *J* = 15.1 Hz, 1H), 2.70–2.57 (m, 2H), 2.39 (dd, *J* = 14.2, 8.4 Hz, 1H), 2.20 (d, *J* = 14.0 Hz, 2H), 2.09–2.01 (m, 2H), 2.00–1.84 (m, 1H), 1.84–1.73 (m, 1H), 1.71–1.60 (m, 1H), 1.30 (t, *J* = 7.1 Hz, 3H), 1.28 (t, *J* = 7.1 Hz, 3H). ^{13}C NMR (101 MHz, CDCl$_3$): δ 176.2 (C=O), 168.0 (C=O), 147.3 (Cq), 137.1 (Cq), 129.1 (2xCH$_{Ar}$), 127.8 (=CH$_2$), 120.6 (2xCH$_{Ar}$), 119.5 (CH$_{Ar}$), 62.6 (Cq), 61.0 (CH$_2$), 60.6 (CH), 38.9 (CH$_2$), 35.4 (CH), 34.9 (CH$_2$), 31.7 (CH$_2$), 29.9 (CH$_2$), 27.3 (CH$_2$), 25.7 (CH$_2$), 14.36 (CH$_3$), 14.32 (CH$_3$). FT-IR (cm^{-1}, neat): 2978, 1715, 1596, 1493, 1370, 1238, 1180, 1087, 1046, 1027, 753, 696. HRMS (ESI) m/z: [M+H]$^+$ Calcd for C$_{22}$H$_{30}$NO$_4$ 372.2169; Found 372.2156. R$_f$ = 0.34 (SiO$_2$, heptanes/EtOAc 85:15).

Phenylpyrrolidine reacted on mono-allylated intermediate
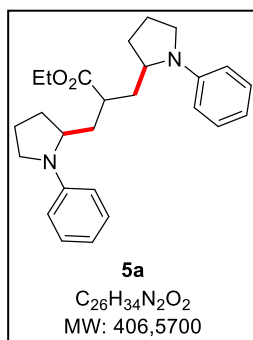
Ethyl 3-(1-phenylpyrrolidin-2-yl)-2-[(1-phenylpyrrolidin-2-yl)methyl]propanoate (5a)

5a
$C_{26}H_{34}N_2O_2$
MW: 406,5700

In an oven-dried vial were added under N_2 ethyl 2-(benzenesulfonylmethyl)prop-2-enoate (50.9 mg, 0.20 mmol), Ir(dtbbpy)(ppy)$_2$]PF$_6$ (3.7 mg, 0.004 mmol), and cesium acetate (46.1 mg, 0.24 mmol). The vial was evacuated and filled with nitrogen (x 3), and 1-phenylpyrrolidine (0.057 mL, 0.40 mmol) was added via a syringe. 1,2-dichloroethane (2.00 mL) was

added. The resulting yellow solution was placed in front of a 390 nm LED and stirred for 16 h. The reaction mixture was diluted with sat. NaHCO$_3$ (5 mL) and the phase were separated. The aqueous phase was extracted with DCM (3 x 5 mL) and the combined organic phases were dried over Na$_2$SO$_4$, filtered, and concentrated under reduced pressure to give the crude product as an orange oil. Purification by flash column chromatography (neutral Alox, heptanes/EtOAc 100:0 to 99:1) afforded the title compound as a colorless oil (22.9 mg, 0.056 mmol, 28%, dr n.d.).

^{1}H NMR (400 MHz, CDCl$_3$): δ 7.25–7.20 (m, 4H, 3 diastereoisomers), 6.69–6.63 (m, 6H, 3 diastereoisomers), 4.33 (q, J = 7.1 Hz, 2H, 1 diastereoisomer), 4.20–4.11 (m, 1H, 1 diastereoisomer), 4.05 (dq, J = 10.4, 6.9 Hz, 1H, 1 diastereoisomer), 3.85 (q, J = 7.1 Hz, 2H, 1 diastereoisomer), 3.82–3.77 (m, 1H, 3 diastereoisomers), 3.65–3.58 (m, 1H, 3 diastereoisomers), 3.46–3.37 (m, 2H, 3 diastereoisomers), 3.19–3.10 (m, 2H, 3 diastereoisomers), 2.44–2.52 (m, 1H, 3 diastereoisomers), 2.26–1.26 (m, 12H, 3 diastereoisomers), 1.41 (t, J = 7.1 Hz, 3H, 1 diastereoisomers), 1.24 (t, J = 7.2 Hz, 3H, 1 diastereoisomers), 1.04 (t, J = 7.2 Hz, 3H, 1 diastereoisomers).

^{13}C NMR (101 MHz, CDCl$_3$): δ 175.4 (C=O, 3 diasteroisomers), 147.3 (Cq, 3 diasteroisomers), 129.4, 115.90, 115.83, 112.14, 112.03, 111.99, 60.9 (CH$_2$, 1 diasteroisomer), 60.8 (CH$_2$, 1 diasteroisomer), 60.6 (CH$_2$, 1 diasteroisomer), 56.8 (3x2CH, 3 diasteroisomers), 48.8 (2CH$_2$, 1 diasteroisomer), 48.54 (2CH$_2$, 1 diasteroisomer), 48.47 (2CH$_2$, 1 diasteroisomer), 41.44 (CH, 1 diasteroisomer), 41.32 (CH, 1 diasteroisomer), 41.28 (CH, 1 diasteroisomer), 36.7, 36.6, 36.2, 35.3, 30.8, 30.7, 30.3, 30.2, 29.8, 23.75, 23.69, 23.5, 14.6 (CH$_3$, 1 diasteroisomer), 14.3 (CH$_3$, 1 diasteroisomer), 14.0 (CH$_3$, 1 diasteroisomer).

FT-IR (cm^{-1}, neat): 2959, 1725, 1596, 1504, 1363, 1344, 1157, 991, 745, 692. HRMS (ESI) m/z: [M+H]$^+$ Calcd for C$_{26}$H$_{35}$N$_2$O$_2$ 407.2693. Found 407.2683. R$_f$ = 0.28 (pentane/Et$_2$O 96:4).

EtO$_2$C

CO$_2$Et

N

CO$_2$Me

C$_{27}$H$_{37}$NO$_6$
MW: 471,5940
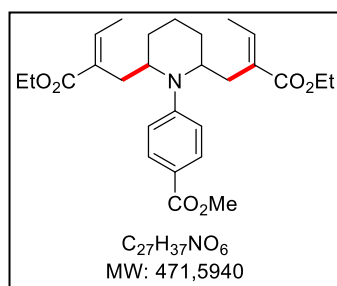
Methyl 4-[2,6-bis[(Z)-2-ethoxycarbonylbut-2-enyl]-1-piperidyl]benzoate

Following **General Procedure C** with ethyl 3-acetoxy-2-methylene-butanoate (41.0 mg, 0.22 mmol) and methyl 4-(1-piperidyl)benzoate (43.9 mg, 0.20 mmol) reacting for 3 hours. Purification by flash column chromatography (SiO$_2$, heptanes/EtOAc 80:20) followed by trituration in pentane afforded the product as a white solid (14.4 mg, 0.03 mmol, 15%, one diastereoisomer isolated, *cis/trans* relationship not assigned).

^{1}H NMR (300 MHz, CDCl$_3$): δ 7.97 (d, J = 8.8 Hz, 2H), 7.32 (d, J = 8.8 Hz, 2H), 7.02 (q, J = 7.1 Hz, 2H), 4.26 (q, J = 7.1 Hz, 4H), 4.19–4.10 (m, 2H), 3.86 (s, 3H), 2.73 (t, J = 13.1 Hz, 2H), 2.56 (dd, J = 13.4, 3.7 Hz,

2H), 1.90 (d, J = 7.2 Hz, 6H), 1.88–1.76 (m, 1H), 1.69–1.44 (m, 5H), 1.36 (t, J = 7.1 Hz, 6H). ^{13}C NMR (101 MHz, CDCl$_3$): δ 167.8 (2xC=O), 167.6 (C=O), 152.3 (Cq), 139.9 (2xCH=), 131.5 (2xCH$_{Ar}$), 131.1 (2xCq), 118.3 (Cq), 113.7 (2xCH$_{Ar}$), 60.9 (2xCH$_2$), 52.0 (2xCH), 51.6 (CH$_3$), 29.4 (2xCH$_2$), 26.9 (2xCH$_2$), 16.2 (CH$_2$), 15.0 (2xCH$_3$), 14.5 (2xCH$_3$). FT-IR (cm^{-1}, neat): 3029, 1691, 1599, 1260, 1192, 1103, 737. HRMS (ESI) m/z: [M+H]$^+$ Calcd for C$_{27}$H$_{38}$O$_6$N 472.2694. Found 472.2677. Mp 126.3–127.5 °C. R$_f$ = 0.14 (pentane/Et$_2$O 80:20).

C$_{19}$H$_{25}$NO$_4$
MW: 331,41
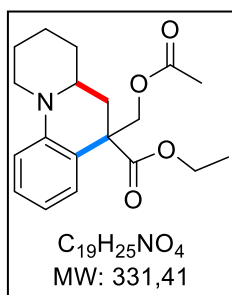
Product of radical addition on the aromatic ring before reduction and elimination of the acetate group. dr 3.3:1. Relative configuration not assigned.

Major diastereoisomer:

^{1}H NMR (400 MHz, CDCl$_3$): δ 7.14 (ddd, J = 8.7, 7.1, 1.7 Hz, 1H), 7.09 (dd, J = 7.8, 1.7 Hz, 1H), 6.87 (dd, J = 8.6, 1.2 Hz, 1H), 6.66 (td, J = 7.5, 1.2 Hz, 1H), 4.60–4.28 (m, 2H), 4.20 (q, J = 7.1 Hz, 2H), 3.97–3.89 (m, 1H), 2.88 (tt, J = 10.9, 2.8 Hz, 1H), 2.57 (td, J = 12.4, 2.8 Hz, 1H), 2.47 – 2.35 (m, 1H), 2.10 (d, J = 2.9 Hz, 1H), 2.06 (s, 3H), 1.89–1.78 (m, 2H), 1.78–1.71 (m, 1H), 1.70–1.55 (m, 1H), 1.45–1.36 (m, 2H), 1.23 (t, J = 7.1 Hz, 3H). ^{13}C NMR (101 MHz, CDCl$_3$): δ 173.7 (C=O), 170.8 (C=O), 146.8 (Cq$_{Ar}$), 129.0 (CH$_{Ar}$), 128.0 (CH$_{Ar}$), 120.8 (Cq$_{Ar}$), 117.7 (CH$_{Ar}$), 113.6 (CH$_{Ar}$), 67.6 (CH$_2$), 61.4 (CH$_2$), 51.9 (CH), 48.7 (Cq), 47.7 (CH$_2$), 34.3 (CH$_2$), 33.7 (CH$_2$), 26.1 (CH$_2$), 24.0 (CH$_2$), 21.0 (CH$_3$), 14.2 (CH$_3$).

Characteristic peaks of the minor diastereoisomer:

^{1}H NMR (400 MHz, CDCl$_3$): δ 7.38 (dd, J = 7.9, 1.6 Hz, 1H), 6.90 (dd, J = 8.8, 1.2 Hz, 1H), 6.72 (ddd, J = 8.1, 7.2, 1.2 Hz, 1H), 4.78 (d, J = 10.7 Hz, 1H), 3.88 (d, J = 2.4 Hz, 0H), 3.05 (tt, J = 11.0, 2.7 Hz, 1H), 2.10 (d, J = 2.9 Hz, 2H). ^{13}C NMR (101 MHz, CDCl$_3$): δ 173.7 (C=O), 170.8 (C=O), 147.8 (Cq$_{Ar}$), 128.7 (CH$_{Ar}$), 128.4 (CH$_{Ar}$), 117.8 (CH$_{Ar}$), 113.8 (CH$_{Ar}$), 70.8 (CH$_2$), 53.2 (CH), 47.8 (CH$_2$), 47.0 (Cq$_{aliph.}$), 37.5 (CH$_2$), 33.8 (CH$_2$), 26.1 (CH$_2$), 23.8 (CH$_2$), 21.0 (CH$_3$).

On the mix:

FT-IR (cm^{-1}, neat): 2933, 1725 (two peaks), 1600, 1493, 1448, 1220, 1033, 749, 735. HRMS (ESI) m/z: [M+H]$^+$ Calcd for C$_{19}$H$_{26}$O$_4$N 332.1856. Found 332.1854. R$_f$ = 0.39 (SiO$_2$, heptanes/EtOAc 80:20).

Towards the synthesis of optically activ tropane and homotropane alkaloids using the radical [3+3]-annulation – Unpublished results

Retention of chiral information throughout the radical process

Synthesis of the starting material [24]
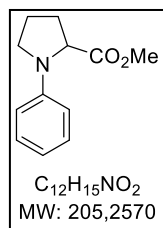
Methyl 1-phenylpyrrolidine-2-carboxylate. In an oven-dried flask containing a solution of pyrrolidine-2-carboxylic acid (5.0 g, 43.4 mmol) and bromobenzene (5.2 mL, 49.5 mmol) in DMF (50 mL) were added under a nitrogen flow CuI (827 mg, 4.34 mmol) and K_2CO_3 (18 g, 130 mmol) with strong magnetic stirring. The mixture was heated at 100 °C for 24 h. After cooling to 0 °C (internal temperature) and diluting with DMF (30 mL), Me_2SO_4 (5.5 mL, 65.1 mmol) was added. The temperature rose to ~8 °C and the mixture was further stirred at 0 °C for 8 h, before being poured into ice-water (200 g, 1/1). Et_2O (200 mL) was added, and the organic phase was separated. The aqueous phase was extracted with Et_2O (2 x 200 mL). The combined organic phase was washed with 2 M HCl (2 x 100 mL) and brine (1 x 100 mL), and dried over Na_2SO_4. After filtration and evaporation *in vacuo*, the residual solvents and impurities were removed by vacuum distillation (1.4 mbar, 35 °C vapor temperature) to give crude product as a dark brown oil. Further purification by fcc (SiO_2, heptanes/EtOAc = 93:7) afforded the title compound as a pale-yellow oil (1.84 g, 8.96 mmol, **21%).**

Structure label: $C_{12}H_{15}NO_2$, MW: 205,2570, with CO₂Me group (N-phenylpyrrolidine-2-carboxylate methyl ester).

^{1}H NMR (300 MHz, CDCl$_3$) δ 7.26–7.18 (m, 2H), 6.72 (tt, *J* = 7.3, 1.0 Hz, 1H), 6.56 (dt, *J* = 7.8, 1.1 Hz, 2H), 4.26 (dd, *J* = 8.3, 2.3 Hz, 1H), 3.71 (s, 3H), 3.60 (ddd, *J* = 11.6, 6.5, 3.4 Hz, 1H), 3.37 (dt, *J* = 8.5, 7.3 Hz, 1H), 2.39–1.98 (m, 4H). The physical and spectral data are in accordance with literature data.[24]

Alternative protocol for the synthesis of the racemic product:
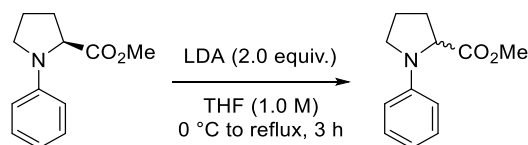
To a mixture of N-isopropylpropan-2-amine (3.4 mL, 24.0 mmol, 2.4 equiv.) in THF (5 mL) at -78°C was added dropwise *n*BuLi (2.50 m, 8.0 mL, 20.0 mmol). After 15 minutes, a solution of methyl (2S)-1-phenylpyrrolidine-2-carboxylate (2.05 g, 10 mmol, 1 quiv.) in THF (5 mL) was added dropwise to the flask. The cooling bath was removed, and the reaction mixture allowed to warm up to room temperature. The mixture was then heated at reflux for 3 h. An aliquot was taken and quenched with D_2O to follow the deprotonation step. After complete deprotonation was achieved, the reaction mixture was quenched with NH$_4$Cl (40 mL) and then extracted with Et_2O (3 x 25mL). The combined

organic phases were washed with NaHCO$_3$ (1 x 40 mL) and brine (1 x 40 mL), dried with Na$_2$SO$_4$, and evaporated under reduced pressure. Purification by flash column chromatography on silica gel (heptanes/EtOAc 88:12) afforded the title compound (1.57 g, 7.6 mmol, 76%) as pale-yellow oil. All spectral data in accordance with above description. [α]$_D$ = 0.10 (c = 1.00, CHCl$_3$, 20 °C).
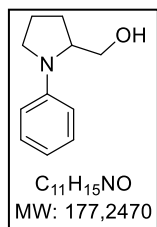
(1-phenylpyrrolidin-2-yl)methanol. Into a 50-mL, three-neck flask equipped with a condenser and a thermometer were added THF (15 mL) and LiAlH$_4$ (544 mg, 14.3 mmol) in small portions with caution. A solution of methyl 1-phenylpyrrolidine-2-carboxylate (1.84 g, 8.96 mmol) in THF (5 mL) was added dropwise into the above suspension with strong stirring, the internal temperature not rising above 30 °C. The reaction was heated to reflux until completion of the reaction (3 h). After cooling to 0 °C, 2 M NaOH (7 mL) was added dropwise, and the resulting mixture was refluxed for 1 h. After cooling down to rt, the organic phase was separated and the aqueous phase extracted with Et$_2$O (3 x 20 mL). The combined organic phases were dried over Na$_2$SO$_4$. After filtration and evaporation *in vacuo*, the residual solvents were removed under high vacuum to give the title compound as a pale-yellow very viscous oil (1.52 g, 5.58 mmol, 96%). No further purification was needed.

$C_{11}H_{15}NO$
MW: 177,2470

^{1}H NMR (300 MHz, CDCl$_3$) δ 7.24 (t, *J* = 7.9 Hz, 2H), 6.72 (dd, *J* = 7.8, 5.8 Hz, 3H), 3.86 (ddd, *J* = 8.2, 4.9, 2.8 Hz, 1H), 3.67 (t, *J* = 5.3 Hz, 2H), 3.52 (td, *J* = 8.2, 7.5, 2.1 Hz, 1H), 3.23 – 3.09 (m, 1H), 2.15 – 1.93 (m, 4H), 1.60 (d, *J* = 5.9 Hz, 1H). The physical and spectral data are in accordance with literature data.[24]
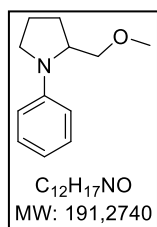
2-(methoxymethyl)-1-phenyl-pyrrolidine. In an oven-dried, 250-mL, two-neck flask equipped with a magnetic stirrer and a thermometer was dissolved (1-phenylpyrrolidin-2-yl)methanol (1.52 g, 8.58 mmol) in THF (40 mL). NaH (60.0 %, 854 mg, 22.3 mmol) was added at rt in 3 portions. A solution of methyl methanesulfonate (1.53 mL, 18.0 mmol) in THF (15 mL) was added dropwise so that the internal temperature of the RM did not rise over 35 °C. The reaction mixture was stirred until completion f reaction (12 h). The mixture was slowly treated with 2 M NaOH (22 mL) at rt, and extracted with Et$_2$O (2 x 40 mL). The organic phase was dried over Na$_2$SO$_4$, filtered, and evaporated *in vacuo* to give crude product as a colorless oil. Purification by distillation (3.5x10^{-2} mbar, 35 °C vapor temperature is excess Me$_2$SO$_4$, 45 °C vapor temperature is expected product) afforded the clean title compound as a colorless oil (1.23 g, 6.43 mmol, 75 %). All spectral data in accordance with literature data.[24]

$C_{12}H_{17}NO$
MW: 191,2740

^{1}H NMR (300 MHz, CDCl$_3$) δ 7.30 – 7.20 (m, 2H), 6.75 – 6.61 (m, 3H), 3.88 (d, *J* = 35.0 Hz, 1H), 3.54 (dd, *J* = 9.4, 3.4 Hz, 1H), 3.50 – 3.41 (m, 2H), 3.39 (s, 3H), 3.20 (t, *J* = 9.1 Hz, 1H), 3.17 – 3.08 (m, 1H), 2.12 – 1.91 (m, 4H). ^{13}C NMR (75 MHz, CDCl$_3$) δ 147.7, 129.4, 116.1, 112.1, 73.2, 59.3, 58.3, 48.6, 29.1, 23.5.

IR (neat, cm^{-1}) 2873, 1596, 1503, 1360, 1108, 743, 690. HRMS (ESI) calculated for $C_{12}H_{17}ON$, [M+H]$^+$ = 192.1383. Found: [M+H]$^+$ = 192.1381. [α]$_D$ = -163 (c 1.10, CHCl$_3$, 20 °C). HPLC trace:

- *Racemic product* (1 mL/min flow rate)

```
                                    Inj Volume : 5.000 µl
Method          : C:\Chem32\1\Data\ECO\ECO_CH2OMe substrate_full study 2021-12-10 12-30-47\C_
                  04-modKU.M (Sequence Method)
Last changed    : 10.12.2021 12:30:47 by SYSTEM
Method Info     : 1% iPrOH in hexanes. Column: chiral OD-H.

Additional Info : Peak(s) manually integrated
```
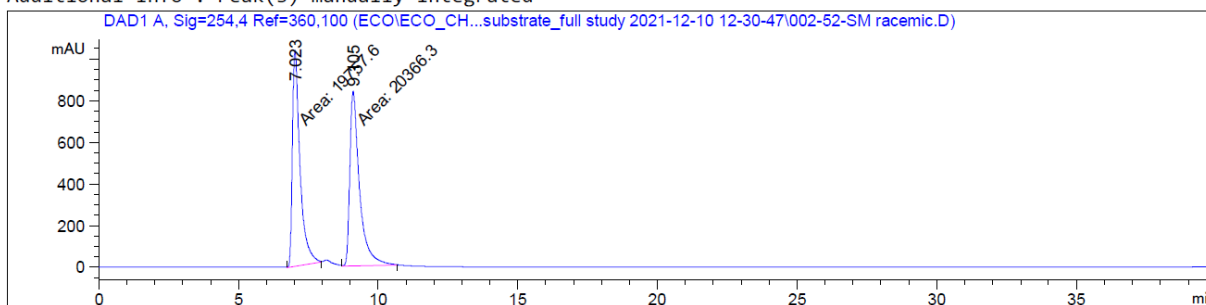


```
Signal 1: DAD1 A, Sig=254,4 Ref=360,100

Peak RetTime Type  Width     Area       Height     Area
  #   [min]        [min]   [mAU*s]      [mAU]        %
----|-------|----|-------|----------|----------|--------|
  1   7.023 MM    0.3172 1.97576e4  1038.10474  49.2415
  2   9.105 MM    0.4041 2.03663e4   840.07397  50.7585

Totals :                4.01238e4   1878.17871
```

- *Optically active product* (1 mL/min flow rate)

```
                                    Inj Volume : 5.000 µl
Method          : C:\Chem32\1\Data\ECO\ECO_CH2OMe substrate_full study 2021-12-10 12-30-47\C_
                  04-modKU.M (Sequence Method)
Last changed    : 10.12.2021 12:30:47 by SYSTEM
Method Info     : 1% iPrOH in hexanes. Column: chiral OD-H.

Additional Info : Peak(s) manually integrated
```
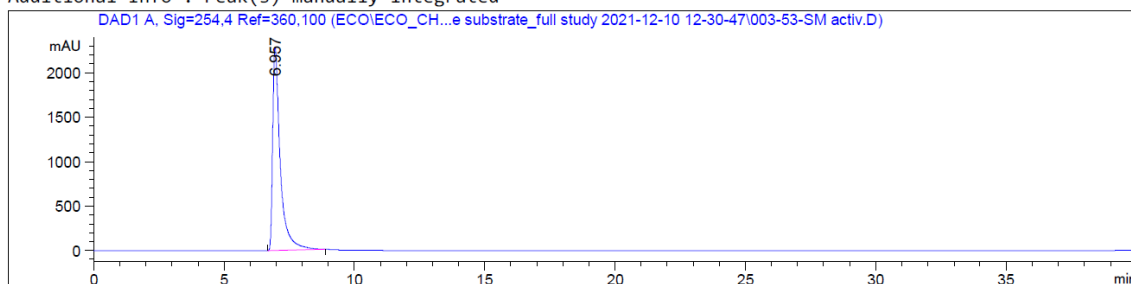


```
Signal 1: DAD1 A, Sig=254,4 Ref=360,100

Peak RetTime Type  Width     Area       Height     Area
  #   [min]        [min]   [mAU*s]      [mAU]        %
----|-------|----|-------|----------|----------|--------|
  1   6.957 BB    0.2965 4.62686e4  2282.31128 100.0000

Totals :                4.62686e4   2282.31128
```

Synthesis of the mono-allylated intermediate 2g

Ethyl 2-[[5-(methoxymethyl)-1-phenyl-pyrrolidin-2-yl]methyl]prop-2-enoate (2g). In an oven-dried 25-mL seal-tube were successively added (2S)-2-(methoxymethyl)-1-phenyl-pyrrolidine (191 mg, 1.00 mmol), ethyl 2-(acetoxymethyl)prop-2-enoate (189 mg, 1.10 mmol), [Ir{dF(CF$_3$)ppy}$_2$(dtbpy)]PF$_6$ (5.6 mg, 0.005 mmol, 1 mol%) and cesium acetate (231 mg, 1.2 mmol). The vial was sealed and evacuated/refilled with N$_2$ (x 3). Finally, dry and degassed 1,2-dichloroethane (20.0 mL, 0.05 M) was added. The resulting yellow mixture was placed in front of a 390 nm blue LED (5 cm distance) and stirred until completion of the reaction (10 min, TLC monitoring pentane/Et$_2$O 8:2). The reaction mixture was diluted with sat. NaHCO$_3$ (30 mL). The aqueous phase was extracted with DCM (3 x 50 mL) and the combined organic phases were dried over Na$_2$SO$_4$, filtered, and concentrated under reduced pressure to give crude product as an orange oil. Purification by flash column chromatography on silica gel (pentane/Et$_2$O 95:5) allowed to recover the starting material (49.7 mg, 26% recovered SM) and the desired product in a mix with the unreacted trap. Further purification can be achieved by flash column chromatography on silica gel (toluene/EtOAc 98:2) to obtain the title compound as a white solid (128.3 mg, 0.42 mmol, 42%, *cis/trans* = 23:77). Note that the trap can also be removed using Kugelrohr distillation.

GC – t$_{R\text{-}trans}$ = 9.78 min. t$_{R\text{-}cis}$ = 9.83 min. R$_f$: 0.34 (toluene/EtOAc 98:2). The diastereoisomers cannot be separated on normal phase SiO$_2$.

Chromatogram and Results					

Injection Details

Injection Name:	ECO-5-153-F2	Run Time (min):	20.67
Vial Number:	4	Injection Volume:	1.00
Injection Type:	Unknown	Channel:	GC1_FID
Calibration Level:		Wavelength:	n.a.
Instrument Method:	GC1-FAST	Bandwidth:	n.a.
Processing Method:	Basic Quantitative	Dilution Factor:	1.0000
Injection Date/Time:	09/Dec/21 12:03	Sample Weight:	1.0000

Integration Results

No.	Peak Name	Retention Time min	Area mV*min	Height mV	Relative Area %	Relative Height %
1		9.783	43.976	2137.632	78.45	76.88
2		9.825	12.081	642.965	21.55	23.12
Total:			56.056	2780.598	100.00	100.00

Image 2: GC determination of the cis/trans ratio by GC.

The diastereoisomers were separated on a reverse phase preparative system (acidic conditions).
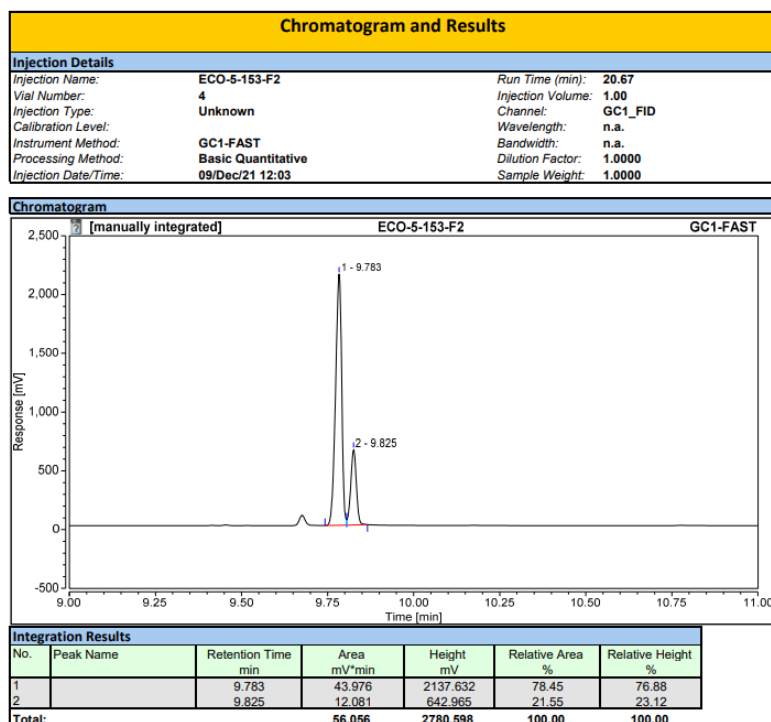
The mixture of diastereoisomers (130 mg) was dissolved in a mix of solution D [100% MeCN + 1% TFA] and solution A [100% H₂O + 1% TFA]. The 15-mL solution was centrifugated and loaded on a Waters PrepLC System (30% D in A to 100% A over 70 minutes at a flow rate of 20 mL/min). The minor diastereoisomer was recovered with 45% D in A. The major diastereoisomer was recovered with 65% D in A. The solvent was evaporated on a lyophilisation system overnight and the TFA-salt was taken in EtOAc (10 mL) and aq. sat. NaHCO₃ (10 mL). The phases were separated and the aqueous phase extracted with EtOAc (2 x 10 mL). A short filtration on silica gel afforded the clean fractions.

*Characterization of the trans diastereoisomer (**2g-trans**)*

2g-trans
C₁₈H₂₅NO₃
MW: 303,4020
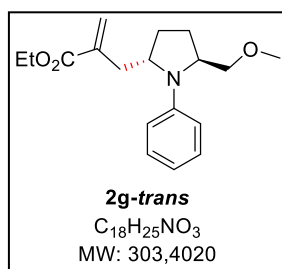
Appearance: white solid. ^{1}H NMR (400 MHz, CDCl₃): δ 7.29 – 7.20 (m, 2H), 6.82 (d, J = 8.1 Hz, 2H), 6.66 (t, J = 7.3 Hz, 1H), 6.26 (d, J = 1.4 Hz, 1H), 5.57 (br s, 1H), 4.26 (qd, J = 7.1, 1.7 Hz, 2H), 4.07 (ddd, J = 10.3, 6.9, 2.8 Hz, 1H), 4.01 (td, J = 8.3, 2.6 Hz, 1H), 3.53 (dt, J = 9.3, 2.8, 1.1 Hz, 1H), 3.34 (s, 3H), 3.05 (t, J = 9.1 Hz, 1H), 2.98 (d, J = 13.7 Hz, 1H), 2.20 – 2.06 (m, 1H), 2.05 – 1.88 (m, 3H), 1.88 – 1.77 (m, 1H), 1.37 (t, J = 7.1 Hz, 3H). ^{13}C NMR (101 MHz, CDCl₃): δ 167.2 (C=O), 144.9 (Cq), 138.8 (Cq), 129.4 (2x CH Ar), 127.8 (CH₂), 115.8 (CH Ar), 113.8 (2x CH Ar), 71.7 (CH₂), 61.1 (CH₂), 59.2 (CH₃), 57.1 (CH), 56.6 (CH), 33.5 (CH₂), 26.4 (CH₂), 26.3 (CH₂), 14.4 (CH₃). FT-IR (cm⁻¹, neat): 2883, 1704, 1594, 1503, 1363, 1324, 1150, 1110, 948, 741, 697. HRMS (ESI) m/z: Calcd for C₁₈H₂₆NO₃ 304.1907; Found 304.1911. mp = 90.5 – 91.4 °C [α]_D = + 14 (c 1.17, CHCl₃, 20 °C). HPLC trace (1 mL/min flow rate):

○ From the racemic substrate 2-(methoxymethyl)-1-phenyl-pyrrolidine

```
                                       Inj Volume : 10.000 µl
Different Inj Volume from Sample Entry!  Actual Inj Volume : 10.000 µl
Method          : C:\Chem32\1\Data\ECO\ECO_CH2OMe substrate_full study 2021-12-09 16-38-05\C_
                  02-modKU.M (Sequence Method)
Last changed    : 09.12.2021 16:38:05 by SYSTEM
Method Info     : 0.5% iPrOH in hexanes. Column: chiral OD-H.

Additional Info : Peak(s) manually integrated
```



```
Signal 1: DAD1 A, Sig=254,4 Ref=360,100

Peak RetTime Type  Width     Area      Height     Area
  #   [min]        [min]   [mAU*s]     [mAU]       %
----|-------|----|-------|----------|----------|--------|
   1  11.937 MF    0.5277 1.92841e4   609.03387  49.3169
   2  13.658 FM    0.6410 1.98183e4   515.30664  50.6831

Totals :                  3.91024e4  1124.34052
```

○ From the optically active substrate (2S)-2-(methoxymethyl)-1-phenyl-pyrrolidine

```
                                    Inj Volume : 10.000 µl
Different Inj Volume from Sample Entry!  Actual Inj Volume : 10.000 µl
Method          : C:\Chem32\1\Data\ECO\ECO_CH2OMe substrate_full study 2021-12-09 16-38-05\C_
                  02-modKU.M (Sequence Method)
Last changed    : 09.12.2021 16:38:05 by SYSTEM
Method Info     : 0.5% iPrOH in hexanes. Column: chiral OD-H.

Additional Info : Peak(s) manually integrated
```



```
Signal 1: DAD1 A, Sig=254,4 Ref=360,100

Peak RetTime Type  Width     Area       Height      Area
  #   [min]        [min]    [mAU*s]     [mAU]        %
----|-------|----|-------|----------|----------|--------|
  1  11.437  MM   0.5201  3.89087e4  1246.81970  100.0000

Totals :                 3.89087e4  1246.81970
```

From the chiral HPLC it can be concluded that no racemization was observed on the *trans* product.

XRay: a sample of the major diastereoisomer was recrystallized from pentane at room temperature and afforded single crystals suitable for XRay analysis.
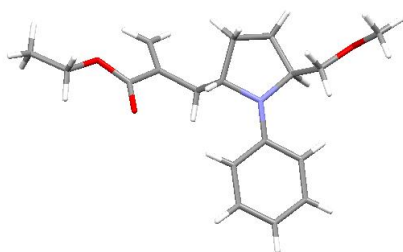
*Characterization of the cis diastereoisomer (***2g-cis***)*

2g-cis
$C_{18}H_{25}NO_3$
MW: 303,4020
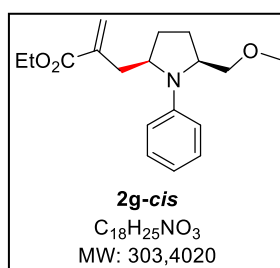
Appearance: colorless oil. ^{1}H NMR (400 MHz, CDCl$_3$): δ 7.30 − 7.21 (m, 2H), 6.88 (d, J = 8.1 Hz, 2H), 6.72 (t, J = 7.3 Hz, 1H), 6.25 (d, J = 1.6 Hz, 1H), 5.63 (br s, 1H), 4.32 − 4.21 (m, 2H), 3.98 − 3.83 (m, 1H), 3.62 (dd, J = 9.4, 3.8 Hz, 1H), 3.41 (s, 3H), 3.26 (t, J = 8.9 Hz, 1H), 3.07 (ddd, J = 13.7, 3.5, 1.3 Hz, 1H), 2.11 (dd, J = 13.6, 10.1 Hz, 1H), 2.05 − 1.88 (m, 3H), 1.83 − 1.71 (m, 1H), 1.37 (t, J = 7.1 Hz, 3H). ^{13}C NMR (101 MHz, CDCl$_3$): δ 167.3 (C=O), 147.7 (Cq), 138.4 (Cq), 129.3 (2x CH Ar), 127.6 (CH$_2$), 116.5 (CH Ar), 112.6 (2x CH Ar), 75.0 (CH$_2$), 61.1 (CH$_2$), 60.8 (CH), 59.4 (CH$_3$), 59.1 (CH), 38.1 (CH$_2$), 29.3 (CH$_2$), 28.0 (CH$_2$), 14.4 (CH$_3$). FT-IR (cm^{-1}, neat): 2976, 2927, 2873,

1710, 1597, 1502, 1364, 1323, 1177, 1154, 1115, 1094, 745, 695. HRMS (ESI) m/z: Calcd for $C_{18}H_{26}NO_3$ 304.1907; Found 304.1904. $[\alpha]_D$ = -116 (c 0.55, CHCl$_3$, 20 °C). HPLC trace (1 mL/min flow rate):

○ From the racemic substrate 2-(methoxymethyl)-1-phenyl-pyrrolidine

```
Different Inj Volume from Sample Entry!  Actual Inj Volume : 10.000 µl
Method          : C:\Chem32\1\Data\ECO\ECO_CH2OMe substrate_full study 2021-12-09 16-38-05\C_
                  02-modKU.M (Sequence Method)
Last changed    : 09.12.2021 16:38:05 by SYSTEM
Method Info     : 0.5% iPrOH on hexanes. Column: chiral OD-H.

Additional Info : Peak(s) manually integrated
```
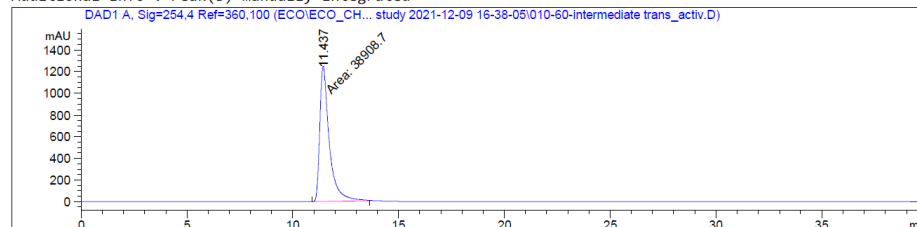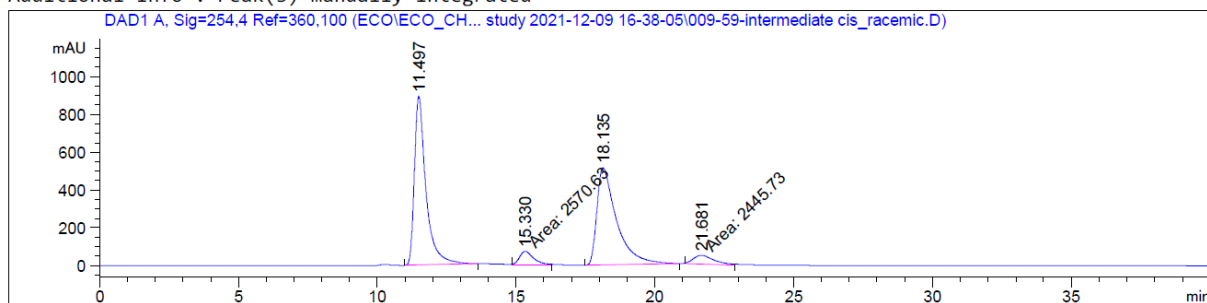


```
Signal 1: DAD1 A, Sig=254,4 Ref=360,100

Peak RetTime Type  Width     Area        Height     Area
  #   [min]        [min]    [mAU*s]      [mAU]       %
----|-------|----|-------|----------|----------|--------|
  1  11.497 BB    0.4250 2.58534e4   892.43542  46.0778
  2  15.330 MM    0.5949 2570.63257   72.01385   4.5816
  3  18.135 BB    0.7085 2.52384e4   513.44415  44.9817
  4  21.681 MM    0.8597 2445.72656   47.41666   4.3589

Totals :                 5.61082e4  1525.31009
```

At t_R 15.33 and 21.68 an impurity is visible (also visible in the NMR).

○ From the optically active substrate (2S)-2-(methoxymethyl)-1-phenyl-pyrrolidine

```
Different Inj Volume from Sample Entry!  Actual Inj Volume : 10.000 µl
Method          : C:\Chem32\1\Data\ECO\ECO_CH2OMe substrate_full study 2021-12-09 16-38-05\C_
                  02-modKU.M (Sequence Method)
Last changed    : 09.12.2021 16:38:05 by SYSTEM
Method Info     : 0.5% iPrOH in hexanes. Column: chiral OD-H.

Additional Info : Peak(s) manually integrated
```
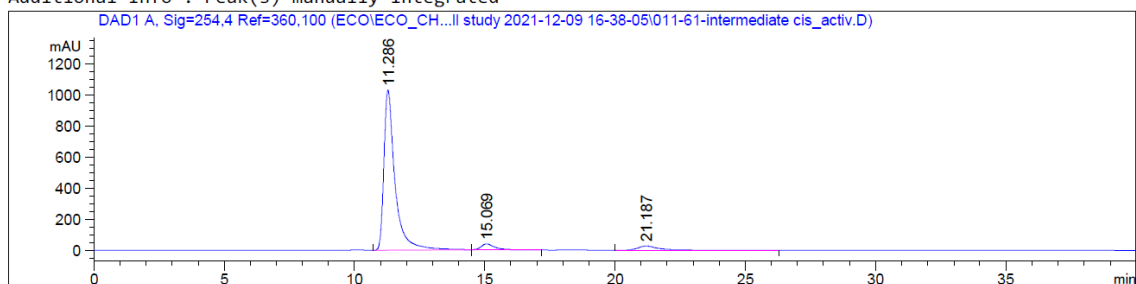
```
Signal 1: DAD1 A, Sig=254,4 Ref=360,100

Peak RetTime Type  Width     Area       Height    Area
  #   [min]        [min]    [mAU*s]      [mAU]      %
----|-------|----|-------|----------|----------|--------|
  1  11.286 BB    0.4308 3.04880e4  1031.51135  91.5937
  2  15.069 BB    0.5239 1340.27454   37.60037   4.0265
  3  21.187 BB    0.7995 1457.85461   26.34755   4.3798

Totals :                 3.32862e4  1095.45927
```

t_R 15.33 and 21.68 = impurity (see also the racemic substrate).

From the chiral HPLC it can be concluded that no racemization was observed on the *cis* product.

Synthesis of the cyclized product 3g

Ethyl 1-(methoxymethyl)-8-phenyl-8-azabicyclo[3.2.1]octane-3-carboxylate (3g). In an oven-dry vial were added under N₂ ethyl 2-[[(5S)-5-(methoxymethyl)-1-phenyl-pyrrolidin-2-yl]methyl]prop-2-enoate (**2g-*trans***) (60.7 mg, 0.20 mmol), [Ir{dF(CF₃)ppy}₂(dtbpy)]PF₆ (2.2 mg, 0.02 mmol, 1 mol%), and cesium acetate (46 mg, 0.24 mmol, 1.2 equiv.). The vial was evacuated and filled with N₂ (x 3), then CH₃CO₂H (11.4 µL, 0.20 mmol, 1.0 equiv.) and degassed 1,2-dichloroethane (4.0 mL, 0.05 M) were successively added. The resulting yellow solution was placed in front of a 390 nm LED and stirred until consumption of the starting material (30 min, TLC monitoring heptanes/EtOAc 8:2). The reaction mixture was diluted with sat. NaHCO₃ (3 mL). The aqueous phase was extracted with DCM (3 x 5 mL) and the combined organic phases were dried over Na₂SO₄, filtered, and concentrated under reduced pressure to give crude product as an orange oil. Purification by flash column chromatography on silica gel (pentane/Et₂O 95:5 to 92:8) afforded the bicyclic product as a colorless oil (39.1 mg, 0.13 mmol, 64%, α/β 9:1). The diastereoisomers could be separated by flash column chromatography on silica gel (heptanes/EtOAc 95:15).

GC – $t_{R-\alpha}$ = 10.19 min. $t_{R-\beta}$ = 10.12 min.

Chromatogram and Results

Injection Details

Injection Name:	ECO-5-154-F2	Run Time (min):	20.67
Vial Number:	1	Injection Volume:	1.00
Injection Type:	Unknown	Channel:	GC1_FID
Calibration Level:		Wavelength:	n.a.
Instrument Method:	GC1-FAST	Bandwidth:	n.a.
Processing Method:	Basic Quantitative	Dilution Factor:	1.0000
Injection Date/Time:	09/Dec/21 11:23	Sample Weight:	1.0000

Chromatogram

Integration Results

No.	Peak Name	Retention Time min	Area mV*min	Height mV	Relative Area %	Relative Height %
1		10.121	5.397	246.384	9.88	10.43
2		10.185	49.211	2115.020	90.12	89.57
Total:			54.608	2361.404	100.00	100.00

Image 3: GC determination of the alpha/beta ratio by GC.

3gα
C$_{18}$H$_{25}$NO$_3$
MW: 303,4020
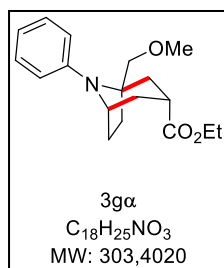
*Characterization of the alpha diastereoisomer (**3gα**)*

Appearance: colorless oil. ^{1}H NMR (400 MHz, CDCl$_3$): δ 7.25–7.17 (m, 2H), 7.02 (d, J = 8.1 Hz, 2H), 6.81 (t, J = 7.2 Hz, 1H), 4.21 (qt, J = 7.1, 3.4 Hz, 3H), 3.65–3.47 (m, 2H), 3.38 (s, 3H), 2.65 (tt, J = 8.0, 2.2 Hz, 1H), 2.28–2.07 (m, 4H), 2.09–1.92 (m, 2H), 1.92–1.79 (m, 1H), 1.73–1.63 (m, 1H), 1.30 (t, J = 7.1 Hz, 3H). ^{13}C NMR (101 MHz, CDCl$_3$): δ 176.1 (C=O), 147.0 (Cq$_{Ar}$), 129.1 (2xCH$_{Ar}$), 119.3 (2xCH$_{Ar}$), 119.2 (CH$_{Ar}$), 77.2 (CH$_2$), 64.2 (Cq$_{aliph}$), 61.0 (CH$_2$), 59.2 (CH$_3$), 58.8 (CH), 35.1 (CH), 33.4 (CH$_2$), 30.1 (CH$_2$), 27.6 (CH$_2$), 25.6 (CH$_2$), 14.3 (CH$_3$). HRMS (ESI) m/z: Calcd for C$_{18}$H$_{26}$NO$_3$ 304.1918; Found 304.1913. FT-IR (cm^{-1}, neat): 2956, 2927, 2874, 1720, 1597, 1493, 1184, 1094, 752, 694. R$_{f-\alpha}$ = 0.24 (heptanes/EtOAc 90:10).

3gβ
C$_{18}$H$_{25}$NO$_3$
MW: 303,4020
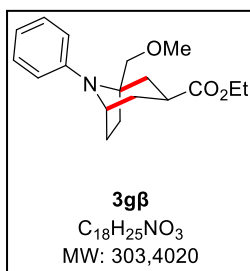
*Characterization of the beta diastereoisomer (**3gβ**)*

Appearance: colorless oil. ^{1}H NMR (400 MHz, CDCl$_3$): δ 7.20 (t, *J* = 7.7 Hz, 2H), 7.01 (d, *J* = 8.1 Hz, 2H), 6.81 (t, *J* = 7.3 Hz, 1H), 4.30 (dt, *J* = 6.4, 2.9 Hz, 1H), 4.08 (q, *J* = 7.1 Hz, 2H), 3.65–3.53 (m, 2H), 3.37 (s, 3H), 2.90 (tt, *J* = 11.9, 5.5 Hz, 1H), 2.24–1.93 (m, 4H), 1.89–1.79 (m, 1H), 1.78–1.58 (m, 3H), 1.22 (t, *J* = 7.1 Hz, 3H).

^{13}C NMR (101 MHz, CDCl$_3$): δ 175.2 (C=O), 146.6 (Cq), 129.1 (2x CH Ar), 119.7 (2x CH Ar), 119.5 (CH Ar), 77.3 (CH$_2$), 64.7 (Cq), 60.6 (CH$_2$), 59.6 (CH), 59.3 (CH$_3$), 36.2 (CH), 34.6 (CH$_2$), 32.3 (CH$_2$), 30.1 (CH$_2$), 26.5 (CH$_2$), 14.4 (CH$_3$). HRMS (ESI) m/z: Calcd for C$_{18}$H$_{26}$NO$_3$ 304.1907; Found 304.1907. FT-IR (cm^{-1}, neat): 2923, 1728, 1598, 1495, 1188, 1101, 1032, 752, 696. R$_{f-β}$ = 0.18 (heptanes/EtOAc 90:10).

HPLC trace (on the mixture of diastereoisomers, α/β 90:10 – 1 mL/min flow rate):

- *From the racemic **2g-trans** ethyl 2-[[5-(methoxymethyl)-1-phenyl-pyrrolidin-2-yl]methyl]prop-2-enoate*

```
Different Inj Volume from Sample Entry!  Actual Inj Volume : 10.000 µl
Method         : C:\Chem32\1\Data\ECO\ECO_CH2OMe substrate_full study 2021-12-09 16-38-05\C_
                 04-modKU.M (Sequence Method)
Last changed   : 09.12.2021 16:38:05 by SYSTEM
Method Info    : 1% iPrOH in hexanes. Column: chiral OD-H.

Additional Info : Peak(s) manually integrated
```
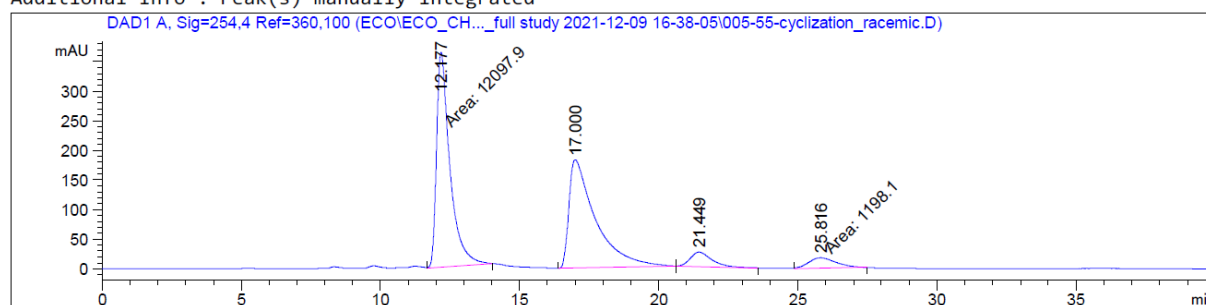


```
Signal 1: DAD1 A, Sig=254,4 Ref=360,100

Peak RetTime Type  Width     Area      Height      Area
  #   [min]        [min]   [mAU*s]     [mAU]        %
----|-------|----|-------|----------|----------|--------|
   1  12.177 MM   0.5560  1.20979e4   362.62241  45.4158
   2  17.000 BB   0.9197  1.20478e4   182.36758  45.2275
   3  21.449 BB   0.7831  1294.34851   24.31332   4.8590
   4  25.816 MM   1.1359  1198.09644   17.57871   4.4977

Totals :                 2.66381e4   586.88202
```

- *From the optically active **2g-trans** ethyl 2-[[(2S)-5-(methoxymethyl)-1-phenyl-pyrrolidin-2-yl]methyl]prop-2-enoate*

```
Different Inj Volume from Sample Entry!  Actual Inj Volume : 10.000 µl
Method          : C:\Chem32\1\Data\ECO\ECO_CH2OMe substrate_full study 2021-12-09 16-38-05\C_
                  04-modKU.M (Sequence Method)
Last changed    : 09.12.2021 16:38:05 by SYSTEM
Method Info     : 1% iPrOH in hexanes. Column: chiral OD-H.

Additional Info : Peak(s) manually integrated
```



```
Signal 1: DAD1 A, Sig=254,4 Ref=360,100

Peak RetTime Type  Width      Area       Height     Area
  #   [min]        [min]    [mAU*s]      [mAU]       %
----|-------|----|-------|----------|----------|--------|
  1  12.700 BB   0.5307 1.79868e4   489.50815  89.5878
  2  26.752 MM   1.2044 2090.48706   28.92874  10.4122

Totals :                 2.00773e4   518.43689
```
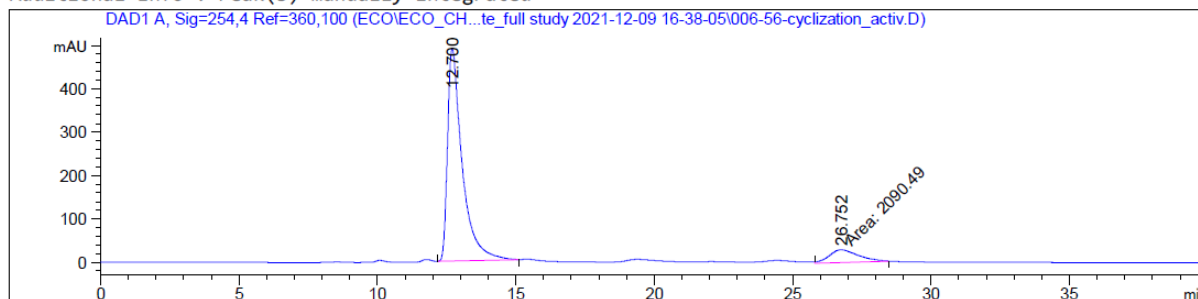
$[\alpha]_D$ = - 2 (c 0.62, CHCl$_3$, 20 °C)

From the chiral HPLC it can be said that no racemization was observed when performing the cyclization on the optically active intermediate.

Cyclization from an optically active mixture of 2g-*cis* and 2g-*trans* isomers (cis/trans 23:77)

Protocol as described above. The resulting mixture of alpha/beta products (90:10) was subjected to chiral HPLC and $[\alpha]_D$ measurements.

$[\alpha]_D$ = - 0.83 (c 1.06, CHCl$_3$, 20 °C)

$$ee = \frac{observed\ [\alpha]_D}{\max[\alpha]_D} = \frac{-0.83}{-2.0} = 0.415\ (41.5\ \%)$$

$$\%(-) = \frac{41.5}{2} + 50 = 70.75\ \%\ (71\ \%)$$

From the $[\alpha]_D$ measurement, the ratio of enantiomers is (-)/(+) = 71:29 (expected ratio: 77:23).

HPLC trace of the mixture of products (1 mL/min flow rate):

```
Different Inj Volume from Sample Entry!  Actual Inj Volume : 10.000 µl
Method          : C:\Chem32\1\Data\ECO\ECO_CH2OMe substrate_full study 2021-12-09 16-38-05\C_
                  04-modKU.M (Sequence Method)
Last changed    : 09.12.2021 16:38:05 by SYSTEM
Method Info:        1% iPrOH in hexanes. Column: chiral OD-H.

Additional Info : Peak(s) manually integrated
```


DAD1 A, Sig=254,4 Ref=360,100 (ECO\ECO_CH...21-12-09 16-38-05\007-57-ECO-5-154 cyclized product_from m.D)
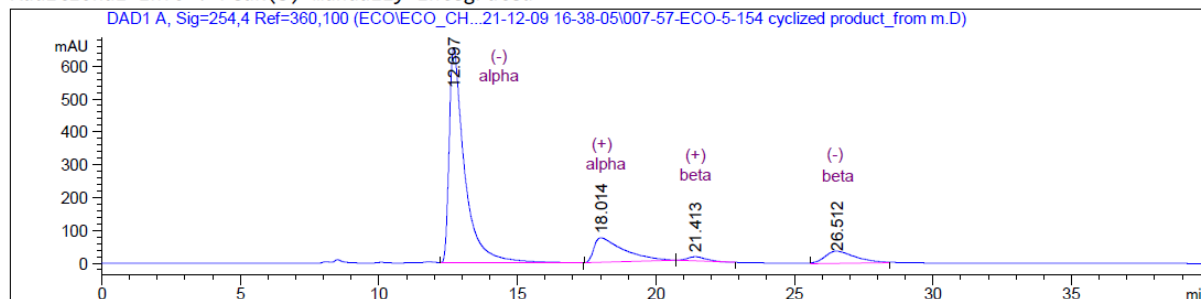
```
Signal 1: DAD1 A, Sig=254,4 Ref=360,100

Peak RetTime Type  Width     Area       Height     Area
  #   [min]        [min]     [mAU*s]     [mAU]        %
----|-------|----|-------|----------|----------|--------|
  1  12.697 BB    0.5537 2.53128e4   653.81750  73.6030
  2  18.014 BB    1.0341 5594.15332   74.49908  16.2663
  3  21.413 BB    0.6936  606.88483   12.62894   1.7647
  4  26.512 MM    1.2786 2877.19092   37.50516   8.3661

Totals :                 3.43911e4   778.45068
```

From the chiral HPLC measurement, the ratio of enantiomers is (-)/(+) = 82:18 (expected ratio: 77:23).

Towards the synthesis of $(+)$–euphococcinine

Synthesis of racemic 6p
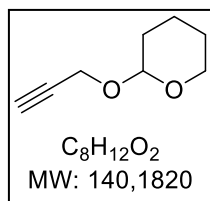
2-prop-2-ynoxytetrahydropyran. A mixture of <u>freshly distilled</u> prop-2-yn-1-ol (5.9 mL, 100 mmol), 3,4-dihydro-2H-pyran (11.8 mL, 130 mmol) and p-TsOH•H_2O (190 mg, 1.00 mmol) was stirred for 1 h at 0 °C. The reaction mixture was directly purified by fcc (SiO_2, pentane:Et_2O 30:1) to afford the title compound as a colorless liquid (12.3 g, 87.5 mmol, 88%).

$C_8H_{12}O_2$
MW: 140,1820

^{1}H NMR (300 MHz, CDCl$_3$) δ 4.82 (t, J = 3.3 Hz, 1H), 4.35–4.16 (m, 2H), 3.84 (ddd, J = 11.4, 8.7, 3.2 Hz, 1H), 3.59–3.48 (m, 1H), 2.41 (t, J = 2.4 Hz, 1H), 1.91–1.75 (m, 1H), 1.76–1.68 (m, 1H), 1.68–1.59 (m, 2H), 1.60–1.43 (m, 2H). ^{13}C NMR (75 MHz, CDCl$_3$) δ 97.0, 79.9, 74.1, 62.1, 54.1, 30.3, 25.5, 19.1. The physical and spectral data are in accordance with reported literature data.[25]

The compound is not stable for a long time in CDCl$_3$. ^{1}H NMR in CD$_2$Cl$_2$ is provided if needed:

^{1}H NMR (300 MHz, CD$_2$Cl$_2$) δ 4.82–4.72 (m, 1H), 4.33–4.10 (m, 2H), 3.88–3.71 (m, 1H), 3.54–3.45 (m, 1H), 2.44 (t, J = 2.4 Hz, 1H), 1.88–1.41 (m, 6H).
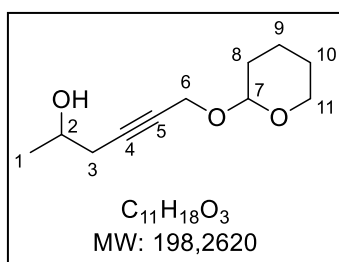
6-tetrahydropyran-2-yloxyhex-4-yn-2-ol. In a three-neck, 1-L round bottom flask equipped with a thermometer and an addition funnel was added the alkyne (2-prop-2-ynoxytetrahydropyran) (14.02 g, 100 mmol) and THF (400 mL). The solution was cooled to -78 °C and nBuLi (2.50 mol/L, 44.0 mL, 110 mmol) was added dropwise *via* the addition funnel.

The structure is labeled with positions 1–11, OH on carbon 2. Formula $C_{11}H_{18}O_3$, MW: 198,2620.

The resultant solution was stirred at the same temperature for 10 minutes, then warmed up to 0 °C for an additional 20 minutes. After cooling back to -78 °C, BF$_3$•Et$_2$O (13.6 mL, 110 mmol) was added and the solution stirred at -78 °C for 10 minutes. A solution of the epoxide (2-methyloxirane) (7.7 mL, 110 mmol) in anhydrous THF (100 mL) was added dropwise *via* the addition funnel, not rising the temperature above -70 °C. The reaction mixture was stirred at -78 °C for 30 minutes, at 0 °C for 30 minutes, and at room temperature for 20 minutes. After it was treated with sat. aq. NH$_4$Cl and aq. ammonia (v/v 2:1, 200 mL), the resultant mixture was stirred at rt for 30 minutes. The mixture was then extracted with Et$_2$O (1 x 300 mL). The combined organic phases were washed with water (200 mL), brine (200 mL), dried over Na$_2$SO$_4$, filtered and concentrated. The crude residue was purified by fcc (SiO$_2$, pentane:Et$_2$O 7:3 to 4:6) to afford the title compound as a colorless oil (11.82 g, 59.6 mmol, 60%) along with recovered alkyne (2.28 g, 16% recovered SM).

^{1}H NMR (300 MHz, CD$_2$Cl$_2$) δ 4.76 (t, J = 3.3 Hz, 1H, H$_7$), 4.32–4.12 (m, 2H, H$_6$), 3.98 – 3.85 (m, 1H, H$_2$), 3.80 (ddd, J = 11.5, 8.5, 3.4 Hz, 1H, H$_{11}$), 3.54–3.43 (m, 1H, H$_{11}$), 2.48–2.24 (m, 2H, H$_3$), 2.16 (d, J = 4.2 Hz, 1H, -OH), 1.88–1.42 (m, 6H, H$_8$, H$_9$, H$_{10}$), 1.21 (d, J = 6.2 Hz, 3H, H$_1$). ^{13}C NMR (75 MHz, CD$_2$Cl$_2$) δ 97.33 & 97.31 (C$_7$), 83.2 (C$_4$), 78.8 (C$_5$), 66.7 (C$_2$), 62.4 (C$_{11}$), 54.89 & 54.87 (C$_6$), 30.8 (C$_9$), 29.7 (C$_3$), 25.8 (C$_{10}$), 22.6 (C$_1$), 19.6 (C$_8$). dr 1:1 estimated on the ^{13}C signals at 97.33 & 97.31, and 54.89 & 54.87. FT-IR (neat, cm-1): 3413, 2941, 2870, 1201, 1114, 1017, 941, 902, 870, 814. HRSM (ESI) m/z calculated for C$_{11}$H$_{18}$O$_3$Na [M+Na]$^+$ = 221.1148. Found 221.1147. R$_f$ = 0.38 (pentane/Et$_2$O 1:1).
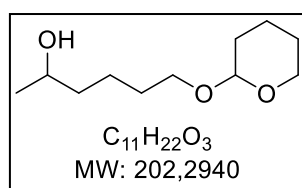
6-tetrahydropyran-2-yloxyhexan-2-ol. Due to the size of the available autoclave, the reaction scale was limited to 20 mmols. Three batches were run successively, then purified together (60 mmol scale total).

The structure shows OH group. Formula $C_{11}H_{22}O_3$, MW: 202,2940.

In a 100-mL erlenmeyer flask were added 6-tetrahydropyran-2-yloxyhex-4-yn-2-ol (3.97 g, 20.0 mmol), EtOAc (100 mL) and palladium (10.0 % on C, 200 mg, 0.19 mmol). The flask was inserted into the autoclave and the pressure of H$_2$ was set to 20 mbar. The reaction mixture was stirred at rt for 30 minutes and TLC indicated completion of reaction. The mixture was filtrated on celite, rinsing with EtOAc. The solvent was evaporated and the crude residue was purified by fcc (SiO$_2$, pentane:Et$_2$O 3:2 to 1:1) to give the title compound as a colorless oil (9.51 g, 47.0 mmol, 79%). A major side product proved to be the ketone at position 2 (6-tetrahydropyran-2-yloxyhexan-2-one, 1.56 g, 7.81 mmol, 13%), whose formation increased with the scale-up.

Spectral data of 6-tetrahydropyran-2-yloxyhexan-2-ol. Note that the product is not stable in CDCl$_3$ overnight. ^{1}H NMR (300 MHz, CDCl$_3$) δ 4.55 (t, J = 4.3, 2.7 Hz, 1H), 3.91–3.66 (m, 3H), 3.53–3.43 (m, 1H), 3.38 (dt, J = 9.7, 6.4 Hz, 1H), 1.88–1.29 (m, 12H), 1.17 (d, J = 6.2 Hz, 3H). ^{13}C NMR (75 MHz, CDCl$_3$) δ 99.04, 99.01, 68.06, 68.03, 67.6, 62.50, 62.47, 39.19, 39.17, 30.9, 29.77, 29.75, 25.58, 23.59, 23.6, 22.61, 22.56, 19.81, 19.78. dr 1:1 estimated on the ^{13}C signals. R$_f$ = 0.22 (pentane/Et$_2$O 1:1). The physical and spectral data are in accordance with reported literature data.[26]

The ketone side product can easily be reduced back to the alcohol according to the following protocol:


C$_{11}$H$_{20}$O$_3$
MW: 200,2780
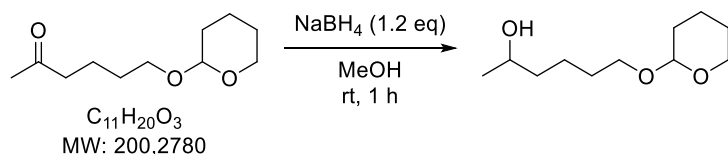
NaBH$_4$ (316 mg, 8.57 mmol) was added to a solution of 6-tetrahydropyran-2-yloxyhexan-2-one (1.56 g, 7.79 mmol) in MeOH (16 mL) at 0 °C. The reaction mixture was allowed to warm up to room temperature and stirred until completion as assessed by TLC (pentane:Et$_2$O 1:1, 1 h). The reaction mixture was cooled down to 0 °C and quenched with water (25 mL). The mixture was extracted with Et$_2$O (2 x 50 mL). The combined organic extracts were dried (Na$_2$SO$_4$), filtered and concentrated to give the crude product as a pale-yellow oil (1.54 g, 7.61 mmol, 98%). The crude product can be engaged without purification in the deprotection step.

Spectral data of 6-tetrahydropyran-2-yloxyhexan-2-one. ^{1}H NMR (400 MHz, CDCl$_3$) δ 4.55 (dd, J = 4.6, 2.8 Hz, 1H), 3.84 (ddd, J = 11.1, 7.6, 3.6 Hz, 1H), 3.73 (dt, J = 9.7, 6.3 Hz, 1H), 3.53–3.45 (m, 1H), 3.37 (dt, J = 9.7, 6.1 Hz, 1H), 2.45 (t, J = 7.2 Hz, 2H), 2.12 (s, 3H), 1.88–1.75 (m, 2H), 1.73–1.44 (m, 10H). ^{13}C NMR (75 MHz, CDCl$_3$) δ 209.1, 99.0, 67.3, 62.5, 43.6, 30.9, 30.0, 29.3, 25.6, 20.8, 19.8. R$_f$ = 0.53 (pentane/Et$_2$O 1:1). The physical and spectral data are in accordance with reported literature data.[26]

C$_6$H$_{14}$O$_2$
MW: 118,1760
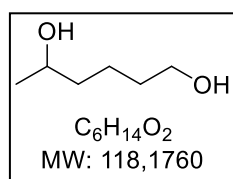
Hexane-1,5-diol. In a 1-L two-neck flask equipped with a refluxing condenser was added 6-tetrahydropyran-2-yloxyhexan-2-ol (10.9 g, 54.0 mmol), MeOH (430 mL), and pTsOH•H$_2$O (364 mg, 1.91 mmol). The mixture was refluxed until completion as assessed by TLC (100% EtOAc, 4 h). The solvent was evaporated and the crude residue purified by fcc (SiO$_2$, 100% EtOAc) to give the title compound as a colorless oil (5.17 g, 43.7 mmol, 81%).

^{1}H NMR (300 MHz, CDCl$_3$) δ 3.88 – 3.74 (m, 1H), 3.65 (t, J = 6.3 Hz, 2H), 2.01 – 1.92 (m, 2H), 1.70 – 1.32 (m, 6H), 1.19 (d, J = 6.2 Hz, 3H). ^{13}C NMR (75 MHz, CDCl$_3$) δ 68.2, 62.8, 38.9, 32.6, 23.7, 22.0. R$_f$ = 0.29 (100% EtOAc). The physical and spectral data are in accordance with reported literature data.[27]

OMs

OMs

C$_8$H$_{18}$O$_6$S$_2$
MW: 274,3460
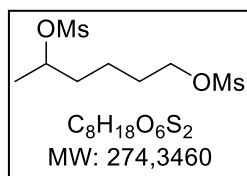
5-methylsulfonyloxyhexyl methanesulfonate. To a solution of hexane-1,5-diol (5.17 g, 43.7 mmol) in DCM (90 mL) was added NEt$_3$ (15.2 mL, 109 mmol). The solution was cooled to -40 °C and MsCl (7.45 mL, 96.2 mmol) was added under vigorous stirring. A white precipitate was immediately formed. After the addition was complete, the mixture was allowed to warm up to 0 °C, stirred at this temperature until completion of reaction (TLC monitoring, 100% EtOAc, 20 min), and then poured into cold 1 N HCl (200 mL). The organic layer was separated, and the aqueous layer was extracted with DCM (2 x 100 mL). The combined organic phases were washed with aq. sat. NaHCO$_3$ (100 mL), dried (Na$_2$SO$_4$), filtered and concentrated. The crude residue was purified by a short fcc (SiO$_2$, 100% Et$_2$O) to afford the title compound as a pale-yellow oil (11.4 g, 41.7 mmol, 95%).

^{1}H NMR (400 MHz, CD$_2$Cl$_2$) δ 4.76 (dqd, J = 7.4, 6.3, 4.9 Hz, 1H, CH-OMs), 4.21 (t, J = 6.4 Hz, 2H, CH$_2$-OMs), 2.99 (s, 3H, OMs), 2.98 (s, 3H, OMs), 1.86 – 1.74 (m, 2H, CH$_2$), 1.74 – 1.60 (m, 2H, CH$_2$), 1.59 – 1.44 (m, 2H, CH$_2$), 1.40 (d, J = 6.3 Hz, 3H, CH$_3$-CH-OMs). ^{13}C NMR (101 MHz, CD$_2$Cl$_2$) δ 80.1 (CH-OMs), 70.4 (CH$_2$-OMs), 39.0 (OMs), 37.6 (OMs), 36.3 (CH$_2$), 29.1 (CH$_2$), 21.6 (CH$_2$), 21.3 (CH$_3$-CH-OMs). FT-IR (neat, cm-1): 1327, 1166, 896. HRMS (ESI) m/z: [M+Na]$^+$ Calcd for C$_8$H$_{18}$O$_6$NaS$_2$ 297.0437. Found 297.0433. R$_f$ = 0.45 (100% Et$_2$O).

6p
C$_{18}$H$_{28}$BNO$_2$
MW: 301,24
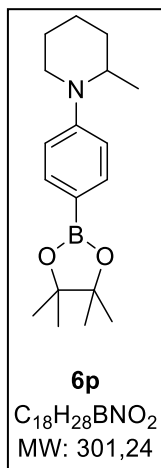
2-methyl-1-[4-(4,4,5,5-tetramethyl-1,3,2-dioxaborolan-2-yl)phenyl]piperidine (6p). This is not an optimized procedure.

^{1}H NMR (300 MHz, CDCl$_3$): δ 7.68 (d, J = 8.6 Hz, 2H), 6.86 (d, J = 8.7 Hz, 2H), 4.23–4.06 (m, 1H), 3.45 (dd, J = 12.5, 4.3 Hz, 1H), 2.95 (t, J = 11.7 Hz, 1H), 1.94–1.70 (m, 2H), 1.70–1.50 (m, 4H), 1.32 (s, 12H), 1.05 (d, J = 6.7 Hz, 3H). ^{11}B NMR (96 MHz, CDCl$_3$): δ 30.9. ^{13}C NMR (75 MHz, CDCl$_3$): δ 153.4 (Cq$_{Ar}$), 136.3 (2xCH$_{Ar}$), 114.7 (2xCH$_{Ar}$), 83.4 (Cq$_{aliph.}$), 49.9 (CH), 42.6 (CH$_2$), 31.2 (CH$_2$), 26.0 (CH$_2$), 25.0 (4xCH$_3$), 19.1 (CH$_2$), 13.4 (CH$_3$). Due to coupling to the quadrupolar ^{11}B and ^{10}B nuclei, the aromatic carbon atom bearing the BPin was not detected. FT-IR (neat, cm^{-1}): 2975, 2931, 1604, 1392, 1360, 1312, 1141, 1091, 960, 861, 819, 655. HRMS (ESI) m/z: Calcd for C$_{18}$H$_{29}$O$_2$NB [M+H]$^+$ = 302.2286. Found: 302.2283. mp = 94.2–95.4 °C. R$_f$ = 0.25 (pentane/Et$_2$O 92:8). Chiral HPLC:

```
====================================================================
Acq. Operator   : SYSTEM                    Seq. Line :    3
Acq. Instrument : 1260NP                     Location :   72
Injection Date  : 02.02.2022 14:02:36            Inj :    1
                                      Inj Volume : 10.000 µl
                                      Actual Inj Volume : 10.000 µl
Method          : C:\Chem32\1\Data\PP\OD-H_ECO-5-135 2022-02-02 11-49-44\C_005-modKU.M (
                  Sequence Method). C = 25% iPrOH in hexanes. A = hexanes. Method: 0.5% C, 95.5% A.
Last changed    : 02.02.2022 11:49:44 by SYSTEM
Method Info     : 0.125% iPrOH in hexanes. Flow: 0.9 mL/min. Column: chiral OD-H.

Additional Info : Peak(s) manually integrated
```
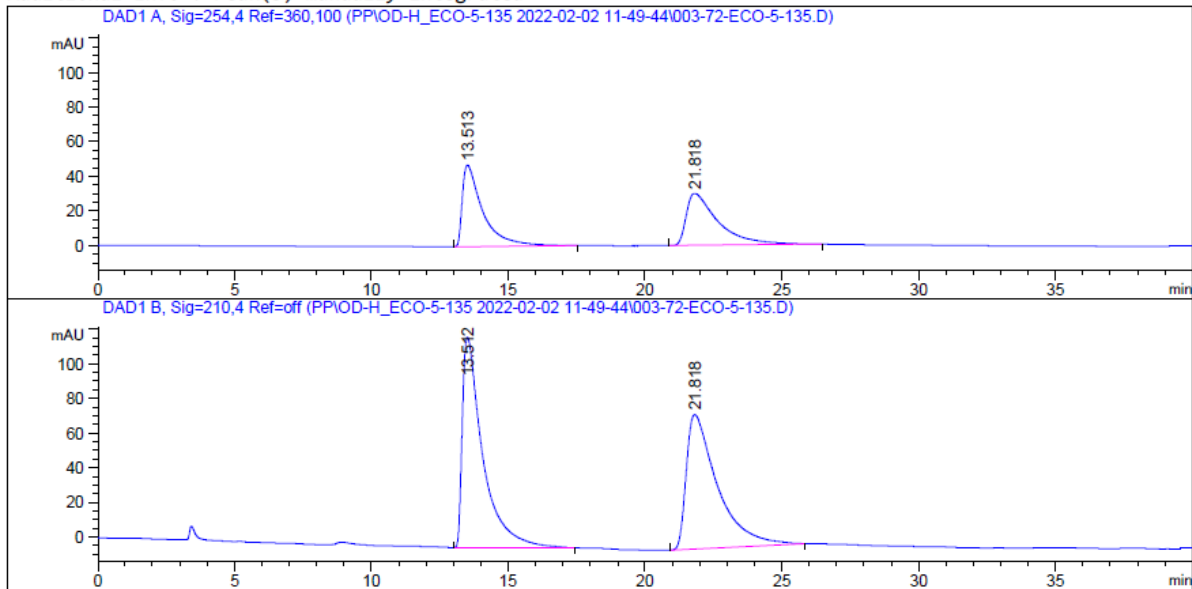
Photoredox reactions for the synthesis of 7p and 8p

6p
1 mmol

1.1 equiv.

7p
40%, dr 6:1

8p
3%, α/β >20:1
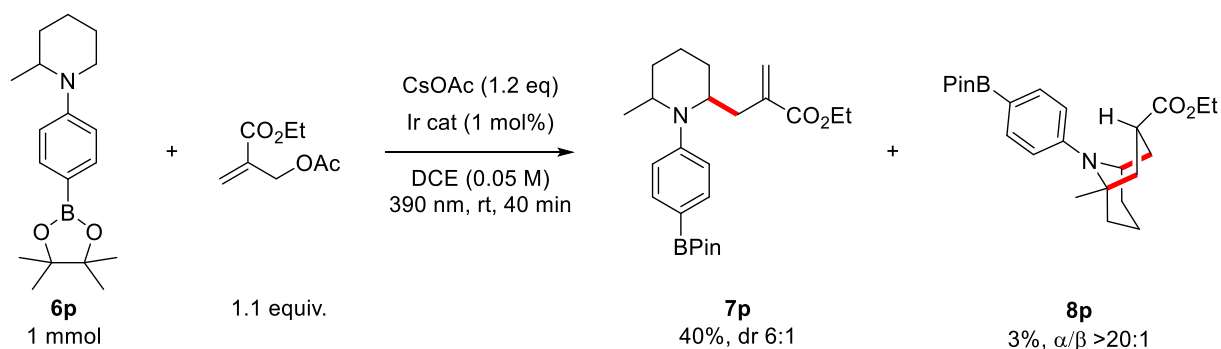
Ethyl 2-[[6-methyl-1-[4-(4,4,5,5-tetramethyl-1,3,2-dioxaborolan-2-yl)phenyl]-2-piperidyl]methyl]prop-2-enoate (7p).

In an oven-dried 25-mL seal-tube were successively added the radical trap (ethyl 2-(acetoxymethyl)prop-2-enoate) (189 mg, 1.10 mmol), 2-methyl-1-[4-(4,4,5,5-tetramethyl-1,3,2-dioxaborolan-2-yl)phenyl]piperidine **6p** (301 mg, 1.00 mmol), [Ir{dF(CF$_3$)ppy}$_2$(dtbpy)]PF$_6$ (5.6 mg, 0.005 mmol, 1 mol%) and cesium acetate (231 mg, 1.2 mmol). The vial was closed with a rubber septum and evacuated/refilled with N$_2$ (x 3). Finally, dry and degassed 1,2-dichloroethane (20.00 mL, 0.05 M) was added. The resulting yellow mixture was placed in front of a 390 nm blue LED (5 cm distance) and stirred until completion of the reaction (TLC monitoring, heptanes:EtOAc 92:8).

R$_f$ values (heptanes/EtOAc 92:8)

Cyclized product 8p

R$_f$ = 0.30

Mono-allylated product 7p

minor dia: R$_f$ = 0.23

major dia: R$_f$ = 0.19

The reaction mixture was diluted with sat. NaHCO$_3$ (30 mL). The aqueous phase was extracted with DCM (3 x 50 mL) and the combined organic phases were dried over Na$_2$SO$_4$, filtered, and concentrated under reduced pressure to give crude product as an orange oil. Purification by flash column chromatography (SiO$_2$, pentane:Et$_2$O 95:5 to 80:20) afforded the mono-allylated product as a colorless oil (167 mg, 0.40 mmol, 40%, dr 6:1).

• *Characterization of 7p (major dia)*

^{1}H NMR (400 MHz, CD$_2$Cl$_2$): δ 7.62 (d, J = 8.9 Hz, 2H), 6.98 (d, J = 8.7 Hz, 2H), 6.20 (d, J = 1.5 Hz, 1H), 5.60–5.54 (m, 1H), 4.21 (q, J = 7.1 Hz, 2H), 3.96–3.79 (m, 2H), 2.53–2.35 (m, 2H), 1.88–1.70 (m, 2H), 1.70–1.53 (m, 3H), 1.53–1.44 (m, 1H), 1.33–1.28 (m, 15H), 1.08 (d, J = 6.6 Hz, 3H). ^{11}B NMR (96 MHz, CD$_2$Cl$_2$): δ 30.7. ^{13}C NMR (101 MHz, CD$_2$Cl$_2$): δ 167.3 (C=O), 151.6 (Cq$_{Ar}$), 139.5 (Cq$_{Ar}$), 136.3 (2xCH$_{Ar}$), 127.3 (CH$_2$), 116.0 (2xCH$_{Ar}$), 83.6 (2xCq$_{aliph.}$), 61.2 (CH$_2$), 53.3 (CH), 49.6 (CH), 35.4 (CH$_2$), 32.3 (CH$_2$), 28.0 (CH$_2$), 25.10 (2xCH$_3$), 25.06 (2xCH$_3$), 19.5 (CH$_3$), 16.8 (CH$_2$), 14.5 (CH$_3$). Due to coupling to the quadrupolar 11B and 10B nuclei, the aromatic carbon atom bearing the BPin was not detected. HRMS (ESI) m/z: [M$^+$H]$^+$ Calcd for C$_{24}$H$_{37}$O$_4$NB 414.2810. Found 414.2806. FT-IR (neat, cm^{-1}): 2941, 2929, 1705, 1602, 1357, 1303, 1265, 1141, 1103, 961, 859, 818, 654.

• *Characterization of **7p** (minor dia)*

^{1}H NMR (400 MHz, CD$_2$Cl$_2$): δ 7.68–7.60 (m, 2H), 7.02–6.96 (m, 2H), 6.13 (d, J = 1.6 Hz, 1H), 5.47 (d, J = 1.6 Hz, 1H), 4.14 (q, J = 7.1 Hz, 2H), 3.74 (dq, J = 12.1, 4.1 Hz, 1H), 3.63 (pd, J = 6.3, 4.0 Hz, 1H), 2.58 (dd, J = 13.5, 3.8 Hz, 1H), 2.41–2.29 (m, 1H), 2.01–1.89 (m, 1H), 1.89–1.74 (m, 1H), 1.73–1.45 (m, 4H), 1.31 (s, 12H), 1.26 (t, J = 7.2 Hz, 3H), 1.04 (d, J = 6.2 Hz, 3H). ^{11}B NMR (96 MHz, CD$_2$Cl$_2$): δ 30.8. ^{13}C NMR (101 MHz, CD$_2$Cl$_2$): δ 167.3 (C=O), 153.1 (Cq$_{Ar}$), 139.5 (Cq$_{Ar}$), 135.6 (2xCH$_{Ar}$), 126.9 (CH$_2$), 121.3 (2xCH$_{Ar}$), 83.7 (2xCq$_{aliph.}$), 61.1 (CH$_2$), 55.9 (CH), 49.4 (CH), 32.4 (CH$_2$ + CH$_2$), 27.3 (CH), 25.09 (2xCH$_3$), 25.06 (2xCH$_3$), 19.1 (CH$_3$), 17.1 (CH$_2$), 14.4 (CH$_3$). Due to coupling to the quadrupolar ^{11}B and ^{10}B nuclei, the aromatic carbon atom bearing the BPin was not detected. HRMS (ESI) m/z: [M$^+$H]$^+$ Calcd for C$_{24}$H$_{37}$O$_4$NB 414.2810. Found 414.2806. FT-IR (neat, cm^{-1}): 2976, 2931, 1714, 1602, 1358, 1142, 1091, 962, 860, 659.

Note: the relative configuration of **7p** has not yet been attributed.

Independent cyclization reaction of 7p to 8p.
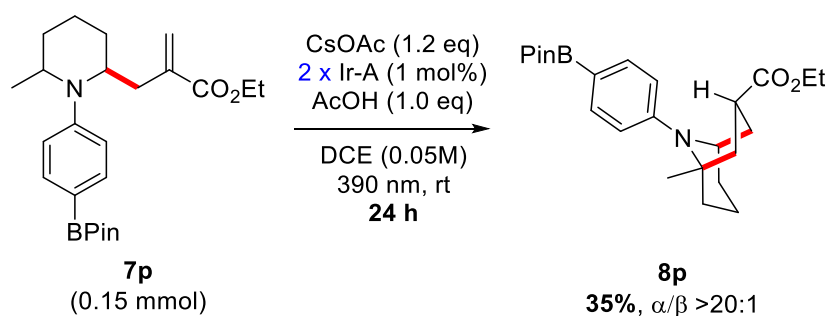
Ethyl 1-methyl-9-[4-(4,4,5,5-tetramethyl-1,3,2-dioxaborolan-2-yl)phenyl]-9-azabicyclo[3.3.1]nonane-3-carboxylate (8p).

Into an oven-dried 5-mL vial was added [Ir{dF(CF$_3$)ppy}$_2$(dtbpy)]PF$_6$ (1.7 mg, 0.0015 mmol) and CsOAc (35 mg, 0.18 mmol). The vial was evacuated and filled with N$_2$ (x 3), and a solution of **7p** (major isomer

only) in DCE (0.05 M, 3.0 mL, 0.15 mmol) was added, followed by acetic acid (8.6 µL, 0.15 mmol). The mixture was shortly sonicated and placed in front of a 390 nm LED for 7 hours. In absence of full starting material conversion, [Ir{dF(CF$_3$)ppy}$_2$(dtbpy)]PF$_6$ (1.7 mg, 0.0015 mmol) in DCE (0.5 mL) was added and the reaction was further stirred for 17 h. The reaction mixture was diluted with sat. NaHCO$_3$ (3 mL). The aqueous phase was extracted with DCM (3 x 5 mL) and the combined organic phases were dried over Na$_2$SO$_4$, filtered, and concentrated under reduced pressure to give crude product as an orange oil. Purification by flash column chromatography (SiO$_2$, heptanes/EtOAc 93:7) afforded the desired product as a colorless oil (21.7 mg, 0.052 mmol, 35%, *α/β > 20:1*).

• *Characterization of the cyclized product_α isomer (β diastereoisomer was detected)*

^{1}H NMR (400 MHz, CD$_2$Cl$_2$): *δ* 7.57 (d, J = 8.2 Hz, 2H), 7.03 (d, J = 8.0 Hz, 2H), 4.09 (q, J = 7.1 Hz, 2H), 3.89 (dq, J = 10.6, 3.6 Hz, 1H), 2.67 (tt, J = 12.5, 6.2 Hz, 1H), 2.28 (dddd, J = 13.3, 10.9, 6.2, 2.1 Hz, 1H), 2.06 – 1.73 (m, 4H), 1.73 – 1.53 (m, 3H), 1.48 – 1.34 (m, 2H), 1.30 (s, 12H), 1.30 (s, 3H), 1.23 (t, J = 7.1 Hz, 3H). ^{11}B NMR (96 MHz, CD$_2$Cl$_2$): *δ* 30.7. ^{13}C NMR (101 MHz, CD$_2$Cl$_2$): *δ* 176.1 (C=O), 154.2 (Cq$_{Ar}$), 135.2 (2xCH$_{Ar}$), 124.5 (2xCH$_{Ar}$), 83.8 (2xCq$_{aliph.}$), 60.6 (CH$_2$), 55.3 (CH), 40.7 (CH$_2$), 38.0 (CH$_2$), 36.4 (CH), 32.4 (CH$_3$), 30.8 (CH$_2$), 28.8 (CH$_2$), 25.1 (4xCH$_3$), 16.9 (CH$_2$), 14.5 (CH$_3$). Due to coupling to the quadrupolar ^{11}B and ^{10}B nuclei, the aromatic carbon atom bearing the BPin was not detected. HRMS (ESI) m/z: [M$^+$H]$^+$ Calcd for C$_{24}$H$_{37}$O$_4$NB 414.2810. Found 414.2806. FT-IR (neat, cm^{-1}): 2926, 1729, 1601, 1356, 1259, 1141, 1091, 960.1, 659. R$_{f-α}$ = 0.14, heptanes/EtOAc 93:7

Investigating different protecting groups

P-8h
C$_{21}$H$_{29}$NO$_4$
MW: 359,4660
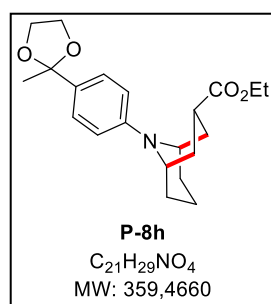
Ethyl 9-[4-(2-methyl-1,3-dioxolan-2-yl)phenyl]-9-azabicyclo[3.3.1]nonane-3-carboxylate (P-8h)

Following *modified general procedure C* with 1-[4-(2-methyl-1,3-dioxolan-2-yl)phenyl]piperidine **P-6h** (49.5 mg, 0.20 mmol) and ethyl 2-(acetoxymethyl)prop-2-enoate (37.9 mg, 0.22 mmol) reacting for 1 hour. Purification by column chromatography (SiO$_2$, pentane/Et$_2$O 80:20) afforded the product as a colorless oil (45.3 mg, 0.13 mmol, 63%, α/β >20:1).

Characterization of the major diastereoisomer:

^{1}H NMR (400 MHz, CDCl$_3$): δ 7.33–7.27 (m, 2H), 6.84–6.75 (m, 2H), 4.28–4.16 (m, 2H), 4.10 (q, J = 7.1 Hz, 2H), 4.06–3.95 (m, 2H), 3.86–3.75 (m, 2H), 2.46–2.28 (m, 3H), 2.01 (qt, J = 13.3, 4.4 Hz, 1H), 1.77 (tt, J = 13.4, 4.4 Hz, 2H), 1.71–1.62 (m, 2H), 1.64 (s, 3H), 1.58–1.50 (m, 1H), 1.50–1.41 (m, 2H), 1.23 (t, J = 7.1 Hz, 3H). ^{13}C NMR (101 MHz, CDCl$_3$): δ 75.9 (C=O), 150.1 (Cq$_{Ar}$), 131.8 (Cq$_{Ar}$), 126.7 (2xCH$_{Ar}$), 113.7

(2xCH$_{Ar}$), 109.1 (Cq$_{aliph.}$), 64.5 (2xCH$_2$), 60.5 (CH$_2$), 47.3 (2xCH), 34.9 (CH), 30.4 (2xCH$_2$), 28.4 (2x CH$_2$), 27.6 (CH$_3$), 14.4 (CH$_3$), 14.3 (CH$_2$). FT-IR (cm^{-1}, neat): 2924, 1722, 1606, 1513, 1402, 1367, 1285, 1243, 1174, 1033, 860, 803. HRMS (ESI) m/z: [M+H]$^+$ Calcd for C$_{21}$H$_{30}$O$_4$N 360.2169; Found 360.2170. R$_f$ = 0.30 (pentane/Et$_2$O 80:20). mp = 85.3 – 87.1 °C.

Characteristic peak of the minor diastereoisomer:

^{1}H NMR (400 MHz, CDCl$_3$): δ 4.36 (br d, J = 10.9 Hz, 3H), 3.35 – 3.25 (m, 1H).

Deprotection of Ethyl 9-[4-(2-methyl-1,3-dioxolan-2-yl)phenyl]-9-azabicyclo[3.3.1]nonane-3-carboxylate (P-8h → 8h). In a 10-ml round-bottom flask were added ethyl 9-[4-(2-methyl-1,3-dioxolan-2-yl)phenyl]-9-azabicyclo[3.3.1]nonane-3-carboxylate (38.8 mg, 0.11 mmol), EtOH (1.5 mL), water (0.5 mL), and sulfuric acid (6 µL, 0.112 mmol). The reaction mixture was stirred at room temperature for 2 hours, and completion of the reaction was assessed by TLC. The ethanol was evaporated under reduced pressure. The residue was taken in EtOAc (10 mL) and made basic by addition of aq. sat. NaHCO$_3$ (10 mL). The aq. phase was extracted with EtOAc (2 x 10 mL). The combined organic phase was dried (Na$_2$SO$_4$), filtered, and evaporated under reduced pressure to give crude product as an oily residue. Purification by column chromatography (SiO$_2$, pentane/Et$_2$O 80:20) afforded ethyl 9-(4-acetylphenyl)-9-azabicyclo[3.3.1]nonane-3-carboxylate as a colorless oil (31.0 mg, 0.10 mmol, **91%**, dr >20:1). Spectral data are in accordance with known product **8h**.

P-8q
C$_{20}$H$_{27}$NO$_4$
MW: 345,4390

Ethyl 9-[4-(1,3-dioxolan-2-yl)phenyl]-9-azabicyclo[3.3.1]nonane-3-carboxylate (P-8q)

Following *modified general procedure C* with 1-[4-(1,3-dioxolan-2-yl)phenyl]piperidine (46.7 mg, 0.20 mmol) and ethyl 2-(acetoxymethyl)prop-2-enoate (37.9 mg, 0.22 mmol) reacting for 1 hour. Purification by column chromatography (SiO$_2$, pentane/Et$_2$O 80:20) afforded the product as a colorless oil (38.8 mg, 0.11 mmol, **56%**, α/β >20:1).
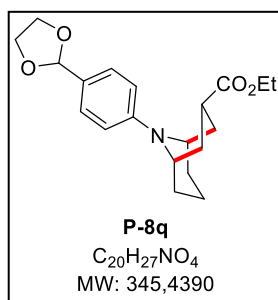
Characterization of the major diastereoisomer:

^{1}H NMR (400 MHz, CD$_2$Cl$_2$): δ 7.35–7.20 (m, 2H), 6.88–6.78 (m, 2H), 5.63 (s, 1H), 4.32–4.19 (m, 2H), 4.15–3.91 (m, 6H), 2.41–2.26 (m, 3H), 2.01 (qt, J = 13.5, 4.3 Hz, 1H), 1.75 (tt, J = 13.3, 4.2 Hz, 2H), 1.70–1.60 (m, 2H), 1.58–1.42 (m, 3H), 1.20 (t, J = 7.1 Hz, 3H). ^{13}C NMR (101 MHz, CD$_2$Cl$_2$): δ 175.8 (C=O), 151.9 (Cq$_{Ar}$), 128.3 (2xCH$_{Ar}$), 126.4 (Cq$_{Ar}$), 113.9 (2xCH$_{Ar}$), 104.4 (CH), 65.6 (2xCH$_2$), 60.6 (CH$_2$), 47.7 (2xCH), 35.2 (CH), 30.6 (2xCH$_2$), 28.7 (2xCH$_2$), 14.6 (CH$_2$), 14.4 (CH$_3$). FT-IR (cm^{-1}, neat): 2926, 1724,

1611, 1517, 1395, 1281, 1177, 1074, 807. HRMS (ESI) m/z: [M+H]$^+$ Calcd for $C_{20}H_{28}O_4N$ 346.2018; Found: 346.2016. R_f = 0.44 (pentane/Et$_2$O 60:40)
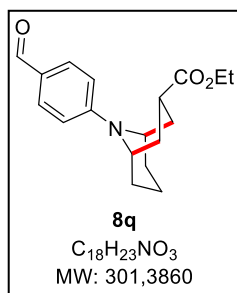
Ethyl 9-(4-formylphenyl)-9-azabicyclo[3.3.1]nonane-3-carboxylate (8q)

In a 10-ml round-bottom flask were added ethyl 9-[4-(1,3-dioxolan-2-yl)phenyl]-9-azabicyclo[3.3.1]nonane-3-carboxylate (38.8 mg, 0.11 mmol), EtOH (1.5 mL), water (0.5 mL), and sulfuric acid (6 µL, 0.112 mmol). The reaction was stirred at rt for 2 hours, and completion of the reaction was assessed by TLC. The ethanol was evaporated under reduced pressure. The residue was taken in EtOAc (10 mL) and made basic by addition of aq. sat. NaHCO$_3$ (10 mL). The aq. phase was extracted with EtOAc (2 x 10 mL). The combined organic phase was dried (Na$_2$SO$_4$), filtered, and evaporated under reduced pressure to give crude product as an oily residue. Purification by column chromatography (SiO$_2$, pentane/Et$_2$O 70:30) afforded ethyl 9-(4-formylphenyl)-9-azabicyclo[3.3.1]nonane-3-carboxylate as a colorless oil (31.7 mg, 0.11 mmol, 94%, α/β >20:1).

Characterization of the major diastereoisomer:

^{1}H NMR (400 MHz, CD$_2$Cl$_2$): δ 9.69 (s, 1H), 7.75–7.60 (m, 2H), 6.96–6.80 (m, 2H), 4.47–4.32 (m, 2H), 4.08 (q, *J* = 7.1 Hz, 2H), 2.44–2.32 (m, 2H), 2.26 (tt, *J* = 12.8, *J* = 5.7 Hz, 1H), 2.05 (qt, *J* = 14.0, 13.4, 13.4, 4.7 Hz, 1H), 1.82–1.66 (m, 4H), 1.62–1.46 (m, 3H), 1.21 (t, *J* = 7.1 Hz, 3H). ^{13}C NMR (101 MHz, CD$_2$Cl$_2$): δ 189.9 (CHO), 175.3 (C=O), 155.1 (Cq$_{Ar}$), 132.5 (2xCH$_{Ar}$), 126.1 (Cq$_{Ar}$), 112.9 (2xCH$_{Ar}$), 60.8 (CH$_2$), 47.7 (2xCH), 35.5 (CH), 30.6 (2xCH$_2$), 28.9 (2xCH$_2$), 14.42 (CH$_2$), 14.39 (CH$_3$). FT-IR (cm^{-1}, neat): 2927, 1724, 1679, 1590, 1554, 1514, 1400, 1286, 1231, 1166, 1042, 811. HRMS (ESI) m/z: [M+Na]$^+$ Calcd for $C_{18}H_{23}O_3NNa$ 324.1581; Found 324.1580. R_f = 0.32 (pentane/Et$_2$O 60:40).

Characteristic peak of the minor diastereoisomer:

^{1}H NMR (400 MHz, CD$_2$Cl$_2$): δ 3.33 (tt, J_{ax-ax} = 12.0, J_{ax-eq} = 6.1 Hz, 1H).

Literature references

1 C. L. Joe and A. G. Doyle, *Angewandte Chemie International Edition*, 2016, **55**, 4040–4043.

2 Q. Su, L. A. Dakin and J. S. Panek, *J. Org. Chem.*, 2007, **72**, 2–24.

3 G. Patel, C. E. Karver, R. Behera, P. J. Guyett, C. Sullenberger, P. Edwards, N. E. Roncal, K. Mensa-Wilmot and M. P. Pollastri, *J. Med. Chem.*, 2013, **56**, 3820–3832.

4 Q. Yin, H. F. T. Klare and M. Oestreich, *Angewandte Chemie International Edition*, 2017, **56**, 3712–3717.

5 A. Noble and D. W. C. MacMillan, *J. Am. Chem. Soc.*, 2014, **136**, 11602–11605.

6 N. Takasu, K. Oisaki and M. Kanai, *Org. Lett.*, 2013, **15**, 1918–1921.

7 Z.-M. Zhang, Y.-T. Xu and L.-X. Shao, *Journal of Organometallic Chemistry*, 2021, **940**, 121683.

8 S. A. Girard, X. Hu, T. Knauber, F. Zhou, M.-O. Simon, G.-J. Deng and C.-J. Li, *Org. Lett.*, 2012, **14**, 5606–5609.

9 R. Sun, Y. Qin and D. G. Nocera, *Angewandte Chemie International Edition*, 2020, **59**, 9527–9533.

10 M. J. Cawley, F. G. N. Cloke, R. J. Fitzmaurice, S. E. Pearson, J. S. Scott and S. Caddick, *Org. Biomol. Chem.*, 2008, **6**, 2820–2825.

11 Q. Zou, C. Wang, J. Smith, D. Xue and J. Xiao, *Chemistry – A European Journal*, 2015, **21**, 9656–9661.

12 D. Chamorro-Arenas, U. Osorio-Nieto, L. Quintero, L. Hernández-García and F. Sartillo-Piscil, *J. Org. Chem.*, 2018, **83**, 15333–15346.

13 M. Quadri, C. Stokes, A. Gulsevin, A. C. J. Felts, K. A. Abboud, R. L. Papke and N. A. Horenstein, *J. Med. Chem.*, 2017, **60**, 7928–7934.

14 A. H. Sandtorv and D. R. Stuart, *Angewandte Chemie International Edition*, 2016, **55**, 15812–15815.

15 N. J. Taylor, E. Emer, S. Preshlock, M. Schedler, M. Tredwell, S. Verhoog, J. Mercier, C. Genicot and V. Gouverneur, *J. Am. Chem. Soc.*, 2017, **139**, 8267–8276.

16 *Org. Synth.*, 2006, **83**, 24.

17 J. Zhang, Y. Li, R. Xu and Y. Chen, *Angewandte Chemie International Edition*, 2017, **56**, 12619–12623.

18 C. Pautigny, S. Jeulin, T. Ayad, Z. Zhang, J.-P. Genêt and V. Ratovelomanana-Vidal, *Advanced Synthesis & Catalysis*, 2008, **350**, 2525–2532.

19 B. M. Trost, M. R. Machacek and H. C. Tsui, *J. Am. Chem. Soc.*, 2005, **127**, 7014–7024.

20 P. V. Ramachandran, T. E. Burghardt and L. Bland-Berry, *J. Org. Chem.*, 2005, **70**, 7911–7918.

21 E. Breuer and D. Melumad, *J. Org. Chem.*, 1973, **38**, 1601–1602.

22 C. Boga, F. Manescalchi and D. Savoia, *Tetrahedron*, 1994, **50**, 4709–4722.

23 D. Taniyama, M. Hasegawa and K. Tomioka, *Tetrahedron Letters*, 2000, **41**, 5533–5536.

24 B. Jiang, Z.-G. Huang and K.-J. Cheng, *Tetrahedron: Asymmetry*, 2006, **17**, 942–951.

25 L. Lempke, T. Fischer, J. Bell, W. Kraus, K. Rurack and N. Krause, *Org. Biomol. Chem.*, 2015, **13**, 3787–3791.

26 A. Nishida, N. Kawahara, M. Nishida and O. Yonemitsu, *Tetrahedron*, 1996, **52**, 9713–9734.

27 P. Calleja, M. Ernst, A. S. K. Hashmi and T. Schaub, *Chemistry – A European Journal*, 2019, **25**, 9498–9503.

Chapter 4

Chapter 4 – Quantum dots as photocatalysts in the radical [3+3]- annulation reaction

After the radical [3+3]-annulation had successfully been developed using iridium photocatalysis, the next milestone of this collaborative project was to use quantum dots as photocatalysts for the same transformation. After a summary of the important results obtained in Grenoble, the results obtained in Bern will be described.

4.1. Description of the quantum dots and of the small-scale reactions – Results obtained in Grenoble

4.1.1. Alpha-vinylation of *N*-phenylpyrrolidine and choice of suitable quantum dots

The developed [3+3] radical annulation is a two-step process following a mono-allylation/cyclization sequence. In order to develop suitable quantum dots, it was decided to focus on a one-step reaction. Because the mono-allylation reaction is not a viable reaction in itself (see Chapter 3, section 3.2), a known vinylation reaction was chosen instead (Scheme 1). This alpha-functionalization of cyclic aniline derivatives was developed by MacMillan[1] with iridium photocatalysis and Weiss[2] and Pillai[3] with quantum dot photocatalysis. The optimization reactions were carried out on 0.001 mmol scale and the reaction outcome determined by UHPLC-MS.
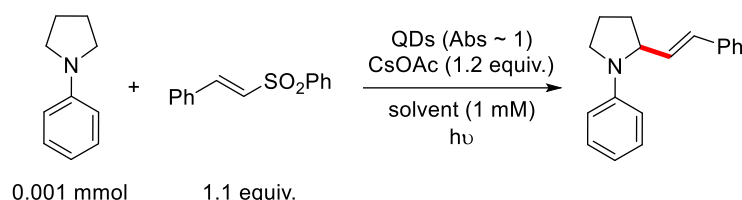
Scheme 1. Model reaction used for the selection of suitable quantum dots carried out in Grenoble.

This optimization work was entirely performed in Grenoble and will not be discussed in detail in this manuscript; the properties of the chosen quantum dots are described in Table 1. The best results obtained with these quantum dots after optimization of the solvent and of the surface ligands are summarized in Table 2.
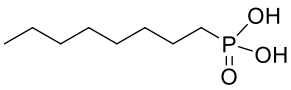
Core CdS	Core CdSe	Core-shell CdS/CdSe (Inverted type-I)	Core-shell InP/ZnS (Type-I)
$\lambda_{exciton}$ = 460 nm D = 5.5 nm $\varepsilon = 1.18 \times 10^6$ M^{-1}cm^{-1} Native ligands: oleic acid	$\lambda_{exciton}$ = 540 nm D = 3.1 nm $\varepsilon = 1.78 \times 10^5$ M^{-1}cm^{-1} Native ligands: oleic acid	$\lambda_{exciton}$ = 530 nm D = 6.35 nm (5.5 nm CdS core and two CdSe layers of 0.42 nm) $\varepsilon = 1.73 \times 10^5$ M^{-1}cm^{-1} Native ligands: oleyl amine	$\lambda_{exciton}$ = 470 nm D = 2.9 nm $\varepsilon = 1.31 \times 10^5$ M^{-1}cm^{-1} Native ligands: oleyl amine
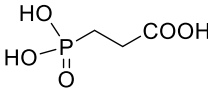
Table 1. Selected quantum dots after optimization on the vinylation reaction, and their properties. $\lambda_{exciton}$ determines the wavelength at which irradiation should be performed. Diameter D was determined by TEM analysis. ε is the extinction coefficient. Native ligands are the ligands present on the as-synthesized quantum dots. For a definition of inverted type-I and type-I core-shell quantum dots, see Chapter 1, figure 10.

Entry	QDs (mol%)	Abs	Surface ligands	Solvent	Irradiation time	Yield
1	CdS (0.1 mol%)	1.1	OlAc + OPAc	TFT	3 h	68%
2	CdSe (0.5 mol%)	0.9	OlAc + OPAc	TFT	4 h	70%
3	CdS/CdSe (0.5 mol%)	0.9	OlAm + OPAc	TFT	4 h	69%
4	Inp/ZnS (0.7 mol%)	0.9	OlAm	TFT	6 h	42%
5	CdS (0.1 mol%)	1.1	PPAc	MeCN	3 h	67%
6	CdSe (0.5 mol%)	0.9	PPAc	MeCN	3 h	71%

Octylphosphonic acid (OPAc)   Phosphopropanoic acid (PPAc)

Table 2. Best results obtained in Grenoble for the alpha-vinylation reaction of N-phenylpyrrolidine. Reactions performed on 0.001 mmol scale. Reaction outcome determined by UHPLC-MS. Structure of the non-native surface ligands.

Of note is the catalyst loading chosen for each quantum dot type in this reaction. In comparing different quantum dots, it is not the catalyst loading that should be kept constant, but the absorbance of the reaction mixture resulting from the quantum dots concentration in solution. On 0.001 mmol scale, the catalyst loading was chosen for each quantum dot type so that the absorbance of the reaction mixture was measured to be around 1. This can be determined using the Beer-Lambert law (see Chapter 1, Eq. 1) since the extinction coefficient of the quantum dots are known. This value was chosen to ensure that the light could efficiently penetrate in the reaction mixture. For example for the CdS QDs, a catalyst loading of 0.1 mol% leads to a quantum dot concentration of 1.0 µM in solution and an absorbance of 1.1. Based on the Beer-Lambert law, it means that before 0.93 cm, 90% of the photons are absorbed. After this length, only 10% of the photons are available for absorption. This is well compatible with the length of the reaction vial for the 0.001 mmol scale reactions (*vide infra*).

Importantly, the optimization of the surface ligands showed that the reaction could be run in α,α,α-trifluorotoluene (TFT) when treating the QDs with octylphosphonic acid ligands (OPAc) *in situ* prior to the reaction (Table 2, entries 1 to 3. See supporting information for the full procedure). Optimization of the equivalents of OPAc showed that 380 equivalents of OPAc should be added compared to the CdS QDs, and 300 equivalents compared to the CdSe and CdS/CdSe QDs. It is thought that the long chain ligands such as oleic acid and oleylamine prevent the accessibility of the substrates to the QD's surface, and that partial exchange with a shorter ligand creates a favorable surface disordering as well as interparticle spacing.[2,4]

4.1.2. Annulation reaction of *N*-phenylpyrrolidine under optimized conditions
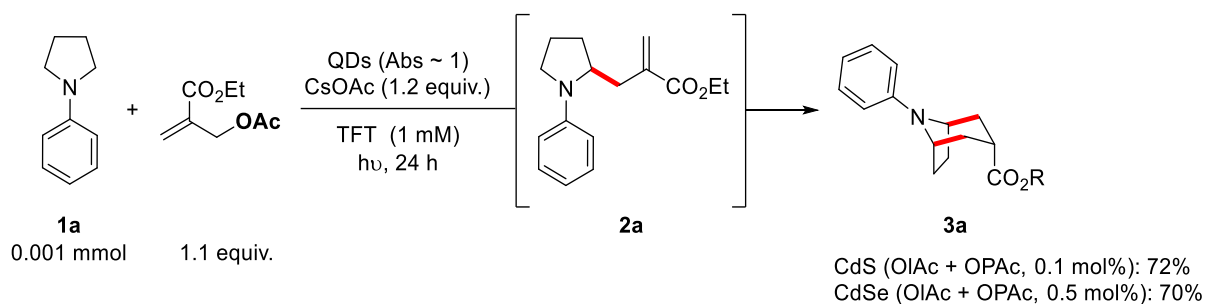
Next, these conditions were used for the targeted radical [3+3] annulation reaction (Table 3). Excellent yields of the cyclized product **3a** were obtained with the CdS, CdSe and CdS/CdSe quantum dots in both α,α,α-trifluorotoluene and acetonitrile. The InP/ZnS quantum dots did not promote the formation of the cyclized product but allowed the formation of the mono-allylated product **2a** in a moderate 42% yield (Table 3, entry 4).
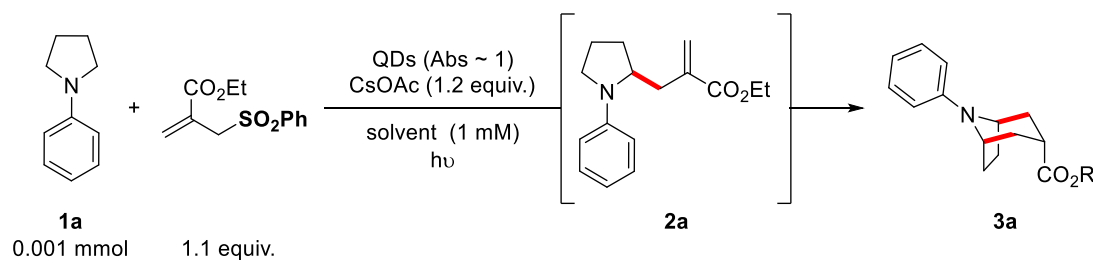
Entry	QDs (mol%)	Abs	Surface ligands	Solvent	Irradiation time	Yield
1	CdS (0.1 mol%)	1.1	OlAc + OPAc	TFT	24 h	**3a**, 75%
2	CdSe (0.5 mol%)	0.9	OlAc + OPAc	TFT	24 h	**3a**, 73%
3	CdS/CdSe (0.5 mol%)	0.9	OlAm + OPAc	TFT	24 h	**3a**, 74%
4	Inp/ZnS (0.7 mol%)	0.9	OlAm	TFT	48 h	**2a**, 42%
5	CdS (0.1 mol%)	1.1	PPAc	MeCN	24 h	**3a**, 74%
6	CdSe (0.5 mol%)	0.9	PPAc	MeCN	24 h	**3a**, 72%

Table 3. Results obtained for the annulation reaction under optimized conditions with the sulfone trap. Reactions performed on 0.001 mmol scale. Reaction outcome determined by UHPLC-MS.

Under these conditions the sulfone radical trap could be replaced by the acetate trap with no loss of yield, as assessed with CdS and CdSe quantum dots in α,α,α-trifluorotoluene (Scheme 2, compare with Table 1 entries 1 and 2).

1a
0.001 mmol   1.1 equiv.

2a

3a

CdS (OlAc + OPAc, 0.1 mol%): 72%
CdSe (OlAc + OPAc, 0.5 mol%): 70%

Scheme 2. Results obtained for the annulation reaction under optimized conditions with the acetate trap. Reactions performed on 0.001 mmol scale. Reaction outcome determined by UHPLC-MS.

4.1.3. Description of the small-scale set-up

The irradiation set-up for this small-scale reaction in Grenoble is a home-made device consisting of a 3D-printed vial holder, a LED of suitable wavelength, and a metallic heat sink to avoid over-heating (Image 1). Depending on the LED, the power was estimated to lie between 10 and 50 mW. The reaction vial is a 2-mL clear glass vial with a PTFE/silicon septum bonded to the cap (commonly called a GC vial, see supporting information for a description of all reaction vessels). It is irradiated from the bottom and agitation is performed *via* a magnetic stirring plate placed on the side. The whole set-up is placed in a nitrogen-filled glovebox. In this whole section, this set-up will be referred to as the "LED set-up", in opposition to the traditional Kessil lamp set-up used for bigger scale reactions.
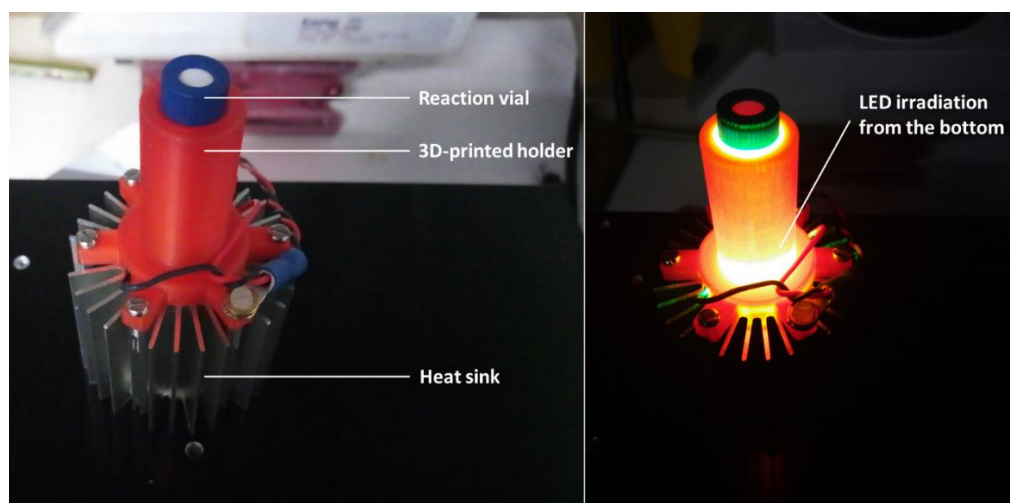
Image 1. Description of the small-scale reaction set-up ("LED set-up"). Maximum volume of 2 mL in a GC vial.

4.2.   Scaling-up the reaction – Results obtained in Bern

Based on the results obtained in Grenoble on 0.001 mmol scale, the focus for the scale-up of the annulation reaction in Bern was put on the CdS and CdSe quantum dots. The CdS/Cdse and InP/ZnS quantum dots will only be briefly discussed.

4.2.1. Challenges

One of the main problems in scaling-up this reaction is the high dilution of 1 mM described to work well on 0.001 mmol scale. To give an order of magnitude, the iridium catalyzed reaction, already quite diluted, is run at a concentration of 50 mM (0.05 M). Concentrating the QD catalyzed reaction while

keeping the catalyst loading constant inevitably leads to a higher quantum dot concentration in solution and therefore, absorbance. This can influence two important parameters: the QD stability and the light penetration in solution. Additionally, the set-up described in Image 1 is only suitable for reaction volumes up to 2 mL. Scaling-up the reaction above this volume necessitates to use a different irradiation set-up. All these parameters have been recognized to be key parameters in photocatalysis[5] and will need to be taken into account in designing an efficient, scaled-up, quantum dot-photocatalyzed reaction.

4.2.2. Preliminary results

Our strategy in scaling-up the reaction was to simultaneously increase the molarity of the reaction and decrease the catalyst loading so as to keep an absorbance value roughly between 4 and 8.

Preliminary results were obtained in collaboration with Alissia Meyer as part of a Bachelor's thesis on the quantum dot photocatalyzed annulation of anilines at the University of Bern.[6] Using CdSe quantum dots in DCM at a decreased catalyst loading of 0.2 mol%, the scale could be increased to 0.05 mmol and 40% NMR yield of the intermediate product was obtained (Figure 1A). The reaction was run in a 3-mL clear glass vial closed with a screw cap, and irradiation was performed with a single Kessil lamp at maximum power (100 W). The reaction was set-up outside the glovebox, degassed by three freeze-and-thaw cycles, and irradiated outside the glovebox for 6 hours. Increasing the reaction time was not investigated at this stage. Blank experiments were run and confirmed that the photocatalyst was necessary for the reaction to occur.

At this point it was envisaged that both the high absorbance (Abs = 8.9) and the irradiation set-up could be problematic for the scale-up of the reaction. Hence reaction conditions closer to the one used for the 0.001 mmol scale were devised. In particular, the absorbance was decreased from 8.9 to 4.45 by reducing by half the catalyst loading. The scale was also reduced so as to accommodate the LED-set up (Figure 1B). Importantly, the reaction was set-up outside but irradiated inside the glovebox. After 24 h of irradiation, no cyclized product was formed and an NMR yield of 34% was obtained for the mono-allylated intermediate, similarly to the previous reaction. Encouragingly however, this reaction performed in Grenoble gave a similar result, showcasing reproducibility between our two laboratories.
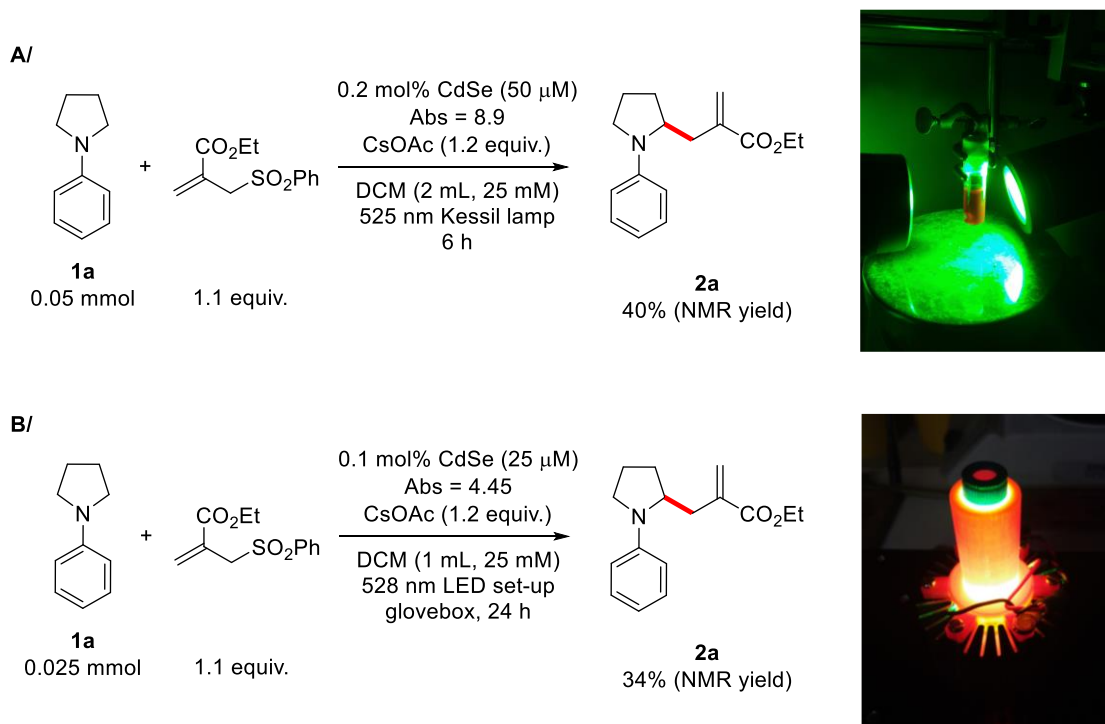
A/

0.2 mol% CdSe (50 µM)
Abs = 8.9
CsOAc (1.2 equiv.)

DCM (2 mL, 25 mM)
525 nm Kessil lamp
6 h

1a
0.05 mmol   1.1 equiv.

2a
40% (NMR yield)

B/

0.1 mol% CdSe (25 µM)
Abs = 4.45
CsOAc (1.2 equiv.)

DCM (1 mL, 25 mM)
528 nm LED set-up
glovebox, 24 h

1a
0.025 mmol   1.1 equiv.

2a
34% (NMR yield)

Figure 1. A/ Reaction conditions and set-up for a 0.05 mmol scale reaction run with CdSe QDs in DCM. B/ 0.025 mmol scale reaction with reduced absorbance and irradiation in small-scale LED set-up.

4.3. Reactions in acetonitrile – Results obtained conjointly in Grenoble and Bern

Next, the reaction was investigated in acetonitrile. In order to stabilize the quantum dots in this solvent, the native ligands were exchanged with phosphopropanoic acid (PPAc) ligands – this exchange was performed in Grenoble. These conditions showed good results for both CdS and CdSe quantum dots on 0.001 mmol scale in Grenoble (respectively 74% and 72% of cyclized product, see Table 3 entries 5 and 6). Scale-up experiments were run conjointly in Grenoble as part of a visit to the CEA laboratories. All reactions were set-up in the CEA LED-set up with CdSe quantum dots dispersed in acetonitrile. Similarly to previous experiments (Figure 1A), a catalyst loading of 0.2 mol% was chosen for a reaction molarity of 25 mM, leading to an absorbance of 8.9. In a first experiment, the reaction was set-up and irradiated inside the nitrogen filled glovebox, leading to an excellent isolated yield of 82% for the cyclized product (Table 4, entry 1). Setting up the reaction outside the glovebox and introducing it, after degassing, inside the glovebox for irradiation led to a significant drop in conversion. The cyclized product was isolated in a modest 38% yield along with 22% of the mono-allylated intermediate (Table 4, entry 2). Importantly, simple degassing by purging with argon for 30 minutes followed by irradiation outside the glovebox led to a messy reaction and only traces of product (Table 4, entry 3). These results clearly indicate a sensitivity of the reaction towards oxygen.
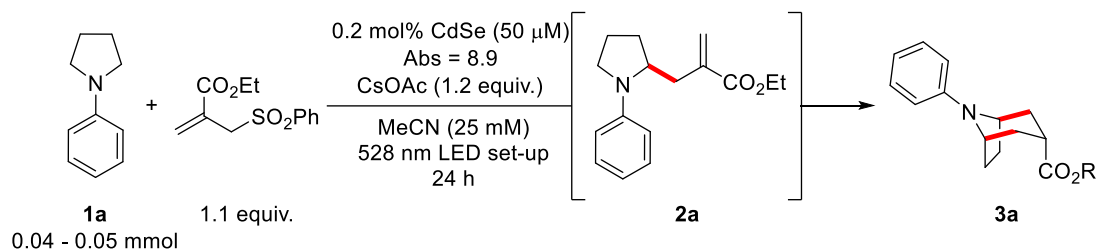
Entry	Scale (mmol)	Set-up and irradiation	Isolated yields
1	0.05	Set-up and irradiation in the glovebox.	**3a**, 82% (α/β 5:1)
2	0.05	Set-up in the glovebox. Irradiation outside the glovebox.	**3a**, 38% (α only) **2a**, 22%
3	0.04	Set-up and irradiation outside the glovebox.	Traces of product

Table 4. 0.05 mmol scale reaction run with CdSe quantum dots in MeCN. Possible contamination of the reaction mixture by air seems to be a crucial parameter inhibiting the reaction.

It was then tried to reproduce these results in Bern. However, these endeavors were only met with failure, even when the reaction was set up and irradiated in the glovebox. NMR yields up to 50% were obtained for the mono-allylated product, but no cyclized product was formed. At this point it is important to mention that technical difficulties arose with the glovebox. Due to a malfunctioning of both the circulation and the analyzers, the oxygen level was high, but not detected. This could partially explain the difficulties to reproduce the results obtained in Grenoble with the same quantum dots. However, independently to this problem, a UV-Vis measurement of a 2.5 μM sample of the quantum dot solution showed an absorbance of 0.11 instead of the expected 0.45 at 540 nm (see supporting information). Additionally, the peak of the first exciton was broad, which confirmed that the photocatalyst had partially decomposed. Stability tests run in Grenoble confirmed the low colloidal stability of these PPAc capped QDs in MeCN. Therefore, and despite good photocatalytic activity, these conditions were not retained for further scale-up experiments.

4.4. Reactions in α,α,α-trifluorotoluene – Results obtained in Bern

Next the scale-up was investigated in α,α,α-trifluorotoluene (TFT). A first set of comparative scaled-up experiments was run in Bern with CdS, CdSe and CdS/CdSe quantum dots under an absorbance of 3.65 in TFT (Table 5). Very promising results were obtained with CdS and CdSe quantum dots with isolated yields of respectively 42% and 56% for the cyclized product (Table 5, entries 1 and 2). Both diastereomers were isolated. Although significantly lower than on 0.001 mmol scale, it should be noted that these yields were obtained with a much-lowered catalyst loading (0.025 mol% instead of 0.1 mol% for CdS QDs, 0.16 mol% instead of 0.5 mol% for CdSe QDs). For the CdS/CdSe quantum dots, the reaction mixture after 24 h of irradiation was significantly messier and the cyclized product was isolated in a low 21% yield. No significant amount of starting material, intermediate or side-product was recovered that could explain the low yield of cyclized product.
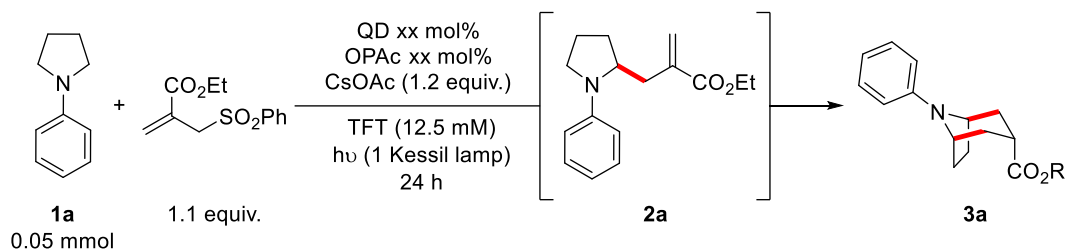
Entry	QD type and loading	OPAc loading	Abs	Isolated yield of 3a
1	CdS (0.025 mol%)	9.5 mol%	3.65	42%, α/β 4.5:1
2	CdSe (0.16 mol%)	48 mol%	3.65	56%, α/β 6:1
3	CdS/CdSe (0.16 mol%)	48 mol%	3.65	21%, α/β 4.5:1

Table 5. Comparative experiment between CdS, CdSe, and CdS/CdSe QDs in TFT with appropriate amounts of OPAc ligands. Reactions were run on 0.05 mmol scale, set-up inside the glovebox and irradiated with one Kessil lamp outside the glovebox.

Hence CdS and CdSe quantum dots were kept as candidates for further optimization on 0.05 mmol scale. Increasing the catalyst loading should for example be beneficial, and we have seen that absorbance values up to 8-9 could be potentially tolerated (see Table 4). Separate optimizations were undertaken with these two types of QDs on 0.05 mmol scale.

4.4.1. CdS quantum dots

The influence of the absorbance of the reaction mixture was investigated by either changing the catalyst loading and keeping the molarity constant, or by keeping the catalyst loading unchanged and modifying the molarity. Other parameters such as leaving group on the trap and equivalent numbers of trap were investigated as well. The results are collected in Table 6 and Table 7.
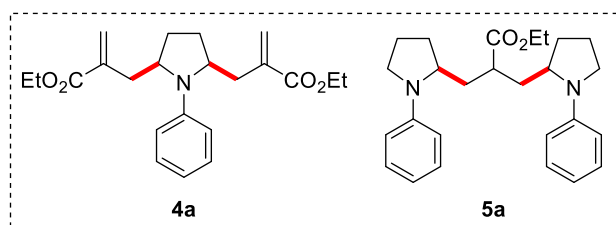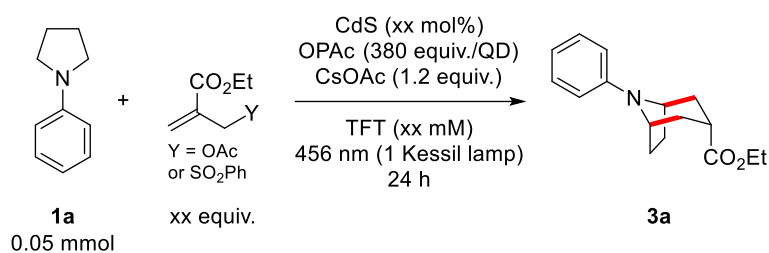
Entry	CdS (mol%)	[1a] (mM)	Abs	Y (equiv)	Isolated yield of 3a	Side product

1	0.025	12.5	3.7	SO₂Ph (1.1)	42% (α/β 4.5:1)	**5a**
2	0.025	12.5	3.7	SO₂Ph (1.4)	27% (α only)	**5a, 4a**
3	0.05	6.25	3.7	SO₂Ph (1.1)	No clean product isolated	n.d.
4	0.05	12.5	7.4	SO₂Ph (1.1)	~ 50% NMR yield[a]	**5a**
5	0.05	12.5	7.4	SO₂Ph (1.4)	49% (α/β 5:1)	None
6	0.05	12.5	7.4	SO₂Ph (1.4)	36% (α only)	**5a**
7	0.05	12.5	7.4	SO₂Ph (2.0)	traces of product	**4a**

Table 6. Optimization of the reaction conditions with CdS quantum dots on 0.05 mmol scale using the sulfone trap. Reactions run in a 8-mL clear glass vial closed with a screw cap. Irradiation with one Kessil lamp (100 W) for 24 hours. When applicable, ^{1}H-NMR yield was determined using ethylene carbonate as a standard. [a]Approximate NMR yield due to unclean reaction; difficulties of purification prevented isolation of the product.

Although an encouraging result was obtained with 0.025 mol% CdS and 1.1 equivalents of the sulfone trap at an absorbance of 3.7 (42%, Table 6, entry 1), the presence of side product **5a** not only decreased the yield of the desired cyclized product but also greatly impaired its purification due to the very similar polarity. Since this side product is formed when too little trap is present, it was first attempted to increase the trap equivalents to 1.4 (Table 6, entry 2). This was unfortunately not beneficial and the major diastereomer was isolated in a low 27% yield. Both **5a** and **4a** were observed in the reaction mixture. Next the catalyst loading was doubled. When keeping the absorbance at 3.7, this resulted in a too low concentration and unclean, inefficient reaction (Table 6, entry 3). Keeping the concentration at 12.5 mM and increasing the absorbance to 7.4 seemed well tolerated at first, as the product was formed in significant amounts as assessed by ^{1}H-NMR analysis of the crude mixture (Table 6, entry 4). However no clean product could be isolated due to the presence of **5a**. At this point, increasing the quantity of radical trap to 1.4 equivalents proved beneficial and the cyclized product was isolated cleanly in 49% yield and a 5:1 diastereomeric ratio (Table 6, entry 5). Unfortunately, the reaction was poorly reproducible and in a duplicate experiment, the major diastereomer was isolated in 36% yield along with side product **5a** (Table 6, compare entries 5 and 6). It has been observed in the iridium-catalyzed reaction that the sulfone radical trap was not stable over long reaction time under the reaction conditions. While this is not a big issue in the iridium-catalyzed reaction due to short reaction times, it might explain why here the number of equivalents needed to be increased. It could also explain the low reproducibility of the reaction in terms of radical trap-related side product formation. With this observation in mind, it was attempted to increase the trap quantity to 2.0 equivalents, however in this case side product **4a** was formed and only traces of cyclized product were observed (Table 6, entry 7). At this point it was not attempted to screen every value between 1.4 and 2.0 equivalents for the sulfone trap.

Instead, the influence of the leaving group was investigated next. This proved to be a crucial parameter in the iridium-catalyzed reaction, and this change was well tolerated in the 0.001 mmol scale reactions as assessed by our collaborators (see Scheme 2). By using the acetate leaving group instead of the sulfone, the reaction was indeed cleaner and 34% of cyclized product could be isolated cleanly (Table 7, entry 1). In line with previous observations, increasing the trap equivalent number from 1.1 to 1.3 proved beneficial and the isolated yield was raised to 50% (Table 7, entry 2). Under these conditions, reducing the catalyst loading to 0.025 mol% induced a significant decrease in yield (Table 7, entry 3).

| Entry	CdS (mol%)	[1a] (mM)	Abs	Y (equiv)	Isolated yield of 3a	Side product
1	0.05	12.5	7.4	OAc (1.1)	34% (α/β 5:1)	None
2	**0.05**	**12.5**	**7.4**	**OAc (1.3)**	**50% (α/β 5:1)**	**None**
3	0.025	12.5	3.7	OAc (1.3)	42% (α/β 3:1)	None

Table 7. Optimization of the reaction conditions with CdS quantum dots on 0.05 mmol scale using the acetate trap. Reactions run in a 8-mL clear glass vial closed with a screw cap. Irradiation with one Kessil lamp (100 W) for 24 hours.

With the optimized conditions in hand, the reproducibility of the reaction with different batches of quantum dots was assessed on 0.05 mmol scale and proved to be excellent (Table 8). With the third batch of quantum dots, the isolated yield was even raised to 58%. Running the reaction in a Schlenk tube gave a similar result. This shows that the "simple" vial set up is suitable for the reaction with CdS quantum dots, but also that it can be replaced by a Schlenk tube, which is a convenient reaction vessel for oxygen sensitive reactions.

CdS batch	Isolated yield
1	50%, α/β 5:1
2	51%, α/β 5:1
3	58%, α/β 6:1 61%, α/β 5.5:1 (in a Schlenk tube, average of 2 runs)

Table 8. Assessment of the reproducibility of the reaction depending on the CdS batch. Reaction conditions as in Table 7, entry 2. Unless otherwise stated, the reaction was run in a 8-mL clear glass vial with a screw cap.

Finally, the optimized reaction conditions were used in a scale up to 0.20 mmol using two lamps for the irradiation. Only a small decrease of yield was observed when going from 0.05 to 0.20 mmol (Scheme 3).

1a   1.3 equiv.   3a

0.05 mmol: **50%**, α/β 5:1
0.20 mmol: **46%**, α/β 6:1
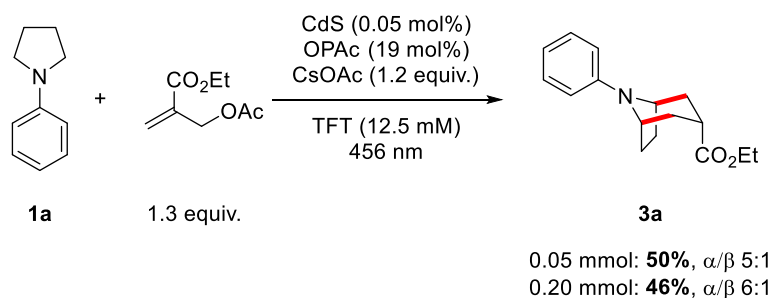
Scheme 3. Scale-up from 0.05 mmol to 0.20 mmol using optimized conditions as in Table 7, entry 2. The 0.05 mmol-scale reaction was irradiated for 24 hours with one Kessil lamp. The 0.20-mmol scale reaction was irradiated for 48 hours with two Kessil lamps.

After precipitation and centrifugation of the QDs, the catalyst used in the 0.20 mmol-scale reaction could be reused and provided the product in 42% isolated yield in a second round (Table 9, entry 2). After a third round, the product was recovered in 35% yield. The decrease in observed diastereoselectivity is due to increased difficulties in purification upon recycling of the quantum dots. Unfortunately, it was difficult to assess the diastereoselectivity of the reaction on the crude mixture due to overlapping signals.

Entry	Round of the CdS QDs	Isolated yield of 3a
1	1st	46% (α/β 6:1)
2	2nd	42% (α/β 4:1)
3	3rd	35% (α/β 4:1)

Table 9. Recycling experiment on 0.20 mmol scale. Reactions were run in a 24-mL clear glass vial with a screw cap and irradiated with two Kessil lamp for 48 hours.

With this reliable reaction in hand, a small substrate scope was undertaken (Figure 2). Phenylpiperidine **6a** was a very good substrate for the iridium-catalyzed reaction but only gave an inseparable mixture of **8a** and **7a** in a 5:1 ratio and total yield of 33% with the CdS QDs (0.20 mmol scale). *Para*-methoxyphenyl piperidine **6e** gave the corresponding cyclized product **8eα** in less than 7% yield along with 9% of **7e** and 17% recovered **6e** on 0.20 mmol scale. *Para*-methoxyphenyl pyrrolidine **1d** gave the corresponding cyclized product **3dα** in a low 25% yield on 0.05 mmol scale. Attempts to run the reaction on 0.20 mmol scale failed to give the desired product all together. No product could be obtained at all from substrate **6g**, presumably due to a too high oxidation potential induced by the ester substituent ($E_{1/2}$ = 0.91 V/SCE in MeCN for the *p*-CO$_2$Me phenylpyrrolidine[7]).
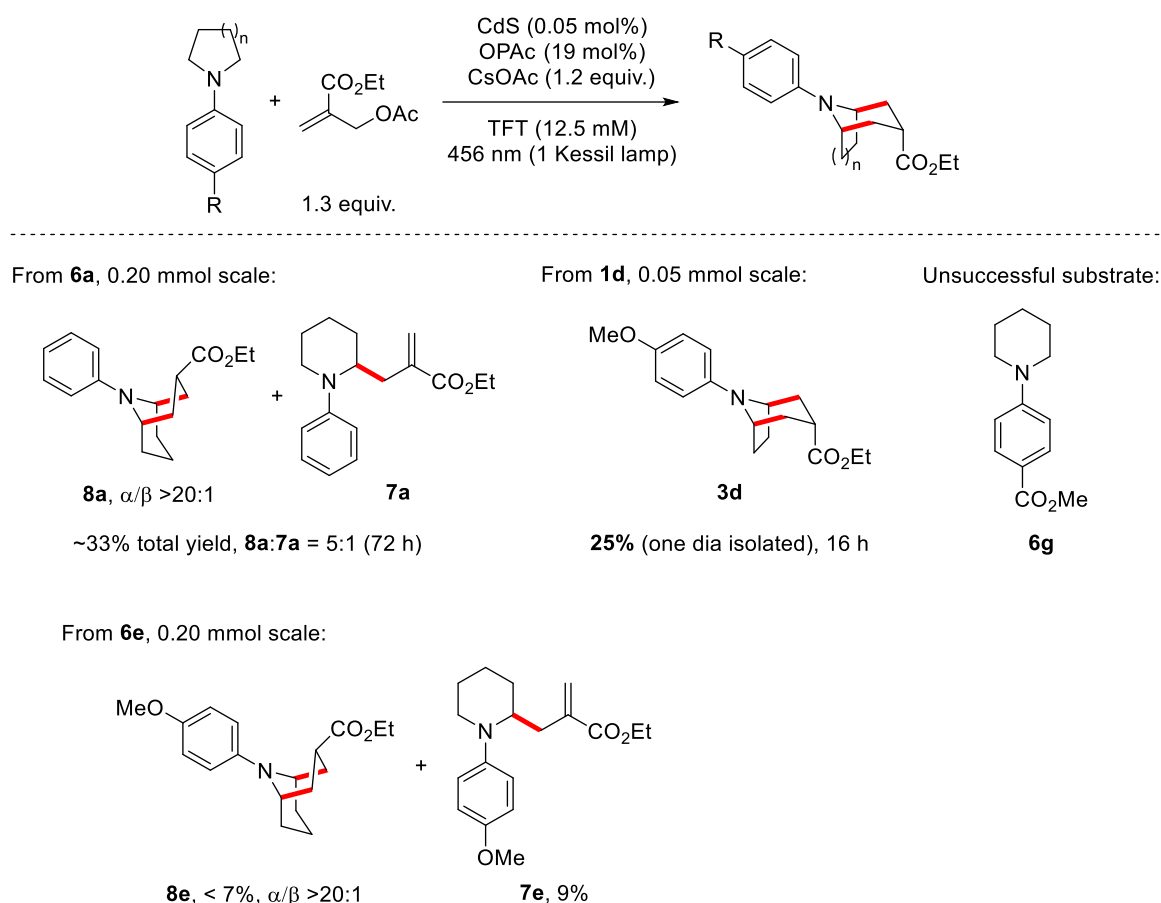
Figure 2. Preliminary substrate scope under optimized conditions with the CdS QDs. 0.20 mmol scale reactions were irradiated with 2 Kessil lamps, 0.05 mmol scale reactions with 1 Kessil lamp.

So far we have been unable to successfully apply the optimized conditions to other substrates than *N*-phenylpyrrolidine, especially on 0.20 mmol scale. This would be the end goal of this study since running a reaction on 0.05 mmol scale is not synthetically useful. Additionally, the low yields obtained on these scales result in very small quantity of product, which calls for difficulties of purification and uncertainties in the isolated yields.

4.4.2. CdSe quantum dots

Following the good result obtained with CdSe QDs on 0.05 mmol scale (56%, see Table 5, entry 2), it was tried to scale up the reaction without further optimization. With the remaining quantity of the CdSe batch (Batch A), a 0.16 mmol scale reaction could be run. After 72 hours of irradiation the cyclized product was only isolated in 28% yield (major diastereomer, Scheme 4).
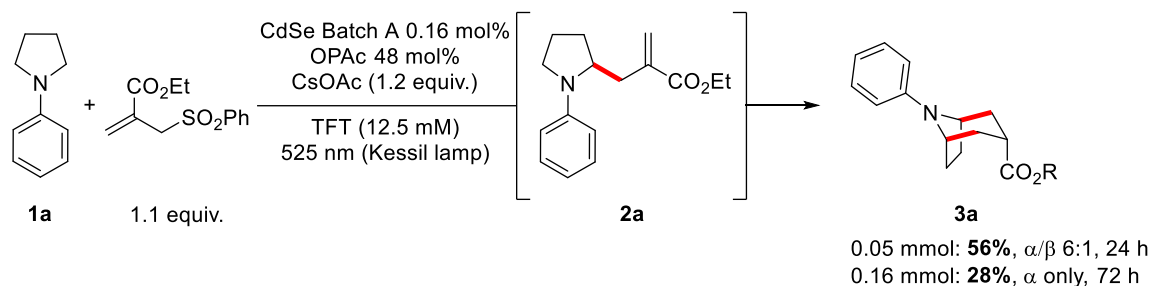
Scheme 4. Scale-up of the CdSe catalyzed reaction from 0.05 to 0.16 mmol. Reaction run in a 8- or 24-mL clear glass vial with a screw cap. One Kessil lamp used for irradiation. Both reactions were run with the same batch of QDs (Batch A).

From the observations made for the CdS QDs, it is clear that several parameters should be investigated for this scale-up, in particular influence of the trap, reaction vessel, number of lamps used for irradiation, and catalyst loading. To this end a new batch of CdSe quantum dots was synthesized in Grenoble and sent to Bern where it was used immediately (Batch B). Unfortunately, this new batch of quantum dots proved completely ineffective in promoting the desired reaction and full recovery of starting material and trap was observed upon prolonged reaction time. The results previously obtained could not be reproduced, even when probing all the above-mentioned parameters (see supporting information for more details). UV-Vis measurements of the CdSe solution showed that the exciton was still present at 540 nm. Additionally, these QDs were effective in promoting the reaction of the more easily oxidizable *para*-methoxyphenyl pyrrolidine substrate **1d** ($E_{1/2}$ = 0.41 V/SCE in MeCN[7]), giving the corresponding cyclized product **3d** in 33% isolated yield after 24 h (major diastereomer, Scheme 5). The yield could be increased to 38% when irradiating for 14 hours instead of 24 hours, from which it can be deduced that the stability of **3d** is an important parameter as well. Running the reaction inside the glovebox did not have any influence on the reaction outcome with this substrate.
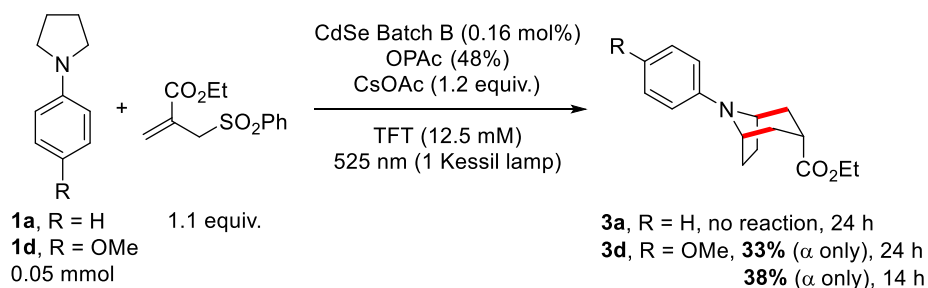

Scheme 5. Batch B of the CdSe QDs is able to catalyze the reaction for the para-methoxyphenyl pyrrolidine derivative **1d**, but not for the simple phenylpyrrolidine substrate **1a**.

Investigations were carried out next to gain understanding on the absence of reaction of **1a** when using Batch B of the CdSe QDs. The irradiation set-up as well as oxygen sensitivity were probed, while keeping all other parameters unchanged (catalyst loading, trap, absorbance, etc). The results are summarized in Table 10. First, the scale was reduced to 0.01-0.02 mmol so that the LED set-up could be used, either inside or outside the glovebox. A first reaction on 0.01 mmol was analyzed qualitatively by TLC and showed that surprisingly, the cyclized product was the main product after 24 hours of irradiation inside the glovebox. This result was confirmed by qualitative NMR analysis on a 0.02 mmol scale reaction (Table 10, entries 1 and 2). Strikingly, as soon as the reaction was taken outside of the glovebox for irradiation, the conversion of the mono-allylated intermediate to the cyclized product was interrupted and a mix of **2a** and **3a** was recovered in a 1:1.3 ratio (Table 10, entries 3). This is in accordance with the hypothesis of an oxygen sensitivity when using substrate **1a** with the CdSe quantum dots. The absence of such sensitivity observed for **1d** could be due to a stronger driving force

for hole transfer, possibly overcoming a competition with traces of oxygen in the reaction mixture. The same experiment was then carried out using a Kessil lamp instead of the LED set-up for the irradiation outside the glovebox. A very similar result was obtained (Table 10, entries 3 and 4). This rules out a strong dependence of the reaction outcome on the irradiation set-up, at least on 0.02 mmol scale.

The influence of the reaction scale was visible when running the reaction on 0.05 mmol in a screw-cap vial. The conversion stopped before any formation of **3a**, and **2a** was formed in 25% yield along with 25% recovered pyrrolidine (^{1}H-NMR analysis of the crude mixture, Table 10, entry 5). Unfortunately, a change of reaction vessel was inevitable when going from 0.02 to 0.05 mmol scale and so it is unclear if this drop in conversion is the result of an inefficient irradiation or a vessel-related issue, or both. Quite surprisingly, this entry is in all point similar to the test reaction that was run when first receiving this batch of QDs, for which no conversion had been observed at all (Scheme 5). When running the reaction is a Schlenk tube on the bench, or in the glovebox, the mono-allylated intermediate **2a** was formed in respectively 65% and 60% NMR yield (Table 10, entries 6 and 7). Between the very first experiment run with Batch B and these last results, exactly one month had passed during which the quantum dots had been stored in the glovebox. We hypothesized that during this month, a better deaeration of the QD solution had been achieved, finally promoting a reaction.
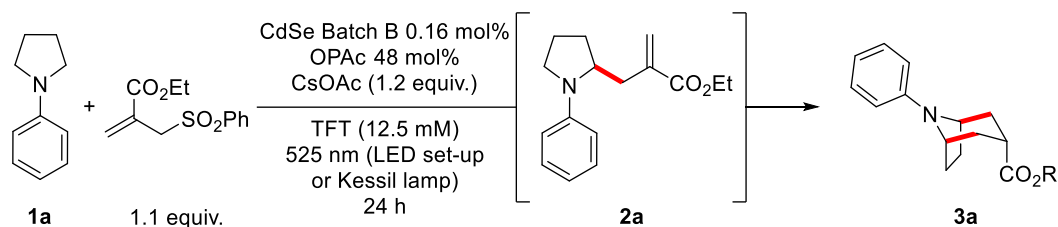
Entry	Irradiation set-up	Environnement of irradiation	Scale	TLC analysis	NMR analysis[a]
1	LED set-up (GC vial)	Glovebox	0.01 mmol	**3a** main product	--
2	LED set-up (GC vial)	Glovebox	0.02 mmol	**3a** main product	**3a** main product. **1a** and **2a** not observed
3	LED set-up (GC vial)	Bench	0.02 mmol	No completion	**2a:3a** ~ 1:1.3
4	Kessil lamp (GC vial)	Bench	0.02 mmol	No completion	**2a:3a** ~ 1:1
5	Kessil lamp (screw cap vial)	Bench	0.05 mmol	No completion	**1a,** 25% recovered **2a,** 25% **3a,** 0%
6	Kessil lamp (Schlenk tube)	Bench	0.05 mmol	No completion	**2a,** 65% (45%)[b]
7	Kessil lamp (screw cap vial)	Glovebox	0.05 mmol	No completion	**2a,** 60% (37%)[b]

Table 10. Investigation of the CdSe photocatalytic activity with phenylpyrrolidine and the sulfone trap. [a] ^{1}H-NMR yields determined using ethylene carbonate as a standard. [b] isolated yields.

This hypothesis was tested on a third batch of CdSe (Batch C). The reaction as in Table 10, entry 7 was repeated with Batch C and failed to give any product. The QDs were stored in the glovebox for a month and the reaction was repeated, unfortunately no reaction occurred and both starting material and trap were fully recovered. The reaction with **1d** was however reproducible and gave the desired cyclized

product **3d** in 35% isolated yield after 14 hours of irradiation (α diastereomer only, compare with Scheme 5).

The behavior of the CdSe quantum dots on 0.05 mmol scale with **1a** is not yet fully understood and important problems of reproducibility remain. An intricate combination of parameters appears to be at play, and it is possible that only slight changes in these parameters lead to a complete shut down of the reaction. For these reasons, CdSe quantum dots do not seem to be good candidates for the scale-up of the [3+3] radical annulation. No further substrate scope was undertaken with this photocatalyst.

4.4.3. InP/ZnS quantum dots

The InP/ZnS quantum dots have been shown to selectively form the mono-allylated product on 0.001 mmol scale (Table 3), which is an interesting reactivity that could complement previous catalysts. So far however, the reaction could not be reproduced on 0.05 mmol scale in Bern. Further experiments are on-going to resolve this matter.

4.5. Conclusion and outlook

Problems of scale-up have been partially solved in the [3+3] radical annulation of phenylpyrrolidine **1a** with CdS quantum dots grafted with oleic acid and octylphosphonic acid ligands in α,α,α-trifluorotoluene. The scale of the reaction could be increased to 0.20 mmol and the recyclability of the quantum dots was demonstrated. However, limitations remain in the scope of this quantum dot photocatalyzed reaction. Using CdSe, CdS/CdSe or InP/ZnS quantum dots could not solve these limitations so far.

To better understand the behavior of the quantum dots in the [3+3] radical annulation reaction, it could be interesting to thoroughly study the cyclization step separately, which has not been done so far. We have shown during the study of the reaction with iridium catalysis that the second step was sluggish without the presence of the acetic acid liberated during the mono-allylation step. If under the quantum dot photocatalysis conditions the acetic acid cannot participate in the acceleration of the second step, for example because of interference by the ligands, this could significantly impair the overall reactivity.

Other important parameters to investigate further are the irradiation intensity, especially in the case of the Kessil lamps which have only been used at their maximum power (100 W). Moreover, the addition of non-negligeable amounts of OPAc ligands in the reaction mixture when the reaction is run in TFT could significantly increase the acidity of the solution. It should be tried to increase the equivalent of base in these cases.

To solve the problem of attenuation of the light intensity because of the high absorption by the photocatalyst, a main issue in our scaled-up reaction, it should be tried to minimize the path length of the light in the reaction vessel. The optimal solution to do so is certainly by running reactions in flow.[5,8] To this end a suitable homogeneous base was tested on the iridium photocatalyzed reaction. Tetrabutylammonium acetate proved to be a suitable base for the reaction and gave the desired cyclized product **3a** in 48% yield and diastereomeric ratio of 4.3:1 (Scheme 6).
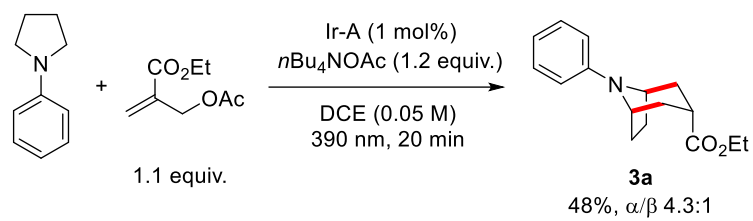
Scheme 6. Iridium catalyzed model reaction using nBu$_4$NOAc instead of CsOAc as base. Reaction mixture fully homogeneous.

References

1 A. Noble and D. W. C. MacMillan, *J. Am. Chem. Soc.*, 2014, **136**, 11602–11605.

2 Z. Zhang, K. Edme, S. Lian and E. A. Weiss, *Journal of the American Chemical Society*, 2017, **139**, 4246–4249.

3 I. N. Chakraborty, S. Roy, G. Devatha, A. Rao and P. P. Pillai, *Chem. Mater.*, 2019, **31**, 2258–2262.

4 M. C. Weidman, Q. Nguyen, D.-M. Smilgies and W. A. Tisdale, *Chem. Mater.*, 2018, **30**, 807–816.

5 T. Noël and E. Zysman-Colman, *Chem Catalysis*, 2022, **2**, 468–476.

6 A. Meyer, *Quantum dots as photocatalysts for the radical annulation of amines*, 2021.

7 E. Colson, J. Andrez, A. Dabbous, F. Dénès, V. Maurel, J.-M. Mouesca and P. Renaud, , DOI:10.26434/chemrxiv-2021-gq1jb-v2.

8 E. B. Corcoran, J. P. McMullen, F. Lévesque, M. K. Wismer and J. R. Naber, *Angewandte Chemie International Edition*, 2020, **59**, 11964–11968.

Supporting information

Table of contents

General information

For iridium catalyzed reactions, all the glassware was oven-dried at 160 °C or flame-dried under vacuum, assembled hot and allowed to cool under a positive pressure of nitrogen. For quantum dot catalyzed reactions, the glassware was not dried. Unless otherwise stated, all reactions were performed under nitrogen atmosphere. Non-aqueous reagents were transferred under nitrogen *via* syringe or in the glovebox with a micropipette. Silica gel 60 Å (230–400 mesh particle size, SiliCycle) was used for flash column chromatography. Thin layer chromatography (TLC) was performed on 0.25 mm silica gel 60 with fluorescent indicator UV 254; visualization under UV light (254 nm) or by staining with a solution of potassium permanganate [$KMnO_4$ (3 g), K_2CO_3 (20 g) and NaOH 5% (3 mL) in H_2O (300 mL)] and subsequent heating.

Instrumentation

^1H, ^{13}C and ^{11}B NMR spectra were recorded on a 300 MHz spectrometer (^1H: 300 MHz, ^{13}C: 75 MHz, ^{11}B: 96 MHz, ^{19}F: 282 MHz) and on a 400 MHz spectrometer (^1H: 400 MHz, ^{13}C: 101 MHz) operating at 22 °C, unless otherwise stated. Chemical shifts (δ) were reported in parts per million with the residual solvent peak used as an internal standard ($CHCl_3$: δ = 7.26 ppm and C_6H_6: δ = 7.16 ppm for ^1H NMR spectra and $CDCl_3$: δ = 77.0 ppm and C_6D_6: δ = 128.0 ppm for ^{13}C NMR spectra). The following abbreviations were used to explain the multiplicities: s (singlet), d (doublet), t (triplet), q (quadruplet), p (pentuplet), hx (hexuplet), hp (heptuplet), m (multiplet), br (broad). The prefix app (apparent) was added when different coupling constants appeared accidentally equal. Coupling constants J are reported in Hz and with an accuracy of one unit of the last digit. HRMS analyses were recorded on a hybrid quadrupole time-of-flight mass spectrometer using positive electrospray and on a double-focusing magnetic sector mass spectrometer using electron impact (70 eV). Mass spectra were measured in electron impact (EI) mode at 70 eV, with solid probe inlet, source temperature of 200 °C, acceleration voltage of 5 kV, and resolution of 2'500. The instrument was scanned between m/z 50 and 1000 at scan rate of 2 s / decade in the magnetic scan mode. Perfluorokerosene served for calibration. Infrared spectra were recorded neat on an FT-IR spectrometer equipped with a Golden Gate Single Reflection Diamond ATR System and are reported in wave numbers (cm^{-1}). Kessil lamps were used for photoredox reactions and were run at maximum power (100 W) 5 cm away from reaction vessel with a cooling fan.

Materials

Unless otherwise stated, all reagents were obtained from commercial sources and used without further purification. α,α,α-trifluorotoluene and 1,2-dichloroethane were bought dry and used without further purification. Acetonitrile and DCM were first distilled then filtered over two columns of dried

alumina under a positive pressure of argon. Acetone was HPLC grade. Solvents for extraction and flash column chromatography were of technical grade and were distilled prior to use, then stored in glass bottles. Commercial iridium photocatalysts (Strem) were used without purification. Unless otherwise stated, quantum dots were used as received from our collaborators.

Description of the reaction vessels for the QD photocatalyzed reactions

"GC vial"

0.01 – 0.02 mmol scale
2-mL clear glass vial with a PTFE/silicon septum bonded to the cap

"screw cap glass vial"

0.05 mmol scale
MN 702096.
8.0 mL, 16.6x61.0 mm.
Polypropylene cap with silicone/PTFT septum. MN 702114.

0.20 mmol scale
MN 702099.
24.0 mL, 22.7x86.0 mm.
Polypropylene cap with silicone/PTFT septum. MN 702116.

"Schlenk tube"

0.05 mmol scale
Schlenk tube with high vacuum valve and hose connector, 10 mL.
Valve size: 0-8 mm.
0.20 mmol scale:
A 25-mL Schlenk tube can be used.

Synthesis of reference products for Grenoble

Starting materials **1a**, **1c**, **1d**, **6a**, **6e**, **6g**, **6j** as well as intermediate **2a** have been described in Chapter 3.

Reactions leading to **2c**, **2d**, **7a**, **7e**, **7g** and **7j** are non-optimized procedures. These compounds are new products – their NMR spectra are in appendix.
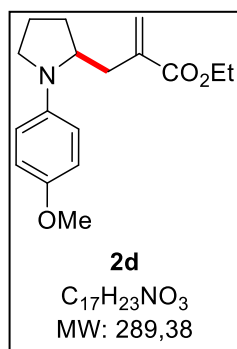

2c
$C_{18}H_{23}NO_4$
MW: 317,38
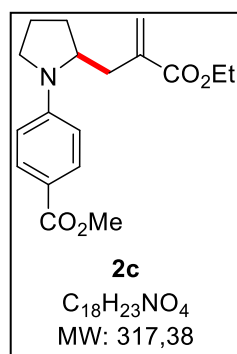
Methyl 4-[2-(2-ethoxycarbonylallyl)pyrrolidin-1-yl]benzoate (2c)

In an oven-dried 10 mL-vial were successively added ethyl 2-(benzenesulfonylmethyl)prop-2-enoate (153 mg, 0.60 mmol), methyl 4-pyrrolidin-1-ylbenzoate **1c** (41.1 mg, 0.20 mmol), Ir(dFppy)₃ (3.1 mg, 0.004 mmol, 2 mol%) and cesium acetate (76.8 mg, 0.40 mmol). The vial was closed with a rubber septum and evacuated/refilled with N_2 (x 3). Finally, dry and degassed 1,2-dichloroethane (2.00 mL, 0.1 M) was added. The resulting yellow mixture was placed in front of a 390 nm blue LED (5 cm distance) and stirred until **1c** was consumed (TLC monitoring, 16 h). The reaction mixture was diluted with sat. $NaHCO_3$ (3 mL). The aqueous phase was extracted

with DCM (3 x 5 mL) and the combined organic phases were dried over Na$_2$SO$_4$, filtered, and concentrated under reduced pressure to give crude product as an orange oil. Purification by flash column chromatography (neutral Alox, heptanes/EtOAc 95:5 to 90:10) afforded **2c** as a colorless oil (15.6 mg, 0.049 mmol, 25%).

^{1}H NMR (300 MHz, CDCl$_3$): δ 7.91 (d, J = 9.0 Hz, 2H), 6.73 (d, J = 9.0 Hz, 2H), 6.28 (d, J = 1.5 Hz, 1H), 5.61 (brs, 1H), 4.36–4.18 (m, 2H), 4.05 (ddd, J = 13.0, 6.0, 3.2 Hz, 1H), 3.85 (s, 3H), 3.48 (ddd, J = 10.3, 7.7, 2.8 Hz, 1H), 3.25 (td, J = 9.4, 7.5 Hz, 1H), 2.90 (ddd, J = 13.6, 3.6, 1.3 Hz, 1H), 2.18–1.95 (m, 3H), 1.94–1.81 (m, 2H), 1.37 (t, J = 7.1 Hz, 3H). ^{13}C NMR (75 MHz, CDCl$_3$): δ 167.7 (C=O), 167.0 (C=O), 150.3 (Cq), 138.2 (Cq), 131.6 (2x CH Ar), 128.2 (CH$_2$), 116.7 (Cq), 111.3 (2x CH Ar), 61.2 (CH$_2$), 57.4 (CH), 51.6 (CH$_3$), 48.2 (CH$_2$), 35.2 (CH$_2$), 28.9 (CH$_2$), 22.9 (CH$_2$), 14.4 (CH$_3$). FT-IR (cm^{-1}, neat): 2948, 1701, 1602, 1522, 1434, 1376, 1270, 1179, 1104, 958, 768. HRMS (ESI) m/z: [M+H]$^+$ Calcd for C$_{18}$H$_{24}$NO$_4$ 318.1700; Found 318.1691. R$_f$ = 0.61 (heptanes/EtOAc 60:40).
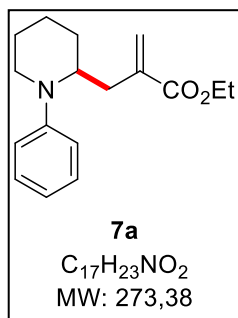

2d
C$_{17}$H$_{23}$NO$_3$
MW: 289,38

Methyl 2-[[1-(4-methoxyphenyl)pyrrolidin-2-yl]methyl]prop-2-enoate (2d)

In an oven-dried 10 mL-vial were successively added ethyl 2-(benzenesulfonylmethyl)prop-2-enoate (76.3 mg, 0.30 mmol), 1-(4-methoxyphenyl)pyrrolidine **1d** (53.2 mg, 0.30 mmol), [Ir{dF(CF$_3$)ppy}$_2$(dtbpy)]PF$_6$ (6.7 mg, 0.006 mmol, 2 mol%) and cesium acetate (173 mg, 0.90 mmol, 3.0 equiv.). The vial was closed with a rubber septum and evacuated/refilled with N$_2$ (x 3). Finally, dry and degassed 1,2-dichloroethane (3.00 mL, 0.1 M) was added. The resulting yellow mixture was placed in front of a 390 nm blue LED (5 cm distance) and stirred until **1d** was consumed (TLC monitoring, 2 h). The reaction mixture was diluted with sat. NaHCO$_3$ (3 mL). The aqueous phase was extracted with DCM (3 x 5 mL) and the combined organic phases were dried over Na$_2$SO$_4$, filtered, and concentrated under reduced pressure to give crude product as an orange oil. Purification by flash column chromatography (SiO$_2$, heptanes/EtOAc 95:5) afforded **2d** as a pale-yellow oil (17.2 mg, 0.059 mmol, 20%).

^{1}H NMR (300 MHz, CDCl$_3$): δ 6.91–6.84 (m, 2H), 6.77–6.70 (m, 2H), 6.25 (d, J = 1.6 Hz, 1H), 5.60 (brs, 1H), 4.36–4.17 (m, 2H), 3.93–3.82 (m, 1H), 3.76 (s, 3H), 3.42 (ddd, J = 8.8, 7.6, 2.7 Hz, 1H), 3.13 (td, J = 8.9, 7.0 Hz, 1H), 2.91 (ddd, J = 13.8, 3.3, 1.4 Hz, 1H), 2.15–1.89 (m, 3H), 1.89–1.80 (m, 2H), 1.36 (t, J = 7.1 Hz, 3H). ^{13}C NMR (75 MHz, CDCl$_3$): δ 167.3 (C=O), 150.9 (Cq), 142.3 (Cq), 138.8 (Cq), 127.6 (CH$_2$), 115.2 (2x CH Ar), 112.9 (2x CH Ar), 61.0 (CH$_2$), 57.8 (CH), 56.1 (CH$_3$), 49.1 (CH$_2$), 35.9 (CH$_2$), 29.2 (CH$_2$), 23.3 (CH$_2$), 14.4 (CH$_3$). FT-IR (cm^{-1}, neat): 2949, 1708, 1511, 1238, 1039, 810. HRMS (ESI) m/z: [M+Na]$^+$ Calcd for C$_{17}$H$_{23}$NO$_3$Na 312.1570; Found 312.1563. R$_f$ = 0.39 (heptanes/EtOAc 90:10).

Ethyl 2-[(1-phenyl-2-piperidyl)methyl]prop-2-enoate (7a)

In an oven-dried 10 mL-vial were successively added ethyl 2-(benzenesulfonylmethyl)prop-2-enoate (153 mg, 0.60 mmol), 1-phenylpiperidine **6a** (32.2 mg, 0.20 mmol), Ir(dFppy)₃ (3.1 mg, 0.004 mmol, 2 mol%) and cesium acetate (76.8 mg, 0.40 mmol). The vial was closed with a rubber septum and evacuated/refilled with N₂ (x 3). Finally, dry and degassed 1,2-dichloroethane (2.00 mL, 0.1 M) was added. The resulting yellow mixture was placed in front of a 390 nm blue LED (5 cm distance) and stirred until **1c** was consumed (TLC monitoring, 16 h). The reaction mixture was diluted with sat. NaHCO₃ (3 mL). The aqueous phase was extracted with DCM (3 x 5 mL) and the combined organic phases were dried over Na₂SO₄, filtered, and concentrated under reduced pressure to give crude product as an orange oil. Purification by flash column chromatography (neutral Alox, heptanes/EtOAc 99:1 to 98:2) afforded **7a** as a colorless oil (5.4 mg, 0.02 mmol, 10%).

¹H NMR (300 MHz, CDCl₃): δ 7.28–7.18 (m, 2H), 7.00–6.91 (m, 2H), 6.77 (tt, *J* = 7.2, 1.1 Hz, 1H), 6.17 (d, *J* = 1.6 Hz, 1H), 5.54–5.50 (brm, 1H), 4.19 (q, *J* = 7.1 Hz, 2H), 4.17–4.06 (m, 1H), 3.44–3.33 (m, 1H), 3.08–2.95 (m, 1H), 2.61–2.46 (m, 2H), 1.82–1.51 (m, 6H), 1.30 (t, *J* = 7.1 Hz, 3H). ¹³C NMR (75 MHz, CDCl₃): δ 167.3 (C=O), 150.9 (Cq), 139.0 (Cq), 129.2 (2x CH Ar), 127.0 (CH₂), 118.6 (CH Ar), 116.5 (2x CH Ar), 60.9 (CH₂), 54.8 (CH), 43.6 (CH₂), 30.0 (CH₂), 27.3 (CH₂), 25.7 (CH₂), 19.2 (CH₂), 14.3 (CH₃). FT-IR (cm⁻¹, neat): 2933, 2854, 1713, 1597, 1501, 1250, 1174, 1145, 1027, 752, 691. HRMS (ESI) m/z: [M+H]⁺ Calcd for C₁₇H₂₄NO₂ 274.1802; Found 274.1789. R_f = 0.41 (heptanes/EtOAc 90:10).
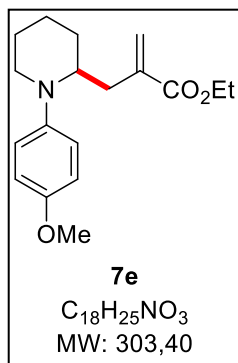
Ethyl 2-[[1-(4-methoxyphenyl)-2-piperidyl]methyl]prop-2-enoate (7e)

In an oven-dried 10 mL-vial were successively added ethyl 2-(acetoxymethyl)prop-2-enoate (48.3 mg, 0.28 mmol), 1-(4-methoxyphenyl)piperidine **6e** (38.3 mg, 0.20 mmol), [Ir{dF(CF₃)ppy}₂(dtbpy)]PF₆ (4.5 mg, 0.004 mmol, 2 mol%) and cesium acetate (46.1 mg, 0.24 mmol). The vial was closed with a rubber septum and evacuated/refilled with N₂ (x 3). Finally, dry and degassed 1,2-dichloroethane (2.00 mL, 0.1 M) was added. The resulting yellow mixture was placed in front of a 390 nm blue LED (5 cm distance) and stirred until **6e** was consumed (TLC monitoring, 3 h). The reaction mixture was diluted with sat. NaHCO₃ (3 mL). The aqueous phase was extracted with DCM (3 x 5 mL) and the combined organic phases were dried over Na₂SO₄, filtered, and concentrated under reduced pressure to give crude product as an orange oil. Purification by flash column chromatography (SiO₂, pentane/Et₂O 90:10) afforded **7e** as a colorless oil (10.1 mg, 0.033 mmol, 17%).

^{1}H NMR (300 MHz, CDCl$_3$): δ 7.05–6.89 (m, 2H), 6.88–6.78 (m, 2H), 6.15 (d, J = 1.6 Hz, 1H), 5.47 (brs, 1H), 4.17 (q, J = 7.1 Hz, 2H), 3.77 (s, 3H), 3.77–3.69 (m, 1H), 3.14–2.92 (m, 2H), 2.55–2.30 (m, 2H), 1.85–1.44 (m, 6H), 1.28 (t, J = 7.1 Hz, 3H). ^{13}C NMR (75 MHz, CDCl$_3$): δ 167.3 (C=O), 153.9 (Cq), 145.4 (Cq), 139.0 (Cq), 127.0 (CH$_2$), 120.4 (2x CH Ar), 114.5 (2x CH Ar), 60.8 (CH$_2$), 56.8 (CH), 55.7 (CH$_3$), 47.6 (CH$_2$), 31.1 (CH$_2$), 28.3 (CH$_2$), 26.0 (CH$_2$), 20.3 (CH$_2$), 14.3 (CH$_3$). FT-IR (cm^{-1}, neat): 2931, 1713, 1508, 1241, 1039. HRMS (ESI) m/z: [M+H]$^+$ Calcd for C$_{18}$H$_{25}$NO$_3$ 304.1907; Found 304.1894. R$_f$ = 0.38 (pentane/Et$_2$O 80:20).

7g
C$_{19}$H$_{25}$NO$_4$
MW: 331,41
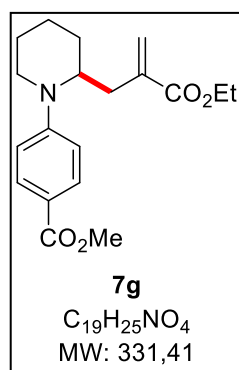
Methyl 4-[2-(2-ethoxycarbonylallyl)-1-piperidyl]benzoate (7g)

In an oven-dried 10 mL-vial were successively added ethyl 2-(acetoxymethyl)prop-2-enoate (37.9 mg, 0.22 mmol), methyl 4-(1-piperidyl)benzoate **6g** (43.9 mg, 0.20 mmol), [Ir{dF(CF$_3$)ppy}$_2$(dtbpy)]PF$_6$ (2.2 mg, 0.004 mmol, 2 mol%) and cesium acetate (46.1 mg, 0.24 mmol). The vial was closed with a rubber septum and evacuated/refilled with N$_2$ (x 3). Finally, dry and degassed 1,2-dichloroethane (4.00 mL, 0.05 M) was added. The resulting yellow mixture was placed in front of a 390 nm blue LED (5 cm distance) and stirred until **6g** was consumed (TLC monitoring, 5 min). The reaction mixture was diluted with sat. NaHCO$_3$ (3 mL). The aqueous phase was extracted with DCM (3 x 5 mL) and the combined organic phases were dried over Na$_2$SO$_4$, filtered, and concentrated under reduced pressure to give crude product as an orange oil. Purification by flash column chromatography (SiO$_2$, pentane/Et$_2$O 95:5 to 90:10) afforded **7g** as a colorless oil (6.5 mg, 0.020 mmol, 10%) along with **8g** (22.4 mg, 0.068 mmol, 34%).

^{1}H NMR (400 MHz, CDCl$_3$): δ 7.93–7.82 (m, 2H), 6.91–6.82 (m, 2H), 6.18 (d, J = 1.5 Hz, 1H), 5.56 (q, J = 1.1 Hz, 1H), 4.40–4.31 (m, 1H), 4.20 (q, J = 7.1 Hz, 2H), 3.85 (s, 3H), 3.69–3.59 (m, 1H), 3.06 (td, J = 12.7, 3.2 Hz, 1H), 2.67–2.54 (m, 2H), 1.81–1.52 (m, 6H), 1.30 (t, J = 7.1 Hz, 3H). ^{13}C NMR (101 MHz, CDCl$_3$): δ 167.4 (C=O), 167.1 (C=O), 153.8 (Cq), 138.3 (Cq), 131.4 (2x CH Ar), 127.6 (CH$_2$), 118.1 (Cq), 113.2 (2x CH Ar), 61.0 (CH$_2$), 53.2 (CH), 51.6 (CH$_3$), 41.8 (CH$_2$), 30.9 (CH$_2$), 27.1 (CH$_2$), 25.4 (CH$_2$), 18.6 (CH$_2$), 14.4 (CH$_3$). FT-IR (cm^{-1}, neat): 2933, 1704, 1600, 1517, 1434, 1285, 1249, 1185, 1175, 1104, 1024, 918, 769. HRMS (ESI) m/z: [M+H]$^+$ Calcd for C$_{19}$H$_{26}$NO$_4$ 332.1856; Found 332.1866. R$_f$ = 0.35 (pentane/Et$_2$O 80:20).
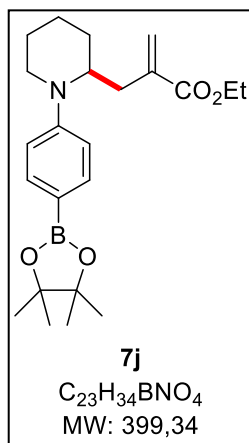
Ethyl 2-[[1-[4-(4,4,5,5-tetramethyl-1,3,2-dioxaborolan-2-yl)phenyl]-2-piperidyl]methyl]prop-2-enoate (7j)

In an oven-dried 10 mL-vial were successively added ethyl 2-(acetoxymethyl)prop-2-enoate (37.9 mg, 0.22 mmol), 1-[4-(4,4,5,5-tetramethyl-1,3,2-dioxaborolan-2-yl)phenyl]piperidine **6j** (57.4 mg, 0.20 mmol), [Ir{dF(CF$_3$)ppy}$_2$(dtbpy)]PF$_6$ (2.2 mg, 0.004 mmol, 2 mol%) and cesium acetate (46.1 mg, 0.24 mmol). The vial was closed with a rubber septum and evacuated/refilled with N$_2$ (x 3). Finally, dry and degassed 1,2-dichloroethane (4.00 mL, 0.05 M) was added. The resulting yellow mixture was placed in front of a 390 nm blue LED (5 cm distance) and stirred until **8j** started to be formed (TLC monitoring, 5 min, interruption before complete consumption of **6j**). The reaction mixture was diluted with sat. NaHCO$_3$ (3 mL). The aqueous phase was extracted with DCM (3 x 5 mL) and the combined organic phases were dried over Na$_2$SO$_4$, filtered, and concentrated under reduced pressure to give crude product as an orange oil. Purification by flash column chromatography (SiO$_2$, pentane/Et$_2$O 93:7) afforded **7j** in a mix with **8j**. After a second purification, partial separation afforded 4.8 mg of **7j** for characterization. Yield was not determined.

7j
C$_{23}$H$_{34}$BNO$_4$
MW: 399,34

^{1}H NMR (400 MHz, CDCl$_3$): δ 7.71–7.62 (m, 2H), 6.93–6.84 (m, 2H), 6.17 (d, J = 1.5 Hz, 1H), 5.53 (d, J = 1.5 Hz, 1H), 4.33–4.24 (m, 1H), 4.19 (q, J = 7.1 Hz, 2H), 3.55 (dt, J = 13.1, 3.8, 3.1 Hz, 1H), 3.09–2.94 (m, 1H), 2.64–2.49 (m, 2H), 1.81–1.44 (m, 6H), 1.32 (s, 12H), 1.30 (t, J = 7.4 Hz, 3H). ^{11}B NMR (96 MHz, CDCl$_3$): δ + 30. ^{13}C NMR (101 MHz, CDCl$_3$): δ 167.2 (C=O), 152.9 (Cq), 138.7 (Cq), 136.3 (2x CH Ar), 127.2 (CH$_2$), 114.1 (2x CH Ar), 83.3 (2x Cq), 60.9 (CH$_2$), 53.7 (CH), 42.2 (CH$_2$), 30.2 (CH$_2$), 27.1 (CH$_2$), 25.5 (CH$_2$), 25.01 (2x CH$_3$), 24.98 (2x CH$_3$), 18.9 (CH$_2$), 14.4 (CH$_3$). Due to coupling to the quadrupolar ^{11}B and ^{10}B nuclei, the aromatic carbon atom bearing the BPin was not detected. FT-IR (cm^{-1}, neat): 2977, 2930, 1712, 1602, 1398, 1358, 1249, 1141, 1092, 860, 816, 655. HRMS (ESI) m/z: [M+H]$^+$ Calcd for C$_{23}$H$_{35}$NO$_4$B 400.2654; Found 400.2667. R$_f$ = 0.30 (pentane/Et$_2$O 90:10).

CdSe quantum dots in MeCN

General Procedure F – Experiments run in Grenoble on 0.04-0.05 mmol scale

In a GC vial equipped with a stirring bar were successively added phenylpyrrolidine (7.1 μL, 1.0 equiv., 0.05 mmol), ethyl 2-(benzenesulfonylmethyl)prop-2-enoate (14.0 mg, 0.055 mmol), CsOAc (12 mg, 0.06 mmol) and the CdSe QDs (50 μM in MeCN, 2.00 mL, 0.02 mol%). If the reaction was set up outside the glovebox, the reaction mixture was degassed by bubbling argon for 30 minutes. The reaction vial was irradiated in the LED set-up (528 nm) for 24 hours. The light pink solution containing precipitated quantum dots was quantitatively transferred with MeCN to an Eppendorf tube for centrifugation (4000

rpm, 7 minutes). The supernatant was transferred into a round-bottom flask. To the remaining precipitate was added additional MeCN and centrifugation was performed (4000 rpm, 7 minutes). The supernatant was transferred to the round-bottom flask, evaporated under reduced pressure, and dried under high vacuum to give the crude product as a crystalline solid. Ethylene carbonate (0.5 equiv., 0.025 mmol) was added to the crude residue, and the whole mixture was dissolved in CDCl$_3$ (Eurisotop 99.8%) for ^{1}H-NMR determination of the NMR yield. Flash column chromatography (SiO$_2$, heptanes/EtOAc = 98:2 to 95:5) afforded the desired product.

Note: it was noticed during the work-up and subsequent crude NMR analysis that the quantum dot solution was contaminated by DMF, a solvent used during the QD's synthesis. The amount of DMF compared to acetonitrile was not determined.

Main text Table 3, entry 1: Following general procedure F (0.05 mmol) in a nitrogen-filled glovebox at all times. The reaction vial was only taken out of the glovebox at the end of the reaction for work-up and column.

^{1}H-NMR yield (2.56 mg (0.029 mmol) of standard): 77%, α/β 5.7:1 (**3a**)

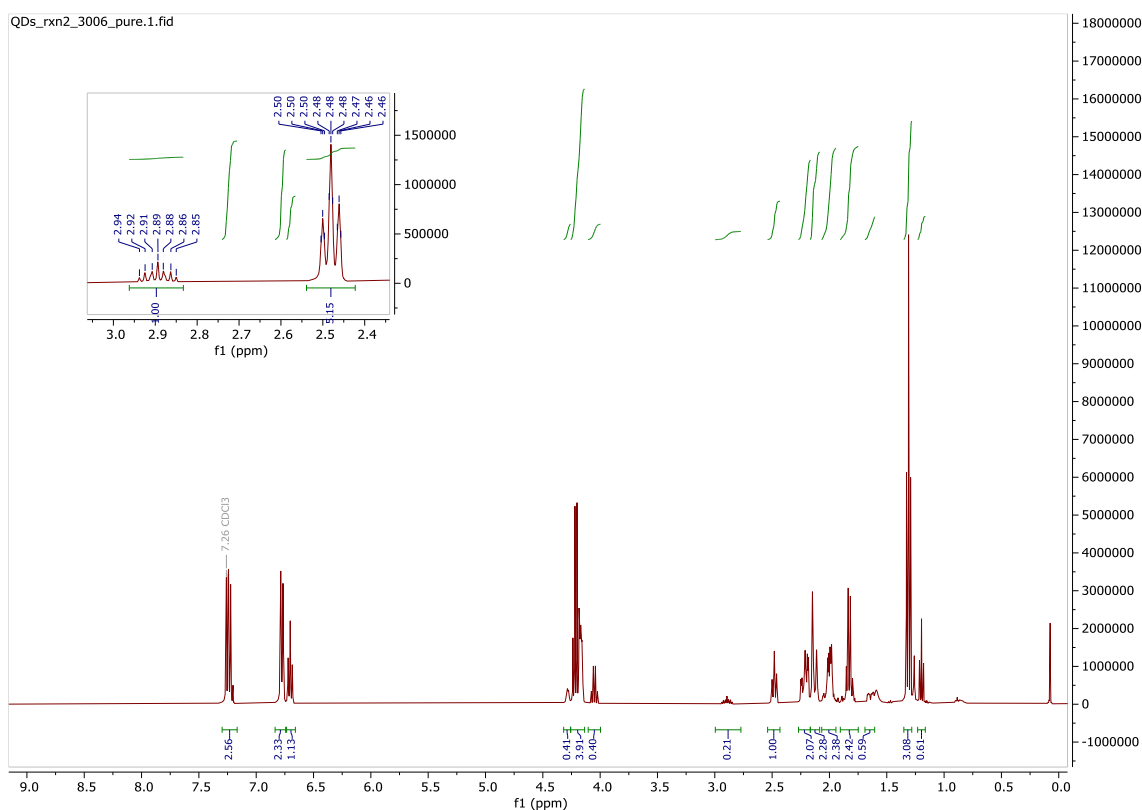Isolated yield: 10.6 mg, 0.041 mmol (82%, α/β 5.3:1, **3a**)

Image 1. ^{1}H-NMR spectrum of isolated product **3a** using CdSe QDs in MeCN, both diastereomers recovered together. Spectral data are in accordance with previously described product.

Main text Table 3, entry 2: Following general procedure F (0.05 mmol), setting up the reaction inside the nitrogen-filled glovebox. The reaction vial was taken out of the glovebox to be irradiated on the bench.

^{1}H-NMR yield (2.19 mg (0.025 mmol) of standard): 36%, α/β n.d. (**3a**); 25% (**2a**).

Isolated yield: 4.90 mg, 0.019 mmol (38%, **3aα**); 2.80 mg, 0.011 mmol (22%, **2a**).

Main text Table 3, entry 3: Following general procedure F (0.037 mmol), setting-up and irradiating the reaction outside the glovebox. Deaeration by bubbling argon for 30 minutes prior to irradiation.

Messy reaction crude. **1a** and **2a** are visible in the spectrum. ^{1}H-NMR yields could not be determined. No purification was carried out.

UV-Vis analysis of the CdSe solution in MeCN used in Bern

The CdSe stock solution (50 µM in MeCN) was diluted by 20. To do so, 0.1 mL of the stock solution was taken with a graduated pipette and added to a 2-mL graduated flask. The flask was filled up to 2 mL by addition of dry MeCN so as to obtain a solution where $[CdSe] = 2.5 \ \mu M$. A blank was measured, and the absorbance of the solution was measured from 200 to 800 nm.[1]

Since by the Beer-Lambert law $A = \varepsilon l [QD]$ and $\varepsilon_{CdSe} = 1.78 \times 10^5 \ M^{-1} cm^{-1}$ at 540 nm, the expected value for the absorbance measured at 540 should be 0.44. The actual measured value gave and absorbance of 0.11 at 540 nm and the exciton was broad.

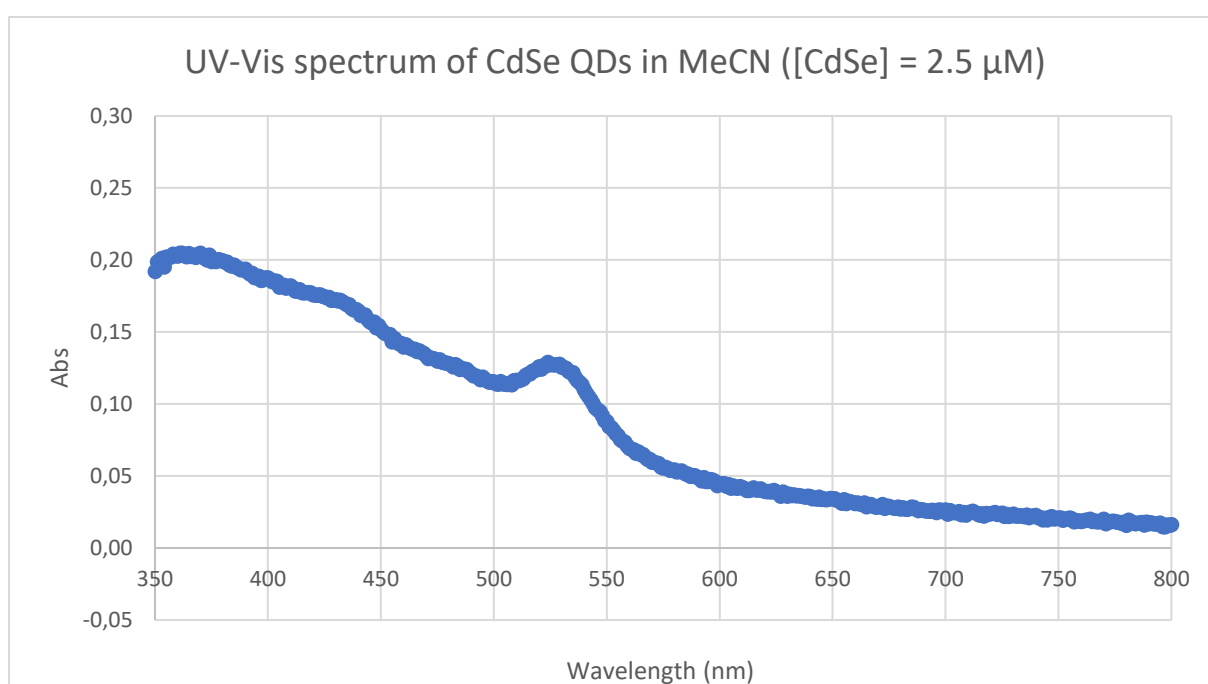[1] At the DCBP, this is done on the apparatus belonging to the Häner group.

Image 2. UV-Vis absorbance spectrum of the CdSe QDs in MeCN.

Quantum dots in α,α,α-trifluorotoluene

### General Procedure G – Reactions in TFT with OPAc ligands

Solutions of the appropriate starting material, trap, and OPAc ligands were prepared in dry α,α,α-trifluorotoluene outside the glovebox. The vials containing the solutions were closed with a septum. Teflon tape and parafilm were applied around the septa, and the solutions were thoroughly degassed by gently bubbling N_2 for 30 minutes. Then, the needles were removed and an additional layer of teflon tape and parafilm was applied around and on the septa. These "sealed" vials were introduced in the antechamber of an argon-filled glovebox. Vacuum was slowly applied and kept at minimal pressure for 2-3 minutes. Then the antechamber was slowly refilled with argon, and the same cycled was repeated at least three times. Finally, the vials were introduced in the glovebox and the septa were replaced by screw caps. A stock of dry α,α,α-trifluorotoluene should be introduced in the glovebox as well, after degassing by gently bubbling N_2 for 60 minutes. While the solvent can be stored in the glovebox for indefinite time*, the reagent solutions shouldn't be stored for more than a week, especially the radical trap solutions which should be freshly prepared.*

The reactions were entirely set up in the glovebox in the appropriate reaction vessels (see optimization tables).

At the end of the reaction, the solution was quantitatively transferred and distributed into two 15-mL Falcon tubes for 0.05 mmol scale reactions, or four 15-mL Falcon tubes for 0.20 mmol scale reactions, using acetone as a solvent. Acetone induces the precipitation of the quantum dots and after

centrifugation (4000 rpm, 7 minutes) the supernatant can be collected, rinsing with acetone. The gathered supernatants were evaporated under reduced pressure and the residue was dried under high vacuum. Flash column chromatography (SiO$_2$, pentane:Et$_2$O) afforded the pure products.

CdS – Representative protocol for a 0.05 mmol scale reaction (Table 5, entry 8 and Table 6)
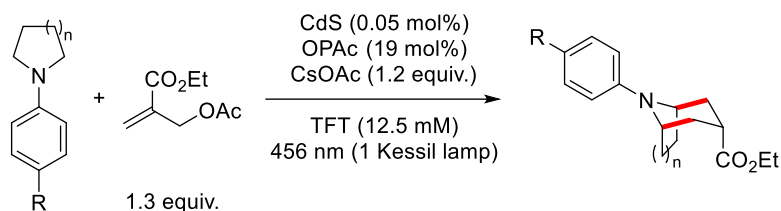
In the reaction vessel equipped with a stirring bar were added the CdSe QDs (20 µM in TFT, 1.250 mL, 0.05 mol%) and the OPAc ligands (50 mM in TFT, 0.190 mL, 19 mol%). Additional α,α,α-trifluorotoluene was added so that the total end volume of the reaction mixture reached 4 mL (12.5 mM, 2.250 mL). The solution was stirred in the dark in the glovebox for 1 h 30. Then, the starting material (1 M in TFT, 50 µL, 0.05 mmol), the radical trap ethyl 2-(acetoxymethyl)prop-2-enoate (0.250 M in TFT, 0.260 mL, 1.3 equiv.) and CsOAc (12 mg, 1.2 equiv.) were added. The vial was tightly closed. A layer of Teflon tape and parafilm was added around the cap. The vial was taken out of the glovebox for irradiation under a 456 nm Kessil lamp for 24 hours. A ventilator was used. When a Schlenk tube was used, no Teflon tape and/or parafilm was used. The protocol was unchanged when scaling up the reaction to 0.20 mmol, except that two Kessil lamps were used opposite to each other, and the reaction time was doubled. Work-up and purification as previously described.

CdSe – Representative protocol for a 0.05 mmol scale reaction (Scheme 5)
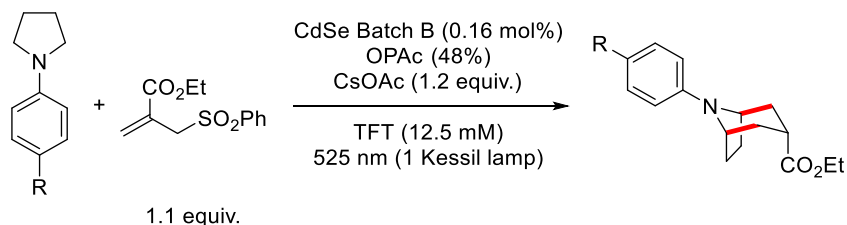
In the reaction vessel equipped with a stirring bar were added the CdSe QDs (50 µM in TFT, 1.600 mL, 0.16 mol%) and the OPAc ligands (50 mM in TFT, 0.480 mL, 48 mol%). Additional α,α,α-trifluorotoluene was added so that the total end volume of the reaction mixture reached 4 mL (12.5 mM, 1.764 mL). The solution was stirred in the dark in the glovebox for 1 h 30. Then, the starting material (1 M in TFT, 50 µL, 0.05 mmol), the radical trap ethyl 2-(benzenesulfonylmethyl)prop-2-enoate (0.520 M in TFT,

0.106 mL, 1.1 equiv.) and CsOAc (12 mg, 1.2 equiv.) were added. The vial was tightly closed. A layer of Teflon tape and parafilm was added around the cap. The vial was taken out of the glovebox for irradiation under a 525 nm Kessil lamp for 24 hours. A ventilator was used. Work-up and purification as previously described.

Three rounds of CdS photocatalysis

For the first round of the CdS QDs, **general procedure G** was followed on 0.20 mmol scale. Work-up and purification were carried out as described to afford the desired product as a white crystalline solid (23.7 mg, 0.091 mmol, 46%, α/β 6:1). The four Falcon tubes containing the recovered quantum dots as a yellow powder were loosely closed and introduced in the glovebox *via* at least three evacuation cycles in the antechamber. They were used within 24 hours for the next round.
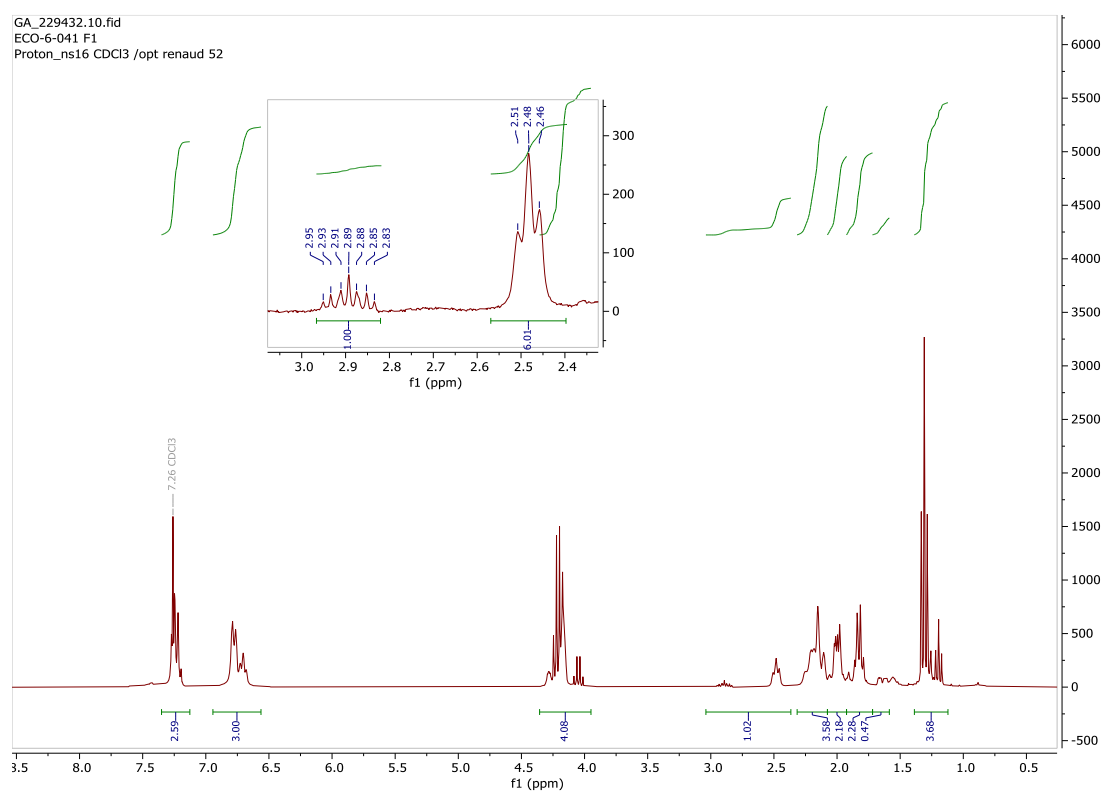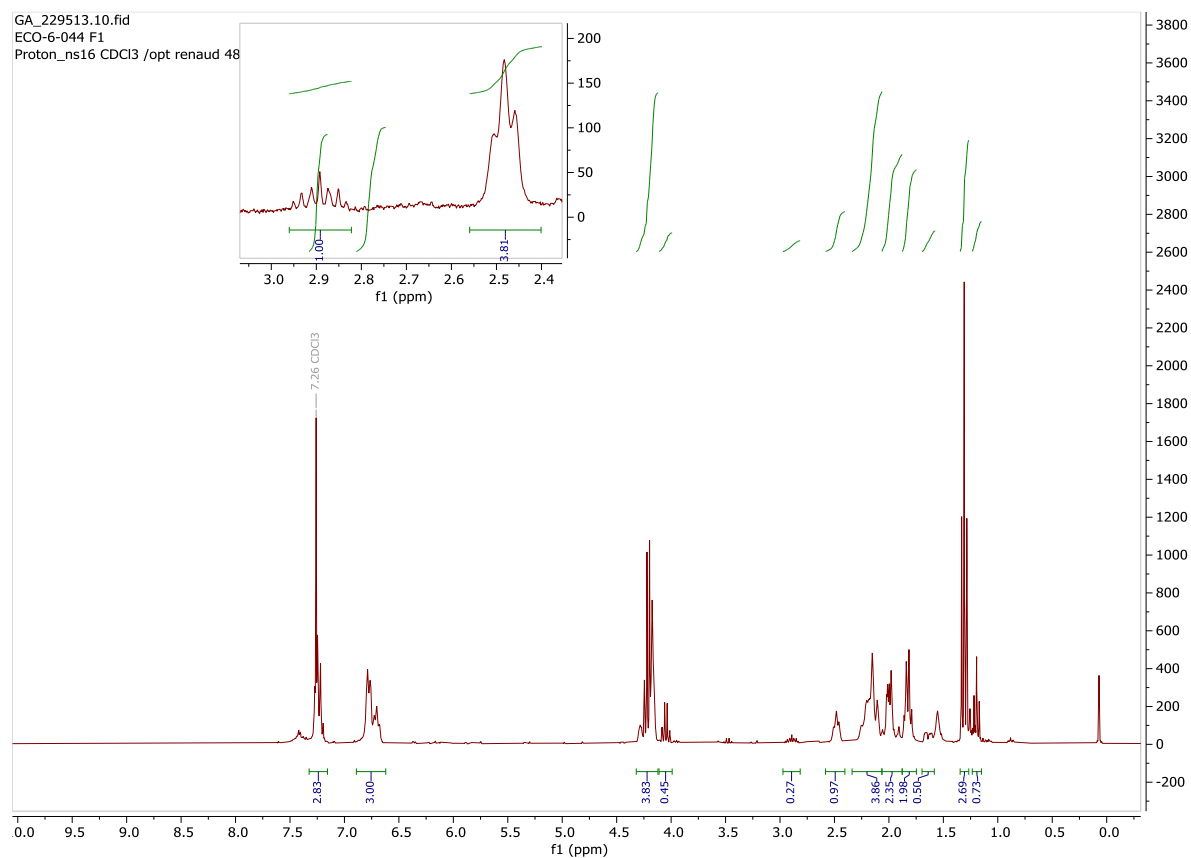

Image 3. ^{1}H-NMR spectrum of the isolated product after the first round of the CdS QDs on 0.20 mmol scale.

In the second round of the CdS QDs, the powder was solubilized in α,α,α-trifluorotoluene and transferred to the reaction vial. The quantity of TFT used for this step should be known so as to comply with the necessary volume to be achieved for the reaction (16 mL in total). The solubilization of the powder QDs can be difficult at this point, so not 100% of the QDs were transferred for the 2nd run. Because the OPAc are already grafted on the quantum dots, no additional ligands were added. No changes in the procedure otherwise. Work-up and purification were carried out as described to afford the desired product as a white crystalline solid (21.5 mg, 0.083 mmol, 42%, α/β 4:1). The four Falcon

tubes containing the recovered quantum dots as a yellow powder were loosely closed and introduced in the glovebox *via* at least three evacuation cycles in the antechamber. They were used within 24 hours for the next round.

Image 4. ^{1}H-NMR spectrum of the isolated product after the second round of the CdS QDs on 0.20 mmol scale

Third round of the QDs performed exactly as the second round. Work-up and purification were carried out as described to afford the desired product as a white crystalline solid (18.3 mg, 0.071 mmol, 35%, α/β 4:1). Not only the yield started to drop significantly, but also the purity of the product started to be compromised.

GA_229726.10.fid
ECO-6-055 F1
Proton_ns16 CDCl3 /opt renaud 14
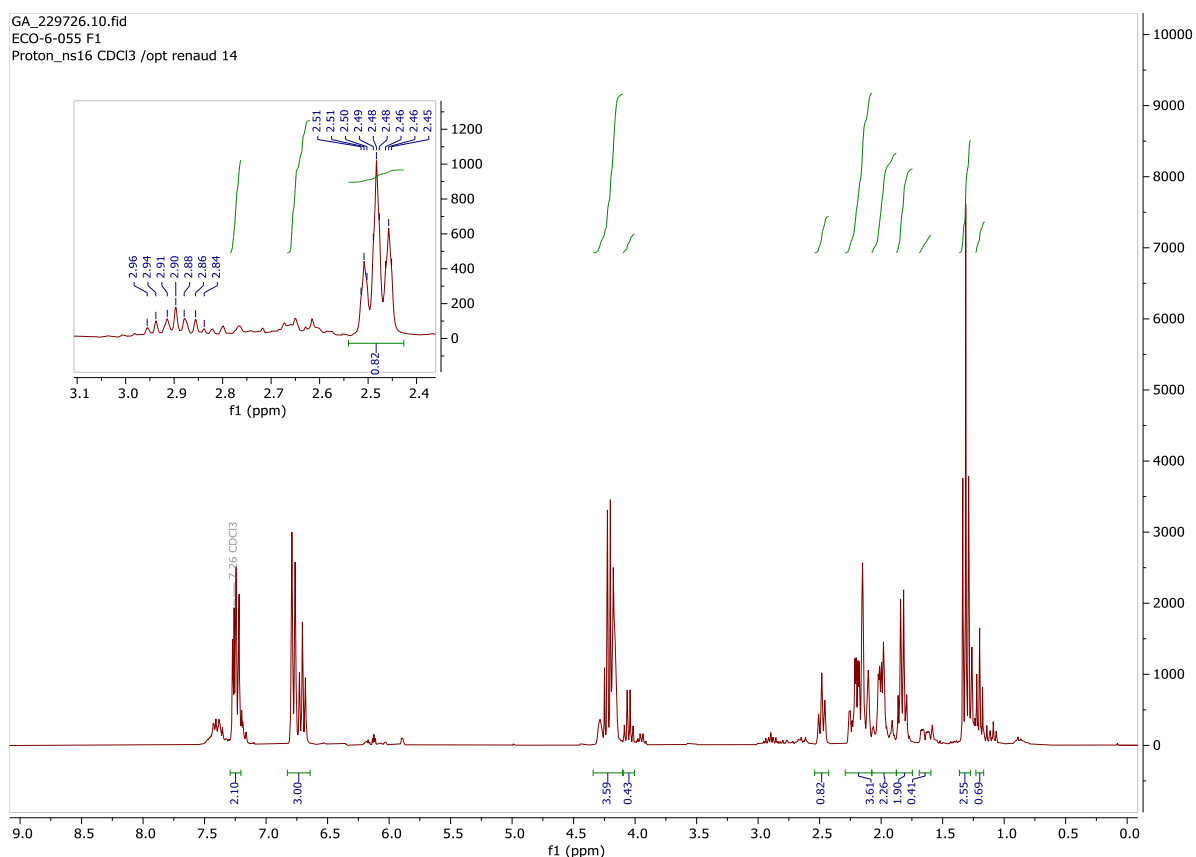
Image 5. ^{1}H-NMR spectrum of the isolated product after the third round of the CdS QDs on 0.20 mmol scale

Preliminary substrate scope using the CdS QDs

8a
C$_{17}$H$_{23}$NO$_2$
MW: 273,3760
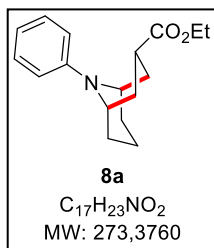
Ethyl 9-phenyl-9-azabicyclo[3.3.1]nonane-3-carboxylate (8a)

Following **General Procedure G** with 1-phenylpiperidine **6a** (0.20 mmol) and CdS QDs. Purification by flash column chromatography (SiO$_2$, heptanes/EtOAc 90:10) afforded the products **7a** and **8a** as an inseparable mix (18.5 mg, 34%, **7a:8a** ~ 5:1).

8e
C$_{18}$H$_{25}$NO$_3$
MW: 303,4020
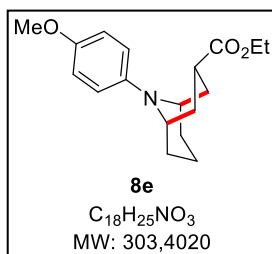
Ethyl 9-(4-methoxyphenyl)-9-azabicyclo[3.3.1]nonane-3-carboxylate (8e)

Following **General Procedure G** with 1-(4-methoxyphenyl)piperidine **6e** (0.20 mmol) and CdS QDs. Purification by flash column chromatography (SiO$_2$, pentane/Et$_2$O 96:4) afforded **8eα** as a colorless oil (4.4 mg, 0.014 mmol, 7%, α/β >20:1). The reaction also afforded compound **7e** in low yield (5.4 mg, 0.018 mmol, 9%).

^{1}H NMR (300 MHz, CDCl$_3$): δ 6.80 (s, 4H), 4.17–4.10 (m, 2H), 4.10 (q, *J* = 7.1 Hz, 2H), 3.75 (s, 3H), 2.47 (tt, *J* = 12.4, 5.9 Hz, 1H), 2.42–2.26 (m, 2H), 2.00 (qt, *J* = 13.3, 4.4 Hz, 1H), 1.79 (tt, *J* = 13.2, 4.3 Hz, 2H),

1.65 (ddd, J = 14.0, 12.3, 3.5 Hz, 2H), 1.58–1.49 (m, 1H), 1.49–1.39 (m, 2H), 1.23 (t, J = 7.1 Hz, 3H).

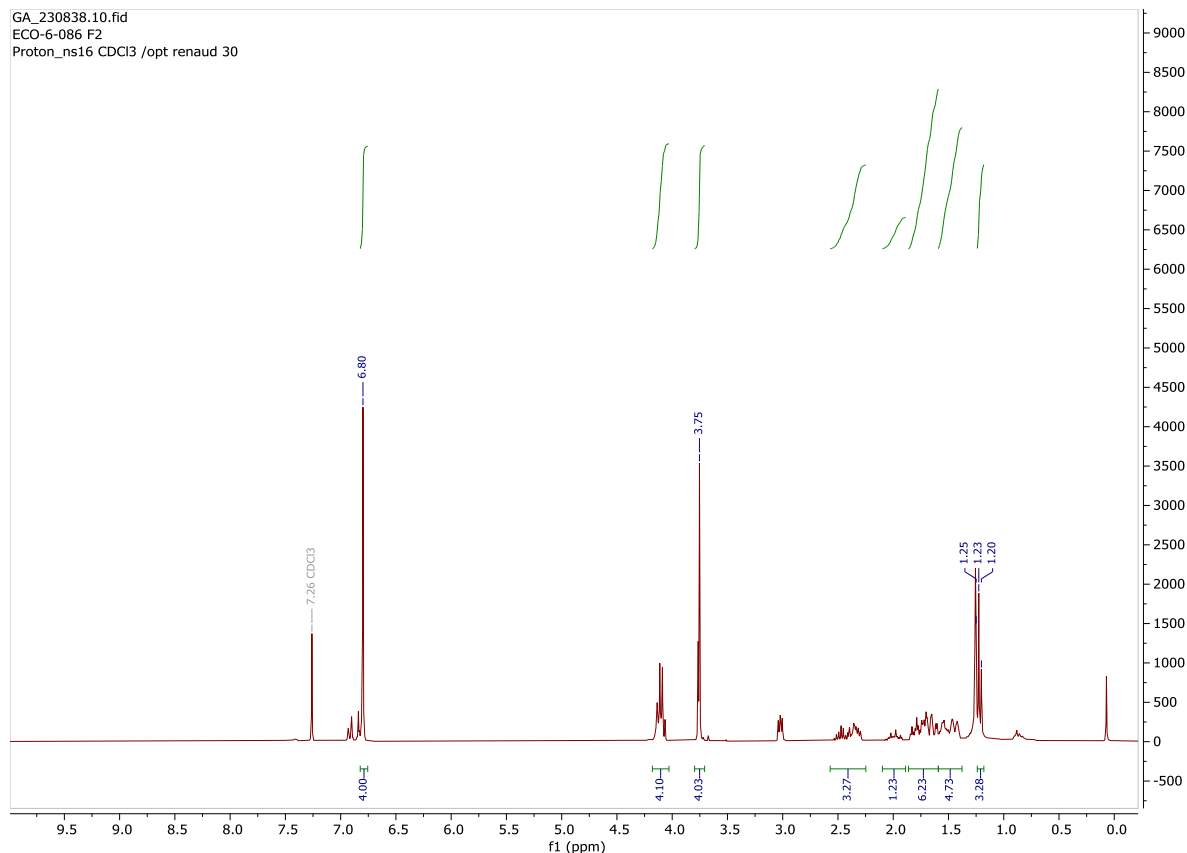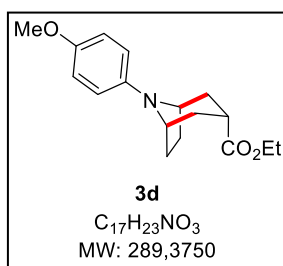Spectral data in accordance with previously described product.

*Image 6. ^{1}H-NMR spectrum of **8e** obtained from the CdS catalyzed reaction on 0.2 mmol scale*

Ethyl 8-(4-methoxyphenyl)-8-azabicyclo[3.2.1]octane-3-carboxylate (3d)

Following **General Procedure G** with 1-(4-methoxyphenyl)pyrrolidine **1d** (0.05 mmol) and CdS QDs. Purification by flash column chromatography (SiO$_2$, heptanes/EtOAc 92:8) afforded the product as a white solid (3.4 mg, 0.012 mmol, 24%, only the α diastereomer was recovered).

3d
C$_{17}$H$_{23}$NO$_3$
MW: 289,3750

^{1}H NMR (300 MHz, CDCl$_3$): δ 6.87–6.80 (m, 2H), 6.76–6.69 (m, 2H), 4.20 (q, J = 7.1 Hz, 2H), 4.11–4.04 (m, 2H), 3.76 (s, 3H), 2.48 (tt, J = 7.8, 1.6 Hz, 1H), 2.21 (ddd, J = 14.4, 7.8, 3.2 Hz, 2H), 2.21 (ddd, J = 14.5, 3.2, 1.5 Hz, 2H), 2.00–1.95 (m, 2H), 1.85–1.75 (m, 2H), 1.30 (t, J = 7.1 Hz, 3H). Spectral data in accordance with previously described product.
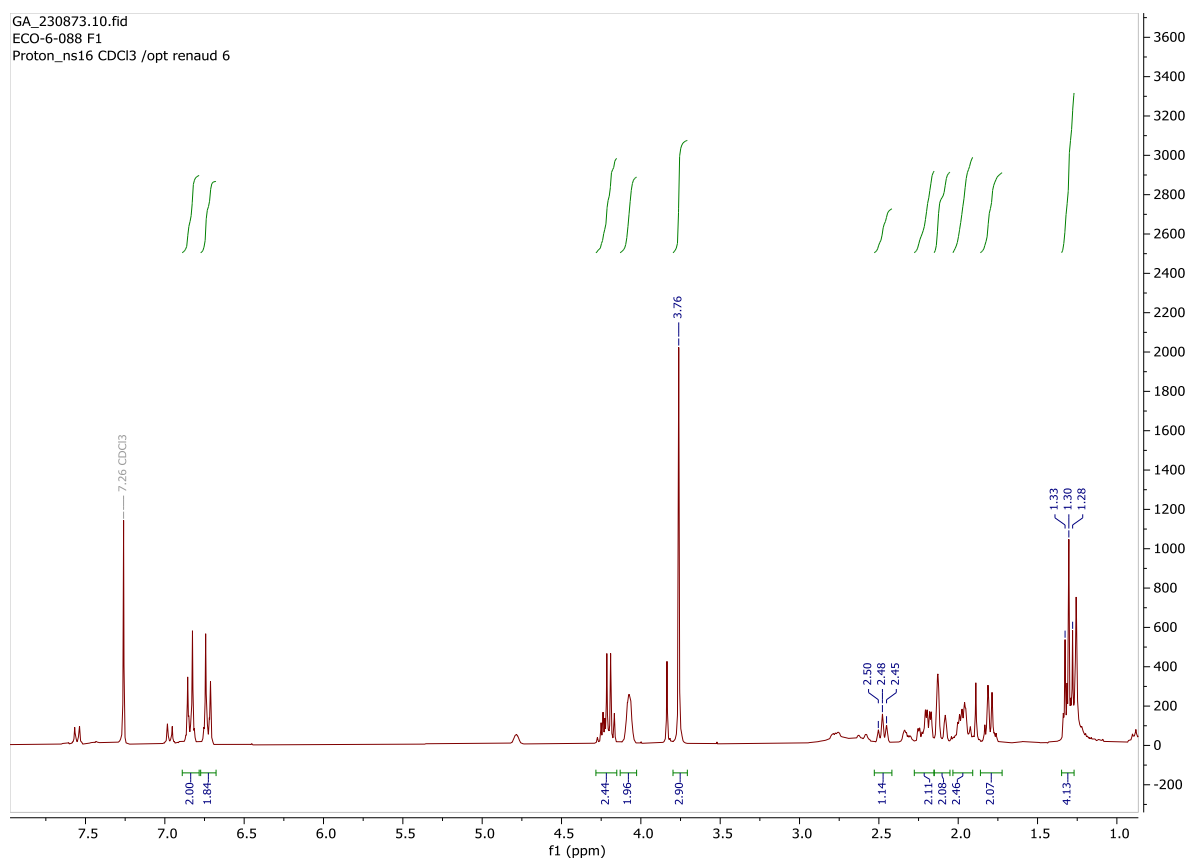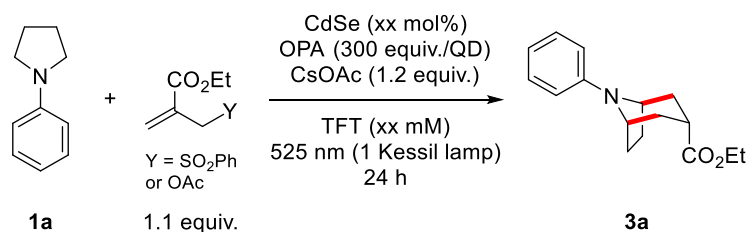
GA_230873.10.fid
ECO-6-088 F1
Proton_ns16 CDCl3 /opt renaud 6

*Image 7. ^{1}H-NMR spectrum of **3d** obtained from the CdS catalyzed reaction on 0.05 mmol scale*

CdSe quantum dots

Additional results

Entry	Scale (mmol)	CdSe (mol%)	[1a] (mM)	Abs	Y	Yield (isolated)
Batch A						
1	0.05	0.16	12.5	3.7	SO₂Ph	56%, dr 6 :1
2	0.16ᵃ	0.16	12.5	3.7	SO₂Ph	28%, α only
Batch B						
3	0.05	0.16	12.5	3.7	SO₂Ph	no reaction
4	0.05	0.16	12.5	3.7	OAc	no reaction

5	0.05 (no OPAc)	0.16	12.5	3.7	SO$_2$Ph	no reaction
6	0.05	0.08	12.5	1.85	SO$_2$Ph	no reaction

Table 1. Investigation of the CdSe photocatalytic activity - Batch B. ^{a}72 h irradiation time.

Under exact same conditions, Batch B and Batch A gave a very different result (Table 1, entries 1 and 3). Switching the sulfone trap to the acetate trap did not promote the reaction (Table 1, entry 4). To rule out a potentially deleterious influence of the OPAc ligands, a reaction was run without adding the ligands to the reaction mixture (Table 1, entry 5). No reaction was observed. Finally, a reaction with an absorbance close to 1 was carried out by reducing the catalyst loading. This was done to favor light penetration in the reaction mixture and to avoid QD aggregation upon reaction. Unfortunately, no starting material conversion was observed either.

*Reactivity with **1d***
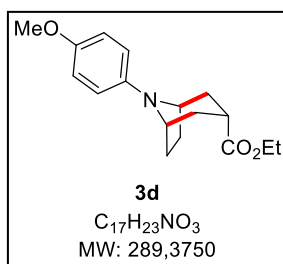
3d
C$_{17}$H$_{23}$NO$_3$
MW: 289,3750

Ethyl 8-(4-methoxyphenyl)-8-azabicyclo[3.2.1]octane-3-carboxylate (3d)

Following **General Procedure G** with 1-(4-methoxyphenyl)pyrrolidine **1d** (0.05 mmol), ethyl 2-(benzenesulfonylmethyl)prop-2-enoate (1.1 equiv.) and CdSe QDs (Batch A, B or C), reacting for 14 hours. Purification by flash column chromatography (SiO$_2$, heptanes/EtOAc 92:8) afforded the product as a white solid (5.5 mg, 0.019 mmol, 38%, only the α diastereomer was recovered).

^{1}H NMR (300 MHz, CDCl$_3$): δ 6.87–6.80 (m, 2H), 6.76–6.69 (m, 2H), 4.20 (q, *J* = 7.1 Hz, 2H), 4.11–4.04 (m, 2H), 3.76 (s, 3H), 2.48 (tt, *J* = 7.8, 1.6 Hz, 1H), 2.21 (ddd, J = 14.4, 7.8, 3.2 Hz, 2H), 2.21 (ddd, *J* = 14.5, 3.2, 1.5 Hz, 2H), 2.00–1.95 (m, 2H), 1.85–1.75 (m, 2H), 1.30 (t, *J* = 7.1 Hz, 3H). Spectral data in accordance with previously described product.
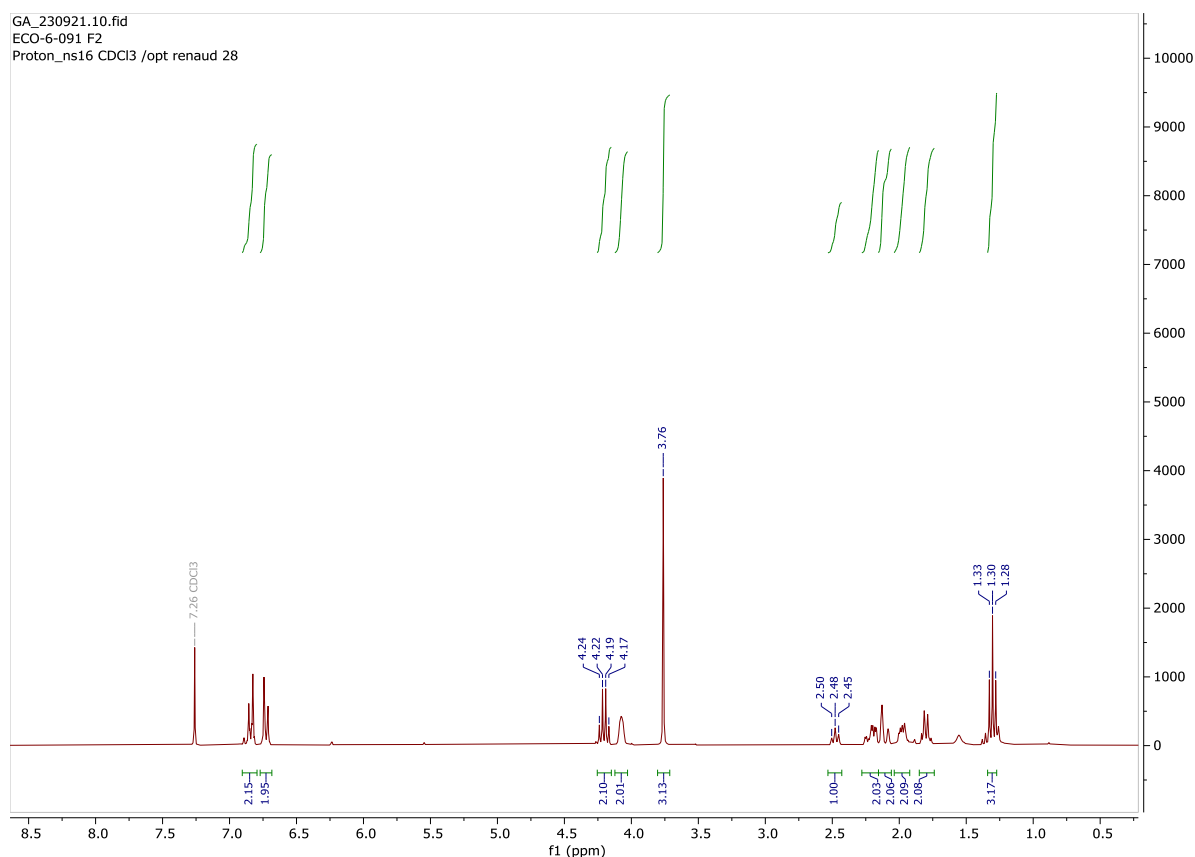
*Image 8. ¹H-NMR spectrum of **3d** obtained from the CdSe catalyzed reaction on 0.05 mmol scale with the sulfone trap.*

In table 5, optimization with the CdS QDs showed that the acetate trap was best used in 1.3 equivalent excess. These conditions were used with the CdSe quantum dots in the reaction of **1d**, in an attempt to increase to yield of **3d** (Scheme 1). With the sulfone trap, 35 to 38% yield had be obtained, depending on the batch of CdSe. With Batch B of the CdSe quantum dots, the acetate trap was not beneficial for the reaction of **1d** toward **3d**. The reaction appeared to be slowlier than with the sulfone trap and after 24 hours, 32% NMR yield of **3d** was obtained. In contrary to the reaction with the sulfone trap, 20% NMR yield of **2d** was obtained as well, which brings the total productive yield to 52%. Unfortunately, the conversion of **2a** to **3d** could not be pushed further.
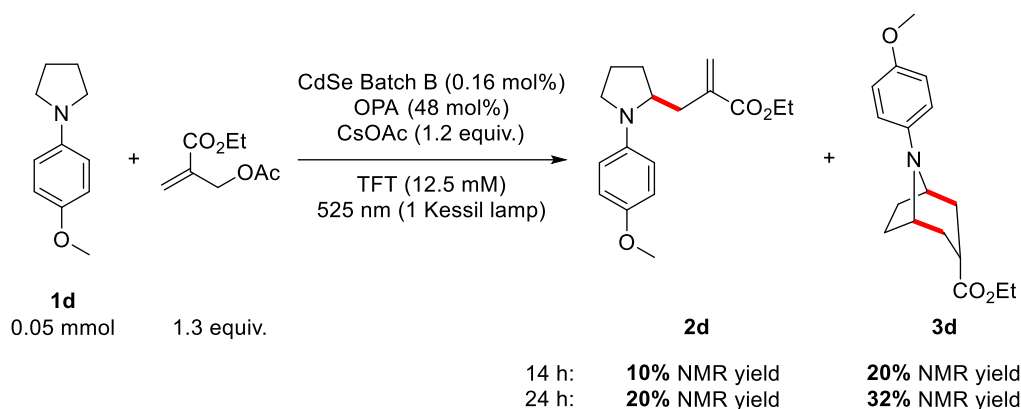
*Scheme 1. Use of the acetate trap with **1d** and CdSe QDs (Batch B). Reaction as in General Procedure G with ethyl 2-(acetoxymethyl)prop-2-enoate (1.3 equiv.) instead of the sulfone trap. ^{1}H-NMR yields determined using ethylene carbonate as a standard.*

Iridium catalyzed reaction with *n*Bu₄OAc

3aα
C₁₆H₂₁NO₂
MW: 259,3490
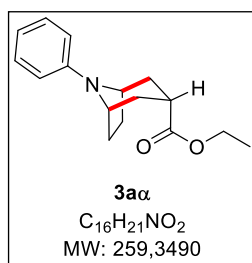
Ethyl 8-phenyl-8-azabicyclo[3.2.1]octane-3-carboxylate (3a)

In an oven-dried 10 mL-vial were successively added ethyl 2-(acetoxymethyl)prop-2-enoate (37.9 mg, 0.22 mmol), [Ir{dF(CF₃)ppy}₂(dtbpy)]PF₆ (2.2 mg, 0.02 mmol, 1 mol%) and *n*Bu₄NOAc (72.4 mg, 0.24 mmol). The vial was closed with a rubber septum and evacuated/refilled with N₂ (x 3). 1-phenylpyrrolidine (29 μL, 0.20 mmol) was added *via* a Hamilton syringe. Finally, dry and degassed 1,2-dichloroethane (4.00 mL, 0.05 M) was added. The resulting yellow mixture was placed in front of a 390 nm blue LED (5 cm distance) and stirred until completion of the reaction (TLC monitoring, 20 minutes). The reaction mixture was diluted with sat. NaHCO₃ (3 mL). The aqueous phase was extracted with DCM (3 x 5 mL) and the combined organic phases were dried over Na₂SO₄, filtered, and concentrated under reduced pressure to give crude product as an orange oil. Purification by flash column chromatography (SiO₂, pentane/Et₂O 90:10) afforded the bicyclic product **3a** as a crystalline white solid (24.7 mg, 0.095 mmol, 48%, α/β 4.3:1).

^{1}H NMR (300 MHz, CDCl₃): δ 7.29–7.20 (m, 2H), 6.78 (d, J = 8.1 Hz, 2H), 6.71 (t, J = 7.2 Hz, 1H), 4.21 (q, J = 7.2 Hz, 2H), 4.17–4.15 (m, 2H), 2.48 (tt, J = 7.7, 1.8 Hz, 1H, -CH-CO2Et), 2.28–2.17 (m, 2H), 2.17–2.09 (m, 2H), 2.04–1.96 (m, 2H), 1.88–1.78 (m, 2H), 1.31 (t, J = 7.1 Hz, 3H). Spectra data in accordance with previously described product.
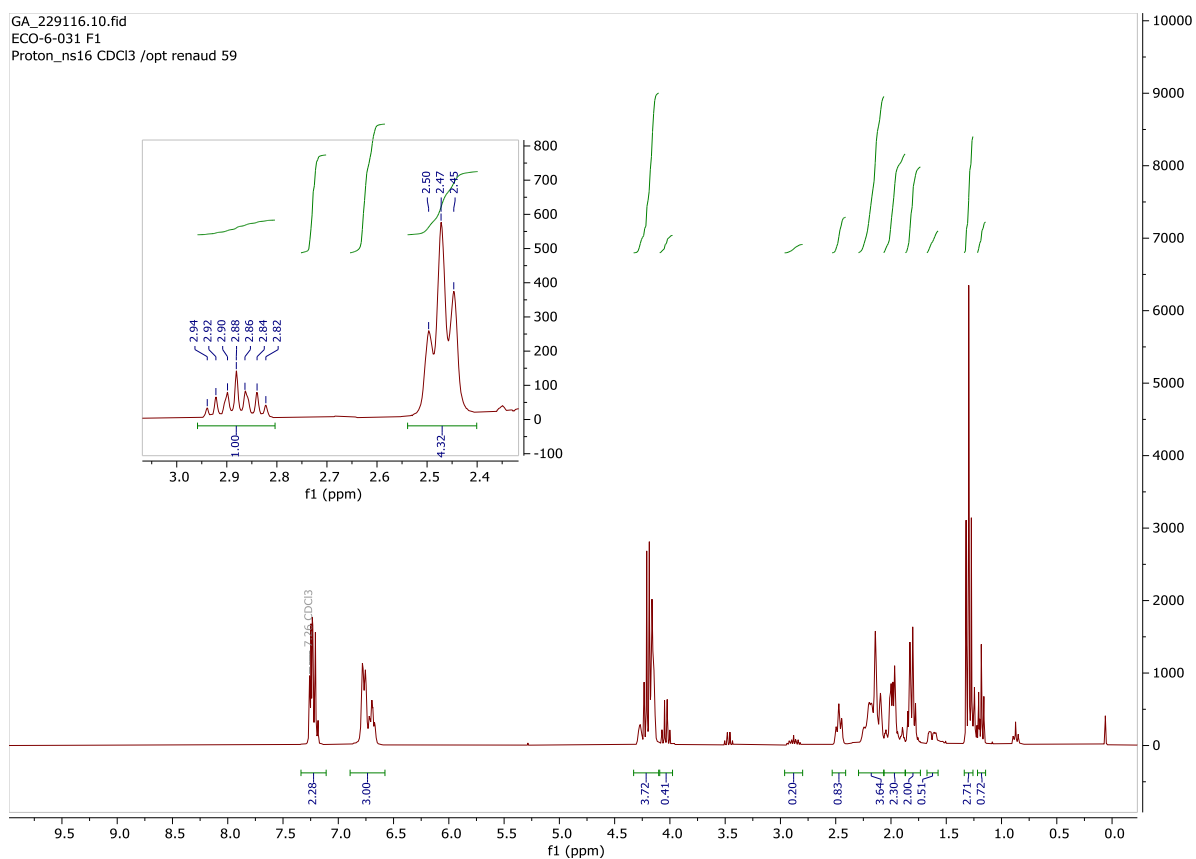
GA_229116.10.fid
ECO-6-031 F1
Proton_ns16 CDCl3 /opt renaud 59

*Image 9. ^{1}H-NMR spectrum of product **1a** obtained from the iridium photocatalyzed reaction with nBu$_4$Ac as the base.*

Declaration of consent

on the basis of Article 18 of the PromR Phil.-nat. 19

Name/First Name:

Registration Number:

Study program:

Bachelor ☐   Master ☐   Dissertation ☐

Title of the thesis:

Supervisor:

I declare herewith that this thesis is my own work and that I have not used any sources other than those stated. I have indicated the adoption of quotations as well as thoughts taken from other authors as such in the thesis. I am aware that the Senate pursuant to Article 36 paragraph 1 litera r of the University Act of September 5th, 1996 and Article 69 of the University Statute of June 7th, 2011 is authorized to revoke the doctoral degree awarded on the basis of this thesis.

For the purposes of evaluation and verification of compliance with the declaration of originality and the regulations governing plagiarism, I hereby grant the University of Bern the right to process my personal data and to perform the acts of use this requires, in particular, to reproduce the written thesis and to store it permanently in a database, and to use said database, or to make said database available, to enable comparison with theses submitted by others.

Place/Date

Signature